EDITOR'S PICK 2021: HIGHLIGHTS IN CELL DEATH AND SURVIVAL

EDITED BY: Craig Michael Walsh and You-Wen He
PUBLISHED IN: Frontiers in Cell and Developmental Biology

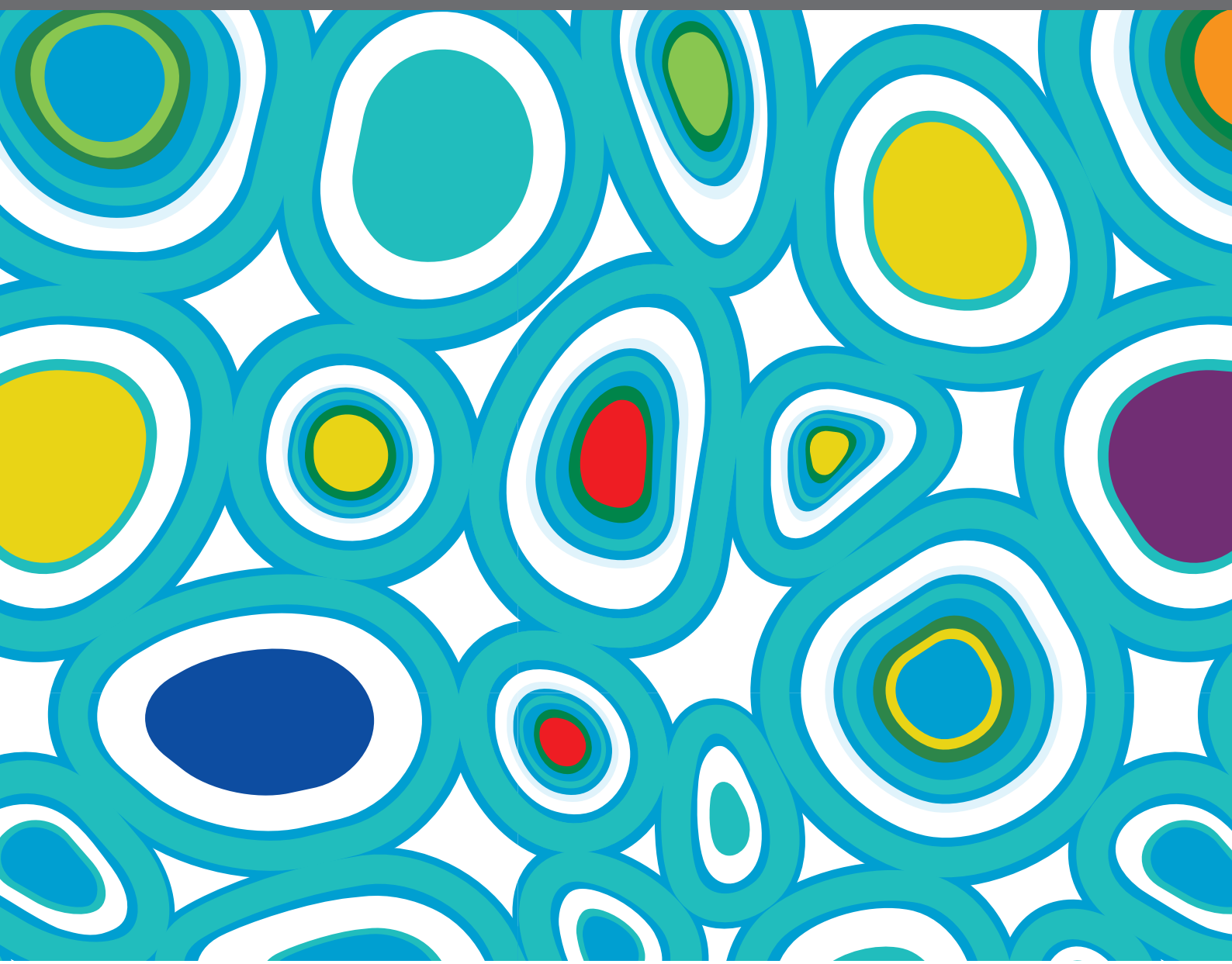

frontiers Research Topics

ISSN 1664-8714
ISBN 978-2-88974-575-3
DOI 10.3389/978-2-88974-575-3

About Frontiers

Frontiers is more than just an open-access publisher of scholarly articles: it is a pioneering approach to the world of academia, radically improving the way scholarly research is managed. The grand vision of Frontiers is a world where all people have an equal opportunity to seek, share and generate knowledge. Frontiers provides immediate and permanent online open access to all its publications, but this alone is not enough to realize our grand goals.

Frontiers Journal Series

The Frontiers Journal Series is a multi-tier and interdisciplinary set of open-access, online journals, promising a paradigm shift from the current review, selection and dissemination processes in academic publishing. All Frontiers journals are driven by researchers for researchers; therefore, they constitute a service to the scholarly community. At the same time, the Frontiers Journal Series operates on a revolutionary invention, the tiered publishing system, initially addressing specific communities of scholars, and gradually climbing up to broader public understanding, thus serving the interests of the lay society, too.

Dedication to Quality

Each Frontiers article is a landmark of the highest quality, thanks to genuinely collaborative interactions between authors and review editors, who include some of the world's best academicians. Research must be certified by peers before entering a stream of knowledge that may eventually reach the public - and shape society; therefore, Frontiers only applies the most rigorous and unbiased reviews.
Frontiers revolutionizes research publishing by freely delivering the most outstanding research, evaluated with no bias from both the academic and social point of view. By applying the most advanced information technologies, Frontiers is catapulting scholarly publishing into a new generation.

What are Frontiers Research Topics?

Frontiers Research Topics are very popular trademarks of the Frontiers Journals Series: they are collections of at least ten articles, all centered on a particular subject. With their unique mix of varied contributions from Original Research to Review Articles, Frontiers Research Topics unify the most influential researchers, the latest key findings and historical advances in a hot research area! Find out more on how to host your own Frontiers Research Topic or contribute to one as an author by contacting the Frontiers Editorial Office: frontiersin.org/about/contact

EDITOR'S PICK 2021: HIGHLIGHTS IN CELL DEATH AND SURVIVAL

Topic Editors:
Craig Michael Walsh, University of California, Irvine, United States
You-Wen He, Duke University, United States

Citation: Walsh, C. M., He, Y.-W., eds. (2022). Editor's Pick 2021: Highlights in Cell Death and Survival. Lausanne: Frontiers Media SA. doi: 10.3389/978-2-88974-575-3

Table of Contents

frontiers | Frontiers in Cell and Developmental Biology

EDITORIAL
published: 09 May 2022
doi: 10.3389/fcell.2022.887688

Editorial: Editor's Pick 2021: Highlights in Cell Death and Survival

You-Wen He[1]* *and Craig M. Walsh*[2]*

[1]Department of Immunology, Duke University School of Medicine, Durham, NC, United States, [2]Department of Molecular Biology and Biochemistry, Sue and Bill Gross Stem Cell Research Center, University of California, Irvine, Irvine, CA, United States

Keywords: cell death, autophagy, survival, T lymphocyte, antitumor immunity, immunotherapy

Editorial on the Research Topic

Editor's Pick 2021: Highlights in Cell Death and Survival

The Cell Death and Survival section of the Frontiers in Cell and Developmental Biology was launched in year 2013 to serve as an open-access venue for outstanding research and commentary in the field. This section has witnessed a dramatic increase in manuscript submission and publication of high-quality original research manuscripts and reviews addressing important Research Topic in cell death and survival in the last year. The published papers in our section cover a broad swath of topics in the area cell death and survival, from fundamental molecular and cellular biology to clinical application of cell death and survival principles. To give the broad readership of this journal an overview of the activities in the section, a Research Topic called Editor's Pick for section editors to highlight significant contributions to the field provides a brief introduction to some of the cutting edge research and influential reviews in our section. Due to a limit on the number of papers allowed for Editor's pick, many high-quality research manuscripts and insightful reviews published in our section deserve as much attention. We highlight the following publications to showcase the breadth and depth of these scholarly contributions to our section. Moreover, we thank all contributors to our section and know that the growth in Frontiers in Cell and Developmental Biology has been driven by these important contributions.

The function of the Bcl-2 family member Bok (Bcl-2 related ovarian killer) remains mysterious. Although Bok was initially classified as a pro-apoptotic protein due to its sequence homology to Bax and Bak, accumulating evidence suggests that Bok is involved in many other cellular functions (Naim and Kaufmann). Szczesniak et al. used TurboID-mediated proximity labeling to probe the Bok interactome. They reported that Bok interacts with, and is proximal to proteins involved in various cellular functions such as mitochondrial fission, endoplasmic reticulum-plasma membrane junctions, and surprisingly, Mcl-1. The physical and functional interactions between Bok and Mcl-1 were further verified. Importantly, these authors showed that Bok interactome is distinct from those of Mcl-1 and Bak. This report has provided important functional insights into Bok in apoptotic and non-apoptotic intracellular processes and will instigate additional research into this important area.

The serine/threonine kinase 35 (STK35) was known to be upregulated in colorectal cancer (CRC) but its function in tumorigenesis was unknown (Capra et al., 2006). Yang et al. reported that STK35 expression is negatively associated with CRC patient survival. In a series of gain- and loss-of-function experiments, the investigators demonstrated that STK35 inhibits tumor cell apoptosis and increases glycolysis by activating the AKT pathway. Importantly, STK35 overexpression renders CRC tumors resistant to 5-FU chemotherapy. This study suggests that STK35 may be used as a prognostic biomarker and therapeutic target for CRC diagnosis and treatment.

Immune checkpoint inhibitors such as anti-PD-1 and PD-L1 antibodies have revolutionized cancer therapy by overcoming immune exhaustion (Lei et al.). Zhang et al. investigated the expression and prognostic value of a newly identified immune checkpoint receptor Human

OPEN ACCESS

Edited and reviewed by:
Amanda Gay Fisher, Medical Research Council, United Kingdom

***Correspondence:**
You-Wen He
youwen.he@duke.edu
Craig M. Walsh
cwalsh@uci.edu

Specialty section:
This article was submitted to Cell Death and Survival, a section of the journal Frontiers in Cell and Developmental Biology

Received: *01 March 2022*
Accepted: *21 April 2022*
Published: *09 May 2022*

Citation:
He Y-W and Walsh CM (2022) Editorial: Editor's Pick 2021: Highlights in Cell Death and Survival. Front. Cell Dev. Biol. 10:887688. doi: 10.3389/fcell.2022.887688

endogenous retrovirus-H Long terminal repeat-Associating protein 2 (HHLA2) in 22 types of solid tumors. HHLA2 was reported to be expressed in all 22 tumors at the mRNA level and 12 types of these tumors at the protein level. Furthermore, HHLA2 was found to have the highest transcript levels in kidney clear cell carcinoma (KIRC) and was positively correlated with better survival and high CD8 expression in this group of patients. This study reveals a potential immunotherapeutic target for KIRC treatment.

Cellular senescence, a stable exit from the cell cycle in response to different stresses and cellular replication, is tightly linked to physiological and pathological processes such as aging and cancer (Herranz and Gil, 2018). Premature senescence may contribute to early thymus involution and immune dysregulation in Down Syndrome patients (Marcovecchio et al., 2021). Yu et al. found that transient ectopic expression of a repressive epigenetic modulator, DNA methyltransferase 3-like (DNMT3L), delays the premature senescence progression in mouse embryonic fibroblasts. The authors further investigated molecular mechanisms underlying DNMT3L-mediated chromatin surveillance through epigenetic regulation. This study is significant as a new epigenetic reinforcement strategy may be used for overcoming premature senescence in a variety of diseases.

Hypoxic ischemic encephalopathy (HIE) causes severe disability and death in ~400,000 newborns worldwide each year (Victor et al., 2021). Xiong et al. studied the molecular network regulating neuronal cell death after HIE and identified a novel long non-coding RNA (lncRNA) Vi4 (TCONS00044054) as a key regulator of neuron survival and apoptosis after HIE. Furthermore, the investigators demonstrated that a regulatory network consisting of Vi4, miR-185-5p, and the target gene Igfbp3 plays an important role in neuronal death and survival after HIE, highlighting potential strategies for therapeutic intervention of HIE.

Bioactive compounds including baicalein, baicalin, wogonin and wognoside from the roots of the medicinal plant *Scutellaria baicalensis* have potent antitumor activities (Banik et al., 2022). Huang et al. studied the antitumor activities of baicalein and baicalin in melanoma cells. These authors showed that baicalein and baicalin inhibits proliferation and induces apoptosis and senescence in melanoma cells. Mechanistically, baicalein and baicalin were found to inhibit tumor cell glucose uptake and metabolism by downregulating the mTOR/HIF-1α signaling pathway. This study suggests a potential for baicalein and baicalin as novel chemotherapy drugs.

Human aldo-keto reductase 1B10 (AKR1B10) may play roles in gastrointestinal (GI) tract function and be involved in GI cancers and inflammatory bowel diseases (Endo et al., 2021). Wang et al. characterized mice lacking AKR1B8, the mouse ortholog of human AKR1B10. The investigators found that the integrity of the intestinal epithelial barrier in AKR1B8 deficient mice was severely disrupted. Furthermore, innate and adaptive immune cell populations in the colon of AKR1B8 deficient mice were dramatically altered in composition and function. This study suggests that AKR1B8 is vital to the maintenance of intestinal epithelial barrier and normal immunity within the colon.

Autophagy plays an essential in regulating T lymphocyte survival and homeostasis (McLeod et al., 2012). Xia et al. investigated the T cell compartment in Beclin 1/Atg6 conditional knockout mice and found a diminished naïve T cell population, increased effector T cells and MDSCs, and severe colitis in aged mice. Interestingly, the reduced population of naïve T cells was rescued by crossing the conditional Beclin 1/Atg6 KO mice onto a TCR transgenic background, which also led to a normalized population of effector T cells. These data provide support for context-dependent roles of Beclin1/Atg6 in T lymphocyte survival and differentiation.

Intratumoral administration of immunotherapies has the potential to maximize immune activating capability and minimize systemic toxicities of immunotherapeutic agents (Melero et al., 2021). Hu et al. tested the antitumor activities of intratumorally injected IL-27 using recombinant adeno-associated virus (rAAV)-based delivery. The authors demonstrated that intratumoral injection of rAAV-IL-27 led to strong antitumor activities in several mouse tumor models. The investigators further showed that IL-27 induces infiltration of $CD8^+$ T cells and CXCR3 expression and imparts synergistic antitumor activities with anti-PD-1 administration or adoptively transferred T cells. These interesting preclinical data suggest that intratumoral delivery of IL-27 may be useful alone or in combination with other therapies for cancer treatment.

In addition to the above nine original research papers, we would like to highlight several insightful reviews published in our section. One example focused on ionizing radiation as a major cancer treatment modality, highlighting its ability to induce ferroptosis and alter fatty acid metabolism in tumor cells. Yuan et al. reviewed the pathways between ionizing radiation and ferroptosis and the critical roles of fatty acid metabolism in radiation-induced ferroptosis in tumor cells. Importantly, the authors provided thoughtful perspectives on the implications of the interplay between fatty acid metabolism, ferroptosis and ionizing radiation for future clinical development of novel cancer treatment modalities. Many clinical drugs have known cardiotoxicities due to their ability to induce various forms of cell death in cardiomyocytes. Ma et al. first reviewed the different forms of cell death including apoptosis, autophagy, necrosis, necroptosis, pyroptosis and ferroptosis in cardiomyocytes. These authors further analyzed the underlying mechanisms of cardiomyocyte death induced by three major classes of clinical therapeutics: anti-tumor, anti-diabetic, and anti-viral drugs. This review has offered both an excellent theoretical overview and practical guidance for physicians in therapeutic application of these clinical drugs. In a more targeted review by Zhai et al., the roles of one specific form of cell death, ferroptosis, in cardiomyopathy are discussed in depth. The potential for utilizing the ferroptosis pathway as a diagnostic and therapeutic target for patients suffering from cardiomyopathy was carefully analyzed. T lymphocytes are essential for the antitumor efficacies of immunotherapies. However, primary and acquired resistance to immunotherapies are common and may be at least partially caused by T cell dysfunction in the tumor microenvironment of cancer patients. Zhang et al. provided a comprehensive update on the molecular mechanisms of T cell dysfunction and exhaustion in the tumor microenvironment and potential strategies to overcome these

defects. In summary, the above reviews have provided timely information and thoughtful insights in a wide array of topics with high scientific and clinical significance.

REFERENCES

Banik, K., Khatoon, E., Harsha, C., Rana, V., Parama, D., Thakur, K. K., et al. (2022). Wogonin and its Analogs for the Prevention and Treatment of Cancer: A Systematic Review. *Phytother. Res.* 31, 1–27. Epub 2022/02/02. doi:10.1002/ptr.7386

Capra, M., Nuciforo, P. G., Confalonieri, S., Quarto, M., Bianchi, M., Nebuloni, M., et al. (2006). Frequent Alterations in the Expression of Serine/Threonine Kinases in Human Cancers. *Cancer Res.* 66 (66), 8147–8154. Epub 2006/08/17. doi:10.1158/0008-5472.CAN-05-3489

Endo, S., Matsunaga, T., and Nishinaka, T. (2021). The Role of AKR1B10 in Physiology and Pathophysiology. *Metabolites* 11, 11. Epub 2021/06/03. doi:10.3390/metabo11060332

Herranz, N., and Gil, J. (2018). Mechanisms and Functions of Cellular Senescence. *J. Clin. Invest* 128 (128), 1238–1246. Epub 2018/04/03. doi:10.1172/JCI95148

Marcovecchio, G. E., Ferrua, F., Fontana, E., Beretta, S., Genua, M., Bortolomai, I., et al. (2021). Premature Senescence and Increased Oxidative Stress in the Thymus of Down Syndrome Patients. *Front. Immunol.* 12, 669893. Epub 2021/06/19. doi:10.3389/fimmu.2021.669893

McLeod, I. X., Jia, W., and He, Y.-W. (2012). The Contribution of Autophagy to Lymphocyte Survival and Homeostasis. *Immunol. Rev.* 249, 195–204. Epub 2012/08/15. doi:10.1111/j.1600-065x.2012.01143.x

Melero, I., Castanon, E., Alvarez, M., Champiat, S., and Marabelle, A. (2021). Intratumoural Administration and Tumour Tissue Targeting of Cancer Immunotherapies. *Nat. Rev. Clin. Oncol.* 18, 558–576. Epub 2021/05/20. doi:10.1038/s41571-021-00507-y

Victor, S., Rocha-Ferreira, E., Rahim, A., Hagberg, H., and Edwards, D. (2021). New Possibilities for Neuroprotection in Neonatal Hypoxic-Ischemic Encephalopathy. *Eur. J. Pediatr. Nov.* 24. Epub 2021/11/26. doi:10.1007/s00431-021-04320-8

AUTHOR CONTRIBUTIONS

Both Y-WH and CW wrote this editorial.

Conflict of Interest: The authors declare that the research was conducted in the absence of any commercial or financial relationships that could be construed as a potential conflict of interest.

Publisher's Note: All claims expressed in this article are solely those of the authors and do not necessarily represent those of their affiliated organizations or those of the publisher, the editors, and the reviewers. Any product that may be evaluated in this article, or claim that may be made by its manufacturer, is not guaranteed or endorsed by the publisher.

frontiers in Cell and Developmental Biology

REVIEW
published: 11 February 2020
doi: 10.3389/fcell.2020.00017

T Cell Dysfunction and Exhaustion in Cancer

Zhen Zhang[1†], Shasha Liu[1†], Bin Zhang[2], Liang Qiao[3], Yi Zhang[4] and Yi Zhang[1,5,6,7]*

[1] Biotherapy Center, The First Affiliated Hospital of Zhengzhou University, Zhengzhou, China, [2] Department of Hematology/Oncology, School of Medicine, Northwestern University, Chicago, IL, United States, [3] Department of Microbiology and Immunology, Stritch School of Medicine, Health Sciences Division, Loyola University Chicago, Maywood, IL, United States, [4] Fels Institute for Cancer Research and Molecular Biology, Lewis Katz School of Medicine, Temple University, Philadelphia, PA, United States, [5] Cancer Center, The First Affiliated Hospital of Zhengzhou University, Zhengzhou, China, [6] Henan Key Laboratory for Tumor Immunology and Biotherapy, Zhengzhou, China, [7] School of Life Sciences, Zhengzhou University, Zhengzhou, China

Tumor immunotherapy is a promising therapeutic strategy for patients with advanced cancers. T cells are key mediators of antitumor function that specifically recognize and react to tumor-expressing antigens and have proven critical for cancer immunotherapy. However, T cells are not as effective against cancer as expected. This is partly because T cells enter a dysfunctional or exhausted state, which is characterized by sustained expression of inhibitory receptors and a transcriptional state distinct from that of functional effector or memory T cells. T cell dysfunction induces the out of control of tumors. Recently, T cell dysfunction has been investigated in many experimental and clinical settings. The molecular definition of T cell dysfunction and the underlying causes of the T cell dysfunction has been advanced regardless of the fact that the pathways involved are not well elucidated, which proposing promising therapeutic opportunities in clinic. In this review, we will discuss the recent advances in the molecular mechanisms that affect TME and induce T cell dysfunction, and the development of promising immunotherapies to counteract the mechanisms of tumor-induced T cell dysfunction. Better understanding these underlying mechanisms may lead to new strategies to improve the clinical outcome of patients with cancer.

Keywords: T cells dysfunction, intrinsic factors, extrinsic factors, tumor microenvironment, cancer immunotherapy

OPEN ACCESS

Edited by:
Bin Li,
Shanghai Jiao Tong University School of Medicine, China

Reviewed by:
Shengtao Zhou,
West China Second University Hospital of Sichuan University, China
Lianjun Zhang,
Center of Systems Medicine, Chinese Academy of Medical Sciences, Suzhou Institute of Systems Medicine (ISM), China

***Correspondence:**
Yi Zhang
yizhang@zzu.edu.cn

† These authors have contributed equally to this work

Specialty section:
This article was submitted to Cell Death and Survival, a section of the journal Frontiers in Cell and Developmental Biology

Received: *05 October 2019*
Accepted: *10 January 2020*
Published: *11 February 2020*

Citation:
Zhang Z, Liu S, Zhang B, Qiao L, Zhang Y and Zhang Y (2020) T Cell Dysfunction and Exhaustion in Cancer. Front. Cell Dev. Biol. 8:17. doi: 10.3389/fcell.2020.00017

INTRODUCTION

Cancer immunotherapy is a transformative strategy that utilizes the immune system of the body to treat cancer. T cells destruct tumor cells by recognizing and reacting to tumor-associated antigens through their T cell receptors (TCRs) (Kishton et al., 2017). Considerable progress has been made in the development of immunotherapy techniques that enhance T cell anti-tumor immunity,

Abbreviations: ARG-1, arginase-1; CAFs, cancer-associated fibroblasts; CAR, chimeric antigen receptor; CAR-T, chimeric antigen receptor-engineered T cells; ETC, endogenous peripheral blood-derived T cells; EZH2, enhancer of zeste homolog 2; FAO, fatty acid oxidation; Glut-1, glycosis transporter-1; ICB, immune checkpoint blockers; IDO, indoleamine 2,3-dioxygenase-1; IFN-γ, interferon-γ; IL-2, interleukin-2; iNOS, inducible nitric oxide synthase; LAG-3, lymphocyte activation gene 3; MDSCs, myeloid derived suppressor cells; MPE, malignant pleural effusion; NSCLC, non-small cell lung cancer; OXPHOS, oxidative phosphorylation; PA-MSHA, *Pseudomonas aeruginosa*-mannose- sensitive hemagglutinin; PD-1, programed cell death 1; PD-L1, programed cell death ligand 1; ROS, reactive oxygen species; TAMs, tumor-associated macrophages; TCR, T cell receptor; TCR-T, TCR-engineered T cells; TGF-β, transforming growth factor-β; TIGIT, immunoreceptor tyrosine-based inhibitory motif domain; TIL, tumor infiltrated lymphocytes; TIM-3, T-cell immunoglobulin domain and mucin domain protein 3; TLR4, toll like receptor 4; TME, tumor microenvironment; TNF-α, tumor necrosis factor-α; Tregs, T regulatory cells.

including adoptive transfer of tumor infiltrating lymphocytes (TILs), endogenous peripheral blood-derived T cells (ETC), chimeric antigen receptor-engineered T cells (CAR-T), and TCR-engineered T cells (TCR-T). In addition, neoantigen vaccines and checkpoint blockade therapies using anti-programed cell death 1 (PD-1) and anti-PD-ligand 1 (PD-L1) have shown potent therapeutic effects in patients with advanced cancer (Chapuis et al., 2016b; Yee and Lizee, 2017; Boyiadzis et al., 2018; Yee, 2018; Riley et al., 2019). These encouraging results demonstrate that T cell-based cancer therapies offer great promise in inducing complete responses in patients against several types of cancer (Maude et al., 2014; Yee et al., 2015). However, many patients who have responded to T cell-based therapies do not achieve durable clinical responses. Mechanisms underlying resistance or short-term response to these therapies remain largely unknown. Some studies suggest that the efficacy of immunotherapy is limited by the generation of dysfunctional T cells in the tumor microenvironment (TME) (Thommen and Schumacher, 2018; Vodnala et al., 2019). Indeed, negative regulators that mediate T cell dysfunction have been identified in mice and humans. For example, treatment with anti-PD-1/PD-L1 and anti-CTLA-4 immune checkpoint inhibitors reinvigorate dysfunctional TILs and augment their anti-tumor effects (Wherry and Kurachi, 2015; Zarour, 2016; Miller et al., 2019; Wang et al., 2019a). Thus, a better understanding of the mechanisms underlying T cell dysfunction in the TME may lead to novel therapeutic interventions for patients with cancer.

Recent studies have shown that the exhaustion and functional impairment of T cells in the TME is a defining feature of many cancers (Jiang et al., 2015). The TME consists of cancer cells as well as immunosuppressive cells and their associated cytokines, i.e., interleukin-10 (IL-10) and transforming growth factor-β (TGF-β) that facilitate tumor progression and mediate T cell dysfunction. Many studies have shown that dysfunctional $CD8^+$ T cells in cancer are characterized by high expression levels of inhibitory receptors, including PD-1, TIM-3, LAG-3 and immunoreceptor tyrosine-based inhibitory motif domain (TIGIT), which are positively associated with T cell exhaustion. In addition, these dysfunctional $CD8^+$ T cells show impaired production of effector cytokines, such as IL-2, IFN-γ and tumor necrosis factor-α (TNF-α) (Chauvin et al., 2015; Wang et al., 2017). Moreover, T cell dysfunction results in impaired proliferation and decreased production of effector molecules in response to tumor antigens. In this review, we discuss the characteristics of T cell dysfunction in cancer with an aim to elucidate the molecular mechanisms through which TME-derived factors mediate T cell dysfunction factors, and this may promote the exploration of novel strategies for restoring intratumoral T cell function, which can further enhance immunotherapy efficacy.

HALLMARKS OF T CELL DYSFUNCTION IN CANCER

Within the heterogeneous TME, T cells are a major part of the immune infiltrate. The intratumoral T cell population comprises naive, memory, effector and regulatory T cells (Treg) (Hashimoto et al., 2018). Upon stimulation by an antigen, TCRs activate a cell-intrinsic program that guides T cell differentiation into cytotoxic effector cells capable of clearing the antigen. Following the peak of effector cell expansion and the clearance of the specific antigen, most effector T cells die, with the exception of a small number of memory T cells that survive and provide long-term protection against the antigen (Chang et al., 2014). However, when antigen-experienced T cells are chronically exposed to the same antigen, substantial alterations in T cell activation and differentiation may occur, leading to T cell "dysfunction" or "exhaustion" (Wherry, 2011; Schietinger and Greenberg, 2014). A previous study has shown that the tumor-specific T cell dysfunctional exhaustion state is initiated early after tumor initiation and antigen encounter in a murine model (Schietinger et al., 2016). Dysfunctional $CD8^+$ T cells are characterized by a loss of effector functions, such as cytotoxicity and proliferation. In addition, the upregulation of immune checkpoints and changes in transcriptional and metabolic molecules have been described as hallmarks of T cell dysfunction (**Table 1**). For example, the single cell RNA sequencing of tumoral T cells from melanoma and lung cancer indicated that T cells expressed genes such as *PDCD1* and *LAG3* that are associated with T cell dysfunction (Guo et al., 2018; Li H. et al., 2019). Nevertheless, T cell function can be successfully reinvigorated by blocking PD-1 or PD-L1, highlighting the critical role of PD-1/PD-L1 axis in T cell dysfunction. However, activated and functional $CD8^+$ T cells can also overexpress PD-1 in cancer patients (Fourcade et al., 2010), and not all PD-1^+ cells might respond equally to anti-PD-1 therapy (Thommen et al., 2018). It has reported that PD-1^+CD$38^+$$CD8^+$ T cells are a population of dysfunctional cells that fail to respond to anti-PD-1 therapy (Verma et al., 2019). Meanwhile, the TME contains a variety of cell types and cytokines (**Table 1**) that take part in tumor progression, which could contribute to T cell dysfunction (Xia et al., 2019). Therefore, there is growing interest in the identification of the molecular signatures and characteristics that are associated with dysfunctional T cells in cancer (**Figure 1**).

INTRINSIC FACTORS THAT INDUCED T CELL DYSFUNCTION

Transcription Factors

It has become increasingly clear that several transcriptional factors, including NR4A1, TOX, Eomes, T-bet, Prdm1 (Blimp-1), NFAT and BATF, regulate the PD-1 expression and are implicated in T cell exhaustion and dysfunction (Wang et al., 2017; Liu X. et al., 2019). For example, NR4A1 was found highly expressed in tolerant or dysfunctional T cells in a mouse model. Overexpression of NR4A1 inhibits effector T cell differentiation, whereas deletion of NR4A1 overcomes T cell tolerance and increases T cell proliferation, enhancing anti-tumor effects. Moreover, expression levels of PD-1 and TIM-3 in T cells were found significantly decreased in NR4A1$^{-/-}$ mice. A mechanistic analysis suggested that NR4A1 is preferentially recruited to binding sites of the transcription factor activator protein 1 (AP-1), where it inhibits effector gene expression by reducing AP-1 function. These findings indicate that NR4A1 is important for

TABLE 1 | Core molecular regulation of T cell dysfunction or exhaustion.

Intrinsic factors	Function	References
NR4A	Transcriptional factor that highly expresses in dysfunctional T cells, which can impair anti-tumor effects of T cells and induce PD-1 and TIM-3 expression.	Liu X. et al., 2019
TOX	High-mobility group (HMG)-box transcription factor that regulates the progression of T cell dysfunction and the maintenance of exhausted T cells.	Alfei et al., 2019; Wang et al., 2019d
TCF-1	Transcriptional factor that supports stem-cell function of PD-1$^+$ TILs and the formation of exhausted T cell progenitors, which are described that express TCF1 and intermediate amounts of PD-1 (PD-1^{int}).	Chen Z. et al., 2019
Eomes	Transcriptional factor that correlates with T cell exhaustion by inducing co-inhibitory molecule B7 superfamily member 1(B7S1) pathway.	Li et al., 2018c
NFAT	A key regulator of T cell activation, can induce exhaustion, which is also the upstream of NR4A and TOX.	Martinez et al., 2015
BATF	Transcription factor that impairs T cell proliferation and cytokine secretion during HIV infection in a pathway downstream of PD-1.	Quigley et al., 2010
Blimp-1	Transcription factor that drives T cells toward a dysfunctional phenotype during chronic LCMV infection.	Hwang et al., 2016
DNMT3A	Epigenetic factor that involves a *de novo* exhaustion-specific DNA methylation pattern, which is important to format the exhausted program.	Ghoneim et al., 2017
mTOR	Metabolic checkpoint that regulates glycolysis via transcription factors including HIF-1α and c-Myc, enhancing the expression of inhibitory receptors in T cells.	Le Bourgeois et al., 2018
TGF-β	Cytokine that induces the expression of TIM-3, PD-1 and CTLA-4 in T cells, and inhibits the secretion of IFN-γ and Granzyme-B.	Wang et al., 2019d
IL-10	Cytokine that suppresses IFN-γ secretion in CD8$^+$ TILs. IL-10 blockade enhances the effects of anti-PD-1 therapy in expanding antigen-specific CD8$^+$ T cells.	Brooks et al., 2008; Li L. et al., 2019

inducing T cell dysfunction and represents a promising target for augmenting cancer immunotherapy (Liu X. et al., 2019).

Recently, the high-mobility group (HMG)-box transcription factor TOX was reported as a critical regulator in the progression of T cell dysfunction and the maintenance of exhausted T cells during chronic infection (Alfei et al., 2019). Several studies also showed that TOX may have a role in mediating transcriptional and epigenetic reprograming that are critical for the exhausted CD8$^+$ T cells responses in cancer (Khan et al., 2019). Although the formation of effector and memory T cells is not dependent on TOX, the formation of exhausted T cells was failure without TOX. Robust expression of TOX can translate continuous stimulation that induces T cell exhaustion (Khan et al., 2019). Moreover, TOX and TOX2 as well as NR4A family members are highly induced PD-1 and TIM-3 expression in CAR$^+$ TILs. TOX and TOX2 deficient CAR$^+$ TILs can prevent tumor growth and prolong survival of tumor-bearing mice (Seo et al., 2019). In a mouse model of hepatocellular carcinoma (HCC), TOX was upregulated in exhausted CD8$^+$ T cells, impairing their anti-tumor function. The underlying mechanism involves a TOX-induced decrease in PD-1 degradation and promotion of PD-1 endocytic recycling to the cell surface. Knocking down TOX in tumor-specific CD8$^+$ T cells promoted the anti-tumor effects of these T cells, exhibiting the synergetic role of anti-PD-1therapy (Wang et al., 2019d).

TCF-1 has been implicated in the formation of memory precursor T cells mediated by Wnt signaling pathway (Jeannet et al., 2010). Similarly, TCF-1 is also required for the stem-like functions of TCF1$^+$PD-1$^+$ TILs, which were detected in the blood of patients with melanoma and who had responded to checkpoint blockade (Siddiqui et al., 2019). Most notably, TCF-1 enhances Bcl2 expression via c-Mycb and supports the establishment of exhausted T cell progenitors (Chen Z. et al., 2019). These progenitor cells were described that express TCF1 and intermediate amounts of PD-1 (PD-1^{int}). These TCF1$^+$PD-1^{int} cells give rise to dysfunctional TCF1$^-$PD-1^{hi} TIM-3$^+$ cells, which show resistance to PD-1 blocking therapy. Moreover, TCF1$^+$PD-1^{int} cell survival can be boost by upregulating TOX expression (Mann and Kaech, 2019). Scott found that TOX-deficient tumor-specific T cells failed to persist in cancers, and hypothesized that TOX-induced exhaustion serves as a negative feedback mechanism that prevents activation-induced T cell death and overstimulation of antigen-specific T cells (Scott et al., 2019). These findings suggest that TOX may play a two-blade function in T cell dysfunction or exhaustion.

T-bet and Eomes were found to operate in contrasting ways to facilitate the effector versus memory CD8$^+$ T cell fates (Chang et al., 2014). Enhanced T-bet expression fosters effector differentiation of antigen-specific CD8$^+$ T cells toward the terminally differentiated fate. In contrast, Eomes is highly expressed in memory T cells and is considered important for the maintenance of memory T cells (Knudson et al., 2017). Notably, recently studies identified high expression levels of Eomes in exhausted CD8$^+$ T cells during chronic lymphocytic choriomeningitis virus (LCMV) infection. Interestingly, the CD8$^+$ T cells producing high levels of Eomes also expressed high levels of PD-1. These Eomes^{hi}PD-1^{hi} CD8$^+$ T cells co-expressed other inhibitory receptors and displayed limited proliferative capacity (Li et al., 2018b). In addition, Eomes is directly involved in exhaustion of CD8$^+$ TILs via the co-inhibitory molecule B7 superfamily member 1(B7S1) pathway (Li et al., 2018c). However, how increased expression of Eomes promotes CD8$^+$ T cell exhaustion remains elusive.

Studies have shown that NFAT, a key regulator of T cell activation, can induce hyporesponsiveness (anergy and

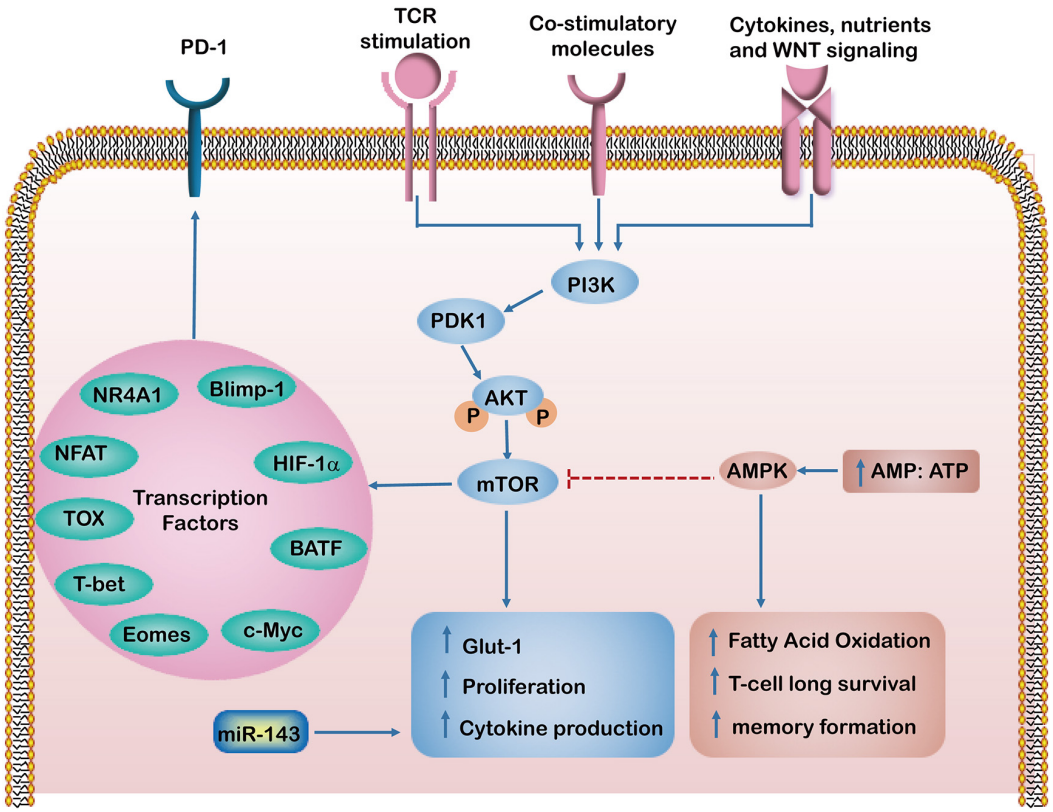

FIGURE 1 | The intrinsic factors regulating T cell dysfunction. In response to T cell receptors (TCRs), co-stimulatory and growth factor cytokines activate PI3K/Akt/mTOR signaling pathways, which induce glucose transporter-1 (Glut-1) expression and enhance T cell proliferation and cytokine production. Activation of mTOR leads to the expression of downstream transcriptional regulators such as HIF-1α and c-Myc. However, an increased AMP to ATP ratio activates AMP-activated protein kinase (AMPK), which in turn inhibits mTOR activity and enhances fatty acid oxidation, which maintains long term T-cell survival and formation of memory T cells. The Transcription factors such as HIF-1α, NR4A1, TOX, Eomes, T-bet, Blimp-1, NFAT and BATF regulate PD-1 expression and have been implicated in T cell exhaustion and dysfunction.

exhaustion) in both $CD4^+$ and $CD8^+$ T cells, if it does not bind AP-1 transcription factors (Martinez et al., 2015). Moreover, TOX and NR4A are important for the transcriptional program of $CD8^+$ T cell exhaustion downstream of NFAT (Seo et al., 2019). Intriguingly, BATF, a transcription factor of the AP-1 family, was found to impair T cell proliferation and cytokine secretion during HIV infection in a pathway downstream of PD-1 (Quigley et al., 2010). Similarly, Blimp-1 was found to drive T cells toward a dysfunctional phenotype during chronic LCMV infection (Hwang et al., 2016). Further identifying how these transcription factors are integrated together to mediate $CD4^+$ and $CD8^+$ T cell exhaustion or dysfunction will provide molecular insights into T cell responses and immunity.

Epigenetic Factors

Emerging evidence indicates that epigenetic states and chromatin landscapes are closely associated with the functional state of dysfunctional or exhausted $CD8^+$ T cells, which are abnormally expressed PD-1 (Pauken et al., 2016; Sen et al., 2016; Kartikasari et al., 2018). Epigenetic components including DNA methylation and histone modifications could control PD-1 expression and T cell exhaustion. For example, DNA methylation enzymes such as DNMT1 and DNMT3B are significantly upregulated in exhausted T cells (Schietinger et al., 2016). Meanwhile, DNA methyltransferase 3A (DNMT3A) has been demonstrated to functionally establish a *de novo* exhaustion-specific DNA methylation pattern. Inhibition of DNMT3A in these T cells can promote their differentiation toward memory cells. Critically, observations from studies of chronic viral infections indicated a critical role for the demethylation at the promoter region of PD-1 locus in mediating T cell dysfunction (Ghoneim et al., 2017). Inhibition of DNA methylation leads to a revitalized effect on the function of exhausted T cells.

The most widely studied histone lysine methylation sites in T cells are histone 3 lysine 4 (H3K4), and H3K27. H3K4 methylation is associated with transcriptional activation, and H3K27 trimethylation is associated with the repression of genes important for T-cell differentiation and survival (Liu H. et al., 2019). When TCR stimulation and IL-6 or IL-12 treatment were combined, both $H3K4^{me1}$ and H3K27 acetylation were contributed to increased PD-1 expression (Bally et al., 2016). Moreover, overexpression of miR-155 significantly enhances polycomb repressor complex 2 (PRC2), which restrains T cell exhaustion and sustains $CD8^+$ T cell antitumor responses

(Ji et al., 2019). Additionally, EZH2 is a catalytic subunit of PRC2 that can alter gene expression by trimethylating H3K27 (Zhao et al., 2016; He et al., 2017). In a recent study, EZH2 was found to control the polyfunctionality and differentiation of effector T cells (He et al., 2017). Interestingly, inhibition of EZH2 in ovarian and colorectal cancer patients resulted in increased of CXCL9 and CXCL10 production and augmented the infiltration of T cells that eliminate tumors (Nagarsheth et al., 2016; Jones et al., 2018). EZH2 represses the expression of tumor suppressor genes in various cancer cells, thereby promoting cell invasion and driving tumor progression (Bohrer et al., 2010; Hayashi et al., 2011). Thus, EZH2 may be a promising target for cancer immunotherapy (Wang et al., 2019c). Meanwhile, treatment with JQ1-α specific inhibitor of the histone acetylation reader bromodomain-containing protein 4 (BRD4)-results in decreased PD-L1 expression on tumor cells and macrophages, which is correlated with an increase in antitumor T cell activity (Zhu et al., 2016). These findings indicate that pharmacological manipulation of epigenetic mechanisms can alter T cell exhaustion or dysfunction in a clinically relevant manner. Thus, therapies employing hypomethylating agents and PD-1 blockade are a promising strategy in cancer patients.

Metabolic Factors

The metabolic program is a set of biochemical reactions that allows T cells to acquire and utilize nutrients necessary for their survival, proliferation, and functions (Chang et al., 2015). It has been shown that effector T cells use glycolysis for anabolic metabolism for their growth and proliferation. In contrast, memory T cells switch to a non-proliferative form of metabolism, using FAO as a predominant metabolic program and obtaining ATP mainly via OXPHOS (Pearce et al., 2013). Interestingly, the link between antigenic stimulation and metabolic pathway activation appears to be altered in dysfunctional T cells (Le Bourgeois et al., 2018; Sugiura and Rathmell, 2018). Recently, metabolic checkpoints (e.g., AMPK, Myc, HIF-1α and mTOR) that control T cell differentiation have been highlighted as a novel therapeutic targets for immune modulation (Chang and Pearce, 2016). AMPK is a heterotrimeric serine/threonine kinase complex that senses the intracellular AMP/ATP ratio. Activated AMPK can enhance FAO and simultaneously inhibit glucose and mTOR activity. This results in maintaining long-term T cell survival and memory formation (Ma et al., 2017). A previous study demonstrated that the abrogation of phosphoenolpyruvate carboxykinase (Pck1)–glycogen–pentose phosphate pathway (PPP) decreases GSH/GSSG ratios and increases levels of ROS levels, leading to impairment of memory $CD8^+$ T cell formation (Ma et al., 2018). Our previous work demonstrated that miR-143 enhances the anti-tumor effects of $CD8^+$ T cells by promoting memory T cell differentiation and metabolism reprograming by inhibiting of glycolysis targeting glucose transporter-1 (Glut-1) (Zhang et al., 2018). TCR signaling, together with costimulatory molecules and growth factor cytokines, activates phosphatidylinositide 3 kinase (PI3K)/Akt/mTOR signaling pathways, which induce Glut-1 and enhance T cell proliferation and cytokine production (Salmond, 2018). Furthermore, activation of the mTOR pathway and engagement of glycolysis lead to the expression of downstream transcriptional regulators such as HIF-1α and c-Myc, enhancing the expression of inhibitory receptors on T cells (Le Bourgeois et al., 2018). Meanwhile, suppression of Akt and mTOR is required for augmenting activity of the transcription factor FoxO1. Importantly, FoxO1 sustains PD-1 expression, which promotes the differentiation of terminally exhausted T cells (Staron et al., 2014). Therefore, these intrinsic metabolic factors regulate T cell metabolism and activate pathways involved in effector function and exhaustion.

EXTRINSIC FACTORS: TUMOR MICROENVIRONMENT

Apart from T cell self-regulation, the interaction between other cells or cytokines in the TME is another important factor that induces T cell dysfunction. Various types of cancers and cytokines compose the TME, including tumor cells, immunosuppressive cells, stromal cells, IL-6 and IL-10, to name a few, which collectively form a complex of immunosuppressive network. These TME components exert potent effects on limiting T cell differentiation and driving T cell dysfunction. In addition, tumor cells and immunosuppressive cells within TME produced highly reactive soluble oxygen and toxic metabolites, which inhibit T cell responses (Maimela et al., 2019). Thus, it is challenging to precisely define the relative contribution of these potential extrinsic factors to T cell function and differentiation in the TME (**Figure 2**).

MYELOID DERIVED SUPPRESSOR CELLS

Myeloid-derived suppressor cells (MDSCs) play pivotal roles in promoting tumor progression and contribute to immunosuppressive function (Ostrand-Rosenberg, 2010; Li et al., 2018e). MDSCs are a heterogeneous group of pathologically activated immature myeloid cells in the TME. The various mechanisms implicated in MDSC-mediated immune suppression include the release of high levels of arginase (ARG)-1, inducible nitric oxide synthase (iNOS), reactive oxygen species (ROS) and cyclooxygenase-2 (COX2) (Chen J. et al., 2019). For example, ARG-1 and iNOS, either separately or in combination, are used by MDSCs to impede $CD8^+$ T cells response to antigens. Indeed, expression of ARG-1 has been reported to decrease CD3ζ-chain biosynthesis, thus impairing T cell function (Rodriguez et al., 2002). In addition, NO alone can suppress $CD8^+$ T cells by inhibiting the phosphorylation and activation of JAK3 and STAT5 transcription factors, as well as inducing T-cell apoptosis (Wu et al., 2015). Elevated levels of ROS in the TME was involved in limiting T cell growth, differentiation, and ultimately promoting the exhaustion of T cells. ROS produced by MDSCs and other cells may interact with T cells and cause oxidative stress which may induce $CD8^+$ T cell hypo-responsiveness in cancer (Chen et al., 2016).

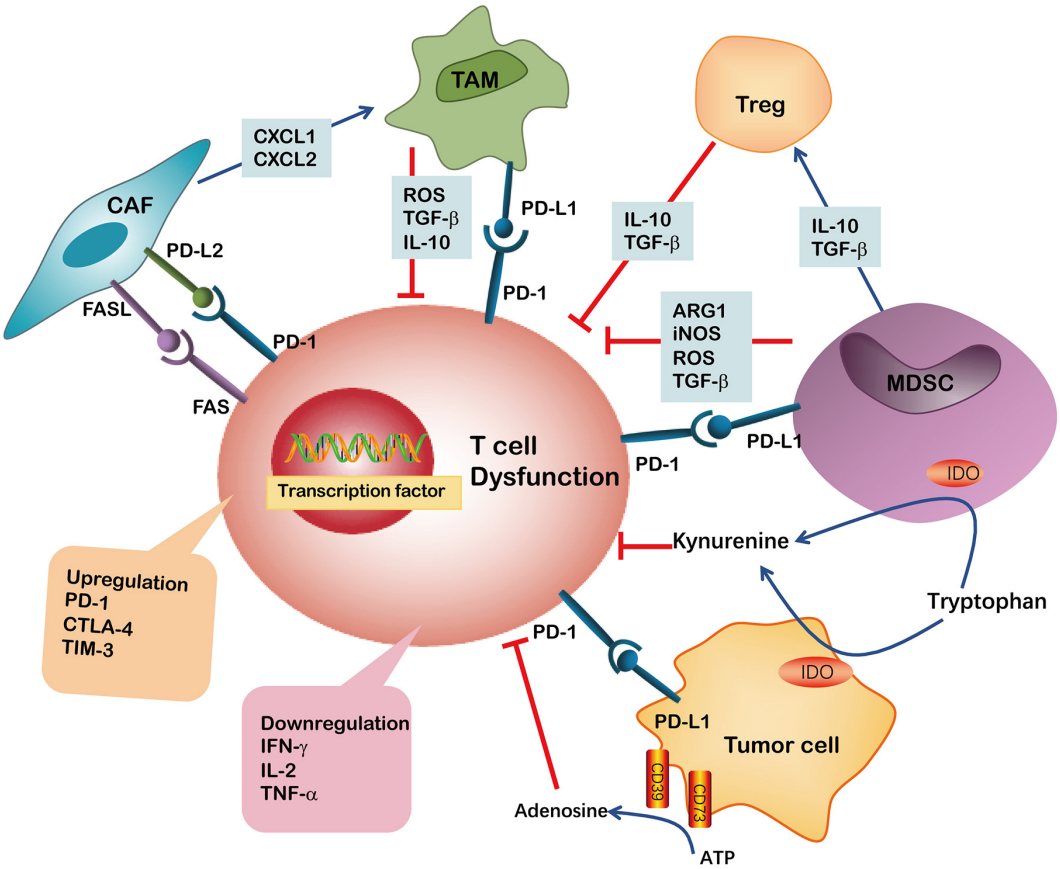

FIGURE 2 | Immunosuppressive cells or factors have been implicated in CD8$^+$ T cell dysfunction in TME. The ARG1, iNOS, TGF-β and ROS are secreted by MDSCs or TAMs and induce CD8$^+$ T cell dysfunction. Both MDSCs and tumor cells may suppress CD8$^+$ T cell proliferation through IDO hydrolyzation of tryptophan in the presence of IFN-γ. Kynurenine inhibits CD8$^+$ T cell activation. MDSCs may additionally produce immunosuppressive cytokines like IL-10, TGF-β and induce Tregs. The upregulation of PD-L1 on MDSCs, TAMs and tumor cells induced CD8$^+$ T cell exhaustion by binding to PD-1 on T cells. Tumor cells also express CD39 and CD73 on their surface, facilitating the metabolism of extracellular ATP into AMP and finally into adenosine, which induce CD8$^+$ T cell dysfunction. CAFs are involved in impairing anti-tumor T cell responses by secreting chemokines such as CXCL1 and CXCL2 to tumors and polarizing them toward the M2 phenotype. Furthermore, the expression of PD-L2 or FASL on CAFs bind to corresponding PD-1 and FAS receptors, respectively, causing CD8$^+$ T cell dysfunction.

Interestingly, MDSCs produce high levels of IDO, which catabolizes tryptophan and generates kynurenine. Depletion of tryptophan and induction of kynurenine lead to blockade of clonal expansion of activated T cells. Experimental studies indicate that IDO hydrolyzation of tryptophan represents an important mechanism by which MDSCs suppress proliferation and survival of tumor infiltrating CD8$^+$ T cells and CD8$^+$ T cells homed to the lymph nodes. Other reports demonstrated that STAT3-dependent IDO expression mediates immunosuppressive effects of MDSCs in breast cancer, in which MDSCs dramatically inhibit the proliferation of CD8$^+$ T cells and their production of IFN-γ (Yu et al., 2013). Data from our previous studies indicate that CD11b$^+$CD33$^+$ MDSCs in tumor tissues from NSCLC patients express surface ectonucleotidases CD39 and CD73. Moreover, TGF-β stimulates CD39 and CD73 expression, thereby inhibiting autologous CD8$^+$ T cell proliferation and function (Li et al., 2017). Thus, MDSCs play an important role in repressing CD8$^+$ T cell proliferation thus inducing CD8$^+$ T-cell exhaustion in TME.

TUMOR-ASSOCIATED MACROPHAGES

Macrophages play a critical role in innate immunity and are responsible for defending the host against foreign pathogens. They can be further classified into pro-inflammatory M1 or anti-inflammatory M2 macrophages. M1 cells are characterized by the high expression of various pro-inflammatory cytokines and contribute to promoting the Th1 response. They also have strong microbicidal and tumoricidal activity (Sica and Mantovani, 2012; Ambade et al., 2016). M2 cells, also known as alternatively activated macrophages, are activated by Th2 cytokines (e.g., IL-4, IL-10, and IL-13) and secret high levels of anti-inflammatory cytokines such as IL-10, and TGF-β. M2 macrophages primarily contribute to immune-suppression and favor tumor promotion (Liu S. et al., 2019).

Tumor-associated macrophages (TAMs) are generally characterized as an M2-like macrophage phenotype in TME. They can be identified by the expression of CD163, CD204 or CD206 in human derived TAMs, and F4/80, CD163, CD206,

ARG1 or Ym1 in murine-derived TAMs (Cassetta et al., 2016; Chen Y. et al., 2017; Benner et al., 2019). TAMs often accelerate the progression of untreated cancer and negatively influence the efficacy of anticancer drugs, including checkpoint blockade immunotherapies. Therefore, TAMs are shown to be closely correlated with a poor prognosis of patients with cancer. Li and colleagues demonstrated that TAMs-secreted IL-10 promotes cancer stem cell-like properties and tumor growth in NSCLC; High levels of IL-10 are associated with a poor prognosis of NSCLC patients (Yang and Zhang, 2017). TAMs can induce immunosuppression mainly through several ways: (1) TAMs may induce the expression of PD-L1 in monocytes, which binds to PD-1 on the surface of $CD8^+$ T cells, inducing T cell exhaustion; (2) TAMs secret numerous immunosuppressive cytokines and factors, including IL-10, TGF-β and ROS, which induce $CD8^+$ TIL exhaustion and dysfunction; and (3) TAMs can directly inhibit $CD8^+$ T cells cytotoxicity through the depletion of the amino acids, such as L-arginine and tryptophan. In addition, these functions indicate that TAMs produce high levels of IDO to inhibit $CD8^+$ T cells cytotoxicity. Collectively, TAMs are a highly active subset of immunosuppressive cells promoting tumor survival and immune evasion (Jiang et al., 2015; Yang and Zhang, 2017).

Efforts are underway to either deplete M2 cells or convert the M2 phenotype into M1 cells (inflammatory) in most tumors. In a mouse model of ovarian cancer, it was shown that tumor rejection by CAR-T cells required the presence of M1 macrophages, suggesting that tumor-reactive T cells were not sufficient to completely eliminate the tumor on their own (Yeku et al., 2017). We have recently reported that M1 macrophages converted from M2 macrophages by *Pseudomonas aeruginosa*-mannose-sensitive hemagglutinin (PA-MSHA) can enhance the anti-tumor immune response. This effect primarily relies on activation of toll like receptor 4 (TLR4) (Yang et al., 2015).

CANCER ASSOCIATED FIBROBLASTS

Cancer-associated fibroblasts (CAFs), the most abundant stromal population, secrete immunomodulatory factors in TME and are emerging as suppressive mediators of T cell immunity. CAFs can recruit myeloid cells to tumors via the secretion of chemokines such as CXCL1 and CXCL2 to tumors. They can also polarize these recruited myeloid cells toward the M2 phenotype (Zhen et al., 2017). Similarly, CAFs can further bolster the immunosuppressive TME by recruiting MDSCs and Tregs. Thus, the crosstalk between CAFs and other cells contributes to the immunosuppressive TME. Other studies revealed a new biological function for CAFs, showing that these cells directly suppress anti-tumor T-cell responses by a mechanism dependent on immune checkpoint activation. One of the underlying mechanisms was the upregulation of FAS/FASL and PD-1/PD-L2 on $CD8^+$ T cells and CAFs, respectively, which drives the dysfunction of tumor-specific $CD8^+$ T cells (Lakins et al., 2018). Targeting CAFs or CAFs-related pathways can be considered as a powerful strategy for attenuating stromal barriers and promoting cancer immunotherapy.

SOLUBLE MEDIATORS

Immunosuppressive cytokines in TME can be produced by tumor cells, MDSCs or CAFs and are crucial factors that mediate T-cell exhaustion and dysfunction (Chen J. et al., 2017). For example, the TGF-β signaling pathway plays an important role in tumor suppression and paradoxically, plays a role in tumor promotion. In general, TGF-β mediates tumor suppression via the inhibition of cancer cell proliferation and induction of cancer stem cell senescence by diminishing their self-renewing capability during the early stages of tumor development. Additionally, TGF-β promotes tumor progression and metastasis through the modulation of immune responses in later stages (Colak and Ten Dijke, 2017). TGF-β derived TAMs exert its function by inducing TIM-3, PD-1 and CTLA-4 expression in T cells and inhibiting IFN-γ and Granzyme-B secretion in a dose-dependent manner. Treatment with anti-TGF-β antibody restored the impaired T cell cytotoxic function in MPE. Furthermore, inhibiting TGF-β signaling in $CD8^+$ T cells using dominant negative receptors can improve the function of exhausted cells (Wang et al., 2019b).

IL-10 in TME is primarily secreted by cancer cells, TAMs, natural killer cells (NK) and $CD4^+$ Tregs (Landskron et al., 2014). A study of patients with ovarian carcinoma demonstrated that the tumor-infiltrating follicular regulatory T (Tfr) cells exhibit significantly upregulated IL-10 expression, which is negatively associated with IFN-γ secretion in $CD8^+$ TILs (Li L. et al., 2019). In chronic viral infections, PD-1 blockade augments IL-10R expression by antigen-specific $CD8^+$ T cells, thereby increasing their sensitivity to the immunosuppressive effects of endogenous IL-10. Conversely, IL-10 blockade strengthens the effects of PD-1 blockade in expanding antigen-specific $CD8^+$ T cells and reinforcing their function. Thus, IL-10 and PD-1 pathways act synergistically through distinct pathways to suppress T cell survival and function (Brooks et al., 2008).

CANCER IMMUNOTHERAPY AND T CELL DYSFUNCTION IN THE TME

As the pivotal player in the adaptive immune system, T cells can recognize and eliminate tumor cells. However, tumor cells evade from the immune attack once the T cells enter dysfunctional state. The emergence of engineered T cells as a form of cancer therapy marks the beginning of a new era in medicine, providing a transformative way to combat tumors (Mikkilineni and Kochenderfer, 2017). To date, CD19-targeted CAR T-cell therapy has been largely successful in hematological malignancies, showing up to 90% complete response in relapsed or treatment-refractory acute lymphoblastic leukemia (ALL) patients (Maude et al., 2014). However, despite extensive research, the efficacy of CAR-T cell therapy on controlling solid tumors is limited effects due to the influence of TME (Yu et al., 2017; Li et al., 2018d; Yan et al., 2019). Studies suggest that solid tumors may induce hyporesponsiveness of CAR-T cells (Irving et al., 2017; Martinez and Moon, 2019). Three CAR-T cell trials that targeted IL13Rα2, Her2/CMV and EGFRvIII showed poor T cell persistence and an inability to prolong

overall survival of patients with glioma (Brown et al., 2016; Ahmed et al., 2017; O'Rourke et al., 2017; Migliorini et al., 2018). Compared with pre-infusion tumor tissues, post-CAR-T cell infusion tumor specimens show markedly upregulated expression of many immunosuppressive molecules, particularly IDO1 and Foxp3, and in some cases, IL-10, PD-L1, and/or TGF-β (O'Rourke et al., 2017). Lim and June (2017) suggested that the TME of solid tumors is hostile for CAR-T cells, reporting that even though CAR-T cells successfully penetrate into the tumor, they are exposed to numerous suppressive factors and tumor-associated stromal cells, which contribute to limiting their function. Additionally, these infused CAR-T cells express high levels of PD-1, T-cell immunoglobulin domain and mucin domain protein 3 (TIM3) and CTLA-4, indicating that they become exhausted or dysfunctional cells (Lim and June, 2017).

Recent studies have identified the crucial role that NR4As play in mediating exhaustion of CAR-T cells. In the NR4A-knocked out mice, CAR-T cells demonstrated low expression levels of inhibitory receptors and increased anti-tumor activity *in vivo* (Chen J. et al., 2019). Other studies have demonstrated the critical roles of that metabolic barriers play in the TME. Low glucose levels in the TME produce particular challenges for memory CAR-T cells. Thus, novel strategies are needed to assist CAR-T cells in overcoming the immunosuppressive microenvironment presented of many solid tumors.

Cancer neoantigens are derived from random somatic mutations in tumor tissues and are attractive targets for cancer immunotherapies (Chu et al., 2018). Neoantigen-based personalized cancer vaccines have recently shown marked therapeutic potential in both preclinical and early phase clinical studies. Although the number of patients with advanced melanoma treated by neoantigen vaccines is small, results from several phase I clinical trials are quite encouraging. Reportedly, neoantigen-pulsed dendritic cells may induce neoantigen-specific T-cell responses in these patients. A phase I/Ib glioblastoma trial also verified that the circulating polyfunctional neoantigen-specific $CD4^+$ and $CD8^+$ T cell responses were generated in these patients (Ott et al., 2017). However, cancer types with a low mutation burden may not be eligible for this vaccine therapy. Meanwhile, the complicated TME possesses numerous immunosuppressive mechanisms that result in immune escape.

Importantly, tumor cell clones can generate tumors that recapitulated T cell-inflamed and non-T-cell-inflamed TMEs upon implantation in immunocompetent mice, with characteristic patterns of infiltration by immune cell subsets. CXCL1 was identified as a determinant of the non-T-cell-inflamed microenvironment, and ablation of CXCL1 promoted T cell infiltration and sensitivity to immunotherapy (Li et al., 2018a). Furthermore, lower expression levels of co-stimulatory molecules and higher expression levels of co-inhibitory receptors, such as PD-L1, have been shown to be correlated with T-cell dysfunction. Therefore, many efforts are currently focused on addressing challenges in the development of neoantigen-based cancer vaccines for wide clinical applications. Notably, two melanoma patients that experienced disease relapse after successful neoantigen vaccine treatments, and later, achieved complete response after subsequent anti-PD-1 antibody treatment (Ott et al., 2017).

One of the most popular and successful strategies to combat T cell exhaustion is the use of checkpoint inhibitors. The ICB such as anti-PD-1, anti-PD-L1 and anti-CTLA-4 are currently approved by the U.S. FDA for various of caner types. However, the response rate of ICB therapy is less than 30% in solid tumors. First, PD-1 expression levels have a distinct role in contributing to T cell dysfunction or resisting to PD-1 blockade. While intratumoral PD-1^{high} $CD8^+$ subsets share the properties of co-expression of inhibitory receptors and loss of effector function, these populations secreted high levels of CXCL13, which can recruit immune cells to TME. Moreover, the presence of PD-1^{high} T cells was strongly predictive for clinical outcome in a small number of NSCLC patients treated with anti-PD-1 (Thommen et al., 2018). Second, cancers that are non-responsive to checkpoint blockade therapies usually already have decreased numbers of T cells infiltrating their tumors. Infiltrating T cells often co-express multiple inhibitory markers, and expression of the corresponding ligands is evident in tumor cells. In addition, factors beyond tumor genomics influence cancer development and therapeutic responses, including host factors such as the gastrointestinal (gut) microbiome and obesity (Gopalakrishnan et al., 2018; Popovic et al., 2018; Wang et al., 2019e). For example, the frequency of $CD8^+$ TILs expressing PD-1and TIM3 is higher in the diet-induced obese mice (DIO) than that in control mice. Anti-PD-1 monotherapy had minimal to no effect on control mice but significantly reduced tumor burden and significantly improved the survival of DIO mice. It remains to be clinically described whether the environment in the obese state results in greater T cell function once checkpoint blockade is applied (Wang et al., 2019e). More importantly, understanding the relationship between heterogeneous dysfunctional T cells and the TME may significantly impact on the success of therapies like checkpoint blockade and could lead to the production of more functional CAR-T cells.

REVERSING T CELL DYSFUNCTION BY COMBINATION CANCER IMMUNOTHERAPY

Great efforts have been made to characterize the intrinsic properties of dysfunctional T cells. Additionally, transcriptional regulators as well as metabolic and epigenetic factors have been investigated as possible targets to improve the anti-tumor efficacy of immunotherapies (**Figure 3**). New treatment strategies employing epigenetic drugs and immune checkpoint blockade therapies have been investigated in an effort to reverse T cell dysfunction. For instance, in a mouse model of epithelial ovarian cancer, the DNA methyltransferase and histone deacetylase inhibitors (DNMTi and HDACi, respectively) can reduce the immunosuppressive microenvironment through type I IFN signaling and improve response to anti-PD-1 therapy. Addition of HDACi and DNMTi 5-azacytidine (AZA) enhances the modulation of the immune microenvironment, specifically increasing T cell activation and reducing the percentage of macrophage *in vivo* (Stone et al., 2017).

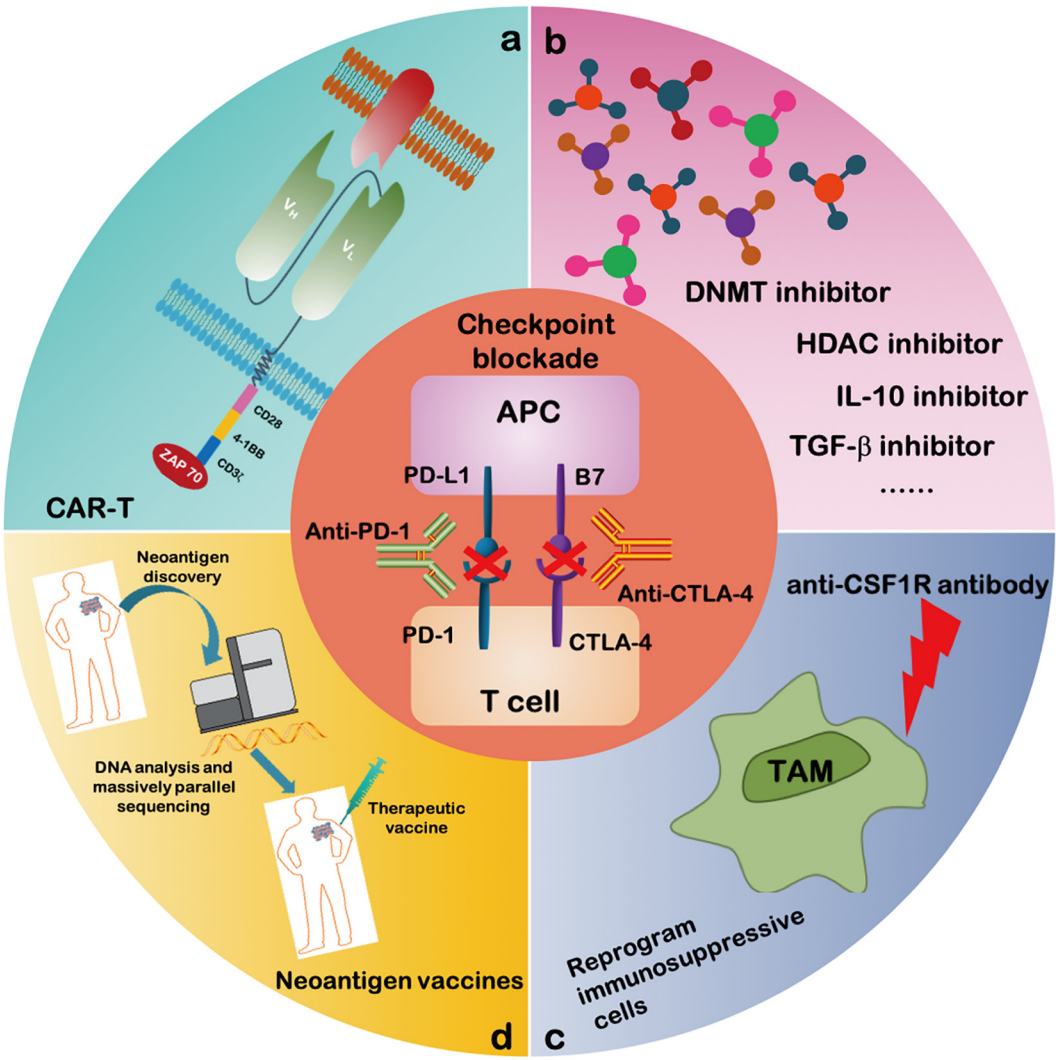

FIGURE 3 | Combinatorial therapeutic strategies to reverse the T cell dysfunction. A growing number of studies propose to evaluate the efficacy of immune checkpoint blockade antibodies together with: **(a)** CAR-T cell therapy; **(b)** inhibitors of soluble mediators targeting IL-10, TGF-β, DNA methyltransferase and histone deacetylase; **(c)** CSF1R antibody targeting activating receptors on TAMs to inhibit the polarization of TAM; and **(d)** neoantigen vaccines.

Recent studies have also provided evidence that classical immune checkpoints can interact with metabolic checkpoints. In a mouse sarcoma model, glucose consumption by tumors metabolically restricts T cells, leading to their dampened mTOR activity and facilitating cancer progression. It was also discovered that PD-L1 blockade can act directly on tumor cells to inhibit mTOR activity, increasing extracellular glucose availability (Chang et al., 2015). These findings suggest that immune checkpoint blockades counteract T cell dysfunction not only by preventing intrinsic T-cell inhibitory signals but also by increasing T cell metabolic fitness. Meanwhile, the AMPK activator metformin, a first-line treatment drug for type 2 diabetes, was reported to have anti-cancer activity. In a mouse model, metformin was found to increase the number of $CD8^+$ TILs and protected them from apoptosis and exhaustion characterized. Thus, a direct effect of metformin on $CD8^+$ T cells is critical for protecting against the T cell exhaustion in TME. Thus, the combined use of metformin and cancer vaccines can improve TILs multifunctionality (Eikawa et al., 2015).

However, whether the combination of ICB and metformin can restore the dysfunctional T cells remains unclear. Transcriptional profiling of dysfunctional T cells revealed a set of transcription factors that are altered in expression compared with effector or memory T cells. Indeed, a growing list of transcription factors that can regulate the expression of inhibitory receptors has been identified, highlighting potential targets for immunotherapy. Two reports have identified NR4A transcription factors as key mediators of T cell function and demonstrated that NR4A deficiency leads to the downregulation of PD-1, which is functionally similar to the effects of PD-1 blockade (Chen J. et al., 2019; Liu X. et al., 2019). Thus, inhibiting the function of NR4A in TILs or CAR-T cells could be a promising strategy in cancer

immunotherapy, similar to combination therapies with ICB against CTLA-4 or GITR (glucocorticoid-induced tumor necrosis factor receptor–related protein) antibodies. Additionally, TOX has been defined as an important transcription factor in regulating T cell exhaustion. Possibly, reducing TOX expression in combination with anti-PD-1 therapy can potentially provide a more effective strategy of abrogating the TOX-dependent pathway of $CD8^+$ T cell exhaustion. Emerging data from a clinical study reported limited clinical activity for anti-GITR monotherapy but potentially promising data for the combination therapy. Combination treatments aimed at PD-1 inhibition and activation of GITR, decrease $CD8^+$ T cell dysfunction and induce a highly proliferative precursor effector memory T cell phenotype (Wang et al., 2018). Monotherapy with CTLA-4 leads to disease control in 20–28% of patients with metastatic melanoma. However, the maintenance of T cell responses triggered by anti-CTLA-4 alone is in most cases insufficient to successfully eradicate tumors, and durable long-term complete remissions (CRs) are seen in a minority of patients. Similarly, adoptive transfer of peripheral blood-derived antigen-specific cytotoxic T cells (CTLs) alone is generally insufficient to eliminate tumors, whereas IL-21-primed CTLs with characteristics of a long-lived memory phenotype may enhance T cell survival after infusion to patients. Thus, the anti-CTLA-4 combined with IL-21-primed CTLs results in long term T cell persistence and durable anti-tumor function (Chapuis et al., 2016a,b).

Importantly, cancer immunotherapies aim to reinvigorate T cell function as well as target immunosuppressive and tumor-promoting pathways mediated by TME (**Figure 3**). Several specific strategies that target TME are being investigated in combination with ICB therapies in order to improve T cell mediated immunotherapy. Recently, there has been a significant new interest in using macrophage modulators to optimize TAMs. An anti-CSF1R antibody was shown to reprogram TAM polarization and improve the responses to ICB therapy in pancreatic cancer (Cassetta and Kitamura, 2018). Other strategies are focused on inhibiting MDSC function and depleting and/or reprograming MDSCs to enhance the efficacy of checkpoint agents. A clinical trial showed MDSC frequencies as potential biomarkers and reported on their correlation with clinical outcomes of melanoma patients treated with ipilimumab (Meyer et al., 2014). Interestingly, a host of cytokines released by immune and tumor cells have been found to negatively contribute to immunosuppression and have therefore been targeted toward reprograming the immunosuppressive TME. Thus, a combined treatment of IL-10 or TGF-β inhibitor(s) with ICB represents a promising strategy for immunotherapy strategy (Zarour, 2016).

CONCLUSION

CAR-T cells, neoantigen vaccines and immune checkpoint-modulating agents have increasingly been proven successful in driving antitumor immune responses. Despite these rapid advances in cancer immunotherapy, enormous challenges remain for the future development of cancer therapy for wide clinical applications. Most clinical and preclinical studies using immunotherapy have been focused on T cell exhaustion and dysfunction in TME. In this review, we discussed the unique transcriptional programs and the metabolic and epigenetic factors underlying tumor-induced T cell dysfunction, with the hope that a clearer understanding of TME may enable the development of novel targeted therapeutics, improving the efficacy of immunotherapies. Moreover, the following aspects should be given more attention, (1) identification of mechanisms that convert immunologically cold tumors to T cell rich hot tumors; (2) agents or strategies that reverse T cell exhaustion, and/or reprogram an otherwise immunosuppressive TME must be employed together with immune checkpoint modulators to achieve a robust and durable clinical response; and (3) utilizing RNA sequencing or NanoString tumor expression profiles, to identify gene signatures of T cell dysfunction and predict the outcome of patients treated with checkpoint modulators. This will aid in identifying new targets and advance our fundamental understanding of new targets or the optimal combination therapies for cancer patients.

AUTHOR CONTRIBUTIONS

ZZ, SL, and YZ (sixth author) conceptualized this review, decided on the content, and wrote the manuscript. ZZ and SL prepared the figures. BZ, LQ, and YZ (fifth author) revised this review. All authors approved the final version of the manuscript and agreed to be accountable for all aspects of the work.

FUNDING

This study was supported by the National Key Research and Development Program of China (No. 2018YFC1313400) and the National Natural Science Foundation of China (Grant Nos. U1804281, 81771781, 81773046, 81702810, and 81773060).

ACKNOWLEDGMENTS

We thank Dr. Cassian Yee (Departments of Melanoma Medical Oncology and Immunology, University of Texas MD Anderson Cancer Center) for his valuable comments.

REFERENCES

Ahmed, N., Brawley, V., Hegde, M., Bielamowicz, K., Kalra, M., Landi, D., et al. (2017). HER2-specific chimeric antigen receptor-modified virus-specific T cells for progressive glioblastoma: a phase 1 dose-escalation trial. *JAMA Oncol.* 3, 1094–1101. doi: 10.1001/jamaoncol.2017.0184

Alfei, F., Kanev, K., Hofmann, M., Wu, M., Ghoneim, H. E., Roelli, P., et al. (2019). TOX reinforces the phenotype and longevity of exhausted T cells in chronic viral infection. *Nature* 571, 265–269. doi: 10.1038/s41586-019-1326-9

Ambade, A., Satishchandran, A., Saha, B., Gyongyosi, B., Lowe, P., Kodys, K., et al. (2016). Hepatocellular carcinoma is accelerated by NASH

involving M2 macrophage polarization mediated by hif-1alphainduced IL-10. *Oncoimmunology* 5:e1221557. doi: 10.1080/2162402x.2016.1221557

Bally, A. P., Austin, J. W., and Boss, J. M. (2016). Genetic and epigenetic regulation of PD-1 expression. *J. Immunol.* 196, 2431–2437. doi: 10.4049/jimmunol.1502643

Benner, B., Scarberry, L., Suarez-Kelly, L. P., Duggan, M. C., Campbell, A. R., Smith, E., et al. (2019). Generation of monocyte-derived tumor-associated macrophages using tumor-conditioned media provides a novel method to study tumor-associated macrophages in vitro. *J. Immunother. Cancer* 7:140. doi: 10.1186/s40425-019-0622-0

Bohrer, L. R., Chen, S., Hallstrom, T. C., and Huang, H. (2010). Androgens suppress EZH2 expression via retinoblastoma (RB) and p130-dependent pathways: a potential mechanism of androgen-refractory progression of prostate cancer. *Endocrinology* 151, 5136–5145. doi: 10.1210/en.2010-0436

Boyiadzis, M. M., Dhodapkar, M. V., Brentjens, R. J., Kochenderfer, J. N., Neelapu, S. S., Maus, M. V., et al. (2018). Chimeric antigen receptor (CAR) T therapies for the treatment of hematologic malignancies: clinical perspective and significance. *J. Immunother. Cancer* 6:137. doi: 10.1186/s40425-018-0460-5

Brooks, D. G., Ha, S. J., Elsaesser, H., Sharpe, A. H., Freeman, G. J., and Oldstone, M. B. (2008). IL-10 and PD-L1 operate through distinct pathways to suppress T-cell activity during persistent viral infection. *Proc. Natl. Acad. Sci. U.S.A.* 105, 20428–20433. doi: 10.1073/pnas.0811139106

Brown, C. E., Alizadeh, D., Starr, R., Weng, L., Wagner, J. R., Naranjo, A., et al. (2016). Regression of glioblastoma after chimeric antigen receptor T-cell therapy. *N. Engl. J. Med.* 375, 2561–2569. doi: 10.1056/NEJMoa1610497

Cassetta, L., and Kitamura, T. (2018). Targeting tumor-associated macrophages as a potential strategy to enhance the response to immune checkpoint inhibitors. *Front. Cell. Dev. Biol.* 6:38. doi: 10.3389/fcell.2018.00038

Cassetta, L., Noy, R., Swierczak, A., Sugano, G., Smith, H., Wiechmann, L., et al. (2016). Isolation of mouse and human tumor-associated macrophages. *Adv. Exp. Med. Biol.* 899, 211–229. doi: 10.1007/978-3-319-26666-4_12

Chang, C. H., and Pearce, E. L. (2016). Emerging concepts of T cell metabolism as a target of immunotherapy. *Nat. Immunol.* 17, 364–368. doi: 10.1038/ni.3415

Chang, C. H., Qiu, J., O'Sullivan, D., Buck, M. D., Noguchi, T., Curtis, J. D., et al. (2015). Metabolic competition in the tumor microenvironment is a driver of cancer progression. *Cell* 162, 1229–1241. doi: 10.1016/j.cell.2015.08.016

Chang, J. T., Wherry, E. J., and Goldrath, A. W. (2014). Molecular regulation of effector and memory T cell differentiation. *Nat. Immunol.* 15, 1104–1115. doi: 10.1038/ni.3031

Chapuis, A. G., Lee, S. M., Thompson, J. A., Roberts, I. M., Margolin, K. A., Bhatia, S., et al. (2016a). Combined IL-21-primed polyclonal CTL plus CTLA4 blockade controls refractory metastatic melanoma in a patient. *J. Exp. Med.* 213, 1133–1139. doi: 10.1084/jem.20152021

Chapuis, A. G., Roberts, I. M., Thompson, J. A., Margolin, K. A., Bhatia, S., Lee, S. M., et al. (2016b). T-cell therapy using interleukin-21-primed cytotoxic T-cell lymphocytes combined with cytotoxic T-cell lymphocyte antigen-4 blockade results in long-term cell persistence and durable tumor regression. *J. Clin. Oncol.* 34, 3787–3795. doi: 10.1200/jco.2015.65.5142

Chauvin, J. M., Pagliano, O., Fourcade, J., Sun, Z., Wang, H., Sander, C., et al. (2015). TIGIT and PD-1 impair tumor antigen-specific CD8(+) T cells in melanoma patients. *J. Clin. Invest.* 125, 2046–2058. doi: 10.1172/jci80445

Chen, J., Lopez-Moyado, I. F., Seo, H., Lio, C. J., Hempleman, L. J., Sekiya, T., et al. (2019). NR4A transcription factors limit CAR T cell function in solid tumours. *Nature* 567, 530–534. doi: 10.1038/s41586-019-0985-x

Chen, J., Ye, Y., Liu, P., Yu, W., Wei, F., Li, H., et al. (2017). Suppression of T cells by myeloid-derived suppressor cells in cancer. *Hum. Immunol.* 78, 113–119. doi: 10.1016/j.humimm.2016.12.001

Chen, X., Song, M., Zhang, B., and Zhang, Y. (2016). Reactive oxygen species regulate T cell immune response in the tumor microenvironment. *Oxid. Med. Cell. Longev.* 2016:1580967. doi: 10.1155/2016/1580967

Chen, Y., Zhang, S., Wang, Q., and Zhang, X. (2017). Tumor-recruited M2 macrophages promote gastric and breast cancer metastasis via M2 macrophage-secreted CHI3L1 protein. *J. Hematol. Oncol.* 10:36. doi: 10.1186/s13045-017-0408-0

Chen, Z., Ji, Z., Ngiow, S. F., Manne, S., Cai, Z., Huang, A. C., et al. (2019). TCF-1-centered transcriptional network drives an effector versus exhausted CD8 T cell-fate decision. *Immunity* 51, 840–855.e5. doi: 10.1016/j.immuni.2019.09.013

Chu, Y., Liu, Q., Wei, J., and Liu, B. (2018). Personalized cancer neoantigen vaccines come of age. *Theranostics* 8, 4238–4246. doi: 10.7150/thno.24387

Colak, S., and Ten Dijke, P. (2017). Targeting TGF-β signaling in cancer. *Trends Cancer* 3, 56–71. doi: 10.1016/j.trecan.2016.11.008

Eikawa, S., Nishida, M., Mizukami, S., Yamazaki, C., Nakayama, E., and Udono, H. (2015). Immune-mediated antitumor effect by type 2 diabetes drug, metformin. *Proc. Natl. Acad. Sci. U.S.A.* 112, 1809–1814. doi: 10.1073/pnas.1417636112

Fourcade, J., Sun, Z., Benallaoua, M., Guillaume, P., Luescher, I. F., Sander, C., et al. (2010). Upregulation of Tim-3 and PD-1 expression is associated with tumor antigen-specific CD8+ T cell dysfunction in melanoma patients. *J. Exp. Med.* 207, 2175–2186. doi: 10.1084/jem.20100637

Ghoneim, H. E., Fan, Y., Moustaki, A., Abdelsamed, H. A., Dash, P., Dogra, P., et al. (2017). De novo epigenetic programs inhibit PD-1 blockade-mediated T cell rejuvenation. *Cell* 170, 142–157.e19. doi: 10.1016/j.cell.2017.06.007

Gopalakrishnan, V., Spencer, C. N., Nezi, L., Reuben, A., Andrews, M. C., Karpinets, T. V., et al. (2018). Gut microbiome modulates response to anti-PD-1 immunotherapy in melanoma patients. *Science* 359, 97–103. doi: 10.1126/science.aan4236

Guo, X., Zhang, Y., Zheng, L., Zheng, C., Song, J., Zhang, Q., et al. (2018). Global characterization of T cells in non-small-cell lung cancer by single-cell sequencing. *Nat. Med.* 24, 978–985. doi: 10.1038/s41591-018-0045-3

Hashimoto, M., Kamphorst, A. O., Im, S. J., Kissick, H. T., Pillai, R. N., Ramalingam, S. S., et al. (2018). CD8 T cell exhaustion in chronic infection and cancer: opportunities for interventions. *Annu. Rev. Med.* 69, 301–318. doi: 10.1146/annurev-med-012017-043208

Hayashi, S., Kumai, T., Matsuda, Y., Aoki, N., Sato, K., Kimura, S., et al. (2011). Six-transmembrane epithelial antigen of the prostate and enhancer of zeste homolog 2 as immunotherapeutic targets for lung cancer. *J. Transl. Med.* 9:191. doi: 10.1186/1479-5876-9-191

He, S., Liu, Y., Meng, L., Sun, H., Wang, Y., Ji, Y., et al. (2017). Ezh2 phosphorylation state determines its capacity to maintain CD8(+) T memory precursors for antitumor immunity. *Nat. Commun.* 8:2125. doi: 10.1038/s41467-017-02187-8

Hwang, S., Cobb, D. A., Bhadra, R., Youngblood, B., and Khan, I. A. (2016). Blimp-1-mediated CD4 T cell exhaustion causes CD8 T cell dysfunction during chronic toxoplasmosis. *J. Exp. Med.* 213, 1799–1818. doi: 10.1084/jem.20151995

Irving, M., Vuillefroy de Silly, R., Scholten, K., Dilek, N., and Coukos, G. (2017). Engineering chimeric antigen receptor T-cells for racing in solid tumors: don't forget the fuel. *Front. Immunol.* 8:267. doi: 10.3389/fimmu.2017.00267

Jeannet, G., Boudousquie, C., Gardiol, N., Kang, J., Huelsken, J., and Held, W. (2010). Essential role of the Wnt pathway effector Tcf-1 for the establishment of functional CD8 T cell memory. *Proc. Natl. Acad. Sci. U.S.A.* 107, 9777–9782. doi: 10.1073/pnas.0914127107

Ji, Y., Fioravanti, J., Zhu, W., Wang, H., Wu, T., Hu, J., et al. (2019). miR-155 harnesses Phf19 to potentiate cancer immunotherapy through epigenetic reprogramming of CD8(+) T cell fate. *Nat. Commun.* 10:2157. doi: 10.1038/s41467-019-09882-8

Jiang, Y., Li, Y., and Zhu, B. (2015). T-cell exhaustion in the tumor microenvironment. *Cell Death Dis.* 6:e1792. doi: 10.1038/cddis.2015.162

Jones, B. A., Varambally, S., and Arend, R. C. (2018). Histone methyltransferase EZH2: a therapeutic target for ovarian cancer. *Mol. Cancer Ther.* 17, 591–602. doi: 10.1158/1535-7163.mct-17-0437

Kartikasari, A. E. R., Prakash, M. D., Cox, M., Wilson, K., Boer, J. C., Cauchi, J. A., et al. (2018). Therapeutic cancer vaccines-T cell responses and epigenetic modulation. *Front. Immunol.* 9:3109. doi: 10.3389/fimmu.2018.03109

Khan, O., Giles, J. R., McDonald, S., Manne, S., Ngiow, S. F., Patel, K. P., et al. (2019). TOX transcriptionally and epigenetically programs CD8(+) T cell exhaustion. *Nature* 571, 211–218. doi: 10.1038/s41586-019-1325-x

Kishton, R. J., Sukumar, M., and Restifo, N. P. (2017). Metabolic regulation of T cell longevity and function in tumor immunotherapy. *Cell Metab.* 26, 94–109. doi: 10.1016/j.cmet.2017.06.016

Knudson, K. M., Pritzl, C. J., Saxena, V., Altman, A., Daniels, M. A., and Teixeiro, E. (2017). NFkappaB-Pim-1-eomesodermin axis is critical for maintaining CD8

T-cell memory quality. *Proc. Natl. Acad. Sci. U.S.A.* 114, E1659–E1667. doi: 10.1073/pnas.1608448114

Lakins, M. A., Ghorani, E., Munir, H., Martins, C. P., and Shields, J. D. (2018). Cancer-associated fibroblasts induce antigen-specific deletion of CD8 (+) T cells to protect tumour cells. *Nat. Commun.* 9:948. doi: 10.1038/s41467-018-03347-0

Landskron, G., De la Fuente, M., Thuwajit, P., Thuwajit, C., and Hermoso, M. A. (2014). Chronic inflammation and cytokines in the tumor microenvironment. *J. Immunol. Res.* 2014:149185. doi: 10.1155/2014/149185

Le Bourgeois, T., Strauss, L., Aksoylar, H. I., Daneshmandi, S., Seth, P., Patsoukis, N., et al. (2018). Targeting T cell metabolism for improvement of cancer immunotherapy. *Front. Oncol.* 8:237. doi: 10.3389/fonc.2018.00237

Li, H., van der Leun, A. M., Yofe, I., Lubling, Y., Gelbard-Solodkin, D., van Akkooi, A. C. J., et al. (2019). Dysfunctional CD8 T cells form a proliferative, dynamically regulated compartment within human melanoma. *Cell* 176, 775–789.e18. doi: 10.1016/j.cell.2018.11.043

Li, J., Byrne, K. T., Yan, F., Yamazoe, T., Chen, Z., Baslan, T., et al. (2018a). Tumor cell-intrinsic factors underlie heterogeneity of immune cell infiltration and response to immunotherapy. *Immunity* 49, 178–193.e7. doi: 10.1016/j.immuni.2018.06.006

Li, J., He, Y., Hao, J., Ni, L., and Dong, C. (2018b). High levels of eomes promote exhaustion of anti-tumor CD8(+) T cells. *Front. Immunol.* 9:2981. doi: 10.3389/fimmu.2018.02981

Li, J., Lee, Y., Li, Y., Jiang, Y., Lu, H., Zang, W., et al. (2018c). Co-inhibitory molecule B7 superfamily member 1 expressed by tumor-infiltrating myeloid cells induces dysfunction of anti-tumor CD8(+) T cells. *Immunity* 48, 773–786.e5. doi: 10.1016/j.immuni.2018.03.018

Li, J., Li, W., Huang, K., Zhang, Y., Kupfer, G., and Zhao, Q. (2018d). Chimeric antigen receptor T cell (CAR-T) immunotherapy for solid tumors: lessons learned and strategies for moving forward. *J. Hematol. Oncol.* 11:22. doi: 10.1186/s13045-018-0568-6

Li, L., Ma, Y., and Xu, Y. (2019). Follicular regulatory T cells infiltrated the ovarian carcinoma and resulted in CD8 T cell dysfunction dependent on IL-10 pathway. *Int. Immunopharmacol.* 68, 81–87. doi: 10.1016/j.intimp.2018.12.051

Li, L., Wang, L., Li, J., Fan, Z., Yang, L., Zhang, Z., et al. (2018e). Metformin-induced reduction of CD39 and CD73 blocks myeloid-derived suppressor cell activity in patients with ovarian cancer. *Cancer Res.* 78, 1779–1791. doi: 10.1158/0008-5472.can-17-2460

Li, J., Wang, L., Chen, X., Li, L., Li, Y., Ping, Y., et al. (2017). CD39/CD73 upregulation on myeloid-derived suppressor cells via TGF-βeta-mTOR-HIF-1 signaling in patients with non-small cell lung cancer. *Oncoimmunology* 6:e1320011. doi: 10.1080/2162402x.2017.1320011

Lim, W. A., and June, C. H. (2017). The principles of engineering immune cells to treat cancer. *Cell* 168, 724–740. doi: 10.1016/j.cell.2017.01.016

Liu, H., Li, P., Wei, Z., Zhang, C., Xia, M., Du, Q., et al. (2019). Regulation of T cell differentiation and function by epigenetic modification enzymes. *Semin. Immunopathol.* 41, 315–326. doi: 10.1007/s00281-019-00731-w

Liu, S., Zhang, C., Maimela, N. R., Yang, L., Zhang, Z., Ping, Y., et al. (2019). Molecular and clinical characterization of CD163 expression via large-scale analysis in glioma. *Oncoimmunology* 8:1601478. doi: 10.1080/2162402x.2019.1601478

Liu, X., Wang, Y., Lu, H., Li, J., Yan, X., Xiao, M., et al. (2019). Genome-wide analysis identifies NR4A1 as a key mediator of T cell dysfunction. *Nature* 567, 525–529. doi: 10.1038/s41586-019-0979-8

Ma, E. H., Poffenberger, M. C., Wong, A. H., and Jones, R. G. (2017). The role of AMPK in T cell metabolism and function. *Curr. Opin. Immunol.* 46, 45–52. doi: 10.1016/j.coi.2017.04.004

Ma, R., Ji, T., Zhang, H., Dong, W., Chen, X., Xu, P., et al. (2018). A Pck1-directed glycogen metabolic program regulates formation and maintenance of memory CD8(+) T cells. *Nat. Cell Biol.* 20, 21–27. doi: 10.1038/s41556-017-0002-2

Maimela, N. R., Liu, S., and Zhang, Y. (2019). Fates of CD8+ T cells in tumor microenvironment. *Comput. Struct. Biotechnol. J.* 17, 1–13. doi: 10.1016/j.csbj.2018.11.004

Mann, T. H., and Kaech, S. M. (2019). Tick-TOX, it's time for T cell exhaustion. *Nat. Immunol.* 20, 1092–1094. doi: 10.1038/s41590-019-0478-y

Martinez, G. J., Pereira, R. M., Aijo, T., Kim, E. Y., Marangoni, F., Pipkin, M. E., et al. (2015). The transcription factor NFAT promotes exhaustion of activated CD8(+) T cells. *Immunity* 42, 265–278. doi: 10.1016/j.immuni.2015.01.006

Martinez, M., and Moon, E. K. (2019). CAR T cells for solid tumors: new strategies for finding, infiltrating, and surviving in the tumor microenvironment. *Front. Immunol.* 10:128. doi: 10.3389/fimmu.2019.00128

Maude, S. L., Frey, N., Shaw, P. A., Aplenc, R., Barrett, D. M., Bunin, N. J., et al. (2014). Chimeric antigen receptor T cells for sustained remissions in leukemia. *N. Engl. J. Med.* 371, 1507–1517. doi: 10.1056/NEJMoa1407222

Meyer, C., Cagnon, L., Costa-Nunes, C. M., Baumgaertner, P., Montandon, N., Leyvraz, L., et al. (2014). Frequencies of circulating MDSC correlate with clinical outcome of melanoma patients treated with ipilimumab. *Cancer Immunol. Immunother.* 63, 247–257. doi: 10.1007/s00262-013-1508-5

Migliorini, D., Dietrich, P. Y., Stupp, R., Linette, G. P., Posey, A. D. Jr., and June, C. H. (2018). CAR T-cell therapies in glioblastoma: a first look. *Clin. Cancer Res.* 24, 535–540. doi: 10.1158/1078-0432.ccr-17-2871

Mikkilineni, L., and Kochenderfer, J. N. (2017). Chimeric antigen receptor T-cell therapies for multiple myeloma. *Blood* 130, 2594–2602. doi: 10.1182/blood-2017-06-793869

Miller, B. C., Sen, D. R., Al Abosy, R., Bi, K., Virkud, Y. V., LaFleur, M. W., et al. (2019). Subsets of exhausted CD8(+) T cells differentially mediate tumor control and respond to checkpoint blockade. *Nat. Immunol.* 20, 326–336. doi: 10.1038/s41590-019-0312-6

Nagarsheth, N., Peng, D., Kryczek, I., Wu, K., Li, W., Zhao, E., et al. (2016). PRC2 epigenetically silences Th1-type chemokines to suppress effector T-cell trafficking in colon cancer. *Cancer Res.* 76, 275–282. doi: 10.1158/0008-5472.can-15-1938

O'Rourke, D. M., Nasrallah, M. P., Desai, A., Melenhorst, J. J., Mansfield, K., Morrissette, J. J. D., et al. (2017). A single dose of peripherally infused EGFRvIII-directed CAR T cells mediates antigen loss and induces adaptive resistance in patients with recurrent glioblastoma. *Sci. Transl. Med.* 9:eaaa0984. doi: 10.1126/scitranslmed.aaa0984

Ostrand-Rosenberg, S. (2010). Myeloid-derived suppressor cells: more mechanisms for inhibiting antitumor immunity. *Cancer Immunol. Immunother.* 59, 1593–1600. doi: 10.1007/s00262-010-0855-8

Ott, P. A., Hu, Z., Keskin, D. B., Shukla, S. A., Sun, J., Bozym, D. J., et al. (2017). An immunogenic personal neoantigen vaccine for patients with melanoma. *Nature* 547, 217–221. doi: 10.1038/nature22991

Pauken, K. E., Sammons, M. A., Odorizzi, P. M., Manne, S., Godec, J., Khan, O., et al. (2016). Epigenetic stability of exhausted T cells limits durability of reinvigoration by PD-1 blockade. *Science* 354, 1160–1165. doi: 10.1126/science.aaf2807

Pearce, E. L., Poffenberger, M. C., Chang, C. H., and Jones, R. G. (2013). Fueling immunity: insights into metabolism and lymphocyte function. *Science* 342:1242454. doi: 10.1126/science.1242454

Popovic, A., Jaffee, E. M., and Zaidi, N. (2018). Emerging strategies for combination checkpoint modulators in cancer immunotherapy. *J. Clin. Invest.* 128, 3209–3218. doi: 10.1172/jci120775

Quigley, M., Pereyra, F., Nilsson, B., Porichis, F., Fonseca, C., Eichbaum, Q., et al. (2010). Transcriptional analysis of HIV-specific CD8+ T cells shows that PD-1 inhibits T cell function by upregulating BATF. *Nat. Med.* 16, 1147–1151. doi: 10.1038/nm.2232

Riley, R. S., June, C. H., Langer, R., and Mitchell, M. J. (2019). Delivery technologies for cancer immunotherapy. *Nat. Rev. Drug Discov.* 18, 175–196. doi: 10.1038/s41573-018-0006-z

Rodriguez, P. C., Zea, A. H., Culotta, K. S., Zabaleta, J., Ochoa, J. B., and Ochoa, A. C. (2002). Regulation of T cell receptor CD3zeta chain expression by L-arginine. *J. Biol. Chem.* 277, 21123–21129. doi: 10.1074/jbc.M110675200

Salmond, R. J. (2018). mTOR regulation of glycolytic metabolism in T cells. *Front. Cell. Dev. Biol.* 6:122. doi: 10.3389/fcell.2018.00122

Schietinger, A., and Greenberg, P. D. (2014). Tolerance and exhaustion: defining mechanisms of T cell dysfunction. *Trends Immunol.* 35, 51–60. doi: 10.1016/j.it.2013.10.001

Schietinger, A., Philip, M., Krisnawan, V. E., Chiu, E. Y., Delrow, J. J., Basom, R. S., et al. (2016). Tumor-specific T cell dysfunction is a dynamic antigen-driven differentiation program initiated early during tumorigenesis. *Immunity* 45, 389–401. doi: 10.1016/j.immuni.2016.07.011

Scott, A. C., Dundar, F., Zumbo, P., Chandran, S. S., Klebanoff, C. A., Shakiba, M., et al. (2019). TOX is a critical regulator of tumour-specific T cell differentiation. *Nature* 571, 270–274. doi: 10.1038/s41586-019-1324-y

Sen, D. R., Kaminski, J., Barnitz, R. A., Kurachi, M., Gerdemann, U., Yates, K. B., et al. (2016). The epigenetic landscape of T cell exhaustion. *Science* 354, 1165–1169. doi: 10.1126/science.aae0491

Seo, H., Chen, J., Gonzalez-Avalos, E., Samaniego-Castruita, D., Das, A., Wang, Y. H., et al. (2019). TOX and TOX2 transcription factors cooperate with NR4A transcription factors to impose CD8(+) T cell exhaustion. *Proc. Natl. Acad. Sci. U.S.A.* 116, 12410–12415. doi: 10.1073/pnas.1905675116

Sica, A., and Mantovani, A. (2012). Macrophage plasticity and polarization: in vivo veritas. *J. Clin. Invest.* 122, 787–795. doi: 10.1172/jci59643

Siddiqui, I., Schaeuble, K., Chennupati, V., Fuertes Marraco, S. A., Calderon-Copete, S., Pais Ferreira, D., et al. (2019). Intratumoral Tcf1(+)PD-1(+)CD8(+) T cells with stem-like properties promote tumor control in response to vaccination and checkpoint blockade immunotherapy. *Immunity* 50, 195–211.e10. doi: 10.1016/j.immuni.2018.12.021

Staron, M. M., Gray, S. M., Marshall, H. D., Parish, I. A., Chen, J. H., Perry, C. J., et al. (2014). The transcription factor FoxO1 sustains expression of the inhibitory receptor PD-1 and survival of antiviral CD8(+) T cells during chronic infection. *Immunity* 41, 802–814. doi: 10.1016/j.immuni.2014.10.013

Stone, M. L., Chiappinelli, K. B., Li, H., Murphy, L. M., Travers, M. E., Topper, M. J., et al. (2017). Epigenetic therapy activates type I interferon signaling in murine ovarian cancer to reduce immunosuppression and tumor burden. *Proc. Natl. Acad. Sci. U.S.A.* 114, E10981–E10990. doi: 10.1073/pnas.1712514114

Sugiura, A., and Rathmell, J. C. (2018). Metabolic barriers to T cell function in tumors. *J. Immunol.* 200, 400–407. doi: 10.4049/jimmunol.1701041

Thommen, D. S., Koelzer, V. H., Herzig, P., Roller, A., Trefny, M., Dimeloe, S., et al. (2018). A transcriptionally and functionally distinct PD-1(+) CD8(+) T cell pool with predictive potential in non-small-cell lung cancer treated with PD-1 blockade. *Nat. Med.* 24, 994–1004. doi: 10.1038/s41591-018-0057-z

Thommen, D. S., and Schumacher, T. N. (2018). T cell dysfunction in cancer. *Cancer Cell* 33, 547–562. doi: 10.1016/j.ccell.2018.03.012

Verma, V., Shrimali, R. K., Ahmad, S., Dai, W., Wang, H., Lu, S., et al. (2019). PD-1 blockade in subprimed CD8 cells induces dysfunctional PD-1(+)CD38(hi) cells and anti-PD-1 resistance. *Nat. Immunol.* 20, 1231–1243. doi: 10.1038/s41590-019-0441-y

Vodnala, S. K., Eil, R., Kishton, R. J., Sukumar, M., Yamamoto, T. N., Ha, N. H., et al. (2019). T cell stemness and dysfunction in tumors are triggered by a common mechanism. *Science* 363:eaau0135. doi: 10.1126/science.aau0135

Wang, B., Zhang, W., Jankovic, V., Golubov, J., Poon, P., Oswald, E. M., et al. (2018). Combination cancer immunotherapy targeting PD-1 and GITR can rescue CD8(+) T cell dysfunction and maintain memory phenotype. *Sci. Immunol.* 3:eaat7061. doi: 10.1126/sciimmunol.aat7061

Wang, C., Singer, M., and Anderson, A. C. (2017). Molecular dissection of CD8(+) T-cell dysfunction. *Trends Immunol.* 38, 567–576. doi: 10.1016/j.it.2017.05.008

Wang, D., Lin, J., Yang, X., Long, J., Bai, Y., Yang, X., et al. (2019a). Combination regimens with PD-1/PD-L1 immune checkpoint inhibitors for gastrointestinal malignancies. *J. Hematol. Oncol.* 12:42. doi: 10.1186/s13045-019-0730-9

Wang, D., Yang, L., Yue, D., Cao, L., Li, L., Wang, D., et al. (2019b). Macrophage-derived CCL22 promotes an immunosuppressive tumor microenvironment via IL-8 in malignant pleural effusion. *Cancer Lett.* 452, 244–253. doi: 10.1016/j.canlet.2019.03.040

Wang, X., Brea, L. T., and Yu, J. (2019c). Immune modulatory functions of EZH2 in the tumor microenvironment: implications in cancer immunotherapy. *Am. J. Clin. Exp. Urol.* 7, 85–91.

Wang, X., He, Q., Shen, H., Xia, A., Tian, W., Yu, W., et al. (2019d). TOX promotes the exhaustion of antitumor CD8(+) T cells by preventing PD1 degradation in hepatocellular carcinoma. *J. Hepatol.* 71, 731–741. doi: 10.1016/j.jhep.2019.05.015

Wang, Z., Aguilar, E. G., Luna, J. I., Dunai, C., Khuat, L. T., Le, C. T., et al. (2019e). Paradoxical effects of obesity on T cell function during tumor progression and PD-1 checkpoint blockade. *Nat. Med.* 25, 141–151. doi: 10.1038/s41591-018-0221-5

Wherry, E. J. (2011). T cell exhaustion. *Nat. Immunol.* 12, 492–499.

Wherry, E. J., and Kurachi, M. (2015). Molecular and cellular insights into T cell exhaustion. *Nat. Rev. Immunol.* 15, 486–499. doi: 10.1038/nri3862

Wu, A. A., Drake, V., Huang, H. S., Chiu, S., and Zheng, L. (2015). Reprogramming the tumor microenvironment: tumor-induced immunosuppressive factors paralyze T cells. *Oncoimmunology* 4:e1016700. doi: 10.1080/2162402x.2015.1016700

Xia, A., Zhang, Y., Xu, J., Yin, T., and Lu, X. J. (2019). T cell dysfunction in cancer immunity and immunotherapy. *Front. Immunol.* 10:1719. doi: 10.3389/fimmu.2019.01719

Yan, Z., Li, L., Wang, W., OuYang, B., Cheng, S., Wang, L., et al. (2019). Clinical efficacy and tumor microenvironment influence in a dose-escalation study of anti-CD19 chimeric antigen receptor T cells in refractory B-cell non-Hodgkin's lymphoma. *Clin. Cancer Res.* 25, 6995–7003. doi: 10.1158/1078-0432.Ccr-19-0101

Yang, L., Wang, F., Wang, L., Huang, L., Wang, J., Zhang, B., et al. (2015). CD163+ tumor-associated macrophage is a prognostic biomarker and is associated with therapeutic effect on malignant pleural effusion of lung cancer patients. *Oncotarget* 6, 10592–10603. doi: 10.18632/oncotarget.3547

Yang, L., and Zhang, Y. (2017). Tumor-associated macrophages: from basic research to clinical application. *J. Hematol. Oncol.* 10:58. doi: 10.1186/s13045-017-0430-2

Yee, C. (2018). Adoptive T cell therapy: points to consider. *Curr. Opin. Immunol.* 51, 197–203. doi: 10.1016/j.coi.2018.04.007

Yee, C., Lizee, G., and Schueneman, A. J. (2015). Endogenous T-cell therapy: clinical experience. *Cancer J.* 21, 492–500. doi: 10.1097/ppo.0000000000000158

Yee, C., and Lizee, G. A. (2017). Personalized therapy: tumor antigen discovery for adoptive cellular therapy. *Cancer J.* 23, 144–148. doi: 10.1097/ppo.0000000000000255

Yeku, O. O., Purdon, T. J., Koneru, M., Spriggs, D., and Brentjens, R. J. (2017). Armored CAR T cells enhance antitumor efficacy and overcome the tumor microenvironment. *Sci. Rep.* 7:10541. doi: 10.1038/s41598-017-10940-8

Yu, J., Du, W., Yan, F., Wang, Y., Li, H., Cao, S., et al. (2013). Myeloid-derived suppressor cells suppress antitumor immune responses through IDO expression and correlate with lymph node metastasis in patients with breast cancer. *J. Immunol.* 190, 3783–3797. doi: 10.4049/jimmunol.1201449

Yu, S., Li, A., Liu, Q., Li, T., Yuan, X., Han, X., et al. (2017). Chimeric antigen receptor T cells: a novel therapy for solid tumors. *J. Hematol. Oncol.* 10:78. doi: 10.1186/s13045-017-0444-9

Zarour, H. M. (2016). Reversing T-cell dysfunction and exhaustion in cancer. *Clin. Cancer Res.* 22, 1856–1864. doi: 10.1158/1078-0432.ccr-15-1849

Zhang, T., Zhang, Z., Li, F., Ping, Y., Qin, G., Zhang, C., et al. (2018). miR-143 regulates memory T cell differentiation by reprogramming T cell metabolism. *J. Immunol.* 201, 2165–2175. doi: 10.4049/jimmunol.1800230

Zhao, E., Maj, T., Kryczek, I., Li, W., Wu, K., Zhao, L., et al. (2016). Cancer mediates effector T cell dysfunction by targeting microRNAs and EZH2 via glycolysis restriction. *Nat. Immunol.* 17, 95–103. doi: 10.1038/ni.3313

Zhen, Z., Tang, W., Wang, M., Zhou, S., Wang, H., Wu, Z., et al. (2017). Protein nanocage mediated fibroblast-activation protein targeted photoimmunotherapy to enhance cytotoxic T cell infiltration and tumor control. *Nano Lett.* 17, 862–869. doi: 10.1021/acs.nanolett.6b04150

Zhu, H., Bengsch, F., Svoronos, N., Rutkowski, M. R., Bitler, B. G., Allegrezza, M. J., et al. (2016). BET bromodomain inhibition promotes anti-tumor immunity by suppressing PD-L1 expression. *Cell Rep.* 16, 2829–2837. doi: 10.1016/j.celrep.2016.08.032

Conflict of Interest: The authors declare that the research was conducted in the absence of any commercial or financial relationships that could be construed as a potential conflict of interest.

frontiers in Cell and Developmental Biology

ORIGINAL RESEARCH
published: 04 March 2020
doi: 10.3389/fcell.2020.00103

Transient DNMT3L Expression Reinforces Chromatin Surveillance to Halt Senescence Progression in Mouse Embryonic Fibroblast

Yoyo Chih-Yun Yu[1], Tony ZK Hui[2,3], Tzu-Hao Kao[1], Hung-Fu Liao[1], Chih-Yi Yang[1], Chia-Chun Hou[4], Hsin-Ting Hsieh[1], Jen-Yun Chang[1], Yi-Tzang Tsai[1], Marina Pinskaya[5], Kai-Chien Yang[6], Yet-Ran Chen[7], Antonin Morillon[5], Mong-Hsun Tsai[1] and Shau-Ping Lin[1,4,7,8†]*

[1] Institute of Biotechnology, National Taiwan University, Taipei, Taiwan, [2] Department of Microbiology and Immunology, University of British Columbia, Vancouver, BC, Canada, [3] Canada's Michael Smith Genome Sciences Centre, British Columbia Cancer Agency, Vancouver, BC, Canada, [4] Center for Systems Biology, National Taiwan University, Taipei, Taiwan, [5] ncRNA, Epigenetic and Genome Fluidity, CNRS UMR 3244, Sorbonne Université, PSL University, Institut Curie, Centre de Recherche, Paris, France, [6] Graduate Institute and Department of Pharmacology, National Taiwan University School of Medicine, Taipei, Taiwan, [7] Agricultural Biotechnology Research Center, Academia Sinica, Taipei, Taiwan, [8] Research Center for Developmental Biology and Regenerative Medicine, Taipei, Taiwan

OPEN ACCESS

Edited by:
Nu Zhang,
The University of Texas Health Science Center at San Antonio, United States

Reviewed by:
Lei Chen,
Eastern Hepatobiliary Surgery Hospital, China
Shruti Mishra,
The University of Texas Health Science Center at San Antonio, United States

***Correspondence:**
Shau-Ping Lin
shaupinglin@ntu.edu.tw

†ORCID:
Shau-Ping Lin
0000-0003-3423-991X

Specialty section:
This article was submitted to Cell Death and Survival, a section of the journal Frontiers in Cell and Developmental Biology

Received: 09 November 2019
Accepted: 07 February 2020
Published: 04 March 2020

Citation:
Yu YC-Y, Hui TZK, Kao T-H, Liao H-F, Yang C-Y, Hou C-C, Hsieh H-T, Chang J-Y, Tsai Y-T, Pinskaya M, Yang K-C, Chen Y-R, Morillon A, Tsai M-H and Lin S-P (2020) Transient DNMT3L Expression Reinforces Chromatin Surveillance to Halt Senescence Progression in Mouse Embryonic Fibroblast. Front. Cell Dev. Biol. 8:103. doi: 10.3389/fcell.2020.00103

Global heterochromatin reduction, which is one of the hallmarks of senescent cells, is associated with reduced transposable element repression and increased risk of chromatin instability. To ensure genomic integrity, the irreparable cells in a population exit permanently from the cell cycle, and this process is termed "senescence." However, senescence only blocks the expansion of unwanted cells, and the aberrant chromatin of senescent cells remains unstable. Serendipitously, we found that the transient ectopic expression of a repressive epigenetic modulator, DNA methyltransferase 3-like (DNMT3L) was sufficient to delay the premature senescence progression of late-passage mouse embryonic fibroblasts (MEFs) associated with a tightened global chromatin structure. DNMT3L induces more repressive H3K9 methylation on endogenous retroviruses and downregulates the derepressed transposons in aging MEFs. In addition, we found that a pulse of ectopic DNMT3L resulted in the reestablishment of H3K27me3 on polycomb repressive complex 2 (PRC2)-target genes that were derepressed in old MEFs. We demonstrated that ectopic DNMT3L interacted with PRC2 in MEFs. Our data also suggested that ectopic DNMT3L might guide PRC2 to redress deregulated chromatin regions in cells undergoing senescence. This study might lead to an epigenetic reinforcement strategy for overcoming aging-associated epimutation and senescence.

Keywords: senescence, epigenetics, DNA methyltransferase 3-like (DNMT3L), polycomb repressive complex 2 (PRC2), chromatin surveillance, transposable element (TE)

Abbreviations: ANOVA, analysis of variance; BSA, bovine serum albumin; ChEA, ChIP Enrichment Analysis; ChIP, chromatin immunoprecipitation; co-IP, coimmunoprecipitation; DEGs, differentially expressed genes; DMEM, Dulbecco's modified Eagle's medium; DNMTs, DNA methyltransferases; DNMT3L, DNA methyltransferase 3-like; DOX, doxycycline; ERVs, endogenous retroviruses; HDAC, histone deacetylases; IP, Immunoprecipitation; KO, knockout; MEFs, mouse embryonic fibroblasts; PCA, principal component analysis; PMSF, phenylmethylsulfonyl fluoride; PRC2, polycomb repressive complex 2; RFP, red fluorescent protein; RT-qPCRs, reverse transcription and quantitative polymerase chain reactions; SASP, senescence-associated secretory phenotype; SDS-PAGE, sodium dodecyl sulfate–polyacrylamide gel electrophoresis; SEMs, standard errors of the mean; TE, transposable element; WB, Western blot.

BACKGROUND

Cellular senescence is a major response to irreversible damage acquired in response to stress or replication mistakes (d'Adda, 2008; Hernandez-Segura et al., 2018). Senescent cells exhibit permanent cell-cycle arrest and substantial chromatin remodeling (Cruickshanks et al., 2013; Tchkonia et al., 2013). The number of senescent cells in tissues increases with age (Spaulding et al., 1997; Krishnamurthy et al., 2004; Herbig et al., 2006; Krizhanovsky et al., 2008; Vidal et al., 2012; Waaijer et al., 2012), and the rate of their accumulation predicts the lifespan of mice (Jurk et al., 2014). The secretions from senescent cells lead to a senescence-associated secretory phenotype (SASP), which might contribute to aging-associated tissue dysfunction or the development of a cancerous niche in old tissue (Coppe et al., 2010; Castro-Vega et al., 2015; Buhl et al., 2019; Lopes-Paciencia et al., 2019). A recent study showed that the transplantation of senescent cells into mice leads to the early onset of aging-related phenotypes (Xu et al., 2017, 2018), which supports the current hypothesis that senescence can be a driver of aging (Krtolica et al., 2001; Sturmlechner et al., 2017; Lewis-McDougall et al., 2019).

Emerging studies suggest the elimination of senescent cells to extend the healthspan (Baker et al., 2011, 2016; Xu et al., 2015; Palmer et al., 2019). The Kirkland research group initiated a quest for specific activation of the programed death of senescent cells (Zhu et al., 2015), which has resulted in interest in the identification of various senolytic compounds or drugs that can kill senescent cells of specific cell lineages (Zhu et al., 2017; Fuhrmann-Stroissnigg et al., 2018; Cherif et al., 2019; Justice et al., 2019). In addition, it has been found that several emerging senomorphic drugs can suppress SASP (Bitto et al., 2016; de Cecco et al., 2019). The current senotherapeutic interventions basically focus on pre-existing senescent cells (Myrianthopoulos, 2018; Kim and Kim, 2019), whereas the process for safely slowing the emergence of senescence is poorly understood.

Senescence can be activated by reaching the Hayflick limit (telomere shortening to a critical length) (Hayflick and Moorhead, 1961; Hayflick, 1965) or stressors (Serrano et al., 1997; Wang et al., 2009; Luo et al., 2011; Suram et al., 2012; de Magalhaes and Passos, 2018). In addition to the continuous attrition of telomere length accompanied by cell division, aging cells approaching senescence display a less-stringent chromatin architecture and epigenetic control (Pal and Tyler, 2016; Xie et al., 2018; Benayoun et al., 2019), and these features can be accelerated by stress induced by stochastic replication mistakes, environmental stimuli, oncogene activation or signals produced by pre-existing senescent cells (Hodny et al., 2010; Nelson et al., 2012; Benayoun et al., 2015). Therefore, many cells enter senescence before reaching the Hayflick limit (Spaulding et al., 1997; Rubin, 2002; Toussaint et al., 2002; Parrinello et al., 2003; Hewitt et al., 2012; Suram et al., 2012), and this process is known as premature senescence.

The gradual loss of chromatin organization during aging is associated with perinuclear-chromatin detachment (associated with the depletion of the nuclear-envelope protein lamin B1) (Guelen et al., 2008; McCord et al., 2013), reductions in histone core proteins (H3 and H4) (O'Sullivan et al., 2010), and changes in trimethylation markers on histone H3 lysines (H3K4me3, H3K9me3, and H3K27me3) resulting from the reconfiguration of chromatin regulators during aging (Pal and Tyler, 2016). These features contribute to a decline in the maintenance of heterochromatin (inactivated, condensed chromatin state), which is a hallmark of senescent cells (de Cecco et al., 2013a; Pal and Tyler, 2016).

Heterochromatin is mainly concentrated on repeat sequences, including transposable elements (TEs), which constitute a major fraction of the mammalian genome (Lander et al., 2001; Mouse Genome Sequencing Consortium et al., 2002). TE derepression is frequently observed during cellular aging and cancer development (Belancio et al., 2010; de Cecco et al., 2013a,b, 2019). The reactivation of TEs in somatic cells reflects the increases in heterochromatin loss and global chromatin relaxation observed with aging (Orr, 2016; Pal and Tyler, 2016). Elevated chromatin accessibility leads to genomic instability, which can serve as a prelude to senescence. Therefore, the enhancement of chromatin surveillance might allow prolongation of the healthspan of a cell, and the appropriate perturbation of chromatin modifiers reportedly extends the lifespan of invertebrate models (Pal and Tyler, 2016; Sen et al., 2016; Benayoun et al., 2019; Mahmoudi et al., 2019).

Serendipitously, we discovered that the transient ectopic expression of a repressive epigenetic modulator, DNA methyltransferase 3-like (DNMT3L), was sufficient to delay the senescence progression of late-passage mouse embryonic fibroblasts (MEFs). MEFs usually enter senescence after approximately 10 passages when cultured *in vitro* under standard cultural conditions with ambient oxygen (20%), and these cells still contain relatively long telomeres (Parrinello et al., 2003). Therefore, MEFs are considered a useful model for the study of premature senescence independent of telomere shortening (Cristofalo et al., 2000).

DNMT3L is a well-studied TE suppressor (Liao et al., 2012). In addition to the maintenance of heterochromatin obtained with endogenous DNMT3L in germ cells, we discovered that ectopic DNMT3L expression can recruit a repressive chromatin-modifying complex to stimulate *de novo* repressive histone modification markers on newly infected retroviruses and endogenous retroviruses (ERVs) in MEFs (Kao et al., 2014). This finding resonates with DNMT3L's known function of facilitating the epigenetic repression of TE-associated regions during germ cell development after the physiological genome-wide erasure of repressive epigenetic markers (Bourc'his and Bestor, 2004; Hata et al., 2006; Hu et al., 2008).

In this study, we discovered that the transient expression of DNMT3L in MEFs is sufficient to sustain the proliferation activity of cells for at least 40 passages *in vitro* under standard 20% oxygen culture conditions. To gain insights into the mechanism underlying this phenomenon, we examined several factors associated with the aging process, including the

quantities of the nuclear envelope-binding protein lamin B1, histone proteins, and repressive H3K9me3 markers on ERVs and the expression level of selected TEs. To understand the effect of DNMT3L on aging-associated single-copy genes, we further performed a cDNA microarray analysis of young, old and DNMT3L-treated MEFs and characterized the properties of DNMT3L-responsive genes that are derepressed in old MEFs. Our data suggest that chromatin surveillance enhancement might constitute one of the mechanisms underlying the DNMT3L-induced halting of senescence progression in aging MEFs. This type of study might lead to the development of an epigenetic reinforcement strategy that could mitigate aging-associated epimutation and prevent premature senescence.

RESULTS

A Pulse of Ectopic DNMT3L Delays Premature Senescence in Mouse Embryonic Fibroblasts

Here, we demonstrated for the first time that transient DNMT3L expression in late-passage MEFs was sufficient to extend the proliferative activities of these cells. Intriguingly, transient DNMT3L expression in early passage MEFs failed to delay senescence (**Supplementary Figure S1**). This observation indicated that this DNMT3L-dependent resistance to senescence was restrictive to the presenescent cellular environment in MEFs. We therefore determined the expression timing of *Dnmt3l* in MEFs in a restrictive range of passages based on the percentage of Ki67-positive cells (actively dividing cells) (**Figure 1A**). Old/presenescent MEFs steadily proliferated after transient exposure to DNMT3L. We termed the cells after a DNMT3L pulse as "DNMT3L-treated MEFs" (the representative passages used in this paper were at least 10 passages after transient DNMT3L expression, when DNMT3L was no longer present). The DNMT3L-treated MEFs sustained robust cell division for over 40 passages and were still growing well after 40 passages, whereas MEFs transfected with a mock expression vector (used as a control) barely showed any division within five passages after the transfection. Compared with the flat and irregular shapes of old/presenescent MEFs, the DNMT3L-treated MEFs bulged in the center and had smaller nuclei (**Figure 1B**). Remarkably, the DNMT3L-treated MEFs showed around 80% enrichment in Ki67-positive cells, and this finding is similar to that found for young MEFs, which can be defined as 80% Ki67-positive cells (**Figures 1C,D**). BrdU-positive cells were also significantly enriched in DNMT3L-treated MEF (similar to that found in young MEFs) comparing with old/presenescent MEFs, indicating active DNA replication after the DNMT3L pulse (**Supplementary Figure S2**). The growth curve of the DNMT3L-treated MEFs was closer to that of young MEFs than to that of old/presenescent MEFs and was clearly different from that of senescent MEFs (**Figure 1E**). The Ki67 index and growth curve of the DNMT3L-treated MEFs suggested that transient DNMT3L expression restored the proliferative ability of old/presenescent MEFs.

The DNMT3L-Induced Halting of the Senescence Machinery Might Be Partly Due to Maintenance of the Nuclear Architecture

The quantity of the nuclear envelope-binding protein lamin B1 and the associated heterochromatin usually declines during the aging process, and these decreases are associated with reductions in the total nucleosome numbers. The transient treatment of aging MEFs with DNMT3L not only induced long-term proliferation activity but also significantly restored the lamin B1 and H3 expression levels (**Figures 2A–D**), which suggested reinforcement of the condensed global chromatin structure. These results indicated that the transient expression of DNMT3L in presenescent MEFs enabled the halting of senescence progression partly via the maintenance of sufficient levels of nuclear lamina protein and nucleosomes.

A Pulse of Ectopic DNMT3L Enhances H3K9me3 on ERVs in a Long-Term Manner

We previously found that the H3K9me3 marks on two TE families, Class I and II ERVs, were significantly elevated in DNMT3L-expressing MEFs at 48 hr post-*Dnmt3l* transfection (Kao et al., 2014). After this immediate response, we found a global elevation of H3K9me3 in DNMT3L-treated MEFs (**Figure 3A**) and a long-term maintenance of H3K9me3 enrichment in all three classes of ERVs in DNMT3L-treated MEFs for at least 10 passages after a DNMT3L pulse administered once ectopic DNMT3L was no longer detectable (**Figure 3B**). In addition, most of the selected TE subfamilies included in the RT-qPCR analysis were derepressed in old MEFs compared with their expression in young MEFs. The great majority of the derepressed TE subfamilies were downregulated after DNMT3L treatment (data not shown). Although DNMT3L protein is not detectable in MEFs, the above findings suggested a long-term effect carried over from prior ectopic DNMT3L expression.

DNMT3L Treatment Partly Reverses Aberrant Gene Expression During the Aging Process in MEFs

To understand the impacts of DNMT3L exposure on single-copy genes in old MEFs, we compared the annotated gene expression patterns of young, old/presenescent and DNMT3L-treated MEFs through a microarray analysis. The pairwise Spearman correlation matrix showed that the gene expression levels were similar between young and old MEFs (**Supplementary Figure S3**). The genes upregulated in young compared with old MEFs were largely associated with proliferation-related pathways (**Supplementary Figure S4a**), whereas the genes upregulated in old MEFs were enriched in other pathways and included

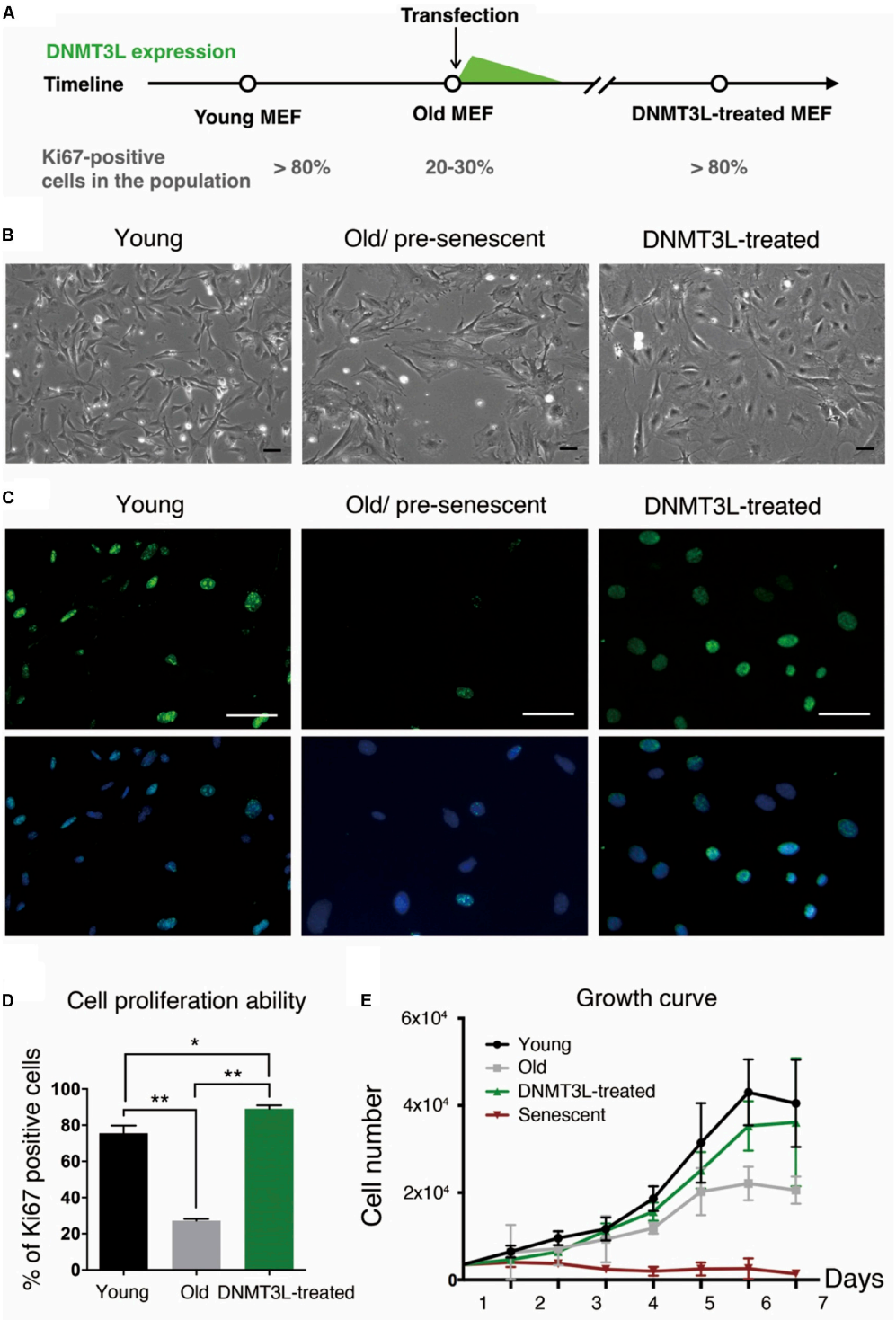

FIGURE 1 | Ectopic DNMT3L pulse restored the proliferation ability of aging MEFs. **(A)** Timeline of the sampling time points and the ectopic DNMT3L expression timing. The percentage of Ki67-positive cells in the population indicated the stage of cells. **(B)** Representative bright-field microscopy images of young, old/presenescent and DNMT3L-treated MEFs as labeled. Scale bar = 10 μm. **(C)** Representative Ki67-immunofluorescence images of the indicated cells. Green: Ki67 (proliferating cells); blue: Hoechst 33342 (nuclei). Bar = 10 μm. **(D)** Frequency distribution of proliferating cells among the three cell types based on the percentage of Ki67–positive nuclei. Mean ± SEM, $n = 3$. Asterisks indicate averages with significantly differences at $^{*}p < 0.05$ or $^{**}p < 0.01$, as determined by Student's *t*-test. **(E)** Growth curve of the labeled cell populations. The black lines indicate the young MEFs; the gray lines indicate the old/presenescent MEFs; the green lines indicate the DNMT3L-treated MEFs; and the dark-red lines indicate the senescent MEFs. The cells were initially seeded at 5000 per well in a 24-well tissue culture plate (mean ± SEM, $n = 6$).

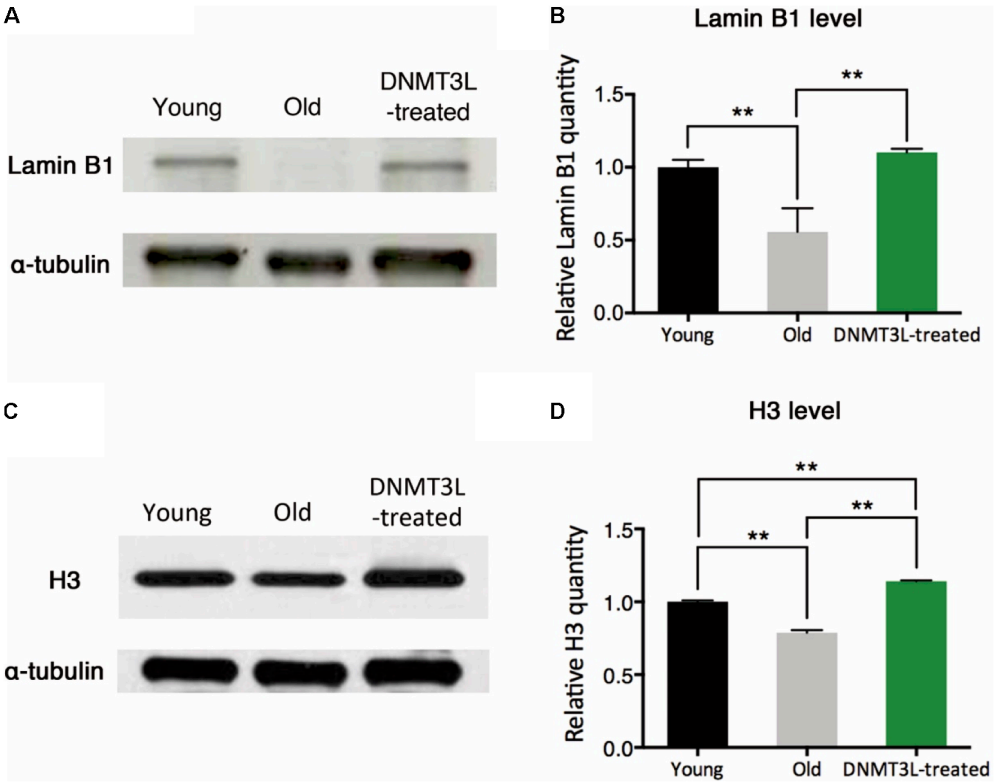

FIGURE 2 | DNMT3L treatment restored the nuclear envelope-binding and histone core proteins that decreased during cellular aging. **(A)** Western blot analysis of extracts from young, old/presenescent and DNMT3L-treated MEFs using anti–lamin B1 and anti–α-tubulin antibodies. The distribution of the α-tubulin quantity was relatively stable among populations of young, old/presenescent and DNMT3L-treated MEFs with the same cell number. **(B)** Statistical results from repeated immunoblots assessing the relative quantity of lamin B1 normalized by α-tubulin. Mean ± SEM, $n = 3$. Asterisks indicate averages with significant differences at $^{**}p < 0.01$, as determined by Student's *t*-test. **(C)** Western blot analysis of extracts from the same set of cell lines using anti–H3 and anti–α-tubulin antibodies. **(D)** Statistical results from repeated immunoblots assessing the relative quantity of H3 normalized by α-tubulin. Mean ± SEM, $n = 3$. Asterisks indicate significant differences at $^{**}p < 0.01$, Student's *t*-test.

genes negatively regulated by Sirt1, genes associated with oxidative stress-induced senescence, and genes associated with SASPs (**Supplementary Figure S4b**). Intriguingly, a significant proportion of the genes that were differentially expressed between young and old MEFs were also affected by DNMT3L treatment. We found 1006 differentially expressed genes (DEGs) between young and old MEFs, and 556 of these DEGs also showed differential expression before and after the DNMT3L pulse (**Supplementary Figure S5**). The hypergeometric *p*-value of this overlap was less than 2×10^{-16}, which suggested that DNMT3L exerted a significant impact on genes that exhibit altered expression among passages. We found that DNMT3L treatment partly reversed the cellular aging-related transcriptome changes in MEFs during the aging process. Among the 556 genes whose expression was affected by both prolonged passages and DNMT3L treatment, 82.7% exhibited a young cell-like expression pattern after DNMT3L treatment (**Supplementary Figures S6a–d**). Intriguingly, the majority of the genes upregulated in old MEFs were re-repressed after DNMT3L treatment. We also performed proteomic analysis on the young, old, and DNMT3L-treated MEFs. The changes in the protein expression patterns were highly associated with the DEGs identified in the microarray analysis (data not shown).

DNMT3L Enhances the Repression of Derepressed PRC2-Targeted Genes in Old MEFs and Globally Reinforces H3K27me3 Markers

To identify the repressive machinery lost during aging, we focused on the genes repressed in young MEFs and derepressed in old MEFs. We first defined a set of genes with expression levels below a manually positioned cutout line in young MEFs (**Figure 4A**). These genes represented those that properly maintained the repressed/silenced machinery at early passages (**Figure 4B**). Among the 19,116 genes that were expressed at low levels in young MEFs, we then spotted 419 hits that were overexpressed by more than 1.5-fold in old MEFs.

Among these 419 hits, only 11% were continuously upregulated after DNMT3L treatment, and half of the remaining 89% were downregulated after the treatment (**Figure 4C**). This distribution suggested that ectopic DNMT3L mainly played a repressive role on the genes derepressed in old MEFs, resulting in

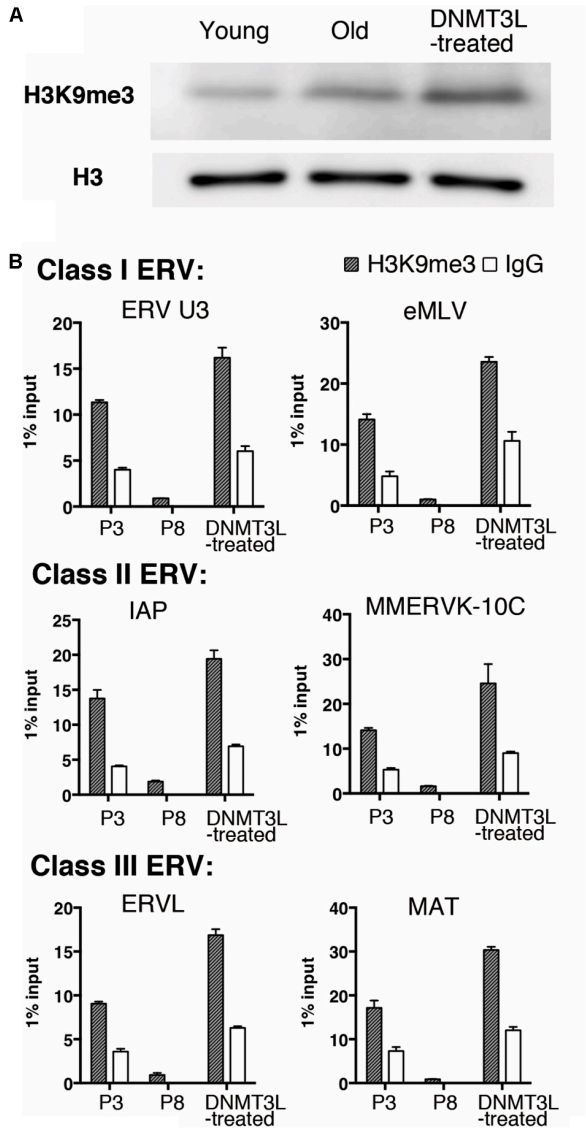

FIGURE 3 | Ectopic DNMT3L established a long-term effect on global H3K9me3 elevation and H3K9me3 enrichment on ERVs. **(A)** Western blot analysis of extracts from young, old/presenescent and DNMT3L-treated MEFs using anti–H3K9me3 antibody. Anti–H3 antibodies were used to indicate the relative expression on nucleosomes among samples. **(B)** ChIP-qPCR with anti-H3K9me3 antibody was used to assess the enrichment of H3K9me3 on representative Class I to Class III ERVs in the indicated cells. Mean ± SEM, $n = 3$. Rabbit IgG was used as a negative control.

establishment of a "young cell-like" pattern, which is consistent with the primarily repressive function attributed to DNMT3L.

According to ChIP Enrichment Analysis (ChEA) 2016 (a gene list enrichment analysis tool from Enrichr), SUZ12, a PRC2 member responsible for establishment of the H3K27me3 repressive marker, showed a significantly higher potential to be one of the binding factors for genes re-repressed after DNMT3L treatment. MTF2, a polycomb group (PcG) protein that recruits PRC2 to induce an enhancement in H3K27me3 methylation activity, was also in the list of top five proteins with a significant adjusted *p*-value (**Figure 4D**). The microarray data showed that the RNA expression levels of *Suz12*, *Mtf2* and *Trp53* were downregulated in old MEFs compared with those in both young and DNMT3L-treated MEFs, whereas *Nr0b1* and *Jarid2* maintained similar levels among all of the samples (**Supplementary Figure S7**).

Additionally, the above-described genes derepressed in old MEFs and re-repressed after DNMT3L treatment were subjected to Encode Histone Modification 2015 (another gene list enrichment analysis tool from Enrichr). These genes are mainly found to be marked by H3K27me3 in various mouse somatic cell lineages (**Figure 4D**). We performed a Western blotting analysis to measure the overall levels of SUZ12 and H3K27me3 in young, old and DNMT3L-treated MEFs (**Figure 4E**). SUZ12 was slightly downregulated in old MEFs and upregulated in DNMT3L-treated MEFs compared with its expression in young MEFs, which was consistent with the *Suz12* RNA expression levels obtained in the microarray analysis (**Supplementary Figure S7**). Among these cells, old MEFs showed the lowest levels of both H3 and H3K27me3 (**Figures 2C,D**, **4F,H**). After normalization based on alpha-tubulin, the H3K27me3 level was globally increased in DNMT3L-treated MEFs (**Figure 4F**). Our data suggested that DNMT3L can enhance the repressive regulation of genes that lose H3K27me3 repression during aging and reinforce the global H3 and H3K27me3 levels.

Ectopic DNMT3L Interacts With SUZ12 and Restores H3K27me3 in the Promoters of Derepressed PRC2 Target Genes

The above-described data support the hypothesis that DNMT3L mitigates the derepression of PRC2-target genes that showed a loss of H3K27me3 suppression during aging. Based on the global elevation of SUZ12 and H3K27me3 after DNMT3L treatment in MEFs, and as DNMT3L and EZH2 interaction has been observed in ES cells before (Neri et al., 2013), we hypothesized that DNMT3L might facilitate the re-establishment of H3K27me3 markers on derepressed PRC2 target genes.

To test whether DNMT3L can recruit PRC2, we examined whether PRC2 and ectopic DNMT3L can be precipitated in the same complex in MEFs through a coimmunoprecipitation (co-IP) assay. Due to the lack of a suitable IP-grade anti-DNMT3L antibody, we constructed a lentiviral vector encoding N-terminal FLAG-tagged DNMT3L under the control of a doxycycline-inducible promoter. Young MEFs were transduced, selected using puromycin and treated with doxycycline at the time point corresponding to the 30% Ki67 index described previously (**Supplementary Figure S8a**). The expression of exogenous *Dnmt3l* was well controlled by doxycycline (**Figure 5A** and **Supplementary Figure S8b**). As expected, DNMT3L coprecipitated the PRC2 member SUZ12 (**Figure 5B**). Consistently, the immunoprecipitation of SUZ12 with anti-SUZ12 antibody revealed the presence of DNMT3L and EZH2, another PRC2 member (as a control), in the pull-down lysate (**Figure 5C**). We also observed HDAC1 in the IP-SUZ12

pull-down complex in MEFs and observed enrichment of the HDAC1-SUZ12 interaction in the DNMT3L-expressing MEFs (data not shown).

We randomly selected some genes from those derepressed in old MEFs and re-repressed after DNMT3L treatment (**Figure 6A**) and measured the H3K27me3 levels at their promoters in young, old and DNMT3L-treated MEFs through ChIP. The analysis of the genes that were re-repressed after DNMT3L treatment and showed a loss of H3K27me3 in old MEFs revealed that their H3K27me3 levels were significantly restored in DNMT3L-treated MEFs (**Figure 6B**). The trends found for repressive H3K27me3 among young, old and DNMT3L-treated MEFs were negatively-correlated with the mRNA abundance of each gene tested (**Figures 6A,B**).

We then tested whether DNMT3L re-establishes H3K27me3 in the derepressed PRC2 targets through a ChIP-qPCR assay using an anti-FLAG antibody to assess the DNMT3L occupancy on chromatin (using the doxycycline-induced DNMT3L-expressing MEFs described in **Supplementary Figure S8**). The signal for DNMT3L binding was slightly enriched in the tested promoters or exon1 regions in the FLAG-DNMT3L-expressing MEFs compared with that in the RFP-expressing MEFs (used as a negative control; **Figure 6C**). Together with the potential ability of DNMT3L to interact with PRC2, these data suggested that DNMT3L might be involved in the accumulation of H3K27me3 on the regulatory regions in genes that show a loss of PRC2 repression in old MEFs (**Figures 5**, **6**).

In conclusion, we discovered that the transient expression of DNMT3L in old MEFs induced long-term H3K9me3 enrichment on ERV sequences and might guide the PRC2 complex to a panel of aging-associated derepressed genes and thereby introduce H3K27me3. These repressive phenomena might represent a stronger surveillance of chromatin signatures and were associated with the halting of senescence progression (**Figure 7**).

DISCUSSION

Accompanying the global relaxation of epigenetic control, an aging cell leaning toward senescence undergoes changes in its nuclear architecture, shifts in its epigenetic modifier/modification patterns, and subsequent transcriptional alterations, including TE reactivation. In this study, we demonstrated that the transient expression of DNMT3L can halt senescence progression in aging cells. It is also sufficient to restore the global core histone protein and lamin B1, which are significantly reduced in old MEFs, and to tighten up the genomic regions that show a loss of proper repression machinery in presenescent cells.

A loss of histone core proteins during aging has been observed in various species (O'Sullivan et al., 2010; Pal and Tyler, 2016; Song and Johnson, 2018), and this loss resulted in a reduction of genomic stringency. The supply of additional histone H3 and H4 partially reverses the transcriptional defects in aging cells and extends the lifespan of budding yeast (Dang et al., 2009; Feser et al., 2010). In this study, we demonstrated that the transient expression of *Dnmt3l* in presenescent cells can restore nuclear structure-related components, including global histone H3 and lamin B1. The ectopic expression of human *Dnmt3l* also elevates the expression of H3 and lamin B1 in late-passage Hs68, which are primary human foreskin fibroblasts. Consistent with our findings in MEFs, restoration after *Dnmt3l* expression was only observed in the presenescent population and not in the early passages of human fibroblasts (data not shown). Lamin B1 depletion is a remarkable feature in senescent cells. The knockdown of lamin B1 epitomizes the chromatin landscape observed in replicative senescent cells, including the emergence of heterochromatin H3K27me3-diminished regions (Shah et al., 2013) and the redistribution of the constitutive heterochromatin marker H3K9me3 (Sadaie et al., 2013).

In addition to lamin B1 restoration, we found that DNMT3L partially fixed the aberrant H3K27me3 and H3K9me3 landscape and redressed the silencing modifications in the examined gene regions. In senescent cells, transcriptional downregulation of the PRC2 member EZH2 leads to a loss of H3K27me3 and the activation of PRC2-mediated genes (Bracken et al., 2007; Maertens et al., 2009). A recent finding showed that PRC redistribution could be caused by the recruitment of PRCs to sites of DNA damage (Ginjala et al., 2011). A more comprehensive investigation combining genomic organization and functional annotation data from multiple studies linked the abnormal PRC2 signature to poised promoter and heterochromatin depletion in aging-associated regions (Dozmorov, 2015). These data highlighted PRC2 as a key regulator of age-related processes and suggested that repairing the PRC2 signature might be a novel approach against aging. Consistent with this concept, we found an association between the halting of senescence progression and the regaining of H3K27me3 markers on derepressed PRC2 targets in presenescent MEFs after transient *Dnmt3l* expression. The upregulation of SUZ12 in DNMT3L-treated MEFs may contribute to the increased accumulation of H3K27me3 (**Figures 4F,G**). The correction of the PRC2 signature is therefore considered at least one of the critical factors for extending the cellular healthspan.

In proliferating cells, many tumor-suppressor genes or senescence effectors are silenced by PRC2 (e.g., p16 and the *CDKN2A* gene at the INK4A locus), and in senescent cells, the transcriptional downregulation of EZH2 leads to a loss of H3K27me3 and the activation of PRC2-mediated genes (Bracken et al., 2007; Maertens et al., 2009). Although we did not observe a significant decrease in PRC2 levels in our presenescent MEFs, we found a loss of H3K27me3 in certain PRC2 targets. The previously demonstrated DNA damage induced PRC redistribution (Ginjala et al., 2011), supports our speculation of PRC2 relocalization during aging. These findings indicated that PRC2-mediated silencing might be a critical inhibitor of senescence. Additionally, the PRC2 members EZH2 and EED are known to interact with histone deacetylases (HDAC) 1 and 2 (van der Vlag and Otte, 1999; Caretti et al., 2004; Tonini et al., 2004), which suggests that based on the cellular context, transcriptional repression

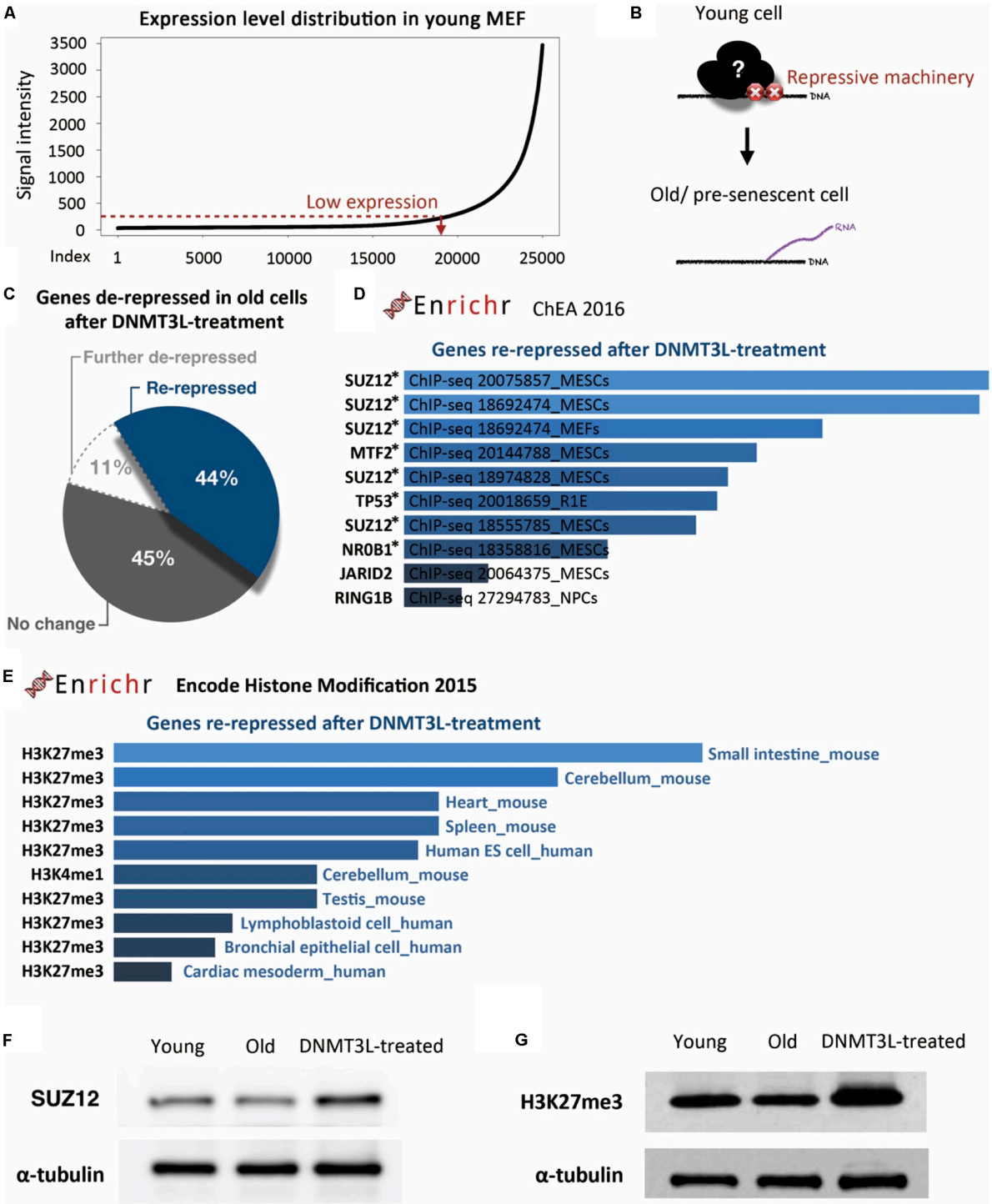

FIGURE 4 | DNMT3L treatment enhanced the repression of derepressed PRC2-targeted genes in old MEFs and globally reinforced H3K27me3 markers. **(A)** The distribution of gene expression in young MEFs was determined by a microarray analysis. According to the curve, we manually defined a threshold for the probe signal intensity below 100 as indicating a gene with low expression. The following analysis focused on these low-expression genes that lose repression in old MEFs. **(B)** Illustration of the genes with aging-associated loss of repression and their original repressor in young MEFs. **(C)** Pie chart indicating the change in genes derepressed in old MEFs after DNMT3L treatment. **(D)** The top 10 potential consensus transcriptional regulators of genes derepressed in old MEFs and re-repressed after a DNMT3L pulse are listed. The gene set described above was submitted to Enrichr and aligned with the ChEA 2016 database. All the listed regulators, SUZ12, MTF2, TP53, NR0B1, JARID2, and RING1, have significant hits with $p < 0.05$. The asterisks indicate the genes with p-values < 0.05. **(E)** Most-consensus histone modification of the genes described above in other cell lineages according to Encode Histone Modification 2015 (Enrichr). The listed markers in each dataset have a significance of $p < 0.05$. **(F,G)** Western blot analysis of extracts from young, old/presenescent and DNMT3L-treated MEFs with anti-SUZ12 and anti-H3K27me3 antibodies. The quantity of α-tubulin represents the loading control of similar cell numbers.

by the PRC2 complex might be mediated through HDACs. This result is consistent with our observation of the nuclear relocalization of HDAC1 after DNMT3L treatment (Kao et al., 2014). The cytoplasmic mislocalization of the nuclear protein HDAC1 has been described as a characteristic of cellular aging that is also linked to heterochromatin loss during aging (Willis-Martinez et al., 2010).

In addition to the DNMT3L-PRC2 activity observed in the present study, we previously found that ectopic DNMT3L expression in MEFs also triggers the formation of the DNMT3L-DNMT3A-KAP1-HDAC1-SETDB1 complex, which is linked to H3K9me3 repressive modifications at least on Class I and Class II ERVs (Kao et al., 2014), two well-known TE families. A specific point mutation of DNMT3L that breaks the DNMT3L-H3 tail or DNMT3L- DNMT3A interaction abolishes the formation of this complex (Kao et al., 2014). The interaction between DNMT3L and DNMT3A has been well demonstrated in germ cell development and stem cell differentiation. Without DNA methyltransferase activity, DNMT3L modulates chromatin by interpreting histone modifications and facilitating DNMT3A and DNMT3B for *de novo* DNA methylation (Ooi et al., 2007). The loss of DNA methylation in *Dnmt3l*-knockout (KO) male mouse germ cells leads to histone hyperacetylation and H3K9 demethylation, which consequently results in a loss of heterochromatin at the specific developmental stage of germ cells (Webster et al., 2005). According to microarray data from young, old and DNMT3L-treated MEFS, the transcription levels of *Kap1*, *Hdac1*, and *Setdb1* were lower in old MEFs and elevated in DNMT3L-treated MEFs, whereas *Dnmt3a* was expressed at similar low levels in all the samples (**Supplementary Figure S9**). The KAP1, HDAC1 and SETDB1 proteins in the ectopic DNMT3L-mediated repressive complex were all correlated with heterochromatin maintenance. KAP1 coordinates the assembly of a macromolecular complex containing chromatin-remodeling proteins (Sripathy et al., 2006; Iyengar and Farnham, 2011) and mediates heterochromatin-packaging repression on LINE1 (a well-known TE family). The KAP1-mediated repression of TEs fails with stress and age (van Meter et al., 2014). HDAC proteins govern heterochromatin at every cell phase (Murakami, 2013), and SETDB1 is a KAP1-associated H3K9-specific tri-methyltransferase (Schultz et al., 2002). The DNMT3L-mediated recruitment of DNMT3A-KAP1-HDAC1-SETDB1 and the elevated H3K9me3 markers on ERVs suggested the enforcement potential of heterochromatin maintenance on TEs in old MEFs (**Figure 7**).

The loss of heterochromatin that accompanies aging leads to a relaxed chromatin state, which potentially increases the risk of TE transposition and thereby jeopardizes the genomic stability (Pal and Tyler, 2016). In a young healthy individual, transposition rarely occurs in somatic cells. However, TE reactivation is frequently found in aging or cancer cells due to global epigenetic drift (de Cecco et al., 2013a,b, 2019; van Meter et al., 2014; Kaczkowski et al., 2016). Active TEs can affect gene expression by disrupting the promoter, enhancer, or gene body with new insertions or by introducing novel regulatory sequences (Inouye et al., 1984; Saigo, 1984; Saigo et al., 1984). Even without transposition, aberrant TE activation leads to transcriptome deregulation through the activation of neighboring genes via their strong promoters or the attraction of repressive chromatin modifiers and the spreading of repressive signatures across neighboring genomic regions. Therefore, enhancement of the heterochromatic silencing of repeat elements could be key to maintaining the healthspan. The gain-of-function effect of ectopic DNMT3L on TE repression observed in our current study was consistent with our previous DNMT3L loss-of-function study using *Dnmt3l*-KO embryo-derived MEFs (Liao et al., 2015). MEFs derived from *Dnmt3l*-KO embryos have an accelerated premature senescence phenotype, which is associated with a global reduction in repressive H3K9me3 and H3K27me3 markers (Liao et al., 2015). We further developed bioinformatic pipelines to quantify the representation of each TE subfamily from our published strand-specific RNA-seq datasets of *Dnmt3l*−/− and *Dnmt3l*+/+ littermate-derived MEFs (Liao et al., 2015). We found that more than 90% of the differentially expressed TE subfamilies were upregulated in *Dnmt3l*-KO MEFs (**Supplementary Table S1**). These findings described above suggest that a long-term effect of DNMT3L-expressing progenitor cells can still impact a cell type with no detectable DNMT3L.

Not surprisingly, the expression of most of the tested genes increased after DNMT3L treatment, and the genes with enriched expression in young cells were found to be more involved in pathways related to proliferation. The pathway enriched with DNMT3L-affected genes that are derepressed during aging is less cataloged, and the stochastic errors that sporadically occur during cellular aging might be one explanation for this finding. Intriguingly, the transcription factors predicted from the set of genes that were downregulated after DNMT3L treatment and derepressed in old cells are involved in the pluripotency network. In stem cells, the pluripotent-associated proteins regulate autophagy (Sotthibundhu et al., 2018), and whether a similar regulation tends to self-rescue cells at the initiation of presenescence remains unclear. In addition to the pluripotency factor-target genes, TRP53-target genes were mostly upregulated in presenescent cells, expressed at lower levels in the young population and downregulated after DNMT3L treatment. TRP53 is best known as a tumor suppressor (Sotthibundhu et al., 2018) because it can either activate or repress genes. Intriguingly, we found that the expression of *Trp53* was sustained in DNMT3L-treated MEFs (**Supplementary Figure S7**), which indicated that the restored proliferation ability of DNMT3L-treated MEFs was unlikely due to the "silencing of Trp53" that is frequently found in cancers.

Although DNMT3L-treated MEFs exhibit a restored proliferative ability, the morphology of the DNMT3L-treated MEFs and the spindle-shaped young MEFs were not identical (**Figure 1A**). To provide clues regarding the cell identity of DNMT3L-treated MEFs, we performed a principal component analysis (PCA) to compare approximately 1000 gene expression profiles of other mouse cell lineages, including the immortalized MEF-base cell line 3T3, primary cultured somatic cells, stem cells, and other cancer cells described in a database (data not shown). The results showed that the transcriptomes of DNMT3L-treated MEFs were most similar to those of young

MEFs. To further examine whether the DNMT3L-treated MEFs have fibrosis potential, we examined the expression levels of several representative fibrosis markers (Shih et al., 2018) from our microarray data (**Supplementary Figure S10**) and found no difference among young, old MEF and DNMT3L-treated MEFs in terms of their fibrogenic potential. The results indicated that the DNNMT3L pulse might have some effects on the transcriptional activity of certain extracellular matrix genes (*Col3a1* and *Ctgf*) without affecting markers for fibroblast activity (*Txndc5*, *Acta2,* and *Postn*). Our data showed that most of the fibrogenic protein genes were distinctly regulated in DNMT3L-treated MEFs. This suggested a limited role of DNMT3L in the process of tissue fibrosis. In addition, our transcriptomic data did not link the ectopic expression of *Dnmt3l* to cancer-related outcomes. The tumor formation assay in nude mice gave negative results, disproving a tumorigenic function for *Dnmt3l* in DNMT3L-treated MEFs (data not shown). The relationship between DNA methyltransferases (DNMTs) and tumorigenesis has been widely discussed (Zhang and Xu, 2017). Unlike DNMT1, DNMT3A and DNMT3B, no direct evidence has shown that DNMT3L contributes to carcinogenesis thus far. The current data are unlikely to link DNMT3L-treated MEFs to carcinogenesis, but we are not excluding the possibility that DNMT3L might lead to further unexpected cell fate changes beyond a repair of the chromatin state. Hopefully, our work could pave the way for the identification of more precise targets based on the DNMT3L-affected aging-associated network or downstream pathways associated with the resistance to senescence and prolongation of the cellular healthspan.

DNMT3L expression is rarely observed outside of germ cells and embryonic stem cell lineages. In MEFs from passage 1 to passage 8, DNMT3L expression, if any, was under the detection sensitivity for RNA-seq, RT-qPCR and Western, immunocytochemistry (Kao et al., 2014; **Figure 5**; unpublished observations). However, transient ectopic DNM3L expression induced long term effect observed in this study still provides potential physiological and pathological significance. For example, mouse DNMT3L has been demonstrated to be expressed in hematopoietic stem cells (Liu et al., 2013), and potentially have influence on the differentiated blood cell lineages (unpublished observation). In contrast, the Down syndrome associated overexpression of DNMT3L in neural progenitor cells of frontal cortex could underlie one mechanistic cause of the consequential neural disorder (Lu et al., 2016). It is also possible that aberrant transient DNMT3L expression may lead to detrimental effect for cells that need to be cleared out.

In summary, we discovered that transient DNMT3L expression halted senescence in aging/presenescent MEFs via enforcing global and regional chromatin surveillance. DNMT3L treatment of old MEFs restored their nuclear structure to a state closer to that of young cells by upregulating the nuclear envelope protein LaminB1 and histone H3. In addition, DNMT3L recruited the repressive epigenomic modifying complex DNMT3L-DNMT3A-KAP1-SETDB1-HDAC1 and increased H3K9me3 modifications in some ERVs and retrotransposons. DNMT3L also interacted with the PRC2 complex, resulting in increased H3K9me3 modification on a significant proportion of aging-associated derepressed single-copy genes (**Figure 7**). While current anti-aging research and applications place greater emphasis on eliminating senescent cells, we propose the possibility of minimizing the aging-associated relaxation of chromatin surveillance to prolong cellular health span.

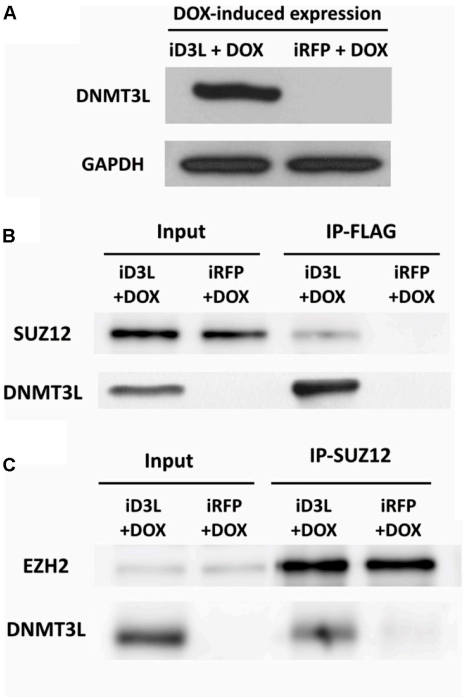

FIGURE 5 | Ectopic DNMT3L interacted with the PRC2 member SUZ12. **(A)** DNM3L or RFP expression was induced by 48 h of treatment with doxycycline (DOX) in lentivirus-infected DOX-inducible MEFs expressing the manufactured gene (**Supplementary Figure S6**). Western blot (WB) analysis of extracts of the same numbers of DNMT3L-expressing- (iD3L + DOX) and red fluorescent protein (RFP)-expressing (iRFP + DOX) MEFs using anti-DNMT3L antibody. Anti-GAPDH antibody was used as a loading control. **(B,C)** Immunoprecipitation (IP) and WB results revealed the interaction between DNMT3L and PRC2 members. Whole-cell extracts from DNMT3L- and RFP-expressing MEFs at 48 h postinduction were subjected to IP with anti–FLAG and anti–SUZ12 antibodies. WB using antibodies against DNMT3L, SUZ12, and EZH2 was performed to detect these proteins in the indicated IP-pulldown lysate extracts. SUZ12 and EZH2 showed equal quantities after a 5% input of both DNMT3L- and RFP-expressing MEFs. The presence of DNMT3L and SUZ12 was found in each protein interaction complex.

EXPERIMENTAL PROCEDURES

Animal Care and Cell Culture

The care of mice and the experimental procedures involving animals were approved by the Institutional Animal Care and Use Committee (IACUC) of National Taiwan University (approval number NTU-104-EL-00031 and NTU-105-EL-00123). Murine embryonic fibroblasts (MEFs) were derived from 13.5- to 14-day prenatal wild−type C57BL/6 mouse embryos and cultured with 5% CO_2 and ambient oxygen (20%) in Dulbecco's modified Eagle's medium (DMEM) (Gibco, CA,

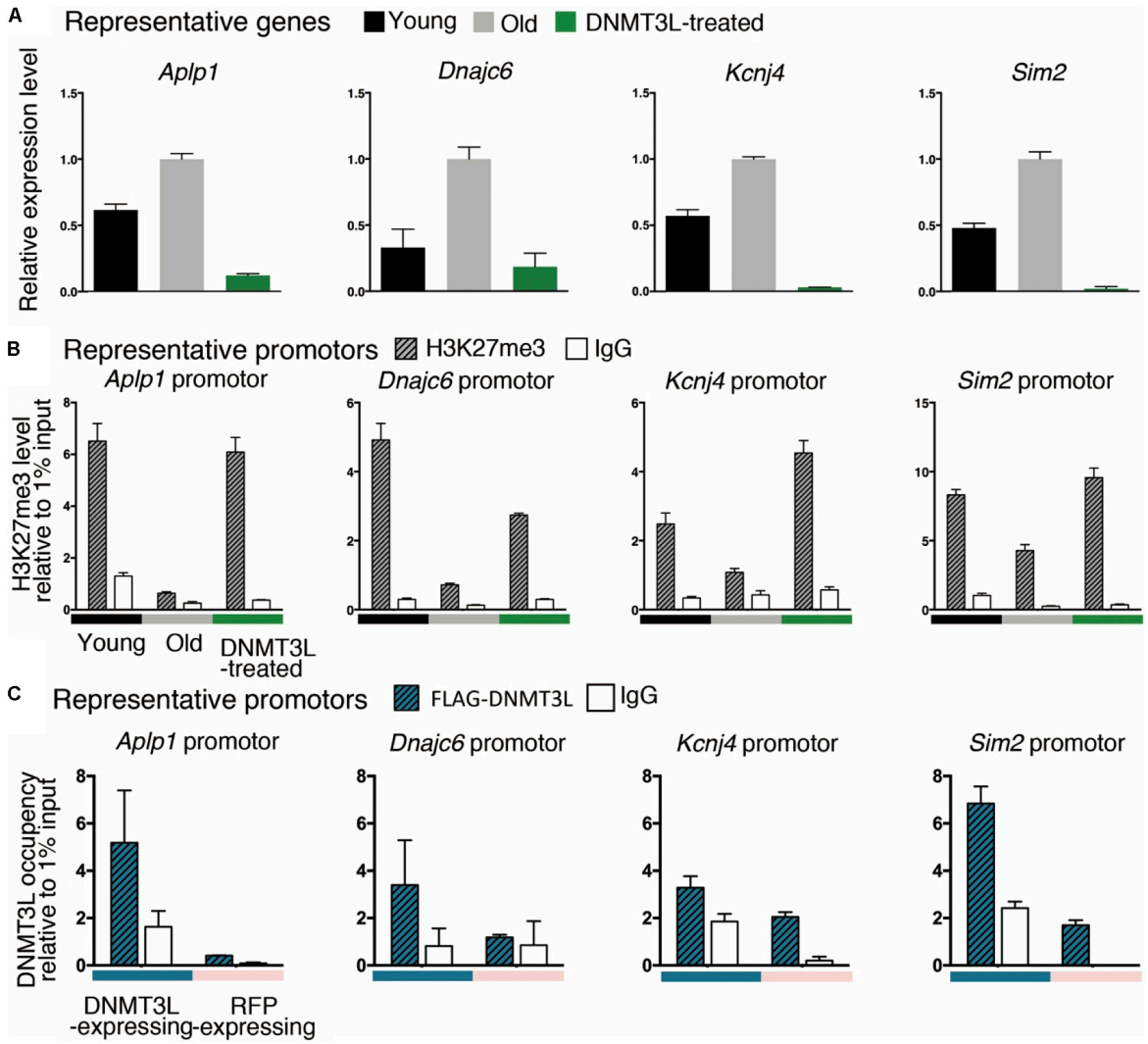

FIGURE 6 | Ectopic DNMT3L pulse restored H3K27me3 on the promoter of PRC2-target genes derepressed in old MEFs. **(A)** An RT-qPCR analysis (±SEM) demonstrated the relative expression of representative genes. The gene expression levels were normalized by *Rplp0*, and three technical repeats were performed. The *y*-axis represents the expression fold-changes relative to the gene expression in old MEFs. Representative genes: *Aplp1, Dnmajc6, Kcnj4,* and *Sim2*. **(B)** Anti-H3K27me3 ChIP-qPCR was performed to demonstrate the enrichment of H3K27me3 on the promoter or exon1 of the represented genes. Negative control: mouse IgG. The RNA expression of representative genes was reciprocally correlated to the accumulation of H3K27me3 in the promoter. **(C)** The occupancy of DNMT3L on the promoter or exon 1 of the represented genes during DNMT3L expression was assessed by ChIP-qPCR with an anti-FLAG antibody. RFP-expressing MEFs served as DNMT3L-negative controls. Mouse IgG was used as the negative control for ChIP.

United States) supplemented with 10% FBS, 100 U/ml penicillin and 100 μg/ml streptomycin.

Transient Ectopic DNMT3L Expression

Mouse DNMT3L or control eGFP was cloned into a constitutive pCAG vector with neomycin resistance. Plasmid DNA was purified and transfected into MEFs using Lipofectamine 2000 (Thermo Fisher, CA, United States) according to the manufacturer's instructions.

Immunocytochemistry (ICC)

The cells were seeded onto poly-L-lysine slides (Thermo Scientific) and cultured overnight. After fixing in 4% PFA for 10 min at room temperature, the cells were washed twice with DPBS, treated with 0.5% Triton X-100 in PBS and blocked in 10% goat serum with 1–2% bovine serum albumin (BSA). After incubation with the primary anti-Ki67 antibody (ab16667), the sections and tubules were incubated with secondary antibodies (1:500 dilution, 715-485-150 DyLight 488 and 211-505-109 DyLight 549, Jackson ImmunoResearch), counterstained with Hoechst 33342 (Sigma) and mounted with mounting medium (Cat. P36934, Invitrogen).

Western Blotting (WB)

Cells were homogenized and lysed with RIPA Buffer (Abcam) containing 1 mM phenylmethylsulfonyl fluoride (Sigma) and

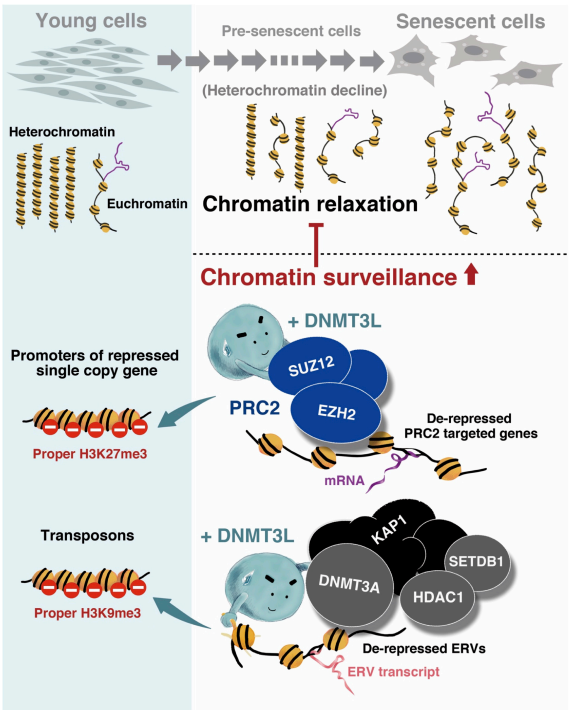

FIGURE 7 | Graphical summary of the mechanism through which ectopic DNMT3L enhances chromatin surveillance and decelerates senescence progression. Global chromatin relaxation is a hallmark of aging cells. Compared with the chromatin structure in young cells, fewer heterochromatin compartments are found in aging cells approaching senescence, which consequently leads to the reactivation of transposable elements (TEs) or abnormal gene expression. The ectopic expression of DNA methyltransferase 3-like (DNMT3L) in aging MEFs enhances chromatin surveillance against heterochromatin loss during cellular aging. DNMT3L mediates repressive chromatin modulators to induce a higher amount of repressive H3K9me3 on endogenous retroviruses (ERVs) and re-establish H3K27me3 on polycomb repressive complex 2 (PRC2)-target genes that were derepressed in old MEFs. The DNMT3L pulse in aging MEFs can partially rescue chromatin relaxation and is sufficient to slow the progression of premature senescence.

Protease Inhibitor Cocktail (Sigma) and centrifuged for 10 min at 16,000 × *g* at 4°C. The protein concentrations of the lysates from total cortical gray matter homogenates were determined by the bicinchoninic acid assay method (Pierce, Rockford, IL, United States). Lysates from equal amounts of cells were separated by sodium dodecyl sulfate–polyacrylamide gel electrophoresis (SDS–PAGE) and transferred to PVDF membranes (Millipore). The membranes were blocked with 5% BSA (Sigma) or 5% milk dissolved in PBST (PBS containing 0.1% Tween-20, Millipore) at room temperature for 2 h. The incubations with the primary antibodies at an appropriate dilution were performed at 4°C overnight with gentle shaking. The membranes were incubated with a horseradish peroxidase-conjugated secondary antibody (1:5000 dilution). The proteins were detected using a chemiluminescent reagent (Millipore) and a BioSpectrum Imaging System (UVP). The protein quantities were quantified by analyzing the images using ImageJ software[1].

[1]https://imagej.nih.gov/ij

The antibodies used for WB were anti–lamin B1 (ab16048), anti–α-tubulin (ab7291), anti–H3 (ab1791), anti-H3K9me3 (ab8898), anti-DNMT3L (E1Y7Q, Cell Signaling #13451), anti-GAPDH (ab181602), anti-SUZ12 (D39F6, Cell Signaling #37373) and anti-EZH2 (AC22, Merck Millipore #17-662) antibodies.

Chromatin Immunoprecipitation (ChIP)

ChIP assays were performed using a LowCell# ChIP kit (Cat. Diagenode). Briefly, 1 × 10^6 freshly collected cells were cross-linked using 1% formaldehyde for 8 min at room temperature, and the cross-linking was arrested with glycine. After centrifugation, the cells were resuspended in lysis buffer supplemented with a protease inhibitor cocktail (Cat. Diagenode) and 20 mM NaBu. The cross-linked chromatin was sheared to lengths of approximately 500 bp by ultrasound (Cat. Diagenode). The sheared chromatin samples were divided into 10 fractions, and each fraction incubated with 4 μg of anti-H3K4me3 (ab8895, Abcam), anti-H3K27me3 (07-449, Millipore) anti-FLAG (Cat. Sigma) or control IgGs (Cat. Diagenode) overnight at 4°C with rotation. The immunoprecipitated DNA was isolated using DNA isolation buffer (Diagenode), and specific genes in the purified DNA were amplified by qPCR and analyzed.

Viral–Mediated Gene Transfer

FLAG-tagged *Dnmt3l* was flanked into the all-in-one inducible lentiviral backbone pAS4.1w.Ppuro-aOn vector using the *Nhe*I and *Eco*RV restriction enzyme cutting sites downstream of the TetOn operator. This constructed, inducible *Dnmt3l*-bearing plasmid and a pAS4.1w.Ppuro-aOn-RFP (control) plasmid were transfected, respectively, into 293T cells with TransIT-2020 transfection reagent (Mirus Bio) for the packaging of pseudotype lentivirus. The DOX-inducible lentiviruses produced were used for the infection of young MEFs. Young P2-P3 MEFs were seeded in 24-well plates at 70% confluence 1 day prior to infection. The MEFs were infected by viral suspension with fresh media containing 8 μg/ml polybrene. Puromycin selection was initiated at 5 μg/ml after 24 h of viral infection. After the non-viral infected MEFs were clearly killed, the selected infected MEFs were continuously cultured in selection medium with 2 μg/ml puromycin. When the number of Ki67-positive cells decreased to 20–30%, ectopic gene expression in the infected old MEFs was induced by treatment with 0.5 μg/ml doxycycline for 48 h, and the cells were then subjected to the following experiments. Additional details are supplied in the Supporting Information.

Immunoprecipitation (IP)

The cells were lysed in NP40 buffer (Invitrogen) supplemented with 1x protease inhibitor cocktail (R1321, Fermentas) and 1 mM phenylmethylsulfonyl fluoride (PMSF). Immunoprecipitation was performed using a Dynabeads kit (Invitrogen) following the manufacturer's recommended protocol. For IP, 50 μg of total protein from DNMT3L/RFP-expressing cells was used for each experiment. The antibodies used for IP were anti–FLAG (M2, Sigma #F3165) and anti–SUZ12 (D39F6, Cell Signaling #3737) antibodies.

Total RNA Extraction and RT-qPCR

The cells were trypsinized from the culture dish and neutralized using an equal volume of culture medium containing 10% FBS. After two washes with DPBS, 500 g of the cells were pelleted in a 1.5-mL microcentrifuge tube and then centrifuged for 5 min at RT. Five hundred microliters of TRIzol® reagent (Cat. 15596018, Invitrogen, Carlsbad, CA, United States) was added to 2×10^6 cells, and the cells were then lysed by pipetting several times in the presence of TRIzol® reagent and homogenized by 1 min of vortexing. RNA purification was accomplished using the RNeasy mini kit (Cat. 74104, QIAGEN, United States), and the RNA was then treated with RNase-Free DNase I Set (Cat. 79254, QIAGEN, United States) while bound to the RNeasy membrane and subjected to "On-Column DNase Digestion" for 30 min at room temperature. The DNA-free RNA was eluted in RNase-free water. For assessment of the total RNA quantity and quality, 1 μl of sample was loaded on a NanoDrop spectrophotometer (NP-1000, NanoDrop, Wilmington, DE, United States) and then subjected to 1% agarose gel electrophoresis or analysis with a bioanalyzer. The RNA was stored at −80°C, and the reverse transcription and quantitative polymerase chain reactions (RT-qPCRs) were performed using a SuperScript First-Strand Synthesis System (Invitrogen) and Roche LightCycler 480II instrument, respectively. The annealing temperature used for all the primers was 60°C (primers are listed in **Supplementary Table S2**).

Statistics

The data are presented as the means ± standard errors of the mean (*SEMs*). The data analyses were performed using unpaired *t*-test or one−way analysis of variance (ANOVA) followed by *post hoc* Tukey's test as appropriate. $p < 0.05$ was considered statistically significant.

DATA AVAILABILITY STATEMENT

All sequencing data are deposited at the GEO repository under the accession number GSE135258.

ETHICS STATEMENT

The animal study was reviewed and approved by the National Taiwan University IACUC.

AUTHOR CONTRIBUTIONS

S-PL, YY, and H-FL conceived and planned the experiments. T-HK discovered the DNMT3L-mediated senescence-moderating phenomenon. YY, T-HK, H-FL, C-YY, J-YC, Y-TT, and H-TH performed the experiments. TH and C-CH performed the bioinformatic analysis. TH discovered the DNMT3L-mediated re-repression of PRC2-target genes in aging cells after DNMT3L treatment. MP and AM provided expertise and resources for transcriptome analysis of *Dnmt3l* KO MEFs. K-CY, Y-RC, and M-HT provided expertise, experimental support and critical comments on fibrosis, proteomic analysis and microarray analysis, respectively. All authors were involved in periodic discussion and critical feedback that helped to shape the research direction. S-PL provided overall funding and full-time supervision. YY and S-PL wrote the manuscript and incorporated comments from co-authors. YY created all the artwork (including graphic summary) in this manuscript.

FUNDING

This work was mainly funded by the Ministry of Science and Technology (MOST), Taiwan (MOST 107-2313-B-002-054-MY3 and MOST 105-2311-B-002 -008) and National Taiwan University (NTU 104R8952-2 and NTU 108L880304).

ACKNOWLEDGMENTS

We thank Dr. Ya-Ping Yen, Dr. Kai-Wei Chang, Dr. Yen-Tzu Tseng, Mr. Pin-Han Hsieh, Mr. Rohan Sitaniya, Mr. Pu-Sheng Hsu, and Mr. Yan-Ru Ju, the members of M-HT's laboratory and Technology Commons in College of Life Science and Center for Systems Biology, National Taiwan University, for their technical support. We also appreciate the insightful comments provided by Dr. Steen Ooi, Prof. Fredric Berger, Prof. Frederic Chedin, and members from the S-PL and AM laboratories.

SUPPLEMENTARY MATERIAL

The Supplementary Material for this article can be found online at: https://www.frontiersin.org/articles/10.3389/fcell.2020.00103/full#supplementary-material

REFERENCES

Baker, D. J., Childs, B. G., Durik, M., Wijers, M. E., Sieben, C. J., Zhong, J., et al. (2016). Naturally occurring p16(Ink4a)-positive cells shorten healthy lifespan. *Nature* 530, 184–189. doi: 10.1038/nature16932

Baker, D. J., Wijshake, T., Tchkonia, T., le Brasseur, N. K., Childs, B. G., van de Sluis, B., et al. (2011). Clearance of p16Ink4a-positive senescent cells delays ageing-associated disorders. *Nature* 479, 232–236. doi: 10.1038/nature10600

Belancio, V. P., Roy-Engel, A. M., Pochampally, R. R., and Deininger, P. (2010). Somatic expression of LINE-1 elements in human tissues. *Nucleic Acids Res.* 38, 3909–3922. doi: 10.1093/nar/gkq132

Benayoun, B. A., Pollina, E. A., and Brunet, A. (2015). Epigenetic regulation of ageing: linking environmental inputs to genomic stability. *Nat. Rev. Mol. Cell Biol.* 16, 593–610. doi: 10.1038/nrm4048

Benayoun, B. A., Pollina, E. A., Singh, P. P., Mahmoudi, S., Harel, I., Casey, K. M., et al. (2019). Remodeling of epigenome and transcriptome landscapes with aging in mice reveals widespread induction of inflammatory responses. *Genome Res.* 29, 697–709. doi: 10.1101/gr.240093.118

Bitto, A., Ito, T. K., Pineda, V. V., le Texier, N. J., Huang, H. Z., Sutlief, E., et al. (2016). Transient rapamycin treatment can increase lifespan and healthspan in middle-aged mice. *eLife* 5:e16351. doi: 10.7554/eLife.16351

Bourc'his, D., and Bestor, T. H. (2004). Meiotic catastrophe and retrotransposon reactivation in male germ cells lacking Dnmt3L. *Nature* 431, 96–99. doi: 10.1038/nature02886

Bracken, A. P., Kleine-Kohlbrecher, D., Dietrich, N., Pasini, D., Gargiulo, G., Beekman, C., et al. (2007). The polycomb group proteins bind throughout the INK4A-ARF locus and are disassociated in senescent cells. *Genes Dev.* 21, 525–530. doi: 10.1101/gad.415507

Buhl, J. L., Selt, F., Hielscher, T., Guiho, R., Ecker, J., Sahm, F., et al. (2019). The senescence-associated secretory phenotype mediates oncogene-induced senescence in pediatric pilocytic astrocytoma. *Clin. Cancer Res.* 25, 1851–1866. doi: 10.1158/1078-0432.CCR-18-1965

Caretti, G., di Padova, M., Micales, B., Lyons, G. E., and Sartorelli, V. (2004). The Polycomb Ezh2 methyltransferase regulates muscle gene expression and skeletal muscle differentiation. *Genes Dev.* 18, 2627–2638. doi: 10.1101/gad.1241904

Castro-Vega, L. J., Jouravleva, K., Ortiz-Montero, P., Liu, W. Y., Galeano, J. L., Romero, M., et al. (2015). The senescent microenvironment promotes the emergence of heterogeneous cancer stem-like cells. *Carcinogenesis* 36, 1180–1192. doi: 10.1093/carcin/bgv101

Cherif, H., Bisson, D. G., Jarzem, P., Weber, M., Ouellet, J. A., and Haglund, L. (2019). Curcumin and o-Vanillin exhibit evidence of senolytic activity in human IVD cells *in vitro*. *J. Clin. Med.* 8:433. doi: 10.3390/jcm8040433

Coppe, J. P., Desprez, P. Y., Krtolica, A., and Campisi, J. (2010). The senescence-associated secretory phenotype: the dark side of tumor suppression. *Ann. Rev. Pathol.* 5, 99–118. doi: 10.1146/annurev-pathol-121808-102144

Cristofalo, V. J., Volker, C., and Allen, R. G. (2000). Use of the fibroblast model in the study of cellular senescence. *Methods Mol. Med.* 38, 23–52. doi: 10.1385/1-59259-070-5:23

Cruickshanks, H. A., McBryan, T., Nelson, D. M., van der Kraats, N. D., Shah, P. P., van Tuyn, J., et al. (2013). Senescent cells harbour features of the cancer epigenome. *Nat. Cell Biol.* 15, 1495–1506. doi: 10.1038/ncb2879

d'Adda, F. F. (2008). Living on a break: cellular senescence as a DNA-damage response. *Nat. Rev. Cancer* 8, 512–522. doi: 10.1038/nrc2440

Dang, W., Steffen, K. K., Perry, R., Dorsey, J. A., Johnson, F. B., Shilatifard, A., et al. (2009). Histone H4 lysine 16 acetylation regulates cellular lifespan. *Nature* 459, 802–807. doi: 10.1038/nature08085

de Cecco, M., Criscione, S. W., Peckham, E. J., Hillenmeyer, S., Hamm, E. A., Manivannan, J., et al. (2013a). Genomes of replicatively senescent cells undergo global epigenetic changes leading to gene silencing and activation of transposable elements. *Aging Cell* 12, 247–256. doi: 10.1111/acel.12047

de Cecco, M., Criscione, S. W., Peterson, A. L., Neretti, N., Sedivy, J. M., and Kreiling, J. A. (2013b). Transposable elements become active and mobile in the genomes of aging mammalian somatic tissues. *Aging* 5, 867–883. doi: 10.18632/aging.100621

de Cecco, M., Ito, T., Petrashen, A. P., Elias, A. E., Skvir, N. J., Criscione, S. W., et al. (2019). L1 drives IFN in senescent cells and promotes age-associated inflammation. *Nature* 566, 73–78. doi: 10.1038/s41586-018-0784-9

de Magalhaes, J. P., and Passos, J. F. (2018). Stress, cell senescence and organismal ageing. *Mech. Ageing Dev.* 170, 2–9. doi: 10.1016/j.mad.2017.07.001

Dozmorov, M. G. (2015). Polycomb repressive complex 2 epigenomic signature defines age-associated hypermethylation and gene expression changes. *Epigenetics* 10, 484–495. doi: 10.1080/15592294.2015.1040619

Feser, J., Truong, D., Das, C., Carson, J. J., Kieft, J., Harkness, T., et al. (2010). Elevated histone expression promotes life span extension. *Mol. Cell* 39, 724–735. doi: 10.1016/j.molcel.2010.08.015

Fuhrmann-Stroissnigg, H., Niedernhofer, L. J., and Robbins, P. D. (2018). Hsp90 inhibitors as senolytic drugs to extend healthy aging. *Cell Cycle* 17, 1048–1055. doi: 10.1080/15384101.2018.1475828

Ginjala, V., Nacerddine, K., Kulkarni, A., Oza, J., Hill, S. J., Yao, M., et al. (2011). BMI1 is recruited to DNA breaks and contributes to DNA damage-induced H2A ubiquitination and repair. *Mol. Cell Biol.* 31, 1972–1982. doi: 10.1128/MCB.00981-10

Guelen, L., Pagie, L., Brasset, E., Meuleman, W., Faza, M. B., Talhout, W., et al. (2008). Domain organization of human chromosomes revealed by mapping of nuclear lamina interactions. *Nature* 453, 948–951. doi: 10.1038/nature06947

Hata, K., Kusumi, M., Yokomine, T., Li, E., and Sasaki, H. (2006). Meiotic and epigenetic aberrations in Dnmt3L-deficient male germ cells. *Mol. Reprod. Dev.* 73, 116–122. doi: 10.1002/mrd.20387

Hayflick, L. (1965). The limited *in vitro* lifetime of human diploid cell strains. *Exp. Cell Res.* 37, 614–636. doi: 10.1016/0014-4827(65)90211-9

Hayflick, L., and Moorhead, P. S. (1961). The serial cultivation of human diploid cell strains. *Exp. Cell Res.* 25, 585–621. doi: 10.1016/0014-4827(61)90192-6

Herbig, U., Ferreira, M., Condel, L., Carey, D., and Sedivy, J. M. (2006). Cellular senescence in aging primates. *Science* 311:1257. doi: 10.1126/science.1122446

Hernandez-Segura, A., Nehme, J., and Demaria, M. (2018). Hallmarks of cellular senescence. *Trends Cell Biol.* 28, 436–453. doi: 10.1016/j.tcb.2018.02.001

Hewitt, G., Jurk, D., Marques, F. D., Correia-Melo, C., Hardy, T., Gackowska, A., et al. (2012). Telomeres are favoured targets of a persistent DNA damage response in ageing and stress-induced senescence. *Nat. Commun.* 3:708. doi: 10.1038/ncomms1708

Hodny, Z., Hubackova, S., and Bartek, J. (2010). Cytokines shape chemotherapy-induced and 'bystander' senescence. *Aging* 2, 375–376. doi: 10.18632/aging.100171

Hu, Y. G., Hirasawa, R., Hu, J. L., Hata, K., Li, C. L., Jin, Y., et al. (2008). Regulation of DNA methylation activity through Dnmt3L promoter methylation by Dnmt3 enzymes in embryonic development. *Hum. Mol. Genet.* 17, 2654–2664. doi: 10.1093/hmg/ddn165

Inouye, S., Yuki, S., and Saigo, K. (1984). Sequence-specific insertion of the *Drosophila* transposable genetic element 17.6. *Nature* 310, 332–333. doi: 10.1038/310332a0

Iyengar, S., and Farnham, P. J. (2011). KAP1 protein: an enigmatic master regulator of the genome. *J. Biol. Chem.* 286, 26267–26276. doi: 10.1074/jbc.R111.252569

Jurk, D., Wilson, C., Passos, J. F., Oakley, F., Correia-Melo, C., Greaves, L., et al. (2014). Chronic inflammation induces telomere dysfunction and accelerates ageing in mice. *Nat. Commun.* 2:4172. doi: 10.1038/ncomms5172

Justice, J. N., Nambiar, A. M., Tchkonia, T., le Brasseur , N. K., Pascual, R., Hashmi, S. K., et al. (2019). Senolytics in idiopathic pulmonary fibrosis: results from a first-in-human, open-label, pilot study. *EBiomedicine* 40, 554–563. doi: 10.1016/j.ebiom.2018.12.052

Kaczkowski, B., Tanaka, Y., Kawaji, H., Sandelin, A., Andersson, R., Itoh, M., et al. (2016). Transcriptome analysis of recurrently deregulated genes across multiple cancers identifies new pan-cancer biomarkers. *Cancer Res.* 76, 216–226. doi: 10.1158/0008-5472.CAN-15-0484

Kao, T. H., Liao, H. F., Wolf, D., Tai, K. Y., Chuang, C. Y., Lee, H. S., et al. (2014). Ectopic DNMT3L triggers assembly of a repressive complex for retroviral silencing in somatic cells. *J. Virol.* 88, 10680–10695. doi: 10.1128/JVI.01176-14

Kim, E. C., and Kim, J. R. (2019). Senotherapeutics: emerging strategy for healthy aging and age-related disease. *BMB Rep.* 52, 47–55. doi: 10.5483/bmbrep.2019.52.1.293

Krishnamurthy, J., Torrice, C., Ramsey, M. R., Kovalev, G. I., Al-Regaiey, K., Su, L., et al. (2004). Ink4a/Arf expression is a biomarker of aging. *J. Clin. Investig.* 114, 1299–1307. doi: 10.1172/jci22475

Krizhanovsky, V., Xue, W., Zender, L., Yon, M., Hernando, E., and Lowe, S. W. (2008). Implications of cellular senescence in tissue damage response, tumor suppression, and stem cell biology. *Cold Spring Harb. Symp. Quant. Biol.* 73, 513–522. doi: 10.1101/sqb.2008.73.048

Krtolica, A., Parrinello, S., Lockett, S., Desprez, P. Y., and Campisi, J. (2001). Senescent fibroblasts promote epithelial cell growth and tumorigenesis: a link between cancer and aging. *Proc. Natl. Acad. Sci. U.S.A.* 98, 12072–12077. doi: 10.1073/pnas.211053698

Lander, E. S., Linton, L. M., Birren, B., Nusbaum, C., Zody, M. C., Baldwin, J., et al. (2001). Initial sequencing and analysis of the human genome. *Nature* 409, 860–921. doi: 10.1038/35057062

Lewis-McDougall, F. C., Ruchaya, P. J., Domenjo-Vila, E., Teoh, T. S., Prata, L., Cottle, B. J., et al. (2019). Aged-senescent cells contribute to impaired heart regeneration. *Aging Cell* 18:e12931. doi: 10.1111/acel.12931

Liao, H. F., Mo, C. F., Wu, S. C., Cheng, D. H., Yu, C. Y., Chang, K. W., et al. (2015). Dnmt3l-knockout donor cells improve somatic cell nuclear transfer reprogramming efficiency. *Reproduction* 150, 245–256. doi: 10.1530/REP-15-0031

Liao, H. F., Tai, K. Y., Chen, W. S., Cheng, L. C., Ho, H. N., and Lin, S. P. (2012). Functions of DNA methyltransferase 3-like in germ cells and beyond. *Biol. Cell* 104, 571–587. doi: 10.1111/boc.201100109

Liu, L., Souto, J., Liao, W., Jiang, Y., Li, Y., Nishinakamura, R., et al. (2013). Histone lysine-specific demethylase 1 (LSD1) protein is involved in Sal-like

protein 4 (SALL4)-mediated transcriptional repression in hematopoietic stem cells. *J. Biol. Chem.* 288, 34719–34728. doi: 10.1074/jbc.M113.506568

Lopes-Paciencia, S., Saint-Germain, E., Rowell, M. C., Ruiz, A. F., Kalegari, P., and Ferbeyre, G. (2019). The senescence-associated secretory phenotype and its regulation. *Cytokine* 117, 15–22. doi: 10.1016/j.cyto.2019.01.013

Lu, J., Mccarter, M., Lian, G., Esposito, G., Capoccia, E., Delli-Bovi, L. C., et al. (2016). Global hypermethylation in fetal cortex of Down syndrome due to DNMT3L overexpression. *Hum. Mol. Genet.* 25, 1714–1727. doi: 10.1093/hmg/ddw043

Luo, W., Xiong, W., Zhou, J., Fang, Z., Chen, W., Fan, Y., et al. (2011). Laminar shear stress delivers cell cycle arrest and anti-apoptosis to mesenchymal stem cells. *Acta Biochim. Biophys. Sin.* 43, 210–216. doi: 10.1093/abbs/gmr004

Maertens, G. N., El Messaoudi-Aubert, S., Racek, T., Stock, J. K., Nicholls, J., Rodriguez-Niedenfuhr, M., et al. (2009). Several distinct polycomb complexes regulate and co-localize on the INK4a tumor suppressor locus. *PLoS One* 4:e6380. doi: 10.1371/journal.pone.0006380

Mahmoudi, S., Xu, L., and Brunet, A. (2019). Turning back time with emerging rejuvenation strategies. *Nat. Cell Biol.* 21, 32–43. doi: 10.1038/s41556-018-0206-0

McCord, R. P., Nazario-Toole, A., Zhang, H., Chines, P. S., Zhan, Y., Erdos, M. R., et al. (2013). Correlated alterations in genome organization, histone methylation, and DNA-lamin A/C interactions in Hutchinson-Gilford progeria syndrome. *Genome Res.* 23, 260–269. doi: 10.1101/gr.138032.112

Mouse Genome Sequencing Consortium Waterston, R. H., Lindblad-Toh, K., Birney, E., Rogers, J., Abril, J. F., et al. (2002). Initial sequencing and comparative analysis of the mouse genome. *Nature* 420, 520–562. doi: 10.1038/nature01262

Murakami, Y. (2013). Histone deacetylases govern heterochromatin in every phase. *EMBO J.* 32, 2301–2303. doi: 10.1038/emboj.2013.154

Myrianthopoulos, V. (2018). The emerging field of senotherapeutic drugs. *Future Med. Chem.* 10, 2369–2372. doi: 10.4155/fmc-2018-0234

Nelson, G., Wordsworth, J., Wang, C., Jurk, D., Lawless, C., Martin-Ruiz, C., et al. (2012). A senescent cell bystander effect: senescence-induced senescence. *Aging Cell* 11, 345–349. doi: 10.1111/j.1474-9726.2012.00795.x

Neri, F., Krepelova, A., Incarnato, D., Maldotti, M., Parlato, C., Galvagni, F., et al. (2013). Dnmt3L antagonizes DNA methylation at bivalent promoters and favors DNA methylation at gene bodies in ESCs. *Cell* 155, 121–134. doi: 10.1016/j.cell.2013.08.056

Ooi, S. K., Qiu, C., Bernstein, E., Li, K., Jia, D., Yang, Z., et al. (2007). DNMT3L connects unmethylated lysine 4 of histone H3 to *de novo* methylation of DNA. *Nature* 448, 714–717. doi: 10.1038/nature05987

Orr, W. C. (2016). Tightening the connection between transposable element mobilization and aging. *Proc. Natl. Acad. Sci. U.S.A.* 113, 11069–11070. doi: 10.1073/pnas.1613350113

O'Sullivan, R. J., Kubicek, S., Schreiber, S. L., and Karlseder, J. (2010). Reduced histone biosynthesis and chromatin changes arising from a damage signal at telomeres. *Nat. Struct. Mol. Biol.* 17, 1218–1225. doi: 10.1038/nsmb.1897

Pal, S., and Tyler, J. K. (2016). Epigenetics and aging. *Sci. Adv.* 2:e1600584. doi: 10.1126/sciadv.1600584

Palmer, A. K., Xu, M., Zhu, Y., Pirtskhalava, T., Weivoda, M. M., Hachfeld, C. M., et al. (2019). Targeting senescent cells alleviates obesity-induced metabolic dysfunction. *Aging Cell* 18:e12950. doi: 10.1111/acel.12950

Parrinello, S., Samper, E., Krtolica, A., Goldstein, J., Melov, S., and Campisi, J. (2003). Oxygen sensitivity severely limits the replicative lifespan of murine fibroblasts. *Nat. Cell Biol.* 5, 741–747. doi: 10.1038/ncb1024

Rubin, H. (2002). The disparity between human cell senescence *in vitro* and lifelong replication *in vivo*. *Nat. Biotechnol.* 20, 675–681. doi: 10.1038/nbt0702-675

Sadaie, M., Salama, R., Carroll, T., Tomimatsu, K., Chandra, T., Young, A. R., et al. (2013). Redistribution of the Lamin B1 genomic binding profile affects rearrangement of heterochromatic domains and SAHF formation during senescence. *Genes Dev.* 27, 1800–1808. doi: 10.1101/gad.217281.113

Saigo, K. (1984). Structure and evolution of movable genetic elements in eukaryotes. *Seikagaku* 56, 371–387.

Saigo, K., Kugimiya, W., Matsuo, Y., Inouye, S., Yoshioka, K., and Yuki, S. (1984). Identification of the coding sequence for a reverse transcriptase-like enzyme in a transposable genetic element in *Drosophila melanogaster*. *Nature* 312, 659–661. doi: 10.1038/312659a0

Schultz, D. C., Ayyanathan, K., Negorev, D., Maul, G. G., and Rauscher, F. J. III (2002). SETDB1: a novel KAP-1-associated histone H3, lysine 9-specific methyltransferase that contributes to HP1-mediated silencing of euchromatic genes by KRAB zinc-finger proteins. *Genes Dev.* 16, 919–932. doi: 10.1101/gad.973302

Sen, P., Shah, P. P., Nativio, R., and Berger, S. L. (2016). Epigenetic mechanisms of longevity and aging. *Cell* 166, 822–839. doi: 10.1016/j.cell.2016.07.050

Serrano, M., Lin, A. W., McCurrach, M. E., Beach, D., and Lowe, S. W. (1997). Oncogenic ras provokes premature cell senescence associated with accumulation of p53 and p16INK4a. *Cell* 88, 593–602. doi: 10.1016/s0092-8674(00)81902-9

Shah, P. P., Donahue, G., Otte, G. L., Capell, B. C., Nelson, D. M., Cao, K., et al. (2013). Lamin B1 depletion in senescent cells triggers large-scale changes in gene expression and the chromatin landscape. *Genes Dev.* 27, 1787–1799. doi: 10.1101/gad.223834.113

Shih, Y. C., Chen, C. L., Zhang, Y., Mellor, R. L., Kanter, E. M., Fang, Y., et al. (2018). Endoplasmic reticulum protein TXNDC5 augments myocardial fibrosis by facilitating extracellular matrix protein folding and redox-sensitive cardiac fibroblast activation. *Circ Res.* 122, 1052–1068. doi: 10.1161/CIRCRESAHA.117.312130

Song, S., and Johnson, F. B. (2018). Epigenetic mechanisms impacting aging: a focus on histone levels and telomeres. *Genes* 9:E201. doi: 10.3390/genes9040201

Sotthibundhu, A., Promjuntuek, W., Liu, M., Shen, S., and Noisa, P. (2018). Roles of autophagy in controlling stem cell identity: a perspective of self-renewal and differentiation. *Cell Tissue Res.* 374, 205–216. doi: 10.1007/s00441-018-2829-7

Spaulding, C. C., Walford, R. L., and Effros, R. B. (1997). The accumulation of non-replicative, non-functional, senescent T cells with age is avoided in calorically restricted mice by an enhancement of T cell apoptosis. *Mech. Ageing Dev.* 93, 25–33. doi: 10.1016/s0047-6374(96)01808-8

Sripathy, S. P., Stevens, J., and Schultz, D. C. (2006). The KAP1 corepressor functions to coordinate the assembly of *de novo* HP1-demarcated microenvironments of heterochromatin required for KRAB zinc finger protein-mediated transcriptional repression. *Mol. Cell Biol.* 26, 8623–8638. doi: 10.1128/mcb.00487-06

Sturmlechner, I., Durik, M., Sieben, C. J., Baker, D. J., and van Deursen, J. M. (2017). Cellular senescence in renal ageing and disease. *Nat. Rev. Nephrol.* 13, 77–89. doi: 10.1038/nrneph.2016.183

Suram, A., Kaplunov, J., Patel, P. L., Ruan, H., Cerutti, A., Boccardi, V., et al. (2012). Oncogene-induced telomere dysfunction enforces cellular senescence in human cancer precursor lesions. *EMBO J.* 31, 2839–2851. doi: 10.1038/emboj.2012.132

Tchkonia, T., Zhu, Y., van Deursen, J., Campisi, J., and Kirkland, J. L. (2013). Cellular senescence and the senescent secretory phenotype: therapeutic opportunities. *J. Clin. Investig.* 123, 966–972. doi: 10.1172/jci64098

Tonini, T., Bagella, L., D'Andrilli, G., Claudio, P. P., and Giordano, A. (2004). Ezh2 reduces the ability of HDAC1-dependent pRb2/p130 transcriptional repression of cyclin A. *Oncogene* 23, 4930–4937. doi: 10.1038/sj.onc.1207608

Toussaint, O., Royer, V., Salmon, M., and Remacle, J. (2002). Stress-induced premature senescence and tissue ageing. *Biochem. Pharmacol.* 64, 1007–1009. doi: 10.1016/s0006-2952(02)01170-x

van der Vlag, J., and Otte, A. P. (1999). Transcriptional repression mediated by the human polycomb-group protein EED involves histone deacetylation. *Nat. Genet.* 23, 474–478. doi: 10.1038/70602

van Meter, M., Kashyap, M., Rezazadeh, S., Geneva, A. J., Morello, T. D., Seluanov, A., et al. (2014). SIRT6 represses LINE1 retrotransposons by ribosylating KAP1 but this repression fails with stress and age. *Nat. Commun.* 5:5011. doi: 10.1038/ncomms6011

Vidal, M. A., Walker, N. J., Napoli, E., and Borjesson, D. L. (2012). Evaluation of senescence in mesenchymal stem cells isolated from equine bone marrow, adipose tissue, and umbilical cord tissue. *Stem Cells Dev.* 21, 273–283. doi: 10.1089/scd.2010.0589

Waaijer, M. E., Parish, W. E., Strongitharm, B. H., van Heemst, D., Slagboom, P. E., de Craen, A. J., et al. (2012). The number of p16INK4a positive cells in human skin reflects biological age. *Aging Cell* 11, 722–725. doi: 10.1111/j.1474-9726.2012.00837.x

Wang, C., Jurk, D., Maddick, M., Nelson, G., Martin-Ruiz, C., and von Zglinicki, T. (2009). DNA damage response and cellular senescence in tissues of aging mice. *Aging Cell* 8, 311–323. doi: 10.1111/j.1474-9726.2009.00481.x

Webster, K. E., O'Bryan, M. K., Fletcher, S., Crewther, P. E., Aapola, U., Craig, J., et al. (2005). Meiotic and epigenetic defects in Dnmt3L-knockout mouse spermatogenesis. *Proc. Natl. Acad. Sci. U.S.A.* 102, 4068–4073. doi: 10.1073/pnas.0500702102

Willis-Martinez, D., Richards, H. W., Timchenko, N. A., and Medrano, E. E. (2010). Role of HDAC1 in senescence, aging, and cancer. *Exp. Gerontol.* 45, 279–285. doi: 10.1016/j.exger.2009.10.001

Xie, K., Ryan, D. P., Pearson, B. L., Henzel, K. S., Neff, F., Vidal, R. O., et al. (2018). Epigenetic alterations in longevity regulators, reduced life span, and exacerbated aging-related pathology in old father offspring mice. *Proc. Natl. Acad. Sci. U.S.A.* 115, E2348–E2357. doi: 10.1073/pnas.1707337115

Xu, M., Bradley, E. W., Weivoda, M. M., Hwang, S. M., Pirtskhalava, T., Decklever, T., et al. (2017). Transplanted senescent cells induce an osteoarthritis-like condition in mice. *J. Gerontol. A Biol. Sci. Med. Sci.* 72, 780–785. doi: 10.1093/gerona/glw154

Xu, M., Palmer, A. K., Ding, H., Weivoda, M. M., Pirtskhalava, T., White, T. A., et al. (2015). Targeting senescent cells enhances adipogenesis and metabolic function in old age. *eLife* 4:e12997. doi: 10.7554/eLife.12997

Xu, M., Pirtskhalava, T., Farr, J. N., Weigand, B. M., Palmer, A. K., Weivoda, M. M., et al. (2018). Senolytics improve physical function and increase lifespan in old age. *Nat. Med.* 24, 1246–1256. doi: 10.1038/s41591-018-0092-9

Zhang, W., and Xu, J. (2017). DNA methyltransferases and their roles in tumorigenesis. *Biomark. Res.* 5:1. doi: 10.1186/s40364-017-0081-z

Zhu, Y., Doornebal, E. J., Pirtskhalava, T., Giorgadze, N., Wentworth, M., Fuhrmann-Stroissnigg, H., et al. (2017). New agents that target senescent cells: the flavone, fisetin, and the BCL-XL inhibitors. A1331852 and A1155463. *Aging* 9, 955–963. doi: 10.18632/aging.101202

Zhu, Y., Tchkonia, T., Pirtskhalava, T., Gower, A. C., Ding, H., Giorgadze, N., et al. (2015). The Achilles' heel of senescent cells: from transcriptome to senolytic drugs. *Aging Cell* 14, 644–658. doi: 10.1111/acel.12344

Conflict of Interest: The authors declare that the research was conducted in the absence of any commercial or financial relationships that could be construed as a potential conflict of interest.

frontiers in Cell and Developmental Biology

ORIGINAL RESEARCH
published: 27 March 2020
doi: 10.3389/fcell.2020.00210

Intra-Tumoral Delivery of IL-27 Using Adeno-Associated Virus Stimulates Anti-tumor Immunity and Enhances the Efficacy of Immunotherapy

Aiyan Hu[1,2,3†], Miao Ding[1†], Jianmin Zhu[1,2,3], Jin-Qing Liu[2,3], Xueliang Pan[4], Kalpana Ghoshal[2,3] and Xue-Feng Bai[2,3]*

[1] Institute of Pediatric Translational Medicine, Shanghai Children's Medical Center, Shanghai Jiao Tong University School of Medicine, Shanghai, China, [2] Department of Pathology, The Ohio State University Wexner Medical Center, Columbus, OH, United States, [3] The Comprehensive Cancer Center, The Ohio State University Wexner Medical Center, Columbus, OH, United States, [4] Center for Biostatistics, The Ohio State University, Columbus, OH, United States

IL-27 is an anti-inflammatory cytokine that has been shown to have potent anti-tumor activity. We recently reported that systemic delivery of IL-27 using recombinant adeno-associated virus (rAAV) induced depletion of Tregs and significantly enhanced the efficacy of cancer immunotherapy in a variety of mouse tumor models. A potential caveat of systemic delivery of IL-27 using rAAV is that there is no practical method to terminate IL-27 production when its biological activity is no longer needed. Therefore, in this work, we tested if directly injecting AAV-IL-27 into tumors could lead to similar anti-tumor effect yet avoiding uncontrolled IL-27 production. We found that high levels of IL-27 was produced in tumors and released to peripheral blood after AAV-IL-27 intra-tumoral injection. AAV-IL-27 local therapy showed potent anti-tumor activity in mice bearing plasmacytoma J558 tumors and modest anti-tumor activity in mice bearing B16.F10 tumors. Intra-tumoral injection of AAV-IL-27 induced infiltration of immune effectors including $CD8^+$ T cells and NK cells into tumors, caused systemic reduction of Tregs and stimulated protective immunity. Mechanistically, we found that IL-27 induced T cell expression of CXCR3 in an IL-27R-dependent manner. Additionally, we found that AAV-IL-27 local therapy had significant synergy with anti-PD-1 or T cell adoptive transfer therapy. Importantly, in mice whose tumors were completely rejected, IL-27 serum levels were significantly reduced or diminished. Thus, intra-tumoral injection of AAV-IL-27 is a feasible approach that can be used alone and in combination with anti-PD-1 antibody or T cell adoptive transfer for the treatment of cancer.

Keywords: IL-27, recombinant adeno-associated virus, B16 melanoma, J558 plasmacytoma, Tregs, PD-1 blockade therapy, T cell adoptive transfer

OPEN ACCESS

Edited by:
Guangyong Peng,
Saint Louis University, United States

Reviewed by:
Fan Pan,
Johns Hopkins University, United States
Yukai He,
Augusta University, United States

****Correspondence:***
Xue-Feng Bai
Xue-Feng.Bai@osumc.edu

† These authors have contributed equally to this work

Specialty section:
This article was submitted to Cell Death and Survival, a section of the journal Frontiers in Cell and Developmental Biology

Received: *05 February 2020*
Accepted: *11 March 2020*
Published: *27 March 2020*

Citation:
Hu A, Ding M, Zhu J, Liu J-Q, Pan X, Ghoshal K and Bai X-F (2020) Intra-Tumoral Delivery of IL-27 Using Adeno-Associated Virus Stimulates Anti-tumor Immunity and Enhances the Efficacy of Immunotherapy. Front. Cell Dev. Biol. 8:210. doi: 10.3389/fcell.2020.00210

INTRODUCTION

Cancer immunotherapies based on blockade of immune checkpoints (Phan et al., 2003; Topalian et al., 2012; Hamid et al., 2013) have achieved significant success. However, a majority of patients with advanced cancer are not sensitive to this type of immunotherapy. Although factors responsible for cancer resistance to immunotherapy are not fully understood, the

following factors are considered important. *First*, lack of pre-existing T cell infiltration in the tumor microenvironment (TME) is considered to be the most important factor for anti-PD-1 resistance (Tumeh et al., 2014). *Second*, although not well-established in human cancer, regulatory T cells (Tregs) in the TME contribute to anti-PD-1 resistance in mouse models (Ngiow et al., 2015). Tregs expand in cancer patients and are enriched in cancer lesions (Curiel et al., 2004). *Third*, although not absolute, tumor expression of PD-L1 is another potentially important factor. In cancer types such as non-small cell lung carcinoma, bladder cancer and melanoma, PD-L1 immunohistochemistry has identified patients with a higher likelihood of treatment response (Topalian, 2017). Thus, developing novel strategies that can overcome these limitations is critical to enhancing the efficacy of current cancer immunotherapies.

Although the role of IL-27 in tumor immunity has been appreciated for more than a decade, developing IL-27 into a therapeutic to enhance tumor immunity has not been well achieved. Recombinant adeno-associated viral vectors (rAAV) are highly versatile gene delivery agents for gene therapy. The lack of immunogenicity and toxicity make rAAV the vector of choice for human clinical trials (Aalbers et al., 2011). Recently (Zhu et al., 2018), we have produced IL-27-expressing rAAV (AAV-IL-27) that can efficiently produce IL-27 in recipient mice and made the following novel observations. First, AAV-IL-27 significantly inhibits the growth of a broad-spectrum of tumor types in mice. Second, AAV-IL-27 treatment results in dramatic reduction of Tregs without causing autoimmunity. Third, AAV-IL-27 therapy shows strong synergy with PD-1 antibody in inhibiting tumor growth.

A potential caveat of systemic delivery of IL-27 using rAAV is that there is no practical method to terminate IL-27 production when its biological activity is no longer needed. In this study, we tested the approach of directly injecting AAV-IL-27 into tumors and determined its anti-tumor efficacy. We found that intra-tumoral administration of AAV–IL-27 induces infiltration of immune effectors including $CD8^+$ T cells and NK cells into tumors, causes systemic reduction of Tregs and stimulates protective immunity. Mechanistically, we found that AAV-IL-27 induces T cell expression of CXCR3 in an IL-27R-dependent manner. Additionally, we found that AAV-IL-27 local therapy has significant synergy with anti-PD-1 or T cell adoptive transfer therapy. Importantly, in mice whose tumors were completely rejected, IL-27 serum levels were significantly reduced or diminished.

MATERIALS AND METHODS

Mice and Tumor Cells

C57BL/6, BALB/c, and $IL27R^{-/-}$ mice were purchased from The Jackson Laboratory and were maintained in the animal facilities of the Ohio State University. $Stat1^{-/-}$ BALB/c mice were described before (Zhu et al., 2018). B16.F10 melanoma cells and plasmacytoma J558 cells were originally obtained from ATCC and used after a few passages *in vitro*. These cancer cells were maintained in RPMI1640 medium (Gibco) supplemented with 100 μg/ml penicillin, 100 μg/ml streptomycin, and 10% FBS (Gibco).

Treatment of Mice With Tumors Using AAV

Production of rAAV-IL-27 has been described previously (Zhu et al., 2018). To establish tumors in mice, indicated numbers of cancer cells were injected into each C57BL6 or BALB/c mouse s.c. in 100 μl of PBS. AAV-IL-27 or AAV-ctrl viruses were diluted in PBS containing the indicated quantity of AAV virus, and were injected into the established tumors in a total volume of 50 μl. The length and width of tumors were measured using a digital caliper every 2 or 3 days. The tumor volume was calculated according to the formula volume (V) = $ab^2/2$, where a represents length and b represents width. In some experiments, starting on the day of AAV treatment, mice were also treated with 250 μg/mouse of anti-PD-1 (RMP1-14) or an isotype-matched control antibody (anti-rat IgG2a; 2A3) i.p. at 3-day intervals for up to 4 times. Anti-PD-1 antibody and isotype-matched control antibody were purchased from BioXcell.

Flow Cytometry

FITC-, PE-, PE-CY7, APC-, APC-CY7 or Percp-labeled antibodies to CD3 (145-2C11), CD45 (30-F11), CD4 (GK1.5), CD8α (53-6.7), CD11b (M1/70), CD11c (N418), B220 (RA36B2), CD25 (PC61), NK1.1 (PK136), PD-L1 (MIH5), FoxP3 (NRRF-30), IFN-γ (XMG1.2), TNF-α (MAb11), CD49 (DX5), and CXCR3 (CXCR3-173) and isotype-matched control antibodies were purchased from Biolegend (antibodies to CD3, CD4, CD8, CD45,CD11b, CD11c, B220, CD25, PD-L1, FoxP3, IFN-γ, TNF-α, CD49, CXCR3, and control antibodies) or BD Biosciences (antibodies to NK1.1 and control antibodies). For identification of cellular phenotypes, disassociated cells from tumors or spleens were suspended in PBS containing 1% bovine serum albumin and incubated with the antibodies on ice for 30 min. Cells were fixed in 1% paraformaldehyde in PBS after washing. For intracellular cytokine staining, cells were stimulated in culture medium for 4 h in the presence of Leukocyte Activation Cocktail, with BD Golgi^{Stop} (1: 500; BD Biosciences). Viable cells were then fixed and permeabilized with transcription staining buffer set (eBioscience) and stained with respective antibodies to cytokines. FoxP3 staining was performed according to manufacturer's protocol (eBioscience). Stained cells were analyzed on a FACSCalibur or FACS Canton flow cytometer, and data were analyzed using the flowjo software.

ELISA

ELISA kit for the detection of IL-27 was purchased from eBiosciences. Standard procedures were followed to detect releases of cytokines in supernatants of cultured cells in a variety of settings or blood of AAV-treated mice.

Real Time RT-PCR

Quantitative real-time PCR was performed using previously determined conditions (Liu et al., 2013). The relative amount of mRNA was calculated by plotting the Ct (cycle number) and

the average relative expression for each group was determined using the comparative method ($2^{-\Delta\ \Delta\ Ct}$). The following primers were used for amplifying IL-27 and β-actin genes: IL-27: 5′-TCTGAGGTTCAGGGCTATGT-3′(forward) and 5′- TCAGGGAAACATTGGGAAGATG-3′(reverse); β-actin: 5′- GAGACCTTCAACACCCCAGC-3′ (forward) and 5′-ATGTCACGCACGATTTCCC-3′ (reverse).

Cytotoxicity Assay

A flow cytometry-based cytotoxicity assay was used to measure *in vitro* cellular cytotoxicity of tumor-infiltrating lymphocytes (TILs) to J558 target cells as previously described (Liu et al., 2013).

Generation of Tumor-Infiltrating Lymphocytes and Adoptive Transfer

Tumor infiltrating $CD8^+$ T cells were isolated from established J558 tumors. Briefly, 5×10^6 J558 cells diluted in PBS were injected into BALB/c mice s.c. in a volume of 100 ul. When tumors reached 1 cm in length, mice were sacrificed and mouse tumors were dissected, ground to single cell suspensions. $CD8^+$ TILs were isolated by using CD8 MicroBeads (MACS) and cultured in RPMI 1640 (Gibico) with 10% fetal calf serum, 2-mercaptoethanol(invitrogen), HEPES(invitrogen), penicillin/streptomycin (invitrogen), recombinant human IL-2 (50IU/ml, Peprotech), and 20 ng/ml anti-CD3 antibody (2C11, Biolegend) in the presence of 2×10^6/ml irradiated syngeneic splenocytes (2000 rad). TIL cultures were split when confluent and reseeded at $2–3 \times 10^5$/ml in culture medium. To treat mice with established J558 tumors, 5×10^6 *in vitro*-cultured TIL $CD8^+$ cells were injected into each tumor-bearing mice i.v.

Statistics

One way ANOVA, student's *t* test and log-rank tests were used for statistical analyses. The GraphPad Prism software was used for all the analyses.

RESULTS

Intra-Tumoral Administration of AAV-IL-27 Inhibits Tumor Growth and Stimulates Anti-tumor Immunity

To determine if AAV is a suitable vector for tumor local delivery of therapeutics, we generated rAAV vectors that express GFP (AAV–GFP) and tested if AAV-GFP could infect B16 melanoma cells. After incubation with AAV-GFP for 48 h, more than 60% B16 melanoma cells expressed GFP (**Figures 1A,B**). Moreover, injection of AAV-GFP into established B16 tumors resulted in the GFP expression at the injection sites (**Supplementary Figure S1**). Thus, it appears that B16 melanoma cells are sensitive to AAV infection *in vitro* and *in vivo*. Next, we tested if IL-27 expressing rAAV (AAV-IL-27) infection of B16 cells could lead to IL-27 production. As shown in **Figure 1C**, AAV-IL-27 infected B16 cells dose-dependently, as quantified for IL-27 mRNA by qPCR. AAV-IL-27 infection of B16 cells also resulted in release of IL-27 protein in the culture supernatant, as determined by ELISA after 48 h incubation (**Figure 1D**). To determine if AAV-IL-27 intra-tumoral delivery leads to IL-27 production *in vivo*, we directly injected AAV-IL-27 into established B16 tumors in C57BL/6 mice and examined IL-27 in blood samples at different times after AAV-IL-27 injection. As shown in **Figure 1E**, AAV–IL-27 intra-tumor administration resulted in IL-27 production in tumors. We could also detect sustained IL-27 production in blood after AAV-IL-27 intra-tumoral injection (**Figure 1F**). Similarly, we found that AAV-IL-27 could also infect mouse plasmacytoma J558 cells *in vitro* (**Figure 1G**), which resulted in IL-27 protein production during *in vitro* culture (**Figure 1H**). Injection of AAV-IL-27 into established J558 tumors in mice also resulted in IL-27 production in tumors (**Figure 1I**) and blood (**Figure 1J**). Thus, intra-tumoral injection of AAV-IL-27 resulted in IL-27 production in tumors, which was subsequently released to blood.

To test if intra-tumoral delivery of AAV-IL-27 inhibits tumor growth, we injected AAV–IL-27 into B16 melanoma tumors in mice at various doses. At lower doses, AAV-IL-27 did not inhibit B16 tumor growth significantly (**Figures 2A,B**), while at a higher doses (**Figure 2C**), intra-tumoral injection of AAV-IL-27 significantly inhibited the growth of B16 tumors. Similarly, at a lower dose, injection of AAV-IL-27 into established J558 tumors resulted in a slight inhibition of tumor growth (**Figure 2D**), while at a high dose, mice had nearly complete tumor rejection (**Figure 2E**) with long term tumor free survival (**Figure 2F**). We examined blood IL-27 levels in two typical mice whose tumors were not rejected or completely rejected, and found that tumor rejection also resulted in IL-27 reduction (**Figure 2G**). Moreover, we found mice that rejected J558 tumors were completely resistant to J558 tumor cell re-challenging (**Figure 2H**). Thus, AAV–IL-27 intra-tumoral delivery is not only an effective treatment in experimental mouse tumor models, it also induces protective immunity.

Intra-Tumoral Administration of AAV-IL-27 Enhances Accumulation of T and NK Cells in Tumors and Causes Systemic Reduction of Tregs

To determine if intra-tumoral administration of AAV–IL-27 altered the tumor immune microenvironment, we examined the cellular components of tumor-infiltrating leukocytes in tumors from AAV–IL-27 or AAV-ctrl virus–treated mice using flow cytometry. As shown in **Supplementary Figure S2A** and **Figure 3A**, AAV–IL-27 intra-tumoral treatment significantly increased the percentage of $CD45^+$ leukocytes and $CD3^+$ T cells in B16 tumors. AAV–IL-27 treatment also enhanced tumor infiltration of $CD3^-NK1.1^+$ NK cells. We found that AAV–IL-27 treatment slightly decreased $CD4^+$ T cells and significantly increased the infiltration of $CD8^+$ T cells into B16 tumors. Moreover, we found that T cells, particularly $CD8^+$ T cells in B16 tumors receiving AAV-IL-27 treatment produced more IFN-γ (**Figure 3B**). Similarly, we found that injection of AAV-IL-27 into established J558 tumors resulted in more

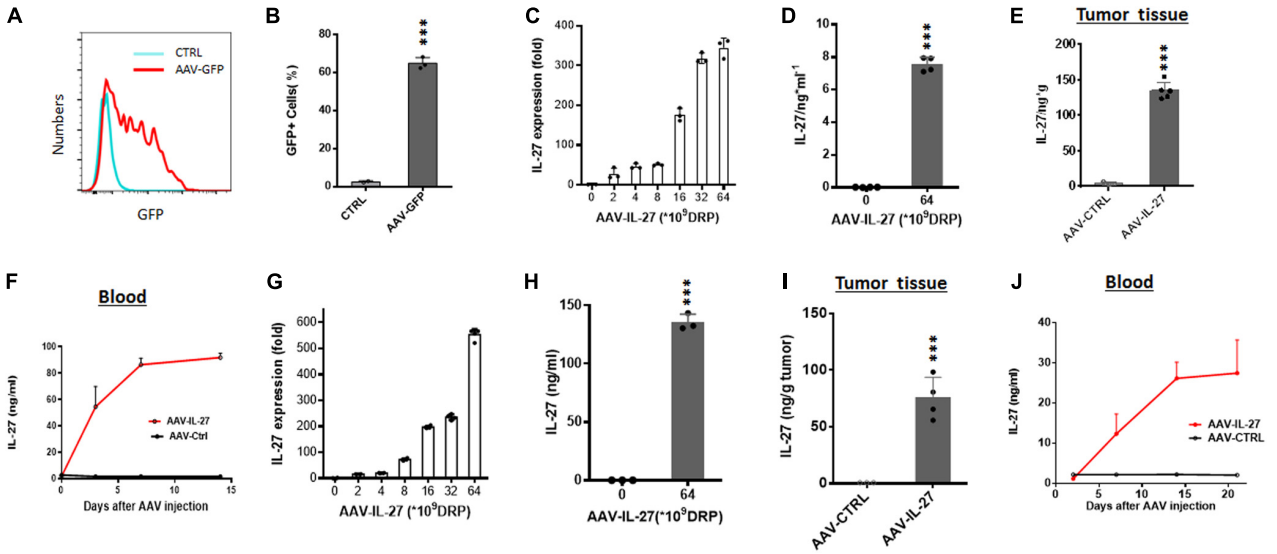

FIGURE 1 | AAV can efficiently infect tumor cells *in vitro* and *in vivo*. **(A,B)** B16.F10 melanoma cells were incubated with AAV-GFP at a concentration of 5×10^9 DRP (DNase resistant particles) for 48 h and GFP-positive melanoma cells were analyzed and quantified by flow cytometry. **(C,D)** B16.F10 melanoma cells were infected with AAV-IL-27 at various concentrations, and the expression of IL-27 mRNA **(C)** in melanoma cells and IL-27 protein **(D)** in the cell culture supernatants were quantified by qPCR or ELISA. **(E,F)** AAV-IL-27 was directly injected into established B16 melanoma tumors in C57BL/6 mice and the blood samples were collected at different time points. Mice were sacrificed 2 weeks after AAV injection and the concentrations of IL-27 in tumor tissues **(E)** and blood **(F)** were quantified by ELISA. **(G,H)** J558 plasmacytoma cells were infected with AAV-IL-27 at various concentrations, and the expression of IL-27 mRNA **(G)** in J558 cells and IL-27 protein **(H)** in the cell culture supernatants were quantified by qPCR or ELISA. **(I–J)** AAV-IL-27 was directly injected into established J558 tumors in BALB/c mice and the blood samples were collected at different time points. Mice were sacrificed 3 weeks after AAV injection and the concentrations of IL-27 in tumor tissues **(I)** and blood **(J)** were quantified by ELISA. Data are expressed as Mean ± SD of 3-5 samples in each group/per time point. $^*P < 0.05$, $^{**}P < 0.01$, $^{***}P < 0.001$ by one-way ANOVA or student's *t* test.

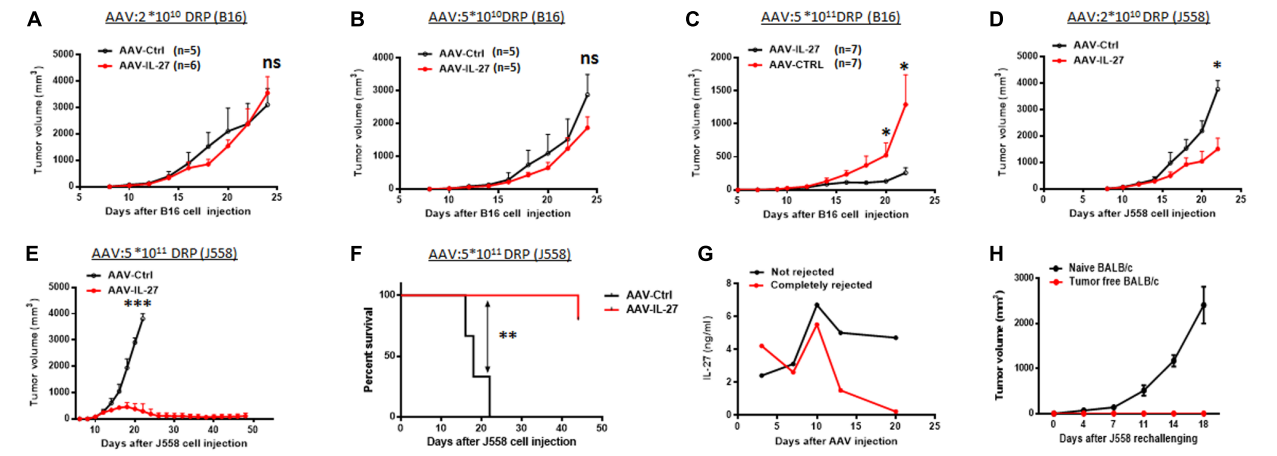

FIGURE 2 | Intra-tumoral injection of AAV-IL-27 inhibits tumor growth and stimulates protective immunity in mice. **(A–C)** B16.F10 cells (2×10^5 cells) were injected into C57BL/6 mice s.c. 7 days later, AAV-IL-27 or AAV-ctrl virus were directly injected into the established tumors at the indicated dose. **(D–F)** J558 cells (5×10^6 cells) were injected into BALB/c mice s.c. Five days later, mice were treated with AAV-IL-27 or AAV-ctrl virus intra-tumorally at the indicated doses. Tumor volume changes **(A–E)** and mice survival **(F)** were recorded. **(G)** Serum IL-27 concentrations in mice with J558 tumors or mice whose tumors were rejected. **(H)** J558 cells were injected into mice whose tumors were rejected after AAV-IL-27 therapy or naïve BALB/c mice, and tumor growth was compared. Data shown represent 2–3 experiments with similar results. ns: no significant difference. $^*P < 0.05$, $^{**}P < 0.01$, $^{***}P < 0.001$by One-way ANOVA or Log-rank test.

$CD45^+$ leukocyte infiltration. Among the $CD45^+$ population, $CD3^+$, $CD4^+$, $CD8^+$ T cells, and $CD3^-CD49b^+$ NK cells had increased (**Supplementary Figure S2B** and **Figure 3C**), and tumor infiltrating $CD4^+$ and $CD8^{++}$T cells produced more IFN-γ in AAV-IL-27 treated tumors (**Supplementary Figure S3A** and **Figure 3D**).

We previously showed that i.m. injection of AAV-IL-27 leads to systemic IL-27 production, which caused depletion

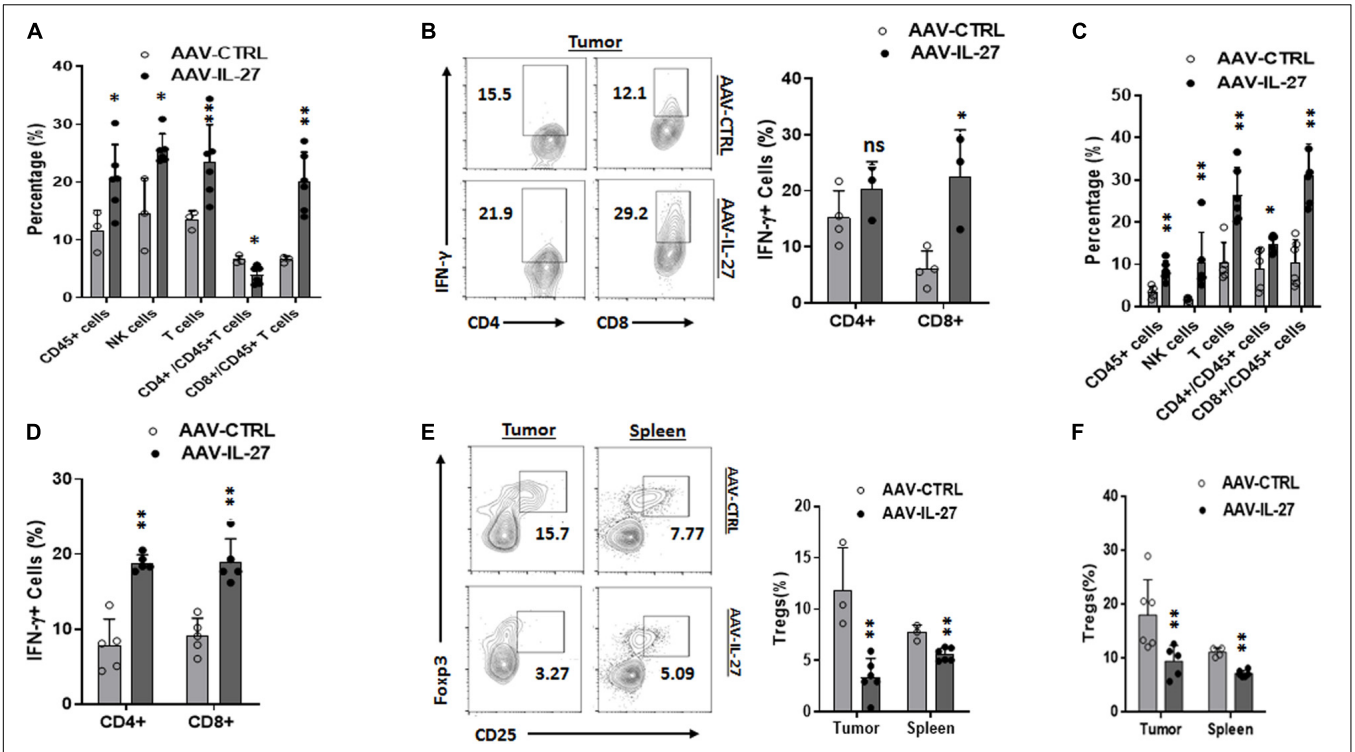

FIGURE 3 | Intra-tumoral injection of AAV–IL-27 alters tumor immune microenvironment. **(A,B)** B16.F10 cells (2×10^5) were injected into C57BL/6 mice s.c. Seven days later, mice were treated with AAV-IL-27 or AAV-ctrl virus intra-tumorally at a dose of 2×10^{11} DRP/mouse. Mice were sacrificed on day 21, and populations of tumor infiltrating lymphocytes **(A)** and IFN-γ production by tumor infiltrating T cells **(B)** were analyzed by flow cytometry. **(C,D)** J558 cells (5×10^6) were injected into BALB/c mice s.c. Seven days later, mice were treated with AAV-IL-27 or AAV-ctrl virus intra-tumorally at a dose of 5×10^{10} DRP/mouse, and mice were sacrificed on day 21, and populations of tumor infiltrating lymphocytes **(C)** and IFN-γ production by tumor infiltrating T cells **(D)** were analyzed by flow cytometry. Data are expressed as Mean ± SD and represent 3–5 experiments with similar results. ns: no significant difference; $^*P < 0.05$, $^{**}P < 0.01$, $^{***}P < 0.001$ by One-way ANOVA. **(E,F)** $CD4^+CD25^+FoxP3^+$ Tregs in tumors and spleens in mice bearing B16 **(E)** or J558 tumors **(F)**. B16 and J558 tumor establishment and treatment conditions were the same as described above **(A–D)**. Mononuclear cells from tumors and spleens were analyzed by flow cytometry. $^{**}P < 0.01$ by One-way ANOVA.

of Tregs in peripheral lymphoid organs and tumors (Zhu et al., 2018). To determine if intra-tumoral injection of AAV-IL-27 depletes Tregs, we used flow cytometry to examine Tregs in spleens and tumors from treated mice. As shown in **Figure 3E**, intra-tumoral injection of AAV-IL-27 resulted in reduction of Tregs both in tumors and spleens. Similarly, we also found that AAV-IL-27 injection into established J558 tumors resulted in reduction of Tregs in both tumors and spleens (**Supplementary Figure S3B** and **Figure 3F**). Thus, intra-tumoral delivery of AAV–IL-27 induces systemic reduction of Tregs, and increases tumor infiltration of T and NK cells and enhances their effector functions.

AAV-IL-27 Treatment Induces T Cell Expression of CXCR3

Since AAV-IL-27 treated tumors had increased infiltration of T cells, we examined whether increased recruitment of T cells into tumors was a mechanism. CXCR3, a chemokine receptor for the interferon-inducible chemokines CXCL9, CXCL10, and CXCL11, is known to play key roles in T cell trafficking to tumors (Franciszkiewicz et al., 2012). We therefore examined if AAV-IL-27 intra-tumoral injection induced CXCR3 in T cells. As shown in **Figure 4A**, we detected significant levels of CXCR3 in $CD4^+$and especially $CD8^+$ T cells in spleens of AAV-ctrl treated mice. AAV-IL-27 treatment significantly increased the expression of CXCR3 in both spleen $CD4^+$ and $CD8^+$ T cells. In tumors, IL-27-induced CXCR3 expression was only found on T cells, especially $CD8^+$ T cells, but not on other leukocytes (**Figure 4B**). Similarly, intra-tumoral injection of AAV-IL-27 into established J558 tumors resulted in induction of CXCR3 spleen and tumor T cells (**Supplementary Figure S4** and **Figure 4C**). To determine if induction of CXCR3 is IL-27-specific, we treated WT and IL-$27R^{-/-}$ mice with AAV-IL-27 or AAV-ctrl virus, and found that AAV-IL-27 only induced CXCR3 in $CD4^+$ and $CD8^+$ T cells in WT, but not IL-$27R^{-/-}$ mice (**Supplementary Figure S5A** and **Figure 4D**). Interestingly, we found that AAV-IL-27-induced CXCR3 expression in T cells was independent of Stat1, because AAV-IL-27-treatment could induce CXCR3 expression in T cells from $Stat1^{-/-}$ mice (**Supplementary Figure S5B** and **Figure 4E**). Finally, we found that co-culture of tumor-antigen P1A-specific P1CTL cells (Bai et al., 2003) with IL-27 *in vitro* resulted in significant upregulation of CXCR3 in P1CTL cells (**Figure 4F**), suggesting that IL-27 can directly induce CXCR3 in tumor-specific T cells.

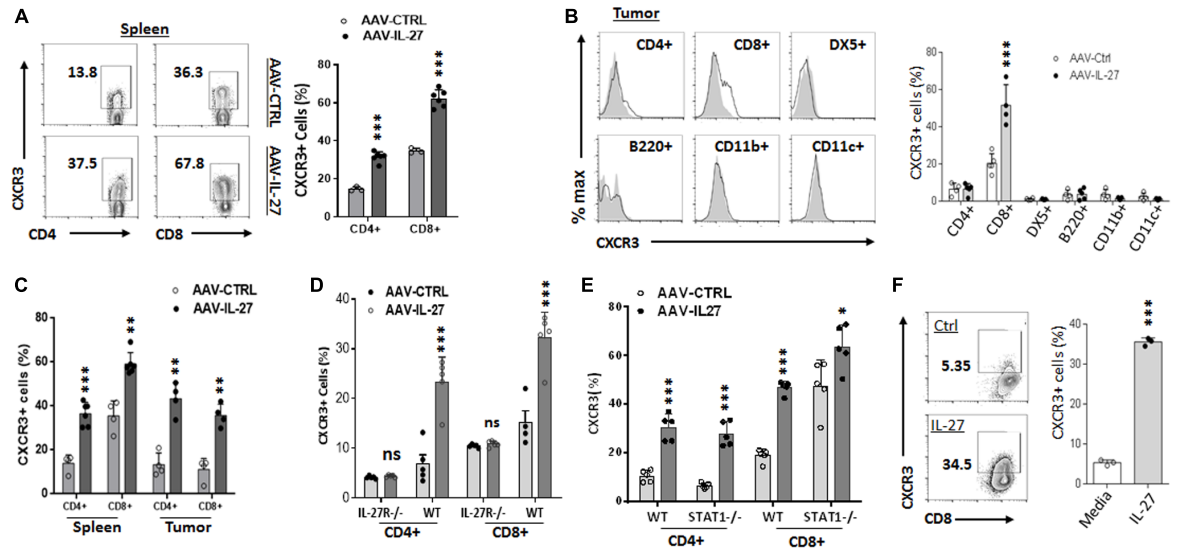

FIGURE 4 | AAV–IL-27 therapy induces CXCR3 expression in T cells. **(A,B)** C57BL6 mice were injected with B16.F10 tumor cells (2×10^5/mouse) s.c. 7 days later, mice were treated with AAV–IL-27 or AAV-ctrl virus intra-tumorally at a dose of 2×10^{11} DRP/mouse. Three weeks after AAV injection, mice were sacrificed and their spleens **(A)** and tumors **(B)** were analyzed for the expression of CXCR3 in T lymphocytes and other leukocytes by flow cytometry. **(C)** J558 cells (5×10^6) were injected into BALB/c mice s.c. Five days later, mice were treated with AAV-IL-27 or AAV-ctrl virus intra-tumorally at a dose of 1×10^{11} DRP/mouse. Three weeks after viral injection, mice were sacrificed and their spleens and tumors were analyzed for the expression of CXCR3 in T lymphocytes by flow cytometry. **(D)** C57BL6 and IL-27R$^{-/-}$ mice were injected with B16.F10 tumor cells (2×10^5/mouse) s.c. Seven days later, mice were treated with AAV–IL-27 or AAV-ctrl virus intra-tumorally at a dose of 2×10^{11} DRP/mouse. 21 days after viral injection, mice were sacrificed and their spleens were analyzed for T cell expression of CXCR3 by flow cytometry. **(E)** AAV-IL-27 or AAV-ctrl virus (2×10^{11} DRP/mouse) was injected into Stat1$^{-/-}$ or control BALB/c mice i.m. Three weeks after AAV injection, T cell expression of CXCR3 in spleens was analyzed by flow cytometry. **(F)** Spleen cells from P1CTL Tg mice were activated with P1A peptide (0.1 μg/ml) for 5 days *in vitro* in the presence or absence of IL-27 (50 ng/ml), and CXCR3 expression on P1CTL cells were analyzed by flow cytometry on day 5. Ns: no significant difference. ***$P < 0.001$ by One-way ANOVA.

AAV–IL-27 Intra-Tumoral Delivery Overcomes Anti–PD-1 Resistance

We previously found that i.m. injection of AAV-IL-27 could induce PD-L1 expression in T cells, which unexpectedly overcome tumor resistance to anti-PD-1 therapy (Zhu et al., 2018). To test if intra-tumoral delivery of AAV-IL-27 induced PD-L1 in T cells, we analyzed PD-L1 expression in T cells in treated mice using flow cytometry. We found that CD4$^+$ and CD8$^+$ T cells in spleens and tumors of mice receiving AAV–IL-27 intra-tumoral treatment indeed upregulated PD-L1 expression (**Figures 5A,B**). To determine if IL-27–induced PD-L1 expression in T cells prevented the effectiveness of IL-27 local therapy, C57BL6 mice with established B16 tumors received the following treatments: AAV-ctrl virus + control mAb; AAV-ctrl virus + anti–PD-1; AAV–IL-27 virus + control mAb or AAV–IL-27 virus + anti–PD-1. Antibodies were injected into mice at a dose of 250 μg/mouse i.p. at 3-day intervals starting on day 10 (**Figure 5C**). As shown in **Figure 5D**, we found that B16 tumors grew progressively in mice treated with AAV-ctrl + ctrl Ab and AAV-ctrl + anti–PD-1; while in AAV–IL-27 + ctrl Ab–treated mice, slight inhibition of tumor growth was observed. AAV–IL-27 + anti–PD-1–treatment most significantly inhibited tumor growth, which also resulted in significantly reduced tumor weight at the end of the experiment (**Figure 5E**). We used a similar regimen to treat mice with established J558 tumors. A suboptimal dose of AAV (2×10^{10}DRP) was used since high dose AAV-IL-27 could induced complete tumor rejection. As shown in **Figure 5F**, mice treated with AAV–IL-27 + control mAb showed reduced tumor growth compared with mice treated with AAV-ctrl virus + control mAb or AAV-ctrl virus + anti–PD-1. Most significant inhibition of tumor growth was observed in mice treated with AAV–IL-27 + anti–PD-1. Overall, AAV–IL-27/anti–PD-1 combination therapy resulted in tumor-free survival of 70% of mice (**Figure 5G**). We collected serum from some mice receiving combined treatment on days 18 and 39, during which time their tumors reached peak followed by tumor volume reduction. As shown in **Figure 5H**, significant reduction of IL-27 in blood was observed when the tumor volume decreased or disappeared. Thus, in the two tumor models that are resistant to anti–PD-1 therapy, we found that AAV-IL-27 local therapy and anti–PD-1 combination could induce complete tumor rejection or better tumor growth inhibition when a low dose of AAV-IL-27 was used.

AAV-IL-27 Intra-Tumoral Administration Significantly Enhances Anti-tumor Efficacy of Tumor Infiltrating T Cells

Adoptive transfer of tumor infiltrating T cells (TILs) is an effective therapy for cancer patients (Rosenberg and Restifo, 2015). Our previous research (Liu et al., 2013) suggests that IL-27 significantly enhances the survival of tumor antigen specific

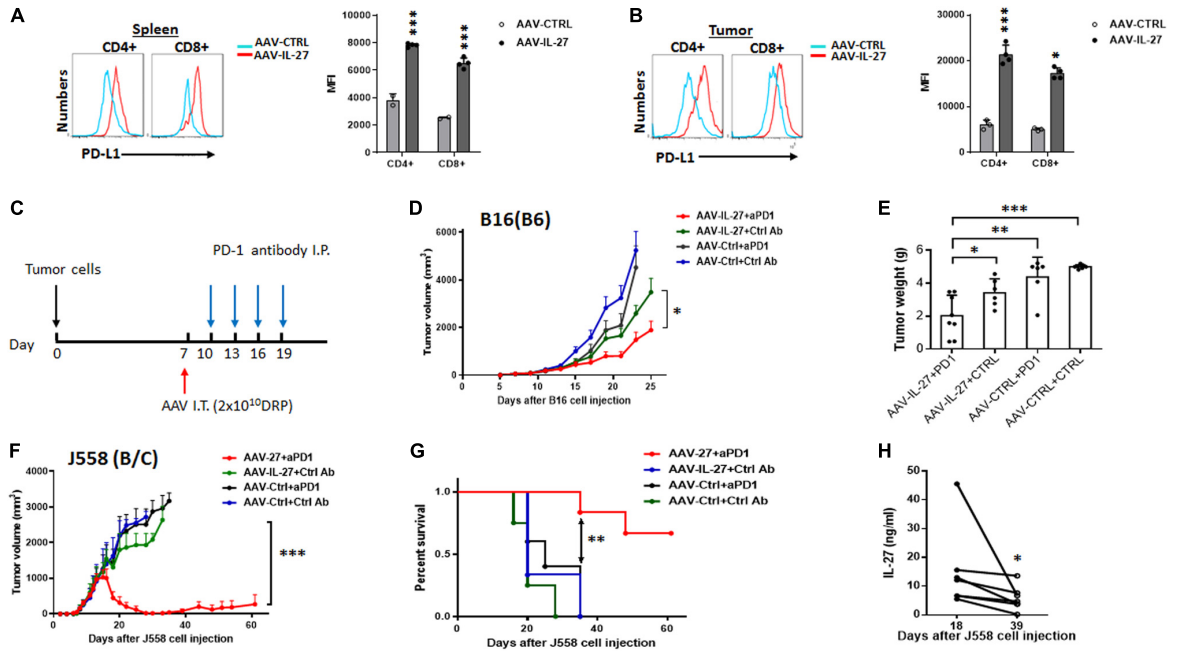

FIGURE 5 | Intra-tumoral injection of AAV–IL-27 induces PD-L1 expression in T cells and enhances tumor sensitivity to anti-PD-1 therapy. **(A,B)** Flow cytometry analysis of $CD4^+$ and $CD8^+$ T cells in spleen **(A)** and tumors **(B)** from C57BL6 mice that were treated intra-tumorally with AAV-IL-27 or AAV-ctrl virus. Average mean fluorescence intensity (MFI) of PD-L1 expression in T cells from each group of mice was also shown. **(C)** Schematic diagram of intra-tumoral AAV-IL-27 and anti-PD-1 combination therapy. Mice are injected with tumor cells s.c. Seven days later, mice with established tumors are treated with AAV–IL-27 or AAV-ctrl virus intra-tumorally. Starting on day 10, mice are also treated with 250 μg/mouse of anti–PD-1 (RMP1-14) or an isotype-matched control antibody (2A3) i.p. at 3-day intervals for up to 4 times. **(D,E)** Synergy of anti-PD-1 and intra-tumoral AAV-IL-27 in inhibiting the growth of B16.F10 melanoma. AAV–IL-27 or AAV-ctrl virus intra-tumoral treatment were at a dose of 2×10^{11} DRP/mouse. Tumor volume changes **(D)** and mice tumor weight **(E)** were recorded. **(F,G)** Synergy of anti-PD-1 and intra-tumoral AAV-IL-27 in inhibiting the growth of J558 tumors. AAV-IL-27 or AAV-ctrl virus intra-tumoral treatments were at a dose of 5×10^{10} DRP/mouse. Tumor volume changes **(F)** and mice survival **(G)** were recorded. Data were expressed as Mean ± SD of at least five mice in each group. Data shown represent 2–3 experiments with similar results. Ns: no significant difference. $^*P < 0.05$, $^{**}P < 0.01$, $^{***}P < 0.001$ by One-way ANOVA or Log-rank test. **(H)** IL-27 concentration in peripheral blood from BALB/c mice receiving intra-tumoral AAV-IL-27 and anti-PD-1 combination therapy were examined.

$CD8^+$ T cells *in vivo*, which indicates that AAV-IL-27 intra-tumoral administration could also be used as an adjuvant for T cell adoptive transfer therapy for cancer. We first generated tumor infiltrating lymphocytes (TILs) from established J558 tumors by MACS beads-based purification of $CD8^+$ T cells followed by *in vitro* expansion. As shown in **Figure 6A**, TILs generated this way were of >97% purity. The TIL $CD8^+$ T cells showed strong cytotoxicity to J558 tumor cells (**Figure 6B**), and produced TNF-α and IFN-γ upon co-culture with J558 tumor cells (**Figure 6C**). To determine if AAV-IL-27 intra-tumoral delivery enhances T cell adoptive transfer therapy, we first injected J558 cells into BALB/c mice to establish tumors and treatments were carried out as outlined in **Figure 6D**. AAV-IL-27 or AAV-ctrl virus was injected into tumors on day 5 when the tumors were established. On day 7, TIL $CD8^+$ T cells were injected i.v. into mice treated with AAV-IL-27 or AAV-ctrl. As shown in **Figure 6E**, mice treated with AAV–IL-27 + TIL $CD8^+$ T cells showed most significant tumor growth inhibition compared with mice treated with AAV-ctrl virus + TIL cells or AAV-IL-27 or AAV-ctrl alone. Prolonged survival of mice (**Figure 6F**) were observed in AAV-IL-27/TIL $CD8^+$ T cell combination–treated mice. Thus, AAV-IL-27 intra-tumoral delivery showed significant synergy with T cell adoptive transfer therapy.

DISCUSSION

A critical problem for systemic delivery of cytokines for cancer therapy is toxicity (Waldmann, 2018). For instance, IL-2 is the first effective immunotherapy of human cancer but it is also known to be very toxic (Rosenberg, 2014). IL-12 exhibits potent anti-tumor activity (Colombo and Trinchieri, 2002) via promoting Th1/Tc1 response (Colombo and Trinchieri, 2002; Del Vecchio et al., 2007) and enhancing T cell trafficking to tumors through induction of chemokines (Hu et al., 2018). However, systemically delivered IL-12 causes fatal toxicity (Car et al., 1995; Ryffel, 1997). To avoid this problem, researchers have designed various strategies (Kerkar et al., 2010; Zhang et al., 2015; Zhao et al., 2019) to target IL-12 to tumors. However, unless IL-12 is confined to tumor site, systemic toxicity appears to be unavoidable (Momin et al., 2019). As an IL-12 family of cytokine, IL-27 shares some similarities with IL-12. For instance, IL-27 also promotes Th1/Tc1 responses and induces T cell infiltration into tumors via a variety of mechanisms (Yoshimoto et al., 2015; Zhu et al., 2018). However, unlike IL-12, IL-27 is considered to be a cytokine with low toxicity (Yoshimoto et al., 2015). Indeed, we recently reported (Zhu et al., 2018) that systemic delivery of IL-27 using rAAV could inhibit tumor growth and significantly

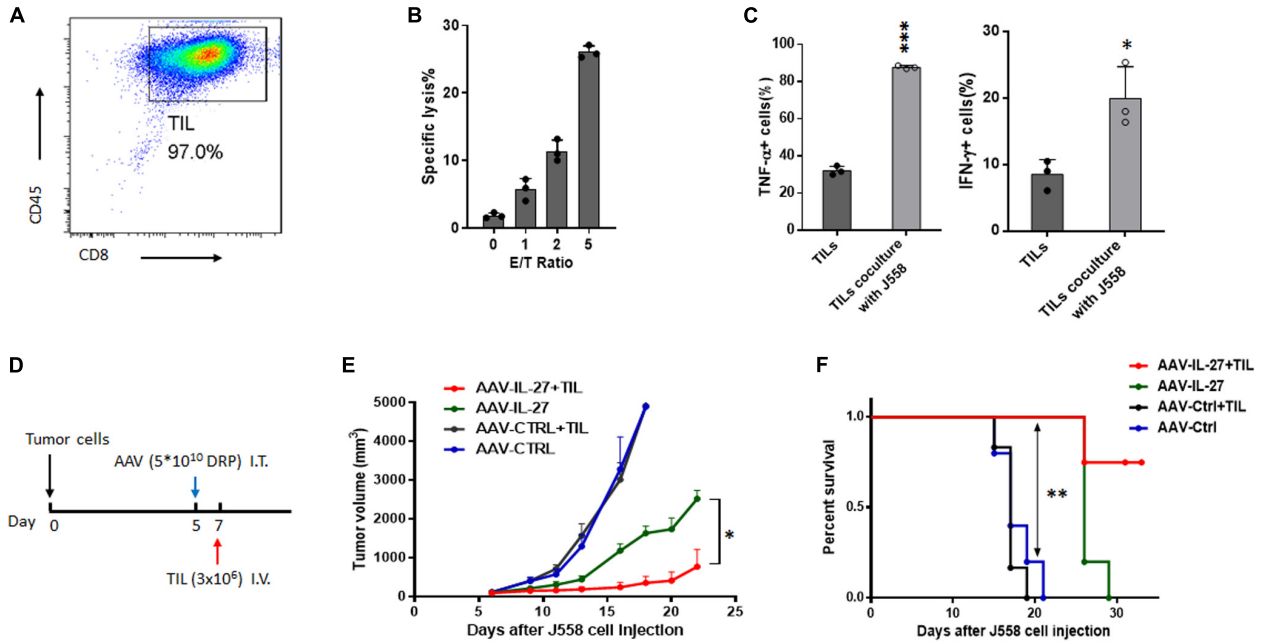

FIGURE 6 | Intra-tumoral injection of AAV–IL-27 enhances tumor-infiltrating T lymphocyte therapy. **(A)** Flow cytometry analysis of tumor-infiltrating lymphomcyte (TILs) isolated and expanded from J558 tumors grown in BALB/C mice. **(B)** TIL effector functions were quantify by flow cytometry-based cytotoxicity assay. **(C)** TILs from J558 tumors produced IFN-γ and TNF-α upon co-culture with J558 tumor cells *in vitro*. **(D)** Schematic diagram of intra-tumoral AAV-IL-27 and adoptive transfer of TILs. Mice were injected with J558 tumor cells s.c. Five days later, tumor-bearing mice were treated with AAV–IL-27 or AAV-ctrl virus intra-tumorally followed by injection of TIL T cells i.v. **(E,F)** Tumor growth **(E)** and survival of mice **(F)** bearing J558 tumors treated with intra-tumoral AAV-IL-27 and TILs. Data shown represent three independent experiments with $n = 5$ mice per group. $^{*}P < 0.05$, $^{**}P < 0.01$ by One-way ANOVA or Log-rank test.

enhance cancer immunotherapy in a variety of mouse tumor models without causing significant toxicity. Although our study (Zhu et al., 2018) suggests that high concentrations of IL-27 in blood were very well tolerized by mice, a potential caveat of systemic delivery of IL-27 using rAAV is that there is no practical method to terminate IL-27 production when its biological activity is no longer needed. To avoid this problem, we tested direct injection of AAV-IL-27 into tumors in this study. We found that in mice receiving AAV-IL-27 intra-tumoral injection, IL-27 was produced in tumors and released to blood. However, in mice whose tumors were completely rejected, IL-27 serum levels were significantly reduced or diminished (**Figures 2G**, 5H). These results suggest that intra-tumoral injection of AAV-IL-27 could (1) achieve similar efficacy as AAV-IL-27 systemic administration and (2) avoid the unwanted problem of continued high level IL-27 production. Thus, intra-tumoral delivery of AAV-IL-27 appears to be a feasible approach for enhancing anti-tumor immunity.

In this study, we found that intra-tumoral injection of AAV-IL-27 enhanced NK cells and especially $CD8^+$ T cell infiltration in tumors. Moreover, we found that intra-tumoral AAV-IL-27 injection caused reduction of Tregs both in peripheral lymphoid organs and tumors. In a previous study (Zhu et al., 2018), we reported that systemic delivery of AAV-IL-27 led to depletion of Tregs in peripheral lymphoid organs and tumors via down-regulation of IL-2 signaling. Since intra-tumoral injection of AAV-IL-27 results in IL-27 release to blood, we believe the same mechanism applies here. We also observed that in mice that rejected J558 tumors, protective immunity was established (**Figure 2H**). This result suggests that intra-tumoral injection of AAV-IL-27 induces long term anti-tumor immunity in protected mice. We believe a number of mechanisms, including Treg reduction-induced additional T cell priming and IL-27 induced T memory stem cells (Liu et al., 2017), are responsible for induction of T cell memory.

Increased expression of CXCR3 in peripheral T cells suggests that increased T cell trafficking of T cells into tumors is the major mechanism for enhanced T cell infiltration into tumors after AAV-IL-27 intra-tumoral injection. In this case, $CXCR3^+$ tumor-specific T cells accumulate into tumors through interaction with CXCR3 ligands (CXCL9, CXCL10, and CXCL11) (Franciszkiewicz et al., 2012). Previously, IL-27 was shown to induce CXCR3 in Tregs (Hall et al., 2012). In this study, we show that IL-27 directly induces CXCR3 expression in conventional T cells including tumor antigen specific $CD8^+$ T cells (**Figure 4**). Since IL-27 activates the Stat1-T-bet axis (Hibbert et al., 2003; Kamiya et al., 2004), and T-bet directly transactivates CXCR3 (Beima et al., 2006; Lewis et al., 2007), we postulated that IL-27 directly induces T cell expression of CXCR3 via IL-27R-Stat1-T-bet axis. Unexpectedly, we found that in the absence of Stat1, IL-27 could still induce CXCR3 in both $CD4^+$ and $CD8^+$ T cells (**Figure 4E**). These results suggest that IL-27 can also signal through transcription factors other than Stat1 in T cells to induce CXCR3. Regardless of the mechanisms, our study

suggests that intra-tumoral injection of AAV-IL-27 enhances CXCR3-mediated T cell infiltration and directly enhances T cell effector functions.

IL-27 is known to induce T cell expression of PD-L1 (Hirahara et al., 2012), and PD-L1-PD-1 interaction among T cells may inhibit T cell effector functions thereby limiting IL-27-mediated anti-tumor efficacy. However, our recent study (Zhu et al., 2018) suggests that this same activity renders tumors more susceptible to anti-PD-1 therapy. In this work, we found that (1) intra-tumoral delivery of AAV-IL-27 also induced PD-L1 in T cells in peripheral lymphoid organs and tumors, and (2) AAV-IL-27 and anti-PD-1 showed synergy in inhibiting tumor growth (**Figure 5**). Thus, the limitation of IL-27-induced PD-L1 expression in T cells can serve as an opportunity for developing novel combination therapy.

Adoptive transfer of TIL T cells is a well-established therapy for patients with solid tumors such as melanoma (Rosenberg and Restifo, 2015). In a standard protocol, a pretreatment of recipients with chemotherapy drugs is usually needed to deplete Tregs and make room for T cell homeostatic proliferation (Dudley et al., 2005). Consistent with this notion, we found that adoptive transfer of TILs alone was insufficient to induce tumor regression in non-lymphopenic mice (**Figure 6E**). However, intra-tumoral injection of AAV-IL-27 showed significant synergy with TIL therapy in the absence of pretreatment of recipient mice. This outcome is due to a number of mechanisms. First, as described above, IL-27-induced CXCR3 upregulation can enhance T cell trafficking into tumors. Second, IL-27 can directly stimulate TIL T cells, enhancing their survival ability and IFN-γ production, as we previously demonstrated (Liu et al., 2013; Li et al., 2015). Third, IL-27-mediated depletion of Tregs can bypass the need of lymphodepletion prior to T cell transfer. Nevertheless, our results suggest that intra-tumoral injection of AAV-IL-27 in combination with TIL adoptive transfer is a potential combination for cancer therapy.

Taken together, we evaluated if directly injecting AAV-IL-27 into tumors could lead to inhibition of tumor growth. In the two tumor models (B16.F10 and J558) tested, intra-tumoral delivery of high dose AAV-IL-27 showed potent anti-tumor activity in mice bearing plasmacytoma J558 tumors and modest anti-tumor activity in mice bearing B16.F10 tumors. Importantly, in mice whose tumors were completely rejected, IL-27 serum levels were significantly reduced or diminished, and protective immunity was established. Moreover, we found that intra-tumoral injection of AAV-IL-27 showed significant synergy with anti-PD-1 antibody or T cell adoptive transfer therapy in inhibiting tumor growth. Thus, intra-tumoral delivery of AAV-IL-27 is a feasible approach for enhancing anti-tumor immunity and can be used alone and in combination with anti-PD-1 antibody or T cell adoptive transfer for the treatment of cancer.

DATA AVAILABILITY STATEMENT

All datasets generated for this study are included in the article/**Supplementary Material**.

ETHICS STATEMENT

The animal study was reviewed and approved by Ohio State University Animal Care and Use Committee.

AUTHOR CONTRIBUTIONS

AH and MD performed most of the experiments. JZ helped and performed flow cytometry analysis. J-QL produced rAAV and helped with mouse work. XP helped with statistical analysis. KG helped with experimental design. X-FB generated funding support, designed experiments, analyzed data and wrote the manuscript.

FUNDING

This work was supported by a grant (R01CA229254) from National Cancer Institute and an IDEA award from the intramural research program at OSU Comprehensive Cancer Center (OSUCCC). This project was also supported by the OSUCCC Biostatistics and Analytical Cytometry supported in part by NCI grant P30 CA016058. MD was supported by young investigator awards from China Natural Science Foundation (81803074) and postdoctoral Science Foundation (2018M632140).

SUPPLEMENTARY MATERIAL

The Supplementary Material for this article can be found online at: https://www.frontiersin.org/articles/10.3389/fcell.2020.00210/full#supplementary-material

FIGURE S1 | Immunofluorescence analysis of GFP expression from tumors receiving AAV-GFP. Mice with established B16 tumors were treated with AAV-GFP ($5*10^9$DRP), 7 days later, the injection sites of tumor tissues were examined for the expression of GFP under a confocal microscope. Upper panel: tumor tissue from an untreated tumor; lower panel: tumor tissue from an AAV-GFP treated tumor.

FIGURE S2| Representative flow cytometry data showing analysis of tumor infiltrating leukocytes. **(A)** B16.F10 cells (2×10^5) were injected into C57BL/6 mice s.c. Seven days later, mice were treated with AAV-IL-27 or AAV-ctrl virus intra-tumorally at a dose of 2×10^{11} DRP/mouse. Mice were sacrificed on day 21, and populations of tumor infiltrating leukocytes were analyzed by flow cytometry. **(B)** J558 cells (5×10^6) were injected into BALB/c mice s.c. Seven days later, mice were treated with AAV-IL-27 or AAV-ctrl virus intra-tumorally at a dose of 5×10^{10} DRP/mouse, and mice were sacrificed on day 21, and populations of tumor infiltrating leukocytes were analyzed by flow cytometry. Data shown are representative of 3–5 experiments.

FIGURE S3 | Representative flow cytometry data showing analysis of IFN-γ producing T cells **(A)** and Tregs **(B)** in mice bearing J558 tumors. Data are representative of three experiments with similar results.

FIGURE S4 | Flow cytometry analysis of CXCR3 expression in T cells from mice bearing J558 tumors. Data are representative of three experiments with similar results.

FIGURE S5 | Flow cytometry analysis of CXCR3 expression in T cells from IL-27R$^{-/-}$ and Stat1$^{-/-}$ mice. **(A)** C57BL6 and IL-27R$^{-/-}$ mice were injected with B16.F10 tumor cells (2×10^5/mouse) s.c. 7 days later, mice were treated

with AAV–IL-27 or AAV-ctrl virus intra-tumorally at a dose of 2×10^{11} DRP/mouse. 21 days after viral injection, mice were sacrificed and their spleens were analyzed for T cell expression of CXCR3 by flow cytometry. **(B)** AAV-IL-27 or AAV-ctrl virus was injected into Stat1$^{-/-}$ or control BALB/c mice i.m. Three weeks after AAV injection, T cell expression of CXCR3 in spleens was analyzed by flow cytometry. Data are representative of two experiments with similar results.

REFERENCES

Aalbers, C. J., Tak, P. P., and Vervoordeldonk, M. J. (2011). Advancements in adeno-associated viral gene therapy approaches: exploring a new horizon. *F1000 Med. Rep.* 3:17. doi: 10.3410/M3-17

Bai, X. F., Liu, J., Li, O., Zheng, P., and Liu, Y. (2003). Antigenic drift as a mechanism for tumor evasion of destruction by cytolytic T lymphocytes. *J. Clin. Invest.* 111, 1487–1496.

Beima, K. M., Miazgowicz, M. M., Lewis, M. D., Yan, P. S., Huang, T. H., and Weinmann, A. S. (2006). T-bet binding to newly identified target gene promoters is cell type-independent but results in variable context-dependent functional effects. *J. Biol. Chem.* 281, 11992–12000.

Car, B. D., Eng, V. M., Schnyder, B., LeHir, M., Shakhov, A. N., Woerly, G., et al. (1995). Role of interferon-gamma in interleukin 12-induced pathology in mice. *Am. J. Pathol.* 147, 1693–1707.

Colombo, M. P., and Trinchieri, G. (2002). Interleukin-12 in anti-tumor immunity and immunotherapy. *Cytokine Growth. Factor. Rev.* 13, 155–168.

Curiel, T. J., Coukos, G., Zou, L., Alvarez, X., Cheng, P., Mottram, P., et al. (2004). Specific recruitment of regulatory T cells in ovarian carcinoma fosters immune privilege and predicts reduced survival. *Nat. Med.* 10, 942–949.

Del Vecchio, M., Bajetta, E., Canova, S., Lotze, M. T., Wesa, A., Parmiani, G., et al. (2007). Interleukin-12: biological properties and clinical application. *Clin. Cancer Res.* 13, 4677–4685.

Dudley, M. E., Wunderlich, J. R., Yang, J. C., Sherry, R. M., Topalian, S. L., Restifo, N. P., et al. (2005). Adoptive cell transfer therapy following non-myeloablative but lymphodepleting chemotherapy for the treatment of patients with refractory metastatic melanoma. *J. Clin. Oncol.* 23, 2346–2357.

Franciszkiewicz, K., Boissonnas, A., Boutet, M., Combadiere, C., and Mami-Chouaib, F. (2012). Role of chemokines and chemokine receptors in shaping the effector phase of the antitumor immune response. *Cancer Res.* 72, 6325–6332. doi: 10.1158/0008-5472.CAN-12-2027

Hall, A. O., Beiting, D. P., Tato, C., John, B., Oldenhove, G., and Lombana, C. G. (2012). The cytokines interleukin 27 and interferon-gamma promote distinct Treg cell populations required to limit infection-induced pathology. *Immunity* 37, 511–523. doi: 10.1016/j.immuni.2012.06.014

Hamid, O., Robert, C., Daud, A., Hodi, F. S., Hwu, W. J., Kefford, R., et al. (2013). Safety and tumor responses with lambrolizumab (anti-PD-1) in melanoma. *N. Engl. J. Med.* 369, 134–144.

Hibbert, L., Pflanz, S., De Waal Malefyt, R., and Kastelein, R. A. (2003). IL-27 and IFN-alpha signal via Stat1 and Stat3 and induce T-Bet and IL-12Rbeta2 in naive T cells. *J. Interferon Cytokine Res.* 23, 513–522.

Hirahara, K., Ghoreschi, K., Yang, X. P., Takahashi, H., Laurence, A., Vahedi, G., et al. (2012). Interleukin-27 priming of T cells controls IL-17 production in trans via induction of the ligand PD-L1. *Immunity* 36, 1017–1030. doi: 10.1016/j.immuni.2012.03.024

Hu, J., Sun, C., Bernatchez, C., Xia, X., Hwu, P., Dotti, G., et al. (2018). T-cell homing therapy for reducing regulatory T cells and preserving effector T-cell function in large solid tumors. *Clin. Cancer Res.* 24, 2920–2934. doi: 10.1158/1078-0432.CCR-17-1365

Kamiya, S., Owaki, T., Morishima, N., Fukai, F., Mizuguchi, J., and Yoshimoto, T. (2004). An indispensable role for STAT1 in IL-27-induced T-bet expression but not proliferation of naive CD4+ T cells. *J. Immunol.* 173, 3871–3877.

Kerkar, S. P., Muranski, P., Kaiser, A., Boni, A., Sanchez-Perez, L., Yu, Z., et al. (2010). Tumor-specific CD8+ T cells expressing interleukin-12 eradicate established cancers in lymphodepleted hosts. *Cancer Res.* 70, 6725–6734. doi: 10.1158/0008-5472.CAN-10-0735

Lewis, M. D., Miller, S. A., Miazgowicz, M. M., Beima, K. M., and Weinmann, A. S. (2007). T-bet's ability to regulate individual target genes requires the conserved T-box domain to recruit histone methyltransferase activity and a separate family member-specific transactivation domain. *Mol. Cell. Biol.* 27, 8510–8521.

Li, M. S., Liu, Z., Liu, J. Q., Zhu, X., Liu, Z., and Bai, X. F. (2015). The Yin and Yang aspects of IL-27 in induction of cancer-specific T-cell responses and immunotherapy. *Immunotherapy* 7, 191–200. doi: 10.2217/imt.14.95

Liu, Z., Liu, J. Q., Talebian, F., Wu, L. C., Li, S., and Bai, X. F. (2013). IL-27 enhances the survival of tumor antigen-specific CD8+ T cells and programs them into IL-10-producing, memory precursor-like effector cells. *Eur. J. Immunol.* 43, 468–479. doi: 10.1002/eji.201242930

Liu, Z., Wu, L., Zhu, J., Zhu, X., Zhu, J., Liu, J. Q., et al. (2017). Interleukin-27 signalling induces stem cell antigen-1 expression in T lymphocytes in vivo. *Immunology* 152, 638–647. doi: 10.1111/imm.12805

Momin, N., Mehta, N. K., Bennett, N. R., Ma, L., Palmeri, J. R., Chinn, M. M., et al. (2019). Anchoring of intratumorally administered cytokines to collagen safely potentiates systemic cancer immunotherapy. *Sci. Transl. Med.* 11:eaaw2614. doi: 10.1126/scitranslmed.aaw2614

Ngiow, S. F., Young, A., Jacquelot, N., Yamazaki, T., Enot, D., Zitvogel, L., et al. (2015). A threshold level of intratumor CD8+ T-cell PD1 expression dictates therapeutic response to anti-PD1. *Cancer Res.* 75, 3800–3811. doi: 10.1158/0008-5472.CAN-15-1082

Phan, G. Q., Yang, J. C., Sherry, R., Hwu, P., Topalian, S. L., Schwartzentruber, D. J., et al. (2003). Cancer regression and autoimmunity induced by cytotoxic T lymphocyte-associated antigen-4 blockade in patients with metastatic melanoma. *Proc. Natl. Acad. Sci. U.S.A.* 100, 8372–8377.

Rosenberg, S. A. (2014). IL-2: the first effective immunotherapy for human cancer. *J. Immunol.* 192, 5451–5458. doi: 10.4049/jimmunol.1490019

Rosenberg, S. A., and Restifo, N. P. (2015). Adoptive cell transfer as personalized immunotherapy for human cancer. *Science* 348, 62–68. doi: 10.1126/science.aaa4967

Ryffel, B. (1997). Interleukin-12: role of interferon-gamma in IL-12 adverse effects. *Clin. Immunol. Immunopathol.* 83, 18–20.

Topalian, S. L. (2017). Targeting immune checkpoints in cancer therapy. *JAMA* 318, 1647–1648.

Topalian, S. L., Hodi, F. S., Brahmer, J. R., Gettinger, S. N., Smith, D. C., McDermott, D. F., et al. (2012). Safety, activity, and immune correlates of anti-PD-1 antibody in cancer. *N. Engl. J. Med.* 366, 2443–2454. doi: 10.1056/NEJMoa1200690

Tumeh, P. C., Harview, C. L., Yearley, J. H., Shintaku, I. P., Taylor, E. J., Robert, L., et al. (2014). PD-1 blockade induces responses by inhibiting adaptive immune resistance. *Nature* 515, 568–571. doi: 10.1038/nature13954

Waldmann, T. A. (2018). Cytokines in cancer immunotherapy. *Cold Spring Harb. Perspect. Biol.* 10:a028472. doi: 10.1101/cshperspect.a028472

Yoshimoto, T., Chiba, Y., Furusawa, J., Xu, M., Tsunoda, R., Higuchi, K., et al. (2015). Potential clinical application of interleukin-27 as an antitumor agent. *Cancer Sci.* 106, 1103–1110. doi: 10.1111/cas.12731

Zhang, L., Morgan, R. A., Beane, J. D., Zheng, Z., Dudley, M. E., Kassim, S. H., et al. (2015). Tumor-infiltrating lymphocytes genetically engineered with an inducible gene encoding interleukin-12 for the immunotherapy of metastatic melanoma. *Clin. Cancer Res.* 21, 2278–2288. doi: 10.1158/1078-0432.CCR-14-2085

Zhao, Q., Hu, J., Mitra, A., Cutrera, J., Zhang, W., Zhang, Z., et al. (2019). Tumor-targeted IL-12 combined with tumor resection yields a survival-favorable immune profile. *J. Immunother. Cancer* 7:154. doi: 10.1186/s40425-019-0631-z

Zhu, J., Liu, J. Q., Shi, M., Cheng, X., Ding, M., Zhang, J. C., et al. (2018). IL-27 gene therapy induces depletion of Tregs and enhances the efficacy of cancer immunotherapy. *JCI Insight* 3:e98745. doi: 10.1172/jci.insight.98745

Conflict of Interest: The authors declare that the research was conducted in the absence of any commercial or financial relationships that could be construed as a potential conflict of interest.

frontiers in Cell and Developmental Biology

ORIGINAL RESEARCH
published: 19 May 2020
doi: 10.3389/fcell.2020.00280

Over-Expression and Prognostic Significance of HHLA2, a New Immune Checkpoint Molecule, in Human Clear Cell Renal Cell Carcinoma

Zhen Zhang[1†], Jinyan Liu[1†], Chaoqi Zhang[2], Feng Li[1], Lifeng Li[1], Dan Wang[1], Damini Chand[3], Fangxia Guan[4], Xingxing Zang[3] and Yi Zhang[1,4,5,6]**

[1] Biotherapy Center, The First Affiliated Hospital of Zhengzhou University, Zhengzhou, China, [2] Department of Thoracic Surgery, National Cancer Center/Cancer Hospital, Chinese Academy of Medical Sciences and Peking Union Medical College, Beijing, China, [3] Department of Microbiology and Immunology, Albert Einstein College of Medicine, Bronx, NY, United States, [4] School of Life Sciences, Zhengzhou University, Zhengzhou, China, [5] Cancer Center, The First Affiliated Hospital of Zhengzhou University, Zhengzhou, China, [6] Key Laboratory for Tumor Immunology and Biotherapy of Henan Province, Zhengzhou, China

OPEN ACCESS

Edited by:
Jiyan Zhang,
Independent Researcher, Beijing, China

Reviewed by:
Yuan Wei,
Sun Yat-sen University, China
Lianjun Zhang,
Suzhou Institute of Systems Medicine (ISM), China

***Correspondence:**
Xingxing Zang
xingxing.zang@einstein.yu.edu
Yi Zhang
yizhang@zzu.edu.cn

[†] These authors have contributed equally to this work

Specialty section:
This article was submitted to Cell Death and Survival, a section of the journal Frontiers in Cell and Developmental Biology

Received: 28 January 2020
Accepted: 31 March 2020
Published: 19 May 2020

Citation:
Zhang Z, Liu J, Zhang C, Li F, Li L, Wang D, Chand D, Guan F, Zang X and Zhang Y (2020) Over-Expression and Prognostic Significance of HHLA2, a New Immune Checkpoint Molecule, in Human Clear Cell Renal Cell Carcinoma. Front. Cell Dev. Biol. 8:280. doi: 10.3389/fcell.2020.00280

HHLA2, a newly identified B7 family member, regulates T cell functions. However, the expression and prognostic value of HHLA2 in solid tumors is ill defined. This study aimed to reveal the expression landscape of HHLA2 in various solid tumors, and to evaluate its prognostic value in kidney clear cell carcinoma (KIRC). Using The Cancer Genome Atlas (TCGA) database, we investigated the expression pattern of HHLA2 across 22 types of cancer. HHLA2 and CD8 protein expression was determined via immunohistochemistry (IHC). KIRC-specific findings were further analyzed with R software and the prognostic value was validated on tissue microarrays. HHLA2 was widely expressed in cancers at both the mRNA and protein levels. Among all tested tumors, KIRC showed the highest transcript level of HHLA2, and HHLA2 levels were significantly higher in tumor tissues than in matched normal samples, as evidenced by both TCGA and IHC data. HHLA2 was also positively correlated with survival rates in KIRC based on TCGA and clinical data. Receiver operating characteristic curves data showed the prognostic value of HHLA2 for patients with KIRC in TCGA. Moreover, HHLA2 was positively correlated with immune-related genes, while HHLA2 and CD8 expression exhibited a consistent trend in KIRC tumor samples. In conclusion, HHLA2 is highly expressed in KIRC and predicts a favorable survival outcome, highlighting that it may work as a potential target for KIRC therapy.

Keywords: KIRC, HHLA2, CD8$^+$ T cells, TCGA, tissue microarrays

Abbreviations: BLCA, bladder urothelial carcinoma; BRCA, breast invasive carcinoma; CESC, cervical squamous cell carcinoma and endocervical adenocarcinoma; COAD, colon adenocarcinoma; CNAs, copy number variations; CTLA-4, cytotoxic T-lymphocyte-associated protein 4; ESCA, esophageal carcinoma; GBM, glioblastoma multiforme; GO, gene ontology; HNSC, head and neck squamous cell carcinoma; IHC, immunohistochemistry; KICH, kidney chromophobe; KIRC, kidney renal cell carcinoma; KIRP, kidney papillary cell carcinoma; LGG, brain lower grade glioma; LIHC, liver hepatocellular carcinoma; LUAD, lung adenocarcinoma; LUSC, lung squamous cell carcinoma; MHC, the major histocompatibility complex; OV, ovarian serous cystadenocarcinoma; PAAD, pancreatic adenocarcinoma; PCPG, pheochromocytoma and paraganglioma; PD-1, programmed cell death 1; PRAD, prostate adenocarcinoma; RCC, renal cell carcinoma; READ, rectum adenocarcinoma; SARC, sarcoma; SKCM, skin cutaneous melanoma; TCGA, The Cancer Genome Atlas; THYM, thymoma.

INTRODUCTION

Renal cell carcinoma (RCC) accounts for 3% of adult malignant tumors and ranks as the most lethal of all urologic cancers (Ferlay et al., 2015). Nearly 95% of RCC cases are clear cell KIRC, KIRP, and KICH (Shuch et al., 2015). Among these three types, KIRC shows strong resistance when treated with traditional therapies, including chemotherapy and radiotherapy, with a < 20% 2-year survival rate for metastatic patients (Chen et al., 2016; Han et al., 2017). During the last decade, immunotherapy has attracted attention due to the important role of the immune system in cancer (Schumacher and Schreiber, 2015; Ribas and Wolchok, 2018). It has been clearly demonstrated that once an antigen is presented through the MHC, a simultaneous signal is required to determine the type of T cell response. A costimulatory signal induces T cell activation while a coinhibitory signal results in T cell inhibition (Shi et al., 2019). In one mechanism of tumor evasion from the immune system, tumor cells express coinhibitory ligands that result in T cell exhaustion and blunt the immune response (Chen et al., 2018; Zhang et al., 2020). By targeting this phenomenon, immune checkpoint blockade therapy (ICBT), can unleash the breaks in the immune system and induce long-lasting responses (Hato et al., 2014; Marin-Acevedo et al., 2018a). With these advances in immunotherapy, patients with KIRC have been treated with PD-1 inhibitors; however, the limited expression of PD-Ll limits application of this therapy in the clinic (Shi et al., 2019). Thus, identifying a more suitable target in KIRC to improve immunotherapy efficacy is necessary.

The B7 and CD28 family have attracted increasing attention for their important roles in determining T cell fate. Inhibiting coinhibitory checkpoints using ICBT has been regarded as a promising method for controlling tumors, and many studies have demonstrated its efficacy (Li et al., 2018; Marin-Acevedo et al., 2018b). The most studied are PD-1 and CTLA-4, which have been approved by the FDA for the treatment of blood tumors (Hirano et al., 2005; Yu et al., 2016; Chau, 2017). Although this approach has provided encouraging results, the clinical responses are far from perfect for patients with solid cancers (Pardoll, 2012; Topalian et al., 2012; Abril-Rodriguez and Ribas, 2017); the underlying mechanisms resulting in treatment failure are complicated. Thus, exploring new targets may help increase the efficacy of ICBT. HHLA2 (B7H7/B7-H5/B7y), a newly defined B7 family member (Zhao et al., 2013), is a co-inhibitory molecule expressed in multiple cancers, including lung, breast and pancreatic cancers as well as melanoma, and osteosarcoma and shows limited expression in normal tissues. While HHLA2 expression is associated with worse survival in patients with osteosarcoma (Koirala et al., 2016), its expression and significance of HHLA2 is ill defined in other types of solid tumors (Janakiram et al., 2015b). Therefore, in this study, we aimed to reveal the expression pattern and potential prognostic value of HHLA2 in various solid tumors.

MATERIALS AND METHODS

The Cancer Genome Atlas (TCGA) Database

HHLA2 transcriptome data from 22 types of solid tumors in TCGA dataset were obtained from the website of the Cancer Genomics Browser of the University of California Santa Cruz[1]. The following tumor types were selected: KIRC (n = 534), READ (n = 95), KIRP (n = 291), COAD (n = 288), PAAD (n = 179), LUAD (n = 517), ESCA (n = 185), LUSC (n = 502), OV (n = 308), PRAD (n = 498), LGG (n = 530), THYM (n = 120), HNSC (n = 522), CESC (n = 305), PCPG (n = 184), LIHC (n = 373), KICH (n = 66), GBM (n = 167), BLCA (n = 407), SKCM (n = 473), SARC (n = 263), BRCA (n = 1104). We also retrieved KIRC normal sample (n = 72) data from TCGA. Only primary patients were enrolled in this study while recurrent ones were excluded.

Gene Expression Omnibus (GEO) Datasets

Normalized data of a previous Affymetrix HG-U133A 2.0 gene expression array that compared gene expression in KIRC tumors and matched adjacent normal tissues was downloaded from the GEO[2]. Specifically, 101 and 72 pairs of normal and matched cancer samples were obtained from GSE40435 and GSE53757, respectively. While 63 cases of normal samples and 67 cases of cancer samples were obtained from GSE46699. Network Analyst software was used to re-analyze the data.

DNA Methylation Analysis

We collected DNA methylation datasets from 319 KIRC cases in TCGA program. Methylation measurements were performed using the Illumina Human Methylation 450 platform (Illumina, San Diego, CA, United States). HHLA2 gene expression values from KIRC tumor tissues were also extracted. Pearson's product-moment correlation between HHLA2 gene expression levels and methylation of its CpG islands was evaluated. Data analysis was performed using R software[3]. Data analysis was completed by using MEXPRESS[4].

Patients and Samples

All paraffin-embedded tumor tissue specimens (n = 250) were collected from patients with KIRC, who underwent surgery at the First Affiliated Hospital of Zhengzhou University. Normal and tumor tissue microarrays (TMAs) were purchased from Shang Hai Outdo Biotech for the analysis of HHLA2 expression in human tissues. The diameter of the tissue chip was 1 mm. The types of tumors in TMAs were listed as follows: KIRC, STAD, COAD, LUAD, BLCA, BRCA, ESCA, PAAD, UCEC, READ, THCA, and CESC. TMA construction has been previously

[1]https://genome-cancer.ucsc.edu/

[2]https://www.ncbi.nlm.nih.gov/geo/info/datasets.html

[3]https://www.r-project.org

[4]http://mexpress.be

described in detail (Nocito et al., 2001). This study was approved by the Ethics Committee of the First Affiliated Hospital of Zhengzhou, Henan, China.

Immunohistochemistry (IHC) Staining

To examine HHLA2 expression in tumors and matched normal tissue, samples from cancer patients were obtained from the First Affiliated Hospital of Zhengzhou University. Tumor tissues were incubated in 4% paraformaldehyde (PFA) overnight, then embedded in paraffin, and sectioned at a thickness of 4 μm. For staining, the slides were deparaffinized and rehydrated, followed by antigen retrieval. The sections were then blocked with 5% BSA in PBS and incubated with anti-HHLA2 mAb (2 μg/mL, 1:500; clone 566.1, IgG1) (Cheng et al., 2017) or anti-CD8 (1:200; ab93278; Abcam, Cambridge, United Kingdom) monoclonal antibodies at 4°C overnight. The next day signal amplification was performed using an ABC HRP Kit (Zhongshanjinqiao Biotechnology, Beijing, China) and the samples were counter-stained with hematoxylin. Following dehydration with a graded ethanol series and clearing with xylene, the sections were imaged using a microscope (Leica, Wetzlar, Germany). Non-immune immunoglobulin G (IgG) was used as negative control. To analyze HHLA2 and CD8 expression, 5 to 10 fields were analyzed per patient sample. Marker density was scored independently by two investigators as follows: 0, negative; 1, weak; 2, moderate; or 3, strong. When tumor samples were tabulated, those with moderate and strong staining for HHLA2 or CD8 were considered the high expression group, while those with negative and weak expression were considered the low expression group.

Gene Ontology (GO) Analysis

Immune-correlated genes were shared by TCGA dataset. Using DAVID Bioinformatics Resources 6.8[5], function annotation was performed and the optimal related genes (top 600 genes ranked by Pearson |R|) were identified for analysis. Then, the groups on the network to the cluster distribution over the terms was visualized using the Cytoscape plugin (ClueGO plugin).

Statistical Analysis

Statistical analysis was mainly performed by using R software[3]. All data are presented as mean ± SD. The association between HHLA2 expression and clinical parameters was analyzed using the χ^2 test (age, sex, tumor grade, and stage) or Student's *t*-test [overall survival, (OS)]. Univariate and multivariate analyses were performed using Cox proportional hazard model. Statistical analysis was also performed using the GraphPad Prism v6.0 (GraphPad Software, La Jolla, CA, United States). For the analysis of TCGA data, continuous variables were dichotomized for OS before running a log-rank test by employing optimal cutoff values. Comparison of the Kaplan–Meier survival curves between HHLA2 or CD8 expression high and low expression groups was performed using log-rank test. *P*-values < 0.05 were considered statistically significant.

[5]http://david.ncifcrf.gov/

RESULTS

The Expression Landscape of HHLA2 in Different Types of Solid Tumors

Accumulating evidence has shown that the B7 family of ligands provides coinhibitory or costimulatory signals that determine T cell fate (Schildberg et al., 2016). As the most recently discovered ligand of the B7 family, HHLA2 has attracted increasing attention (Janakiram et al., 2017). However, the expression pattern of HHLA2 in solid tumors is not well-defined. To comprehensively analyze the expression pattern of HHLA2 expression in solid tumors, we analyzed its transcriptome expression from TCGA data. As shown in **Figure 1A**, HHLA2 mRNA was widely expressed in 22 types of solid tumors and showed had expression in seven tumors including KIRC, READ, KIRP, COAD, PAAD, LUAD, ESCA according to the mean value. To further validate these findings, we performed IHC using TMAs. Consistent with TCGA data, HHLA2 was widely expressed in 12 types of solid tumors in protein level, including KIRC, READ, COAD, BRCA, PAAD, LUAD, ESCA, CESC, STAD, BLCA, UCEC, and THCA (**Figure 1B**). Furthermore, HHLA2 showed highly positive expression (**Figure 1C**) and positive intensity (**Figure 1D**). Taken together, these results demonstrate that HHLA2 was widely expressed in human solid cancers, and that it had high positive rate and expression in KIRC.

HHLA2 Is Highly Expressed in Tumor Tissues and Predicts Good Outcomes in KIRC Patients

Given high positive rate and expression intensity of HHLA2 observed in KIRC samples, we next explored the significance of HHLA2 expression in patients with KIRC. First, we analyzed HHLA2 expression in KIRC tumors and matched normal tissues from TCGA dataset and found that HHLA2 expression is significantly higher expression in KIRC tumor tissues than in matched normal samples. Similar results were obtained with the GEO dataset (**Figure 2A**, all $P < 0.01$), indicating that HHLA2 is overexpressed in KIRC tumors. To investigate the potential significance of accumulated HHLA2, we divided the KIRC cohort ($n = 531$) into HHLA2-high and low expression groups and evaluated the prognostic value. Patients with high HHLA2 expression had a significantly longer survival time than those patients with low expression. When patients were divided into stage I–II and III–IV groups, similar results were obtained for both groups (**Figure 2B**, all $P < 0.01$). We further compared the clinical characteristics (including age, sex, clinical stage, and tumor grade) between HHLA2-high and low groups and observed statistically significant differences in tumor grade and survival; no significant differences were detected for other clinical features (**Table 1**). Furthermore, the univariate and multivariate Cox regression model using TCGA data revealed that age, tumor grade, clinical stage, and HHLA2 expression were independent prognostic factors for OS of patients with KIRC (**Table 2**). Evaluation of the correlation between tumor HHLA2 and

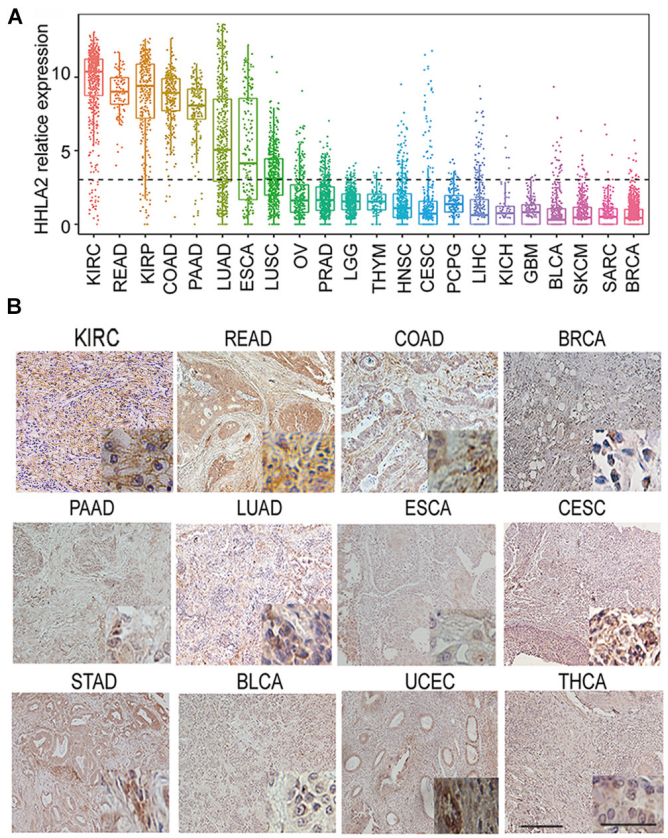

C

The expression of HHLA2 in human cancers.

Types (positive/total cases)			
KIRC (23/25)	READ (25/30)	COAD (12/15)	BRCA (26/30)
PAAD (11/15)	LUAD (23/30)	ESCA (13/15)	CESC (25/30)
STAD (13/15)	BLCA (56/60)	UCEC (29/34)	THCA (28/30)

D

The analysis of HHLA2 score in the positive staining samples.

Tumor types	total cases	HHLA2 (each score/total cases, %)		
		3	2	1
KIRC	23	8/23 (34.8)	5/23 (21.7)	10/23 (43.4)
READ	25	3/25 (12.0)	15/25 (60)	7/25 (28.0)
COAD	15	2/15 (13.3)	7/15 (46.7)	3/15 (20.0)
BRCA	26	5/26 (19.2)	12/26 (46.2)	9/26 (36.0)
PAAD	11	2/11 (18.2)	4/11 (36.3)	5/11 (45.5)
LUAD	23	7/23 (30.4)	7/23 (30.4)	9/23 (39.1)
ESCA	13	3/13 (23.1)	4/13 (30.8)	6/13 (46.2)
CESC	25	11/25 (44.0)	12/25 (48.0)	2/25 (8.0)
STAD	13	4/13 (30.8)	8/13 (61.5)	1/13 (7.6)
BLCA	56	21/56 (37.5)	17/56 (30.4)	18/56 (32.1)
UCEC	29	7/29 (24.1)	12/29 (41.4)	10/29 (34.5)
THCA	28	13/28 (46.4)	13/28 (46.4)	2/28 (7.1)

FIGURE 1 | The expression landscape of HHLA2 in different types of solid tumors. **(A)** mRNA gene expression of HHLA2 in 22 tumor types was analyzed by using the mRNA-sequencing data from the TCGA database. **(B)** Representative IHC of HHLA2 expression in 12 types of tumor tissues. Full-sized images were acquired at 10 × and zoomed-in images were originally acquired at 40 × . **(C)** HHLA2 protein expression in human cancers detected by immunohistochemistry via tissue microarrays; positive cases were analyzed. **(D)** The HHLA2 score was evaluated in each sample based on positive staining and intensity. A summary of HHLA2 score in human cancers was listed.

clinicopathologic parameters in KIRC patients from two TAMs (n = 90 and n = 150) and 250 clinical samples revealed that tumor grade was correlated with HHLA2 expression in the validation 1 (n = 150) and 2 (n = 250) groups (**Table 3**). In addition, the area under the curve (AUC) of HHLA2 from TCGA and GEO data sets were 86.9, 71.4, 80.1, and 82.9%, respectively (**Figure 2C**), supporting HHLA2 as a prognostic marker in KIRC.

We further examined protein expression of HHLA2 in TMAs and analyzed its correlation with patient prognosis. HHLA2 positive expression was defined as positive membranous and cytoplasmic staining (**Figure 2D**, staining scores of 0, 1, 2, or 3) as previous report (Cheng et al., 2017). HHLA2 showed significantly higher expression in tumor tissues than that of the matched normal samples in both cohort 1 (paired, n = 90) and cohort 2 (paired, n = 30) (**Figures 2E,F**). Kaplan–Meier curves was used to analyze the correlation between HHLA2 expression and OS, which showed that patients in the HHLA2-high group had longer survival rates than those of patients in the HHLA2-low group in both cohort 1 and 2 (**Figure 2G**), which was consistent with TCGA data. Together, these results demonstrated that HHLA2 was highly expressed in the tumor sites, and that increased expression is positively correlated with OS of patients with KIRC.

Analysis of the Potential Genetic and Epigenetic Alterations Associated With HHLA2 Dysregulation

We next investigated the underlying mechanism underlying HHLA2 expression that induced abnormalities of HHLA2 in KIRC. Copy number alterations (CNAs) are an important mechanism of oncogene activation in cancer (Curtis et al., 2012). To reveal whether CNAs are responsible for the abnormal expression of HHLA2 in KIRC, we analyzed data from 415 cases with CNAs available in TCGA dataset. Different patterns of CNAs were observed in the HHLA2-high and low groups. Specifically, the proportion of the diploid normal copy was higher in the HHLA2-high group (75.9%, 186/245, **Figure 3A**) than in the HHLA2-low group (48.2%, 135/280, **Figure 3B**). The proportion of single copy deletions showed the opposite trend, with 41.4 and 11.4% in the HHLA2-low and high groups, respectively (**Figures 3A,B**). No differences were observed for homozygous deletion, low-level copy number amplification, and

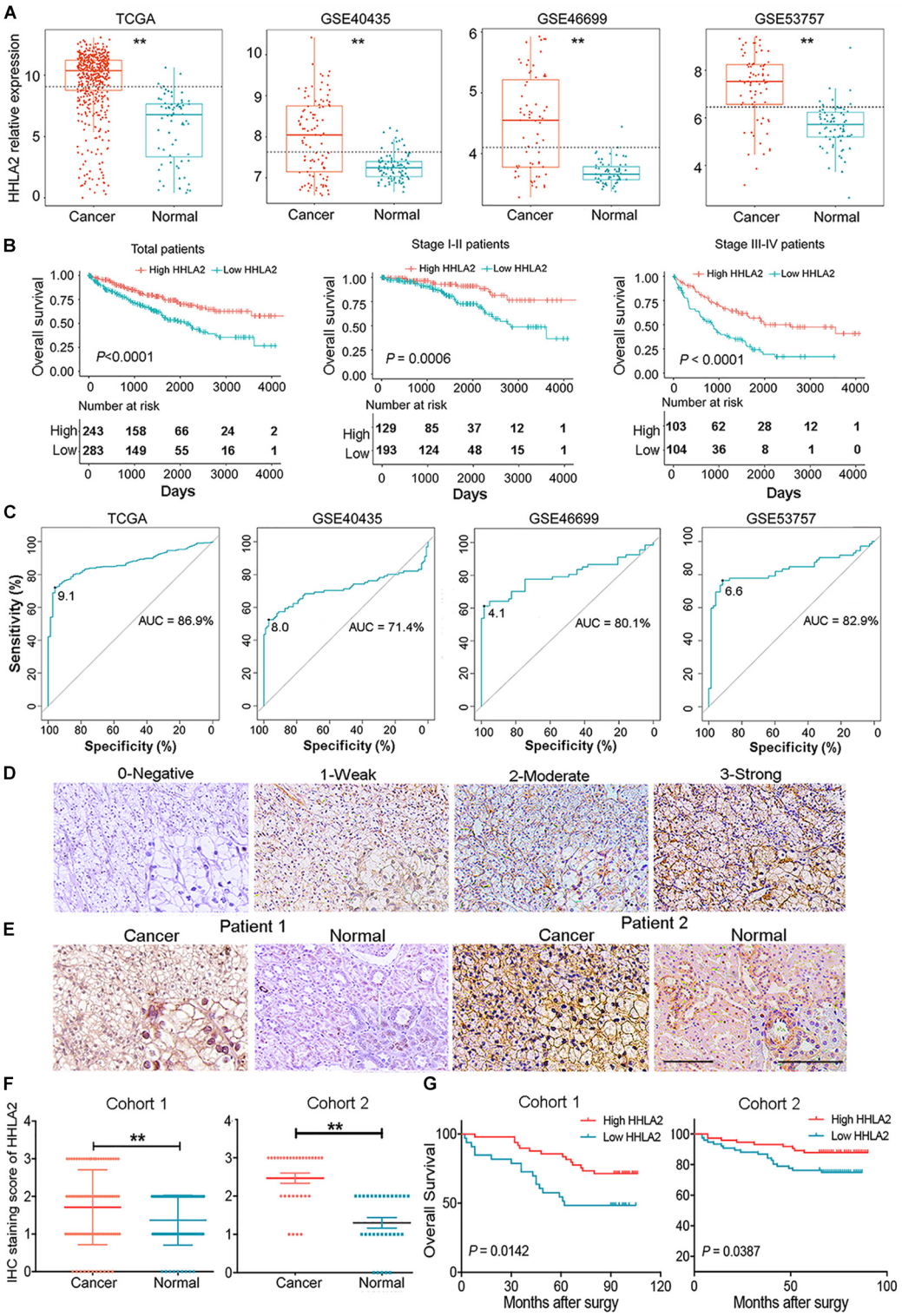

FIGURE 2 | HHLA2 is highly expressed in tumor tissues and is a positive prognostic marker for patients with KIRC. **(A)** Compared with normal tissues, HHLA2 expression was higher in tumor tissues from patients with KIRC, based on TCGA and GEO datasets. **(B)** HHLA2 expression levels were positively correlated with the survival rates in KIRC from TCGA dataset. **(C)** The ROC curve of HHLA2 was analyzed by using the data from TCGA and GEO. **(D)** Evaluation of the HHLA2 score. Magnification, 10 and 20×. **(E)** Normal and tumor tissues from patients with KIRC were stained determine HHLA2 protein expression. **(F)** The HHLA2 score was significantly higher in the tumor tissues than that in normal samples from the KIRC patients (TMAs numbered Hkid-CRC180 Sur-01 was defined as cohort 1 and HkidE180 Su02 defined as cohort 2). **(G)** IHC staining showed that HHLA2 expression is positively correlated with survival time of patients with KIRC. $^{**}P < 0.01$. Score 0, negative; 1, low expression; 2, moderate expression; and 3, high expression.

TABLE 1 | Comparison of clinical characteristics between low HHLA2 group and high HHLA2 group in KIRC cohort.

Variable	Case NO. (%)	HHLA2		*P*
		Low	High	
Sample	531	266	265	
Age (year)				0.075
≤60	264	122	142	
>60	267	144	123	
Gender				0.192
Male	345	180	165	
Female	186	86	100	
Grade				0.001
G1	13	6	7	
G2	229	110	119	
G3	205	89	116	
G4	76	54	22	
Unknown	8	7	1	
Tumor stage				0.168
T1	271	137	134	
T2	69	35	34	
T3	180	85	95	
T4	11	9	2	
Clinical stage				0.888
I	265	134	131	
II	57	30	27	
III	123	58	65	
IV	84	43	41	
Unknown	2	1	1	
Distant metastases				0.341
Yes	107	58	49	
No	422	207	215	
Unknown	2	1	1	
Lymph node metastasis				0.629
Yes	291	143	148	
No	240	123	117	
Survival state				0.001
Alive	356	160	196	
Dead	175	106	69	

TABLE 2 | Univariate and multivariate regression analyses for predicting overall survival in KIRC cohort.

Variable	Univariate		Multivariate	
	HR (95% CI)	*P*	HR (95% CI)	*P*
Age	1.8 (1.3–2.5)	<0.001	1.6 (1.2–2.2)	0.005
Gender	1.1 (0.8–1.5)	0.690	1.1 (0.8–1.5)	0.553
Laterality	0.7 (0.5–1.0)	0.028	0.9 (0.6–1.2)	0.407
Tumor grade	2.3 (1.8–2.8)	<0.001	1.4 (1.1–1.8)	0.003
Clinical stage	1.8 (1.6–2.1)	<0.001	1.8 (1.1–2.9)	0.013
Tumor stage	1.9 (1.6–2.2)	<0.001	0.8 (0.5–1.2)	0.288
Lymph node metastasis	0.9 (0.8–1.1)	0.257	0.9 (0.8–1.1)	0.225
Distant metastasis	4.3 (3.1–5.8)	<0.001	1.3 (0.7–2.6)	0.427
HHLA2 mRNA level	0.9 (0.8–0.9)	<0.001	0.8 (0.8–0.9)	<0.001

high-level copy number amplification between the two groups (**Figures 3A,B**).

Apart from CNAs, studies integrating DNA-methylation profiles and gene expression data have shown that methylation at different genomic regions is associated with gene expression levels (Diaz-Lagares et al., 2016; Chen G. et al., 2019). CpG DNA methylation is considered perhaps the most fundamental molecular phenomenon determining chromatin accessibility to the transcriptional machinery, thereby regulating gene expression (Chen G. et al., 2019). To investigate whether DNA methylation results in HHLA2 dysfunction, we examined status of 12 CpG sites of 319 KIRC cases in TCGA. Only seven CpG sites had associated data; among them, five CpG sites, including cg02059214, cg02124498, cg08817540, cg10431989, and cg11326415, showed a negative correlation with HHLA2 expression; the other two sites were positively correlated with HHLA2 (**Figure 3C**). We then employed the Pearson correlation coefficient and found that HHLA2 expression was negatively correlated with the above-mentioned five CpG sites (**Figure 3D**, all $P < 0.01$). Collectively, these data demonstrated the potential function of CNAs or DNA methylation in regulating the abnormal expression of HHLA2 in KIRC, highlighting the need for further investigation of the underlying mechanism.

HHLA2 Is Positively Correlated With the Inflammatory Activities

Given that HHLA2 expression in KIRC is strongly associated with prognosis, we theorized that HHLA2 expression may be regulated by inflammatory responses, leading to enhanced survival rates. To identify the HHLA2 associated immune signature in KIRC, gene sets associated with the immune response[6] were selected. We found 600 genes in TCGA dataset that were strongly correlated with HHLA2 expression (Pearson $|R| > 0.5$), and thus were eligible for further analysis. As most genes were positively correlated with HHLA2 expression (**Figure 4A**), we performed GO analysis to clarify their biofunctions. The results showed that these genes positively related to HHLA2 were significantly enriched in IFN-γ production, cell chemotaxis, and cytokine-mediated signaling pathway (**Figure 4B**). Thus, HHLA2 expression appears positively correlated with immune-related genes and immune responses in KIRC.

To gain a further understanding of HHLA2-related inflammatory activities, we chose seven clusters that were subsequently defined as metagenes from TCGA dataset. These genes represented different types of inflammatory and immune responses, and most clusters were positively associated with HHLA2 expression except for IgG, which was mainly associated with the activities of B lymphocytes (**Figure 4C**). To assess these cluster data, seven metagenes were generated using the gene sets variation analysis (GSVA) results of corresponding gene clusters. Then the correlogram was used to display relationships between variables, based on the Pearson *r* values between HHLA2 and the seven metagenes (**Figure 4D**). HHLA2 was positively correlated with MHC-II, MHC-I, STAT1 and LCK, but was negatively associated with IgG, consistent with what was observed in

[6]http://amigo.geneontology.org/amigo/landing

TABLE 3 | Clinicopathologic characteristics of HHLA2 expression in KIRC patients from the discovery and validation groups.

Parameter	Discovery cohort (n = 90)			Validation cohort 1 (n = 150)			Validation cohort 2 (n = 250)		
	HHLA2 Low	HHLA2 High	*P*	HHLA2 Low	HHLA2 High	*P*	HHLA2 Low	HHLA2 High	*P*
Age[a] (year)			0.800			0.899			0.776
<65	25	34		61	60		92	90	
≥65	14	17		15	14		33	35	
Gender[a]			0.966			0.977			0.241
Female	17	22		22	21		52	43	
Male	22	29		54	53		73	82	
Tumor grade[a]			0.448			<0.001			0.006
I	15	25		38	22		52	57	
II	17	21		19	43		40	53	
III	7	5		18	9		30	10	
IV	0	0		1	0		4	5	
Stage[a]			0.357			0.305			0.891
I	28	32		61	61		96	98	
II	7	11		7	9		16	18	
III	3	1		7	4		8	6	
IV	0	2		1	0		3	2	
Unknown	1	5		0	0		2	1	
Overall survival[b] (months)	63.94	84.22	0.014	63.63	73.10	0.039	34.50	39.76	<0.001

[a] χ^2 *test;* [b] *Student's t-test.*

Figure 4A. Together, these results suggested that HHLA2 is positively correlated with inflammatory activities in KIRC.

HHLA2 Is Not Simultaneously Expressed With Other B7-CD28 Family Members

We next examined whether HHLA2 is co-expressed with other B7 family members, including CD80, CD86, CD274, CD276, ICOSLG, PDCD1LG2, and VTCN1. Pearson correlation coefficient analysis was performed with these factors in the TCGA database. Interestingly, we observed that HHLA2 showed no obvious correlation with CD80, CD86, CD274, CD276, ICOSLG, PDCD1LG2, or VTCN1 (**Figure 5A**), indicating that HHLA2 expression is not co-expressed with other B7 family members. Considering that B7 family members must bind to cognate CD28 family receptors expressed on T cells—e.g., CD80/CD86 binds to CD28—to regulate T cell function (Ville et al., 2015). Thus, we analyzed the correlation between HHLA2 expression with CD28 family, including CD28, CTLA-4, PDCD1, TMIGD2 and ICOS. Surprisingly, no obvious correlation was observed between HHLA2 and any CD28 family member (**Figure 5B**), suggesting that HHLA2 is not co-expressed with the CD28 family (Zhao et al., 2013).

It is well-known that activated immune response and inflammatory responses represent a good prognosis for patients with cancer. Tumor necrosis factor (TNF), a pleiotropic cytokine and a major mediator of apoptosis as well as inflammation and immunity, is a component of the immune response (Cervera-Carrascon et al., 2017). Accordingly, we analyzed the correlation between HHLA2 expression and the TNF family, including CD40, CD40L, TNFRSF4, TNFSF9, TNFRSF9, TNFSF18 and TNRFRSF14. A limited correlation was observed between HHLA2 and TNFSF9, while no clear correlation was observed with other family members (**Figure 5C**). As for other immune checkpoints such as LAG3, HAVCR2, CD47, ENTPD1, NTSE and IDO1, we found that none were strongly correlated with HHLA2 (**Figure 5D**). These results indicated that HHLA2 is not co-expressed with other B7 or CD28 family members, suggesting that it may work as an independent immune checkpoint in those patients with low expression of other well-defined immune checkpoints.

HHLA2 and CD8 Are Positively Correlated With the Prognosis of Patients With KIRC

Next, we investigated why HHLA2 overexpression in the KIRC tumor sites is correlated with good prognosis. Accumulating evidence has demonstrated that high levels of $CD8^+$ T cells predict good prognosis for cancer patients (McKinney et al., 2010). Thus, to assess HHLA2 correlation with CD8, we analyzed CD8 and HHLA2 expression in TMAs of discovery and validation cohorts, with IgG as the negative control (**Figure 6A**). We found that CD8 showed significantly higher expression in tumor sites than in the matched normal samples (**Figure 6B**). This pattern was validated in the discovery cohort (**Figure 6C**, $n = 30$, $P < 0.01$). Furthermore, we divided the patients into two groups according to CD8 expression and found that CD8 levels were positively correlated with the survival time (**Figure 6D**, $n = 150$, $P < 0.01$). In validation cohort ($n = 250$), we divided the patients into two groups based on HHLA2 levels and subsequently analyzed CD8 expression. CD8 levels were significantly upregulated in tumor tissues of the HHLA2-high group compared with the HHLA2-low group

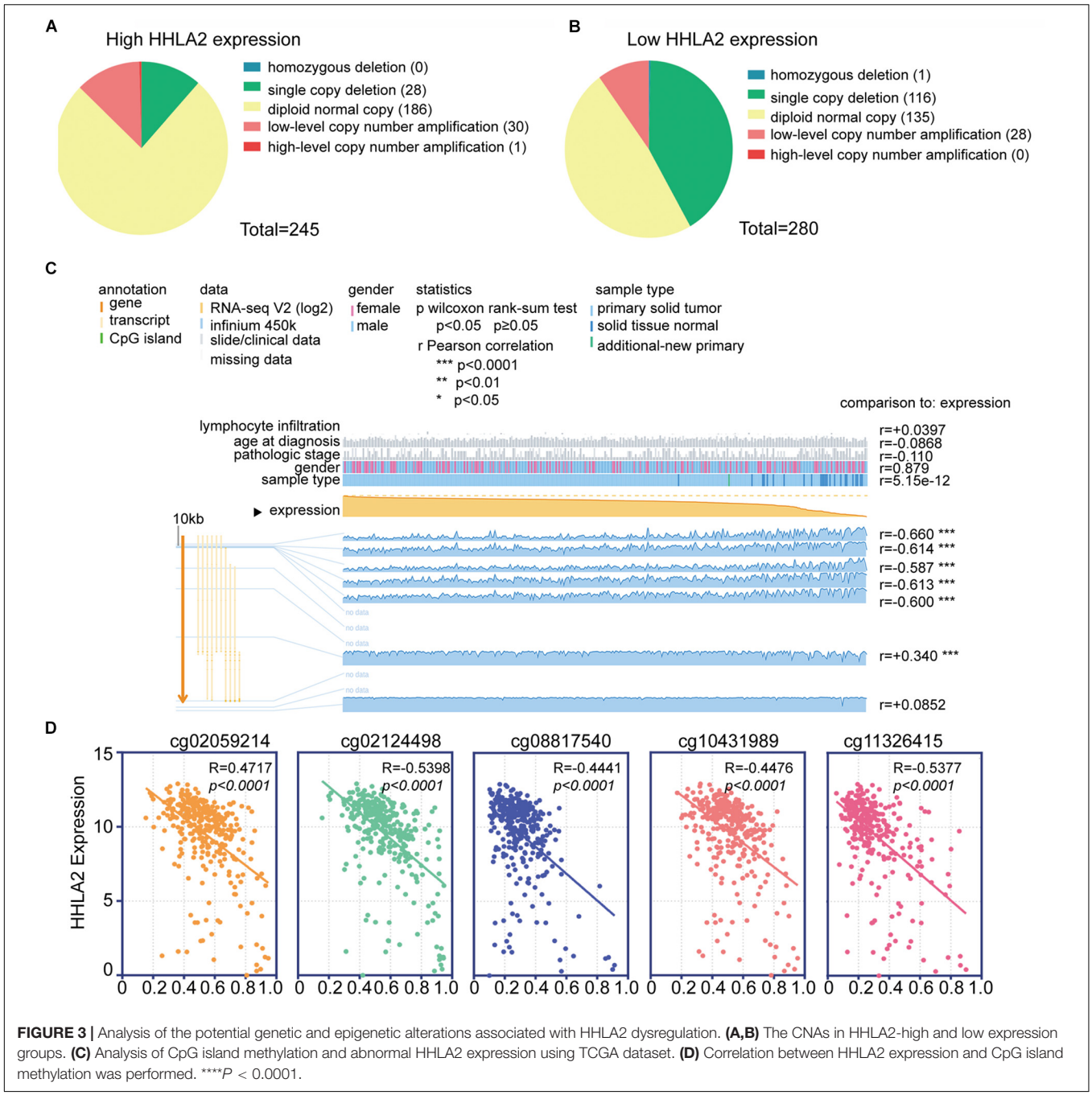

FIGURE 3 | Analysis of the potential genetic and epigenetic alterations associated with HHLA2 dysregulation. **(A,B)** The CNAs in HHLA2-high and low expression groups. **(C)** Analysis of CpG island methylation and abnormal HHLA2 expression using TCGA dataset. **(D)** Correlation between HHLA2 expression and CpG island methylation was performed. ****$P < 0.0001$.

(**Figures 6E,F**, $n = 250$, $P < 0.01$). A similar trend was observed in the validation cohort (**Figure 6G**, $P < 0.0001$). Together, these findings suggested that HHLA2 expression is not associated with CD8, while CD8 expression predicts a good prognosis in KIRC.

DISCUSSION

In the present study, we reported here that HHLA2 can be potentially utilized as a new target for immunotherapy of KIRC. We demonstrated that HHLA2 is widely expressed in a variety of solid tumors, including KIRC, READ, BRCA, and COAD among others. HHLA2 exhibited significantly higher expression in KIRC tumor tissues than in matched normal samples. This abnormal expression may be induced by CNAs or DNA methylation. In tumor sites, HHLA2 expression is positively correlated with survival time. Subsequently, we found that HHLA2 is positively correlated with immune-related activities, but its expression is independent of other B7 and CD28 family members. Finally, by employing clinical samples of patients with KRC, we demonstrated that HHLA2 is positively correlated with

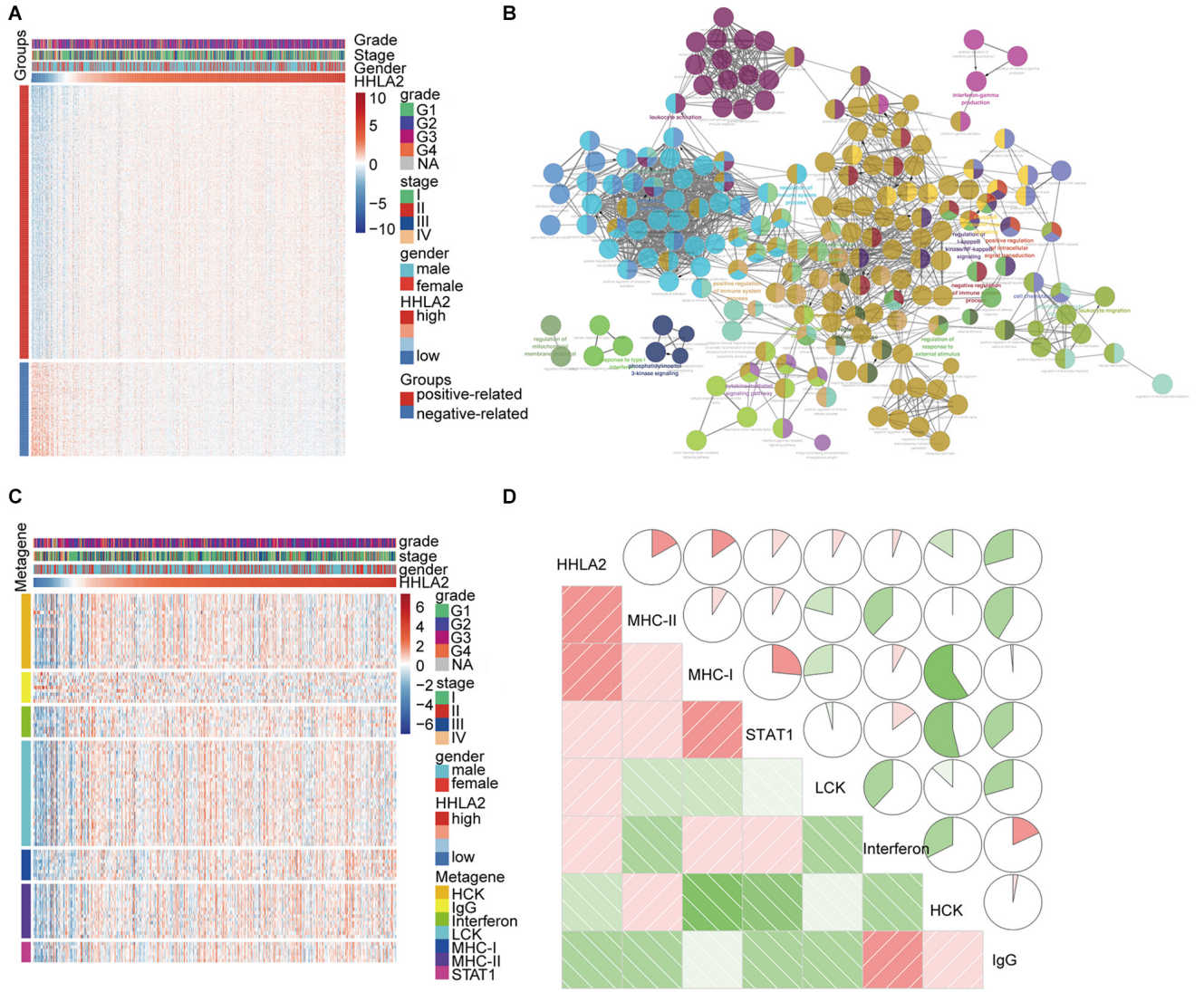

FIGURE 4 | HHLA2 is positively correlated with an inflammatory gene expression profile. **(A)** HHLA2 correlation with inflammatory genes. **(B)** Gene ontology analysis of HHLA2 expression in KIRC. **(C)** HHLA2 correlation with immune responses from clusters derived from the TCGA data. **(D)** Correlation analysis between HHLA2 and immune-related genes using TCGA data.

CD8 and predicts a good prognosis. These findings indicate the prognostic value of HHLA2 in KIRC and highlight it as a potential target in those patients with limited PD-1 or other well-defined immune checkpoint expression.

HHLA2 belongs to the B7 family and conveys coinhibitory or costimulatory signals through binding to its receptors (Janakiram et al., 2015b). Here, we employed TCGA database and TMAs to investigate the expression pattern of HHLA2 in a several cancer types. Our results showed that HHLA2 was widely expressed in multiple tumor types and HHLA2 protein expression was detected in 12 commonly diagnosed tumors, including breast cancer, lung cancer, and others, several cancers such as colon and rectum cancer exhibited HHLA2 levels in tumor sites, which is in contrast to a previous study (Janakiram et al., 2015a). This discrepancy in expression patterns of HHLA2 in tumors may be explained by the different cohorts and the lack of positive correlation with the B7 family. In our study, patients with KIRC showed higher levels of HHLA2 in cancer tissues than in normal kidney tissue, based on TCGA data. Further analysis showed a positive correlation between higher HHLA2 expression and improved OS. In addition, we extended our analysis to TMAs from 90 patients with KIRC. Consistent with the data from the TCGA dataset, the results demonstrated that high HHLA2 levels in tumors were correlated with a better outcome, supporting the prognostic value of HHLA2 in KIRC.

Specific mechanisms, such as CNAs and DNA methylation, are known to regulate the expression of certain immune-related genes (Diaz-Lagares et al., 2016; Chen G. et al., 2019). Here, we found a significant difference in the proportion of CNAs

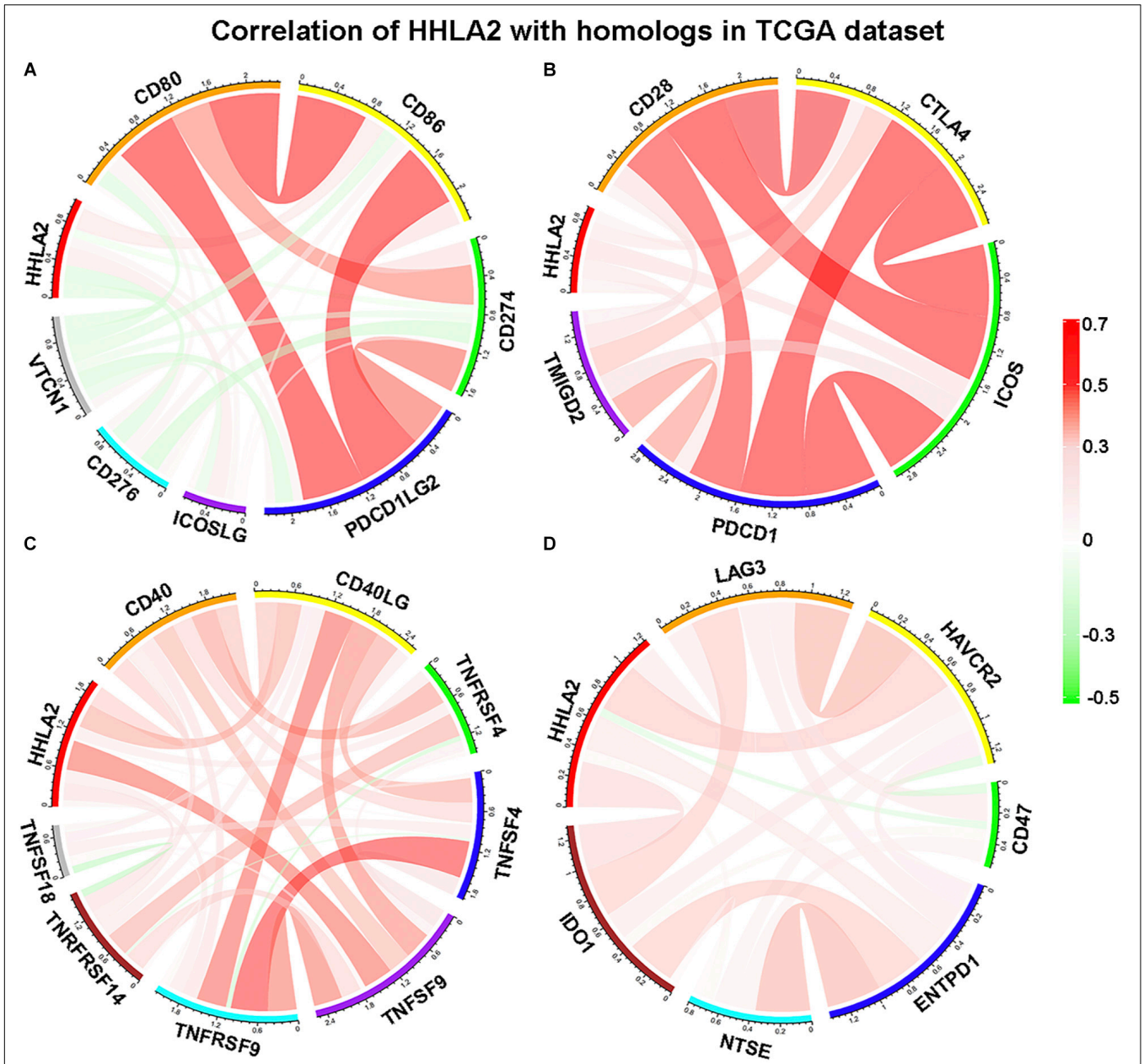

FIGURE 5 | HHLA2 expression is not co-expressed with B7 or CD28 family. The B7 family **(A)**, CD28 family **(B)** and other immune check points **(C,D)** were used to analyze the correlation with HHLA2.

between HHLA2-high and low groups, suggesting that CNAs may contribute to HHLA2 dysfunction. Indeed, the important role of CNAs in immune responses has been previously reported (Miao et al., 2018). Additionally, we observed that increased DNA methylation showed remarkedly correlation with abnormal HHLA2 expression; similarly, a role for DNA methylation in regulating immune response was also previously reported (Aznar et al., 2018). We further revealed that HHLA2 is positively correlated with immune-related responses, such as IFN-γ production and cell chemotaxis. Indeed, the increased expression of HHLA2 on monocytes, macrophages and B cells after stimulation with lipopolysaccharide and IFN-γ has been described (Janakiram et al., 2015b).

Cancer immunotherapy has entered into a new phase since the discovery of drugs that can interfere with specific immune checkpoints. One of the most reported is the checkpoint proteins are PD-1 and its ligand, PD-L1. However, the clinical efficacy of PD-1/PD-L1 monoclonal antibodies relies on their target expression in the tumor microenvironment, exhibiting limited responses in patients with low PD-1/PD-L1 levels (Herbst et al., 2016; Akinleye and Rasool, 2019). Thus, exploring new immune checkpoint targets is important.

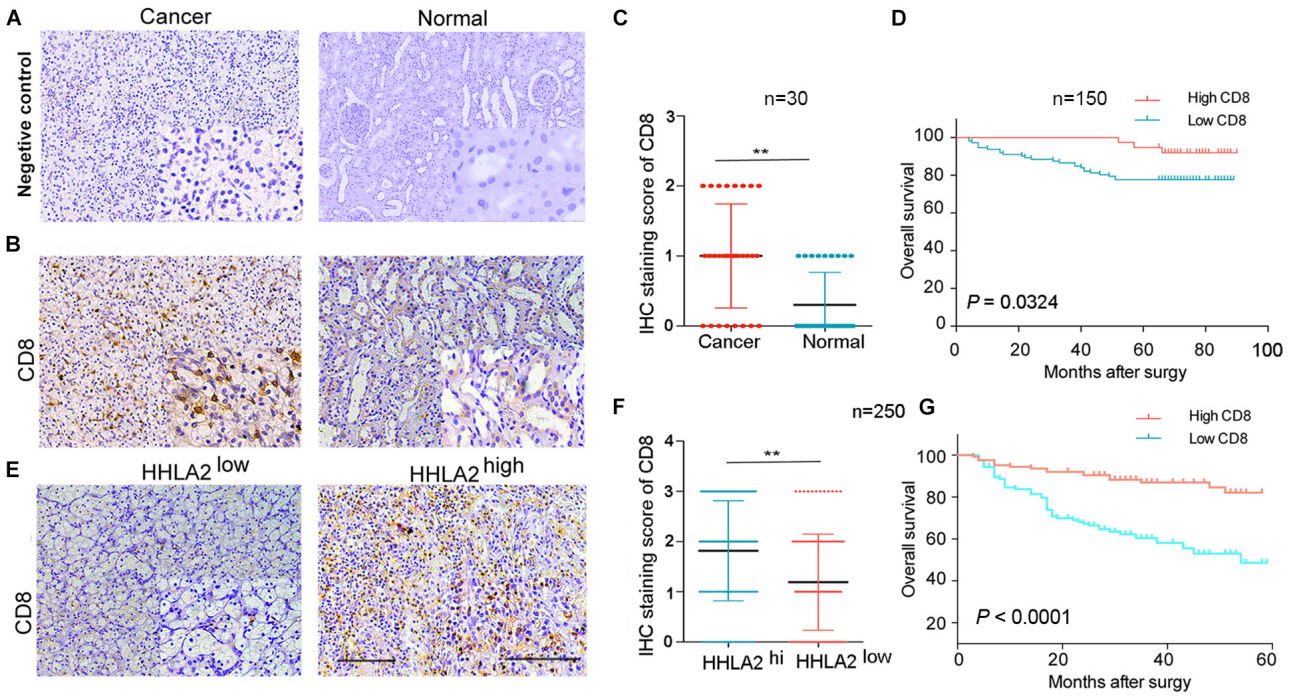

FIGURE 6 | HHLA2 and CD8 are positively correlated with the prognosis of patients with KIRC. **(A)** IHC staining negative control. **(B)** Tumors from a cohort of patients with KIRC (n = 180) were stained for CD8 expression at the protein level. **(C)** IHC score of CD8 in normal and tumor tissues form patients with KIRC (paired, n = 30). **(D)** High CD8 expression is correlated with a good prognosis (n = 150). **(E)** CD8 showed high expression in tumor tissues with high HHLA2 expression. **(F)** IHC score of HHLA2 in tumor tissues form HHLA2-high and low patient groups (n = 250). **(G)** High CD8 expression is correlated with a good prognosis (n = 250). $^{**}P < 0.01$ (two-tailed Student's t-test).

Herein, we found that HHLA2 expression is not co-expressed with other B7 or CD28 family members, suggesting that there are numerous factors involved in immune checkpoint expression. Considering the limited correlation of HHLA2 with other immune checkpoints, HHLA2 may represent a good immunotherapeutic target for patients with low levels of PD-L1 or other well-studied checkpoints.

Several studies have reported that HHLA2 is a negative indicator in colon, lung and pancreatic cancers (Cheng et al., 2017; Zhu and Dong, 2018; Yan et al., 2019). The poor prognostic value of HHLA2 was also reported in clear cell RCC (Chen D. et al., 2019; Chen L. et al., 2019). However, increased HHLA2 expression was associated with better post-surgical prognosis in pancreatic and ampullary cancers when using a different anti-HHLA2 antibody clone for IHC (Boor et al., 2020). Herein, we also observed that HHLA2 is a positive predictor in KIRC. Patients with high HHLA2 showed longer survival rates, contradicting previous studies. In KIRC samples, we observed accumulated $CD8^+$ T cells in KIRC samples, which secrete IFN-γ. The inducible expression of HHLA2 by cytokines (IFN-γ) has been previously reported (Janakiram et al., 2015b), suggesting that the accumulated effector $CD8^+$ T cells can elevate HHLA2 levels. Additionally, HHLA2 was reported to stimulate T cells by interacting with its receptor TMIGD2 (Zhu et al., 2013). Thus, this positive loop between HHLA2 and IFN-γ-secreting $CD8^+$ T cells may contribute to its good prognosis in KIRC. Nevertheless, HHLA2 expression on tumor cells has also been reported to stimulate tumor angiogenesis through interactions with TMIGD2 on the endothelium, which may result in a poor prognosis (Janakiram et al., 2015b). These opposing functions highlight that the expression and distribution of HHLA2 and its receptors may determine the reactions and immune responses in tumor microenvironment, further affecting the prognosis. The different datasets or cohorts used in these studies may also lead to the contradictory prognostic value of HHLA2 in cancers. A similar phenomenon was observed for PD-L1 expression and its prognostic significance in various tumors. In colorectal, breast, and ovary cancers, PD-L1 expression represents a better outcome (Darb-Esfahani et al., 2016; Li et al., 2016; Kitano et al., 2017), whereas worse prognostic outcomes were observed in gastrointestinal, esophageal, and pancreatic cancers as well as glioma and hepatocellular carcinoma (Ohaegbulam et al., 2015; Wang et al., 2016; Liu et al., 2017). This highlights that the prognostic value and clinical significance of HHLA2 expression in various cancers may be complex and affected by many factors. It has also been reported that HHLA2 protein is constitutively expressed on the surface of human monocytes and is induced on B cells (Zhao et al., 2013; Janakiram et al., 2015a). However, the HHLA2 expression in B cells or monocytes was not evaluated in our study. Whether the HHLA2 derived from host cells

has an impact on patient survival remains unclear. Therefore, further research is necessary to determine the impacts on patient survival of HHLA2 expression derived from host and malignant cells.

CONCLUSION

To our knowledge, this is the first work to explore the different prognostic impacts of HHLA2 in solid tumors. We also explored the mechanisms underlying the up-regulation of HHLA2, which predicts a favorable outcome for KIRC. Based on the results, we can speculate that high expression of HHLA2 in KIRC may accompany improved renal function. Furthermore, the positive impact of HHLA2 in KIRC may be explained by a compensatory up-regulation of this molecule in tumor microenvironment, which fights the tumor via an activated immune response. Taking these findings into consideration, immunotherapy based on HHLA2 expression may further improve the prognosis of patients with high HHLA2 expression.

Our study has several limitations. The exact mechanism underlying HHLA2 expression dysfunction was not well-illustrated, which warrants further research. Moreover, there was a limited investigation of HHLA2 receptors as we mainly focused on HHLA2 itself. Nevertheless, this study is the first to show that HHLA2, a newly discovered immune checkpoint ligand, is highly expressed in KIRC and predicts a good prognosis, suggesting it as a potential therapeutic target for patients with KIRC in the clinic.

DATA AVAILABILITY STATEMENT

Publicly available datasets were analyzed in this study. This data can be found here: https://genomecancer.ucsc.edu/.

ETHICS STATEMENT

The studies involving human participants were reviewed and approved by Ethics Committee of First Affiliated Hospital of Zhengzhou. The patients/participants provided their written informed consent to participate in this study.

AUTHOR CONTRIBUTIONS

YZ and XZ conceived and designed this project. ZZ and JL performed experiments and acquired data. ZZ, JL, CZ, FL, LL, DW, DC, and FG analyzed data. All authors participated in writing or revising the manuscript.

FUNDING

This work was supported by grants from the National Key Research and Development Program of China (Grant No. 2018YFC1313400) and the National Natural Science Foundation of China (Grant Nos. U1804281 and 81771781).

REFERENCES

Abril-Rodriguez, G., and Ribas, A. (2017). SnapShot: immune checkpoint inhibitors. *Cancer Cell* 31, 848.e1–848.e1. doi: 10.1016/j.ccell.2017.05.010

Akinleye, A., and Rasool, Z. (2019). Immune checkpoint inhibitors of PD-L1 as cancer therapeutics. *J. Hematol. Oncol.* 12:92. doi: 10.1186/s13045-019-0779-775

Aznar, M. A., Labiano, S., Diaz-Lagares, A., Molina, C., Garasa, S., Azpilikueta, A., et al. (2018). CD137 (4-1BB) costimulation modifies DNA methylation in CD8(+) T cell-relevant genes. *Cancer Immunol. Res.* 6, 69–78. doi: 10.1158/2326-6066.cir-17-0159

Boor, P. P. C., Sideras, K., Biermann, K., Hosein Aziz, M., Levink, I. J. M., Mancham, S., et al. (2020). HHLA2 is expressed in pancreatic and ampullary cancers and increased expression is associated with better post-surgical prognosis. *Br. J. Cancer* 8, 1211–1218. doi: 10.1038/s41416-020-0755-754

Cervera-Carrascon, V., Santos, J., Siurala, M., Havunen, R., Sorsa, S., and Hemminki, A. (2017). 51P Delivering complete responses against solid tumors by checkpoint blockade enabled with tumor necrosis factor alpha and interleukin-2 armed adenoviruses. *Oncoimmunology* 28(Suppl._11):mdx711.032.

Chau, I. (2017). Clinical development of PD-1/PD-L1 immunotherapy for gastrointestinal cancers: facts and hopes. *Clin. Cancer Res.* 23, 6002–6011. doi: 10.1158/1078-0432.ccr-17-0020

Chen, D., Chen, W., Xu, Y., Zhu, M., Xiao, Y., Shen, Y., et al. (2019). Upregulated immune checkpoint HHLA2 in clear cell renal cell carcinoma: a novel prognostic biomarker and potential therapeutic target. *J. Med. Genet.* 56, 43–49. doi: 10.1136/jmedgenet-2018-105454

Chen, G., Chen, H., Ren, S., Xia, M., Zhu, J., Liu, Y., et al. (2019). Aberrant DNA methylation of mTOR pathway genes promotes inflammatory activation of immune cells in diabetic kidney disease. *Kidney Int.* 96, 409–420. doi: 10.1016/j.kint.2019.02.020

Chen, L., Zhu, D., Feng, J., Zhou, Y., Wang, Q., Feng, H., et al. (2019). Overexpression of HHLA2 in human clear cell renal cell carcinoma is significantly associated with poor survival of the patients. *Cancer Cell Int.* 19:101.

Chen, W., Hill, H., Christie, A., Kim, M. S., Holloman, E., Pavia-Jimenez, A., et al. (2016). Targeting renal cell carcinoma with a HIF-2 antagonist. *Nature* 539, 112–117. doi: 10.1038/nature19796

Chen, X., Wang, L., Li, P., Song, M., Qin, G., Gao, Q., et al. (2018). Dual TGF-beta and PD-1 blockade synergistically enhances MAGE-A3-specific CD8(+) T cell response in esophageal squamous cell carcinoma. *Int. J. Cancer* 143, 2561–2574. doi: 10.1002/ijc.31730

Cheng, H., Janakiram, M., Borczuk, A., Lin, J., Qiu, W., Liu, H., et al. (2017). HHLA2, a new immune checkpoint member of the B7 family, is widely expressed in human lung cancer and associated with EGFR mutational status. *Clin. Cancer Res.* 23, 825–832. doi: 10.1158/1078-0432.ccr-15-3071

Curtis, C., Shah, S. P., Chin, S. F., Turashvili, G., Rueda, O. M., Dunning, M. J., et al. (2012). The genomic and transcriptomic architecture of 2,000 breast tumours reveals novel subgroups. *Nature* 486, 346–352. doi: 10.1038/nature10983

Darb-Esfahani, S., Kunze, C. A., Kulbe, H., Sehouli, J., Wienert, S., Lindner, J., et al. (2016). Prognostic impact of programmed cell death-1 (PD-1) and PD-ligand 1 (PD-L1) expression in cancer cells and tumor-infiltrating lymphocytes in ovarian high grade serous carcinoma. *Oncotarget* 7:1486.

Diaz-Lagares, A., Crujeiras, A. B., Lopez-Serra, P., Soler, M., Setien, F., Goyal, A., et al. (2016). Epigenetic inactivation of the p53-induced long noncoding RNA TP53 target 1 in human cancer. *Proc. Natl. Acad. Sci. U.S.A.* 113, E7535–E7544. doi: 10.1073/pnas.1608585113

Ferlay, J., Soerjomataram, I., Dikshit, R., Eser, S., Mathers, C., Rebelo, M., et al. (2015). Cancer incidence and mortality worldwide: sources, methods and major patterns in GLOBOCAN 2012. *Int. J. Cancer* 136, E359–E386. doi: 10.1002/ijc.29210

Han, G., Zhao, W., Song, X., Kwok-Shing Ng, P., Karam, J. A., Jonasch, E., et al. (2017). Unique protein expression signatures of survival time in kidney renal clear cell carcinoma through a pan-cancer screening. *BMC Genomics* 18(Suppl. 6):678. doi: 10.1186/s12864-017-4026-4026

Hato, T., Goyal, L., Greten, T. F., Duda, D. G., and Zhu, A. X. (2014). Immune checkpoint blockade in hepatocellular carcinoma: current progress and future directions. *Hepatology* 60, 1776–1782. doi: 10.1002/hep.27246

Herbst, R. S., Baas, P., Kim, D.-W., Felip, E., Pérez-Gracia, J. L., Han, J.-Y., et al. (2016). Pembrolizumab versus docetaxel for previously treated, PD-L1-positive, advanced non-small-cell lung cancer (KEYNOTE-010): a randomised controlled trial. *Lancet* 387, 1540–1550. doi: 10.1016/s0140-6736(15)01281-7

Hirano, F., Kaneko, K., Tamura, H., Dong, H., Wang, S., Ichikawa, M., et al. (2005). Blockade of B7-H1 and PD-1 by monoclonal antibodies potentiates cancer therapeutic immunity. *Cancer Res.* 65, 1089–1096.

Janakiram, M., Chinai, J. M., Fineberg, S., Fiser, A., Montagna, C., Medavarapu, R., et al. (2015a). Expression, clinical significance, and receptor identification of the Newest B7 family member HHLA2 protein. *Clin. Cancer Res.* 21, 2359–2366. doi: 10.1158/1078-0432.ccr-14-1495

Janakiram, M., Chinai, J. M., Zhao, A., Sparano, J. A., and Zang, X. (2015b). HHLA2 and TMIGD2: new immunotherapeutic targets of the B7 and CD28 families. *Oncoimmunology* 4:e1026534. doi: 10.1080/2162402x.2015.1026534

Janakiram, M., Shah, U. A., Liu, W., Zhao, A., Schoenberg, M. P., and Zang, X. (2017). The third group of the B7-CD 28 immune checkpoint family: HHLA 2, TMIGD 2, B7x, and B7-H3. *Immunol. Rev.* 276, 26–39. doi: 10.1111/imr.12521

Kitano, A., Ono, M., Yoshida, M., Noguchi, E., Shimomura, A., Shimoi, T., et al. (2017). Tumour-infiltrating lymphocytes are correlated with higher expression levels of PD-1 and PD-L1 in early breast cancer. *ESMO Open* 2:e000150. doi: 10.1136/esmoopen-2016-000150

Koirala, P., Roth, M. E., Gill, J., Chinai, J. M., Ewart, M. R., Piperdi, S., et al. (2016). HHLA2, a member of the B7 family, is expressed in human osteosarcoma and is associated with metastases and worse survival. *Sci. Rep.* 6:31154. doi: 10.1038/srep31154

Li, Y., Liang, L., Dai, W., Cai, G., Xu, Y., Li, X., et al. (2016). Prognostic impact of programed cell death-1 (PD-1) and PD-ligand 1 (PD-L1) expression in cancer cells and tumor infiltrating lymphocytes in colorectal cancer. *Mol. Cancer* 15:55.

Li, Z., Song, W., Rubinstein, M., and Liu, D. (2018). Recent updates in cancer immunotherapy: a comprehensive review and perspective of the 2018 China Cancer Immunotherapy Workshop in Beijing. *J. Hematol. Oncol.* 11:142. doi: 10.1186/s13045-018-0684-683

Liu, Y., Cheng, Y., Xu, Y., Wang, Z., Du, X., Li, C., et al. (2017). Increased expression of programmed cell death protein 1 on NK cells inhibits NK-cell-mediated anti-tumor function and indicates poor prognosis in digestive cancers. *Oncogene* 36, 6143–6153. doi: 10.1038/onc.2017.209

Marin-Acevedo, J. A., Dholaria, B., Soyano, A. E., Knutson, K. L., Chumsri, S., and Lou, Y. (2018a). Next generation of immune checkpoint therapy in cancer: new developments and challenges. *J. Hematol. Oncol.* 11:39. doi: 10.1186/s13045-018-0582-588

Marin-Acevedo, J. A., Soyano, A. E., Dholaria, B., Knutson, K. L., and Lou, Y. (2018b). Cancer immunotherapy beyond immune checkpoint inhibitors. *J. Hematol. Oncol.* 11:8. doi: 10.1186/s13045-017-0552-556

McKinney, E. F., Lyons, P. A., Carr, E. J., Hollis, J. L., Jayne, D. R., Willcocks, L. C., et al. (2010). A CD8+ T cell transcription signature predicts prognosis in autoimmune disease. *Nat. Med.* 16, 586–591. doi: 10.1038/nm.2130

Miao, D., Margolis, C. A., Vokes, N. I., Liu, D., Taylor-Weiner, A., Wankowicz, S. M., et al. (2018). Genomic correlates of response to immune checkpoint blockade in microsatellite-stable solid tumors. *Nat. Genet.* 50, 1271–1281. doi: 10.1038/s41588-018-0200-2

Nocito, A., Kononen, J., Kallioniemi, O. P., and Sauter, G. (2001). Tissue microarrays (TMAs) for high-throughput molecular pathology research. *Int. J. Cancer* 94, 1–5. doi: 10.1002/ijc.1385

Ohaegbulam, K. C., Assal, A., Lazar-Molnar, E., Yao, Y., and Zang, X. (2015). Human cancer immunotherapy with antibodies to the PD-1 and PD-L1 pathway. *Trends Mol. Med.* 21, 24–33. doi: 10.1016/j.molmed.2014.10.009

Pardoll, D. M. (2012). The blockade of immune checkpoints in cancer immunotherapy. *Nat. Rev. Cancer* 12, 252–264. doi: 10.1038/nrc3239

Ribas, A., and Wolchok, J. D. (2018). Cancer immunotherapy using checkpoint blockade. *Science* 359, 1350–1355. doi: 10.1126/science.aar4060

Schildberg, F. A., Klein, S. R., Freeman, G. J., and Sharpe, A. H. (2016). Coinhibitory pathways in the B7-CD28 ligand-receptor family. *Immunity* 44, 955–972. doi: 10.1016/j.immuni.2016.05.002

Schumacher, T. N., and Schreiber, R. D. (2015). Neoantigens in cancer immunotherapy. *Science* 348, 69–74. doi: 10.1126/science.aaa4971

Shi, X., Zhang, D., Li, F., Zhang, Z., Wang, S., Xuan, Y., et al. (2019). Targeting glycosylation of PD-1 to enhance CAR-T cell cytotoxicity. *J. Hematol. Oncol.* 12:127. doi: 10.1186/s13045-019-0831-835

Shuch, B., Amin, A., Armstrong, A. J., Eble, J. N., Ficarra, V., Lopez-Beltran, A., et al. (2015). Understanding pathologic variants of renal cell carcinoma: distilling therapeutic opportunities from biologic complexity. *Eur. Urol.* 67, 85–97. doi: 10.1016/j.eururo.2014.04.029

Topalian, S. L., Hodi, F. S., Brahmer, J. R., Gettinger, S. N., Smith, D. C., McDermott, D. F., et al. (2012). Safety, activity, and immune correlates of anti-PD-1 antibody in cancer. *N. Engl. J. Med.* 366, 2443–2454. doi: 10.1056/NEJMoa1200690

Ville, S., Poirier, N., Blancho, G., and Vanhove, B. (2015). Co-stimulatory blockade of the CD28/CD80-86/CTLA-4 balance in transplantation: impact on memory T cells? *Front. Immunol.* 6:411. doi: 10.3389/fimmu.2015.00411

Wang, Z., Zhang, C., Liu, X., Wang, Z., Sun, L., Li, G., et al. (2016). Molecular and clinical characterization of PD-L1 expression at transcriptional level via 976 samples of brain glioma. *Oncoimmunology* 5:e1196310. doi: 10.1080/2162402x.2016.1196310

Yan, H., Qiu, W., de Gonzalez, A. K. K., Wei, J.-S., Tu, M., Xi, C.-H., et al. (2019). HHLA2 is a novel immune checkpoint protein in pancreatic ductal adenocarcinoma and predicts post-surgical survival. *Cancer Lett.* 442, 333–340. doi: 10.1016/j.canlet.2018.11.007

Yu, G. T., Bu, L. L., Zhao, Y. Y., Mao, L., Deng, W. W., Wu, T. F., et al. (2016). CTLA4 blockade reduces immature myeloid cells in head and neck squamous cell carcinoma. *Oncoimmunology* 5:e1151594. doi: 10.1080/2162402x.2016.1151594

Zhang, Z., Liu, S., Zhang, B., Qiao, L., Zhang, Y., and Zhang, Y. (2020). T cell dysfunction and exhaustion in cancer. *Front. Cell. Dev. Biol.* 8:17. doi: 10.3389/fcell.2020.00017

Zhao, R., Chinai, J. M., Buhl, S., Scandiuzzi, L., Ray, A., Jeon, H., et al. (2013). HHLA2 is a member of the B7 family and inhibits human CD4 and CD8 T-cell function. *Proc. Natl. Acad. Sci. U.S.A.* 110, 9879–9884. doi: 10.1073/pnas.1303524110

Zhu, Y., Yao, S., Iliopoulou, B. P., Han, X., Augustine, M. M., Xu, H., et al. (2013). B7-H5 costimulates human T cells via CD28H. *Nat. Commun.* 4:2043. doi: 10.1038/ncomms3043

Zhu, Z., and Dong, W. (2018). Overexpression of HHLA2, a member of the B7 family, is associated with worse survival in human colorectal carcinoma. *Onco Targets Ther.* 11, 1563–1570. doi: 10.2147/OTT.S160493

Conflict of Interest: XZ is an inventor on patent number US10093737 (HHLA2 as a novel inhibitor of human immune system and uses thereof) and patent number US 10280208 (TMIGD2 and its derivatives as blockers or binders of cancer-expressed HHLA2 for immunotherapies).

The remaining authors declare that the research was conducted in the absence of any commercial or financial relationships that could be construed as a potential conflict of interest.

frontiers in Cell and Developmental Biology

REVIEW
published: 03 June 2020
doi: 10.3389/fcell.2020.00434

Molecular Mechanisms of Cardiomyocyte Death in Drug-Induced Cardiotoxicity

Wanjun Ma[1,2], *Shanshan Wei*[1,2], *Bikui Zhang*[1,2]* *and Wenqun Li*[1,2]*

[1] *Department of Pharmacy, The Second Xiangya Hospital, Central South University, Changsha, China,* [2] *Institute of Clinical Pharmacy, Central South University, Changsha, China*

Homeostatic regulation of cardiomyocytes plays a crucial role in maintaining the normal physiological activity of cardiac tissue. Severe cardiotoxicity results in cardiac diseases including but not limited to arrhythmia, myocardial infarction and myocardial hypertrophy. Drug-induced cardiotoxicity limits or forbids further use of the implicated drugs. Such drugs that are currently available in the clinic include anti-tumor drugs (doxorubicin, cisplatin, trastuzumab, etc.), antidiabetic drugs (rosiglitazone and pioglitazone), and an antiviral drug (zidovudine). This review focused on cardiomyocyte death forms and related mechanisms underlying clinical drug-induced cardiotoxicity, including apoptosis, autophagy, necrosis, necroptosis, pryoptosis, and ferroptosis. The key proteins involved in cardiomyocyte death signaling were discussed and evaluated, aiming to provide a theoretical basis and target for the prevention and treatment of drug-induced cardiotoxicity in the clinical practice.

Keywords: cardiotoxicity, cardiomyocytes, cell death, apoptosis, autophagy, necrosis

OPEN ACCESS

Edited by:
Lawrence H. Boise,
Emory University, United States

Reviewed by:
Darren Finlay,
Sanford-Burnham Institute for Medical Research, United States
Chunying Li,
Georgia State University, United States

***Correspondence:**
Bikui Zhang
505995@csu.edu.cn
Wenqun Li
liwq1204@csu.edu.cn

Specialty section:
This article was submitted to Cell Death and Survival, a section of the journal Frontiers in Cell and Developmental Biology

Received: *01 March 2020*
Accepted: *08 May 2020*
Published: *03 June 2020*

Citation:
Ma W, Wei S, Zhang B and Li W (2020) Molecular Mechanisms of Cardiomyocyte Death in Drug-Induced Cardiotoxicity. Front. Cell Dev. Biol. 8:434. doi: 10.3389/fcell.2020.00434

INTRODUCTION

Cardiotoxicity commonly refers to toxicity that has a detrimental impact on the heart, which might finally lead to myocardiopathy such as arrhythmia, myocardial infarction and myocardial hypertrophy. These inevitable side effects, especially of anticancer drugs, are usually the main causes of treatment termination and drug development failure. In addition, modern cancer treatments recommend a combination of multiple agents, almost always leading to synergistic side-effects (Ewer and Ewer, 2015). In the past few decades, more than 10% of clinical drugs were forced out of the market due to cardiovascular side effects, which still hindered the drug development and seriously affected the improvement of patient health. Many studies have revealed that drug-induced myocardial damage may be a stepwise process accompanied by the increase of cardiac biomarkers and structural myocardial deformation, finally resulting in left ventricular ejection fraction (LVEF) decrease (Pistillucci et al., 2015; Patel and Cornell, 2019). Currently, the widely accepted definition of cardiotoxicity is the decline in LVEF of at least 10% to less than 55% (Nicol et al., 2019). Clinical data show that cardiomyocyte death or damage concomitantly takes place with the progression of cardiotoxicity, indicating that drug-induced cardiomyocyte death may be the main cause of cardiotoxicity.

OVERVIEW OF CELL DEATH FORMS

It is widely accepted that cell death, proliferation and differentiation are essential throughout the pathological and physiological processes. Although more than ten types of cell death have been discovered to date, the most common forms of cell death in drug-induced cardiotoxicity are apoptosis, autophagy and necrosis (Galluzzi et al., 2018). In addition, recently discovered cell death forms, such as necroptosis, pyroptosis and ferroptosis, are also involved in drug-induced cardiotoxicity.

Apoptosis

Morphologically, apoptosis is the most widely studied cell death form, exhibiting signs of cell shrinkage, increased cytoplasmic density, decreased mitochondrial membrane potential (MMP) disappearance and changes in permeability. Eventually, intact apoptotic bodies are formed to be efficiently absorbed and degraded by adjacent cells. Based on the underlying mechanisms, apoptosis is divided into intrinsic and extrinsic apoptosis. Intrinsic apoptosis is caused by microenvironment disorders such as DNA damage, excessive oxidative stress, mitotic disaster, loss of growth factor signaling and endoplasmic reticulum (ER) stress (Brumatti et al., 2010; Wu and Bratton, 2013; Czabotar et al., 2014; Roos et al., 2016). B cell lymphoma-2 (Bcl-2) family pro-apoptotic members, such as Bax, Bak, and BH3-only protein, primarily regulate the intrinsic cell apoptosis via their influence on mitochondria. Bcl-2 stimulates mitochondria translocation of Bax/Bak and causes mitochondrial membrane permeabilization, which eventually leads to the release of cytochrome C in the cytoplasm, where the apoptosome forms and caspases cascade reactions arise (Hutt, 2015). Unlike intrinsic apoptosis, the extrinsic apoptosis is mainly initiated by two kinds of plasma membrane receptors including Fas cell surface death receptor (Fas) and tumor necrosis factor receptor (TNF) super family member (TNFR1, TNFRSF10A, and TNFRSF10B) along with their respective homologous ligands. Death-inducing signaling complex (DISC), composed of death ligands and corresponding receptors on the cell membrane, is a receptor proximal protein complex that helps connect the death receptor signaling with caspases cascade reactions. The pro-apoptotic proteins caspase-8 and caspase-10 are recruited and cleaved by upstream caspase enzyme to initiate apoptosis (Barnhart et al., 2003; Yang, 2015).

Autophagy

As a pro-survival mechanism, autophagy occurs in destroying and recovering unwanted or damaged cellular components, playing an essential role in maintaining intracellular metabolic homeostasis (Yang et al., 2017). A series of evidences suggest that the autophagy-activating kinase 1 (ULK-1) initiates autophagy by phosphorylating Beclin1 and activating the vacuolar protein sorting 34 (VPS34) complex (Klionsky et al., 2016). As a critical signaling protein of autophagy, the mammalian target of rapamycin (mTOR) can be activated by nutritional deficiency, growth factor and receptor tyrosine kinase, which subsequently forms mammalian target of rapamycin complex 1 (mTORC1) with several other proteins. The mTORC1 further binds to the ULK-1 complex and blocks ULK-1-mediated Beclin 1 phosphorylation, thus inhibiting autophagy initiation (Jung et al., 2010). In contrast, the adenosine 5-monophosphate activated protein kinase (AMPK) mediates autophagy by decreasing mTOR-related autophagy suppression and phosphorylating the ULK-1 complex at Ser317 and Ser777 (Kim et al., 2011).

Necrosis

In the past few decades, necrosis is typically described as a form of passive and irreversible cell death that is always associated with pathology, usually accompanied by morphological characteristics such as increased membrane permeability, disintegration of organelles and cell swelling. As a traditional cell death form, necrosis occurs usually after the exposure to extreme physical or chemical insults, and therefore is regarded as an accident and unregulated cell death form. With in-depth study, more regulated cell death forms are proposed, including necroptosis, pryoptosis and ferroptosis, which share similar morphological characteristics with necrosis.

Other Regulated Cell Death Forms: Necroptosis, Pryoptosis, and Ferroptosis

In contrast to necrosis, necroptosis is regulated by specific transduction mechanism. Death receptor TNFR1 plays a key role in the development of necroptosis (Kaiser et al., 2013). Activation of TNFR1 can stimulate RIPK1 to further recruit RIPK3 that leads to necrosomes formation (Grootjans et al., 2017). In addition, sequential activation of RIPK3/MLKL is also crucial in necroptosis signaling (Song and Wang, 2013). Phosphorylated MLKL can destroy the plasma membrane and organelles to release inflammatory factors, and elicit an immune response, indicating the occurrence of necroptosis (Galluzzi et al., 2018). It is worth mentioning that caspase-8 plays a suppressing role in necroptosis since it inactivates RIPK1 and RIPK3 (Belmonte et al., 2015; Tummers and Green, 2017).

Pyroptosis, firstly proposed by Cooksonis, is widely recognized as inflammatory and regulated cell death form that usually occurs in defense of exogenous pathogens such as virus, bacteria and fungi (Cookson and Brennan, 2001; Jorgensen and Miao, 2015). Activation of caspases including caspase-1, caspase-3, caspase-4 and caspase-11 is necessary for initiating the pyroptosis, which further specifically cleaves GSDMD or GSDME to generate holes in the membrane and release interleukin-1beta (IL-1β) and IL-18, inducing pyroptosis (Shi et al., 2015; Man et al., 2017). Recent studies have identified a potential relationship between pyroptosis and myocardial injury (Chen et al., 2018).

Unlike pyroptosis, ferroptosis is firstly discovered in carcinoma cells and characterized by the accumulation of iron and lipid reactive oxygen species (ROS), which could deplete anti-oxidases and cause mitochondrial damages, leading to cell death (Sumneang et al., 2020). Moreover, Chen et al. (2019) found that the inhibition of Toll like receptor 4 (TLR4) and triphosphopyridine nucleotide oxidase 4 (NOX4) significantly alleviated ferroptosis. Glutathione peroxidase 4 (GPx4) can

prevent erastin and RSL3-induced ferroptosis via suppressing lipid peroxidation (Imai et al., 2017).

CARDIOMYOCYTE DEATH IN DRUG-INDUCED CARDIOTOXICITY

Multiple evidences have suggested that there is a strong correlation between drug-induced cardiomyocyte death and cardiotoxicity. Here, we will summarize and discuss cardiomyocyte death induced by the drugs listed in **Table 1** and their underlying cell death mechanisms shown in **Figure 1**.

Anticancer Drugs

Doxorubicin (DOX)

Apoptosis

Enhanced production of ROS is recognized as the classic mechanism of DOX induced cardiomyocyte death. ROS consists of both free radicals and non-free radicals derived from oxygen, including superoxide anions (O_2^-), hydrogen peroxide (H_2O_2), hydroxyl radicals (OH^-), ozone (O_3) and singlet oxygen ($^1O_2$) (Zorov et al., 2014). DOX can be reduced to semiquinone by the endothelial nitric oxide synthase (eNOS) and triphosphopyridine nucleotide (NADPH) oxidase, which in turn leads to production of O_2^-, a major free radical that can produce other ROS, such as H_2O_2 and hydroxyl radicals ($OH^·$) (Vasquez-Vivar et al., 1997). This is the main pathway by which DOX treatment generates ROS. Moreover, Deng et al. (2007) found that reactions between DOX and NADPH could produce superoxide in the absence of any enzyme activity, suggesting ROS production may be caused by the chemical interaction of DOX and NADPH. The generated ROS further induced DNA damage, especially DNA single-strand breaks. Previous studies showed that DOX treatment suppressed the DNA binding activity of GATA binding protein 4 (GATA4), an oxidant-sensitive transcription factor that plays an important role in transducing nuclear events (Kim et al., 2003). *In vitro*, DNA breaks activated nuclear poly ADP-ribose polymerase 1 (PARP-1) to induce the synthesis of poly-ADP-ribose and cause ATP consumption by subsequent glycohydrolase reactions and ATP conversion, leading to the collapse of heart energy metabolism (Mukhopadhyay et al., 2009). Scaffold protein Sirt6 was proved to be protective against DOX-induced DNA damage (Brito et al., 2016). In addition to DNA damage, DOX-induced intracellular ion disorder also contributes to ROS production.

A previous study demonstrated that under aerobic conditions, DOX could automatically combine with iron to form DOX-iron complex, which increased the contents of OH^- by self-reduction, contributing to subsequent lipid peroxidation through membrane interactions (Malisza and Hasinoff, 1995). Another study also discovered that the levels of iron and ROS were up-regulated in DOX-treated cardiomyocytes, which finally induced the mitochondrial apoptosis through caspase-3 activation and cytochrome C release (Childs et al., 2002). The participation of intracellular iron in the degradation of hypoxia-inducible factors (HIF) has been demonstrated (Peyssonnaux et al., 2008). Latter research indicated that iron/HIF signaling mediated the cardio-protective effect of dexrazoxane, the unique authorized protectant for DOX-induced cardiotoxicity (Spagnuolo et al., 2011). Paradoxically, DOX-induced ROS increased the synthesis of ferritin and mediated the protective effect of DOX against iron-induced cardiotoxicity (Corna et al., 2004).

In addition, topoisomerase 2 beta (Top2β) was found to involve in ROS formation during DOX treatment (Vejpongsa and Yeh, 2014). Topoisomerase 2 (Top2), consisting of Top2α and Top2β, played a crucial role in DNA replication, transcription, and repair (Wang, 2002). Top2 was considered a target for the anticancer effect of anthracyclines (Zhu et al., 2016). Top2β interaction with DOX caused DNA double-strand breaks and further triggered transcriptome changes in cardiomyocytes (Zhang et al., 2012). The DOX-Top2β combination may inhibit the transcription of peroxisome proliferator-activated receptor gamma coactivator-1 (PGC1) including PGC1α and PGC1β, which play critical roles in mitochondrial biogenesis as antioxidant (Finkel, 2006; Finck and Kelly, 2007). Moreover, mice with cardiomyocyte-specific Top2β conditional knockout ($Top2\beta^{-/-}$) presented less DNA damage and mitochondrial dysfunction as well as oxidative phosphorylation after DOX exposure (Zhang et al., 2012).

Doxorubicin-induced oxidative stress can also stimulate death reporters to combine with corresponding cognate ligands, thereby inducing assembly of the DISC complex, which in turn caused caspase cascades activations and substrates cleavages. A recent study showed that the four death reporters (Fas, TNFR1, DR4, and DR5) were significant increased at the mRNA and protein levels after DOX treatment in induced pluripotent stem cells (iPS) -derived cardiomyocytes (Zhao and Zhang, 2017). One study suggested that ROS-induced up-regulation of cytosolic calcium concentration further elevated the expression of Fas Ligand (Fas L) by stimulating the nuclear factor of activated T-cells (NFAT) signaling (Kalivendi et al., 2005). Moreover, the calcium and calmodulin can conversely bind with eNOS electrons to increase superoxide formation, exacerbating cardiotoxicity (Vasquez-Vivar et al., 1998). Additionally, cardiac fibroblasts exacerbated cardiomyocyte apoptosis by releasing exosomes carrying Fas L in a paracrine manner during DOX treatment. Rosmarinic acid was shown to decrease Fas L secretion by suppressing the level of NFAT activation and metalloproteinase 7 (MMP7) expressions in cardiac fibroblasts, and served a protective role (Zhang et al., 2019). Preclinical experiments demonstrated a decrease in cardiomyocyte death of rats treated with anti-Fas L antibody (Nakamura et al., 2000). Moreover, caspase-8 inhibition blocked Fas L-induced apoptosis, indicating that downstream signaling of apoptosis was mediated by Fas L (Yamaoka et al., 2000). The matricellular protein CCN1 triggered by DOX reacted with integrin $\alpha_6\beta_1$ to promote the activation of p38 mitogen-activated protein kinase (p38-MAPK), which stimulated the release of second mitochondrial activator of caspase (SMAC) and high-temperature requirement protein A2 (HtrA2), synergizing with Fas L to induce cardiomyocytes apoptosis (Hsu and Mo, 2016). As an important receptor in extrinsic apoptosis, TNFR1 was also involved in DOX-related cardiomyocyte death. DOX changed the level of TNFα in H9c2 cells, leading to an increase in TNFR1 expression and a decrease in TNFR2 expression, accompanied by the activation

TABLE 1 | Molecular mechanisms of cardiomyocyte death in drug-induced cardiotoxicity.

Drug type	Drugs	Cell death type	Cell type/animal	Mechanism	References
Anticancer drug	Doxorubicin	Apoptosis	C57BL/6J mice	Cytochrome P450-NADPH-ROS↑-DNA damage	Deng et al., 2007
			Adult cardiac myocytes, HL-1 cardiac muscle cells	GATA4↓-DNA damage	Kim et al., 2003
			Cardiomyocytes; C57BL/6J mice	ROS↑, RNS↑-PARP-1-ATP↓	Mukhopadhyay et al., 2009
			Sprague Dawley (SD) rats	Fe↑-ROS↑-Bcl-2/Bax↓-caspase-3↑, Cytochrome C↑	Childs et al., 2002
			Cardiomyocytes; Mice	Top2β-DNA damage-ROS↑	Zhang et al., 2012
			Pluripotent stem cells-derived cardiomyocytes	TNFR1↑, Fas↑, DR4↑, DR5↑, TRAIL↑	Zhao and Zhang, 2017
			Adult rat cardiomyocytes, Rat H9c2 cardiac cells	ROS↑-Ca^{2+}↑-NFAT↑- Fas L↑-caspase-3/8↑	Kalivendi et al., 2005
			Neonatal rat cardiomyocytes, cardiac fibroblasts; C57/B6 mice	CFs-Fas L exosome release-cardiomyocyte	Zhang et al., 2019
			Primary cardiomyocytes	Fas L↑-caspase-8↑	Yamaoka et al., 2000
			Rat cardiomyoblast H9c2 cells; C57BL/6 mice	ROS↑-CCN1↑-p38-MAPK↑-Smac↑, HtrA2↑-Fas L↑	Hsu and Mo, 2016
			H9c2 cells	TNFα↑-TNFR1↑, TNFR2↓-caspase-8↑, IκBα↓	Chiosi et al., 2007
			Male Wistar rats	ROS↑-NO↑, iNOS↑, Lipid peroxidation-TNFα↑, IL-1β↑, IL-6↑	Akolkar et al., 2017
			SD rats	Ca^{2+}↑-TNFα↑-caspase-9/12↑	Agustini et al., 2016
			Adult Wistar rats	ROS↑-mitochondrial damage	Giulivi et al., 1995
			Neonatal cardiac myocytes	Mn-SOD↓-MMP↓-Bcl-2↓, Bax↑, Cytochrome C↑	Chae et al., 2005
			Kunming mice	Mn-SOD↓-MMP↓, MPT-caspase↑	Li W. J. et al., 2018
			NRCMs; C57BL/6 mice	miR-146a↑-ErbB4↓	Horie et al., 2010
			Primary cardiomyocytes, H9c2 cells	miR-181a↓-Bcl-2↓	Zhao et al., 2018
			H9c2 cells	HO-1↓-Bax↑, Cytochrome C↑	Bernuzzi et al., 2009
			Male wild-type Balb/c mice	p53↑-Bax↑, Cytochrome C↑	Zhang et al., 2011
			H9c2 cells	ROS↑, p53↑-IGF-IR↓, IGFBP-3↑	Fabbi et al., 2015
		Autophagy	H9c2 cells; C57BL/6J mice	ROS↑-LC3II/LC3I↑, Beclin1↑	Zhang et al., 2015
			Adult rat cardiomyocytes	p53↑, p38-MAKP↑, JNK-MAKP↑	Ludke et al., 2017
			Kunming mice	p85↓-phosphorylated AKT↓-phosphorylated mTOR↓	Yu et al., 2017
			MHC-CB7 mice	p53↑-phosphorylated mTOR↓	Zhu et al., 2009
			Adult rat ventricular myocytes (ARVMs); Male Wistar rats	ROS↑-lysosome acidification↓-autophagy flux↑, autophagosomes↑	Dimitrakis et al., 2012
			ARVMs, NRCMs, H9 human embryonic stem Cells induced cardiomyocytes; C57BL/6 mice	lysosome acidification↓, autolysosome degradation↓-damage of autophagic mode	Li et al., 2016
			NRCMs, adult rat cardiomyocytes, adult mouse cardiomyocytes, H9c2 rat embryonic cardiomyoblasts; C57BL/6J mice, SD rats	TFEB↓-lysosomal cathepsin B↓-caspase-3↑	Bartlett et al., 2016
			NRCMs; Wistar rats	HMGB1↑, YAP↓-caspase-3↑	Luo et al., 2018
			NRCMs	GATA4↓-autophagy flux↑-Bcl-2↓, Beclin 1↑	Kobayashi et al., 2010
		Necrosis	Cardiomyocytes; C57BL/6J mice	ROS↑, RNS↑	Mukhopadhyay et al., 2009
			H9c2 cells	nuclear swelling, DNA damage, mitochondrial dysfunction	Rharass et al., 2016
			C57BL/6J mice	ROS↑-autophagy damage	Li et al., 2014
			NRCMs, ARVMs	calpains↑-titin degradation	Lim et al., 2004
			Postnatal rat cardiac myocytes	BNIP3↑-COX1-UCP3 disruption-ROS↑-mitochondrial dysfunction	Dhingra et al., 2014

(Continued)

TABLE 1 | Continued

Drug type	Drugs	Cell death type	Cell type/animal	Mechanism	References
		Necroptosis	Mice	ROS↑-RIPK3 + phosphorylated-CaMKII-MTPT opening	Zhang T. et al., 2016
			Neonatal mouse ventricular myocytes; C57BL/6 mice	p38-MAPK↑-NF-κB↑-RIP1↑-RIP3↑-MLKL↑	Yu et al., 2020
		Pyroptosis	H9c2 cells; C57BL/6J mice	TLR4↑-NLRP3↑-caspase-1↑-IL1β↑, IL-18↑	Singla et al., 2019; Tavakoli et al., 2019
			HL-1 cardiomyocytes; C57BL/6J mice	BNIP3↑-caspase-3↑-GSDME↑	Zheng et al., 2020
			Neonatal rat ventricular cardiomyocytes (NRVCs); H9c2 cells; C57BL/6J mice	Drp1↑-NOX1↑, NOX4↑-NLRP3↑-caspase-1↑	Zeng et al., 2020
			Primary neonatal rat cardiomyocytes; H9c2 cells; Wistar rats	TINCR-lncRNA↑-IGF2BP1↑-NLRP3↑-caspase-3↑-GSDMD-IL1β↑, IL-18↑	Meng et al., 2019
			H9c2 cells; Rats	SIRT1↑-NLRP3↑-caspase-1↑-IL1β↑, IL-18↑	Sun et al., 2020; Zhai et al., 2020
		Ferroptosis	mice	Nrf2↑-Hmox1↑-Fe↑-mitochondrial damage-lipid peroxidation	Fang et al., 2019
			Male SD rats	TLR4↑, NOX4↑	Chen et al., 2019
	Cisplatin	Apoptosis	Cardiomyocytes; C57BL/6 mice	ROS↑-mitochondrial dysfunction, ER stress-caspase-3↑	Ma et al., 2010
			Male Albino rats	mitochondrial DNA injury, nuclear DNA infraction	El-Awady el et al., 2011
	Cyclophosphamide	Apoptosis	Male Wistar rats	sarcoplasmic reticulum dilatation, mitochondrial disruption, nuclear membrane invagination	Lushnikova et al., 2008
			H9c2; Wistar albino rats	acrolein-ROS↑, RNS↑	Nagi et al., 2011; Kurauchi et al., 2017
			Male Wistar albino rats	mitochondrial dysfunction-ATP↓-caspase-3↑	Refaie et al., 2020
			Male Wistar rats	ROS↑-TLR4↑-NF-κB↑	El-Agamy et al., 2017
			Female Wistar albino rats	DNA damage-Bcl2↑, caspase↑	Avci et al., 2017
	5 -Fluorouracil	Apoptosis	ARVMs	ROS↑, GSH↓-lipid peroxidation, MMP-caspase↑	Eskandari et al., 2015
		Autophagy	Human umbilical vein endothelial cells, Human colorectal cancer cells Human cardiac myocytes	autophagosome↑	Focaccetti et al., 2015
			ARVMs	lysosomal membrane leakiness-autophagy damage	Eskandari et al., 2015
	Arsenic trioxide	Apoptosis	Cardiac myocytes; Wistar rats	ROS↑, Ca^{2+}↑	Raghu and Cherian, 2009
			H9c2 cells; Wistar rats	ROS↑-GSH↓, GPx↓, GST↓, SOD↓-lipid peroxidation, MMP↓	Varghese et al., 2017
			H9c2 cells	mitochondrial damage-ATP↓-caspase-3↑	Vineetha et al., 2015
			Male Hy-line chickens	trace elements disorder-mitochondrial damage- Bax caspase-3/8	Li et al., 2019
			ARVMs; Male SD rats	SERCA2a↓-ER stress-CHOP↑, caspase-12↑, GRP78↑	Zhang J.Y. et al., 2016
			Chickens	TNFα↑, NF-κB↑, COX-2↑, iNOS↑	Li et al., 2017
			NRVCs; Wistar albino rats	ROS↑, Ca^{2+}↑-p38↑, JNK MAPK↑-NF-κB↑, IKK↑- PARP, caspase-3↑	Ghosh et al., 2009; Fan et al., 2013
			Human pluripotent stem cells induced cardiomyocytes	gammah2ax↑-DNA damage	Bao et al., 2019
		Autophagy	Culture HL-1 murine atrial cardiomyocytes	Parkin-mitophagy	Watanabe et al., 2014
			Hy-line chickens, carp	PI3K↑-Akt↑-mTORC1↓	Li S. et al., 2018; Zhao et al., 2019
	Trastuzumab	Apoptosis	NRVMs, ARVMs	Bax↑, Bcl-xS↑, Bcl-xL↓-MMP↓-ATP↓-caspase↑	Grazette et al., 2004
			Primary cardiomyocytes	ErbB2↓-DNA damage	Rohrbach et al., 2005

(Continued)

TABLE 1 | Continued

Drug type	Drugs	Cell death type	Cell type/animal	Mechanism	References
			ARVMs	neuregulin-1/ErbB2-phosphorylated Akt ↓	Sawyer et al., 2002
			C3H/HeJ mice	TLR4 -TNFα↑	Yousif and Al-Amran, 2011
			NRVCs	MDM2↓- p53↑	Singh et al., 2011
			Human primary cardiomyocytes	Beclin1↓, Atg 5-12/14↓-EebB1-Y845/ErbB2-Y1248 -ERK/mTOR/ULK-1-ROS↑, mitochondrial dysfunction	Mohan et al., 2016
	Sunitinib	Apoptosis	H9c2; Male C57BL/6NRj mice	ROS↑-mitochondrial damage	Bouitbir et al., 2019
			SD rats	miR-133A↑-phosphorylation of Ask1/MKK7/JNK↓	Cooper et al., 2018
		Autophagy	H9c2 cells	autophagy flux↑	Zhao et al., 2010
	Imatinib	Apoptosis	Primary cardiomyocytes; Mice	GATA4↓-Bcl-2↓, Bcl-xL↓	Maharsy et al., 2014
			H9c2 cells	Sab-JNK-ROS↑, mitochondrial damage-caspase- 3/7/9↑	Chambers et al., 2017
		Autophagy	Neonatal cardiomyocytes	autophagy block-lysosome↑, p62↑	Hu et al., 2012
	Nilotinib	Apoptosis	H9c2 cells	ROS↑, ATF4↑, CHOP↑-MMP↓, caspase-3↑	Lekes et al., 2016
			H9c2 cells	ER stress-JNK↑, phosphorylated Akt↓-phosphorylated GSK3β↓-Nox4/ROS↑	Yang et al., 2018
	Sorafenib	Apoptosis	Zebrafish	Raf-1/B-raf↓-MEK↓-ERK↓	Cheng et al., 2011
	Ponatinib	Apoptosis	NRCMs; Zebrafish	Phosphorylated Akt↓, ERK1/2↓-caspase-3↑	Singh et al., 2019
	Dasatinib	Necroptosis	CCC-HEH-2 human embryonic cardiac tissues	RIP1↑, RIP3↑-HMGB1↑	Xu et al., 2018
	Mitoxantrone	Apoptosis	H9c2 cells	ROS↑-Ca^{2+}↑-MMP↓-ATP↓-caspase-3↑	Rossato et al., 2013
			Neonatal cardiomyocytes H9c2 cells	Top2β↓-DNA damage	Damiani et al., 2018
Antidiabetic drug	Rosiglitazone	Apoptosis	H9c2 cells	NAPHD↑, iNOS↑, SOD↓, GR↓	Mishra et al., 2014
			C57BL/6 mice	ROS↑-mitochondrial dysfunction	He et al., 2014
	Pioglitazone	Apoptosis	Wistar rats	Sphingomyelinase↑, ceramidase↑	Baranowski et al., 2007
			Primary cardiomyocytes	Bax↑, phosphorylated p53↑, phosphorylated vegfr-2↓, Akt↓, mTOR↓	Zhong et al., 2018
Antiviral drug	Zidovudine	Apoptosis	Rats	ROS↑, peroxynitrite↑-DNA breaks-NAD^+-ATP↓	Szabados et al., 1999
			Primary human cardiomyocytes	ROS↑-mitochondrial disruptions-caspase-3/7↑	Gao et al., 2011
			Mice	Fas/Fas L↑-caspase-3↑	Purevjav et al., 2007
		Autophagy	C2C12 myocyte cells	autophagy inhibition-MMP, ROS↑	Lin et al., 2019
		Necrosis	Primary human cardiomyocytes	Zidovudine-PARP↑	Gao et al., 2011
Teratogen	Cyclophosphamide	Apoptosis	Primigravida Swiss Webster mice	DNA fragmentation degradation-caspase-3↑	Mirkes and Little, 1998
			Swiss-Webster mice	p38-MAPK↑-caspases cascade reactions	Mirkes et al., 2000

of caspase-8 and suppression of IκBα (Chiosi et al., 2007). It is noteworthy that vitamin C, a well-known reductant, can evidently decline the levels of TNFα, IL-1β and IL-6 in DOX-treated mice, indicating that oxidation/nitrosation stress may be one of the targets of cardiac protection during DOX treatment (Akolkar et al., 2017). In addition, the intracellular calcium homeostasis protective agent mangiferin was also verified to be able to relieve the up-regulation of TNFα and caspase-9 induced by DOX and stimulates the calcium regulatory gene, preventing myocarditis and apoptosis (Agustini et al., 2016).

Another plausible mechanism is that DOX-induced oxidative stress breaks the oxido-reduction balance of mitochondria in cardiomyocytes. DOX treatment promotes ROS overproduction, which remains inside the mitochondrial membrane and induces mitochondrial dysfunction (Giulivi et al., 1995). DOX caused a down-regulation of antioxidant enzymes such as copper, manganese and zinc superoxide dismutases (SODs), glutathione peroxidase (GSH-Px) and catalase (Costa et al., 2013). This imbalance between oxidation and antioxidation aggravates mitochondrial damage. Therefore, overexpression of antioxidant enzymes can reduce DOX-induced cardiotoxicity. *In vitro*, γ-ray

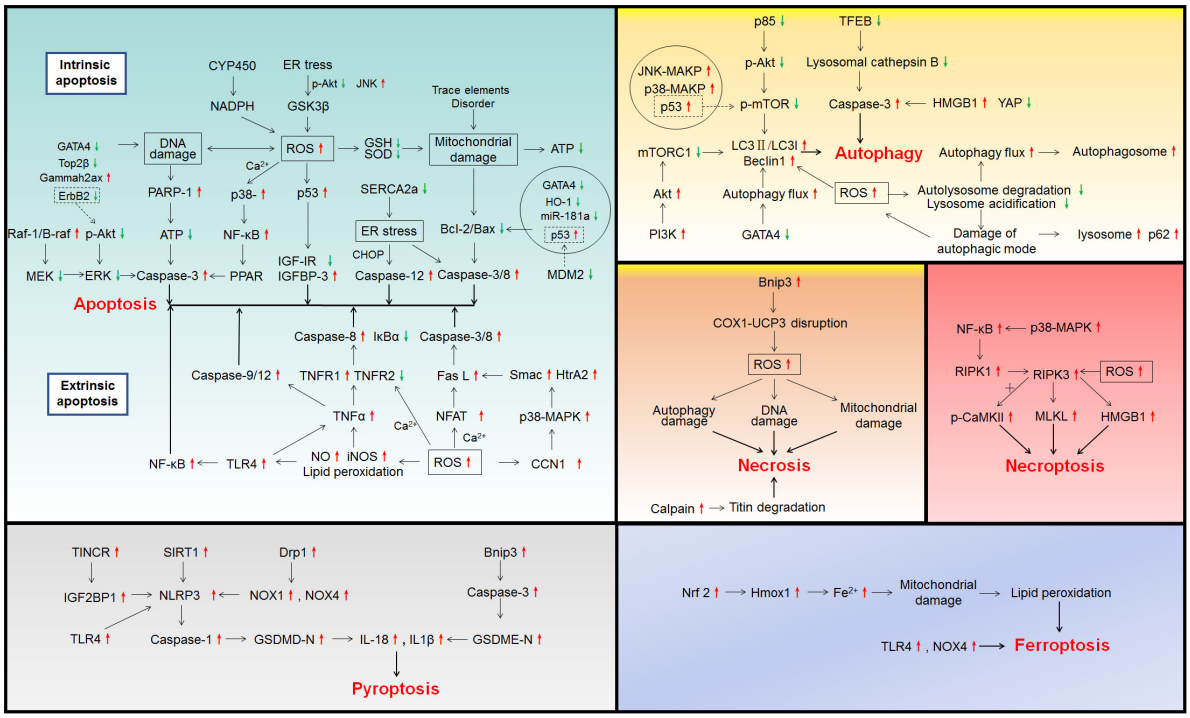

FIGURE 1 | Signaling pathways involved in drug-induced cardiotoxicity.

pre-irradiation increased manganese superoxide dismutase (Mn-SOD) levels in neonatal rat ventricular myocytes (NRCMs), which up-regulated MMP, Bcl-2 expressions, and decreased the Bax expression and cytochrome C release (Childs et al., 2002; Chae et al., 2005). Nevertheless, polysaccharide elevated MMP and restrained mitochondrial permeability transition (MPT) by activating manganese superoxide dismutase (Mn-SOD) and suppressing the subsequent caspases cascade reactions (Li W. J. et al., 2018).

Recent studies demonstrated that DOX could indirectly target some receptors or anti-apoptosis factors by regulating miRNAs. DOX increased the level of miR-146a and induced the targeted inhibition of human epidermal growth factor receptor-4 (ErbB4), which caused cardiomyocyte apoptosis and acute cardiotoxicity (Horie et al., 2010). The miR-181a directly targeted the Bcl-2 transcript and negatively regulated Bcl-2 expression, which mediates the protective effect of propofol against DOX-induced cardiotoxicity *in vitro* and *in vivo* (Zhao et al., 2018). Moreover, miR-29b was found to target 3' untranslated region of Bax and restrained Bax expression, hence alleviating DOX-induced cardiomyocyte apoptosis (Jing et al., 2018).

Several studies showed that varying DOX dosages caused apoptosis through different pathways. A study reported that treatment with a high concentration of DOX (2 μM) tended to promote ROS accumulation, while a lower concentration (0.25 M) was more likely to suppress the expression of haem oxygenase 1 (HO-1). HO-1 down-regulation induced cardiomyocyte apoptosis by activating caspase-3 and the release of mitochondrial cytochrome C (Bernuzzi et al., 2009). Another study found that a high concentration of DOX (1 μM) tended to cause DNA damage, PARP-1 dissociation and grievous apoptosis, and a low concentration of DOX (0.5 μM) could activate the p53-related mitochondrial apoptosis pathway (Cunha-Oliveira et al., 2018). Furthermore, DOX dose-dependently increased p53 expression in H9c2 cells, which inhibits type 1 insulin-like growth factor receptor (IGF-1R) transcription and induces IGF binding protein-3 (IGFBP-3) transcription, resulting in resistance to IGF-1 and contributing to apoptosis (Fabbi et al., 2015). More in-depth study indicated that the regulation of DOX on p53 may involve Sirtuin 1 (SIRT1) -mediated deacetylation of p53 (Zhang et al., 2011).

Autophagy

Autophagy is commonly considered as a conservative and beneficial regulatory process that maintains intracellular homeostasis, which is initially activated to resist DOX-induced cardiotoxicity. Oxidative stress is considered the main inducement for autophagy. As reported, during DOX treatment, ROS increased the ratio of LC3II/LC3I and the level of Beclin 1, both being the bio-markers of autophagy (Zhang et al., 2015). In addition, Dox up-regulated the levels of pro-autophagy factors (p53, p38-MAPK, and JNK-MAPK), and down-regulated the p85 expression, the catalytic subunit of phosphoinosmde-3-kinase (PI3K) as well as Akt phosphorylation (Ludke et al., 2017; Yu et al., 2017).

Even though the autophagy process is indeed initiated by DOX to serve a protective role, it somehow fails to finish the process since overwhelming oxidative stress blocks the

degradation of lysosomes and even causes autophagic cell death, which in fact turns the original protective effect into damage. Under these circumstances, the normal protein degradation of cardiomyocytes was disrupted, and the subsequent increase in ubiquitinated proteins resulted in the accumulation of autophagy flux and autophagosomes (Dimitrakis et al., 2012). Meanwhile, DOX suppressed lysosome acidification and autolysosome degradation, which blocked the autophagic flux and augmented the damage (Li et al., 2016). Moreover, DOX-induced up-regulation of histone deacetylase 6 (HDAC6) decreased α-tubulin acetylation level, giving rise to mitochondrial dysfunction and autophagy flux damage (Song et al., 2018). Lysosome dysfunction was found to involve in the depletion of transcription factor EB (TFEB). DOX can suppress the expression of TFEB and induce the impairment of lysosomal cathepsin B, which subsequently inhibited lysosomal autophagy, increasing the levels of ROS and caspase-3 cleavage (Bartlett et al., 2016).

In addition to ROS-related autophagy, DOX also regulates autophagy-related factors and cause autophagic cell death. High mobility group box 1 (HMGB1) plays a vital role in the process of autophagy. DOX increased HMGB1expression, while silencing HMGB1 could reverse cardiomyocyte damage by attenuating autophagy (Luo et al., 2018). In addition, inhibition of the transcription factor GATA4 was observed in DOX-treated cardiomyocytes, and GATA4 induces the expression of Bcl2, which can interact with Beclin 1 to silence autophagy, decreases the cardiotoxicity (Kobayashi et al., 2010). Moreover, rats treated with 3-methyladenine, a specific inhibitor of autophagy, showed fewer autophagic vacuoles and mitochondrial MPT, but higher levels of Na^+-K^+ ATPase activity and MMP as compared with DOX treatment alone (Lu et al., 2009).

It has been reported that starvation or caloric restriction prior to DOX insult can suppress cardiotoxicity. Caloric restriction attenuated DOX-induced ATP exhaustion and enhances the activity of AMPK, which eventually corrected the harmful autophagy caused by DOX, demonstrating a protective role (Chen et al., 2011). On the contrary, prior starvation mitigated acute DOX-induced cardiotoxicity via further augmenting autophagy (Kawaguchi et al., 2012). In addition, Astragalus polysaccharide and resveratrol can restore autophagy in mice and H9c2 cells through the AMPK/mTOR signaling pathway, alleviating cardiotoxicity (Gu et al., 2016; Cao et al., 2017).

Necrosis

Unlike apoptosis and autophagy, emerging evidence has indicated that cardiomyocyte necrosis is triggered by a high dosage or prolonged exposure to DOX treatment. Dose-dependently elevated by DOX, the accumulation of ROS and peroxynitrite increase the rate of necrosis in cardiomyocyte death (Mukhopadhyay et al., 2009; Fulbright et al., 2015). The commonly used dosages of DOX are ≤20 mg/kg *in vivo* and 1 μM *in vitro*. A single intraperitoneal injection of DOX at 25 mg/kg in mice could immediately cause necrotic death and cardiac insufficiency (Li et al., 2014), and 2 μM DOX can directly induce cardiomyocyte necrosis *in vitro* (Bernuzzi et al., 2009). Moreover, when the cardiomyocytes are exposed to DOX for a long period, initial apoptosis develops into necrosis as the cells preferentially exhibits early DNA impairment and nuclear swelling (Rharass et al., 2016). As discussed above, DOX can destroy the function of lysosomes and disrupt normal autophagy as a result of oxidative stress. Consequently, the delayed autophagy in cardiomyocytes causes more severe apoptotic secondary necrosis (Dimitrakis et al., 2012; Li et al., 2014). These studies further confirm the notion that necrosis arose with extended exposure to DOX treatment.

Moreover, DOX initiates necrotic cell death by regulating necrosis-related intracellular factors. The degradation of titin, a myofilament protein associated with myocardial damage, was induced by DOX, and finally induced cardiomyocyte necrotic death (Lim et al., 2004). In addition, BH3-only protein BNIP3 was activated by DOX to destroy the combination of respiratory chain complex IV subunit 1 (COX1) and uncoupling protein 3 (UCP3), which disrupted respiratory efficiency, eventually leading to necrotic cell death (Dhingra et al., 2014).

Necroptosis

It has been demonstrated that RIPK3 is activated by DOX to bind with phosphorylated-CaMKII, causing the opening of mitochondrial permeability transition pore (MTPT), and resulting in necroptosis (Zhang T. et al., 2016). More importantly, dexrazoxane alleviated Dox-induced inflammation and cardiomyocyte necroptosis through inhibiting p38-MAPK/nuclear factor kappa-B (NF-κB) signal (Yu et al., 2020).

Pyroptosis

The increased secretion of IL-1β and IL-18, activation of TLR4, NLRP3 inflammasome and caspases were found in DOX-treated H9c2 cells, suggesting the occurrence of pyroptosis (Singla et al., 2019). BNIP3, the upstream regulator of cardiomyocyte pyroptosis, can activate caspase-3 and lead to subsequent GSDME cleavage (Zheng et al., 2020). DRP1/NOX signaling was activated to cause mitochondrial damage, which involved in DOX-induced pyrotosis (Zeng et al., 2020). Moreover, up-regulated lncRNA TINCR recruited IGF2BP1 to enhance the NLRP3 expression that mediated Dox-induced pyrotosis (Meng et al., 2019). However, embryonic stem cells-derived exosomes and Heat-shock Protein 22 can reverse the Dox-induced cardiomyocytes pyrotosis via inhibiting TLR4/NLRP3/caspase-1 signaling (Tavakoli et al., 2019; Lan et al., 2020). Moreover, suppression of ROS was also reported to be able to alleviate Dox-induced cardiomyocyte pyrotosis, whose mechanism involved the inhibition of sirtuin 1/NLRP3 signaling pathway (Sun et al., 2020; Zhai et al., 2020).

Ferroptosis

Doxorubicin-induced accumulation of ROS and lipid peroxidation can lead to cardiomyocyte ferroptosis (Koleini et al., 2019). Activation of TLR 4 and NOX 4 has also been proven to promote DOX-induced cardiomyocyte ferroptosis (Chen et al., 2019). Administering DOX to mice induced cardiomyopathy with a rapid, systemic accumulation of nonheme iron via heme degradation by NF-E2-related factor 2 (Nrf2)-mediated up-regulation of heme oxygenase-1 (HMOX1),

indicating the cardio-protective role of targeting ferroptosis for cardiomyopathy prevention (Fang et al., 2019).

Cisplatin

Cisplatin is a chemotherapeutic agent for a vast spectrum of cancers. However, its acute and cumulative cardiotoxicity partially limits anti-tumor treatment and clinical applications (Ma et al., 2010). Cisplatin-treated cardiomyocytes showed mitochondrial abnormalities such as mitochondrial membrane depolarization, inflammatory responses and increased ER stress, which finally stimulated the activity of caspase-3 and induced apoptosis (Chowdhury et al., 2016). In addition, emerging evidences demonstrated a close connection between oxidative stress and cisplatin-induced cardiomyocyte apoptosis. El-Awady el et al. (2011) discovered that cisplatin improved lipid peroxidation, decreased GSH content and suppressed SOD activity, implying oxidative stress induced by cisplatin. Moreover, mitochondrial DNA injury and nuclear DNA damage were observed. Antioxidant natural products such as tutin (vitamin P1), zingerone and cyanidin can inhibit cisplatin-induced inflammatory infiltration, DNA damage, and mitochondrial dysfunction, indicating the key role of oxidative stress in cisplatin-induced cardiomyocyte apoptosis (Qian et al., 2018; Soliman et al., 2018; Topal et al., 2018).

Cyclophosphamide

Cyclophosphamide is commonly applied in the treatment of malignant tumors such as leukemia and lymphoma, and it is also adopted to treat systemic lupus erythaematosus and polymyositis as an immunosuppressor. Because of the dose-dependent manner, cyclophosphamide-induced cardiotoxicity basically coincides with high-dose treatment (Nishikawa et al., 2015; Wadia, 2015). Acrolein, the active metabolite of cyclophosphamide, was confirmed to be mainly responsible for cardiomyocyte death (Conklin et al., 2015; Nishikawa et al., 2015; Kurauchi et al., 2017). The cardiomyocyte injuries caused by cyclophosphamide treatment included sarcoplasmic reticulum dilatation, mitochondrial disruption and nuclear membrane invagination (Lushnikova et al., 2008). Further studies attributed these injuries to oxidative stress, clarifying that acrolein caused oxidative and nitrite stress through the suppression of intracellular GSH and SOD and increase of MDA (Nagi et al., 2011; Kurauchi et al., 2017; Omole et al., 2018). Corresponding lipid peroxidation initiated mitochondrial function damage, which further led to a collapse in APT production and the activation of caspase-3, resulting in apoptosis (Nagi et al., 2011; Refaie et al., 2020). In addition, cyclophosphamide was verified to stimulate TLR4, through which it initiated the TLR4 /NF-κB signaling to trigger an inflammatory reaction, and eventually apoptosis (El-Agamy et al., 2017). Furthermore, DNA damage was observed in cyclophosphamide-treated rats, which were accompanied with activation of caspase-3 and inhibition of Bcl-2 expression (Avci et al., 2017). Antioxidant drugs such as silymarin and curcumin can inhibit cyclophosphamide-induced cardiotoxicity via decreasing the fragments of mitochondrial DNA and nuclear DNA, suggesting that excessive ROS might be responsible for cyclophosphamide-induced DNA injuries.

With the exception of the evidence discussed above, cyclophosphamide acted as a teratogen to injure cardiomyocytes. Cyclophosphamide affected cardiomyocytes developing via DNA fragmentation degradation, caspase-3 activation and PARP cleavage (Mirkes and Little, 1998). Moreover, cyclophosphamide was found to activate the apoptotic pathways, culminating in abnormality of the heart via the p38-MAPK signaling (Mirkes et al., 2000).

Fluorouracil and Capecitabin

5-Fluorouracil, a pyrimidine antimetabolite, is used widely in clinical practice as an anti-tumor treatment for cancers such as intestinal cancer and liver cancer. Capecitabin, a tumor-targeting drug that takes effect after the intracellular transformation into 5-fluorouracil, was regarded as having similar cardiotoxicity. Multiple studies confirmed the cardiotoxicity induced by 5-fluorouracil, which was attributed to the coronary arteries injury (Clavel et al., 1988; Herrmann et al., 2016). Further study suggested that the cardiomyocyte apoptosis might also play an important role in 5-fluorouracil-induced cardiotoxicity (Tsibiribi et al., 2006). 5-Fluorouracil stimulated intracellular oxidative stress by O_2^- generation, which eventually activated the caspases cascade reactions, leading to apoptosis (Lamberti et al., 2012). To further determine the underlying mechanism, Eskandari et al. (2015) discovered that 5-fluorouracil-induced ROS increase was accompanied by the depletion of GSH, a ROS scavenger. Next, the generated ROS mediated lipid peroxidation on mitochondria to decrease MMP, causing mitochondrial dysfunction and caspase-3 activation. Fluoroacetate, the metabolite of 5-fluorouracil, can restrain aconitase to block the tricarboxylic acid cycle, resulting in a mitochondrial energy metabolism crisis (Lischke et al., 2015). Moreover, accumulation of autophagosomes and lysosomal membrane leakiness were observed in 5-fluorouracil-treated human cardiomyocytes, indicating the involvement of autophagic cell death in 5-fluorouracil-induced cardiotoxicity (Eskandari et al., 2015; Focaccetti et al., 2015).

Arsenic Trioxide

Arsenic trioxide represents a breakthrough in the field of acute promyelocytic leukemia therapeutic, but its cardiotoxicity remains an unresolved problem. In the past few decades, numerous studies have proposed that cardiomyocyte apoptosis is induced by ROS, and mitochondrial damage might be the main reason for arsenic trioxide-induced cardiotoxicity (Zhao et al., 2008; Raghu and Cherian, 2009; Vineetha et al., 2015). Arsenic trioxide can increase ROS level and calcium concentration, which was accompanied with cardiomyocyte apoptosis (Raghu and Cherian, 2009). Moreover, ROS generation depleted intracellular antioxidants such as GSH, GSH-Px, glutathione s-transferase (GST) and SOD, which caused lipid peroxidation and decreased MMP (Varghese et al., 2017). In addition, mitochondrial damage such as MTP and mitochondrial swelling was also observed under arsenic trioxide exposure, following by a decrease in oxygen consumption as well as ATP production, resulting in caspase-3 activation and apoptosis (Vineetha et al., 2015). Recently, Li et al. (2019) found that arsenic trioxide interfered with the dynamic balance of trace elements in chicken cardiomyocytes

to break mitochondrial cristae and mitochondrial vacuoles, increasing the expressions of Bax and caspase-3/8. In addition to ROS and mitochondrial damage, calcium imbalance is also involved in arsenic trioxide-induced cardiotoxicity. Arsenic trioxide suppressed the activity of sarcoplasmic reticulum Ca^{2+}-ATPase2a, by which cytoplasmic calcium was taken back to the sarcoplasmic reticulum (Zhang J.Y. et al., 2016). Consequently, the imbalance of calcium homeostasis and ER stress activated C/EBP-homologous protein (CHOP), caspase-12 and GRP78, leading to apoptosis.

By increasing the levels of the inflammatory cytokines TNFα, NF-κB, cyclooxygenase-2 (COX-2) and inducible nitric oxide synthase (iNOS), arsenic trioxides promoted the inflammatory reactions and brought ultrastructural damage to cardiomyocytes (Li et al., 2017). These inflammatory responses partly contributed to heavy metal-related cardiotoxicity (Lakkur et al., 2015). Additionally, it has been determined that arsenic trioxides up-regulates the content of phosphorylated p38 and JNK by oxidative stress stimulation and calcium overload, which further induces NF-κB phosphorylation, caspase-3 activation and PARP cleavage (Ghosh et al., 2009; Fan et al., 2013). Suppression of ROS apparently inhibited the activation of JNK, extracellular regulated protein kinases (ERK), and p38, which eventually reversed cardiomyocyte apoptosis (Miao et al., 2013; Zhang et al., 2017). One recent study reported that arsenic trioxides might induce cardiomyocyte apoptosis through DNA damage, since it dose-dependently increased the content of γH2AX, a sensitive biomarker for DNA breaks (Bao et al., 2019). Moreover, activation of Parkin, an E3 ubiquitin ligase, can inhibit arsenic trioxide-induced cardiotoxicity via the maintenance of mitochondrial as well as cellular homeostasis (Watanabe et al., 2014). It is well known that Parkin-induced ubiquitination of mitochondrial substrates finally leads to mitophagy. Therefore, mitophagy displays a positive role in maintaining cardiac homeostasis during arsenic trioxide exposure. However, a subsequent study demonstrated that arsenic trioxide-induced oxidative stress led to the formation of autophagosomes through PI3K/Akt/mTOR signaling, which resulted in myocardial damage (Li S. et al., 2018; Zhao et al., 2019). Moreover, cardiomyocyte necrosis was also observed under arsenic trioxide exposure (Raghu and Cherian, 2009; Vineetha et al., 2015), but the underlying mechanisms remained unclear.

Trastuzumab

A novel and widely used monoclonal antibody drug, Trastuzumab, is also reported to cause cardiotoxicity, such as cardiac insufficiency and heart failure. Under physiological condition, neuregulin-1 interacted with epidermal growth factor receptor-2 (ErbB2) to allow for the formation of ErbB4/ErbB2 heterodimer, which blocked cell death through an Akt-dependent signaling in cardiomyocytes (Sawyer et al., 2002; Lemmens et al., 2007). Functioning as an inhibitor of ErbB2 receptor, trastuzumab interrupted ErbB4/ErbB2 heterodimerization, thereby leading to apoptosis (Holbro and Hynes, 2004; Rohrbach et al., 2005). Interaction between Trastuzumab and ErbB2 triggered the downstream signal transduction pathways, such as increased levels of Bax and Bcl-xS, decreased Bcl-xL level and caspases cascade activations. Furthermore, the decreased MMP caused by Bcl-xL suppression and subsequent mitochondrial energy catastrophe also contributed to trastuzumab-induced apoptosis (Grazette et al., 2004). Singh et al. (2011) proposed that the cardiotoxicity induced by trastuzumab might stem from its negative regulation of murine double minute 2 (MDM2) and p53. In addition, trastuzumab-induced cardiomyocyte apoptosis was found to be related to inflammatory infiltration (Coppola et al., 2016), and the TLR4-mediated chemokine expressions of TNFα, MCP-1 and ICAM-1 contributed to inflammatory responses induced by trastuzumab (Yousif and Al-Amran, 2011).

A recent study reported that trastuzumab suppressed autophagy, resulting in mitochondrial dysfunction and ROS accumulation (Mohan et al., 2017). Trastuzumab insult inhibited the expressions of Beclin 1, autophagy related gene (Atg) 5-12 and Atg14. Moreover, Trastuzumab stimulated EebB1-Y845 and ErbB2-Y1248 and activated the ERK/mTOR/ULK-1 signaling to supress autophagy (Mohan et al., 2016).

Currently, drug combination therapies with trastuzumab are quite popular among cancer treatment plans. However, the combination therapies show more serious cardiotoxicity compared with single drug remedies. Trastuzumab combining with DOX exacerbated the exhaustion of antioxidant enzymes as well as damage to the mitochondrial structure (Xu et al., 2004). Trastuzumab-induced ErbB2 inhibition further suppressed c-Abl and Arg, which plays an antioxidant role by activating GSH-Px and catalase, thereby increasing DOX-induced cytotoxicity (Belmonte et al., 2015). Additionally, inhibition of the neuregulin-ErbB signaling by trastuzumab restrained the phosphorylation of ERK1/2 and Akt, and eventually exacerbated DOX-induced cardiomyocyte apoptosis and myocardial fiber injury (Sawyer et al., 2002). The underlying mechanism might also include the increased level of iNOS, which contributed to oxidative stress and inflammatory cell infiltration (Milano et al., 2020). Moreover, DOX-trastuzumab combination synergistically repressed Top2β, and eventually resulted in DNA double strand breaks and the ROS overproduction (Jiang et al., 2018). N-Acetyl Cysteine Amide, a ROS scavenger, can attenuate the DOX and trastuzumab-induced cardiac dysfunction (Goyal et al., 2016). Furthermore, paclitaxel-trastuzumab combination was reported to have a worsening effect on cardiomyocyte function, which might result from the inhibition of phosphorylated-ERK1/2. However, no cell death was observed during treatment in addition to myofibrillar structure changes (Pentassuglia et al., 2007).

Tyrosine-Kinase Inhibitors (Sunitinib, Imatinib, Nilotinib, Sorafenib, Ponatinib and Dasatinib)

Tyrosine-kinase inhibitors such as sunitinib, imatinib, nilotinib, sorafenib, ponatinib, and dasatinib are widely applied for chronic myelogenous leukemia and solid tumors, however, an increasing number of studies have reported cardiotoxicity associated with tyrosine-kinase inhibitors. Clinical research observed aberrantly shaped, swollen mitochondria in cardiomyocytes of patients who developed congestive heart after sunitinib treatment (Chu et al., 2007). Bouitbir et al. (2019) demonstrated that the oxidative stress caused by sunitinib was mainly responsible for the mitochondrial

damage and final apoptosis of cardiomyocytes. By suppressing mitochondrial electron transport chain enzyme complexes, sunitinib induced ROS accumulation, which further decreased MMP and destroyed the mitochondrial structure to initiate caspases cascade reactions. In addition, sunitinib was confirmed to increase the expression of miR-133A, and suppress the apoptosis signal-regulating kinase 1 (ASK1)/mitogen activated kinase kinase 7 (MKK7)/JNK signaling to induce apoptosis and myocardial damage (Cooper et al., 2018). The elevation of autophagy flux was observed in sunitinib-treated H9c2 cells, (Zhao et al., 2010), and inhibition of autophagy was demonstrated to attenuate sunitinib-induced cardiotoxicity (Kimura et al., 2017), indicating involvement of autophagy in the cytotoxicity.

Mitochondrial damage was also observed in imatinib-treated cardiomyocytes. Imatinib down-regulates the expression of Bcl-2 and Bcl-xL by suppressing the content of the transcription factor GATA4, resulting in apoptosis. Moreover, aging was verified to be a risk factor during imatinib treatment because of its positive impact on the oxidative stress (Maharsy et al., 2014). In addition, Chambers et al. (2017) showed that imatinib induced oxidative stress and mitochondrial dysfunction via mediating JNK-related mitochondrial signaling and activating caspase-3/7/9. Autophagic death was also reported to be associated with imatinib-induced cardiotoxicity (Hu et al., 2012). Imatinib blocked the autophagic process as indicated by an increased level of lysosomes, which was consistent with the accumulation of p62, a protein degraded by autophagic clearance.

As a second-generation Bcr-Abl inhibitor, nilotinib mediated apoptosis mainly through the accumulation of ROS and ER stress (Doherty et al., 2013). The increase of ROS and ER stress biomarkers (ATF4 and CHOP), was observed in nilotinib-treated H9c2 cells, which subsequently decreased MMP and activated caspase-3, markers of apoptosis (Lekes et al., 2016). Recently, Yang et al. (2018) made further efforts to demonstrate that nilotinib induced ER stress to activate JNK and restrain Akt phosphorylation, which in turn suppressed glycogen synthase kinase-3 beta (GSK3β) phosphorylation and activated NOX4/ROS signaling, resulting in apoptosis.

Few studies reported potential apoptosis mechanisms associated with sorafenib, ponatinib and dasatinib. Cheng et al. (2011) demonstrated that sorafenib induced cardiomyocyte apoptosis and cardiotoxicity by inhibiting the Raf/MEK/ERK signaling. In addition, cardiomyocytes necrosis was observed during high-dose sorafenib treatment with unclear mechanism (Duran et al., 2014). The most recent study reported that ponatinib inhibited phosphorylation of Akt and ERK1/2, which contributed to the activation of pro-apoptotic caspase-3 (Singh et al., 2019). Xu et al. (2018) found that dasatinib dose-dependently up-regulated intracellular HMGB1 to induce cardiomyocyte necroptosis.

Mitoxantrone

With similar structure to DOX, mitoxantrone was thought to be an alternative to DOX with less cardiotoxicity (Herman et al., 1997). However, several studies have also reported mitoxantrone-induced cardiotoxicity. Mitoxantrone induced cardiomyocyte apoptosis associated with oxidative stress and mitochondrial dysfunction. With a time-dependent increase in the content of ROS, mitoxantrone promoted the accumulation of calcium and decreased the MMP, which further caused mitochondrial energy deficiency and activated caspase-3 (Rossato et al., 2013). In addition, DNA strand breaks were observed in apoptotic H9c2 cells treated with mitoxantrone, which was probably mediated by a Top2β-dependent signaling (Wu et al., 2013; Damiani et al., 2018).

Antidiabetic Drugs (Rosiglitazone and Pioglitazone)

Rosiglitazone and pioglitazone, as thiazolidinedione antidiabetic agents, were regarded as protective agents in diabetic cardiomyopathy and ischaemia-reperfusion injury (Cao et al., 2007; Baraka and Abdelgawad, 2010). However, with further expansion of their clinical applications, rosiglitazone and pioglitazone are also found to cause serious side effects such as myocardial hypertrophy and heart failure. It has been reported that rosiglitazone exerts both protective and detrimental effects in rats treated by ischaemia reperfusion (Palee et al., 2013). Although rosiglitazone was known as a PPARγ agonist, it caused cardiotoxicity via oxidative stress-induced mitochondrial dysfunction independent of PPARγ. By increasing the levels of NAPHD and iNOS, rosiglitazone induced oxidative stress accompanied by the exhaustion of antioxidant enzymes such as SOD and glutathione reductase, resulting in cardiotoxicity apoptosis (Mishra et al., 2014). In addition, the oxidative effect caused mitochondrial dysfunction, followed by cardiomyocyte energy deficiency (He et al., 2014). For pioglitazone, a study once reported that pioglitazone up-regulated the levels of sphingomyelinase and ceramidase, a mediator of cardiomyocyte apoptosis (Baranowski et al., 2007). Moreover, by activating Bax and phosphorylated p53 as well as suppressing phosphorylated Akt and mTOR, pioglitazone could induce apoptosis in a VEGFR-2 dependent manner (Zhong et al., 2018).

Antiviral Drug (Zidovudine)

Zidovudine, like other nucleoside reverse transcriptase inhibitors, is widely used for human immunodeficiency virus type 1 (HIV-1) infection. However, side effects such as hypertension and cardiomyopathy limit its long-term application. Zidovudine stimulated the accumulation of ROS and peroxynitrite, which in turn gives rise to single-strand DNA breaks, and eventually results in mitochondrial energy depletion in a NAD^+-dependent manner (Szabados et al., 1999). Zidovudine induced the transport of protein kinase C δ (PKCδ) from the cytosol to the membrane, which promoted the activation of NADPH oxidases (Papparella et al., 2007). Meanwhile, mitochondrial damage is observed after zidovudine treatment (Fiala et al., 2004). Mitochondrial ROS caused by zidovudine played a significant role in mitochondrial disruption-induced apoptosis by activating caspase-3/7 (Ry et al., 2011). Fas/Fas L was also involved in zidovudine-induced cardiomyocytes apoptosis (Purevjav et al., 2007). Besides the above effects, zidovudine was shown to inhibit autophagosome maturation and decrease autophagic flux, leading to mitochondrial membrane polarization and ROS accumulation (Lin et al., 2019).

Zidovudine-induced cardiomyocyte necrosis involved PARP activation (Gao et al., 2011).

PERSPECTIVES AND CONCLUSION

Cardiotoxicity is a major concern when evaluating whether drugs can be put on the market during preclinical research and is an important reason for post-approval drug withdrawal. Even for widely used drugs, cardiotoxicity limits their clinical applications. Fortunately, the mechanisms of cardiotoxicity have gradually come to light in recent years. ROS serves a main driver in drug-induced cardiotoxicity, and thereby many antioxidants have undergone preclinical development or clinically research for cardiotoxicity. For example, dexrazoxane, an iron chelating agent against iron-mediated oxidative stress, is the cardio-protective medicine approved by FDA in July 1995 for preventing anthracycline-induced cardiotoxicity, and now has been widely applied in the clinical practice (Padegimas et al., 2020). In addition, numerous natural antioxidants serve as adjuvant therapies to reduce drug-induced cardiotoxicity, such as berberine, epigallocatechin-3-gallate, and resveratrol (Coelho et al., 2017; Yu et al., 2018).

Recently, immune checkpoint inhibitors including anti-PD-1, anti-PD-L1 and CTLA-4 blockade have attracted a substantial amount of attention, which may revolutionize the treatment of cancer. Ever since the first case of cardiotoxicity induced by ipilimumab (CTLA-4 blockade) was reported in 2013 (Voskens et al., 2013), more and more case reports have indicated immune checkpoint inhibitor-induced cardiotoxicity. Worse still is the underlying mechanism remains unknown, possibly due to the lack of suitable animal models. Immune inflammation and ROS accumulation may play key roles in the immune checkpoint inhibitor-induced cardiotoxicity, which needs to be confirmed by future studies.

To achieve a better treatment effect, combinations of anticancer drugs have been widely applied in the clinical practice, but unfortunately lead to greater cardiotoxicity than with individual drug. Much attention has been paid to trastuzumab combined with DOX for treating women with ErbB2-positive breast cancer. Addition of trastuzumab to adjuvant DOX chemotherapy increases the incidence of cardiotoxicity, and few studies have been conducted to explore the underlying mechanisms, with iNOS or Top2β-mediated oxidative stress being the only acceptable mechanism (Jiang et al., 2018; Milano et al., 2020). To sum up, the mechanisms of drug-induced cardiomyocyte death are not absolutely independent, with the crosstalk and overlap of signaling pathways perplexing and complicating the cardiotoxicity. Therefore, further in-depth mechanisms deserve urgent investigation to avoid synergistic cardiotoxicity.

In this review, we summarized and discussed six cardiomyocyte death forms associated with drug-induced cardiotoxicity, including apoptosis, autophagy, necrosis, necroptosis, pyroptosis and ferroptosis. However, most of studies focused on the apoptosis, and whether the coexistence of multiple cardiomyocyte death forms was a common phenomenon of drug-induced cardiotoxicity remains to be explored. A recent study found that caspase-8 was the molecular switch that controls apoptosis, necroptosis and pyroptosis, and prevented tissue damage during embryonic development and adulthood (Fritsch et al., 2019). Therefore, it may be an interesting and important research topic to explore the contribution of each form and conversion of different forms in drug-induced cardiomyocyte death.

AUTHOR CONTRIBUTIONS

WM and SW wrote the manuscript. BZ and WL revised the manuscript. All authors read and approved the final version of the manuscript for publication.

FUNDING

This work was supported by grants of the National Natural Scientific Foundation of China (Nos. 81703518 and 81973406), the Hunan Provincial Natural Scientific Foundation (No. 2019JJ50849), and the Scientific Research Project of Hunan Provincial Health and Family Planning Commission (No. B20180253).

REFERENCES

Agustini, F. D., Arozal, W., Louisa, M., Siswanto, S., Soetikno, V., Nafrialdi, N., et al. (2016). Cardioprotection mechanism of mangiferin on doxorubicin-induced rats: focus on intracellular calcium regulation. *Pharm. Biol.* 54, 1289–1297. doi: 10.3109/13880209.2015.1073750

Akolkar, G., Da Silva, Dias, D., Ayyappan, P., Bagchi, A. K., Jassal, D. S., et al. (2017). Vitamin C mitigates oxidative/nitrosative stress and inflammation in doxorubicin-induced cardiomyopathy. *Am. J. Physiol. Heart Circ. Physiol.* 313, H795–H809.

Avci, H., Epikmen, E. T., Ipek, E., Tunca, R., Birincioglu, S. S., Aksit, H., et al. (2017). Protective effects of silymarin and curcumin on cyclophosphamide-induced cardiotoxicity. *Exp. Toxicol. Pathol.* 69, 317–327. doi: 10.1016/j.etp.2017.02.002

Bao, Z., Han, Z., Zhang, B., Yu, Y., Xu, Z., Ma, W., et al. (2019). Arsenic trioxide blocked proliferation and cardiomyocyte differentiation of human induced pluripotent stem cells: implication in cardiac developmental toxicity. *Toxicol. Lett.* 309, 51–58. doi: 10.1016/j.toxlet.2019.03.008

Baraka, A., and Abdelgawad, H. (2010). Targeting apoptosis in the heart of streptozotocin-induced diabetic rats. *J. Cardiovasc. Pharmacol. Ther.* 15, 175–181. doi: 10.1177/1074248409356557

Baranowski, M., Blachnio, A., Zabielski, P., and Gorski, J. (2007). Pioglitazone induces de novo ceramide synthesis in the rat heart. *Prostaglandins Other Lipid Mediat.* 83, 99–111. doi: 10.1016/j.prostaglandins.2006.10.004

Barnhart, B. C., Alappat, E. C., and Peter, M. E. (2003). The CD95 type I/type II model. *Semin. Immunol.* 15, 185–193. doi: 10.1016/s1044-5323(03)00031-9

Bartlett, J. J., Trivedi, P. C., Yeung, P., Kienesberger, P. C., and Pulinilkunnil, T. (2016). Doxorubicin impairs cardiomyocyte viability by suppressing transcription factor EB expression and disrupting autophagy. *Biochem. J.* 473, 3769–3789. doi: 10.1042/bcj20160385

Belmonte, F., Das, S., Sysa-Shah, P., Sivakumaran, V., Stanley, B., Guo, X., et al. (2015). ErbB2 overexpression upregulates antioxidant enzymes, reduces

basal levels of reactive oxygen species, and protects against doxorubicin cardiotoxicity. *Am. J. Physiol. Heart Circ. Physiol.* 309, H1271–H1280.

Bernuzzi, F., Recalcati, S., Alberghini, A., and Cairo, G. (2009). Reactive oxygen species-independent apoptosis in doxorubicin-treated H9c2 cardiomyocytes: role for heme oxygenase-1 down-modulation. *Chem. Biol. Interact* 177, 12–20. doi: 10.1016/j.cbi.2008.09.012

Bouitbir, J., Alshaikhali, A., Panajatovic, M. V., Abegg, V. F., Paech, F., and Krahenbuhl, S. (2019). Mitochondrial oxidative stress plays a critical role in the cardiotoxicity of sunitinib: running title: sunitinib and oxidative stress in hearts. *Toxicology* 426:152281. doi: 10.1016/j.tox.2019.152281

Brito, V. B., Nascimento, L. V., Nunes, R. B., Moura, D. J., Lago, P. D., and Saffi, J. (2016). Exercise during pregnancy decreases doxorubicin-induced cardiotoxic effects on neonatal hearts. *Toxicology* 36, 46–57. doi: 10.1016/j.tox.2016.08.017

Brumatti, G., Salmanidis, M., and Ekert, P. G. (2010). Crossing paths: interactions between the cell death machinery and growth factor survival signals. *Cell Mol. Life Sci.* 67, 1619–1630. doi: 10.1007/s00018-010-0288-8

Cao, Y., Shen, T., Huang, X., Lin, Y., Chen, B., Pang, J., et al. (2017). Astragalus polysaccharide restores autophagic flux and improves cardiomyocyte function in doxorubicin-induced cardiotoxicity. *Oncotarget* 8, 4837–4848. doi: 10.18632/oncotarget.13596

Cao, Z., Ye, P., Long, C., Chen, K., Li, X., and Wang, H. (2007). Effect of pioglitazone, a peroxisome proliferator-activated receptor gamma agonist, on ischemia-reperfusion injury in rats. *Pharmacology* 79, 184–192. doi: 10.1159/000100870

Chae, H. J., Kim, H. R., Lee, W. G., Kwak, Y. K., and Kim, W. H. (2005). Radiation protects adriamycin-induced apoptosis. *Immunopharmacol. Immunotoxicol.* 27, 211–232. doi: 10.1081/iph-200067715

Chambers, T. P., Santiesteban, L., Gomez, D., and Chambers, J. W. (2017). Sab mediates mitochondrial dysfunction involved in imatinib mesylate-induced cardiotoxicity. *Toxicology* 382, 24–35. doi: 10.1016/j.tox.2017.03.006

Chen, G., Chelu, M. G., Dobrev, D., and Li, N. (2018). Cardiomyocyte inflammasome signaling in cardiomyopathies and atrial fibrillation: mechanisms and potential therapeutic implications. *Front. Physiol.* 9:1115. doi: 10.3389/fphys.2018.01115

Chen, K., Xu, X., Kobayashi, S., Timm, D., Jepperson, T., and Liang, Q. (2011). Caloric restriction mimetic 2-deoxyglucose antagonizes doxorubicin-induced cardiomyocyte death by multiple mechanisms. *J. Biol. Chem.* 286, 21993–22006. doi: 10.1074/jbc.m111.225805

Chen, X., Xu, S., Zhao, C., and Liu, B. (2019). Role of TLR4/NADPH oxidase 4 pathway in promoting cell death through autophagy and ferroptosis during heart failure. *Biochem. Biophys. Res. Commun.* 516, 37–43. doi: 10.1016/j.bbrc.2019.06.015

Cheng, H., Kari, G., Dicker, A. P., Rodeck, U., Koch, W. J., and Force, T. (2011). A novel preclinical strategy for identifying cardiotoxic kinase inhibitors and mechanisms of cardiotoxicity. *Circ. Res.* 109, 1401–1409. doi: 10.1161/circresaha.111.255695

Childs, A. C., Phaneuf, S. L., Dirks, A. J., Phillips, T., and Leeuwenburgh, C. (2002). Doxorubicin treatment in vivo causes cytochrome C release and cardiomyocyte apoptosis, as well as increased mitochondrial efficiency, superoxide dismutase activity, and Bcl-2:Bax ratio. *Cancer Res.* 62, 4592–4598.

Chiosi, E., Spina, A., Sorrentino, A., Romano, M., Sorvillo, L., Senatore, G., et al. (2007). Change in TNF-alpha receptor expression is a relevant event in doxorubicin-induced H9c2 cardiomyocyte cell death. *J. Interferon Cytokine Res.* 27, 589–597.

Chowdhury, S., Sinha, K., Banerjee, S., and Sil, P. C. (2016). Taurine protects cisplatin induced cardiotoxicity by modulating inflammatory and endoplasmic reticulum stress responses. *Biofactors* 42, 647–664. doi: 10.1002/biof.1301

Chu, T. F., Rupnick, M. A., Kerkela, R., Dallabrida, S. M., Zurakowski, D., Nguyen, L., et al. (2007). Cardiotoxicity associated with tyrosine kinase inhibitor sunitinib. *Lancet* 370, 2011–2019.

Clavel, M., Simeone, P., and Grivet, B. (1988). [Cardiac toxicity of 5-fluorouracil. review of the literature, 5 new cases]. *Presse Med.* 17, 1675–1678.

Coelho, A. R., Martins, T. R., Couto, R., Deus, C., Pereira, C. V., Simoes, R. F., et al. (2017). Berberine-induced cardioprotection and Sirt3 modulation in doxorubicin-treated H9c2 cardiomyoblasts. *Biochim. Biophys. Acta Mol. Basis Dis.* 1863, 2904–2923. doi: 10.1016/j.bbadis.2017.07.030

Conklin, D. J., Haberzettl, P., Jagatheesan, G., Baba, S., Merchant, M. L., Prough, R. A., et al. (2015). Glutathione S-transferase P protects against cyclophosphamide-induced cardiotoxicity in mice. *Toxicol. Appl. Pharmacol.* 285, 136–148. doi: 10.1016/j.taap.2015.03.029

Cookson, B. T., and Brennan, M. A. (2001). Pro-inflammatory programmed cell death. *Trends Microbiol.* 9, 113–114. doi: 10.1016/s0966-842x(00)01936-3

Cooper, S. L., Sandhu, H., Hussain, A., Mee, C., and Maddock, H. (2018). Involvement of mitogen activated kinase kinase 7 intracellular signalling pathway in Sunitinib-induced cardiotoxicity. *Toxicology* 394, 72–83. doi: 10.1016/j.tox.2017.12.005

Coppola, C., Riccio, G., Barbieri, A., Monti, M. G., Piscopo, G., Rea, D., et al. (2016). Antineoplastic-related cardiotoxicity, morphofunctional aspects in a murine model: contribution of the new tool 2D-speckle tracking. *Onco Targets Ther.* 9, 6785–6794. doi: 10.2147/ott.s106528

Corna, G., Santambrogio, P., Minotti, G., and Cairo, G. (2004). Doxorubicin paradoxically protects cardiomyocytes against iron-mediated toxicity: role of reactive oxygen species and ferritin. *J. Biol. Chem.* 279, 13738–13745. doi: 10.1074/jbc.m310106200

Costa, V. M., Carvalho, F., Duarte, J. A., Bastos Mde, L., and Remiao, F. (2013). The heart as a target for xenobiotic toxicity: the cardiac susceptibility to oxidative stress. *Chem. Res. Toxicol.* 26, 1285–1311. doi: 10.1021/tx400130v

Cunha-Oliveira, T., Ferreira, L. L., Coelho, A. R., Deus, C. M., and Oliveira, P. J. (2018). Doxorubicin triggers bioenergetic failure and p53 activation in mouse stem cell-derived cardiomyocytes. *Toxicol. Appl. Pharmacol.* 348, 1–13. doi: 10.1016/j.taap.2018.04.009

Czabotar, P. E., Lessene, G., Strasser, A., and Adams, J. M. (2014). Control of apoptosis by the BCL-2 protein family: implications for physiology and therapy. *Nat. Rev. Mol. Cell Biol.* 15, 49–63. doi: 10.1038/nrm3722

Damiani, R. M., Moura, D. J., Viau, C. M., Brito, V., Moras, A. M., Henriques, J. P., et al. (2018). Influence of PARP-1 inhibition in the cardiotoxicity of the topoisomerase 2 inhibitors doxorubicin and mitoxantrone. *Toxicol. In Vitro* 52, 203–213. doi: 10.1016/j.tiv.2018.06.013

Deng, S., Kruger, A., Kleschyov, A. L., Kalinowski, L., Daiber, A., and Wojnowski, L. (2007). Gp91phox-containing NAD(P)H oxidase increases superoxide formation by doxorubicin and NADPH. *Free Radic. Biol. Med.* 42, 466–473. doi: 10.1016/j.freeradbiomed.2006.11.013

Dhingra, R., Margulets, V., Chowdhury, S. R., Thliveris, J., Jassal, D., Fernyhough, P., et al. (2014). Bnip3 mediates doxorubicin-induced cardiac myocyte necrosis and mortality through changes in mitochondrial signaling. *Proc. Natl. Acad. Sci. U.S.A.* 111, E5537–E5544.

Dimitrakis, P., Romay-Ogando, M. I., Timolati, F., Suter, T. M., and Zuppinger, C. (2012). Effects of doxorubicin cancer therapy on autophagy and the ubiquitin-proteasome system in long-term cultured adult rat cardiomyocytes. *Cell Tissue Res.* 350, 361–372. doi: 10.1007/s00441-012-1475-8

Doherty, K. R., Wappel, R. L., Talbert, D. R., Trusk, P. B., Moran, D. M., Kramer, J. W., et al. (2013). Multi-parameter in vitro toxicity testing of crizotinib, sunitinib, erlotinib, and nilotinib in human cardiomyocytes. *Toxicol. Appl. Pharmacol.* 272, 245–255. doi: 10.1016/j.taap.2013.04.027

Duran, J. M., Makarewich, C. A., Trappanese, D., Gross, P., Husain, S., Dunn, J., et al. (2014). Sorafenib cardiotoxicity increases mortality after myocardial infarction. *Circ. Res.* 114, 1700–1712. doi: 10.1161/circresaha.114.303200

El-Agamy, D. S., Elkablawy, M. A., and Abo-Haded, H. M. (2017). Modulation of cyclophosphamide-induced cardiotoxicity by methyl palmitate. *Cancer Chemother. Pharmacol.* 79, 399–409. doi: 10.1007/s00280-016-3233-1

El-Awady el, S. E., Moustafa, Y. M., Abo-Elmatty, D. M., and Radwan, A. (2011). Cisplatin-induced cardiotoxicity: mechanisms and cardioprotective strategies. *Eur. J. Pharmacol* 650, 335–341. doi: 10.1016/j.ejphar.2010.09.085

Eskandari, M. R., Moghaddam, F., Shahraki, J., and Pourahmad, J. (2015). A comparison of cardiomyocyte cytotoxic mechanisms for 5-fluorouracil and its pro-drug capecitabine. *Xenobiotica* 45, 79–87. doi: 10.3109/00498254.2014.942809

Ewer, M. S., and Ewer, S. M. (2015). Cardiotoxicity of anticancer treatments. *Nat. Rev. Cardiol.* 12, 547–558. doi: 10.1038/nrcardio.2015.65

Fabbi, P., Spallarossa, P., Garibaldi, S., Barisione, C., Mura, M., Altieri, P., et al. (2015). Doxorubicin impairs the insulin-like growth factor-1 system and causes insulin-like growth factor-1 resistance in cardiomyocytes. *PLoS One* 10:e0124643. doi: 10.1371/journal.pone.0124643

Fan, Y., Wang, C., Zhang, Y., Hang, P., Liu, Y., Pan, Z., et al. (2013). Genistein ameliorates adverse cardiac effects induced by arsenic trioxide through preventing cardiomyocytes apoptosis. *Cell Physiol. Biochem.* 31, 80–91. doi: 10.1159/000343351

Fang, X., Wang, H., Han, D., Xie, E., Yang, X., Wei, J., et al. (2019). Ferroptosis as a target for protection against cardiomyopathy. *Proc. Natl. Acad. Sci. U.S.A.* 116, 2672–2680. doi: 10.1073/pnas.1821022116

Fiala, M., Murphy, T., Macdougall, J., Yang, W., Luque, A., Iruela-Arispe, L., et al. (2004). HAART drugs induce mitochondrial damage and intercellular gaps and gp120 causes apoptosis. *Cardiovasc. Toxicol.* 4, 327–337.

Finck, B. N., and Kelly, D. P. (2007). Peroxisome proliferator-activated receptor gamma coactivator-1 (PGC-1) regulatory cascade in cardiac physiology and disease. *Circulation* 115, 2540–2548. doi: 10.1161/circulationaha.107.670588

Finkel, T. (2006). Cell biology: a clean energy programme. *Nature* 444, 151–152. doi: 10.1038/444151a

Focaccetti, C., Bruno, A., Magnani, E., Bartolini, D., Principi, E., Dallaglio, K., et al. (2015). Effects of 5-fluorouracil on morphology, cell cycle, proliferation, apoptosis, autophagy and ROS production in endothelial cells and cardiomyocytes. *PLoS One* 10:e0115686. doi: 10.1371/journal.pone.0115686

Fritsch, M., Gunther, S. D., Schwarzer, R., Albert, M. C., Schorn, F., Werthenbach, J. P., et al. (2019). Caspase-8 is the molecular switch for apoptosis, necroptosis and pyroptosis. *Nature* 575, 683–687. doi: 10.1038/s41586-019-1770-6

Fulbright, J. M., Egas-Bejar, D. E., Huh, W. W., and Chandra, J. (2015). Analysis of redox and apoptotic effects of anthracyclines to delineate a cardioprotective strategy. *Cancer Chemother. Pharmacol.* 76, 1297–1307. doi: 10.1007/s00280-015-2879-4

Galluzzi, L., Vitale, I., Aaronson, S. A., Abrams, J. M., Adam, D., Agostinis, P., et al. (2018). Molecular mechanisms of cell death: recommendations of the nomenclature committee on cell death 2018. *Cell Death. Differ.* 25, 486–541.

Gao, R. Y., Mukhopadhyay, P., Mohanraj, R., Wang, H., Horvath, B., Yin, S., et al. (2011). Resveratrol attenuates azidothymidine-induced cardiotoxicity by decreasing mitochondrial reactive oxygen species generation in human cardiomyocytes. *Mol. Med. Rep.* 4, 151–155.

Ghosh, J., Das, J., Manna, P., and Sil, P. C. (2009). Taurine prevents arsenic-induced cardiac oxidative stress and apoptotic damage: role of NF-kappa B, p38 and JNK MAPK pathway. *Toxicol. Appl. Pharmacol.* 240, 73–87. doi: 10.1016/j.taap.2009.07.008

Giulivi, C., Boveris, A., and Cadenas, E. (1995). Hydroxyl radical generation during mitochondrial electron transfer and the formation of 8-hydroxydesoxyguanosine in mitochondrial DNA. *Arch. Biochem. Biophys.* 316, 909–916. doi: 10.1006/abbi.1995.1122

Goyal, V., Bews, H., Cheung, D., Premecz, S., Mandal, S., Shaikh, B., et al. (2016). The Cardioprotective role of N-Acetyl cysteine amide in the prevention of doxorubicin and trastuzumab-mediated cardiac dysfunction. *Can. J. Cardiol.* 32, 1513–1519. doi: 10.1016/j.cjca.2016.06.002

Grazette, L. P., Boecker, W., Matsui, T., Semigran, M., Force, T. L., Hajjar, R. J., et al. (2004). Inhibition of ErbB2 causes mitochondrial dysfunction in cardiomyocytes: implications for herceptin-induced cardiomyopathy. *J. Am. Coll. Cardiol.* 44, 2231–2238. doi: 10.1016/j.jacc.2004.08.066

Grootjans, S., Vanden Berghe, T., and Vandenabeele, P. (2017). Initiation and execution mechanisms of necroptosis: an overview. *Cell Death. Differ.* 24, 1184–1195. doi: 10.1038/cdd.2017.65

Gu, J., Hu, W., Song, Z. P., Chen, Y. G., Zhang, D. D., and Wang, C. Q. (2016). Resveratrol-induced autophagy promotes survival and attenuates doxorubicin-induced cardiotoxicity. *Int. Immunopharmacol.* 32, 1–7. doi: 10.1016/j.intimp.2016.01.002

He, H., Tao, H., Xiong, H., Duan, S. Z., Mcgowan, F. X., Mortensen, R. M., et al. (2014). Rosiglitazone causes cardiotoxicity via peroxisome proliferator-activated receptor gamma-independent mitochondrial oxidative stress in mouse hearts. *Toxicol. Sci.* 138, 468–481. doi: 10.1093/toxsci/kfu015

Herman, E. H., Zhang, J., Hasinoff, B. B., Clark, J. R., and Ferrans, V. J. (1997). Comparison of the structural changes induced by doxorubicin and mitoxantrone in the heart, kidney and intestine and characterization of the Fe(III)-mitoxantrone complex. *J. Mol. Cell Cardiol.* 29, 2415–2430. doi: 10.1006/jmcc.1997.0477

Herrmann, J., Yang, E. H., Iliescu, C. A., Cilingiroglu, M., Charitakis, K., Hakeem, A., et al. (2016). Vascular toxicities of cancer therapies: the old and the new–an evolving avenue. *Circulation* 133, 1272–1289. doi: 10.1161/circulationaha.115.018347

Holbro, T., and Hynes, N. E. (2004). ErbB receptors: directing key signaling networks throughout life. *Annu. Rev. Pharmacol. Toxicol.* 44, 195–217. doi: 10.1146/annurev.pharmtox.44.101802.121440

Horie, T., Ono, K., Nishi, H., Nagao, K., Kinoshita, M., Watanabe, S., et al. (2010). Acute doxorubicin cardiotoxicity is associated with miR-146a-induced inhibition of the neuregulin-ErbB pathway. *Cardiovasc. Res.* 87, 656–664. doi: 10.1093/cvr/cvq148

Hsu, P. L., and Mo, F. E. (2016). Matricellular protein CCN1 mediates doxorubicin-induced cardiomyopathy in mice. *Oncotarget* 7, 36698–36710. doi: 10.18632/oncotarget.9162

Hu, W., Lu, S., Mcalpine, I., Jamieson, J. D., Lee, D. U., Marroquin, L. D., et al. (2012). Mechanistic investigation of imatinib-induced cardiac toxicity and the involvement of c-Abl kinase. *Toxicol. Sci.* 129, 188–199. doi: 10.1093/toxsci/kfs192

Hutt, K. J. (2015). The role of BH3-only proteins in apoptosis within the ovary. *Reproduction* 149, R81–R89.

Imai, H., Matsuoka, M., Kumagai, T., Sakamoto, T., and Koumura, T. (2017). Lipid peroxidation-dependent cell death regulated by GPx4 and ferroptosis. *Curr. Top. Microbiol. Immunol.* 403, 143–170. doi: 10.1007/82_2016_508

Jiang, J., Mohan, N., Endo, Y., Shen, Y., and Wu, W. J. (2018). Type IIB DNA topoisomerase is downregulated by trastuzumab and doxorubicin to synergize cardiotoxicity. *Oncotarget* 9, 6095–6108. doi: 10.18632/oncotarget.23543

Jing, X., Yang, J., Jiang, L., Chen, J., and Wang, H. (2018). MicroRNA-29b regulates the mitochondria-dependent apoptotic pathway by targeting bax in doxorubicin cardiotoxicity. *Cell Physiol. Biochem.* 48, 692–704. doi: 10.1159/000491896

Jorgensen, I., and Miao, E. A. (2015). Pyroptotic cell death defends against intracellular pathogens. *Immunol. Rev.* 265, 130–142. doi: 10.1111/imr.12287

Jung, C. H., Ro, S. H., Cao, J., Otto, N. M., and Kim, D. H. (2010). mTOR regulation of autophagy. *FEBS Lett.* 584, 1287–1295.

Kaiser, W. J., Sridharan, H., Huang, C., Mandal, P., Upton, J. W., Gough, P. J., et al. (2013). Toll-like receptor 3-mediated necrosis via TRIF. RIP3, and MLKL. *J. Biol. Chem.* 288, 31268–31279. doi: 10.1074/jbc.m113.462341

Kalivendi, S. V., Konorev, E. A., Cunningham, S., Vanamala, S. K., Kaji, E. H., Joseph, J., et al. (2005). Doxorubicin activates nuclear factor of activated T-lymphocytes and Fas ligand transcription: role of mitochondrial reactive oxygen species and calcium. *Biochem. J.* 389, 527–539. doi: 10.1042/bj20050285

Kawaguchi, T., Takemura, G., Kanamori, H., Takeyama, T., Watanabe, T., Morishita, K., et al. (2012). Prior starvation mitigates acute doxorubicin cardiotoxicity through restoration of autophagy in affected cardiomyocytes. *Cardiovasc. Res.* 96, 456–465. doi: 10.1093/cvr/cvs282

Kim, J., Kundu, M., Viollet, B., and Guan, K.-L. (2011). AMPK and mTOR regulate autophagy through direct phosphorylation of Ulk1. *Nat. Cell Biol.* 13, 132–134.

Kim, Y., Ma, A. G., Kitta, K., Fitch, S. N., Ikeda, T., Ihara, Y., et al. (2003). Anthracycline-induced suppression of GATA-4 transcription factor: implication in the regulation of cardiac myocyte apoptosis. *Mol. Pharmacol.* 63, 368–377. doi: 10.1124/mol.63.2.368

Kimura, T., Uesugi, M., Takase, K., Miyamoto, N., and Sawada, K. (2017). Hsp90 inhibitor geldanamycin attenuates the cytotoxicity of sunitinib in cardiomyocytes via inhibition of the autophagy pathway. *Toxicol. Appl. Pharmacol* 329, 282–292. doi: 10.1016/j.taap.2017.06.015

Klionsky, D. J., Abdelmohsen, K., Abe, A., Abedin, M. J., Abeliovich, H., Acevedo Arozena, A., et al. (2016). Guidelines for the use and interpretation of assays for monitoring autophagy (3rd edition). *Autophagy* 12, 1–222.

Kobayashi, S., Volden, P., Timm, D., Mao, K., Xu, X., and Liang, Q. (2010). Transcription factor GATA4 inhibits doxorubicin-induced autophagy and cardiomyocyte death. *J. Biol. Chem.* 285, 793–804. doi: 10.1074/jbc.m109.070037

Koleini, N., Nickel, B. E., Edel, A. L., Fandrich, R. R., Ravandi, A., and Kardami, E. (2019). Oxidized phospholipids in Doxorubicin-induced cardiotoxicity. *Chem. Biol. Interact* 303, 35–39. doi: 10.1016/j.cbi.2019.01.032

Kurauchi, K., Nishikawa, T., Miyahara, E., Okamoto, Y., and Kawano, Y. (2017). Role of metabolites of cyclophosphamide in cardiotoxicity. *BMC Res Notes* 10:406. doi: 10.1186/s13104-017-2726-2

Lakkur, S., Judd, S., Bostick, R. M., Mcclellan, W., Flanders, W. D., Stevens, V. L., et al. (2015). Oxidative stress, inflammation, and markers of cardiovascular health. *Atherosclerosis* 243, 38–43. doi: 10.1016/j.atherosclerosis.2015.08.032

Lamberti, M., Porto, S., Marra, M., Zappavigna, S., Grimaldi, A., Feola, D., et al. (2012). 5-Fluorouracil induces apoptosis in rat cardiocytes through intracellular oxidative stress. *J. Exp. Clin. Cancer Res.* 31:60. doi: 10.1186/1756-9966-31-60

Lan, Y., Wang, Y., Huang, K., and Zeng, Q. (2020). Heat shock protein 22 attenuates doxorubicin-induced cardiotoxicity via regulating inflammation and apoptosis. *Front. Pharmacol.* 11:257. doi: 10.3389/fphar.2020.00257

Lekes, D., Szadvari, I., Krizanova, O., Lopusna, K., Rezuchova, I., Novakova, M., et al. (2016). Nilotinib induces ER stress and cell death in H9c2 cells. *Physiol. Res.* 65, S505–S514.

Lemmens, K., Doggen, K., and De Keulenaer, G. W. (2007). Role of neuregulin-1/ErbB signaling in cardiovascular physiology and disease: implications for therapy of heart failure. *Circulation* 116, 954–960. doi: 10.1161/circulationaha.107.690487

Li, D. L., Wang, Z. V., Ding, G., Tan, W., Luo, X., Criollo, A., et al. (2016). Doxorubicin blocks cardiomyocyte autophagic flux by inhibiting lysosome acidification. *Circulation* 133, 1668–1687. doi: 10.1161/circulationaha.115.017443

Li, S., Wang, W., Niu, T., Wang, H., Li, B., Shao, L., et al. (2014). Nrf2 deficiency exaggerates doxorubicin-induced cardiotoxicity and cardiac dysfunction. *Oxid Med. Cell Longev* 2014:748524.

Li, S., Zhao, H., Wang, Y., Shao, Y., Liu, J., and Xing, M. (2019). Arsenic-induced cardiotoxicity correlates with mitochondrial damage and trace elements imbalance in broiler chickens. *Poult. Sci.* 98, 734–744. doi: 10.3382/ps/pey469

Li, S., Zhao, H., Wang, Y., Shao, Y., Wang, B., Wang, Y., et al. (2018). Regulation of autophagy factors by oxidative stress and cardiac enzymes imbalance during arsenic or/and copper induced cardiotoxicity in *Gallus gallus*. *Ecotoxicol. Environ. Saf.* 148, 125–134. doi: 10.1016/j.ecoenv.2017.10.018

Li, W. J., Zhang, X. Y., Wu, R. T., Song, Y. H., and Xie, M. Y. (2018). Ganoderma atrum polysaccharide improves doxorubicin-induced cardiotoxicity in mice by regulation of apoptotic pathway in mitochondria. *Carbohydr. Polym.* 202, 581–590. doi: 10.1016/j.carbpol.2018.08.144

Li, S. W., Sun, X., He, Y., Guo, Y., Zhao, H. J., Hou, Z. J., et al. (2017). Assessment of arsenic trioxide in the heart of Gallus gallus: alterations of oxidative damage parameters, inflammatory cytokines, and cardiac enzymes. *Environ. Sci. Pollut. Res. Int.* 24, 5781–5790. doi: 10.1007/s11356-016-8223-7

Lim, C. C., Zuppinger, C., Guo, X., Kuster, G. M., Helmes, M., Eppenberger, H. M., et al. (2004). Anthracyclines induce calpain-dependent titin proteolysis and necrosis in cardiomyocytes. *J. Biol. Chem.* 279, 8290–8299. doi: 10.1074/jbc.m308033200

Lin, H., Stankov, M. V., Hegermann, J., Budida, R., Panayotova-Dimitrova, D., Schmidt, R. E., et al. (2019). Zidovudine-mediated autophagy inhibition enhances mitochondrial toxicity in muscle cells. *Antimicrob. Agents Chemother* 63:e01443-18. doi: 10.1128/AAC.01443-18

Lischke, J., Lang, C., Sawodny, O., and Feuer, R. (2015). Impairment of energy metabolism in cardiomyocytes caused by 5-FU catabolites can be compensated by administration of amino acids. *Conf. Proc. IEEE Eng. Med. Biol. Soc.* 2015, 5363–5366.

Lu, L., Wu, W., Yan, J., Li, X., Yu, H., and Yu, X. (2009). Adriamycin-induced autophagic cardiomyocyte death plays a pathogenic role in a rat model of heart failure. *Int. J. Cardiol.* 134, 82–90. doi: 10.1016/j.ijcard.2008.01.043

Ludke, A., Akolkar, G., Ayyappan, P., Sharma, A. K., and Singal, P. K. (2017). Time course of changes in oxidative stress and stress-induced proteins in cardiomyocytes exposed to doxorubicin and prevention by vitamin C. *PLoS One* 12:e0179452. doi: 10.1371/journal.pone.0179452

Luo, P., Zhu, Y., Chen, M., Yan, H., Yang, B., Yang, X., et al. (2018). HMGB1 contributes to adriamycin-induced cardiotoxicity via up-regulating autophagy. *Toxicol. Lett.* 292, 115–122. doi: 10.1016/j.toxlet.2018.04.034

Lushnikova, E. L., Nepomnyashchikh, L. M., Sviridov, E. A., and Klinnikova, M. G. (2008). Ultrastructural signs of cyclophosphamide-induced damage to cardiomyocytes. *Bull. Exp. Biol. Med.* 146, 366–371. doi: 10.1007/s10517-008-0287-z

Ma, H., Jones, K. R., Guo, R., Xu, P., Shen, Y., and Ren, J. (2010). Cisplatin compromises myocardial contractile function and mitochondrial ultrastructure: role of endoplasmic reticulum stress. *Clin. Exp. Pharmacol. Physiol.* 37, 460–465. doi: 10.1111/j.1440-1681.2009.05323.x

Maharsy, W., Aries, A., Mansour, O., Komati, H., and Nemer, M. (2014). Ageing is a risk factor in imatinib mesylate cardiotoxicity. *Eur. J. Heart Fail.* 16, 367–376. doi: 10.1002/ejhf.58

Malisza, K. L., and Hasinoff, B. B. (1995). Production of hydroxyl radical by iron(III)-anthraquinone complexes through self-reduction and through reductive activation by the xanthine oxidase/hypoxanthine system. *Arch. Biochem. Biophys.* 321, 51–60. doi: 10.1006/abbi.1995.1367

Man, S. M., Karki, R., and Kanneganti, T. D. (2017). Molecular mechanisms and functions of pyroptosis, inflammatory caspases and inflammasomes in infectious diseases. *Immunol. Rev.* 277, 61–75. doi: 10.1111/imr.12534

Meng, L., Lin, H., Zhang, J., Lin, N., Sun, Z., Gao, F., et al. (2019). Doxorubicin induces cardiomyocyte pyroptosis via the TINCR-mediated posttranscriptional stabilization of NLR family pyrin domain containing 3. *J. Mol. Cell Cardiol.* 136, 15–26. doi: 10.1016/j.yjmcc.2019.08.009

Miao, X., Tang, Z., Wang, Y., Su, G., Sun, W., Wei, W., et al. (2013). Metallothionein prevention of arsenic trioxide-induced cardiac cell death is associated with its inhibition of mitogen-activated protein kinases activation in vitro and in vivo. *Toxicol. Lett.* 220, 277–285. doi: 10.1016/j.toxlet.2013.04.025

Milano, G., Biemmi, V., Lazzarini, E., Balbi, C., Ciullo, A., Bolis, S., et al. (2020). Intravenous administration of cardiac progenitor cell-derived exosomes protects against doxorubicin/trastuzumab-induced cardiac toxicity. *Cardiovasc. Res.* 116, 383–392.

Mirkes, P. E., and Little, S. A. (1998). Teratogen-induced cell death in postimplantation mouse embryos: differential tissue sensitivity and hallmarks of apoptosis. *Cell Death. Differ.* 5, 592–600. doi: 10.1038/sj.cdd.4400390

Mirkes, P. E., Wilson, K. L., and Cornel, L. M. (2000). Teratogen-induced activation of ERK, JNK, and p38 MAP kinases in early postimplantation murine embryos. *Teratology* 62, 14–25. doi: 10.1002/1096-9926(200007)62:1<14::aid-tera6>3.0.co;2-9

Mishra, P., Singh, S. V., Verma, A. K., Srivastava, P., Sultana, S., and Rath, S. K. (2014). Rosiglitazone induces cardiotoxicity by accelerated apoptosis. *Cardiovasc. Toxicol.* 14, 99–119. doi: 10.1007/s12012-013-9234-y

Mohan, N., Jiang, J., and Wu, W. J. (2017). Implications of autophagy and oxidative stress in trastuzumab-mediated cardiac toxicities. *Austin. Pharmacol. Pharm.* 2:1005.

Mohan, N., Shen, Y., Endo, Y., Elzarrad, M. K., and Wu, W. J. (2016). Trastuzumab, but not pertuzumab, dysregulates HER2 signaling to mediate inhibition of autophagy and increase in reactive oxygen species production in human cardiomyocytes. *Mol. Cancer Ther.* 15, 1321–1331. doi: 10.1158/1535-7163.mct-15-0741

Mukhopadhyay, P., Rajesh, M., Batkai, S., Kashiwaya, Y., Hasko, G., Liaudet, L., et al. (2009). Role of superoxide, nitric oxide, and peroxynitrite in doxorubicin-induced cell death in vivo and in vitro. *Am. J. Physiol. Heart Circ. Physiol.* 296, H1466–H1483.

Nagi, M. N., Al-Shabanah, O. A., Hafez, M. M., and Sayed-Ahmed, M. M. (2011). Thymoquinone supplementation attenuates cyclophosphamide-induced cardiotoxicity in rats. *J. Biochem. Mol. Toxicol.* 25, 135–142. doi: 10.1002/jbt.20369

Nakamura, T., Ueda, Y., Juan, Y., Katsuda, S., Takahashi, H., and Koh, E. (2000). Fas-mediated apoptosis in adriamycin-induced cardiomyopathy in rats: in vivo study. *Circulation* 102, 572–578. doi: 10.1161/01.cir.102.5.572

Nicol, M., Baudet, M., and Cohen-Solal, A. (2019). Subclinical left ventricular dysfunction during chemotherapy. *Cardiac Fail. Rev.* 5, 31–36.

Nishikawa, T., Miyahara, E., Kurauchi, K., Watanabe, E., Ikawa, K., Asaba, K., et al. (2015). Mechanisms of fatal cardiotoxicity following high-dose cyclophosphamide therapy and a method for its prevention. *PLoS One* 10:e0131394. doi: 10.1371/journal.pone.0131394

Omole, J. G., Ayoka, O. A., Alabi, Q. K., Adefisayo, M. A., Asafa, M. A., Olubunmi, B. O., et al. (2018). Protective effect of kolaviron on cyclophosphamide-induced cardiac toxicity in rats. *J. Evid. Based Integr. Med.* 23:2156587218757649.

Padegimas, A., Clasen, S., and Ky, B. (2020). Cardioprotective strategies to prevent breast cancer therapy-induced cardiotoxicity. *Trends Cardiovasc. Med.* 30, 22–28. doi: 10.1016/j.tcm.2019.01.006

Palee, S., Weerateerangkul, P., Chinda, K., Chattipakorn, S. C., and Chattipakorn, N. (2013). Mechanisms responsible for beneficial and adverse effects of rosiglitazone in a rat model of acute cardiac ischaemia-reperfusion. *Exp. Physiol.* 98, 1028–1037. doi: 10.1113/expphysiol.2012.070433

Papparella, I., Ceolotto, G., Berto, L., Cavalli, M., Bova, S., Cargnelli, G., et al. (2007). Vitamin C prevents zidovudine-induced NAD(P)H oxidase activation and hypertension in the rat. *Cardiovasc. Res.* 73, 432–438. doi: 10.1016/j.cardiores.2006.10.010

Patel, V. G., and Cornell, R. F. (2019). Cardiovascular complications associated with multiple myeloma therapies: incidence, pathophysiology, and management. *Curr. Oncol. Rep.* 21:29.

Pentassuglia, L., Timolati, F., Seifriz, F., Abudukadier, K., Suter, T. M., and Zuppinger, C. (2007). Inhibition of ErbB2/neuregulin signaling augments paclitaxel-induced cardiotoxicity in adult ventricular myocytes. *Exp. Cell Res.* 313, 1588–1601. doi: 10.1016/j.yexcr.2007.02.007

Peyssonnaux, C., Nizet, V., and Johnson, R. S. (2008). Role of the hypoxia inducible factors HIF in iron metabolism. *Cell Cycle* 7, 28–32. doi: 10.4161/cc.7.1.5145

Pistillucci, G., Ciorra, A. A., Sciacca, V., Raponi, M., Rossi, R., and Veltri, E. (2015). Troponin I and B-type natriuretic peptide (BNP) as biomarkers for the prediction of cardiotoxicity in patients with breast cancer treated with adjuvant anthracyclines and trastuzumab. *Clin. Terapeutica* 166, E67–E71.

Purevjav, E., Nelson, D. P., Varela, J. J., Jimenez, S., Kearney, D. L., Sanchez, X. V., et al. (2007). Myocardial fas ligand expression increases susceptibility to AZT-induced cardiomyopathy. *Cardiovasc. Toxicol.* 7, 255–263. doi: 10.1007/s12012-007-9004-9

Qian, P., Yan, L. J., Li, Y. Q., Yang, H. T., Duan, H. Y., Wu, J. T., et al. (2018). Cyanidin ameliorates cisplatin-induced cardiotoxicity via inhibition of ROS-mediated apoptosis. *Exp. Ther. Med.* 15, 1959–1965.

Raghu, K. G., and Cherian, O. L. (2009). Characterization of cytotoxicity induced by arsenic trioxide (a potent anti-APL drug) in rat cardiac myocytes. *J. Trace Elem. Med. Biol.* 23, 61–68. doi: 10.1016/j.jtemb.2008.10.001

Refaie, M. M. M., Shehata, S., El-Hussieny, M., Abdelraheem, W. M., and Bayoumi, A. M. A. (2020). Role of ATP-sensitive potassium channel (KATP) and eNOS in mediating the protective effect of nicorandil in cyclophosphamide-induced cardiotoxicity. *Cardiovasc. Toxicol.* 20, 71–81. doi: 10.1007/s12012-019-09535-8

Rharass, T., Gbankoto, A., Canal, C., Kursunluoglu, G., Bijoux, A., Panakova, D., et al. (2016). Oxidative stress does not play a primary role in the toxicity induced with clinical doses of doxorubicin in myocardial H9c2 cells. *Mol. Cell. Biochem.* 413, 199–215. doi: 10.1007/s11010-016-2653-x

Rohrbach, S., Muller-Werdan, U., Werdan, K., Koch, S., Gellerich, N. F., and Holtz, J. (2005). Apoptosis-modulating interaction of the neuregulin/erbB pathway with anthracyclines in regulating Bcl-xS and Bcl-xL in cardiomyocytes. *J. Mol. Cell Cardiol.* 38, 485–493. doi: 10.1016/j.yjmcc.2004.12.013

Roos, W. P., Thomas, A. D., and Kaina, B. (2016). DNA damage and the balance between survival and death in cancer biology. *Nat. Rev. Cancer* 16, 20–33. doi: 10.1038/nrc.2015.2

Rossato, L. G., Costa, V. M., Vilas-Boas, V., De Lourdes Bastos, M., Rolo, A., Palmeira, C., et al. (2013). Therapeutic concentrations of mitoxantrone elicit energetic imbalance in H9c2 cells as an earlier event. *Cardiovasc. Toxicol.* 13, 413–425. doi: 10.1007/s12012-013-9224-0

Ry, G., Mukhopadhyay, P., Mohanraj, R., Wang, H., Horváth, B., and Yin, S. (2011). Resveratrol attenuates azidothymidine-induced cardiotoxicity by decreasing mitochondrial reactive oxygen species generation in human cardiomyocytes. *Mol. Med. Rep.* 4, 151–155.

Sawyer, D. B., Zuppinger, C., Miller, T. A., Eppenberger, H. M., and Suter, T. M. (2002). Modulation of anthracycline-induced myofibrillar disarray in rat ventricular myocytes by neuregulin-1beta and anti-erbB2: potential mechanism for trastuzumab-induced cardiotoxicity. *Circulation* 105, 1551–1554. doi: 10.1161/01.cir.0000013839.41224.1c

Shi, J., Zhao, Y., Wang, K., Shi, X., Wang, Y., Huang, H., et al. (2015). Cleavage of GSDMD by inflammatory caspases determines pyroptotic cell death. *Nature* 526, 660–665. doi: 10.1038/nature15514

Singh, A. P., Glennon, M. S., Umbarkar, P., Gupte, M., Galindo, C. L., Zhang, Q., et al. (2019). Ponatinib-induced cardiotoxicity: delineating the signalling mechanisms and potential rescue strategies. *Cardiovasc. Res.* 115, 966–977. doi: 10.1093/cvr/cvz006

Singh, K. K., Shukla, P. C., Quan, A., Lovren, F., Pan, Y., Wolfstadt, J. I., et al. (2011). Herceptin, a recombinant humanized anti-ERBB2 monoclonal antibody, induces cardiomyocyte death. *Biochem. Biophys. Res. Commun.* 411, 421–426. doi: 10.1016/j.bbrc.2011.06.169

Singla, D. K., Johnson, T. A., and Tavakoli Dargani, Z. (2019). Exosome treatment enhances anti-inflammatory M2 macrophages and reduces inflammation-induced pyroptosis in doxorubicin-induced cardiomyopathy. *Cells* 8:1224. doi: 10.3390/cells8101224

Soliman, A. F., Anees, L. M., and Ibrahim, D. M. (2018). Cardioprotective effect of zingerone against oxidative stress, inflammation, and apoptosis induced by cisplatin or gamma radiation in rats. *Naunyn Schmiedebergs Arch. Pharmacol.* 391, 819–832. doi: 10.1007/s00210-018-1506-4

Song, B. W., and Wang, L. (2013). [Necroptosis: a programmed cell necrosis]. *Sheng Li Ke Xue Jin Zhan* 44, 281–286.

Song, R., Yang, Y., Lei, H., Wang, G., Huang, Y., Xue, W., et al. (2018). HDAC6 inhibition protects cardiomyocytes against doxorubicin-induced acute damage by improving alpha-tubulin acetylation. *J. Mol. Cell Cardiol.* 124, 58–69. doi: 10.1016/j.yjmcc.2018.10.007

Spagnuolo, R. D., Recalcati, S., Tacchini, L., and Cairo, G. (2011). Role of hypoxia-inducible factors in the dexrazoxane-mediated protection of cardiomyocytes from doxorubicin-induced toxicity. *Br. J. Pharmacol.* 163, 299–312. doi: 10.1111/j.1476-5381.2011.01208.x

Sumneang, N., Siri-Angkul, N., Kumfu, S., Chattipakorn, S. C., and Chattipakorn, N. (2020). The effects of iron overload on mitochondrial function, mitochondrial dynamics, and ferroptosis in cardiomyocytes. *Arch. Biochem. Biophys.* 680:108241. doi: 10.1016/j.abb.2019.108241

Sun, Z., Lu, W., Lin, N., Lin, H., Zhang, J., Ni, T., et al. (2020). Dihydromyricetin alleviates doxorubicin-induced cardiotoxicity by inhibiting NLRP3 inflammasome through activation of SIRT1. *Biochem. Pharmacol.* 175:113888. doi: 10.1016/j.bcp.2020.113888

Szabados, E., Fischer, G. M., Toth, K., Csete, B., Nemeti, B., Trombitas, K., et al. (1999). Role of reactive oxygen species and poly-ADP-ribose polymerase in the development of AZT-induced cardiomyopathy in rat. *Free Radic. Biol. Med.* 26, 309–317. doi: 10.1016/s0891-5849(98)00199-3

Tavakoli, R., Dargani, Z., and Singla, D. K. (2019). Embryonic stem cell-derived exosomes inhibit doxorubicin-induced TLR4-NLRP3-mediated cell death-pyroptosis. *Am. J. Physiol. Heart Circ. Physiol.* 317, H460–H471.

Topal, I., Ozbek Bilgin, A., Keskin Cimen, F., Kurt, N., Suleyman, Z., Bilgin, Y., et al. (2018). The effect of rutin on cisplatin-induced oxidative cardiac damage in rats. *Anatol. J. Cardiol.* 20, 136–142.

Tsibiribi, P., Bui-Xuan, C., Bui-Xuan, B., Lombard-Bohas, C., Duperret, S., Belkhiria, M., et al. (2006). Cardiac lesions induced by 5-fluorouracil in the rabbit. *Hum. Exp. Toxicol.* 25, 305–309. doi: 10.1191/0960327106ht628oa

Tummers, B., and Green, D. R. (2017). Caspase-8: regulating life and death. *Immunol. Rev.* 277, 76–89. doi: 10.1111/imr.12541

Varghese, M. V., Abhilash, M., Paul, M. V., Alex, M., and Nair, R. H. (2017). Omega-3 fatty acid protects against arsenic trioxide-induced cardiotoxicity in vitro and in vivo. *Cardiovasc. Toxicol.* 17, 109–119. doi: 10.1007/s12012-016-9361-3

Vasquez-Vivar, J., Kalyanaraman, B., Martasek, P., Hogg, N., Masters, B. S., Karoui, H., et al. (1998). Superoxide generation by endothelial nitric oxide synthase: the influence of cofactors. *Proc. Natl. Acad. Sci. U.S.A.* 95, 9220–9225. doi: 10.1073/pnas.95.16.9220

Vasquez-Vivar, J., Martasek, P., Hogg, N., Masters, B. S., Pritchard, K. A., and Kalyanaraman, B. (1997). Endothelial nitric oxide synthase-dependent superoxide generation from adriamycin. *Biochemistry* 36, 11293–11297. doi: 10.1021/bi971475e

Vejpongsa, P., and Yeh, E. T. (2014). Topoisomerase 2beta: a promising molecular target for primary prevention of anthracycline-induced cardiotoxicity. *Clin. Pharmacol. Ther.* 95, 45–52. doi: 10.1038/clpt.2013.201

Vineetha, V. P., Soumya, R. S., and Raghu, K. G. (2015). Phloretin ameliorates arsenic trioxide induced mitochondrial dysfunction in H9c2 cardiomyoblasts mediated via alterations in membrane permeability and ETC complexes. *Eur. J. Pharmacol.* 754, 162–172. doi: 10.1016/j.ejphar.2015.02.036

Voskens, C. J., Goldinger, S. M., Loquai, C., Robert, C., Kaehler, K. C., Berking, C., et al. (2013). The price of tumor control: an analysis of rare side effects of anti-CTLA-4 therapy in metastatic melanoma from the ipilimumab network. *PLoS One* 8:e53745. doi: 10.1371/journal.pone.0053745

Wadia, S. (2015). Acute cyclophosphamide hemorrhagic myopericarditis: dilemma case report. Literature review and proposed diagnostic criteria. *J. Clin. Diagn Res.* 9, Oe01–Oe03.

Wang, J. C. (2002). Cellular roles of DNA topoisomerases: a molecular perspective. *Nat. Rev. Mol. Cell Biol.* 3, 430–440. doi: 10.1038/nrm831

Watanabe, M., Funakoshi, T., Unuma, K., Aki, T., and Uemura, K. (2014). Activation of the ubiquitin-proteasome system against arsenic trioxide cardiotoxicity involves ubiquitin ligase Parkin for mitochondrial homeostasis. *Toxicology* 322, 43–50. doi: 10.1016/j.tox.2014.04.008

Wu, C.-C., and Bratton, S. B. (2013). Regulation of the intrinsic apoptosis pathway by reactive oxygen species. *Antioxid. Redox Signal.* 19, 546–558. doi: 10.1089/ars.2012.4905

Wu, C. C., Li, Y. C., Wang, Y. R., Li, T. K., and Chan, N. L. (2013). On the structural basis and design guidelines for type II topoisomerase-targeting anticancer drugs. *Nucleic Acids Res.* 41, 10630–10640. doi: 10.1093/nar/gkt828

Xu, Y., He, B., Wang, Y. J., and Fu, Q. (2004). [Effect of herceptin combined with Doxorubicin on rat cardiotoxicity]. *Ai Zheng* 23, 367–371.

Xu, Z., Jin, Y., Yan, H., Gao, Z., Xu, B., Yang, B., et al. (2018). High-mobility group box 1 protein-mediated necroptosis contributes to dasatinib-induced cardiotoxicity. *Toxicol. Lett.* 296, 39–47. doi: 10.1016/j.toxlet.2018.08.003

Yamaoka, M., Yamaguchi, S., Suzuki, T., Okuyama, M., Nitobe, J., Nakamura, N., et al. (2000). Apoptosis in rat cardiac myocytes induced by Fas ligand: priming for Fas-mediated apoptosis with doxorubicin. *J. Mol. Cell Cardiol.* 32, 881–889. doi: 10.1006/jmcc.2000.1132

Yang, J. K. (2015). Death effecter domain for the assembly of death-inducing signaling complex. *Apoptosis* 20, 235–239. doi: 10.1007/s10495-014-1060-6

Yang, Q., Wen, L., Meng, Z., and Chen, Y. (2018). Blockage of endoplasmic reticulum stress attenuates nilotinib-induced cardiotoxicity by inhibition of the Akt-GSK3beta-Nox4 signaling. *Eur. J. Pharmacol* 822, 85–94. doi: 10.1016/j.ejphar.2018.01.011

Yang, S., Liu, J., Qu, C., Sun, J., Zhang, B. Q., Sun, Y. R., et al. (2017). [Potassium channels and autophagy]. *Sheng Li Xue Bao* 69, 509–514.

Yousif, N. G., and Al-Amran, F. G. (2011). Novel Toll-like receptor-4 deficiency attenuates trastuzumab (Herceptin) induced cardiac injury in mice. *BMC Cardiovasc. Disord.* 11:62. doi: 0.1186/1471-2261-11-62

Yu, J., Wang, C., Kong, Q., Wu, X., Lu, J. J., and Chen, X. (2018). Recent progress in doxorubicin-induced cardiotoxicity and protective potential of natural products. *Phytomedicine* 40, 125–139. doi: 10.1016/j.phymed.2018.01.009

Yu, W., Sun, H., Zha, W., Cui, W., Xu, L., Min, Q., et al. (2017). apigenin attenuates adriamycin-induced cardiomyocyte apoptosis via the PI3K/AKT/mTOR pathway. *Evid Based Complement. Alternat. Med.* 2017:2590676.

Yu, X., Ruan, Y., Huang, X., Dou, L., Lan, M., Cui, J., et al. (2020). Dexrazoxane ameliorates doxorubicin-induced cardiotoxicity by inhibiting both apoptosis and necroptosis in cardiomyocytes. *Biochem. Biophys. Res. Commun.* 523, 140–146. doi: 10.1016/j.bbrc.2019.12.027

Zeng, C., Duan, F., Hu, J., Luo, B., Huang, B., Lou, X., et al. (2020). NLRP3 inflammasome-mediated pyroptosis contributes to the pathogenesis of non-ischemic dilated cardiomyopathy. *Redox Biol.* 101523. doi: 10.1016/j.redox.2020.101523 [Epub ahead of print].

Zhai, J., Tao, L., Zhang, S., Gao, H., Zhang, Y., Sun, J., et al. (2020). Calycosin ameliorates doxorubicin-induced cardiotoxicity by suppressing oxidative stress and inflammation via the sirtuin 1-NOD-like receptor protein 3 pathway. *Phytother. Res.* 34, 649–659. doi: 10.1002/ptr.6557

Zhang, C., Feng, Y., Qu, S., Wei, X., Zhu, H., Luo, Q., et al. (2011). Resveratrol attenuates doxorubicin-induced cardiomyocyte apoptosis in mice through SIRT1-mediated deacetylation of p53. *Cardiovasc. Res.* 90, 538–545. doi: 10.1093/cvr/cvr022

Zhang, J. Y., Sun, G. B., Luo, Y., Wang, M., Wang, W., Du, Y. Y., et al. (2017). Salvianolic acid A protects H9c2 Cells from arsenic trioxide-induced injury via inhibition of the MAPK signaling pathway. *Cell Physiol. Biochem.* 41, 1957–1969. doi: 10.1159/000472409

Zhang, J. Y., Sun, G. B., Wang, M., Liao, P., Du, Y. Y., Yang, K., et al. (2016). Arsenic trioxide triggered calcium homeostasis imbalance and induced endoplasmic reticulum stress-mediated apoptosis in adult rat ventricular myocytes. *Toxicol. Res.* 5, 682–688. doi: 10.1039/c5tx00463b

Zhang, T., Zhang, Y., Cui, M., Jin, L., Wang, Y., Lv, F., et al. (2016). CaMKII is a RIP3 substrate mediating ischemia- and oxidative stress-induced myocardial necroptosis. *Nat. Med.* 22, 175–182. doi: 10.1038/nm.4017

Zhang, S., Liu, X., Bawa-Khalfe, T., Lu, L. S., Lyu, Y. L., Liu, L. F., et al. (2012). Identification of the molecular basis of doxorubicin-induced cardiotoxicity. *Nat. Med.* 18, 1639–1642. doi: 10.1038/nm.2919

Zhang, X., Zhu, J. X., Ma, Z. G., Wu, H. M., Xu, S. C., Song, P., et al. (2019). Rosmarinic acid alleviates cardiomyocyte apoptosis via cardiac fibroblast in doxorubicin-induced cardiotoxicity. *Int. J. Biol. Sci.* 15, 556–567. doi: 10.7150/ijbs.29907

Zhang, Y. Y., Meng, C., Zhang, X. M., Yuan, C. H., Wen, M. D., Chen, Z., et al. (2015). Ophiopogonin D attenuates doxorubicin-induced autophagic cell death by relieving mitochondrial damage in vitro and in vivo. *J. Pharmacol. Exp. Ther.* 352, 166–174. doi: 10.1124/jpet.114.219261

Zhao, H., Wang, Y., Liu, J., Guo, M., Fei, D., Yu, H., et al. (2019). The cardiotoxicity of the common carp (Cyprinus carpio) exposed to environmentally relevant concentrations of arsenic and subsequently relieved by zinc supplementation. *Environ. Pollut.* 253, 741–748. doi: 10.1016/j.envpol.2019.07.065

Zhao, H., Zhang, X., Zheng, Y., Li, Y., Wang, X., Hu, N., et al. (2018). Propofol protects rat cardiomyocytes from anthracycline-induced apoptosis by regulating MicroRNA-181a In vitro and in vivo. *Oxid Med. Cell Longev* 2018:2109216.

Zhao, L., and Zhang, B. (2017). Doxorubicin induces cardiotoxicity through upregulation of death receptors mediated apoptosis in cardiomyocytes. *Sci. Rep.* 7:44735.

Zhao, X. Y., Li, G. Y., Liu, Y., Chai, L. M., Chen, J. X., Zhang, Y., et al. (2008). Resveratrol protects against arsenic trioxide-induced cardiotoxicity in vitro and in vivo. *Br. J. Pharmacol.* 154, 105–113. doi: 10.1038/bjp.2008.81

Zhao, Y., Xue, T., Yang, X., Zhu, H., Ding, X., Lou, L., et al. (2010). Autophagy plays an important role in sunitinib-mediated cell death in H9c2 cardiac muscle cells. *Toxicol. Appl. Pharmacol.* 248, 20–27. doi: 10.1016/j.taap.2010.07.007

Zheng, X., Zhong, T., Ma, Y., Wan, X., Qin, A., Yao, B., et al. (2020). Bnip3 mediates doxorubicin-induced cardiomyocyte pyroptosis via caspase-3/GSDME. *Life Sci.* 242:117186. doi: 10.1016/j.lfs.2019.117186

Zhong, W., Jin, W., Xu, S., Wu, Y., Luo, S., Liang, M., et al. (2018). Pioglitazone induces cardiomyocyte apoptosis and inhibits cardiomyocyte hypertrophy Via VEGFR-2 signaling pathway. *Arq. Bras. Cardiol.* 111, 162–169.

Zhu, H., Sarkar, S., Scott, L., Danelisen, I., Trush, M. A., Jia, Z., et al. (2016). Doxorubicin redox biology: redox cycling, topoisomerase inhibition, and oxidative stress. *React. Oxyg Species* 1, 189–198. doi: 10.20455/ros.2016.835

Zhu, W., Soonpaa, M. H., Chen, H., Shen, W., Payne, R. M., Liechty, E. A., et al. (2009). Acute doxorubicin cardiotoxicity is associated with p53-induced inhibition of the mammalian target of rapamycin pathway. *Circulation* 119, 99–106. doi: 10.1161/circulationaha.108.799700

Zorov, D. B., Juhaszova, M., and Sollott, S. J. (2014). Mitochondrial reactive oxygen species (ROS) and ROS-induced ROS release. *Physiol. Rev.* 94, 909–950. doi: 10.1152/physrev.00026.2013

Conflict of Interest: The authors declare that the research was conducted in the absence of any commercial or financial relationships that could be construed as a potential conflict of interest.

frontiers in Cell and Developmental Biology

ORIGINAL RESEARCH
published: 25 August 2020
doi: 10.3389/fcell.2020.00836

Baicalein and Baicalin Promote Melanoma Apoptosis and Senescence via Metabolic Inhibition

Lan Huang[1,2], Bo Peng[2†], Yash Nayak[2†], Cindy Wang[2], Fusheng Si[2], Xia Liu[2], Jie Dou[3], Huaxi Xu[1] and Guangyong Peng[2]**

[1] *Department of Immunology, School of Medicine, Jiangsu University, Zhenjiang, China,* [2] *Division of Infectious Diseases, Allergy and Immunology, Department of Internal Medicine, School of Medicine, Saint Louis University, St. Louis, MO, United States,* [3] *State Key Laboratory of Natural Medicines, School of Life Sciences and Technology, China Pharmaceutical University, Nanjing, China*

OPEN ACCESS

Edited by:
Binfeng Lu,
University of Pittsburgh, United States

Reviewed by:
Bin Zhang,
Northwestern University, United States
Ruoning Wang,
Nationwide Children's Hospital, United States
Deliang Cao,
Southern Illinois University Carbondale, United States

***Correspondence:**
Huaxi Xu
xuhx@ujs.edu.cn
Guangyong Peng
guangyong.peng@health.slu.edu

†Present address:
Bo Peng,
Washington University, St. Louis, MO, United States
Yash Nayak,
Washington University, St. Louis, MO, United States

Specialty section:
This article was submitted to Cell Death and Survival, a section of the journal Frontiers in Cell and Developmental Biology

Received: *29 May 2020*
Accepted: *04 August 2020*
Published: *25 August 2020*

Citation:
Huang L, Peng B, Nayak Y, Wang C, Si F, Liu X, Dou J, Xu H and Peng G (2020) Baicalein and Baicalin Promote Melanoma Apoptosis and Senescence via Metabolic Inhibition. Front. Cell Dev. Biol. 8:836. doi: 10.3389/fcell.2020.00836

Malignant melanoma is one of the most common and dangerous skin cancers with a high rate of death every year. Furthermore, N-RAS and B-RAF mutations in melanoma cells increase the difficulties for clinical treatment in patients. Therefore, development of effective and universal drugs against melanoma is urgently needed. Here we demonstrate that baicalein and baicalin, the active components of the Chinese traditional medicinal plant *Scutellaria baicalensis* Georgi, can significantly inhibit melanoma cell growth and proliferation, suppress tumor cell colony formation and migration, as well as induce apoptosis and senescence in melanoma cells. The anti-tumor effects mediated by baicalein and baicalin are independent of N-RAS and B-RAF mutation statuses in melanoma cells. Mechanistically, we identify that the suppression of baicalein and baicalin on melanoma cells is due to inhibition of tumor cell glucose uptake and metabolism by affecting the mTOR-HIF-1α signaling pathway. In addition, we demonstrated that baicalein and baicalin can suppress tumorigenesis and tumor growth *in vivo* in the melanoma model. These studies clearly indicate that baicalein and baicalin can control tumor growth and development metabolically and have great potential as novel and universal drugs for melanoma therapy.

Keywords: baicalein, baicalin, melanoma, N-RAS, B-RAF, apoptosis, senescence, glucose metabolism

INTRODUCTION

Melanoma, a type of skin cancer, is one of the deadly cancers in the world. In the United States, according to the American Cancer Society, there were 91,270 new cases of melanoma, and 9,320 cases were expected to die in 2018 (American Cancer Society, 2018). Great progress has made in diagnosis and treatment with melanoma, but the overall survival of advanced melanoma is still very low. In addition, melanoma with N-RAS and B-RAF mutations has been well-recognized as a challenge that brings out more difficulties for the treatment (Brose et al., 2002; Omholt et al., 2003; Thumar et al., 2014). Furthermore, the status of those mutations is directly associated with the worse prognosis of the cancer patients (Thomas et al., 2015). Although certain activated signaling pathways induced by the mutations, such as RAS-RAF-MAPK have been identified as the promising targets for drug development, the clinical therapeutic effects of target inhibitors are still varied (Flaherty et al., 2010; Nazarian et al., 2010; Kaplan et al., 2011). Importantly, treatments with

some target inhibitors may induce drug resistance and/or promote tumor growth and progression in cancer patients as well as pre-clinical tumor models (Flaherty et al., 2010; Hatzivassiliou et al., 2010; Nazarian et al., 2010; Poulikakos et al., 2010; Kaplan et al., 2011; Kwong et al., 2012). Therefore, development of the unique inhibitors to target specific mutations or universal drugs against melanoma is urgently needed.

Recent studies suggest that many natural products have been developed into promising drugs and applied into clinical trials for various disease treatments including cancers (Cragg et al., 2009; Cragg and Newman, 2013; Stover et al., 2014). Baicalin and its aglycon baicalein are the major flavonoids derived from the edible medicinal plants *Scutellaria baicalensis* Georgi (Xiao et al., 2014). Baicalein and baicalin have been widely used for inflammation and infectious disease treatments (Johnson, 2011; Ding et al., 2014; Moghaddam et al., 2014; de Oliveira et al., 2015; Ji et al., 2015). Furthermore, both baicalein and baicalin are also potent anti-tumor drugs, which have been shown strong anti-tumor effects in various cancers, including in breast cancer, prostate cancer, pancreatic cancer, esophageal squamous cell carcinoma and burkitt lymphoma (Takahashi et al., 2011; Huang et al., 2012; Yu et al., 2013; Zhang et al., 2013; Aryal et al., 2014; Chung et al., 2015; Dou et al., 2018). Both compounds can inhibit the proliferation, migration, adhesion and invasive properties of tumor cells, and induce tumor cell cycle arrest (Chao et al., 2007; Chiu et al., 2011; Takahashi et al., 2011; Aryal et al., 2014; Wang et al., 2015; Gong et al., 2017). We have recently demonstrated that baicalein and baicalin could inhibit human colon cancer cell growth and proliferation *in vitro* and *in vivo* (Dou et al., 2018; Wang et al., 2018). The suppressive effects are due to the induction of colon cancer cell apoptosis and senescence (Dou et al., 2018; Wang et al., 2018). However, whether baicalein and baicalin have anti-tumor effects against melanoma, especially melanoma with mutations is unknown. Furthermore, the molecular mechanism by which the two compounds inhibit cancer is still unclear. A precise understanding of biological functions and mechanisms of these two natural compounds on different types of cancers will provide novel targets for the clinical therapy against cancers including melanoma.

In this study, we explored the anti-tumor effects and related mechanism of baicalein and baicalin in melanoma. We demonstrated that baicalein and baicalin can significantly inhibit both human and mouse melanoma cell growth and proliferation, suppress tumor cell colony formation and migration, as well as induce apoptosis and senescence in melanoma cells. The anti-tumor effects mediated by baicalein and baicalin are independent of N-RAS and B-RAF mutation statuses in melanoma cells. Furthermore, we identified that the suppressive effects mediated by baicalein and baicalin on tumor cells are mechanistically due to the inhibition of tumor cell glucose metabolism, which are molecularly controlled by mTORC1-HIF-1α signaling pathway in melanoma cells. In addition, we demonstrated that baicalein and baicalin can suppress tumorigenesis and tumor growth *in vivo* in the melanoma model. These studies clearly indicate that baicalein and baicalin could be potential novel and universal drugs for melanoma therapy.

RESULTS

Baicalein and Baicalin Inhibit Melanoma Cell Growth and Proliferation

Our previous studies have demonstrated that baicalein and baicalin can suppress colon cancer cell proliferation and growth (Dou et al., 2018; Wang et al., 2018). We further determined whether baicalein and baicalin can inhibit tumor growth of melanoma cells. Three human melanoma cell lines Mel586, SK-MEL-2 (wild type B-RAF and mutant N-RAS), A375 (B-RAF V600E and wild type N-RAS), as well as mouse B16F0 melanoma cell line were cultured in the presence of different concentrations of baicalein and baicalin. Tumor cell growth and proliferation were further determined using cell growth curve and [^{3}H]-thymidine incorporation assays. We found that baicalein and baicalin strongly suppressed tumor growth and proliferation of both human and mouse melanoma cells (Mel586, SK-MEL-2, A375 and B16F0) regardless of the mutation statuses of B-RAF and N-RAS (**Figures 1A,B**). Furthermore, the suppressive effects mediated by the two compounds were in a dose-dependent manner. In addition, baicalein has stronger inhibitory activity on melanoma cell growth and proliferation than that of baicalin. High concentration of baicalein (40 μM) almost completely inhibited human melanoma growth (**Figure 1B**). These results clearly suggest that both baicalein and baicalin strongly suppress melanoma cell proliferation and growth.

Baicalein and Baicalin Inhibit Melanoma Cell Colony Formation, Migration and Adhesion

We then investigated whether baicalein and baicalin have inhibitory effects on the other key biological behaviors of melanoma cells, including colony formation, migration and adhesion capacities. We observed that the numbers and sizes of tumor cell colonies were significantly decreased in SK-MEL-2 and A375 tumor cells after treatment with baicalein or baicalin (**Figures 2A,B**). Furthermore, two different concentrations of baicalein and baicalin markedly suppressed both human and mouse melanoma cell migration at different time points using a wound healing assay (**Figure 2C**). In addition, baicalein and baicalin inhibited the adhesion ability of both human and mouse melanoma cell lines (**Figure 2D**). Consistent with the effect on tumor growth and proliferation, the suppression of melanoma cell colony formation, migration and adhesion is in a dose-dependent manner and regardless of the mutation statuses of B-RAF and N-RAS genes. These results collectively indicate baicalein and baicalin can strongly inhibit tumor cell growth and biological behaviors in melanoma.

Baicalein and Baicalin Induce Apoptosis and Senescence in Melanoma Cells

Our previously studies have shown that baicalein and baicalin can induce colon cancer cell apoptosis and senescence (Dou et al., 2018; Wang et al., 2018). Furthermore, studies from other groups have also shown that baicalein and baicalin induce cancer

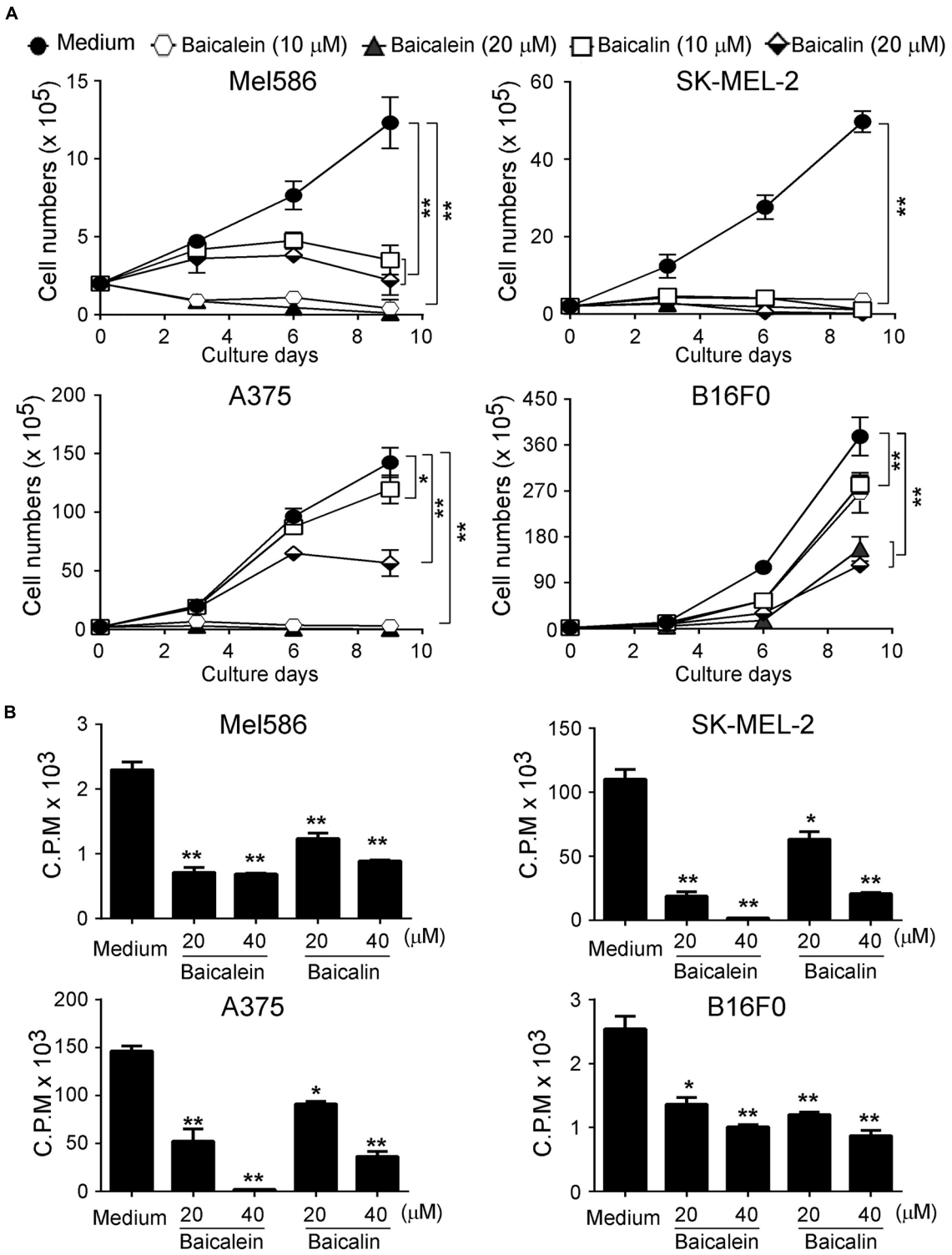

FIGURE 1 | Baicalein and baicalin inhibit both melanoma cell growth and proliferation. Three human melanoma cell lines (Mel586, SK-MEL-2, and A375) and one mouse melanoma cell line (B16F0) were cultured at a started number of 2×10^5/well in 6-well plates, or 5×10^3/well in 96-well plates, and treated with the indicated concentrations of baicalein or baicalin. The cell growth was evaluated at different time points using the cell number counting **(A)**, and cell proliferation was determined using [^{3}H]-thymidine assays **(B)**. Data shown in Panels **(A,B)** are mean ± SD from three independent experiments with similar results. *$p < 0.05$ and **$p < 0.01$ compared with the medium control group.

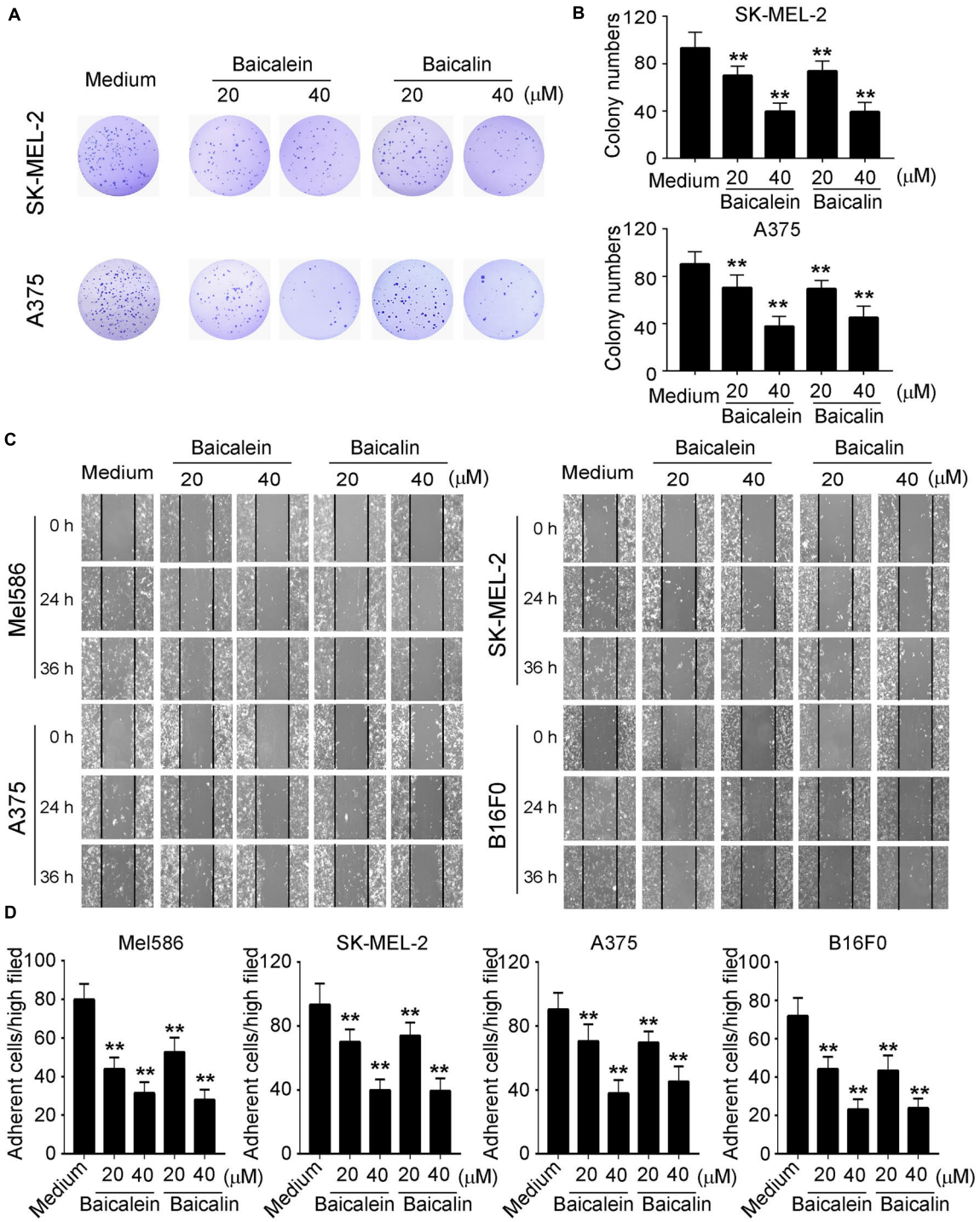

FIGURE 2 | Baicalein and baicalin inhibit melanoma cell colony formation, migration and adhesion. **(A,B)** Baicalein and baicalin treatments dramatically decreased the numbers and sizes of tumor colonies in SK-MEL-2 and A375 cells. 200–500 per well of melanoma cells pre-treated with the indicated concentrations of baicalein or baicalin, were seeded in 6-well plates for culture, and cell colonies counted after 10–14 days of culture. Results shown in the histogram **(B)** are summaries of mean ± SD from three independent experiments. $^{**}p < 0.01$ compared with the medium control group. **(C)** Different concentrations of baicalein and baicalin treatments in both human and mouse melanoma cells significantly inhibited tumor cell migration compared with the medium control group at 24 and 36 h time points in the wound closure assays. Data shown are representatives from three independent experiments with similar results. **(D)** Baicalein and baicalin treatments suppressed the adhesion of melanoma cells. Both human and mouse melanoma cells pretreated with the indicated concentrations of baicalein and baicalin were cultured in the fibronectin-coated plates for 45 min. Adherent cells were counted and averaged in 10 fields at high (×400) magnification with a microscope. Results shown are summaries of mean ± SD from three independent experiments with similar results $^{**}p < 0.01$ compared with the medium control group.

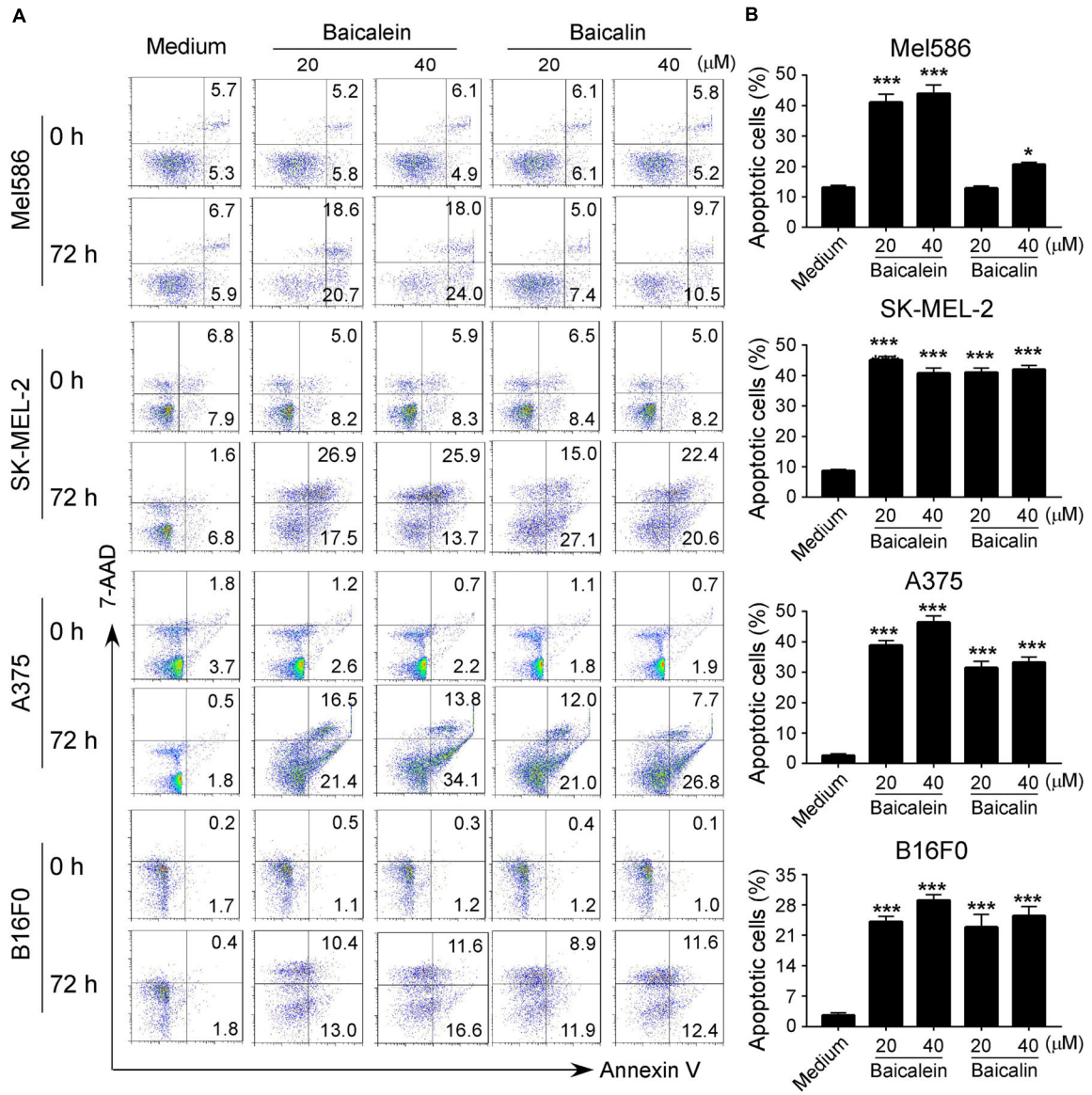

FIGURE 3 | Baicalein and baicalin treatments promote melanoma cell apoptosis. **(A,B)** Significantly increased apoptotic cell populations were induced in both human and mouse melanoma cells after treatments with baicalein and baicalin. Tumor cells were cultured in the presence of indicated concentrations of baicalein and baicalin for 72 h. Apoptosis in treated tumor cells was analyzed after staining with PE-labeled Annexin V and 7-AAD **(A)**. Results shown in the histogram **(B)** are summaries of mean ± SD from three independent experiments. $^{*}p < 0.05$ and $^{***}p < 0.001$, compared with the medium control group.

cell apoptosis in pancreatic cancer, esophageal squamous cell carcinoma and burkitt lymphoma (Takahashi et al., 2011; Huang et al., 2012; Zhang et al., 2013). Therefore, we measured apoptosis and cell death in melanoma cell lines treated by both baicalein and baicalin. We found that culture with medium, melanoma cells contained around 2–10% apoptotic cells (around 10% in Mel586 and SK-MEL-2, and below 5% in A375 and B16F0 tumor cells). Furthermore, consistent with the previous reports in other tumor cells, treatment with baicalein significantly induced tumor cell apoptosis in both human and mouse melanoma cells at 36 and 72 h (**Figures 3A,B** and **Supplementary Figure S1**) (Takahashi et al., 2011; Huang et al., 2012; Zhang et al., 2013; Dou et al., 2018; Wang et al., 2018). We have previously shown that baicalin treatment induced increased senescence rather than apoptosis or cell death in colon cancer cell lines (Dou et al., 2018; Wang et al., 2018). However, our current studies clearly showed that treatment with baicalin also dramatically induced tumor cell apoptosis in both human and mouse melanoma cells, but its effect is less potent than that of baicalein (**Figure 3** and **Supplementary Figure S1**). Interestingly, treatments with baicalein and baicalin also induced some necrotic cell populations in SK-MEL-2 and B16F0 tumor cells (**Figure 3A**).

We then determined whether baicalein and baicalin can induce senescence in melanoma cells, which is another

mechanism involved in the suppressed cell growth and proliferation mediated by baicalin in colon cancer cells (Dou et al., 2018; Wang et al., 2018). The most widely used biomarker for senescent cells is the senescence-associated β-galactosidase (SA-β-Gal) (Ye et al., 2012; Liu et al., 2018). We observed that culture with baicalein and baicalin in human Mel586, SK-MEL-2, and A375 melanoma cells as well as mouse B16F0 melanoma cells significantly increased the numbers of SA-β-Gal$^+$ cells, indicating the induction of tumor cell senescence (**Figures 4A,B**). However, unlike the effect in colon cancer cells, treatment with baicalein induced more senescent cell populations in both human and mouse melanoma cell lines than that of baicalin treatment in those melanoma cells (**Figures 4A,B**). Interestingly, we observed that high concentrations of baicalein and baicalin (above 50 μM) were required to induce senescence in B16F0 mouse melanoma cells compared with those in human melanoma cell lines in *in vitro* treatment (**Figures 4A,B**). These results collectively suggest that baicalein and baicalin treatment in melanoma cells can induce both cell apoptosis and senescence, resulting in the inhibition of tumor cell growth and functions.

Baicalein and Baicalin Suppress Glucose Metabolism in Melanoma Cells

Metabolic dysregulation is one of the characteristic hallmarks of tumor malignancy (Ward and Thompson, 2012; Dang, 2013). Cancer cells often display heightened glucose consumption in the tumor microenvironment. We reasoned that baicalein and baicalin-induced inhibition of tumor proliferation and biological functions may be caused by interfering with cell energy metabolism. We thus investigated the metabolic profile of the melanoma cells treated with baicalein and baicalin (**Figure 5A**). We first determined the glucose uptake ability of melanoma cells in the presence and absence of different concentrations of baicalein and baicalin, using a fluorescent glucose analog D-glucose analog 2-(N-(7-nitrobenz-2-oxa-1,3-diazol-4-yl) amino)-2-deoxy-D-glucose (2-NBDG) labeling assay (Liu et al., 2018; Li et al., 2019). Our results clearly showed that both human and mouse melanoma cells had high glucose uptake abilities. However, treatments with baicalein and baicalin significantly inhibited glucose uptake abilities of four melanoma cell lines no matter of N-RAS and B-RAF mutation statuses (**Figure 5B**). We then determined the effect on key glycolytic enzymes in tumor cells using real-time quantitative PCR analyses (Li et al., 2019). Those molecules include glucose transporters 1 and 3 (Glut1 and Glut3), as well as glycolysis-related enzymes hexokinase 2 (HK2), glucose-6-phosphate isomerase (GPI), phosphofructokinase 1 (PFK1), triosephosphate isomerase 1 (TPI1), enolase 1 (ENO1), pyruvate kinase muscle 2 (PKM2), and lactate dehydrogenase A (LDHα) (**Figure 5A**). Baicalein and baicalin treatments markedly suppressed gene expression of Glut1, Glut3, HK2, TPI, GPI, and PFK1 in both human and mouse melanoma cells (**Figure 5C**). In addition, both baicalein and baicalin inhibited LDHα expression in Mel586, A375, and B16F0 melanoma cells, and ENO1 expression in SK-MEL-2 and A375 cells, as well as partially suppressed PKM2 expression in SK-MEL-2, A375, and B16F0 tumor cells (**Supplementary Figure S2**). To further investigate the causative role of glucose metabolism inhibition in cell senescence and suppression of melanoma cells mediated by these two compounds, we determined whether we can prevent tumor cell senescence mediated by baicalein and baicalin if we promote glucose mentalism through overexpression of Glut1 gene in the melanoma cells. Consistent with the above results, baicalein and baicalin treatments significantly increased melanoma cell senescence. However, transfection of pCDNA-Glut1 plasmid but not control vector in melanoma cells dramatically reversed the senescence in the melanoma cells induced by both baicalein and baicalin treatments (**Figure 5D**). These results collectively suggest that baicalein and baicalin inhibit melanoma tumor growth and function via suppression of tumor cell glucose metabolism.

Down-Regulation of mTORC1-HIF1α Signaling in Melanoma Cells Is Responsible for Glucose Metabolism Inhibition Induced by Baicalein and Baicalin

mTOR signaling pathway plays a central role in metabolic reprogramming of tumor cell growth and proliferation (Sun et al., 2011; Chen et al., 2015). Furthermore, hypoxia-inducible factor 1-alpha (HIF1α) serves as a key transcription factor that performs important functions in regulation of cellular metabolism (Cheng et al., 2014; Pusapati et al., 2016; Salmond, 2018). Our recent studies demonstrated that mTORC1–HIF1α pathway promotes glucose metabolism and glycolysis in Treg cells (Li et al., 2019). We therefore explored the possibility that baicalein and baicalin could inhibit mTORC1–HIF1α signaling pathway and thus result in suppression of glucose metabolism in melanoma cells. To test this possibility, we first analyzed the phosphorylation and activation of mTOR and its downstream substrates p70S6K and 4E-BP1 in melanoma cells treated with or without baicalein and baicalin. We found that both human and mouse melanoma cells have high phosphorylated mTOR and p70S6K cell populations, indicating elevated mTORC1 activity in melanoma tumor cells. However, treatments with baicalein and baicalin significantly suppressed the phosphorylation of mTOR and its downstream substrates p70S6K and 4E-BP1 in the melanoma cell lines, further confirming their inhibition of mTOR signaling in melanoma cells (**Figure 6A**). Consistent with our above and previous results, baicalein had more potent suppressive effect on mTOR signaling in tumor cells than that of baicalin. To further test the possibility that baicalein and baicalin-mediated suppression of melanoma cells involves the mTORC1–HIF1α signaling pathway regulation, we also determined HIF1α protein and mRNA expression in both human and mouse melanoma cells treated with or without the two compounds using the flow cytometry and Real-time PCR analyses. The four melanoma cell lines expressed high levels of HIF1α. Furthermore, treatments with baicalein and baicalin significantly inhibited HIF1α expression in all melanoma cells, suggesting down-regulation of HIF1α pathway in melanoma cells induced by the two compounds (**Figures 6B,C**). All these results suggest

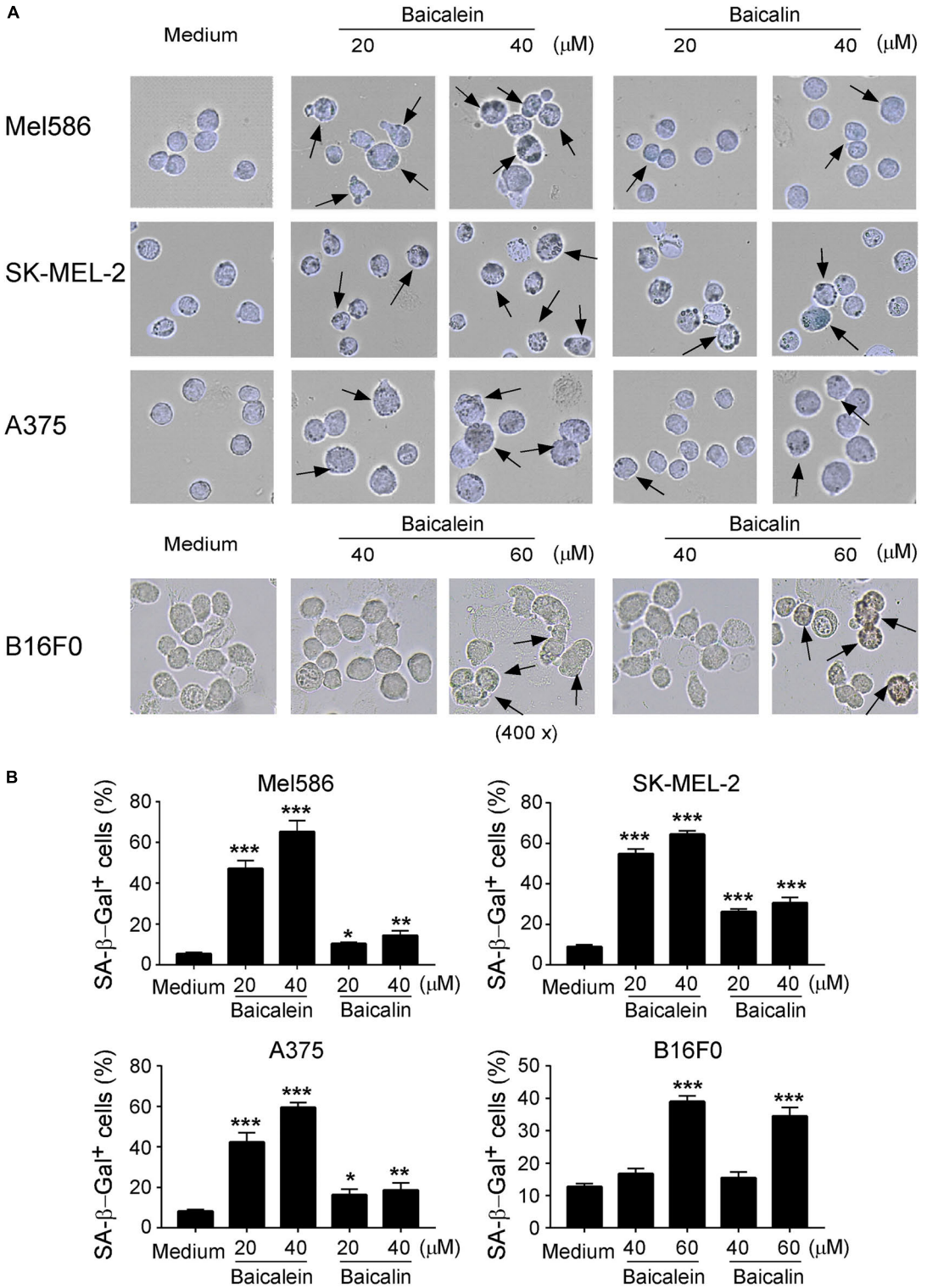

FIGURE 4 | Baicalein and baicalin treatments induce melanoma cell senescence. **(A,B)** Increased senescent cell populations were induced in human and mouse melanoma cells after treatments with baicalein and baicalin. Tumor cells were cultured in the presence of indicated concentrations of baicalein and baicalin for 72 h. Senescent cells were analyzed using the SA-β-Gal activity assay and the SA-β-Gal positive cells were identified with dark blue granules as indicated by the arrows **(A)**. Data in panel **(B)** are mean ± SD from three independent experiments with similar results. $^{*}p < 0.05$, $^{**}p < 0.01$, and $^{***}p < 0.001$, compared with the medium control group.

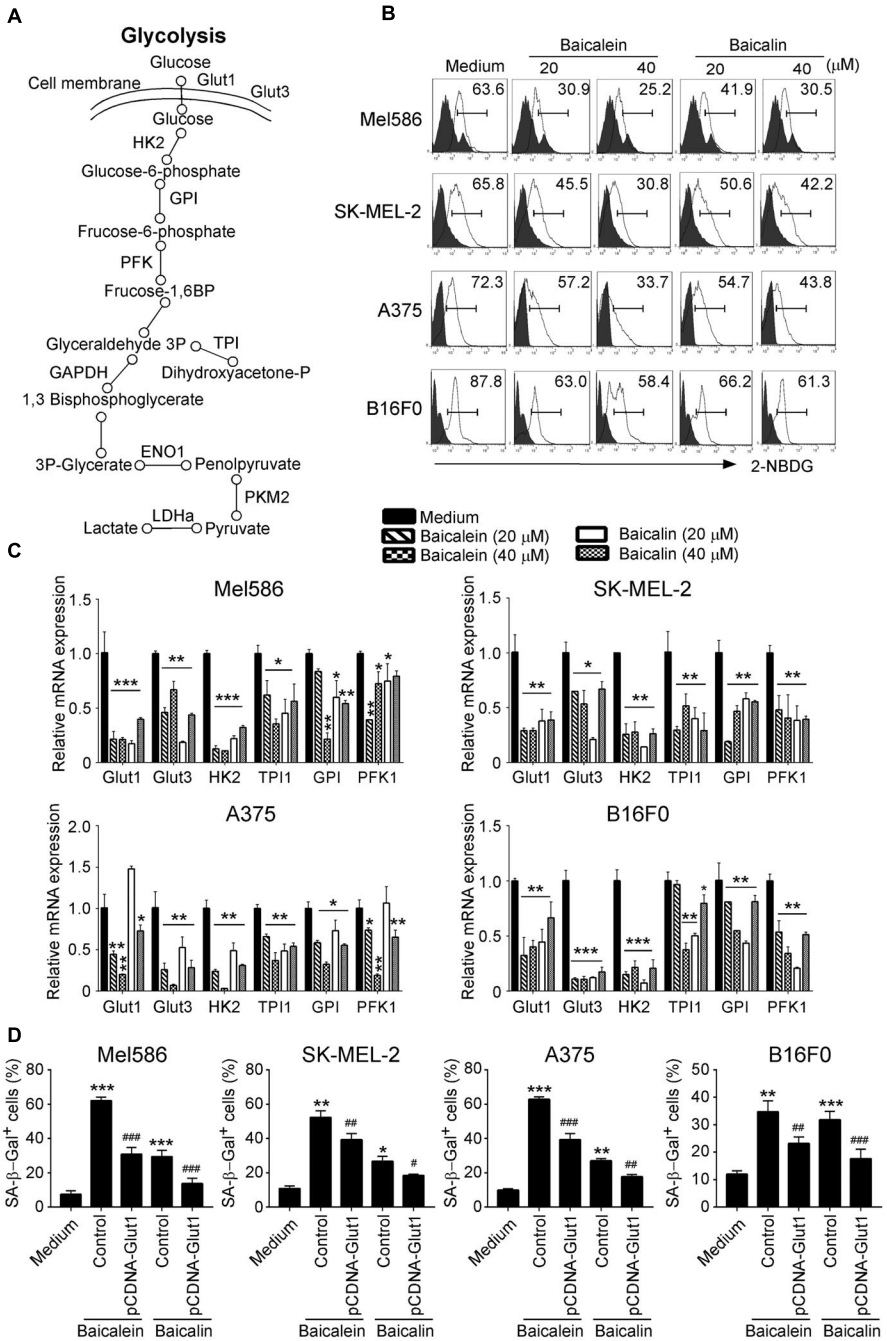

FIGURE 5 | Baicalein and baicalin treatments down-regulate glucose uptake and glycolysis in melanoma cells. **(A)** The sketch map shows the steps and regulations of the key metabolites and enzymes in cell glycolysis. **(B)** Baicalein and baicalin treatments significantly decreased glucose uptake in both human and mouse melanoma cells. Glucose uptake of melanoma cells was determined by the flow cytometry with addition of 2-NBDG (100 μM) for 30 min after 3-day culture with the indicated concentrations of baicalein and baicalin. **(C)** Baicalein and baicalin treatments significantly down-regulated gene expression levels of key glycolytic enzymes in both human and mouse melanoma cells. Melanoma cells were treated with or without indicated concentrations of baicalein and baicalin for 72 h. Total RNA was isolated from the tumor cells and analyzed by real-time PCR. The expression levels of each gene were normalized to β-actin expression levels and adjusted to the levels in untreated tumor cells (medium). Data shown in different melanoma cells are mean ± SD from three independent experiments. $^{*}p < 0.05$, $^{**}p < 0.01$, and $^{***}p < 0.001$, compared with the medium only group. **(D)** Over-expression of Glut1 prevented cell senescence in melanoma cells induced by baicalein and baicalin. Melanoma cells were transfected with pCDNA-Glut1 or control vector plasmids for 24 h, then cultured for 3 days in the presence of baicalein or baicalin (40 μM for Mel586, A375, and SK-mel-2 cells, and 50 μM for B16F0 cells). Senescent cells were analyzed using the SA-β-Gal activity assay. Data shown are mean ± SD from three independent experiments with similar results. $^{*}p < 0.05$, $^{**}p < 0.01$, and $^{***}p < 0.001$, compared with the medium control group. $^{\#}p < 0.05$, $^{\#\#}p < 0.01$, and $^{\#\#\#}p < 0.001$, compared with the respective baicalein or baicalin treatment group.

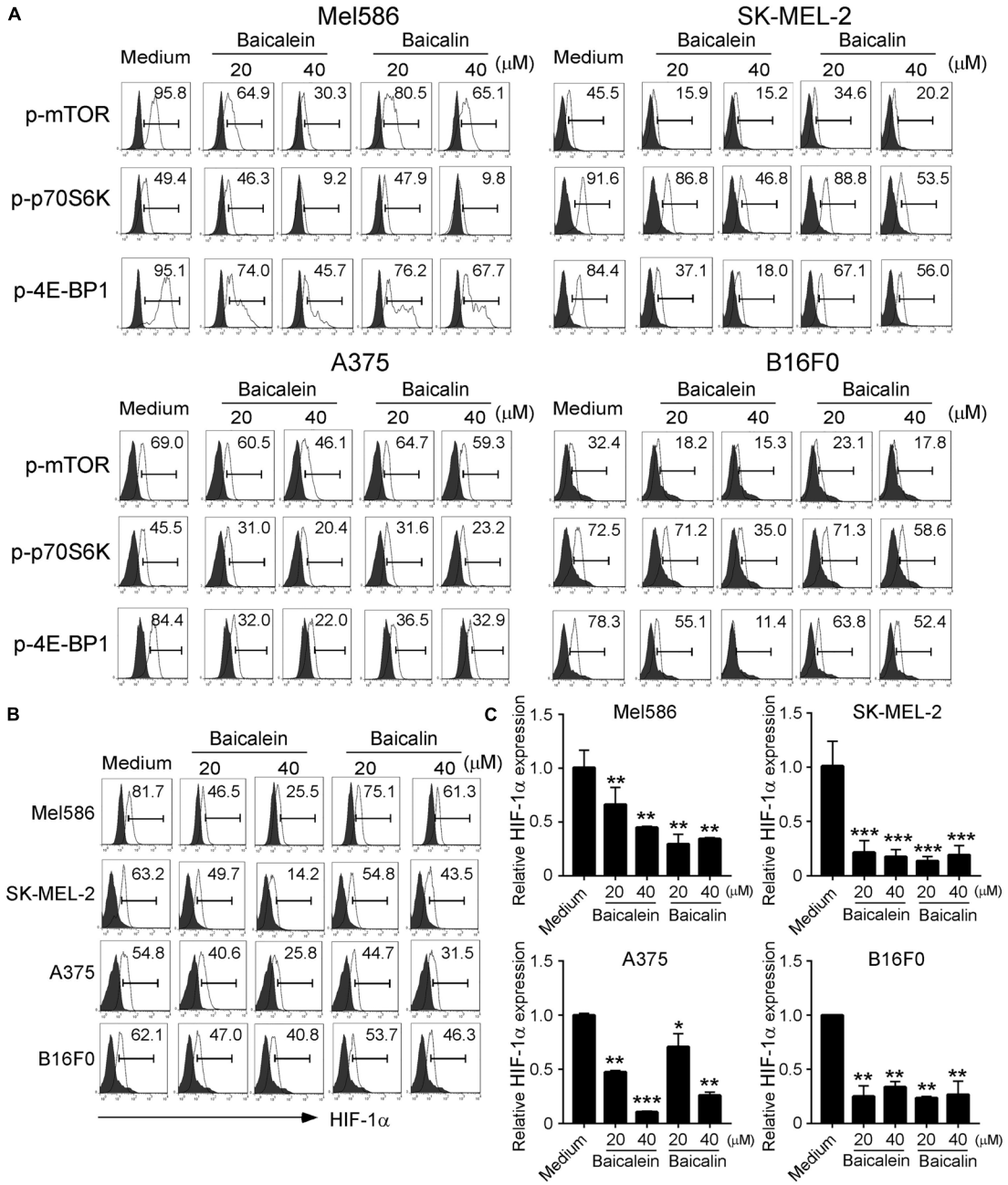

FIGURE 6 | Baicalein and baicalin treatments suppress mTORC1-HIFα signaling in melanoma cells. **(A)** Suppression of phosphorylation and subsequent activation of mTOR signaling in melanoma cells treated with baicalein and baicalin. Melanoma cells were treated with or without indicated concentrations of baicalein and baicalin for 72 h and then phosphorylated mTOR, p70S6K, and 4E-BP1 in tumor cells were determined by the flow cytometry analyses. **(B,C)** Baicalein and baicalin treatments down-regulated HIF1α protein and mRNA expression in melanoma cells. Cell preparation and treatment were identical to panel **(A)**. The protein expression of HIF-1α in treated tumor cells was determined by the flow cytometry **(B)**. Total RNA was isolated from the tumor cells and analyzed by Real-time PCR **(C)**. The gene expression levels of HIF1α were normalized to β-actin expression levels and adjusted to the levels in untreated melanoma cells. Data shown are representatives of mean ± SD from three independent experiments. $^{*}p < 0.05$, $^{**}p < 0.01$, and $^{***}p < 0.001$, compared with the medium only group.

that baicalein and baicalin down-regulate the mTOR-HIFα signaling in tumor cells.

We then confirmed the functional importance of mTOR-HIFα signaling pathway in glucose metabolism suppression and senescence induction in melanoma cells mediated by baicalein and baicalin. We performed a functional rescue experiment with over-expression of the mTOR upstream activator Rheb gene in melanoma cells (retrovirus-based Rheb) (Yang et al., 2017; Li et al., 2019). Activation of mTOR signaling with Retro-Rheb transfection significantly reversed suppression of

gene expression levels of glucose transporters and glycolytic enzymes in melanoma cells induced by baicalein and baicalin (**Figure 7A**). Furthermore, mTOR signaling activation markedly prevented the baicalein and baicalin-induced senescence in both human and mouse melanoma cells (**Figure 7B**). In addition, we activated HIF1α function with the specific pharmacological activator dimethyloxalylglycine (DMOG) and then evaluated glycolysis inhibition and cell senescence induction mediated by baicalein and baicalin (Zhdanov et al., 2015; Cosin-Roger et al., 2017). Consistent with the results from Retro-Rheb transfection, activation of HIF1α signaling with DMOG in tumor cells markedly blocked the inhibition of gene expression of glucose transporters and glycolytic enzymes and prevented induction of senescence in melanoma cells mediated by baicalein and baicalin (**Figures 7A,B**). These results indicate that mTOR-HIF1α axis and its downstream glycolytic program is critical and involved in tumor growth suppression and senescence induction in melanoma cells mediated by baicalein and baicalin.

Baicalein and Baicalin Inhibit Tumorigenesis and Growth of Melanoma *in vivo*

Our *in vitro* studies have clearly demonstrated that baicalein and baicalin could suppress glucose metabolism in melanoma cells, resulting in suppression of tumor cell growth and functions. We next performed complementary *in vivo* studies using mouse melanoma B16F0 cells in the humanized NOD-scid IL2Rγ^{null} (NSG) mouse xenograft models, and explored whether baicalein and baicalin can inhibit tumorigenesis and growth of melanoma *in vivo*. B16F0 melanoma cells were subcutaneously injected into NSG mice. After 4 days post tumor injection (tumor size reached around 5 × 5 mm), baicalein and baicalin (80 mg/kg) were administered through intraperitoneal injection into the tumor-bearing mice, respectively, at every other day for 2 weeks. Tumor growth was evaluated. At the end of experiments (day 17), tumors were isolated from the different groups of the sacrificed mice and weighted. B16F0 tumor cells injected with PBS control grew progressively in NSG mice. However, treatments with both baicalein and baicalin significantly inhibited tumor growth (**Figure 8A**). Furthermore, tumor sizes collected from the baicalein- or baicalin-treated B16F0 groups were much smaller than those in the PBS treatment group (**Figure 8B**). In addition, the average tumor weights obtained from either the baicalein treatment group or baicalin treatment group were much lower than that of control group (**Figure 8C**). Notably, consistent with the results from *in vitro* studies, baicalein had more potent anti-tumor effect than that of baicalin *in vivo*.

In addition to the tumor growth evaluation, we investigated the tumor cell proliferation, senescence and apoptosis mediated by baicalein and baicalin treatments in tumor tissues from different groups. We observed that baicalein and baicalin treatments markedly suppressed tumor cell proliferation as indicated by a decrease of Ki-67^{+} cell populations in tumor tissues (**Figures 8D,E**). Furthermore, baicalein and baicalin treatments also significantly induced increases of both senescent and apoptotic cell populations in tumor tissues as determined with SA-β-Gal and cleaved caspase-3 staining analyses, respectively (**Figures 8F–I**). All these studies collectively indicate that baicalein and baicalin can induce tumor cell senescence and apoptosis, and suppress tumor proliferation and growth *in vivo*. We then further confirmed whether baicalein and baicalin-mediated inhibition of tumor growth *in vivo* is due to suppression of glucose metabolism in tumor cells. We detected the gene expression of the key enzymes involved in glycolysis in tumor tissues obtained from different groups. We observed significantly decreased gene expression levels of glucose transporters Glut1 and Glut3, as well as the key glycolytic enzymes in tumor tissues treated with baicalein or baicalin, further suggesting inhibition of glycolysis in tumor cells (**Supplementary Figure S3**). Collectively, our studies clearly indicate that baicalein and baicalin can suppress tumor cell metabolism, promote cell senescence and apoptosis, and inhibit tumor proliferation and growth *in vitro* and *in vivo*.

DISCUSSION

Melanoma is one of the most common cancers worldwide and has a high rate of death with the advanced disease. Development of novel therapeutic strategies and/or effective drugs is a significant challenge and urgently needed for clinical patients (Brose et al., 2002; Omholt et al., 2003; Thumar et al., 2014). Our current studies have identified that the Chinese traditional medicines baicalein and baicalin are potent anti-tumor agents for melanoma even with N-RAS and B-RAF mutations. Baicalein and baicalin strongly inhibit melanoma cell behaviors and functions, including tumor cell growth and proliferation, as well as colony formation and migration. Mechanistic studies further demonstrated that baicalein and baicalin-mediated suppression of melanoma growth and development is through the inhibition of glucose metabolism in tumor cells, promoting tumor cell apoptosis and senescence. Our studies indicate that baicalein and baicalin could be potentially novel and effective therapeutic drugs for melanoma treatment.

Although significant progress has been made to develop target therapy for melanoma, the mutations on N-RAS and B-RAF occurred in tumor cells have been a significant challenge for successful treatment of melanoma patients (Brose et al., 2002; Omholt et al., 2003; Thumar et al., 2014). Patients with N-RAS and B-RAF mutations have higher incidences of central nervous system (CNS) metastasis in stage IV disease than those with wild-type B-RAF and N-RAS (Flanigan et al., 2013). Furthermore, N-RAS mutation status has been proved to be associated with shorter survival from stage IV melanoma patients and be an independent predictor for clinical outcomes (Ugurel et al., 2007; Jakob et al., 2012). Although many inhibitors have been developed to target the mutations and/or activated signaling pathways, the overall effects of the inhibitors against melanoma are limited in certain types of clinical patients (Brose et al., 2002; Thumar et al., 2014). Moreover, resistance against the target inhibitors and/or activation of alternative survival signaling pathways in cancer cells also keep merging in cancer patients (Nazarian et al., 2010; Villanueva et al., 2010; Gowrishankar et al.,

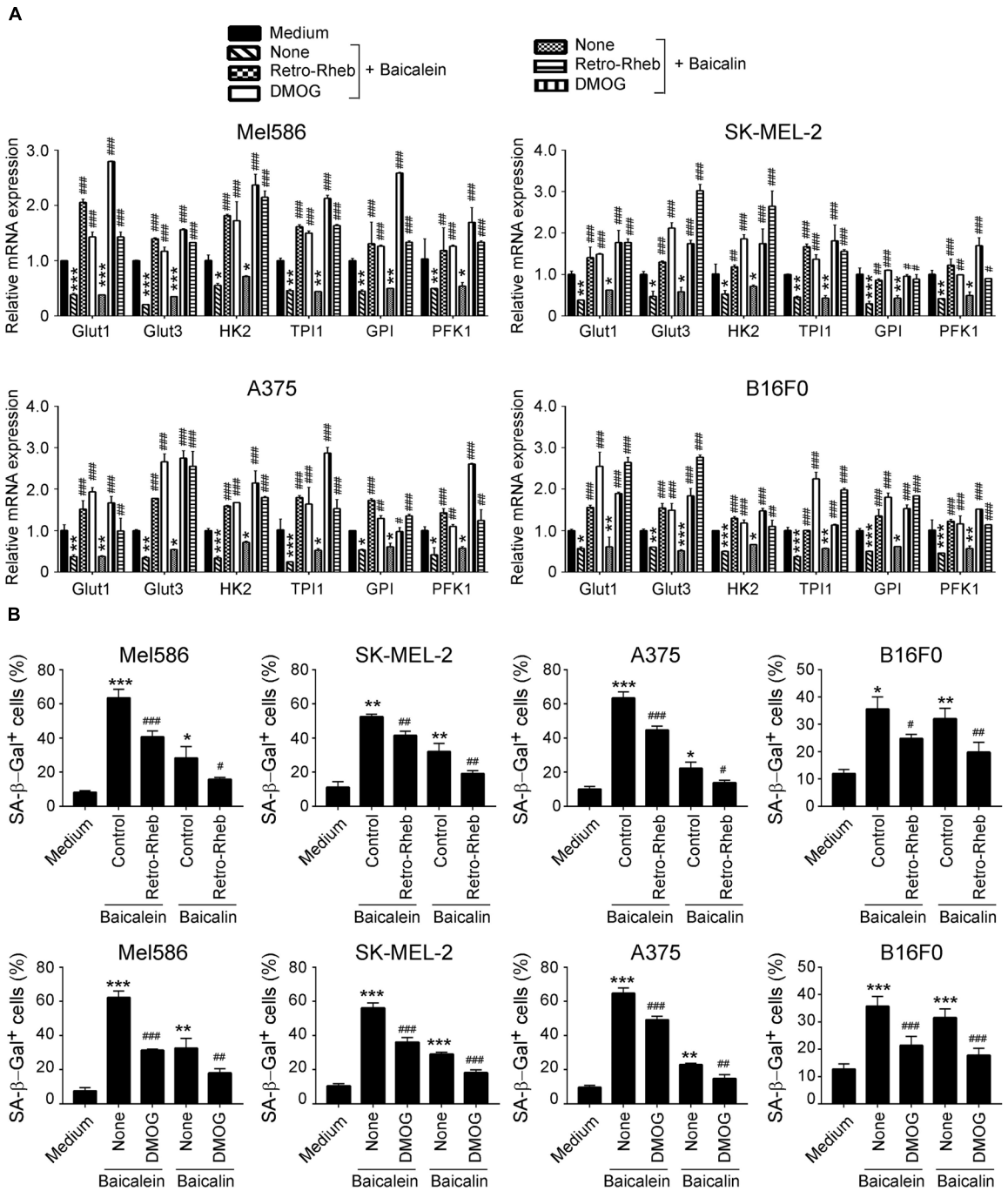

FIGURE 7 | mTORC1-HIFα signaling controls glucose metabolism inhibition and senescence induction in melanoma cells mediated by baicalein and baicalin. **(A)** Activation of mTORC1-HIFα signaling blocked baicalein and baicalin-induced down-regulated gene expression of key glycolytic enzymes in both human and mouse melanoma cells. Melanoma cells were transfected with Retro-Rheb plasmid or pretreated with DMOG (0.1 mM) for 24 h, then cultured for 3 days in the presence of 40 μM of baicalein or baicalin. Total RNA was isolated from the tumor cells and analyzed by Real-time PCR. The expression levels of each gene were normalized to β-actin expression levels and adjusted to the levels in untreated tumor cells (medium). Data shown in different melanoma cells are mean ± SD from three independent experiments. $^{*}p < 0.05$, $^{**}p < 0.01$, and $^{***}p < 0.001$, compared with the medium control group. $^{\#}p < 0.05$, $^{\#\#}p < 0.01$, and $^{\#\#\#}p < 0.001$, compared with the respective baicalein or baicalin treatment group. **(B)** Activation of mTORC1-HIFα signaling prevented senescence induction in melanoma cells mediated by baicalein and baicalin. Cell treatment and procedure are identical to panel **(A)**. Treated melanoma cells were cultured for 3 days in the presence of baicalein or baicalin (40 μM for Mel586, A375, and SK-MEL-2 cells, and 50 μM for B16F0 cells). Senescent cells were analyzed using the SA-β-Gal activity assay. Data shown are mean ± SD from three independent experiments with similar results. $^{*}p < 0.05$, $^{**}p < 0.01$, and $^{***}p < 0.001$, compared with the medium control group. $^{\#}p < 0.05$, $^{\#\#}p < 0.01$, and $^{\#\#\#}p < 0.001$, compared with the respective baicalein or baicalin treatment group.

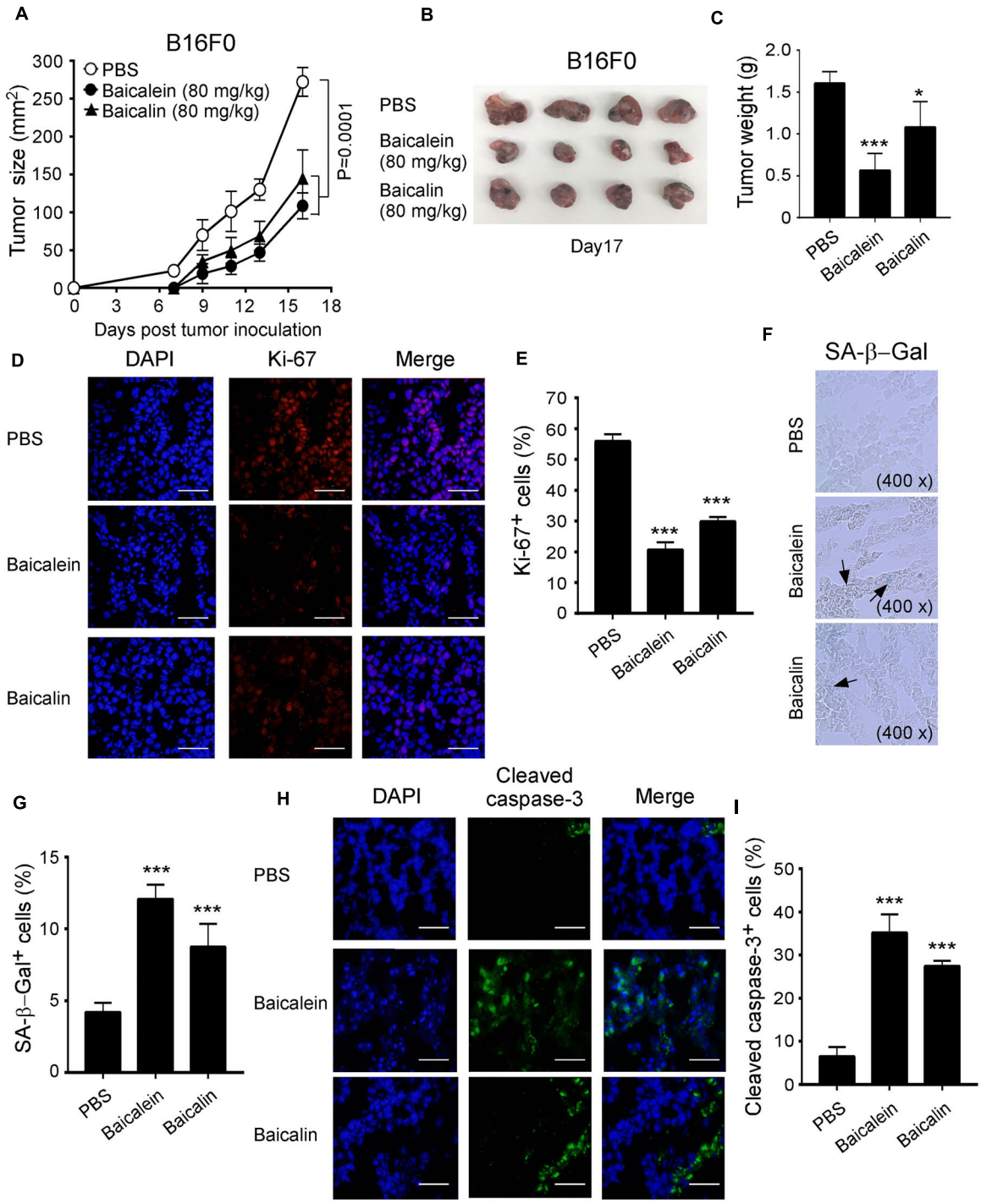

FIGURE 8 | Baicalein and baicalin inhibit tumor growth and tumorigenesis of melanoma *in vivo*. **(A)** Both baicalein and baicalin dramatically inhibited B16F0 melanoma tumor growth in NSG immunodeficient mice. B16F0 cells (1×10^5/mouse) were subcutaneously injected into NSG mice. After 4 days post tumor injection (tumor size reached around 5×5 mm), the tumor-bearing mice were administrated with baicalein (80 mg/kg), baicalin (80 mg/kg), or PBS control through intraperitoneal injection, respectively at every other day for 2 weeks. Tumor volumes were measured and presented as mean ± SD ($n = 4$ mice/group). p values were determined by the one-way analysis of variance (ANOVA). **(B)** Representative image of B16F0 tumors obtained from the indicated groups at the endpoint of the experiments (day 17). **(C)** Treatments with both baicalein and baicalin had much lower tumor weights compared with that of PBS control group. Results shown are mean ± SD of the tumor weights from the indicated groups in the B16F0 model at the endpoint of the experiments (day 17) ($n = 4$ mice/group). $^*p < 0.05$ and $^{***}p < 0.001$, compared with the PBS injection group using unpaired t-test. **(D,E)** Treatments with baicalein and baicalin significantly decreased the Ki-67$^+$ cell populations in tumor tissues at the endpoint of experiment using an immunofluorescence assay. Panel **(D)** are representative images of Ki-67 expression in tumor

(Continued)

FIGURE 8 | Continued
tissues from different groups. Scale bar: 50 μm. Panel **(E)** is the summary of mean ± SD of KI-67$^+$ cell fractions per high microscope field (×400) in the tumor tissues from four mice of each group. ***$p < 0.001$, compared with the PBS control treatment mice using unpaired *t*-test. **(F,G)** Large amounts of senescent tumor cells were observed in the tumor tissues from both treatments of baicalein and baicalin in NSG mice. SA-β-Gal expression was determined in the tumor frozen tissues from different groups at the endpoint of experiment. Panel **(F)** is photomicrographs of SA-β-Gal expression in tumor tissues from different groups as arrows indicated. Panel **(G)** is the summary of mean ± SD of SA-β-Gal$^+$ cell numbers per high microscope field (×400) in the tumor tissues from four mice of each group. ***$p < 0.001$, compared with the PBS treatment control mice using unpaired *t*-test. **(H,I)** Increased apoptotic cells were observed in B16F0 tumor tissues from the treatment groups with baicalein and baicalin. Cell apoptosis in the frozen sections was analyzed by the anti-cleaved caspase-3 staining at the end of experiments. Panel **(H)** are representative images of cleaved caspase-3 expression in tumor tissues from different groups. Scale bar: 50 μm. Panel **(I)** is the summary of mean ± SD of cleaved caspase-3$^+$ cell fractions per high microscope field (×400) in the tumor tissues from four mice of each group. ***$p < 0.001$, compared with the PBS treatment control group using unpaired *t*-test.

2012). In addition, the currently developed inhibitors, such as PLX4720 and PLX4032, show limitations as they could not cure melanoma with both N-RAS and B-RAF mutations (Halaban et al., 2010; Kaplan et al., 2012). These are significantly obstacles for a target therapy against melanoma. Therefore, development of alternative new drugs which can target melanoma cells with or without different types of oncogenic mutations is needed. In fact, many promising drugs have been developed based on the natural products and applied in clinical trials for various disease treatments including cancers (Cragg et al., 2009; Cragg and Newman, 2013; Stover et al., 2014). In our current studies, we utilized different types of melanoma cell lines with/without N-RAS and B-RAF mutations, including Mel586, SK-MEL-2 (wild type B-Raf and mutant N-RAS), A375 (B-RAF V600E and wild type N-RAS), as well as mouse B16F0 melanoma cell line. Our results clearly demonstrated that baicalein and baicalin can significantly inhibit both human and mouse melanoma cancer cell growth and proliferation regardless of N-RAS and B-RAF mutation statuses in tumor cells. In addition, the suppression of melanoma cells is due to the promotion of cancer cell apoptosis and senescence mediated by baicalein and baicalin. All these studies indicate that baicalein and baicalin could be promising and effective drugs targeting different mutants for melanoma therapy.

Scutellaria baicalensis Georgi is one of the most important traditional Chinese medicines, which is widely used for the disease treatments. Baicalein and baicalin are active components of *Scutellaria baicalensis* Georgi. Increasing evidence suggests that baicalein and baicalin have strong anti-tumor effects in various cancers (Takahashi et al., 2011; Huang et al., 2012; Zhang et al., 2013; Aryal et al., 2014; Chung et al., 2015). Our previous studies have further demonstrated that baicalein and baicalin can suppress colon cancer cell proliferation and growth *in vitro* and *in vivo* (Dou et al., 2018; Wang et al., 2018). Thus, exploring anti-tumor efficacy in different cancer types and related mechanisms mediated by baicalein and baicalin will provide critical information for the development of novel strategies for cancer treatment. We have demonstrated that MAPK ERK and p38 signaling pathways are involved in baicalein and baicalin-induced apoptosis and senescence in colon cancer (Dou et al., 2018). Furthermore, we identified that baicalin up-regulates the expression of DEPP (progesterone) and activates its downstream Ras/Raf/MEK/ERK and p16INK4A/Rb signaling pathways by acting as an antioxidant, leading to senescence in colon cancer cells (Wang et al., 2018). In this study, we provide first evidence that baicalein and baicalin can induce melanoma cell apoptosis and senescence, which is consistent with our previous studies shown in colon cancer (Dou et al., 2018; Wang et al., 2018). Importantly, our current studies further identified the metabolic control as a novel molecular mechanism responsible for the tumor suppression mediated by baicalein and baicalin. Increasing evidence suggests that metabolic disorder is a significant hallmark in the malignant tumors which controls the progression of tumor biological behaviors and immune cell functions in the suppressive tumor microenvironment (Biswas, 2015; Yoshida, 2015). Furthermore, the "Warburg effect" has been widely accepted as a common feature of metabolic reprogramming in tumors, and tumor cells depend on aerobic glycolysis for maintaining biosynthesis and functions (Warburg, 1956; Koppenol et al., 2011). In our effort to identify how baicalein and baicalin molecularly inhibit melanoma growth, we demonstrated that baicalein and baicalin can metabolically reprogram melanoma cells via inhibition of glucose uptake and downregulation of the key enzymes in glucose transport and glycolysis in tumor cells. Furthermore, the metabolic inhibition by baicalein and baicalin involves the mTOR-HIF-1α signaling regulation. All the results from both *in vivo* and *in vitro* studies indicate that baicalein and baicalin can rewrite tumor metabolism and have potent anti-tumor effects in melanoma. We will continue our future studies to explore the possibility that combining baicalein or baicalin treatment with other therapeutic strategies including immunotherapy will synergistically enhance anti-tumor efficacy in different melanoma models.

In summary, we report that baicalein and baicalin can significantly inhibit melanoma regardless of mutation statuses *in vitro* and *in vivo*. We further revealed that their anti-tumor effects are mechanistically due to the suppression of cancer cell glucose metabolism and induction of melanoma cell apoptosis and senescence. These data clearly suggest that both baicalein and baicalin have potent anti-tumor effects against melanoma and are potential novel and universal target drugs for melanoma therapy.

MATERIALS AND METHODS

Chemical Compounds

Baicalein (Purity 98.5%) and baicalin (Purity 91.5%) were purchased from the Kanghua Company (Nanjing, Jiangsu, China) and were dissolved in dimethyl sulfoxide (DMSO, Sigma, St. Louis, Mo, United States). A 50 mM stock solution were

prepared and stored in −20°C for the experiments, as we previously described (Dou et al., 2018; Wang et al., 2018).

Melanoma Cell Lines

Human melanoma cell lines (A375 and SK-MEL-2) and mouse melanoma cell line B16F were originally purchased from the American Type Culture Collection (ATCC, Manassas, VA, United States). Human Mel586 were obtained from the National Cancer Institute (NCI). Mel586 and B16F0 cells were maintained in RPMI-1640 medium containing 10% fetal bovine serum (FBS). A375 and SK-MEL-2 were maintained in DMEM medium containing 10% FBS.

Cell Growth and Proliferation Assay

Melanoma cell lines were cultured at a started number of 2×10^5/well in 6-well plates in the presence of different concentrations of baicalein and baicalin in triplicate wells, as we previously described (Dou et al., 2018; Wang et al., 2018). Cell growth was evaluated at different time points using the cell number counting. In addition, cell proliferation was determined using the [^{3}H]-thymidine incorporation assays as we previously described (Ye et al., 2012, 2014). In brief, different numbers of tumor cells (5×10^3, 1×10^4 or 2×10^4) were cultured in 96-well plates in cell assay medium containing 2% FCS in the presence of different concentrations of baicalein and baicalin. After 56 h of culture, [^{3}H]-thymidine was added at a final concentration of 1 μCi/well, followed by an additional 16 h of culture. The incorporation of [^{3}H]-thymidine was measured with a liquid scintillation counter (PerkinElmer, Waltham, MA, United States).

Colony Formation Assay

Two hundred to five hundred per well of melanoma cells treated with different concentrations of baicalein or baicalin, were seeded in 6-well plates and cultured for 10–14 days. Cell colonies were fixed with 4% formaldehyde, stained with 0.5% crystal violet for 15 min at room temperature, washed for several times and then counted under a microscope, as we described previously (Liu et al., 2015; Dou et al., 2018; Wang et al., 2018).

Wound Healing Assay

Melanoma cells were plated in 6-well plates and grown to 60–80% confluence. A wound area was generated by scraping cells with a 10 μl pipette tip across the entire diameter of the dish and extensively rinsed with PBS to remove all cellular debris. The scratches were photographed after additional 24 and 36 h of culture in the presence of different concentrations of baicalein or baicalin. The closure was estimated as the wounded area relative to the initial area (Liu et al., 2015; Dou et al., 2018; Wang et al., 2018).

Adhesion Assay

The flat bottom 96-well plates were coated with fibronectin (10 μl/ml, BD Biosciences) at 4°C overnight and then blocked with 2% BSA in PBS at 37°C for 2 h. Melanoma cells (1×10^5/ml) pre-treated with different concentrations of baicalein or baicalin for 72 h were seeded into fibronectin-pre-coated 96-well plates (10 μl/well) in the medium without FBS and incubated for 45 min. After washing three times with PBS to remove non-adherent cells, the cells attached on the plates were fixed with 4% formaldehyde for 4 min and stained with 0.03% crystal violet for 15 min. Adherent cells were counted and averaged in 10 fields at a high (×400) magnification with a microscope (Liu et al., 2015).

Apoptosis Assays

Melanoma cells were cultured for 36 or 72 h in the presence of different concentrations of baicalein and baicalin, and apoptosis was analyzed after staining with PE-labeled Annexin V and 7-AAD (BD Biosciences, San Diego, CA, United States) (Liu et al., 2015; Dou et al., 2018; Wang et al., 2018). Stained cells were analyzed on a FACSCalibur (BD Bioscience) and the data were analyzed with the FlowJo software (Tree Star, Ashland, OR, United States).

Flow Cytometry Analysis

The expression of mTOR-HIF-1α signaling markers on tumor cells were determined by FACS analysis after staining with anti-human specific antibodies, including anti-phosphorylated mTOR (1:500), p70S6K (1:500), and 4E-BP1 (1:1000), as well as anti-HIF-1α (1:1000) and then secondary anti-rabbit antibody conjugated with either PE or FITC. These antibodies were purchased from Cell Signaling Technology. All stained cells were analyzed on a FACSCalibur flow cytometer (BD Bioscience) and data analyzed with the FlowJo software (Tree Star).

Senescence Associated β-Galactosidase (SA-β-Gal) Staining

Senescence associated β-Galactosidase (SA-β-Gal) activity in tumor cells was detected as we previously described (Dou et al., 2018; Wang et al., 2018). Briefly, melanoma cells were cultured for 3 days in the presence of different concentrations of baicalein or baicalin. For some experiments, tumor cells were transfected with Retro-Rheb, pCDNA-Glut1 or control plasmids, or pretreated with DMOG (0.1 mM, Sigma) for 24 h, then cultured for 3 days in the presence of different concentrations of baicalein or baicalin (Li et al., 2019). Tumor cells were fixed in 3% formaldehyde, and followed to incubate overnight at 37°C with freshly prepared SA-β-Gal staining solution. The stained cells were washed with PBS and examined with a microscope.

Quantitative Real-Time PCR Analysis

Total RNA was extracted from the mouse and human melanoma cells using the Trizol reagent (Invitrogen), and cDNA was transcribed using a SuperScript II RT kit (Invitrogen), both according to the manufacturers' instructions. Expression levels of each gene were determined by reverse-transcription PCR using specific primers, and mRNA levels in each sample were normalized to the relative quantity of β-actin gene expression. All experiments were performed in triplicate. The specific primers used for mouse and human metabolic genes are listed in **Supplementary**

Table S1. All primers were purchased from Integrated DNA Technologies.

Glucose Uptake Assay

Glucose uptake was determined following 20 min incubation of melanoma cells with a fluorescent D-glucose analog 2-[(7-nitrobenz-2-oxa-1,3-diazol-4-yl) amino]-2-deoxy-D-glucose (2-NBDG) (Cayman Chemical), as we previously described (Li et al., 2019). Melanoma cells were pretreated with different concentrations of baicalein and baicalin for 72 h. Treated and untreated melanoma cells were cultured in the glucose-free medium for 30 min, and followed addition of 2-NBDG (100 μM) for 20 min and analyzed with a FACSCalibur flow cytometer (BD Bioscience).

Immunofluorescence Staining in Tissues

Tumor tissues were embedded into OCT and prepared for cryostat sections (4∼8 μm). Frozen slides were recovered to room temperature, washed with PBS and treated with 3% H_2O_2 in PBS for 30 min. The sections were further blocked with 3.7% formaldehyde for 30 min and added the primary antibodies, including anti-Ki-67 (#9129, Cell Signaling Technology), anti-cleaved caspase-3 (#9664, Cell Signaling Technology) at diluted concentrations of 1:50 and 1:400, respectively, under 4°C overnight. The slides were washed with PBS and added a secondary antibody-conjugated with AF594 and DAPI at diluted concentrations of 1:300 and 1:2500, under room temperature for 1 h. The stained slides were analyzed by an immunofluorescence microscopy.

In vivo Tumorigenesis Studies

NOD-scid IL2Rγ^{null} (NSG, 6–8 weeks) immunodeficient mice were purchased from The Jackson Laboratory and maintained in the institutional animal facility. All animal studies have been approved by the Institutional Animal Care Committee. For tumorigenesis studies, B16F0 cells (1×10^5/mouse) were subcutaneously injected into NSG mice. After 4 days post tumor injection (tumor size reached around 5 × 5 mm), the tumor-bearing mice were randomly divided into three groups (n = 4/group) and administrated with baicalein (80 mg/kg), baicalin (80 mg/kg), and PBS control through intraperitoneal injection, respectively, at every other day for 2 weeks. Tumor size was measured with calipers every 2 days. Tumor volume was calculated on the basis of two-dimensional measurements. At the end of experiments (day 17), the mice were sacrificed and tumors were isolated and weighted. Furthermore, tumor tissues were embedded into OCT and prepared for cryostat sections (4∼8 μm), and SA-β-Gal expression, cell proliferation and apoptotic cell populations were assayed, as described above. In addition, parts of tumor issues were grinded and total RNA was extracted, and cDNA was transcribed for RT-PCR experiments.

Statistical Analysis

Statistical analysis was performed with GraphPad Prism5 software. Data are expressed as mean ± standard deviation (SD). For multiple group comparison *in vivo* studies, the one-way analysis of variance (ANOVA) was used, followed by the Dunnett's test for comparing experimental groups against a single control. For single comparison between two groups, paired Student's t-test was used. Non-parametric t-test was chosen if the sample size was too small and did not fit a Gaussian distribution.

DATA AVAILABILITY STATEMENT

The raw data supporting the conclusions of this article will be made available by the authors, without undue reservation.

ETHICS STATEMENT

The animal study was reviewed and approved by the Saint Louis University.

AUTHOR CONTRIBUTIONS

LH, HX, and GP designed research, analyzed the data, prepared figures, and wrote the manuscript. LH, BP, YN, CW, FS, and XL performed the experiments. JD provided the baicalein and baicalin compounds and discussion of the manuscript. All authors contributed to the article and approved the submitted version.

ACKNOWLEDGMENTS

The authors would like to thank Dr. Xu Wu from the Massachusetts General Hospital, Harvard Medical School to provide human melanoma cell lines. The authors also thank Dr. Grant Kolar and Caroline Murphy in the Histology Core at SLU for preparing cryostat sections.

SUPPLEMENTARY MATERIAL

The Supplementary Material for this article can be found online at: https://www.frontiersin.org/articles/10.3389/fcell.2020.00836/full#supplementary-material

FIGURE S1 | Increased apoptotic cell populations are induced in both human and mouse melanoma cells after treatments with baicalein and baicalin. Tumor cells were cultured in the presence of the indicated concentrations of baicalein and baicalin for 36 h. Apoptosis in treated tumor cells was analyzed after staining with PE-labeled Annexin V and 7-AAD. Results shown in the histogram are summaries of mean ± SD from three independent experiments. ***$p < 0.001$, compared with the medium control group.

FIGURE S2 | Baicalein and baicalin treatments significantly down-regulate gene expression levels of key glycolytic enzymes in melanoma cells. Both human and mouse Melanoma cells were treated with or without the indicated concentrations of baicalein and baicalin for 72 h. Total RNA was isolated from the tumor cells and analyzed by Real-time PCR. The expression levels of each gene were normalized to β-actin expression levels and adjusted to the levels in untreated tumor cells (medium). Data shown in different melanoma cells are mean ± SD from three independent experiments. *$p < 0.05$ and **$p < 0.01$, compared with the medium only group.

FIGURE S3 | Baicalein and baicalin treatments down-regulate gene expression levels of key glycolytic enzymes in B16F0 tumor cells *in vivo*. B16F0 cells (1×10^5/mouse) were subcutaneously injected into NSG mice. After 4 days post

tumor injection (tumor size reached around 5 × 5 mm), the tumor-bearing mice were administrated with baicalein (80 mg/kg), baicalin (80 mg/kg), or PBS control through intraperitoneal injection, respectively at every other day for 2 weeks. At the end of experiments, tumor issues were grinded and total RNA was extracted. The expression levels of each gene were normalized to β-actin expression levels and adjusted to the levels in PBS treated group (set as 1). Results shown are mean ± SD from four mice per group. $^{*}p < 0.05$, $^{**}p < 0.01$, and $^{***}p < 0.001$, compared with the PBS treatment control group using unpaired *t*-test.

REFERENCES

American Cancer Society (2018). *Cancer Facts and Figures 2018*. Atlanta, GA: American Cancer Society.

Aryal, P., Kim, K., Park, P. H., Ham, S., Cho, J., and Song, K. (2014). Baicalein induces autophagic cell death through AMPK/ULK1 activation and downregulation of mTORC1 complex components in human cancer cells. *FEBS J.* 281, 4644–4658. doi: 10.1111/febs.12969

Biswas, S. K. (2015). Metabolic reprogramming of immune cells in cancer progression. *Immunity* 43, 435–449. doi: 10.1016/j.immuni.2015.09.001

Brose, M. S., Volpe, P., Feldman, M., Kumar, M., Rishi, I., Gerrero, R., et al. (2002). BRAF and RAS mutations in human lung cancer and melanoma. *Cancer Res.* 62, 6997–7000.

Chao, J. I., Su, W. C., and Liu, H. F. (2007). Baicalein induces cancer cell death and proliferation retardation by the inhibition of CDC2 kinase and survivin associated with opposite role of p38 mitogen-activated protein kinase and AKT. *Mol. Cancer Ther.* 6, 3039–3048. doi: 10.1158/1535-7163.mct-07-0281

Chen, G. Q., Tang, C. F., Shi, X. K., Lin, C. Y., Fatima, S., Pan, X. H., et al. (2015). Halofuginone inhibits colorectal cancer growth through suppression of Akt/mTORC1 signaling and glucose metabolism. *Oncotarget* 6, 24148–24162. doi: 10.18632/oncotarget.4376

Cheng, S. C., Quintin, J., Cramer, R. A., Shepardson, K. M., Saeed, S., Kumar, V., et al. (2014). mTOR- and HIF-1alpha-mediated aerobic glycolysis as metabolic basis for trained immunity. *Science* 345:1250684. doi: 10.1126/science.1250684

Chiu, Y. W., Lin, T. H., Huang, W. S., Teng, C. Y., Liou, Y. S., Kuo, W. H., et al. (2011). Baicalein inhibits the migration and invasive properties of human hepatoma cells. *Toxicol. Appl. Pharmacol.* 255, 316–326. doi: 10.1016/j.taap.2011.07.008

Chung, H., Choi, H. S., Seo, E. K., Kang, D. H., and Oh, E. S. (2015). Baicalin and baicalein inhibit transforming growth factor-beta1-mediated epithelial-mesenchymal transition in human breast epithelial cells. *Biochem. Biophys. Res. Commun.* 458, 707–713. doi: 10.1016/j.bbrc.2015.02.032

Cosin-Roger, J., Simmen, S., Melhem, H., Atrott, K., Frey-Wagner, I., Hausmann, M., et al. (2017). Hypoxia ameliorates intestinal inflammation through NLRP3/mTOR downregulation and autophagy activation. *Nat. Commun.* 8:98.

Cragg, G. M., Grothaus, P. G., and Newman, D. J. (2009). Impact of natural products on developing new anti-cancer agents. *Chem. Rev.* 109, 3012–3043. doi: 10.1021/cr900019j

Cragg, G. M., and Newman, D. J. (2013). Natural products: a continuing source of novel drug leads. *Biochim. Biophys. Acta* 1830, 3670–3695. doi: 10.1016/j.bbagen.2013.02.008

Dang, C. V. (2013). MYC, metabolism, cell growth, and tumorigenesis. *Cold Spring Harb. Perspect. Med.* 3:a014217. doi: 10.1101/cshperspect.a014217

de Oliveira, M. R., Nabavi, S. F., Habtemariam, S., Erdogan Orhan, I., Daglia, M., and Nabavi, S. M. (2015). The effects of baicalein and baicalin on mitochondrial function and dynamics: a review. *Pharmacol. Res.* 100, 296–308. doi: 10.1016/j.phrs.2015.08.021

Ding, Y., Dou, J., Teng, Z., Yu, J., Wang, T., Lu, N., et al. (2014). Antiviral activity of baicalin against influenza A (H1N1/H3N2) virus in cell culture and in mice and its inhibition of neuraminidase. *Arch. Virol.* 159, 3269–3278. doi: 10.1007/s00705-014-2192-2

Dou, J., Wang, Z., Ma, L., Peng, B., Mao, K., Li, C., et al. (2018). Baicalein and baicalin inhibit colon cancer using two distinct fashions of apoptosis and senescence. *Oncotarget* 9, 20089–20102. doi: 10.18632/oncotarget.24015

Flaherty, K. T., Puzanov, I., Kim, K. B., Ribas, A., McArthur, G. A., Sosman, J. A., et al. (2010). Inhibition of mutated, activated BRAF in metastatic melanoma. *N. Engl. J. Med.* 363, 809–819.

Flanigan, J. C., Jilaveanu, L. B., Chiang, V. L., and Kluger, H. M. (2013). Advances in therapy for melanoma brain metastases. *Clin. Dermatol.* 31, 264–281. doi: 10.1016/j.clindermatol.2012.08.008

Gong, W. Y., Zhao, Z. X., Liu, B. J., Lu, L. W., and Dong, J. C. (2017). Exploring the chemopreventive properties and perspectives of baicalin and its aglycone baicalein in solid tumors. *Eur. J. Med. Chem.* 126, 844–852. doi: 10.1016/j.ejmech.2016.11.058

Gowrishankar, K., Snoyman, S., Pupo, G. M., Becker, T. M., Kefford, R. F., and Rizos, H. (2012). Acquired resistance to BRAF inhibition can confer cross-resistance to combined BRAF/MEK inhibition. *J. Invest. Dermatol.* 132, 1850–1859. doi: 10.1038/jid.2012.63

Halaban, R., Zhang, W., Bacchiocchi, A., Cheng, E., Parisi, F., Ariyan, S., et al. (2010). PLX4032, a selective BRAF(V600E) kinase inhibitor, activates the ERK pathway and enhances cell migration and proliferation of BRAF melanoma cells. *Pigment Cell Melanoma Res.* 23, 190–200. doi: 10.1111/j.1755-148x.2010.00685.x

Hatzivassiliou, G., Song, K., Yen, I., Brandhuber, B. J., Anderson, D. J., Alvarado, R., et al. (2010). RAF inhibitors prime wild-type RAF to activate the MAPK pathway and enhance growth. *Nature* 464, 431–435. doi: 10.1038/nature08833

Huang, Y., Hu, J., Zheng, J., Li, J., Wei, T., Zheng, Z., et al. (2012). Down-regulation of the PI3K/Akt signaling pathway and induction of apoptosis in CA46 Burkitt lymphoma cells by baicalin. *J. Exp. Clin. Cancer Res.* 31:48.

Jakob, J. A., Bassett, R. L. Jr., Ng, C. S., Curry, J. L., Joseph, R. W., Alvarado, G. C., et al. (2012). NRAS mutation status is an independent prognostic factor in metastatic melanoma. *Cancer* 118, 4014–4023. doi: 10.1002/cncr.26724

Ji, S., Li, R., Wang, Q., Miao, W. J., Li, Z. W., Si, L. L., et al. (2015). Anti-H1N1 virus, cytotoxic and Nrf2 activation activities of chemical constituents from Scutellaria baicalensis. *J. Ethnopharmacol.* 176, 475–484. doi: 10.1016/j.jep.2015.11.018

Johnson, J. J. (2011). Carnosol: a promising anti-cancer and anti-inflammatory agent. *Cancer Lett.* 305, 1–7. doi: 10.1016/j.canlet.2011.02.005

Kaplan, F. M., Kugel, C. H. III, Dadpey, N., Shao, Y., Abel, E. V., and Aplin, A. E. (2012). SHOC2 and CRAF mediate ERK1/2 reactivation in mutant NRAS-mediated resistance to RAF inhibitor. *J. Biol. Chem.* 287, 41797–41807. doi: 10.1074/jbc.m112.390906

Kaplan, F. M., Shao, Y., Mayberry, M. M., and Aplin, A. E. (2011). Hyperactivation of MEK-ERK1/2 signaling and resistance to apoptosis induced by the oncogenic B-RAF inhibitor, PLX4720, in mutant N-RAS melanoma cells. *Oncogene* 30, 366–371. doi: 10.1038/onc.2010.408

Koppenol, W. H., Bounds, P. L., and Dang, C. V. (2011). Otto Warburg's contributions to current concepts of cancer metabolism. *Nat. Rev. Cancer* 11, 325–337. doi: 10.1038/nrc3038

Kwong, L. N., Costello, J. C., Liu, H., Jiang, S., Helms, T. L., Langsdorf, A. E., et al. (2012). Oncogenic NRAS signaling differentially regulates survival and proliferation in melanoma. *Nat. Med.* 18, 1503–1510. doi: 10.1038/nm.2941

Li, L., Liu, X., Sanders, K. L., Edwards, J. L., Ye, J., Si, F., et al. (2019). TLR8-mediated metabolic control of human treg function: a mechanistic target for cancer immunotherapy. *Cell Metab.* 29, 103–123.

Liu, S., Han, B., Zhang, Q., Dou, J., Wang, F., Lin, W., et al. (2015). Vasohibin-1 suppresses colon cancer. *Oncotarget* 6, 7880–7898. doi: 10.18632/oncotarget.3493

Liu, X., Mo, W., Ye, J., Li, L., Zhang, Y., Hsueh, E. C., et al. (2018). Regulatory T cells trigger effector T cell DNA damage and senescence caused by metabolic competition. *Nat. Commun.* 9:249.

Moghaddam, E., Teoh, B. T., Sam, S. S., Lani, R., Hassandarvish, P., Chik, Z., et al. (2014). Baicalin, a metabolite of baicalein with antiviral activity against dengue virus. *Sci. Rep.* 4:5452.

Nazarian, R., Shi, H., Wang, Q., Kong, X., Koya, R. C., Lee, H., et al. (2010). Melanomas acquire resistance to B-RAF(V600E) inhibition by RTK or N-RAS upregulation. *Nature* 468, 973–977. doi: 10.1038/nature09626

Omholt, K., Platz, A., Kanter, L., Ringborg, U., and Hansson, J. (2003). NRAS and BRAF mutations arise early during melanoma pathogenesis and are preserved throughout tumor progression. *Clin. Cancer Res.* 9, 6483–6488.

Poulikakos, P. I., Zhang, C., Bollag, G., Shokat, K. M., and Rosen, N. (2010). RAF inhibitors transactivate RAF dimers and ERK signalling in cells with wild-type BRAF. *Nature* 464, 427–430. doi: 10.1038/nature08902

Pusapati, R. V., Daemen, A., Wilson, C., Sandoval, W., Gao, M., Haley, B., et al. (2016). mTORC1-dependent metabolic reprogramming underlies escape from

glycolysis addiction in cancer cells. *Cancer Cell* 29, 548–562. doi: 10.1016/j.ccell.2016.02.018

Salmond, R. J. (2018). mTOR regulation of glycolytic metabolism in T cells. *Front. Cell Dev. Biol.* 6:122. doi: 10.3389/fcell.2018.00122

Stover, J. F., Belli, A., Boret, H., Bulters, D., Sahuquillo, J., Schmutzhard, E., et al. (2014). Nitric oxide synthase inhibition with the antipterin VAS203 improves outcome in moderate and severe traumatic brain injury: a placebo-controlled randomized Phase IIa trial (NOSTRA). *J. Neurotrauma* 31, 1599–1606. doi: 10.1089/neu.2014.3344

Sun, Q., Chen, X., Ma, J., Peng, H., Wang, F., Zha, X., et al. (2011). Mammalian target of rapamycin up-regulation of pyruvate kinase isoenzyme type M2 is critical for aerobic glycolysis and tumor growth. *Proc. Natl. Acad. Sci. U.S.A.* 108, 4129–4134. doi: 10.1073/pnas.1014769108

Takahashi, H., Chen, M. C., Pham, H., Angst, E., King, J. C., Park, J., et al. (2011). Baicalein, a component of *Scutellaria baicalensis*, induces apoptosis by Mcl-1 down-regulation in human pancreatic cancer cells. *Biochim. Biophys. Acta* 1813, 1465–1474.

Thomas, N. E., Edmiston, S. N., Alexander, A., Groben, P. A., Parrish, E., Kricker, A., et al. (2015). Association between NRAS and BRAF mutational status and melanoma-specific survival among patients with higher-risk primary melanoma. *JAMA Oncol.* 1, 359–368.

Thumar, J., Shahbazian, D., Aziz, S. A., Jilaveanu, L. B., and Kluger, H. M. (2014). MEK targeting in N-RAS mutated metastatic melanoma. *Mol. Cancer* 13:45. doi: 10.1186/1476-4598-13-45

Ugurel, S., Thirumaran, R. K., Bloethner, S., Gast, A., Sucker, A., Mueller-Berghaus, J., et al. (2007). B-RAF and N-RAS mutations are preserved during short time in vitro propagation and differentially impact prognosis. *PLoS One* 2:e236. doi: 10.1371/journal.pone.0000236

Villanueva, J., Vultur, A., Lee, J. T., Somasundaram, R., Fukunaga-Kalabis, M., Cipolla, A. K., et al. (2010). Acquired resistance to BRAF inhibitors mediated by a RAF kinase switch in melanoma can be overcome by cotargeting MEK and IGF-1R/PI3K. *Cancer Cell* 18, 683–695. doi: 10.1016/j.ccr.2010.11.023

Wang, C. Z., Zhang, C. F., Chen, L., Anderson, S., Lu, F., and Yuan, C. S. (2015). Colon cancer chemopreventive effects of baicalein, an active enteric microbiome metabolite from baicalin. *Int. J. Oncol.* 47, 1749–1758. doi: 10.3892/ijo.2015.3173

Wang, Z., Ma, L., Su, M., Zhou, Y., Mao, K., Li, C., et al. (2018). Baicalin induces cellular senescence in human colon cancer cells via upregulation of DEPP and the activation of Ras/Raf/MEK/ERK signaling. *Cell Death Dis.* 9:217.

Warburg, O. (1956). On the origin of cancer cells. *Science* 123, 309–314.

Ward, P. S., and Thompson, C. B. (2012). Metabolic reprogramming: a cancer hallmark even warburg did not anticipate. *Cancer Cell* 21, 297–308. doi: 10.1016/j.ccr.2012.02.014

Xiao, J. R., Do, C. W., and To, C. H. (2014). Potential therapeutic effects of baicalein, baicalin, and wogonin in ocular disorders. *J. Ocul. Pharmacol. Ther.* 30, 605–614. doi: 10.1089/jop.2014.0074

Yang, H., Jiang, X., Li, B., Yang, H. J., Miller, M., Yang, A., et al. (2017). Mechanisms of mTORC1 activation by RHEB and inhibition by PRAS40. *Nature* 552, 368–373. doi: 10.1038/nature25023

Ye, J., Huang, X., Hsueh, E. C., Zhang, Q., Ma, C., Zhang, Y., et al. (2012). Human regulatory T cells induce T-lymphocyte senescence. *Blood* 120, 2021–2031. doi: 10.1182/blood-2012-03-416040

Ye, J., Ma, C., Hsueh, E. C., Dou, J., Mo, W., Liu, S., et al. (2014). TLR8 signaling enhances tumor immunity by preventing tumor-induced T-cell senescence. *EMBO Mol. Med.* 6, 1294–1311. doi: 10.15252/emmm.201403918

Yoshida, G. J. (2015). Metabolic reprogramming: the emerging concept and associated therapeutic strategies. *J. Exp. Clin. Cancer. Res.* 34:111.

Yu, C., Zhang, Z., Zhang, H., Zhen, Z., Calway, T., Wang, Y., et al. (2013). Pretreatment of baicalin and wogonoside with glycoside hydrolase: a promising approach to enhance anticancer potential. *Oncol. Rep.* 30, 2411–2418. doi: 10.3892/or.2013.2726

Zhang, H. B., Lu, P., Guo, Q. Y., Zhang, Z. H., and Meng, X. Y. (2013). Baicalein induces apoptosis in esophageal squamous cell carcinoma cells through modulation of the PI3K/Akt pathway. *Oncol. Lett.* 5, 722–728. doi: 10.3892/ol.2012.1069

Zhdanov, A. V., Okkelman, I. A., Collins, F. W., Melgar, S., and Papkovsky, D. B. (2015). A novel effect of DMOG on cell metabolism: direct inhibition of mitochondrial function precedes HIF target gene expression. *Biochim. Biophys. Acta* 1847, 1254–1266. doi: 10.1016/j.bbabio.2015.06.016

Conflict of Interest: The authors declare that the research was conducted in the absence of any commercial or financial relationships that could be construed as a potential conflict of interest.

frontiers in Cell and Developmental Biology

ORIGINAL RESEARCH
published: 26 August 2020
doi: 10.3389/fcell.2020.00834

Differential Requirement of Beclin 1 for Regulating the Balance of Naïve and Activated CD4$^+$ T Cells

Rui Xia[1,2,3†], Min Yang[2,4†], Xiaorui Fu[2,5†], Wenwen Du[2], Xin Gao[2], Gang Li[2], Sarangarajan Ranganathan[6], Xueguang Zhang[3], Jingting Jiang[4] and Binfeng Lu[2*]*

[1] Department of Immunology, Institute of Medical Biotechnology, Soochow University, Suzhou, China, [2] Department of Immunology, School of Medicine, University of Pittsburgh, Pittsburgh, PA, United States, [3] Department of Oncology, The Second Affiliated Hospital of Soochow University, Soochow University, Suzhou, China, [4] Department of Oncology, The Third Affiliated Hospital of Soochow University, Changzhou, China, [5] Department of Oncology, The First Affiliated Hospital of Zhengzhou University, Zhengzhou, China, [6] Department of Pathology, UPMC Children's Hospital of Pittsburgh, Pittsburgh, PA, United States

OPEN ACCESS

Edited by:
Guangyong Peng,
Saint Louis University, United States

Reviewed by:
Daolin Tang,
University of Texas Southwestern Medical Center, United States
Jingfang Ju,
Stony Brook Medicine, United States

***Correspondence:**
Rui Xia
xiarui87@163.com
Binfeng Lu
binfeng@pitt.edu

†These authors have contributed equally to this work

Specialty section:
This article was submitted to Cell Death and Survival, a section of the journal Frontiers in Cell and Developmental Biology

Received: 25 June 2020
Accepted: 04 August 2020
Published: 26 August 2020

Citation:
Xia R, Yang M, Fu X, Du W, Gao X, Li G, Ranganathan S, Zhang X, Jiang J and Lu B (2020) Differential Requirement of Beclin 1 for Regulating the Balance of Naïve and Activated CD4$^+$ T Cells. Front. Cell Dev. Biol. 8:834. doi: 10.3389/fcell.2020.00834

Autophagy is highly regulated and plays a multitude of roles during T cell-mediated immune responses. It has been shown that autophagy deficiency in T cells results in a decrease in total T cells, including naïve T cells in young mice, but the mechanism is still not understood. Here, similar to what happened in young mice, we showed that T cell-specific deletion of *Beclin 1/Atg6* (*Becn1* −/−) resulted in decreases in the percentages of CD4$^+$, CD8$^+$, and regulatory T cells in adult mice. In addition, we found that the effector to naïve T cell ratio was increased in older mice. Also, as mice grew older, *Becn1* −/− mice progressively lost weight and developed severe colitis. Analysis of inflamed tissues demonstrated increases in the portion and cytokine production of effector T cells. In contrast, the TCR-transgenic *Becn1* −/− mice had similar numbers of naïve T cells compared to WT controls. Similar to bulk T cells, the TCR-transgenic *Becn1* −/− T cells generated much lower numbers of effector T cells compared to WT controls after activation *in vitro*. These data suggest that autophagy is not required for maintaining the naïve T cell but required for the generation of effector T cells *in vivo*.

Keywords: naive T cell, Beclin 1, effector T cell, colitis, autoimmune, cell death

INTRODUCTION

Autophagy is a highly regulated cellular process during the life cycle of T cells. The numbers of autophagosomes are greatly increased upon T cell activation and are also regulated by cytokines (Li et al., 2006; Pua et al., 2007). Lack of nutrient and inhibition of mTOR can also induce autophagy in activated T cells (Li et al., 2006; Jia and He, 2011). It has been shown that autophagy deficient T cells undergo elevated levels of programmed cell death after activation (Pua et al., 2007; Kovacs et al., 2012). In addition, autophagy is required for the survival of effector CD8$^+$ T cells during viral infection and autoreactive CD4$^+$ T cells during the course of the experimental autoimmune encephalomyelitis (EAE) (Kovacs et al., 2012; Schlie et al., 2015). It has been shown that autophagy blockade in activated T cells resulted in greater levels of apoptotic proteins, leading to increased levels of apoptosis (Kovacs et al., 2012). Despite the evidence for a prosurvival role of autophagy in activated T cells, autophagy has also been shown to promote cell death in a murine T cell line

and HIV-infected human $CD4^+$ T cells (Espert et al., 2006; Li et al., 2006). The exact role of autophagy in T cell survival is therefore dependent on cellular context.

Naïve T cells, characteristically expressing low levels of CD44 and high levels of CD62L, are quiescent, long-lived, and slow-proliferating in immune-intact mice (Sprent and Tough, 1994; Clarke and Rudensky, 2000; Dorfman et al., 2000; Sprent et al., 2008). In mice, the vast majority of the naïve T cell pool is sustained by thymic exodus of recently developed T cells (den Braber et al., 2012). Upon recognition of environmental antigens, naïve T cells are activated, differentiate into effector and memory T cells, and change their surface phenotype to $CD44^{high}$ and $CD62L^{low}$. Thus, the number of naïve T cells is controlled by thymic output, survival of naïve T cells, and activation by MHC/peptide complexes. Autophagy deficiency in T cells results in severely reduced numbers of naïve $CD4^+$ and $CD8^+$ T cells in the secondary lymphoid organs, without affecting thymic T cell development (Pua et al., 2007; Kovacs et al., 2012; Parekh et al., 2013; Wei et al., 2016), suggesting a critical role of autophagy in regulating the number of naïve T cells (Pua et al., 2007; Kovacs et al., 2012; Parekh et al., 2013; Wei et al., 2016). The mechanisms by which autophagy regulates naïve T cells numbers are not understood.

In this study, we investigated the impact of autophagy blockade on naïve and effector/memory T cell populations in adult mice with a deletion of *Beclin 1* in all T cells (*Becn1* −/−). In order to further determine the role of autophagy in naïve T cells, we utilized a TCR transgenic system to prevent naïve T cell activation by environmental antigens. Our study helps to clarify the role of autophagy in homeostasis of naïve T cells and autoimmunity.

RESULTS

Beclin 1 Deficiency in T Cells Led to Severe Reduction in the Percentage of Naïve T Cells, but Greatly Increased Percentages of Effector/Memory T Cells in Adult Mice

Our previous studies have established that Beclin 1 deficiency in T cells resulted in reduction of naïve $CD4^+$ and $CD8^+$ T cells in young mice. We then further examined the long-term effect of Beclin 1 deficiency on total T cell population in adult mice. We observed a significant reduction of the percentage of $CD44^{low}$ $CD62L^{high}$ phenotype naïve T cells in both $CD4^+$ and $CD8^+$ T cells in the spleen and $CD8^+$ T cells in the lymph node of *Becn1* −/− mice compared with WT mice (**Figures 1A–C,E**). We found an increase of the percentage of $CD44^{high}$ $CD62L^{low}$ effector memory T cells in both $CD4^+$ and $CD8^+$ T cells in spleens and lymph nodes of the *Becn1* −/− mice compared with WT mice (**Figures 1A–E**). In addition, we also observed increases in central memory $CD8^+$ T cells in *Becn1* −/− mice compared to WT controls (**Figures 1A–E**). Despite the increase in memory/effector T cells, the percentages of $CD4^+$ and $CD8^+$ T cells were decreased in spleens and lymph nodes (**Figures 1F–H**). Consistent with the role of IL-15 in the expansion and homeostasis of memory T cells, we found an increase in $CD44^{int}$ $CD122^+$ CD4 and CD8 T cells in spleens, lymph nodes, and mesenteric lymph nodes of *Becn1* −/− mice compared with WT control mice (**Figures 1F–L**). Collectively, Beclin 1 deficiency in T cells resulted in decreases in the percentage of naïve T cells and increases in the percentage of effector and memory T cells in adult mice.

Increased Percentages of T Cells Producing Effector Cytokines in *Becn1* −/− Mice

In order to further establish whether effector T cells were increased in *Becn1* −/− mice, we quantified IFN-γ and IL-17 producing $CD4^+$ or $CD8^+$ T cells *ex vivo* (**Figures 2A,B**). We found that the percentage of IFN-γ-producing $CD4^+$ and $CD8^+$ T cells and IL-17-producing $CD4^+$ T cells were much higher in *Becn1* −/− mice than WT mice. These data suggested that active T cell-mediated immune or autoimmune responses were present in in *Becn1* −/− mice.

Beclin 1 Deficiency Decreased the Percentage of Treg

We also examined the percentage of regulatory T cells within the $CD4^+$ T cells. We found no significant difference in the percentage of $Foxp3^+$ T cells within the $CD4^+$ T cells (**Figures 3A,B**). There was also no significant difference in the CD25 expression in the Treg compartment (**Figure 3C**). Since there was a decrease in percentages of total $CD4^+$ T cell numbers, the total percentage of Treg was also smaller in the *Becn1* −/− mice than in WT control mice.

Increased Portions of Myeloid Cells in *Becn1* −/− Mice

Chronic inflammation is usually associated with increases in myeloid derived suppressor cells (MDSC). We quantified the myeloid cells in the spleen. Our data showed a significant increase in the percentages of $CD11b^+$ $Gr\text{-}1^{high}$ MDSC and $CD11b^+$ $Gr\text{-}1^{int}$ MDSC in spleens and lymph nodes of *Becn1* −/− mice compared with WT mice (**Figures 4A–C**). The percentages of $CD11b^+$ $Gr\text{-}1^-$, which contains macrophages and dendritic cells, were not significantly changed between *Becn1* −/− mice and WT control mice. These findings were consistent with a chronic inflammatory condition in adult *Becn1* −/− mice.

Beclin 1 Deficiency in T Cells Led to Severe Colitis in Adult Mice

Defects in autophagy have been found by genetic association studies to confer susceptibility to several autoimmune and inflammatory disorders, particularly inflammatory bowel disease (Jones et al., 2013). We found that *Becn1* −/− mice started to have a lower body weight than WT mice 9 weeks after birth, and this weight loss became more significant as mice aged (**Figure 5A**). We also observed that about 70% of *Becn1* −/− mice ($N > 50$)

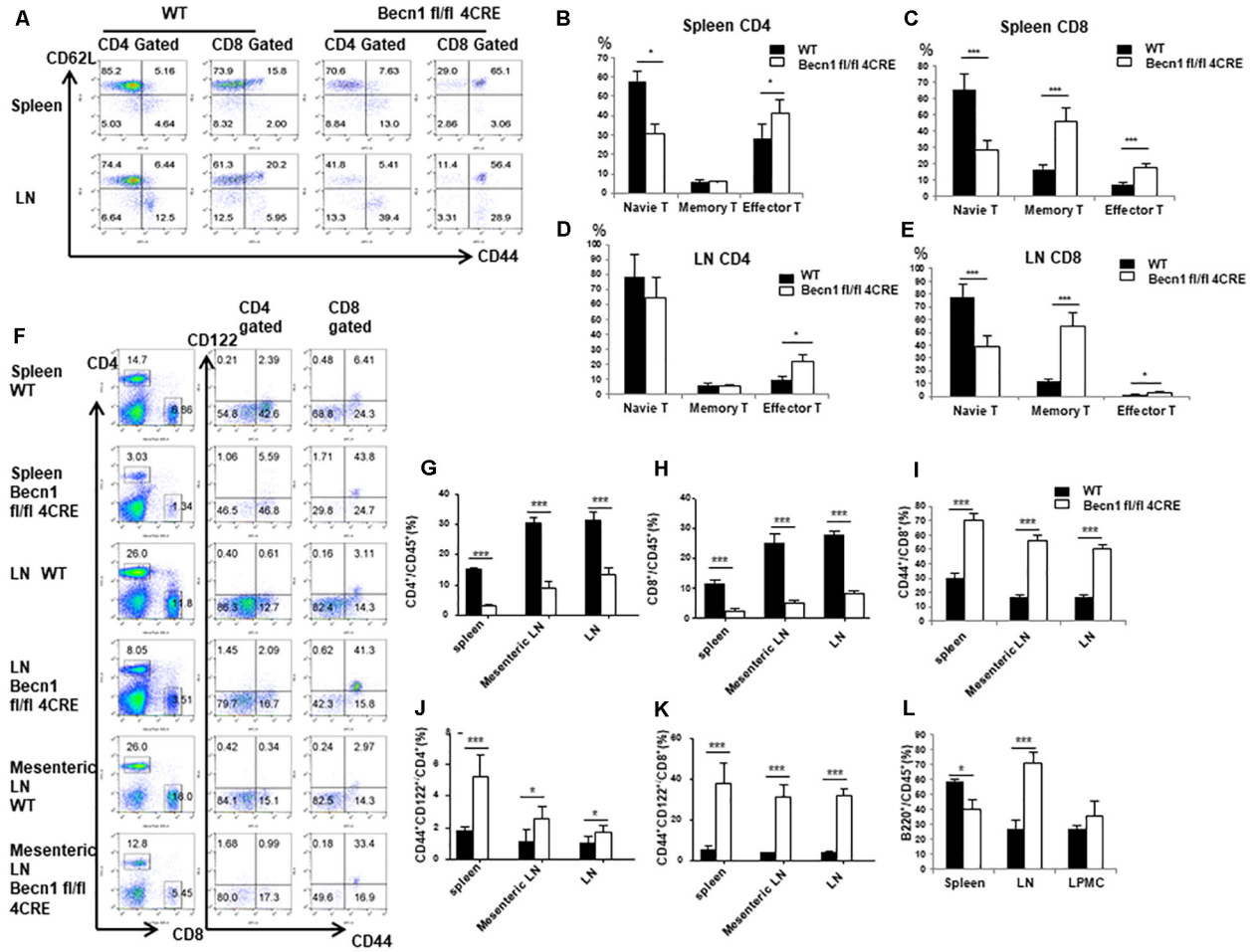

FIGURE 1 | Autophagy blockade in T cells leads to systemic changes in T lymphocytes in secondary lymphoid organs. Lymphocytes were isolated from spleens and lymph nodes from 16-week-old WT and *Becn1* –/– mice. **(A)** Percentages of naïve ($CD44^-$ $CD62L^+$), central memory ($CD44^+$ $CD62L^+$), and effector ($CD44^+$ $CD62L^-$) T cells were analyzed by flow cytometry. **(B–E)** Statistical analysis of percentages of naïve, memory, and effector T cells depicted in panel **(A)**. **(F)** Flow cytometric analysis of percentages of $CD4^+$ and $CD8^+$ T cells (left) and their $CD44^+$ $CD122^+$ proportion (right) in spleens, lymph nodes, and mesenteric lymph nodes from WT and *Becn1* –/– mice. **(G–K)** Statistical analysis of percentages of T cell subsets depicted in panel **(F)**. **(L)** Percentage of B cells in spleens, lymph nodes, and lamina propria from WT and *Becn1* –/– mice. Data are representatives of three independent experiments. At least three control and *Becn1* –/– mice in each experiment. Bar charts represented mean of and error bars represented SEM. $*P < 0.05$, $***P < 0.001$ by Student's *t*-test.

showed rectal prolapse around 4 months after birth (**Figure 5B**). Additionally, we found that the colon of *Becn1* −/− mice were significantly elongated compared with WT mice (**Figure 5B**). This suggested that the *Becn1* −/− mice developed severe colitis. Therefore, Beclin 1 deficiency in T cells resulted in chronic inflammation of the colon.

Since *Becn1* −/− mice developed colitis, we characterized the lamina propria lymphocytes to examine the characteristics of T cells. We observed increased IFN-γ and IL-17 producing $CD4^+$ and IFN-γ producing $CD8^+$ T cells in *Becn1* −/− mice compared to WT mice (**Figures 5C,D**). We also found an increase in the percentage of $Foxp3^+$ $CD4^+$ T cells in the lamina propria (**Figures 5E,F**). We also measured the proliferation of T cells by examining Ki67 expression in $CD4^+$ T cells, $CD8^+$ T cells, and Treg. The proliferative rates were higher for $CD4^+$ T cells and $CD8^+$ T cells from the lamina propria of *Becn1* −/− mice when compared to WT mice (**Figures 5G,H**). In contrast, proliferation rates were similar between WT and *Becn1* −/− Treg in the lamina propria. These data suggest the tissue inflammation in *Becn1* −/− mice was driven by actively proliferating effector T cells.

The TCR Transgene Prevented T Cell Loss and Colitis in *Becn1* −/− Mice

In order to study the effect of Beclin 1 deficiency on naïve CD4 T cells, we bred 2D2.TCR transgene to *Becn1* −/− mice to generate 2D2.*Becn1* −/− mice. As expected, 99% T cells were $CD4^+$ T cells in 2D2.WT and 2D2.*Becn1* −/− mice (**Figure 6A**). Interestingly, the number of $CD4^+$ T cells was similar between 2D2.WT and 2D2.*Becn1* −/− mice (**Figure 6A**). Even around 4 months of age, about 90% of T cells are in the naïve state in both 2D2.WT and 2D2.*Becn1* −/− mice. No colitis was observed in 2D2.WT and 2D2.*Becn1* −/− mice for at least 8 months of age. In addition, IL2

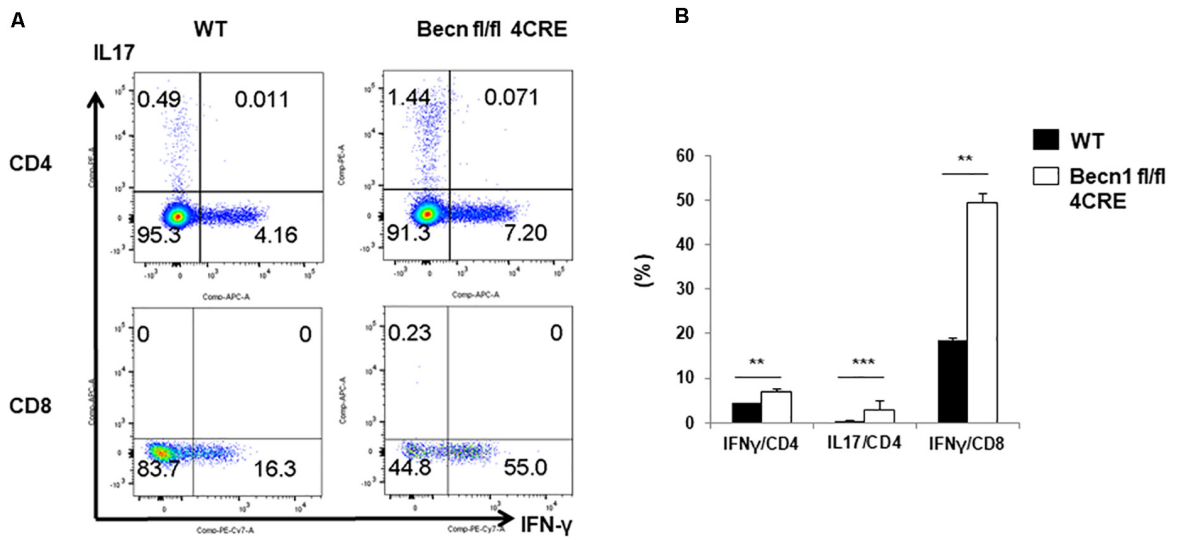

FIGURE 2 | Cytokine production by peripheral CD4 and CD8 T cells. Lymphocytes were isolated from spleens of WT and *Becn1* –/– mice. **(A)** IFN-γ and IL-17 expression by $CD4^+$ and $CD8^+$ T cells were analyzed by flow cytometry. **(B)** Statistical analysis of panel **(A)**. Data are representatives of three independent experiments. Bar charts represented mean of and error bars represented SEM. $^{**}P < 0.01$, $^{***}P < 0.001$ by Student's *t*-test.

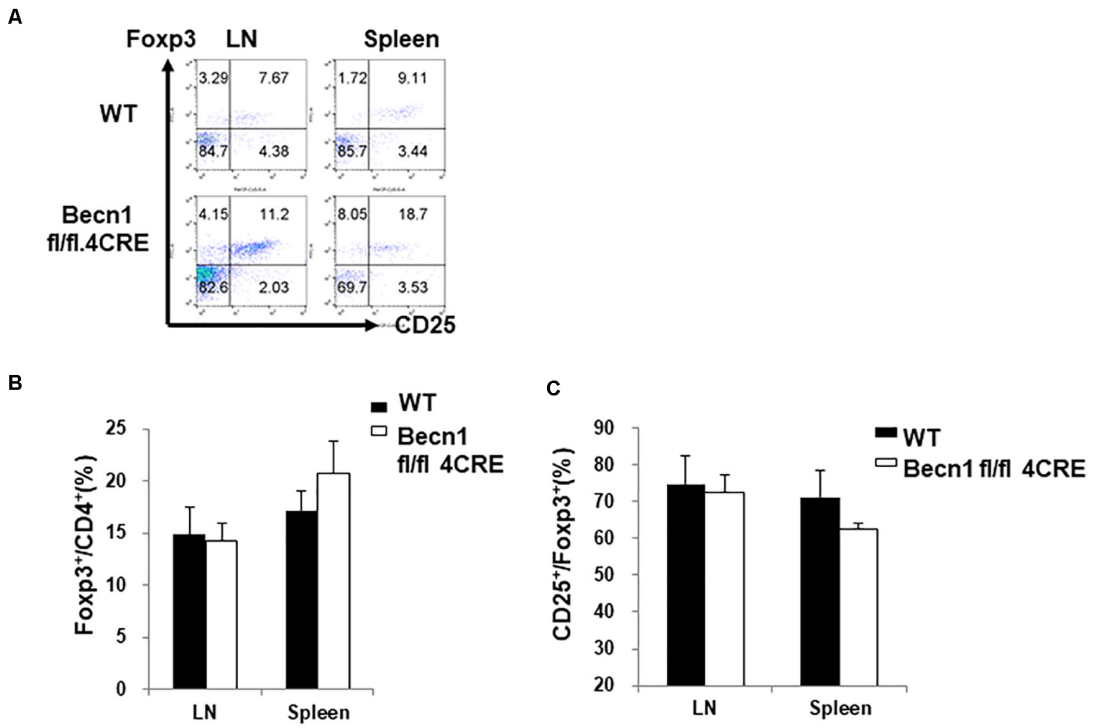

FIGURE 3 | Lack of changes in the percentage of Treg in secondary lymphoid organs. Lymphocytes were isolated from spleens and lymph nodes of WT and *Becn1* –/– mice. **(A)** Flow cytometric analysis of Foxp3 and CD25 expression by $CD4^+$ T cells. Statistical analysis of frequencies of $CD4^+$ $Foxp3^+$ **(B)** and $CD25^+$ $Foxp3^+$ **(C)** T cells. Data are representatives of three independent experiments. Three WT and *Becn1* –/– mice were used for each experiment. Bar charts represented mean of and error bars represented SEM.

production by naïve 2D2 WT and *Becn1* −/− $CD4^+$ T cells was similar (data not shown). Despite the normalization of naïve T cell number *in vivo*, when activated and cultured *in vitro* for 72 h, 2D2.*Becn1* −/− T cells generated much fewer activated live T cells compared to 2D2.WT T cells (**Figure 6B**), suggesting Beclin 1 is required for survival of activated T cells.

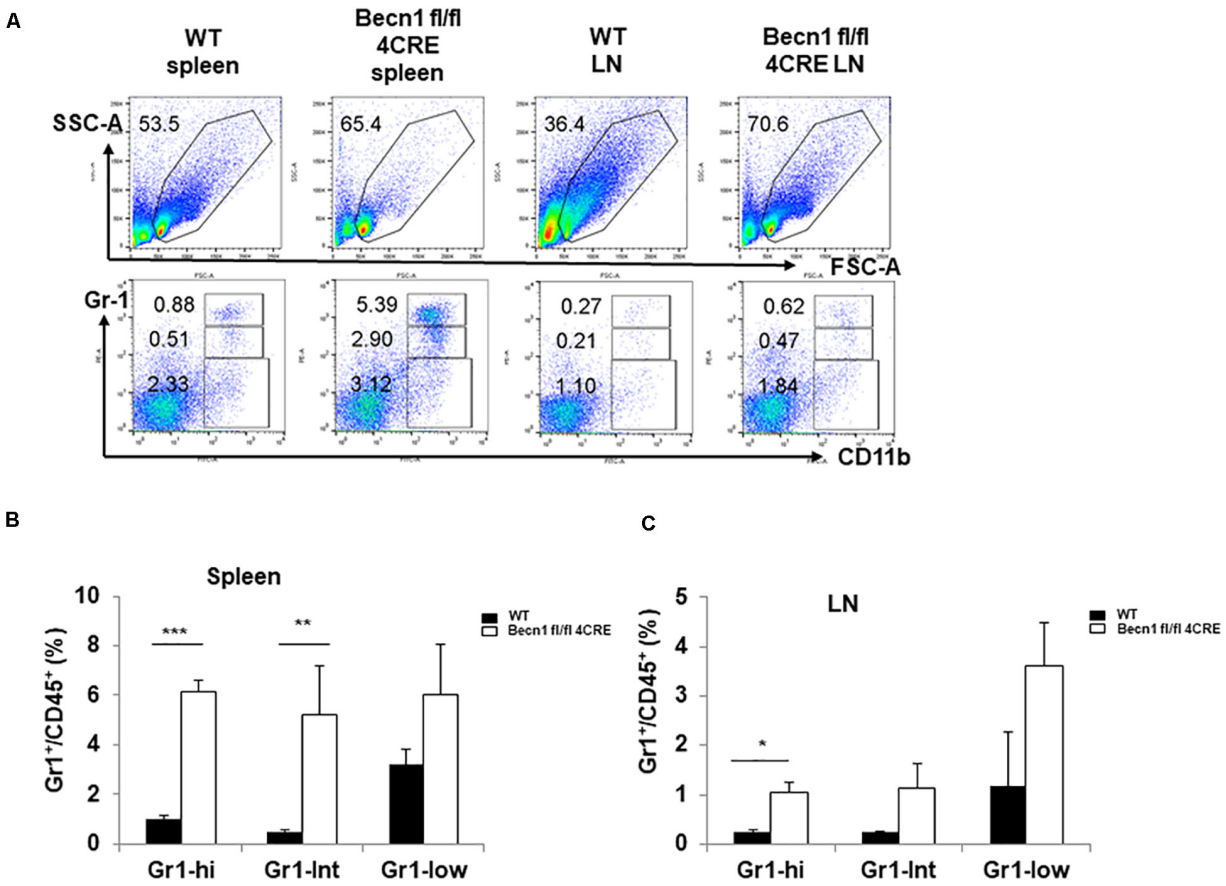

FIGURE 4 | Autophagy blockade in T cells resulted in changes in innate cells. **(A)** The flow cytometric analysis of $CD11b^+$ myeloid cells in spleens and lymph nodes from WT and *Becn1* –/– mice. **(B,C)** Statistical analysis of percentages of myeloid subsets in spleens and lymph nodes from WT and *Becn1* –/– mice. Data are representatives of three independent experiments. Three WT and *Becn1* –/– mice were used for each experiment. Bar charts represented mean of and error bars represented SEM. $^*P < 0.05$, $^{**}P < 0.01$, $^{***}P < 0.001$ by Student's *t*-test. Five WT and *Becn1* –/– mice were used for each experiment. Bar charts represented mean of and error bars represented SEM. $^*P < 0.05$ by Student's *t*-test.

DISCUSSION

The role of autophagy in T cell-mediated immune processes is complicated because of its differential involvement in many functions of T cells and various T cell subsets. Therefore, the exact function of autophagy in T cells needs to be studied in well-defined experimental systems. We found that T cell-specific deletion of *Becn1* resulted in systemic activation of T cells in adult mice, consistent with similar findings by other groups (Parekh et al., 2013; Kabat et al., 2016; Wei et al., 2016). We focused on the gastrointestinal (GI) tract and found strong evidence of colitis that is associated with an increase in the function and number of effector T cells. To further define the role of autophagy in naïve T cells, we generated TCR transgenic mice that had the *Becn1* deletion in T cells. We found that the reduction in the T cell number and systemic inflammation was prevented in the TCR transgenic *Becn1* −/− mice. Our results suggest that, unlike activated T cells, autophagy is not required for the survival of naïve T cells.

It has been suggested that reduction of naïve T cells in autophagy deficient mice is due to defects in naïve T cell homeostasis. Our data obtained using a TCR transgenic system, however, suggest that the development and homeostasis of naïve T cells is normal in T cell-specific autophagy deficient mice. We would like to propose a different explanation for the reduction of total T cell number in *Becn1* −/− mice, which is likely due to the combined effect of Treg deficiency and increased activation of $CD4^+$ and $CD8^+$ T cells. Our new model can reconcile all the published data. It has been reported that the number and functional integrity of Treg is reduced when autophagy is defective (Parekh et al., 2013; Kabat et al., 2016; Marcel and Sarin, 2016; Wei et al., 2016). The deficiency of Treg can result in increased activation of naïve T cells after encountering environmental antigens and self-antigens. Once *Becn1* −/− T cells are activated, they become prone to cell death (Pua et al., 2007; Kovacs et al., 2012). Thus, the increased activation potential of naïve T cells and susceptibility to activation induced cell death in combination lead to the reduction of the number of naïve T cell in the *Becn1* −/− mice.

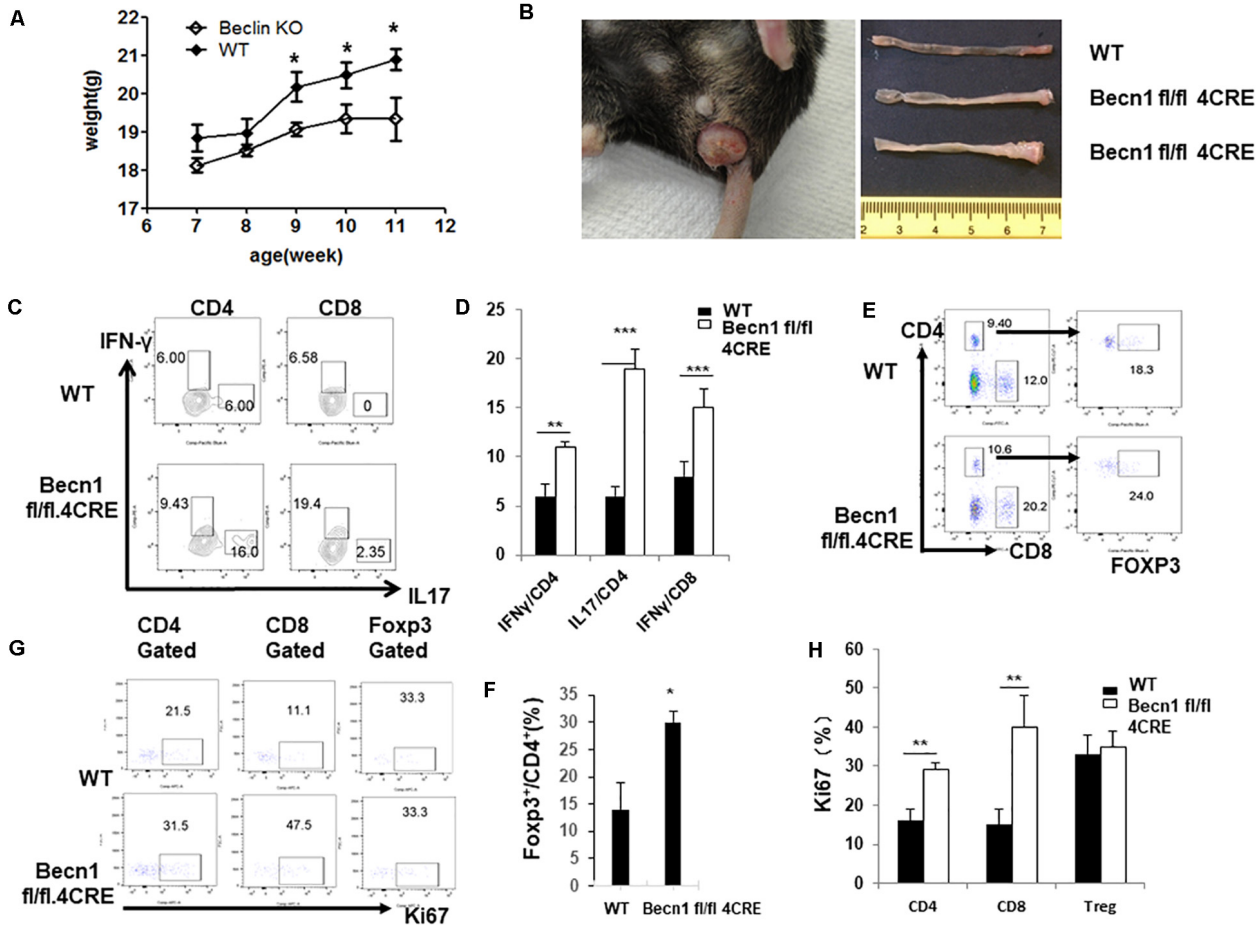

FIGURE 5 | Autophagy-deficient mice developed spontaneous IBD. **(A)** Weight of WT and *Becn1* –/– mice over time ($N = 8$). **(B)** Gross morphology of prolapse from a 16-week-old *Becn1* –/– mouse and control mice (left) and colons from 16-week-old WT and *Becn1* –/– mice (right). **(C)** Lymphocytes were isolated from lamina propria of WT and *Becn1* –/– mice. IFN-γ and IL-17 expression by $CD4^+$ and $CD8^+$ T cells was analyzed by flow cytometry. **(D)** Statistical analysis of panel **(C)**. **(E)** Flow cytometric analysis of Foxp3 expression by $CD4^+$ T cells. **(F)** Statistical analysis of percentages if $Foxp3^+$ $CD4^+$ T cells in WT and *Becn1* –/– mice. **(G)** Ki67 expression by $CD4^+$, $CD8^+$ T, and Treg cells were analyzed by flow cytometry. **(H)** Statistical analysis of panel **(G)**. Data are representatives of three independent experiments. Three WT and *Becn1* –/– mice were used for each experiment. Bar charts represented mean of and error bars represented SEM. $^{**}P < 0.01$, $^{***}P < 0.001$ by Student's *t*-test.

Autophagy genes, such as ATG16L1, have been associated with inflammatory bowel disease (IBD), particularly Crohn's disease (CD) (Hampe et al., 2007; Parkes et al., 2007; Rioux et al., 2007). Dysregulation of both canonical and non-canonical autophagy pathways in Paneth cells, macrophages, and dendritic cells has been shown to contribute to colitis (Saitoh et al., 2008; Cadwell et al., 2010; Chu et al., 2016). Our study suggests that autophagy deficiency in T cell can also potentially contributes to IBD. Although we have established that Beclin 1 plays a crucial role in autophagy in T cells (Kovacs et al., 2012), Beclin 1 has also been shown to have autophagy-independent functions (Kang et al., 2011; Wirawan et al., 2012), which warrants further examination in the future.

Several factors might have collectively contributed to the hyper inflammatory status in adult *Becn1* −/− mice. First, Beclin 1 is required to maintain the number of Treg. Second, Beclin 1 is required for the survival of activated T cells. Therefore, after activation, a majority of T cells undergo apoptosis. This leads to a reduction of total T cells. Third, the resulting lymphopenia allows increased proliferation of effector T cells, which makes large amounts of inflammatory cytokines. Fourth, it is possible that autophagy is differentially required for the function, proliferation, and survival of effector versus central memory T cells. Autophagy blockade might lead to the generation of more effector T cells. This point needs to be carefully examined in the future using appropriate experimental systems.

MATERIALS AND METHODS

Mice

C57BL/6 mice were purchased from the Jackson Laboratory. The T cell-specific Beclin 1 deficient (*Becn1* −/−) mice on the C57BL/6 background were generated as described

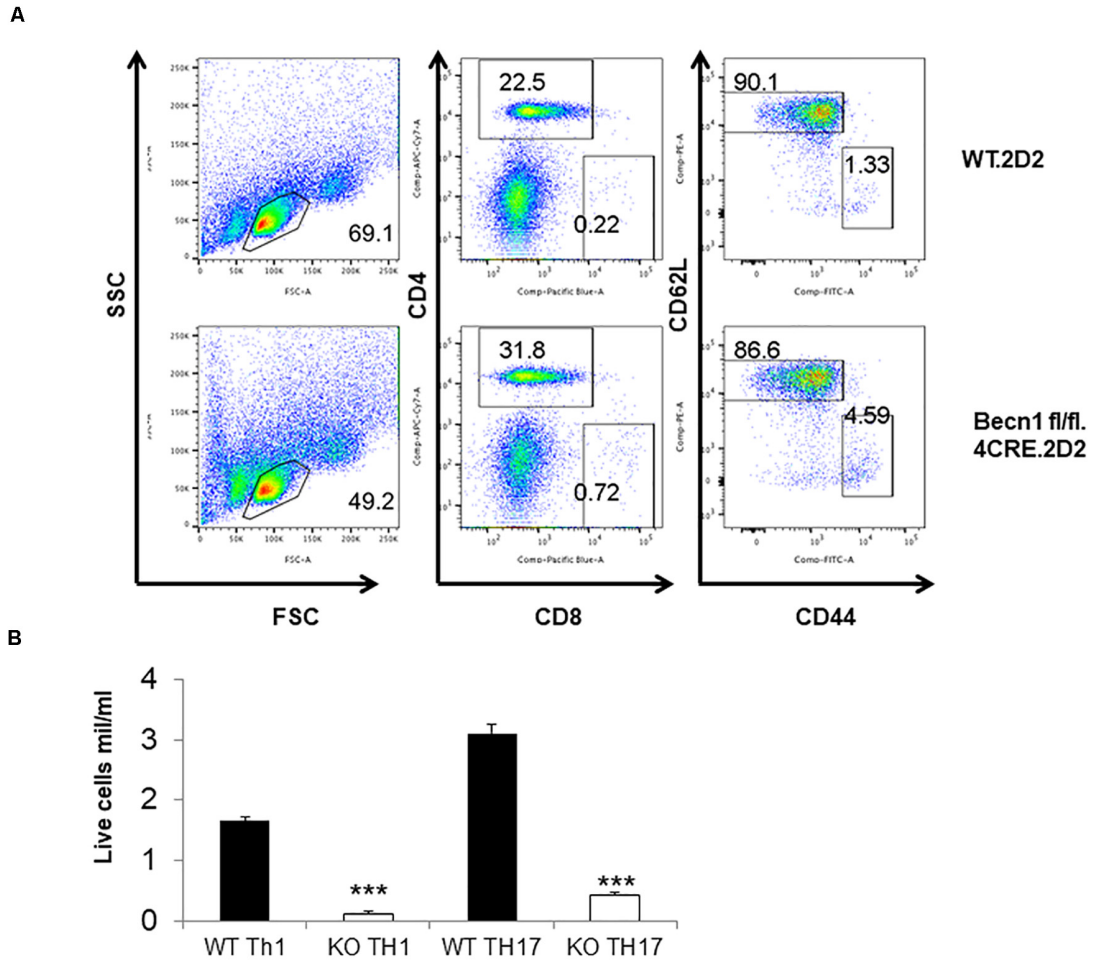

FIGURE 6 | Expression of the TCR transgene normalized the number of CD4$^+$ T cells in *Becn1* –/– mice. **(A)** Splenocytes from 2D2.WT and 2D2.*Becn1* –/– were subject to flow cytometric analysis. **(B)** Naïve CD4$^+$ T cells from 2D2.WT and 2D2. *Becn1* –/– were cultured in the Th1 or Th17 conditions for 4 days. The number of live cells were determined. Bar charts represented mean of and error bars represented SEM. ***$P < 0.001$ by Student's *t*-test.

(Kovacs et al., 2012). 2D2 TCR transgenic mice (Bettelli et al., 2003) were bred with *Becn1* −/− mice and then intercrossed to generate 2D2.*Becn1* −/− mice. All mice were maintained under specific pathogen-free conditions. The Institution Animal Care and Use Committee at University of Pittsburgh has approved all animal work.

Processing of Tissues

Spleens were isolated and mashed completely in Hank's buffer (containing 1% FBS), cells were then treated with ACK lysis buffer and filtered through a 50-μm cell strainer to obtain single cell suspension. Inguinal lymph nodes, axillary lymph nodes, and mesenteric lymph nodes were isolated and mashed completely in Hank's buffer (containing 1% FBS) and then filtered through a 50-μm cell strainer to obtain single cell suspension. For isolation of lamina propria cells, intestines were harvested and Peyer's patches were removed, the intestines were opened longitudinally and the tissues were then minced and incubated in HBSS containing 5 mM EDTA and 1 mM DTT at 37°C for 20 min to remove epithelial cells, villus cells, subepithelial cells, and IELs, which was followed by digestion in RPMI1640 with Liberase TL (0.25 mg/ml, Roche) and DNase I (0.15 mg/ml, Sigma) at 37°C for 30 min. Tissue pieces were then mashed completely in Hank's buffer (containing 1% FBS) and filtered through a 50-μm cell strainer to obtain single cell suspension of lamina propria.

Primary CD4$^+$ T Cells Culture

Mouse naïve CD4$^+$ T cells (CD44$^-$ CD62L$^+$) were purified from spleens and lymph nodes of C57BL/6 mice. These cells were then cultured on 24-well plates pre-coated with 10 μg/ml plate-bound anti-CD3 (clone 145-2C11) and 5 μg/ml plate-bound anti-CD28 mAbs (clone 37.51) in complete RPMI (RPMI 1640 supplemented with 10% heat-inactivated FBS, 2mM-glutamine, 50 μM 2-ME, 100 U/ml penicillin and 100 μg/ml streptomycin) in various polarizing conditions: Th1, huIL-2 (20 U/ml, obtained from the BRB Preclinical Repository), IL-12 (3.4 ng/ml) plus anti-IL-4 (10 μg/ml, clone 11B11, from the BRB Preclinical Repository) and Th17, anti-IL-2Rα

(10 μg/ml, clone PC61, American Type Culture Collection (ATCC), Manassas, VA, United States), IL-23(10 ng/ml), IL-6 (10 ng/ml), TGF-β1 (1 ng/ml), anti-IFN-γ (10 μg/ml, clone XMG 1.2), and anti-IL-4 (10 μg/ml, clone 11B11). At 48 h after the start of culture, cells were transferred to another plate, which was not coated with anti-CD3 or anti-CD28 Abs, with the original culture media (including polarizing cytokines and anti-cytokine Abs). Cells cultured in the Th1 condition were also supplemented with fresh human IL-2 (5 U/ml).

Ex vivo Analysis of Immune Cells in Lymphoid Organs and Lamina Propria

Single cells were made from spleens, lymph nodes and lamina propria isolated from 6–8 week-old female wild type or BECN1 fl/fl mice. Cells were then stained with the following fluorescence-conjugated antibodies: CD45(30F11), CD4(GK1.5), CD8(53-6.7), CD44(IM7), CD62L(MEL-14), CD122(5H4), Ki67(SolA15), IL17(17B7), IFN-γ(XMG1.2) (eBioscience, Inc., San Diego, CA, United States) and p-S6(Cell Signaling). For intracellular cytokine staining, lymphocytes were stimulated with or without 10 ng/ml of PMA and 1 μg/ml of ionomycin (Sigma) for 4 h. Brefeldin A was added for the last 3 h at 10 μg/ml. Cells were transferred to a V-bottom plate, stained with anti-CD45, anti-CD4 and anti-CD8 Ab in Hank's buffer (containing 1% FBS) and then fixed with 2% formaldehyde, which was followed by permeabilization with 0.5% saponin. The cells were subsequently stained with anti-Ki67 and anti-Foxp3 Ab or anti-IL-17 and anti-IFN-γ Ab (eBioscience, Inc., San Diego, CA, United States) or p-S6 Ab. Flow cytometric analysis was performed using a flow cytometer (BD Biosciences) and data were analyzed by using FlowJo (TreeStar).

Statistical Analysis

Statistical analyses were performed using GraphPad Prism 5.0 (GraphPad Software, Inc., San Diego, CA, United States). Differences between experimental groups were analyzed by using student's *t*-test or one-way ANOVA and all *P* values less than 0.05 were considered statically significant.

DATA AVAILABILITY STATEMENT

The raw data supporting the conclusions of this article will be made available by the authors, without undue reservation.

ETHICS STATEMENT

The animal study was reviewed and approved by the University of Pittsburgh.

AUTHOR CONTRIBUTIONS

RX designed the experiments, performed the experiments, analyzed the data, and wrote the manuscript. MY analyzed the data and wrote the manuscript. XF, WD, XG, and GL performed the experiments and analyzed the data. SR performed the pathological analysis. XZ and JJ provided the key reagents and analyzed the data. BL designed the experiments, analyzed the data, and wrote the manuscript. All authors contributed to the article and approved the submitted version.

FUNDING

This work is supported by University of Pittsburgh Start-up Fund (to BL). RX and MY are supported by scholarships from the China Scholarship Council (Numbers 201406920043 and 201706920070).

REFERENCES

Bettelli, E., Pagany, M., Weiner, H. L., Linington, C., Sobel, R. A., and Kuchroo, V. K. (2003). Myelin oligodendrocyte glycoprotein-specific T cell receptor transgenic mice develop spontaneous autoimmune optic neuritis. *J. Exp. Med.* 197, 1073–1081. doi: 10.1084/jem.20021603

Cadwell, K., Patel, K. K., Maloney, N. S., Liu, T. C., Ng, A. C., Storer, C. E., et al. (2010). Virus-plus-susceptibility gene interaction determines Crohn's disease gene Atg16L1 phenotypes in intestine. *Cell* 141, 1135–1145. doi: 10.1016/j.cell.2010.05.009

Chu, H., Khosravi, A., Kusumawardhani, I. P., Kwon, A. H., Vasconcelos, A. C., Cunha, L. D., et al. (2016). Gene-microbiota interactions contribute to the pathogenesis of inflammatory bowel disease. *Science* 352, 1116–1120. doi: 10.1126/science.aad9948

Clarke, S. R., and Rudensky, A. Y. (2000). Survival and homeostatic proliferation of naive peripheral CD4+ T cells in the absence of self peptide:MHC complexes. *J. Immunol.* 165, 2458–2464. doi: 10.4049/jimmunol.165.5.2458

den Braber, I., Mugwagwa, T., Vrisekoop, N., Westera, L., Mogling, R., de Boer, A. B., et al. (2012). Maintenance of peripheral naive T cells is sustained by thymus output in mice but not humans. *Immunity* 36, 288–297. doi: 10.1016/j.immuni.2012.02.006

Dorfman, J. R., Stefanova, I., Yasutomo, K., and Germain, R. N. (2000). CD4+ T cell survival is not directly linked to self-MHC-induced TCR signaling. *Nat. Immunol.* 1, 329–335. doi: 10.1038/79783

Espert, L., Denizot, M., Grimaldi, M., Robert-Hebmann, V., Gay, B., Varbanov, M., et al. (2006). Autophagy is involved in T cell death after binding of HIV-1 envelope proteins to CXCR4. *J. Clin. Invest.* 116, 2161–2172. doi: 10.1172/JCI26185

Hampe, J., Franke, A., Rosenstiel, P., Till, A., Teuber, M., Huse, K., et al. (2007). A genome-wide association scan of nonsynonymous SNPs identifies a susceptibility variant for Crohn disease in ATG16L1. *Nat. Genet.* 39, 207–211. doi: 10.1038/ng1954

Jia, W., and He, Y. W. (2011). Temporal regulation of intracellular organelle homeostasis in T lymphocytes by autophagy. *J. Immunol.* 186, 5313–5322. doi: 10.4049/jimmunol.1002404

Jones, S. A., Mills, K. H., and Harris, J. (2013). Autophagy and inflammatory diseases. *Immunol. Cell Biol.* 91, 250–258. doi: 10.1038/icb.2012.82

Kabat, A. M., Harrison, O. J., Riffelmacher, T., Moghaddam, A. E., Pearson, C. F., Laing, A., et al. (2016). The autophagy gene Atg16l1 differentially regulates Treg and TH2 cells to control intestinal inflammation. *Elife* 5:e12444. doi: 10.7554/eLife.12444

Kang, R., Zeh, H. J., Lotze, M. T., and Tang, D. (2011). The Beclin 1 network regulates autophagy and apoptosis. *Cell Death Differ.* 18, 571–580. doi: 10.1038/cdd.2010.191

Kovacs, J. R., Li, C., Yang, Q., Li, G., Garcia, I. G., Ju, S., et al. (2012). Autophagy promotes T-cell survival through degradation of proteins of the cell death machinery. *Cell Death Differ.* 19, 144–152. doi: 10.1038/cdd.2011.78

Li, C., Capan, E., Zhao, Y., Zhao, J., Stolz, D., Watkins, S. C., et al. (2006). Autophagy is induced in CD4+ T cells and important for the growth factor-withdrawal cell death. *J. Immunol.* 177, 5163–5168. doi: 10.4049/jimmunol.177.8.5163

Marcel, N., and Sarin, A. (2016). Notch1 regulated autophagy controls survival and suppressor activity of activated murine T-regulatory cells. *Elife* 5:e14023. doi: 10.7554/eLife.14023

Parekh, V. V., Wu, L., Boyd, K. L., Williams, J. A., Gaddy, J. A., Olivares-Villagomez, D., et al. (2013). Impaired autophagy, defective T cell homeostasis, and a wasting syndrome in mice with a T cell-specific deletion of Vps34. *J. Immunol.* 190, 5086–5101. doi: 10.4049/jimmunol.1202071

Parkes, M., Barrett, J. C., Prescott, N. J., Tremelling, M., Anderson, C. A., Fisher, S. A., et al. (2007). Sequence variants in the autophagy gene IRGM and multiple other replicating loci contribute to Crohn's disease susceptibility. *Nat. Genet.* 39, 830–832. doi: 10.1038/ng2061

Pua, H. H., Dzhagalov, I., Chuck, M., Mizushima, N., and He, Y. W. (2007). A critical role for the autophagy gene Atg5 in T cell survival and proliferation. *J. Exp. Med.* 204, 25–31. doi: 10.1084/jem.20061303

Rioux, J. D., Xavier, R. J., Taylor, K. D., Silverberg, M. S., Goyette, P., Huett, A., et al. (2007). Genome-wide association study identifies new susceptibility loci for Crohn disease and implicates autophagy in disease pathogenesis. *Nat. Genet.* 39, 596–604. doi: 10.1038/ng2032

Saitoh, T., Fujita, N., Jang, M. H., Uematsu, S., Yang, B. G., Satoh, T., et al. (2008). Loss of the autophagy protein Atg16L1 enhances endotoxin-induced IL-1beta production. *Nature* 456, 264–268. doi: 10.1038/nature07383

Schlie, K., Westerback, A., DeVorkin, L., Hughson, L. R., Brandon, J. M., MacPherson, S., et al. (2015). Survival of effector CD8+ T cells during influenza infection is dependent on autophagy. *J. Immunol.* 194, 4277–4286. doi: 10.4049/jimmunol.1402571

Sprent, J., and Tough, D. F. (1994). Lymphocyte life-span and memory. *Science* 265, 1395–1400. doi: 10.1126/science.8073282

Sprent, J., Cho, J. H., Boyman, O., and Surh, C. D. (2008). T cell homeostasis. *Immunol. Cell Biol.* 86, 312–319. doi: 10.1038/icb.2008.12

Wei, J., Long, L., Yang, K., Guy, C., Shrestha, S., Chen, Z., et al. (2016). Autophagy enforces functional integrity of regulatory T cells by coupling environmental cues and metabolic homeostasis. *Nat. Immunol.* 17, 277–285. doi: 10.1038/ni.3365

Wirawan, E., Lippens, S., Vanden Berghe, T., Romagnoli, A., Fimia, G. M., Piacentini, M., et al. (2012). Beclin1: a role in membrane dynamics and beyond. *Autophagy* 8, 6–17. doi: 10.4161/auto.8.1.16645

Conflict of Interest: The authors declare that the research was conducted in the absence of any commercial or financial relationships that could be construed as a potential conflict of interest.

frontiers in Cell and Developmental Biology

ORIGINAL RESEARCH
published: 08 October 2020
doi: 10.3389/fcell.2020.582695

STK35 Is Ubiquitinated by NEDD4L and Promotes Glycolysis and Inhibits Apoptosis Through Regulating the AKT Signaling Pathway, Influencing Chemoresistance of Colorectal Cancer

*Haojun Yang†, Jie Zhu†, Guangyao Wang, Hanyang Liu, Yan Zhou and Jun Qian**

Department of Gastrointestinal Center, The Affiliated Changzhou No. 2 People's Hospital of Nanjing Medical University, Changzhou, China

OPEN ACCESS

Edited by:
Huijie Bian, Fourth Military Medical University, China

Reviewed by:
Jian Zhang, Fourth Military Medical University, China
Geeta Upadhyay, Uniformed Services University of the Health Sciences, United States

***Correspondence:**
Jun Qian
drqianjun@sina.com

† These authors have contributed equally to this work

Specialty section:
This article was submitted to Cell Death and Survival, a section of the journal Frontiers in Cell and Developmental Biology

Received: *13 July 2020*
Accepted: *14 September 2020*
Published: *08 October 2020*

Citation:
Yang H, Zhu J, Wang G, Liu H, Zhou Y and Qian J (2020) STK35 Is Ubiquitinated by NEDD4L and Promotes Glycolysis and Inhibits Apoptosis Through Regulating the AKT Signaling Pathway, Influencing Chemoresistance of Colorectal Cancer. Front. Cell Dev. Biol. 8:582695. doi: 10.3389/fcell.2020.582695

The development of colorectal cancer (CRC) is often sporadic, but its etiology is multifactorial. Chemoresistance of CRC leads to tumor recurrence and poor prognosis in patients. The phosphorylation of protein kinase B (AKT) can activate metabolic reprogramming toward cellular glycolysis. Serine/threonine kinase 35 (STK35) regulates the cell cycle and is frequently associated with cancer progression, whereas little is known about its specific roles in CRC. In the current study, bioinformatics analyses were performed to investigate the relationship between STK35 and CRC prognosis. STK35 knockdown and overexpressing CRC cells were established to examine its functions in CRC. Fluorouracil (5-FU) was utilized to evaluate the effect of STK35 on CRC chemoresistance. Moreover, co-immunoprecipitation was performed to explore the ubiquitination of STK35. STK35 was highly expressed in CRC, and its protein expression was negatively correlated with the survival of CRC patients. Furthermore, STK35 overexpression could promote glycolysis, suppress apoptosis, upregulate p-AKT, and counteract the antitumor functions of 5-FU and neural precursor cell expressed developmentally downregulated gene 4-like (NEDD4L) in CRC cells. NEDD4L was associated with and could ubiquitinate STK35. STK35 could be a prognostic biomarker for CRC prognosis and has promotive effects on CRC cellular activities, partially through the AKT pathway. Moreover, STK35 also interferes with the chemosensitivity of CRC.

Keywords: STK35, ubiquitination, colorectal cancer, AKT, apoptosis

INTRODUCTION

Colorectal cancer (CRC) remains as one of the most common malignancies, as well as the primary cause of cancer-related deaths worldwide, and its incidence is increasing rapidly among teenagers and adults (Arnold et al., 2017; Siegel et al., 2017). Multiple risk factors, including hereditary components, lifestyle patterns, dietary styles, and environmental influences, are capable of inducing the development and progression of CRC (Brenner et al., 2014). While the tumorigenesis of CRC

is commonly in stepwise mode as sporadic (Fearon and Vogelstein, 1990). Until now, therapeutic approaches, especially chemotherapies, for CRC have been established by targeting the suppression of cell apoptosis and advanced metabolism. However, the intrinsic or acquired chemoresistance of CRC malignant cells restricts the efficacy of chemo-reagents, leading to tumor recurrence and further metastasis (Zheng, 2017). The poor treatment outcomes and prognosis for CRC contribute to the relatively low survival probability of CRC patients, and the current mortality rate ranges from 12 to 87% (stage IV to I) (Cronin et al., 2018).

Generally, CRC cells possess a unique phenotype of global metabolic reprogramming, undergoing aerobic glycolysis (known as the "Warburg effect"), for which glucose serves as the dominant energy source; tumor cells can utilize glucose for the production of pyruvate and adenosine triphosphates (Brown et al., 2018). During the glycolytic process, numerous metabolic intermediates or by-products support the synthesis of macromolecules for rapid cell proliferation (Vander Heiden et al., 2009). Moreover, certain intracellular signaling pathways of glycolysis with genetic drivers also influence other features of cancerous cells (La Vecchia and Sebastian, 2020); for example, the hyperactive phosphatidylinositol-3-OH kinase (PI3K) signal stimulates cell growth (Yu and Grady, 2012), while aberrant tumor protein p53 signaling inhibits apoptosis (Slattery et al., 2019).

The PI3K/protein kinase B (AKT) signaling transduction cascade mediated cell-cycle regulation, as well as proliferation, apoptosis, and differentiation (Osaki et al., 2004). During stable energy conditions, the cellular PI3K/AKT pathway remains catalytically inactive or with limited activity, which ensures a quiescent state for the maintenance of normal cell cycle (Cheung and Rando, 2013; Hung et al., 2017). However, when the cellular glucose level increases, induced growth factors, such as epidermal growth factor, insulin, and insulin-like growth factor, can further activate PI3K, which then phosphorylates and activates AKT (Danielsen et al., 2015). The activation of the PI3K/AKT signaling pathway is associated with nearly 70% of CRC cases, while at the same time, inhibition of the signaling pathway is considered a target for CRC therapy (Malinowsky et al., 2014). In fact, the activated p-AKT can sequentially phosphorylate multiple regulatory proteins, such as cytosolic B cell lymphoma 2-associated death promoter, glycogen synthase kinase 3β, and mouse double minute 2 homolog, as well as nuclear forehead box protein O (Manning and Cantley, 2007). All of these p-AKT downstream proteins are key regulators of normal cell cycle and carcinogenesis, particularly the control of apoptosis and energy metabolism (Nitulescu et al., 2018). Therefore, p-AKT serves as the core factor in the PI3K/AKT signaling pathway, which indicates oncogenic transformation in cells (Chang et al., 2003).

Serine/threonine kinases (STKs) play critical roles through the phosphorylation and activation of relevant effectors, such as cell-cycle regulators, growth factors, and transcription activators, to regulate signaling pathways and cellular homeostasis (Manning et al., 2002; Capra et al., 2006). However, dysregulation of STKs can lead to a deregulated cell cycle, in favor of unlimited cell proliferation, repressed cell apoptosis, and minimized cell differentiation, which facilitate the development of tumors and subsequent metastasis (Freeman and Whartenby, 2004). Although the detailed biological functions of STK35 are still being investigated, STK35 has regulatory roles in cell-cycle modulation, and its abnormal cellular levels are implicated in various human diseases including cancer (Vallenius and Makela, 2002; Goyal et al., 2009). It has also been reported that STK35 is associated with programmed cell death (Yasuda et al., 2012), and *STK35* gene expression is altered in Parkinson disease (Hourani et al., 2008). Furthermore, STK35 is essential for the angiogenesis and migration of endothelial cells (Goyal et al., 2011), as well as cellular apoptosis and proliferation of osteosarcoma (Wu et al., 2018). Moreover, the upregulation of *STK35* has been suggested to be linked with human CRC (Capra et al., 2006), whereas the explicit relationship between them and the specific functions of STK35 in CRC have not been systematically studied.

In the current study, we proposed to explore the correlation between STK35 and prognostic conditions in CRC patients, the roles of STK35 in CRC cellular activities and tumor development, and the possible mechanisms underlying the functions of STK35. We demonstrate that STK35 is highly expressed in CRC tumor tissues and that its expression is positively correlated with the mortality rate of CRC patients. Furthermore, through establishing STK35 knockdown and overexpression in CRC cells, we also reveal that STK35 can interfere with the chemo-sensitivity of CRC cells. We also demonstrate that STK35 promotes both *in vitro* cellular activities and *in vivo* tumor growth of CRC, potentially through regulating the AKT signaling pathway. In addition, TK35 is ubiquitinated by neural precursor cell expressed developmentally downregulated gene 4-like (NEDD4L) and can also counteract the anti-CRC effects of NEDD4L.

MATERIALS AND METHODS

Bioinformatics Analysis

RNA-seq data related to the expression of STK35 and NEDD4L in various cancer patients were acquired from The Cancer Genome Atlas (TCGA) database, including 638 cases for colorectal tumor tissues and 51 cases for non-tumor tissues in patients with CRC, and the GEO database (access id: GSE9348), including 70 cases of tumor tissues and 12 cases of normal tissues. The gene set enrichment analysis (GSEA) algorithm was used to identify pathways that were significantly enriched between STK35 high vs. low expression.

Clinical Samples

A total of 131 CRC patients in The Affiliated Changzhou No. 2 People's Hospital of Nanjing Medical University were enrolled between March 2013 and October 2015. Tumor tissues and their corresponding non-cancerous tissues were collected for storage at −80°C until further analysis. The study was approved by the medical ethics committee of The Affiliated Changzhou No. 2 People's Hospital of Nanjing Medical University, and the study was conducted according to the Declaration of

Helsinki. All patients provided written informed consent prior to participation.

Quantitative Real Time PCR (Q-PCR)

Total RNA was extracted from cells or tissues by TRIzol reagent (Life Technologies, United States) and reverse transcribed to cDNA with PrimeScript kit (Takara Biotechnology, China) in accordance with the manufacturers' protocols. Quantitative real time PCR (Q-PCR) was carried out using SYBR Green PCR Master Mix (Applied Biosystems, United States) on an ABI 9700 real-time PCR system (Applied Biosystems, United States). The primers used were as follows: STK35-F: 5′-CCTGAAGCCAGACAACATCC-3′, STK35-R: 5′-GTCTTGATTGCCCTCTTTGC-3′; NEDD4L-F: 5′-CTCGGTGATGTGGATGTG-3′, NEDD4L-R: 5′-TTCGGCGTCCATGAGTAG-3′; and β-actin-F: 5′-TGGCATCCACGAAACTAC-3′, β-actin-R: 5′-CTTGATCTTCATGGTGCTG-3′. The fold changes at the transcript level were GAPDH-normalized and calculated based on the $2^{-\Delta\Delta CT}$ method.

Immunohistochemistry (IHC)

Formalin-fixed and paraffin-embedded CRC specimens were used for Immunohistochemistry (IHC) staining, as previously described (Zhu et al., 2017). In brief, the target tissues were deparaffinized and rehydrated, followed by heat-induced antigen retrieval with pH 8.0 EDTA. The slides were then stained with primary antibodies (Abcam, United States), including ab237517 against STK35, ab46521 against NEDD4L, and ab81283 against p-AKT, followed by incubation with horseradish peroxidase (HRP)-conjugated anti-IgG secondary antibody D-3004 (Long Island Biotech, China). Immunoreactivity was scored by two investigators using the H-score system based on the percentage of positively stained tumor cells. All patients with more than 25% of positively stained tumor cells were grouped as high-expression, while those with less than 25% were grouped as low-expression.

Cell Culture

Human-origin CRC cell lines (HCT116, LOVO, SW480, SW620, and SW1116) and the normal human intestinal crypt cell line HIEC were obtained from the cell bank of Shanghai Biology Institute (Chinese Academy of Sciences) and cultured in a 5% CO_2 incubator at 37°C. LOVO, SW480, SW620, and SW1116 cells were cultured in RPMI-1640 medium (Life Technologies, United States) supplemented with 10% fetal bovine serum (FBS) (Life Technologies, United States) and 1% penicillin/streptomycin. HCT116 cells were maintained in Dulbecco's Modified Eagle Medium (Life Technologies, United States) supplemented as above.

Gene Overexpression and Knockdown

Serine/threonine kinase 35 and NEDD4L overexpression plasmids were constructed by cloning the coding sequence of STK35 or NEDD4L into pLVX-Puro vectors (Takara Bio Inc., United States). To generate the knockdown clones, synthesized shRNA oligos targeting STK35 were cloned in pLKO.1 plasmids (Addgene, United States). Recombinant plasmids, together with the packaging/envelope plasmids psPAX2 and pMD2.G, were co-transfected to human CRC cells with Lipofectamine 2000 (Invitrogen, United States) in accordance with the manufacturer's instructions. The virus particles were collected after 48 h post-transfection and further transfected into the cells of interest to generate overexpression and knockdown cell lines. The cells transfected with scramble shRNA (shNC) or blank plasmid (Vector) were considered as negative controls.

Western Blot

Proteins were extracted with RIPA lysis buffer with mixed protease inhibitors (Sigma, United States). Proteins (30 μg) were separated on SDS-PAGE gel, followed by transfer to nitrocellulose membrane (MilliporeSigma, United States). The membranes were then blocked with 5% skim milk and incubated at 4°C overnight with the primary antibody: anti-STK35 (ab136695; Abcam, United States), anti-NEDD4L (#2740; Cell Signaling Technology, United States), anti-cleaved caspase-3 (ab2302; Abcam, Cambridge, MA, United States), anti-cleaved caspase-9 (ab2324; Abcam, United States), anti-GLUT1 (ab40084; Abcam, United States), anti-HK-2 (ab209847; Abcam, United States), anti-AKT (#9272; Cell Signaling Technology, United States), anti-p-AKT (#4060; Cell Signaling Technology, United States), or β-actin (#3700; Cell Signaling Technology, United States). Following primary antibody incubation, the membranes were incubated with HRP-conjugated secondary antibody (Beyotime, China). The membranes were visualized by using ChemiDoc Imaging Systems (Bio-Rad, United States).

Cell Viability Assay

Cell viability was analyzed with Cell Counting Kit-8 (CCK-8) (SAB, United States) according to the manufacturer's instructions. Briefly, HCT116, SW480, and SW620 cells transduced with the indicated plasmids were plated in 96-well plates (approximately 3,000 cells/well) and incubated overnight at 37°C, followed by CCK-8 incubation for 1 h at 37°C. The 450-nm optical density (OD) was determined using a multi-plate reader (DNM-9602; Perlong Medical Co., China).

Cell Apoptosis Assay

HCT116, SW480, and SW620 cells were grown in 6-well plates (approximately 5×10^5 cells/well) until they reached 50% confluence. Then, the cells expressing the indicated plasmids were treated with or without 10 μM of AKT inhibitor MK-2206, 200 or 400 μM of fluorouracil (5-FU), or vehicle control for 48 h. Following incubation with 5 μl propidium iodide (PI) and fluorescein isothiocyanate-labeled annexin V (Annexin V-FITC), cell apoptosis was assessed with a FACSArial I flow cytometer (BD Biosciences, United States). Cells that were negative for PI but positive for Annexin V-FITC were counted as apoptotic.

Cellular Activity of Lactate Dehydrogenase (LDH)

The lactate dehydrogenase (LDH) activity in the cell-free cultural supernatants of HCT116, SW480, and SW620 cells

was evaluated using a commercial assay kit A020-1 (Nanjing Jiancheng Bioengineering Institute, China) based on the protocol provided by the manufacturer.

Extracellular Flux (XF) Analysis

The XF24 Extracellular Flux Analyzer (Seahorse, United States) was used to monitor extracellular acidification rates (ECAR) and cellular oxygen consumption rates (OCR) in real time for the estimations of glycolysis and mitochondrial respiration, respectively, as previously described (Guo et al., 2020).

Establishment of Stable Cell Lines for Xenograft Study

Approximately 5×10^6 SW620 cells transduced with shSTK35 or shNC were subcutaneously injected into the armpits of 4- to 5-week-old male nude mice (Beijing HFK Bioscience, China). Tumor measurements were recorded every 3 days. At the 33rd day post-injection, the mice were euthanized, their tumor characteristics were recorded, and the xenografts were collected for further analysis ($n = 6$ per group). The xenografts were subjected to terminal deoxynucleotidyl transferase dUTP nick end labeling (TUNEL). Meanwhile, approximately 5×10^6 SW480 cells transduced with STK35-overexpressing lentivirus or blank lentivirus vector were injected into the same type of mice following the same method. Chemotherapy by 50 mg/kg of 5-FU (once per week) was initiated 12 days after the injection ($n = 6$ per group). At the 33rd day post-injection, the mice were sacrificed for measurement of the tumor size. A total of 80 mice were collected for survival analysis ($n = 20$ per group). Laboratory animal care and procedures were conducted following the animal ethics guidelines of The Affiliated Changzhou No. 2 People's Hospital of Nanjing Medical University.

Immunoprecipitation (IP) and Liquid Chromatography/Mass Spectrometry (LC/MS) Analyses

Cells stably expressing the empty vector or FLAG-tagged STK35 were lysed in precooled RIPA lysis buffer. The cell lysates were then incubated with protein A/G beads (Santa Cruz Biotechnology) for 2 h at 4°C, and the extracts were further incubated overnight with anti-FLAG beads (Sigma-Aldrich) at 4°C. Subsequently, the immunoprecipitated protein complex was eluted using the FLAG peptide (Sigma-Aldrich). Protein samples were resolved by SDS-PAGE for Coomassie Blue staining, and the differentially migrated bands were excised and digested with trypsin for further liquid chromatography/mass spectrometry (LC/MS) analysis.

Co-immunoprecipitation (Co-IP) and Ubiquitination Assays

Cell lysates extracted with RIPA buffer were incubated with anti-STK35 antibody PA5-14082 (Invitrogen), anti-NEDD4L antibody #4013 (Cell Signaling Technology, United States), or IgG antibody sc-2027 (Santa Cruz Biotechnology, United States) overnight at 4°C, followed by 2 h incubation with Protein A/G PLUS-Agarose beads sc-2003 (Santa Cruz Biotechnology, Inc.) at 4°C. The immune-complexes were washed three times with lysis buffer on a magnetic rack and then examined by immunoblotting with anti-STK35 (ab136695; Abcam, United States), anti-NEDD4L (#2740; Cell Signaling Technology, United States), or anti-ubiquitin (ab7780; Abcam, Cambridge, MA, United States) antibodies.

Statistical Analysis

All assays were performed three times, and the quantitative data are displayed as mean ± standard deviation. Statistical analysis was performed by GraphPad Prism 7.0 (GraphPad Software, United States). The comparison between different experimental groups was performed with unpaired *t*-test or ANOVA. Cox's proportional hazards regression model and Kaplan–Meier plotting were applied for calculating the overall or disease-free survival, and the differences between groups were analyzed by a log-rank test. *P*-values < 0.05 were considered statistically significant.

RESULTS

STK35 Expression Was Clinically Correlated With CRC Prognosis

To investigate the relationship between STK35 expression and CRC, we collected related mRNA expression data on CRC patients from both online databases and those of our hospital. According to the datasets from TCGA (**Figure 1A**) and the GSE9348 (**Figure 1B**), the mRNA expression levels of STK35 in tumor tissues of CRC patients were noticeably ($P < 0.001$ and <0.01, respectively) higher than those in normal tissues. Similarly, based on Q-PCR, we also found that the transcriptional level of STK35 in the 131 tumor tissues from CRC patients in our hospital was significantly ($P < 0.001$) higher than that in the 30 normal tissues (**Figure 1C**). However, no substantial correlation was found between mRNA expression (median value = 0.9079) and the overall ($P = 0.095$, HR = 1.510, 95% CI: 0.9107–2.504) or disease-free ($P = 0.1462$, HR = 1.476, 95% CI: 0.8780–2.482) survival rates of the CRC patients (**Supplementary Figure S1**).

Immunohistochemistry staining was used to classified the STK35 protein expression in the CRC patients as high or low, with 78 and 53 cases, respectively (**Figure 1D**), to explore its correlation with CRC. Kaplan–Meier analysis demonstrated that the protein expression of STK35 was significantly correlated with both the overall ($P = 0.0197$, HR = 1.870, 95% CI: 1.105–3.166; **Figure 1E**) and disease-free ($P = 0.0076$, HR = 2.078, 95% CI: 1.214–3.558; **Figure 1F**) survival rates of the CRC patients. Moreover, multivariate analysis revealed that STK35 protein expression was noticeably associated with two clinicopathological parameters in the CRC patients (**Table 1**), including tumor size ($P = 0.016$) and T classification ($P = 0.024$). Multivariate regression analysis demonstrated that STK35 expression was an independent predictor of CRC aggressiveness, with significant HRs for predicting clinical outcome (**Figure 1G**). Collectively, STK35 was upregulated and significantly

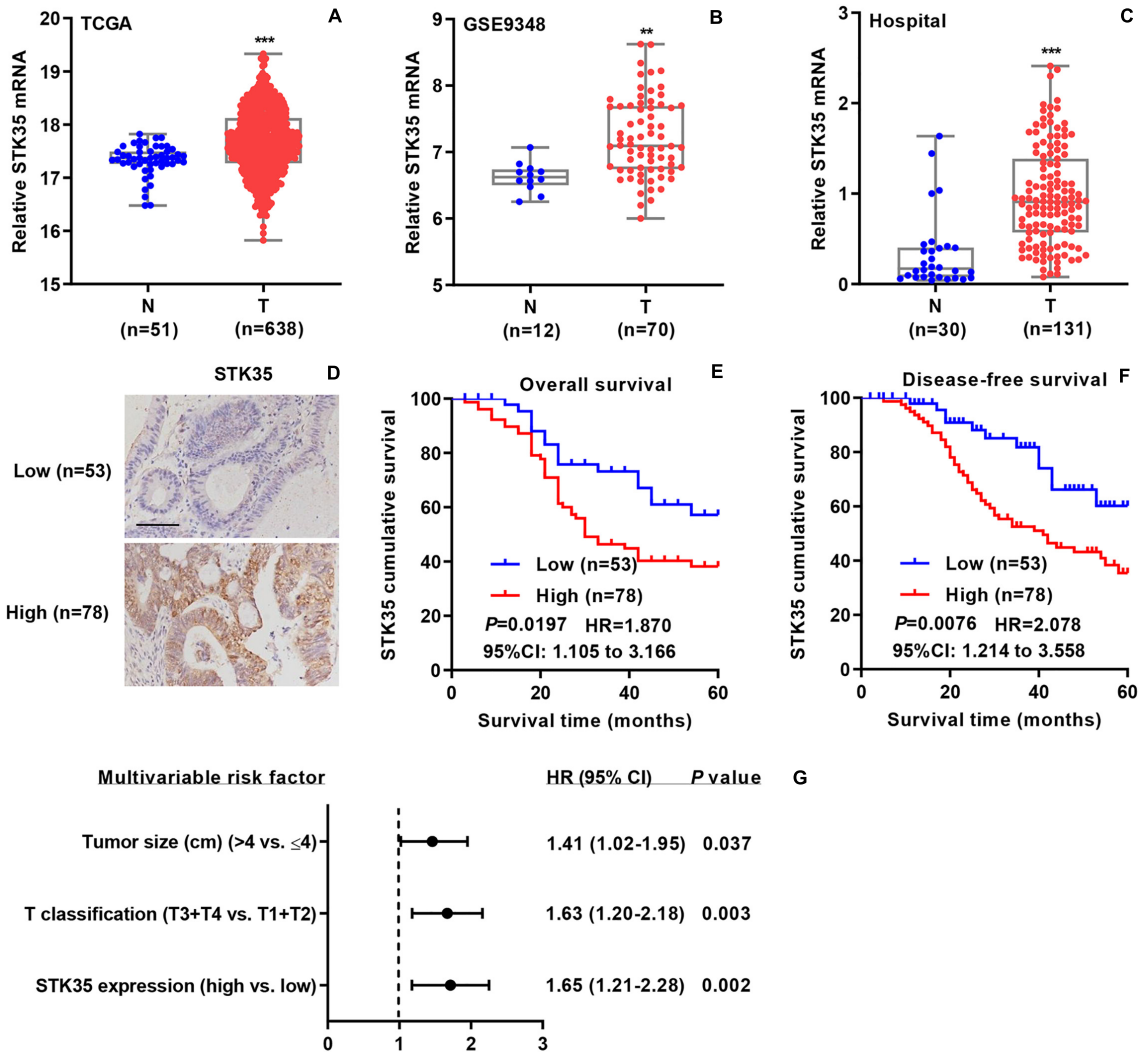

FIGURE 1 | STK35 is clinically relevant in colorectal cancer (CRC). **(A)** STK35 mRNA expression in 638 CRC tissues (T) and 51 normal tissues (N) acquired from TCGA RNA-seq datasets. **(B)** STK35 mRNA expression in 70 CRC tissues (T) and 12 normal tissues (N) acquired from the GSE9348 database. **(C)** STK35 mRNA expression by quantitative RT-PCR in 131 CRC tissues (T) and 30 normal tissues (N) collected at our hospital. **(D)** Representative images of immunohistochemistry staining in CRC samples with differential protein expression of STK35 collected at our hospital. Scale bar: 100 μm. **(E,F)** Kaplan–Meier plots of **(E)** overall survival rate and **(F)** disease-free survival rate of CRC patients based on differential protein expression of STK35. **(G)** Multivariable analysis performed in the hospital cohort. ** $P < 0.01$, *** $P < 0.001$, compared with N.

associated with clinicopathologic characteristics, as well as poor prognosis in human CRC.

STK35 Knockdown Suppressed CRC Cellular Activities and Tumor Growth

We examined both the mRNA and protein levels of STK35 in a normal human intestinal crypt cell line and various CRC cell lines (**Supplementary Figure S2A**), following which, we selected SW620 (**Supplementary Figure S2B**) and HCT116 (**Supplementary Figure S2C**) cells with the highest expression of STK35 for use in gene knockdown experiments.

The viability of SW620 (**Figure 2A**) and HCT116 (**Figure 2B**) cells with STK35 knockdown was substantially ($P < 0.001$) reduced at 48 and 72 h, compared to that of the control cells. On the contrary, STK35 knockdown significantly ($P < 0.001$) increased apoptosis in both SW620 and HCT116 cells compared to control cells (**Figures 2C,D**). We also observed that STK35 knockdown in both SW620 and HCT116 cells significantly ($P < 0.001$) decreased their LDH activities compared to control cells (**Figure 2E**). In addition, the OCR, indicating mitochondrial respiration, and the ECAR, reflecting overall glycolytic flux, were also diminished by STK35 knockdown in both CRC cell lines compared to the control cells (**Figures 2F–I**).

The effect of STK35 on tumor growth was evaluated by subcutaneously injecting nude mice with STK35 knockdown-SW620 cells. We found that in comparison with the control group, the tumor volumes in the SW620 cells with STK35

TABLE 1 | Correlation between the STK35 protein expression and clinicopathological parameters in patients with colorectal cancer.

Clinicopathological parameter	Protein expression of STK35		*P*-value
	Low (*n*=53, 40.4%)	High (*n*=78, 59.6%)	
Gender			
Male	31 (58.5%)	35 (44.9%)	0.126
Female	22 (41.5%)	43 (55.1%)	
Age (years)			
<60	18 (34.0%)	39 (50.0%)	0.069
≥60	35 (66.0%)	39 (50.0%)	
Tumor size (cm)			
≤4	31 (58.5%)	29 (37.2%)	0.016*
>4	22 (41.5%)	49 (62.8%)	
T classification			
T1	8 (15.1%)	4 (5.1%)	0.024*
T2	15 (28.3%)	11 (14.1%)	
T3	13 (24.5%)	24 (30.8%)	
T4	17 (32.1%)	39 (50.0%)	
Histology			
Well	12 (22.6%)	18 (23.1%)	0.326
Moderate	15 (28.3%)	31 (39.7%)	
Poor	26 (49.1%)	29 (37.2%)	

*Differences between groups were determined by the Chi-square test, *P<0.05.*

knockdown-injected mice were notably ($P < 0.001$) reduced from day 24 to 33 (**Figure 3A**). Similarly, STK35 knockdown notably ($P < 0.001$) reduced the tumor weight at day 33 in relation to the control group (**Figure 3B**). In contrast, TUNEL analysis demonstrated that STK35 knockdown could significantly ($P < 0.001$) stimulate apoptosis in xenograft mouse tumors (**Figure 3C**).

STK35 Regulated Apoptosis, Glycolysis, and AKT Signaling in CRC Cells

Gene set enrichment analysis demonstrated that the expression of STK35 was significantly ($P < 0.001$) correlated with cancer cell apoptosis, glycolysis, and AKT pathways (**Figure 4A**). Moreover, Western blot demonstrated that STK35 knockdown in SW620 (**Figures 4B,C**) and HCT116 (**Figures 4D,E**) cells led to increased expression of apoptosis-related proteins, such as cleaved caspase-3 and -9. On the contrary, STK35 knockdown in SW620 (**Figures 4B,C**) and HCT116 (**Figures 4D,E**) cells led to a reduction in the expression of cellular glycolytic-related proteins, including hexokinase 2 (HK-2) and glucose transporter 1 (GLUT1), as well p-AKT in the AKT signaling pathway. The protein levels of AKT were not altered by STK35 knockdown in either of these cell lines (**Figures 4B–E**).

STK35 Overexpression Stimulates CRC Cellular Activities via the AKT Pathway

Based on the protein and mRNA levels of STK35 in the normal human intestinal crypt cell line and various CRC cell lines (**Supplementary Figure S2A**), we selected SW480 cells with the lowest expression of STK35 for gene overexpression experiments (**Supplementary Figure S2D**).

The viability of SW480 cells with STK35 overexpression was significantly ($P < 0.001$) increased at 48 and 72 h compared to that of control cells (**Supplementary Figure S3A** and **Figure 5A**). On the contrary, STK35 overexpression substantially ($P < 0.001$) suppressed the apoptosis of SW480 cells compared to the control cells (**Supplementary Figure S3B** and **Figures 5B,C**). We also observed that STK35 overexpression in SW480 cells significantly ($P < 0.001$) stimulated their LDH activity in relation to the control cells (**Figure 5D**). Both the OCR (**Figure 5E**) and ECAR (**Figure 5F**) were raised in SW480 cells by STK35 overexpression compared to those in the control cells.

We conducted Western blot to further explore the effects of STK35 overexpression on CRC cellular expression of apoptosis-, glycolysis-, and AKT signaling-related proteins. We found that STK35 overexpression in SW480 cells led to downregulation of cellular cleaved caspase-3 and caspase-9 protein levels, but upregulation of GLUT1 and HK-2 proteins (**Figures 5G,H**). STK35 overexpression also upregulated the cellular levels of p-AKT protein in SW480 cells in comparison with the control cells, whereas the levels of AKT protein were unchanged (**Supplementary Figure S3C** and **Figures 5G,H**).

Through treating the cells with the AKT signaling inhibitor MK-2206, we further demonstrated the molecular mechanism by which STK35 participated in modulating CRC cellular activities. MK-2206 treatment of SW480 cells could significantly ($P < 0.001$) suppress the p-AKT protein level (**Figures 5G,H**), lower viability at 48 and 72 h (**Figure 5A**), promote apoptosis (**Figure 5B**), upregulate apoptosis-related proteins (**Figure 5F**), reduce LDH activity (**Figure 5C**), lower the OCR (**Figure 5D**) and ECAR (**Figure 5E**), and downregulate glycolytic-related protein levels (**Figure 5F**) compared to those in the control cells. However, the overexpression of STK35 in MK-2206-treated SW480 cells partially rescued all the observed cellular alterations introduced by the AKT signaling inhibitor at significant levels ($P < 0.001$; **Figure 5**).

STK35 Restricted 5-FU Chemosensitivity of CRC

In order to investigate the influence of STK35 on the chemosensitivity of CRC cells, we treated the indicated CRC cells with 5-FU. The 5-FU treatment stimulated apoptosis in both SW620 (**Figures 6A,B**) and SW480 (**Figures 6C,D**) cells in a dose-dependent manner. However, STK35 knockdown in 5-FU-treated SW620 cells significantly ($P < 0.001$) strengthened the apoptotic–promotive effect of 5-FU (**Figures 6A,B**), while STK35 overexpression in 5-FU-treated SW480 cells partially counteracted the effect of 5-FU at significant levels ($P < 0.01$, $P < 0.001$; **Figures 6C,D**). Following the similar pattern, 5-FU treatment decreased the tumor volumes (**Figure 6E**) and tumor weight (**Figure 6F**) in mice, and simultaneously raised the apoptosis in xenograft mouse tumors (**Figures 6G,H**) and the survival rate of mice (**Figure 6I**). Nevertheless, STK35 overexpression could partially counteract the antitumor effect of 5-FU at significant levels (**Figures 6E–I**).

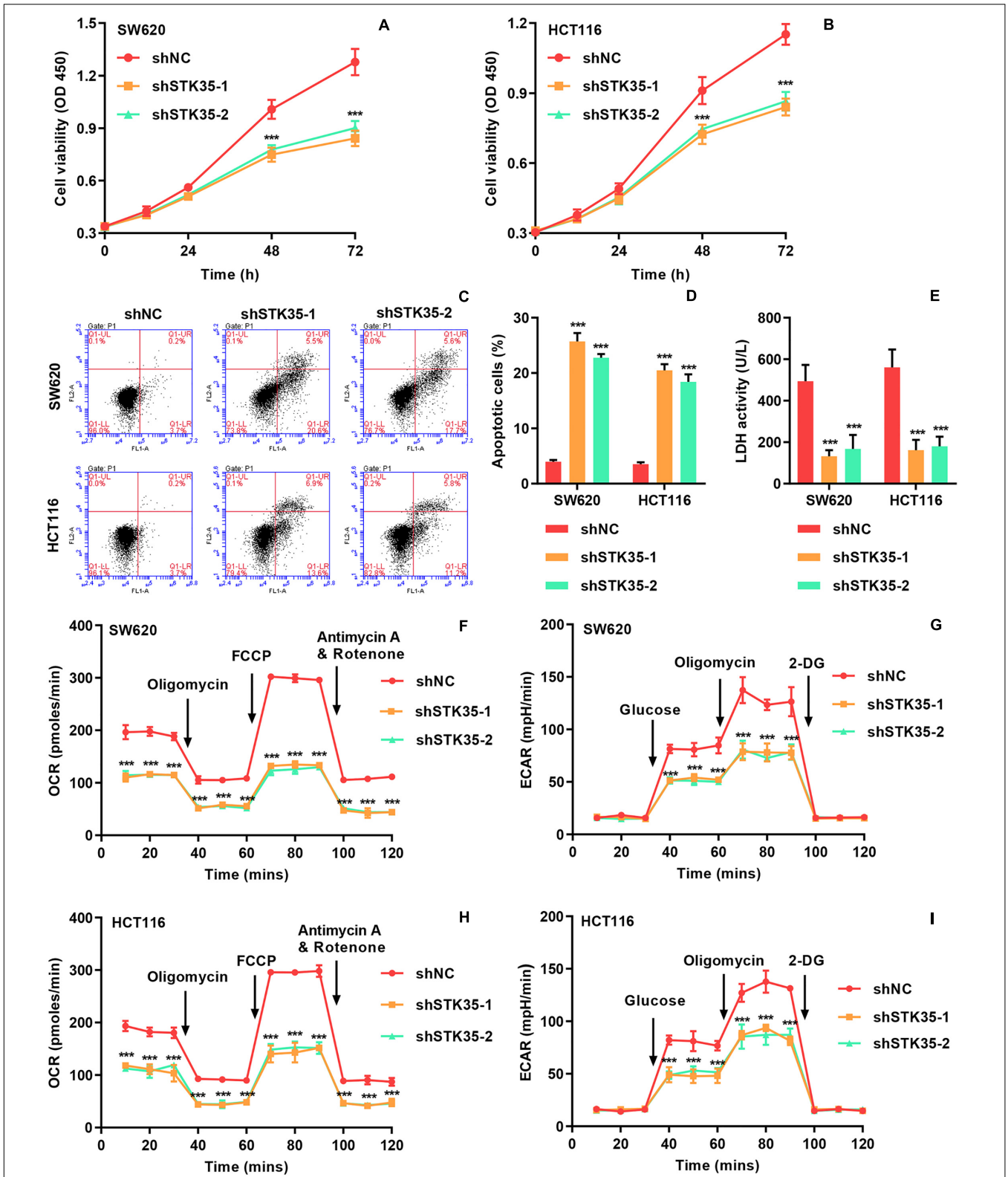

FIGURE 2 | STK35 knockdown inhibits viability and glycolysis but promotes apoptosis in SW620 and HCT116 cells. SW620 and HCT116 cells were transduced with STK35 shRNAs (shSTK35-1 and shSTK35-2) or control scramble shRNA (shNC). **(A,B)** Viability of **(A)** SW620 and **(B)** HCT116 cells assessed by CCK-8. **(C,D)** Assessment and quantification of apoptosis by flow cytometry. **(E)** Cellular LDH levels measured by biochemical analysis. **(F,I)** Energy metabolism of **(F,G)** SW620 and **(H,I)** HCT116 cells reflected by **(F,H)** oxygen consumption rate and **(G,I)** extracellular acidification rate. ***$P < 0.001$, compared with shNC.

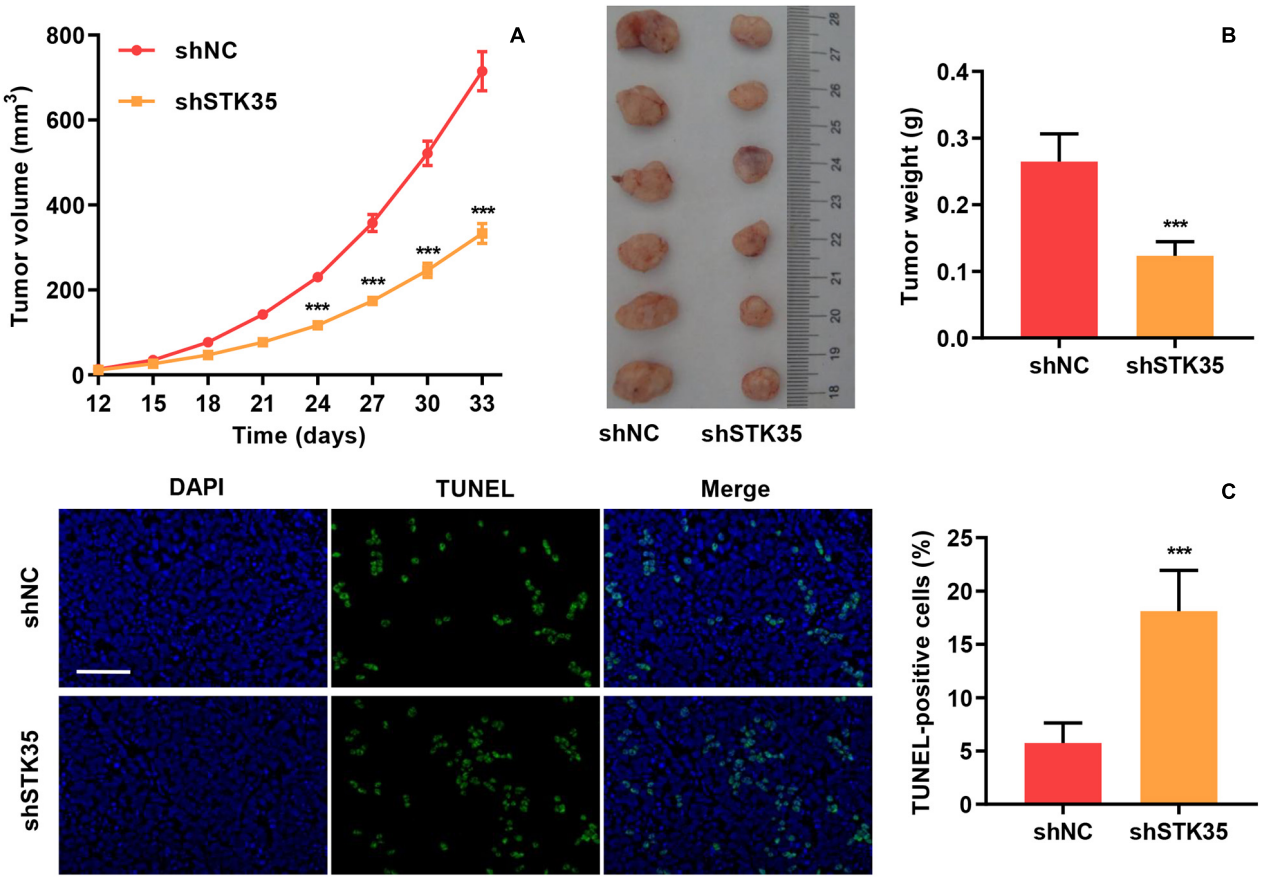

FIGURE 3 | STK35 knockdown constrains tumor growth *in vivo*. SW620 cells stably expressing STK35 shRNAs (shSTK35) or control scramble shRNA (shNC) were subcutaneously injected into male nude mice (n = 6 per group). **(A)** Tumor volumes measured every third day from day 12 to 33. **(B)** Mouse tumor characteristics, including morphology and weight, recorded at day 33. **(C)** Visualization of terminal deoxynucleotidyl transferase dUTP nick end labeling (TUNEL) labeled xenograft mouse tumors and quantification of TUNEL positive cells. Scale bar: 100 μm. ***$P < 0.001$, compared with shNC.

STK35 Inhibited NEDD4L-Mediated Anti-CRC Effects Through Ubiquitination

To investigate STK35 regulation in CRC, we identified candidate proteins associated with STK35 by Co-immunoprecipitation (Co-IP) assay and proteomics analysis. Differentially expressed bands were excised (**Figure 7A**) and identified by LC/MS. Among the proteins with ≥3 peptides identified which may be associated with STK35, NEDD4L, which was previously reported to inhibit CRC, was selected for further investigation. We confirmed the association between STK35 and NEDD4L proteins by Co-IP (**Figure 7B**). Meanwhile, based on the protein and mRNA levels of NEDD4L in the normal human intestinal crypt cell line and various CRC cell lines (**Supplementary Figure S2E**), we selected SW620 cells with the lowest expression of NEDD4L for overexpression experiments (**Supplementary Figure S2F**).

To examine the potential STK35 ubiquitination carried out by NEDD4L, we treated the cells with a proteasome inhibitor MG132. The protein expression of STK35 in NEDD4L-overexpressing SW620 cells was downregulated with no significant effect on the STK35 mRNA level; however, treatment with MG132 could restore its expression back to the normal level in the control cells (**Figure 7C**), suggesting that NEDD4L regulates STK35 levels in a proteasome-dependent manner. Moreover, NEDD4L overexpression in SW620 cells strengthened the ubiquitination of STK35 compared to that of the control cells (**Figure 7D**).

Most importantly, NEDD4L overexpression in SW620 cells increased apoptosis ($P < 0.001$; **Figure 7E**), reduced LDH activity ($P < 0.001$; **Figure 7F**), lowered the OCR (**Figure 7G**) and ECAR (**Figure 7H**), upregulated cleaved caspase-3 and -9 cellular protein levels (**Figures 7I,J**), downregulated GLUT1 and HK-2 protein levels (**Figures 7I,J**), and suppressed the p-AKT protein level (**Figures 7I,J**) in relation to those in the control cells. However, further overexpression of STK35 in NEDD4L-overexpressing SW480 cells significantly ($P < 0.001$) counteracted these observed cellular alterations introduced by NEDD4L overexpression (**Figures 7E–J**).

STK35 Is Clinically Correlated With NEDD4L and p-AKT in CRC Patients

We further explored the relationship between NEDD4L expression and CRC based the mRNA transcriptional data of

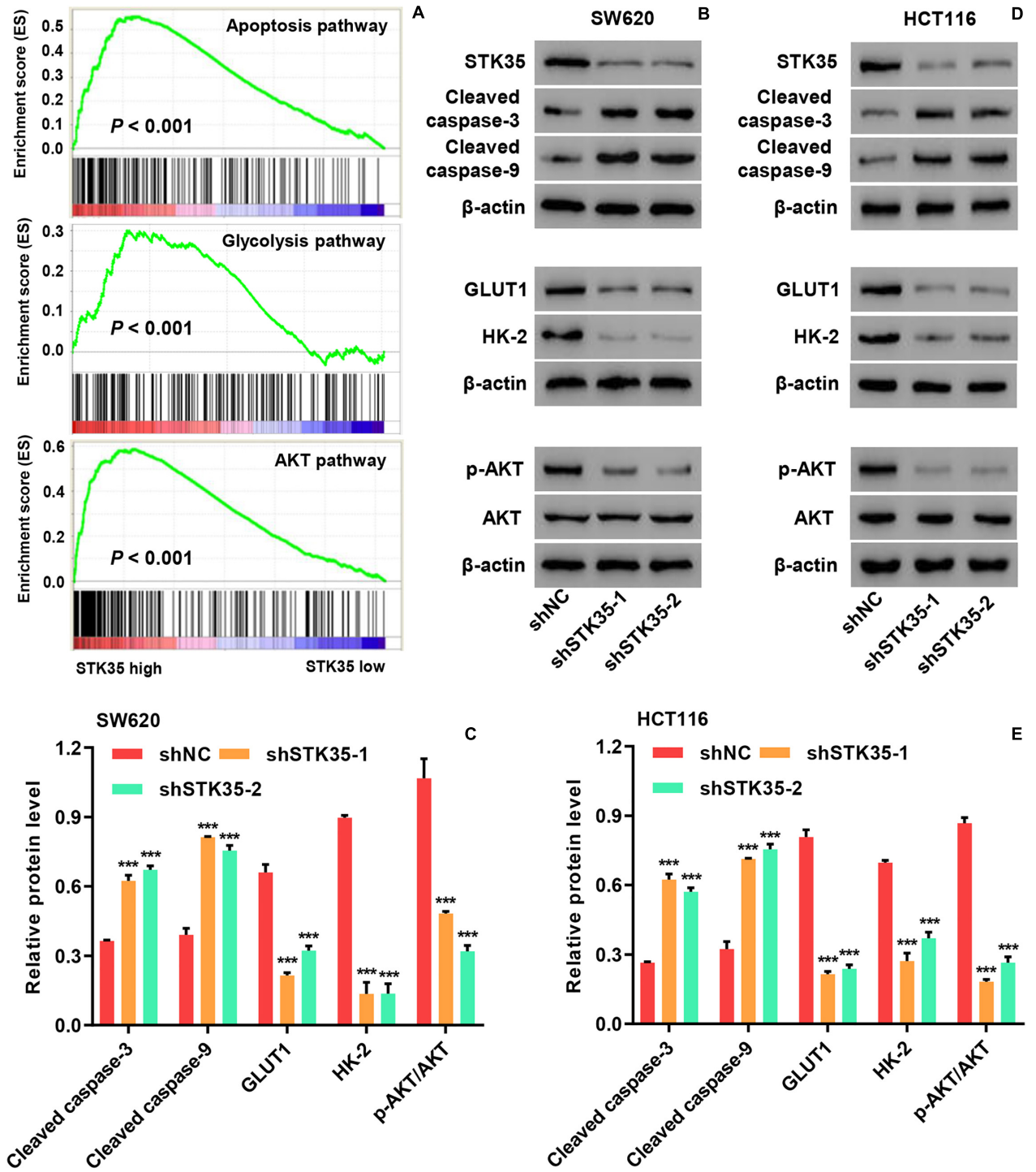

FIGURE 4 | STK35 regulates apoptosis, glycolysis, and AKT signaling in colorectal cancer (CRC). **(A)** Correlation of STK35 high vs. low expression in CRC tissues with genes associated with apoptosis, glycolysis, and AKT pathways, as indicated by gene set enrichment analysis. **(B–E)** Cellular protein levels of STK35, cleaved caspase-3, cleaved caspase-9, GLUT1, HK-2, p-AKT, and AKT in **(B,C)** SW620 and **(D,E)** HCT116 cells transfected with STK35 shRNAs (shSTK35-1 and shSTK35-2) or control scramble shRNA (shNC), assessed by Western blot, with β-actin as the loading control. ***$P < 0.001$, compared with shNC.

CRC patients from both online databases and those of our hospital. According to the datasets from TCGA (**Figure 8A**) and the GSE9348 (**Figure 8B**), the transcript levels of NEDD4L in tumor tissues from CRC patients were significantly ($P < 0.001$) lower than those in normal tissues. Similarly, based on Q-PCR, we also detected that the transcript level of NEDD4L in the 131

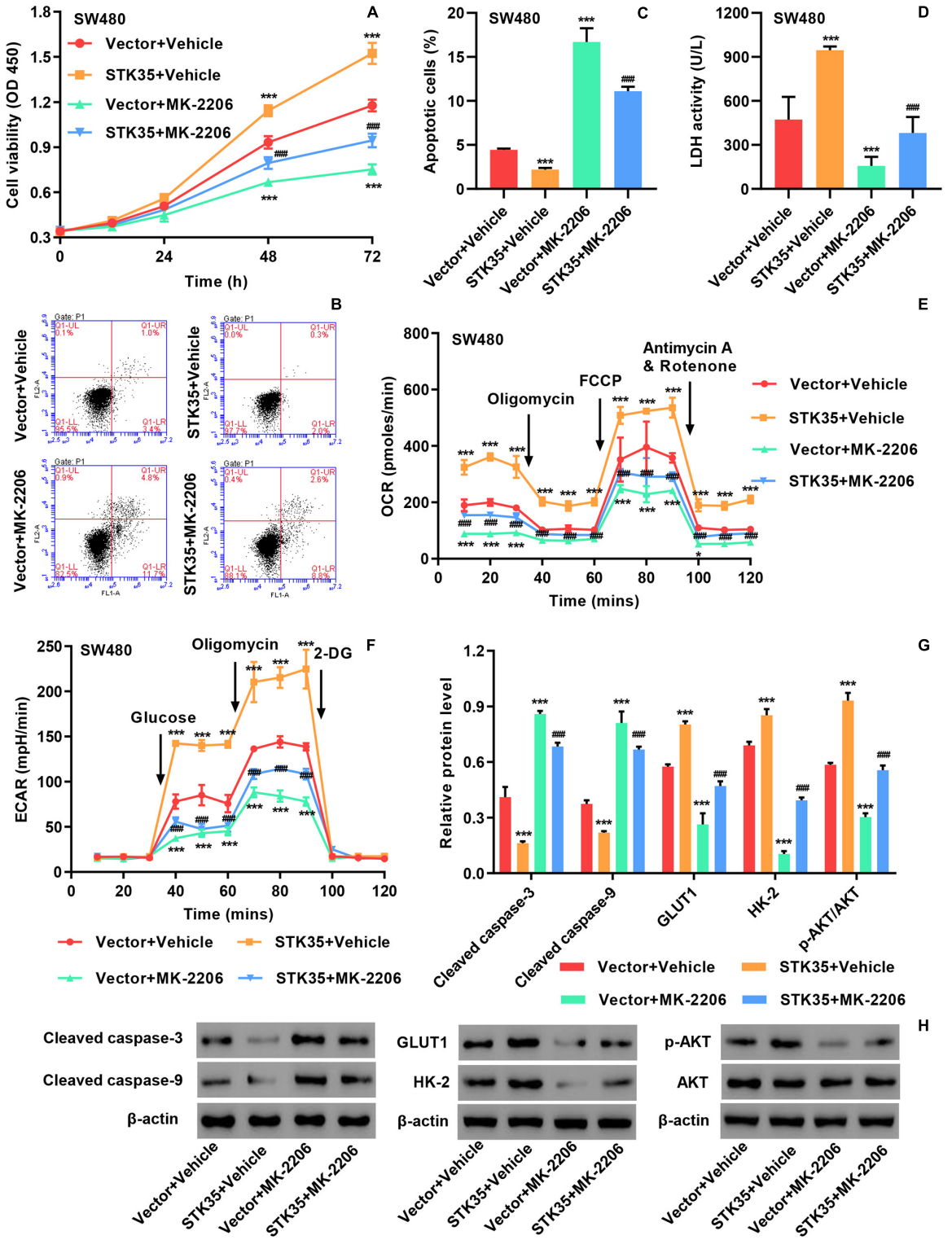

FIGURE 5 | STK35 overexpression promotes viability and glycolysis but inhibits apoptosis in SW480 cells through the AKT signaling pathway. SW480 cells were transduced with STK35 overexpressing lentivirus (STK35) or blank lentivirus (Vector) in the presence of 10 μM AKT inhibitor MK-2206 or control (Vehicle). **(A)** Cell viability assessed by CCK-8. **(B,C)** Cell apoptosis assessed and quantified by flow cytometry. **(D)** Cellular LDH levels measured by biochemical analysis. **(E,F)** Cellular energy metabolism reflected by **(E)** the oxygen consumption rate and **(F)** the extracellular acidification rate. **(G,H)** Cellular protein levels of cleaved caspase-3, cleaved caspase-9, GLUT1, HK-2, p-AKT, and AKT assessed by Western blot, with β-actin as the loading control. $^{*}P < 0.05$, $^{***}P < 0.001$, compared with Vector + Vehicle, $^{\#\#\#}P < 0.001$, compared with STK35 + Vehicle.

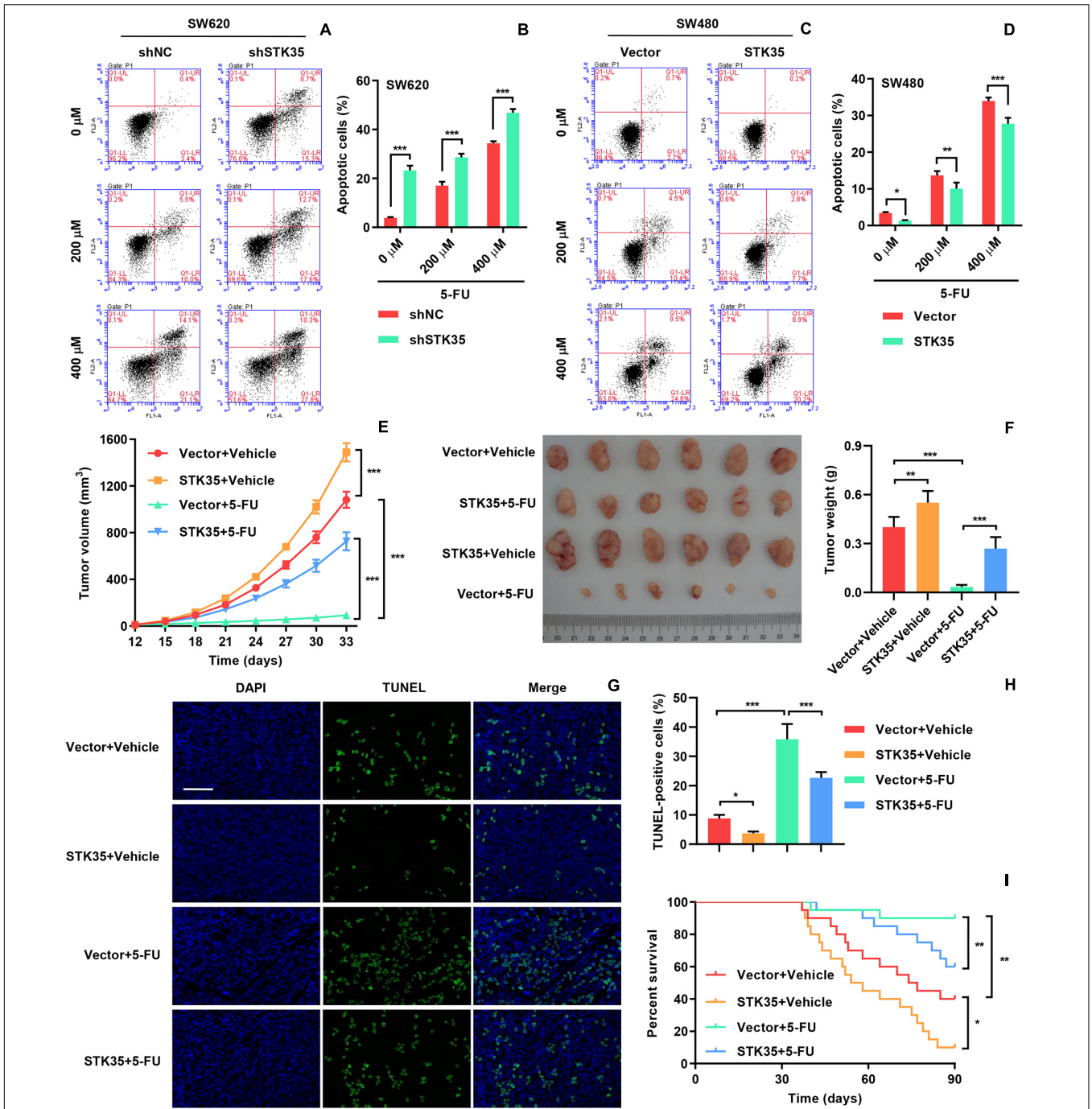

FIGURE 6 | STK35 expression influences chemosensitivity to 5-FU. **(A–D)** SW620 cells stably expressing STK35 shRNAs (shSTK35) or control scramble shRNA (shNC), and SW480 cells transduced with STK35-overexpressing lentivirus (STK35) or blank lentivirus (Vector) were treated with 5-FU (0, 200, and 400 μM) or control (Vehicle) for 48 h. **(A,B)** SW620 and **(C,D)** SW480 apoptosis assessed and quantified by flow cytometry. **(E–I)** SW480 cells transfected with STK35-overexpressing lentivirus (STK35) or blank lentivirus (Vector) following 5-FU chemotherapy were subcutaneously injected into male nude mice ($n = 6$ per group). **(E)** Tumor volumes measured every third day, from days 12 to 33. **(F)** Mouse tumor characteristics, including morphology and weight, recorded at day 33. **(G)** Visualization of terminal deoxynucleotidyl transferase dUTP nick end labeling (TUNEL) labeled xenograft mouse tumors. **(H)** Quantification of TUNEL positive cells. **(I)** Mice survival probability. $^{*}P < 0.05$, $^{**}P < 0.01$, $^{***}P < 0.001$.

tumor tissues from CRC patients in our hospital was substantially ($P < 0.001$) lower than that in the 30 normal tissues (**Figure 8C**). Through IHC staining, we classified the NEDD4L and p-AKT protein expressions in the CRC patients as high or low with 63 and 68, and 67 and 64 cases, respectively (**Figure 8D**). Furthermore, we also revealed significant correlations between

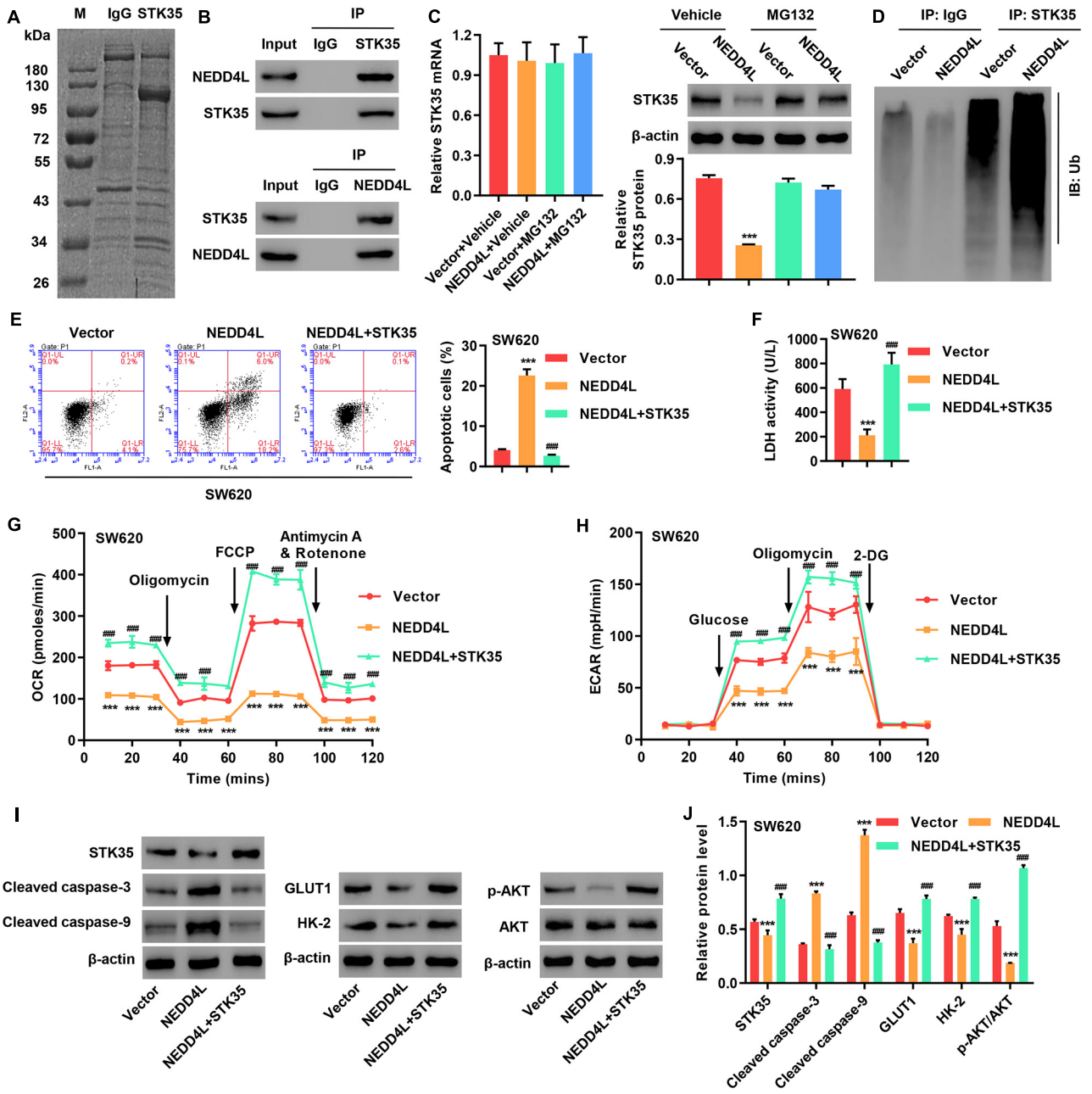

FIGURE 7 | STK35 is ubiquitinated by NEDD4L and inhibits NEDD4L-mediated anti-colorectal cancer function. **(A)** Purification of the STK35 immunocomplex. Proteins were separated by SDS-PAGE and stained with Coomassie Blue. **(B)** Immunoprecipitation was performed with an IgG control, anti-STK35, or anti-NEDD4L antibody, followed by incubation with indicated antibodies. **(C)** Protein and mRNA expression of STK35 in SW620 cells transduced with NEDD4L-overexpressing lentivirus (NEDD4L) or blank lentivirus (Vector) in the presence of 10 μM MG132 or control (Vehicle), measured with western blot and Q-PCR. β-Actin as the loading control. **(D)** NEDD4L-overexpressed SW620 cells immune-precipitated with STK35 or IgG antibody for evaluating ubiquitination. **(E–I)** SW620 cells were transduced with STK35-overexpressing lentivirus (STK35) after NEDD4L-overexpressing lentivirus (NEDD4L) or blank lentivirus (Vector) transfection. **(E)** Cell apoptosis assessed by flow cytometry and quantification accordingly. **(F)** Cellular LDH levels measured by biochemical analysis. **(G,H)** Cellular energy metabolism reflected by **(G)** oxygen consumption rate and **(H)** extracellular acidification rate. **(I,J)** Cellular protein levels of STK35, cleaved caspase-3, cleaved caspase-9, GLUT1, HK-2, p-AKT, and AKT, measured with western blot. β-Actin as the loading control. *** $P < 0.001$, compared with Vector. ### $P < 0.001$, compared with NEDD4L.

STK35 and NEDD4L protein expression ($P = 0.0203$; **Figure 8E**), STK35 and p-AKT protein expression ($P = 0.0012$; **Figure 8F**), and NEDD4L and p-AKT protein expression ($P = 0.0295$; **Figure 8G**).

DISCUSSION

The expression of human STKs have been reported to be frequently modulated in a variety of human cancers, and

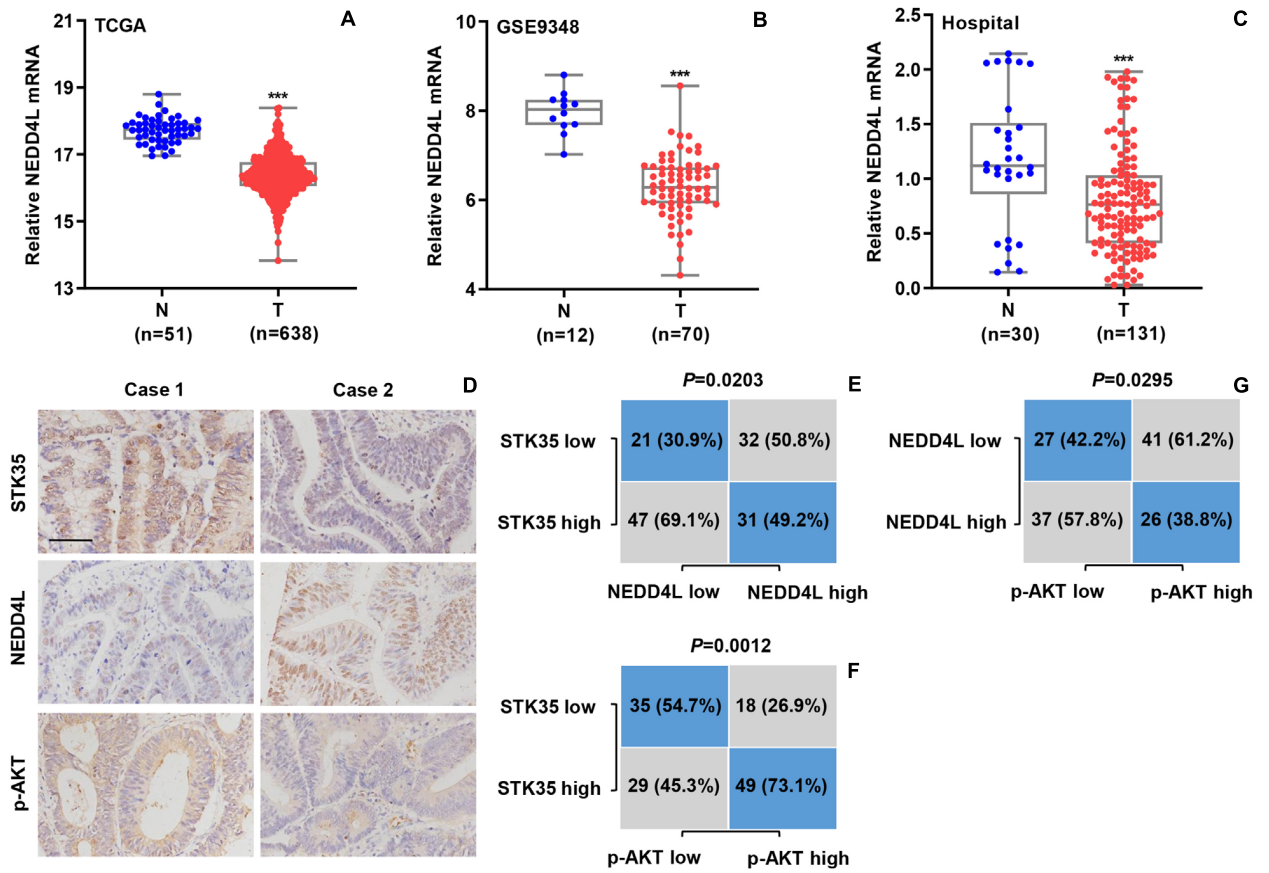

FIGURE 8 | STK35 expression is clinically relevant to NEDD4L and p-AKT in colorectal cancer (CRC). **(A)** NEDD4L expressions in 638 CRC tissues (T) and 51 normal tissues (N) acquired from TCGA RNA-seq datasets. **(B)** NEDD4L expressions in 70 CRC tissues (T) and 12 normal tissues (N) acquired from GSE9348 database. **(C)** NEDD4L expressions assessed by quantitative RT-PCR in 131 CRC tissues (T) and 30 normal tissues (N) collected at our hospital. **(D)** Representative images of immunohistochemistry staining in CRC samples with differential expressions of STK35, NEDD4L, and p-AKT collected at our hospital. Scale bar: 100 μm. **(E–G)** Statistical analyses of CRC tissues for correlation between expressions of **(E)** STK35 and NEDD4L, **(F)** STK35 and p-AKT, and **(G)** NEDD4L and p-AKT. ***$P < 0.001$, compared with N.

particularly, the *STK35* gene is noticeably altered in human CRC (Capra et al., 2006; Goyal et al., 2009; Lu et al., 2017). For the current study, we targeted STK35 based on its regulatory roles in the expression of CDKN2A, with consequent effects on the cell cycle (G1–S phase transition) and programmed cell death (Goyal et al., 2011). Relying on the analyses of patient data collected from both online databases and those of our hospital, we detected a notably higher expression of STK35 in the tumor tissues from CRC patients at both the protein and mRNA levels. Through bioinformatics analysis, the survival probability in patients following CRC diagnosis and treatments was found to be negatively correlated with the protein expression levels of STK35, demonstrating that STK35 could be an indicator of CRC tumor recurrence. This finding is supported by previous reports, which suggested parallel correlations between human STKs and the pathology and prognosis of various types of human cancers, including CRC (Guo et al., 2017; Lu et al., 2017; Sun et al., 2019). Furthermore, multivariate analysis demonstrated a significant association between STK35 protein expression and several CRC clinical parameters, all of which were independently correlated with CRC status in the patients. Together, these results indicate the significance and contribution of STK35 in the clinical management of CRC, for which it could be developed as an efficient prognostic marker.

Previous studies have reported that STK35 and its homolog CLP36 Interacting Kinase 1 Like (Goyal et al., 2009) are capable of regulating a variety of cellular activities in human cancers, in which they have been shown to promote cellular proliferation, migration, and invasion (Yasuda et al., 2012), stimulate the metabolic processes of cancer cells (Zhang et al., 2017), and suppress tumor cell apoptosis (Wu et al., 2018). In the current study, the knockdown of STK35 in CRC cells elevated their apoptotic rate and reduced their proliferation, tumor growth, and energy metabolism, including both mitochondrial respiration and glycolytic flux. In addition, overexpression of STK35 in CRC cells could reduce programmed cell death and increase the tumor-related activities mentioned above. The expression of STK35 was also found to be correlated with cellular apoptosis and glycolysis pathways, which was further confirmed by the elevated apoptotic protein levels and suppressed glycolytic protein levels

in CRC cells caused by STK35 knockdown. Hence, these findings jointly demonstrate that STK35 is an important factor in accelerating oncogenesis and the progression of CRC.

Fluorouracil based or adjuvant chemotherapies are well known for their efficacy in the treatment of cancer, and they have been shown to improve survival probability in patients with cancer especially CRC, as a result of regulating the folate metabolic pathway and inhibiting both DNA and RNA synthesis (Pardini et al., 2011; Hamaya et al., 2015). However, the presence of tumor stem cells possessing chemoresistance, which accounts for approximately 0.05–0.1% of the total tumor cell mass, and harbor unlimited self-renewal competency, is the main cause of failure of cancer chemotherapy (Zeuner et al., 2014). As a matter of fact, a great number of human kinases have been identified as coexistent putative markers of tumor stem cells, which contribute to minimizing 5-FU chemosensitivity in human cancers (Li et al., 2019; Hou et al., 2020). In the current study, we observed the anti-CRC functions of 5-FU in a dose-dependent manner as expected, whereas the overexpression of STK35 in CRC cells partially reversed these effects, such as the promotion of apoptosis, tumor growth inhibition, and survival improvement in an *in vivo* mouse model. Additionally, previous studies have illustrated that reprogrammed glycolysis, as a recognized hallmark for malignancy which generates plentiful intermediate functional products, also contributes to cancer resistance toward therapeutic drugs (Qian et al., 2017; Ma and Zong, 2020), which is in accordance with our findings in the present study. All these results suggest that STK35 is capable of influencing CRC chemoresistance toward 5-FU, partially attributed to its role in the induction of the glycolytic process in cancerous cells, while, to a further extent, targeting STK35 downregulation in CRC patients might improve the efficacy of chemotherapy.

The phosphorylation of AKT, forming p-AKT, is a crucial step for activating the PI3K/AKT signaling pathway in oncogenesis (Chang et al., 2003). Using GSEA, we have identified the positive correlation between STK35 expression and the AKT pathway. The AKT pathway is also involved in modulating chemoresistance of human cancer cells (Deng et al., 2019), which, together with the findings on STK35-CRC resistance toward 5-FU, indicates close relationships among STK35, the AKT signaling pathway, and CRC chemoresistance. Moreover, the knockdown and overexpression of STK35 in CRC cells induced the downregulation and upregulation of cellular p-AKT, respectively, further confirming the connection between STK35 and AKT phosphorylation. Indeed, complete activation of the core molecule AKT, also an STK (Osaki et al., 2004), is fulfilled by the phosphorylation of its threonine Thr308 and serine Ser473 sites (Liao and Hung, 2010). According to previous studies, the phosphorylation of AKT at either site could be effectively modulated by multiple kinases and phosphatases (Zhang et al., 2006; Kanan et al., 2010). In this study, we observed that STK35 overexpression could partly counteract the anti-CRC functions induced by the AKT inhibitor MK-2206, further illustrating that STK35 may promote the activities of CRC cells via its regulatory effect on the AKT pathway. However, further studies are necessary to discover the exact mechanism by which STK35 regulates AKT/p-AKT, either directly or indirectly.

Relying on the results of the proteomics-based analysis, we identified that NEDD4L interacts with STK35, which was further validated by Co-IP. NEDD4L functions as an E3 ubiquitin ligase and plays essential roles in malignancy and tumorigenesis (Rotin and Kumar, 2009). Moreover, NEDD4L was previously reported to inhibit CRC through suppression of the canonical WNT signaling pathway (Tanksley et al., 2013), and its expression could be targeted as either a prognostic or therapeutic biomarker (Ye et al., 2014). We also detected a high transcriptional level of NEDD4L in CRC tumor tissues and found that its overexpression in CRC cells could promote cellular apoptosis, suppress the glycolytic process, influence the expression of key proteins, and modulate the p-AKT protein level. Additionally, NEDD4L is known to catalyze the polyubiquitination of multiple critical kinases, particularly STKs, to regulate the cell cycle and prevent carcinogenesis (Escobedo et al., 2014). In the current study, NEDD4L overexpression in CRC cells downregulated the cellular level of STK35, which was reversed by the proteasome inhibitor MG132, indicating that NEDD4L may also mediate the ubiquitination of STK35. Indeed, the overexpression of NEDD4L in CRC cells intensified STK35 ubiquitination, which unerringly confirmed our speculation. NEDD4L and STK35 have opposite regulatory functions on the PI3K/AKT pathway (Rotin and Kumar, 2009; Ye et al., 2014), the former of which ubiquitinates PI3K and maintains the balanced state of the pathway (Wang et al., 2016), while the latter activates the pathway. Therefore, STK35 overexpression was capable of completely offsetting the observed anti-CRC effects exhibited by NEDD4L overexpression, and it simultaneously recued the cellular p-AKT back to an even higher level. We have also successfully uncovered substantial correlations among the protein expression of STK35, NEDD4L, and p-AKT. These discoveries highlight the NEDD4L-mediated ubiquitination and degradation of STK35, by which STK35 counteracts NEDD4L-induced anticancer functions partially through regulating the AKT signaling pathway.

To the best of our knowledge, the current study is the first to demonstrate the roles of STK35 in CRC and their related molecular mechanisms. In summary, we reveal higher overall expression of STK35 in CRC tissues, its substantial correlation with CRC prognosis, and its suppressive effects on CRC cell apoptosis. In addition, we demonstrate that STK35 promotes CRC cellular viability, energy metabolism, tumor growth, and chemoresistance. We speculate that STK35 could modulate these CRC activities partially through regulating the AKT signaling pathway. Moreover, the E3 ubiquitin ligase NEDD4L was revealed to associate and ubiquitinate STK35, and its anti-CRC functions were found to be counteracted by STK35. Based on these findings, this study establishes the foundation for locating therapeutic targets in CRC therapy and developing CRC prognostic biomarkers in clinical management.

DATA AVAILABILITY STATEMENT

All datasets presented in this study are included in the article/**Supplementary Material**.

ETHICS STATEMENT

The studies involving human participants were reviewed and approved by The Affiliated Changzhou No. 2 People's Hospital of Nanjing Medical University. The patients/participants provided their written informed consent to participate in this study. The animal study was reviewed and approved by The Affiliated Changzhou No. 2 People's Hospital of Nanjing Medical University.

AUTHOR CONTRIBUTIONS

HY and JZ conceived and designed the work. JZ, GW, and HL performed the research and collected and analyzed the data. GW and YZ collected the human tissue samples. HL, YZ, and JQ provided the technical assistance. HY and JQ wrote the manuscript. All authors read and approved the final manuscript.

FUNDING

This study was supported by grants from the National Natural Science Foundation of China for Young Scholars (81700537) and the Major Project of Changzhou Municipal Commission of Health and Family Planning (ZD201606).

SUPPLEMENTARY MATERIAL

The Supplementary Material for this article can be found online at: https://www.frontiersin.org/articles/10.3389/fcell.2020.582695/full#supplementary-material

REFERENCES

Arnold, M., Sierra, M. S., Laversanne, M., Soerjomataram, I., Jemal, A., and Bray, F. (2017). Global patterns and trends in colorectal cancer incidence and mortality. *Gut* 66, 683–691. doi: 10.1136/gutjnl-2015-310912

Brenner, H., Kloor, M., and Pox, C. P. (2014). Colorectal cancer. *Lancet* 383, 1490–1502.

Brown, R. E., Short, S. P., and Williams, C. S. (2018). Colorectal cancer and metabolism. *Curr. Colorectal Cancer Rep.* 14, 226–241. doi: 10.1007/s11888-018-0420-y

Capra, M., Nuciforo, P. G., Confalonieri, S., Quarto, M., Bianchi, M., Nebuloni, M., et al. (2006). Frequent alterations in the expression of serine/threonine kinases in human cancers. *Cancer Res.* 66, 8147–8154. doi: 10.1158/0008-5472.can-05-3489

Chang, F., Lee, J. T., Navolanic, P. M., Steelman, L. S., Shelton, J. G., Blalock, W. L., et al. (2003). Involvement of PI3K/Akt pathway in cell cycle progression, apoptosis, and neoplastic transformation: a target for cancer chemotherapy. *Leukemia* 17, 590–603. doi: 10.1038/sj.leu.2402824

Cheung, T. H., and Rando, T. A. (2013). Molecular regulation of stem cell quiescence. *Nat. Rev. Mol. Cell Biol.* 14, 329–340. doi: 10.1038/nrm3591

Cronin, K. A., Lake, A. J., Scott, S., Sherman, R. L., Noone, A. M., Howlader, N., et al. (2018). Annual report to the nation on the status of cancer, part I: national cancer statistics. *Cancer* 124, 2785–2800. doi: 10.1002/cncr.31551

Danielsen, S. A., Eide, P. W., Nesbakken, A., Guren, T., Leithe, E., and Lothe, R. A. (2015). Portrait of the PI3K/AKT pathway in colorectal cancer. *Biochim. Biophys. Acta* 1855, 104–121. doi: 10.1016/j.bbcan.2014.09.008

Deng, J., Bai, X., Feng, X., Ni, J., Beretov, J., Graham, P., et al. (2019). Inhibition of PI3K/Akt/mTOR signaling pathway alleviates ovarian cancer chemoresistance through reversing epithelial-mesenchymal transition and decreasing cancer stem cell marker expression. *BMC Cancer* 19:618. doi: 10.1186/s12885-019-5824-9

Escobedo, A., Gomes, T., Aragon, E., Martin-Malpartida, P., Ruiz, L., and Macias, M. J. (2014). Structural basis of the activation and degradation mechanisms of the E3 ubiquitin ligase Nedd4L. *Structure* 22, 1446–1457. doi: 10.1016/j.str.2014.08.016

Fearon, E. R., and Vogelstein, B. (1990). A genetic model for colorectal tumorigenesis. *Cell* 61, 759–767. doi: 10.1016/0092-8674(90)90186-i

Freeman, S. M., and Whartenby, K. A. (2004). The role of the mitogen-activated protein kinase cellular signaling pathway in tumor cell survival and apoptosis. *Drug News Perspect.* 17, 237–242. doi: 10.1358/dnp.2004.17.4.829050

Goyal, P., Behring, A., Kumar, A., and Siess, W. (2009). Identifying and characterizing a novel protein kinase STK35L1 and deciphering its orthologs and close-homologs in vertebrates. *PLoS One* 4:e6981. doi: 10.1371/journal.pone.0006981

Goyal, P., Behring, A., Kumar, A., and Siess, W. (2011). STK35L1 associates with nuclear actin and regulates cell cycle and migration of endothelial cells. *PLoS One* 6:e16249. doi: 10.1371/journal.pone.0016249

Guo, Y., Liang, F., Zhao, F., and Zhao, J. (2020). Resibufogenin suppresses tumor growth and Warburg effect through regulating miR-143-3p/HK2 axis in breast cancer. *Mol. Cell Biochem.* 466, 103–115. doi: 10.1007/s11010-020-03692-z

Guo, Z., Peng, G., Li, E., Xi, S., Zhang, Y., Li, Y., et al. (2017). MAP kinase-interacting serine/threonine kinase 2 promotes proliferation, metastasis, and predicts poor prognosis in non-small cell lung cancer. *Sci. Rep.* 7:10612.

Hamaya, Y., Guarinos, C., Tseng-Rogenski, S. S., Iwaizumi, M., Das, R., Jover, R., et al. (2015). Efficacy of adjuvant 5-fluorouracil therapy for patients with EMAST-positive stage II/III colorectal cancer. *PLoS One* 10:e0127591. doi: 10.1371/journal.pone.00127591

Hou, J., Tan, Y., Su, C., Wang, T., Gao, Z., Song, D., et al. (2020). Inhibition of protein FAK enhances 5-FU chemosensitivity to gastric carcinoma via p53 signaling pathways. *Comput. Struct. Biotechnol. J.* 18, 125–136. doi: 10.1016/j.csbj.2019.12.010

Hourani, M., Berretta, R., Mendes, A., and Moscato, P. (2008). Genetic signatures for a rodent model of Parkinson's disease using combinatorial optimization methods. *Methods Mol. Biol.* 453, 379–392. doi: 10.1007/978-1-60327-429-6_20

Hung, Y. P., Teragawa, C., Kosaisawe, N., Gillies, T. E., Pargett, M., Minguet, M., et al. (2017). Akt regulation of glycolysis mediates bioenergetic stability in epithelial cells. *eLife* 6:e27293. doi: 10.7554/eLife.27293

Kanan, Y., Matsumoto, H., Song, H., Sokolov, M., Anderson, R. E., and Rajala, R. V. (2010). Serine/threonine kinase akt activation regulates the activity of retinal serine/threonine phosphatases, PHLPP and PHLPPL. *J. Neurochem.* 113, 477–488. doi: 10.1111/j.1471-4159.2010.06609.x

La Vecchia, S., and Sebastian, C. (2020). Metabolic pathways regulating colorectal cancer initiation and progression. *Semin. Cell Dev. Biol.* 98, 63–70. doi: 10.1016/j.semcdb.2019.05.018

Li, L., Jones, K., and Mei, H. (2019). Doublecotin-Like Kinase 1 increases chemoresistance of colorectal cancer cells through the anti-apoptosis pathway. *J. Stem Cell Res. Ther.* 9:447.

Liao, Y., and Hung, M. C. (2010). Physiological regulation of Akt activity and stability. *Am. J. Transl. Res.* 2, 19–42.

Lu, Y., Tang, J., Zhang, W., Shen, C., Xu, L., and Yang, D. (2017). Correlation between STK33 and the pathology and prognosis of lung cancer. *Oncol. Lett.* 14, 4800–4804. doi: 10.3892/ol.2017.6766

Ma, L., and Zong, X. (2020). Metabolic symbiosis in chemoresistance: refocusing the role of aerobic glycolysis. *Front. Oncol.* 10:5. doi: 10.3389/fonc.2020.00005

Malinowsky, K., Nitsche, U., Janssen, K. P., Bader, F. G., Spath, C., Drecoll, E., et al. (2014). Activation of the PI3K/AKT pathway correlates with prognosis in stage II colon cancer. *Br. J. Cancer* 110, 2081–2089. doi: 10.1038/bjc.2014.100

Manning, B. D., and Cantley, L. C. (2007). AKT/PKB signaling: navigating downstream. *Cell* 129, 1261–1274. doi: 10.1016/j.cell.2007.06.009

Manning, G., Whyte, D. B., Martinez, R., Hunter, T., and Sudarsanam, S. (2002). The protein kinase complement of the human genome. *Science* 298, 1912–1934. doi: 10.1126/science.1075762

Nitulescu, G. M., Van De Venter, M., Nitulescu, G., Ungurianu, A., Juzenas, P., Peng, Q., et al. (2018). The Akt pathway in oncology therapy and beyond (Review). *Int. J. Oncol.* 53, 2319–2331.

Osaki, M., Oshimura, M., and Ito, H. (2004). PI3K-Akt pathway: its functions and alterations in human cancer. *Apoptosis* 9, 667–676. doi: 10.1023/b:appt.0000045801.15585.dd

Pardini, B., Kumar, R., Naccarati, A., Novotny, J., Prasad, R. B., Forsti, A., et al. (2011). 5-Fluorouracil-based chemotherapy for colorectal cancer and MTHFR/MTRR genotypes. *Br. J. Clin. Pharmacol.* 72, 162–163. doi: 10.1111/j.1365-2125.2010.03892.x

Qian, X., Xu, W., Xu, J., Shi, Q., Li, J., Weng, Y., et al. (2017). Enolase 1 stimulates glycolysis to promote chemoresistance in gastric cancer. *Oncotarget* 8, 47691–47708. doi: 10.18632/oncotarget.17868

Rotin, D., and Kumar, S. (2009). Physiological functions of the HECT family of ubiquitin ligases. *Nat. Rev. Mol. Cell Biol.* 10, 398–409. doi: 10.1038/nrm2690

Siegel, R. L., Miller, K. D., Fedewa, S. A., Ahnen, D. J., Meester, R. G. S., Barzi, A., et al. (2017). Colorectal cancer statistics, 2017. *CA Cancer J. Clin.* 67, 177–193. doi: 10.3322/caac.21395

Slattery, M. L., Mullany, L. E., Wolff, R. K., Sakoda, L. C., Samowitz, W. S., and Herrick, J. S. (2019). The p53-signaling pathway and colorectal cancer: interactions between downstream p53 target genes and miRNAs. *Genomics* 111, 762–771. doi: 10.1016/j.ygeno.2018.05.006

Sun, E., Liu, K., Zhao, K., and Wang, L. (2019). Serine/threonine kinase 32C is overexpressed in bladder cancer and contributes to tumor progression. *Cancer Biol. Ther.* 20, 307–320. doi: 10.1080/15384047.2018.1529098

Tanksley, J. P., Chen, X., and Coffey, R. J. (2013). NEDD4L is downregulated in colorectal cancer and inhibits canonical WNT signaling. *PLoS One* 8:e81514. doi: 10.1371/journal.pone.0081514

Vallenius, T., and Makela, T. P. (2002). Clik1: a novel kinase targeted to actin stress fibers by the CLP-36 PDZ-LIM protein. *J. Cell Sci.* 115, 2067–2073.

Vander Heiden, M. G., Cantley, L. C., and Thompson, C. B. (2009). Understanding the Warburg effect: the metabolic requirements of cell proliferation. *Science* 324, 1029–1033. doi: 10.1126/science.1160809

Wang, Z., Dang, T., Liu, T., Chen, S., Li, L., Huang, S., et al. (2016). NEDD4L protein catalyzes ubiquitination of PIK3CA protein and regulates PI3K-AKT signaling. *J. Biol. Chem.* 291, 17467–17477. doi: 10.1074/jbc.m116.726083

Wu, Z., Liu, J., Hu, S., Zhu, Y., and Li, S. (2018). Serine/Threonine Kinase 35, a Target Gene of STAT3, regulates the proliferation and apoptosis of osteosarcoma cells. *Cell Physiol. Biochem.* 45, 808–818. doi: 10.1159/000487172

Yasuda, Y., Miyamoto, Y., Yamashiro, T., Asally, M., Masui, A., Wong, C., et al. (2012). Nuclear retention of importin alpha coordinates cell fate through changes in gene expression. *EMBO J.* 31, 83–94. doi: 10.1038/emboj.2011.360

Ye, X., Wang, L., Shang, B., Wang, Z., and Wei, W. (2014). NEDD4: a promising target for cancer therapy. *Curr. Cancer Drug Targets* 14, 549–556. doi: 10.2174/1568009614666140725092430

Yu, M., and Grady, W. M. (2012). Therapeutic targeting of the phosphatidylinositol 3-kinase signaling pathway: novel targeted therapies and advances in the treatment of colorectal cancer. *Therap. Adv. Gastroenterol.* 5, 319–337. doi: 10.1177/1756283x12448456

Zeuner, A., Todaro, M., Stassi, G., and De Maria, R. (2014). Colorectal cancer stem cells: from the crypt to the clinic. *Cell Stem Cell* 15, 692–705. doi: 10.1016/j.stem.2014.11.012

Zhang, L., Yang, H., Zhang, W., Liang, Z., Huang, Q., Xu, G., et al. (2017). Clk1-regulated aerobic glycolysis is involved in glioma chemoresistance. *J. Neurochem.* 142, 574–588. doi: 10.1111/jnc.14096

Zhang, Q., Adiseshaiah, P., Kalvakolanu, D. V., and Reddy, S. P. (2006). A Phosphatidylinositol 3-kinase-regulated Akt-independent signaling promotes cigarette smoke-induced FRA-1 expression. *J. Biol. Chem.* 281, 10174–10181. doi: 10.1074/jbc.m513008200

Zheng, H. C. (2017). The molecular mechanisms of chemoresistance in cancers. *Oncotarget* 8, 59950–59964. doi: 10.18632/oncotarget.19048

Zhu, W., Li, Z., Xiong, L., Yu, X., Chen, X., and Lin, Q. (2017). FKBP3 promotes proliferation of non-small cell lung cancer cells through regulating Sp1/HDAC2/p27. *Theranostics* 7, 3078–3089. doi: 10.7150/thno.18067

Conflict of Interest: The authors declare that the research was conducted in the absence of any commercial or financial relationships that could be construed as a potential conflict of interest.

frontiers in Cell and Developmental Biology

ORIGINAL RESEARCH
published: 12 February 2021
doi: 10.3389/fcell.2021.632805

Impaired Barrier Function and Immunity in the Colon of Aldo-Keto Reductase 1B8 Deficient Mice

*Xin Wang[1], Ramina Khoshaba[1,2], Yi Shen[1], Yu Cao[1], Minglin Lin[1], Yun Zhu[1], Zhe Cao[1], Duan-Fang Liao[3] and Deliang Cao[1]**

[1] Department of Medical Microbiology, Immunology & Cell Biology, Simmons Cancer Institute, Southern Illinois University School of Medicine, Springfield, IL, United States, [2] Department of Biotechnology, College of Science, University of Baghdad, Baghdad, Iraq, [3] State Key Laboratory of Chinese Medicine Powder and Medicine Innovation in Hunan (incubation), Division of Stem Cell Regulation and Application, Hunan University of Chinese Medicine, Changsha, China

Aldo-keto reductase 1B10 (AKR1B10) is downregulated in human ulcerative colitis (UC) and colorectal cancer, being a potential pathogenic factor of these diseases. Aldo-keto reductase 1B8 (AKR1B8) is the ortholog in mice of human AKR1B10. Targeted AKR1B8 deficiency disrupts homeostasis of epithelial self-renewal and leads to susceptibility to colitis and carcinogenesis. In this study, we found that in AKR1B8 deficient mice, Muc2 expression in colon was diminished, and permeability of colonic epithelium increased. Within 24 h, orally administered FITC-dextran penetrated into mesenteric lymph nodes (MLN) and liver in AKR1B8 deficient mice, but not in wild type controls. In the colon of AKR1B8 deficient mice, neutrophils and mast cells were markedly infiltrated, γδT cells were numerically and functionally impaired, and dendritic cell development was altered. Furthermore, Th1, Th2, and Th17 cells decreased, but Treg and CD8T cells increased in the colon and MLN of AKR1B8 deficient mice. In colonic epithelial cells of AKR1B8 deficient mice, p-AKT (T308 and S473), p-ERK1/2, p-IKBα, p-p65 (S536), and IKKα expression decreased, accompanied with downregulation of IL18 and CCL20 and upregulation of IL1β and CCL8. These data suggest AKR1B8 deficiency leads to abnormalities of intestinal epithelial barrier and immunity in colon.

Keywords: aldo-keto reductase 1B8, intestinal epithelial cells, intestinal immunity, cytokines, AKT and ERK signaling pathways

OPEN ACCESS

Edited by:
Guangyong Peng,
Saint Louis University, United States

Reviewed by:
Xue-Feng Bai,
The Ohio State University, United States
Chuanlin Ding,
University of Louisville, United States

****Correspondence:***
Deliang Cao
dcao@siumed.edu

Specialty section:
This article was submitted to Cell Death and Survival, a section of the journal Frontiers in Cell and Developmental Biology

Received: *24 November 2020*
Accepted: *07 January 2021*
Published: *12 February 2021*

Citation:
Wang X, Khoshaba R, Shen Y, Cao Y, Lin M, Zhu Y, Cao Z, Liao D-F and Cao D (2021) Impaired Barrier Function and Immunity in the Colon of Aldo-Keto Reductase 1B8 Deficient Mice. Front. Cell Dev. Biol. 9:632805. doi: 10.3389/fcell.2021.632805

INTRODUCTION

Colorectal cancer (CRC) ranks at the third in newly diagnosed cancer cases and is the second leading cause of cancer death in U.S (Siegel et al., 2017). Ulcerative colitis (UC) that affects inner layer of large intestine and rectum is prevalent at about 286 per 100,000 in the U.S. (Ng et al., 2017). A variety of risk factors may contribute to UC and CRC development and progression, including genetics, intestinal immunity, and gut microbiota (Tariq and Ghias, 2016). Intestinal epithelium is the key node in the regulatory network of intestinal function and gut health. Intestinal epithelial cells (IECs) mediates gut immunity (Maloy and Powrie, 2011). In addition to being a physical barrier that separates lamina propria from luminal pathogens, IECs can sense and respond to environmental factors by producing cytokines, mucus, and antimicrobial peptides (AMPs), thus controlling intestinal homeostasis (Peterson and Artis, 2014). IEC defects may leads to intestinal permeability and translocation of luminal pathogens, stimulating aberrant immune

response (Salim and Söderholm, 2011). In Ames dwarf mice with a missense mutation in Prop1 gene, retarded development of intestine deters intestinal innate and adaptive immunity (Wang et al., 2018), and in C57BL/6 mice, targeted disruption of aldo-keto reductase 1B8 (*AKR1B8*) gene disturbs self-renewal of colonic cryptic cells and leads to high susceptibility to dextran sulfate sodium (DSS)-induced colitis and associated carcinogenesis (Shen et al., 2015). Therefore, any genetic or hormonal factors that affect epithelial development and function may lead to a series of sequential abnormalities in epithelial cells and intestinal immunity, eventually causing UC and/or colorectal carcinoma (Hanahan and Weinberg, 2011).

Mouse *AKR1B8* is the ortholog of human aldo-keto reductase 1B10 (*AKR1B10*) (Joshi et al., 2010). AKR1B10 protein is primarily expressed in colon and small intestine (Cao et al., 1998; Joshi et al., 2010) and functions as a monomeric cytosolic enzyme with strong activity to α, β-unsaturated carbonyl compounds, protecting the host cells from carbonyl lesions (Yan et al., 2007; Wang et al., 2009; Zhong et al., 2009; Shen et al., 2011). AKR1B10 also mediates *de novo* synthesis of long chain fatty acids and membrane lipids, such as phosphatidylinositol 4,5-bisphosphate (PIP_2) through regulating acetyl-CoA carboxylase-α (ACCA) stability (Ma et al., 2008). PIP_2 is a critical signal molecule that mediates membrane-based signaling transduction, such as, PI3K/AKT and PKC/ERK pathways (Huang et al., 2018). Interestingly, AKR1B10 is lost and may pathogenically contribute to carcinogenesis in CRC (Zu et al., 2017). Data in microarray datasets (GSE39582) showed that AKR1B10 expression decreased in colon adenocarcinomas at all stages (**Supplementary Figure 1A**), and low expression of AKR1B10 was associated with reduced survival rate, being a potential prognostic marker in colorectal cancer (Taskoparan et al., 2017).

AKR1B10 is also downregulated in UC and colitis-associated colorectal cancer (CAC). Data from microarray datasets GSE38713 in GEO exhibited similar results (**Supplementary Figure 1B**). In UC, AKR1B10 expression decreased in both remitted and active UC. However, little is known of the mechanistic role of AKR1B10 deficiency in the development and progression of these human intestinal diseases. In mice, AKR1B8 deficiency leads to susceptibility to colitis and associated carcinogenesis. This is similar to the phenomenon in human cases, where AKR1B10 expression is diminished. In this study, therefore, *AKR1B8* knockout (–/–) mice were used as a model to investigate its role in intestinal epithelial barrier and immunity and the data indicated the importance of AKR1B8 in the intestinal epithelial integrity and innate and adaptive intestinal immunity, suggesting its potential pathogenic contributions in the intestinal diseases, such as UC and CRC.

MATERIALS AND METHODS

Ethics Statement

Animal protocols were approved by Southern Illinois University School of Medicine Laboratory Animal Care and Use Committee (LACUC; Springfield, IL).

Animals

Mice were housed in the animal facility at Southern Illinois University School of Medicine at 24°C ± 0.5°C, 50% ± 10% humidity with 12 h of light from 8:00 am to 8:00 pm and free access to regular diet and tap water. Heterozygous AKR1B8 knockout (+/–) C57BL/6 mice (Shen et al., 2015) were used to produce homozygous *AKR1B8* knockout (–/–) (KO) and littermate wild-type (WT) mice for experimental studies.

In vivo Intestinal Permeability Assay

Intestinal permeability was measured by oral administration of FITC-dextran (40,00 MW; TdB Consultancy) (0.5 g/kg body weight) to mice for 24 h. At indicated time points, mice were euthanized; mesenteric lymph nodes (MLN) and livers were excised and embedded with OTC for cryostat section using a standard procedure (Hanahan and Weinberg, 2011).

Epithelial Crypt, Single Epithelial Cell, and Lamina Propria Leucocyte Isolation

Epithelial crypts (ECs) and lamina propria cells were isolated from colon as previously reported (Wang et al., 2018). Briefly, ECs were collected using HBSS buffer supplemented with 2% FBS, 5 mM EDTA and 1 mM DTT (American Bioanalytical). Single epithelial cell suspensions were made by digestion of crypts in HBSS containing 0.5 mg/ml of dispase II (Roche) at 37°C for 10 min with intermittent shaking. Lamina propria leukocytes (LPLs) were isolated by digestion of lamina propria tissues in Dulbecco's PBS with 10% FBS, 0.5 mg/ml dispase II, 0.5 mg/ml collagenase D (Roche), and 100 U DNase I (Sigma) at 37°C for two consecutive 20 min. LPLs were then recovered by Percoll gradient centrifugation at 1,000 g for 20 min.

Mesenteric Lymph Node and Spleen Cell Isolation

Mesenteric lymph nodes (MLN) and spleens were cut into small pieces and then squeezed with syringe tips. Single cell suspensions were collected from flow-through of the nylon cell strainer. Red blood cells were removed using lysis buffer (Biolegend).

Cell Staining and Flow Cytometry Analysis

Cells were blocked with anti-mouse CD16/CD32 antibody (Clone 93, BioLegend) and then stained with appropriate cell surface marker antibodies, followed by flow cytometry analysis (Harrington et al., 2005). To assess intracellular IFNγ, IL17, IL4, IL10, and IL22, cells were stimulated with 50 ng/ml Phorbol 12-Myristate 13-Acetate (PMA), followed by fixation, permeabilization and staining with appropriate antibodies (Harrington et al., 2005). A True-Nuclear Transcription Factor Buffer Set (BioLegend) was used for intracellular Foxp3, and 7-amino-actinomycin D (7AAD) was applied for dead cell exclusion. Flow cytometry analysis was performed using an Accuri C6 or BD FACS Aria II flow cytometer, and data were analyzed using a FlowJo software (Tree Star). **Supplementary Figures 2, 3** show the gating strategies of tested cells. All antibodies were purchased from Biolegend. CD3 (100235), CD4 (100413), CD8

(100705), CD11B (101229), CD11C (117305), Ly6G (127613), CD45(103107), IFNγ (505809), IL17 (506907), IL4 (144807), IL10 (505013), IL22 (516404).

Immunofluorescent and Mast Cell Staining

Immunofluorescent assays with 4', 6-diamidino-2-phenylindole (DAPI) for nuclear staining were conducted as previously described (Hall et al., 2013). Mast cells were assessed using paraffin-embedded sections stained with 0.5% toluidine blue (pH 0.3) and eosin (Sigma). After mounting, slides were reviewed and photographed under a microscopy (OLYMPUS DP73).

Real-Time RT-PCR

Total RNA extraction and quantitative real-time RT-PCR with SYBR green qPCR mixture were conducted as previously described (Shen et al., 2015). See **Supplementary Table 1** for gene-specific primer sequences.

Western Blot

Soluble protein preparation and Western blotting were conducted as previously described (Shen et al., 2015). Antibodies are purchased from Cell Signaling Biotechnology. AKT (9272S), p-AKT (4060S/13038S), ERK (4695T), p-ERK (9101S), p-p90RSK (11989S), p-MSK1 (9595T), β-actin (4970S), IKKα (61294S), IKKβ (8943S), p-IKKα/β (2697S), p-IKBα (9246S), t-IKBα (9242S), p-P65 (3033S/ 3037), and P65 (8242T).

Statistical Analysis

Unpaired two-tailed Student *t*-test were applied for statistically significant analysis with $p < 0.05$ as statistical significance. All statistical tests were done using GraphPad software (San Diego, CA).

RESULTS

Increased Colon Mucosal Permeability in *AKR1B8* –/– Mice

Muc2 is a major component of luminal mucus that functions as the first barrier to physically separate luminal pathogens from colonic epithelium (Birchenough et al., 2015). Our results showed that in AKR1B8 deficient epithelium, Muc2 expression was diminished and Muc2 expression goblet cells decreased (**Figure 1A**). Oral administration of mice with FITC-labeled dextran showed that the FITC-dextran appeared in MLN and livers within 24 h in *AKR1B8* –/– mice, but not in littermate wild type (WT) controls (**Figure 1B**). These data indicate the impaired barrier function and increased mucosal permeability in the colon of *AKR1B8* –/– mice.

Enhanced Infiltrations of Neutrophils and Mast Cells in the Colon of *AKR1B8* –/– Mice

The impaired barrier function of colon mucosa may allow luminal pathogen invasion and thus activates inflammatory response. Neutrophils are the first responders in host defense. Our data showed that neutrophils increased in colonic lamina propria (cLP) of *AKR1B8* –/– mice compared to wild type littermates (**Figure 2A**, *upper panel*). Immunofluorescent assays confirmed this finding (**Figure 2A**, *lower panel*). Mast cells also increased in the colon of *AKR1B8* –/– mice (**Figure 2B**), and mast cell-specific protease-1 (mMCP-1) and protease-2 (mMCP-2) expression increased by over 2 times in isolated crypts and LPLs (**Figure 2C**). These data suggest that *AKR1B8* deficiency induces infiltration of neutrophils and mast cells in the colon mucosa.

Numerical and Functional Defects of γδT Cells in the Colon of *AKR1B8* –/– Mice

The γδT cells link innate and adaptive immunity, functioning in antigen presentation, cytokine production and bacterial clearance (Bonneville et al., 2010). We further evaluated γδT cells in the colon of *AKR1B8* –/– mice. Results showed that γδT cells decreased in cLP of *AKR1B8* –/– mice (**Figure 3A**, *upper panel*). This was confirmed by immunofluorescent staining assays (**Figure 3A**, *lower panel*). γδT cells function by secretion of IFNγ, IL17, and IL22 (Bonneville et al., 2010). Our results showed the γδT cells that produce IFNγ (**Figure 3B**), IL17 (**Figure 3C**), and IL22 (**Figure 3D**) all decreased. These data indicate the impaired development and function of γδT cells in the colon of *AKR1B8* –/– mice.

Impaired Antigen Presentation in the Colon and MLN of *AKR1B8* –/– Mice

We then assessed professional antigen presentation cells, dendritic cells (DCs) in the colon and mesenteric lymph nodes (MLN) of *AKR1B8* –/– mice (**Supplementary Figure 3**). Results showed that $CD11c^+$ $MHCII^+$ DCs significantly decreased in colon and MLN (**Figure 4A**). $MHCII^+$ DCs are migratory, which develop in colon and migrate to MLN to present antigens to naïve T cells (Guermonprez et al., 2002). We thus investigated subtypes of $MHCII^+$ DCs using CD11b and CD103 markers. Results showed that CD11b and CD103 subtypes of DCs were not notably changed in colon (**Figure 4B**, *left panel*), but $CD11b^-$ $CD103^+$ DCs increased while $CD11b^+$ $CD103^-$ DCs decreased in the MLN of *AKR1B8* –/– mice (**Figure 4B**, *right panel*). These data suggest that AKR1B8 deficiency disturbs the development of $MHCII^+$ DCs in the colon and MLN.

Decreased T Helper Cells but Increased Cytotoxic T Cells in Colon and MLN of *AKR1B8* –/– Mice

Increased mucosal granulocyte infiltrates and abnormal γδT and DC cells in the colon and MLN of *AKR1B8* –/– mice further impaired adaptive immunity. Our data showed that PMA-stimulated cytokine producing T cells altered remarkably in *AKR1B8* –/– mice (**Figure 5**) although the number of total T cells (CD3T) and subtypes (CD4T and CD8T) were not notably changed (**Supplementary Figure 4A**). In the MLN, IFNγ, IL4 and IL17-producing CD4T (i.e., Th1, Th2, and Th17) cells all decreased (**Figure 5A**), but IFNγ and IL17-producing CD8T (Tc1 and Tc17) cells increased while IL4-producing CD8T (Tc2) cells decreased (**Figure 5B**). In the colon of *AKR1B8* –/– mice, IFNγ and IL17-producing CD4T cells also decreased, but IL4-producing CD4T cells (**Supplementary Figure 4B**) and IFNγ, IL17 and IL4-producing CD8T cells (**Supplementary Figure 4C**)

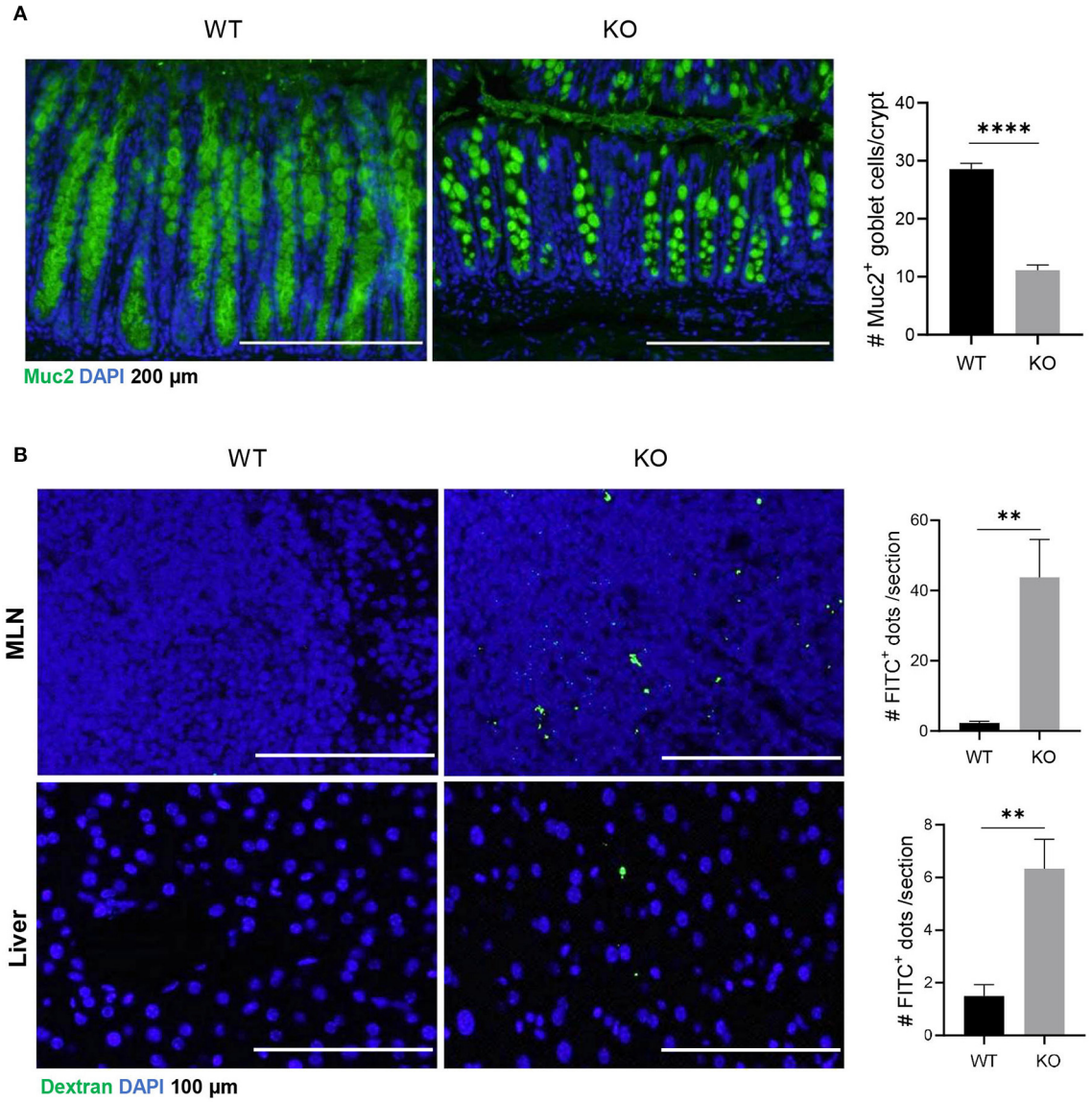

FIGURE 1 | Decreased muc2 expression and increased permeability of colonic epithelium in *AKR1B8 –/–* mice. **(A)** Muc2 expression (green) in colon, detected by immunofluorescent staining. DAPI (blue) was used for nuclear staining. Scale bars, 200 μm. Muc2-producing goblet cells per crypt were counted (*right*). Data indicate mean ± SEM. **(B)** FITC-Dextran in mesenteric lymph nodes (MLN, *upper panel*) and liver (*lower panel*). FITC signals per section were quantitated with an ImageJ software (*right*). Nuclei were stained with DAPI (Blue). Scale bars, 100 μm. WT, wild-type; KO, *AKR1B8 –/–*. *$P < 0.05$; **$P < 0.01$; ***$P < 0.001$; ****$P < 0.0001$.

were not altered. CD4T and CD8T cells are developed and matured in MLN and then disseminated into colon mucosa. This may explain the differential displays of T cells in MLN and colon.

We further investigated Treg cells in *AKR1B8 –/–* mouse colon. Results showed Foxp3$^+$ Treg cells for immune tolerance and suppression increased in MLN of *AKR1B8 –/–* mice (**Figure 5C**) and tended to increase in colon ($p = 0.065$) (**Supplementary Figure 4D**), but IL10-producing Treg cells were not notably changed in MLN and colon (**Figure 5D** and **Supplementary Figure 4E**), indicating a balanced steady status. Together these data suggest that AKR1B8 deficiency alters T cell immunity with decreased CD4T but increased CD8T activity.

Inhibition of AKT, ERK, and NF-κB Signaling Cascades in cECs of *AKR1B8 –/–* Mice

This *AKR1B8 –/–* mouse strain is conventional, and thus we first examined AKR1B8 expression in colon epithelial cells (cECs) and immune cells from MLN. Results showed that AKR1B8 was highly expressed in cECs of wild type mice, but nullified in *AKR1B8 –/–* mice (**Figure 6A**); AKR1B8 was not expressed in immune cells (**Figure 6A**). These data indicate that *AKR1B8* knockout would not have direct effects on immune cells as AKR1B8 is not expressed; and the intestinal immune defects in *AKR1B8 –/–* mice may be derived from cEC deficiency.

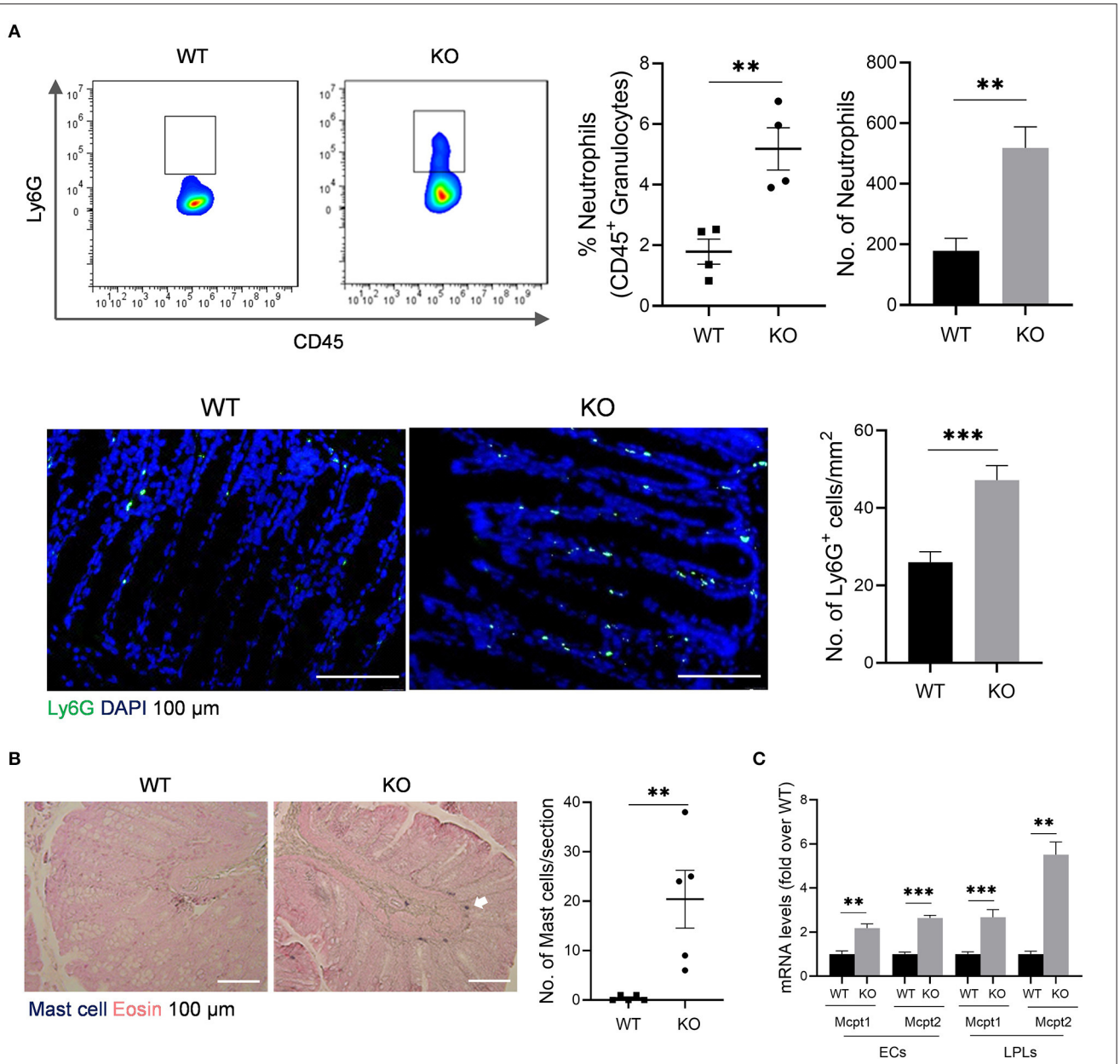

FIGURE 2 | Granulocyte infiltrates in the colon of *AKR1B8 –/–* mice. **(A)** Neutrophils. *Upper panel*: flow cytometry. Lamina propria leukocytes (LPLs) were isolated from colons and subjected to flow cytometry analysis as described in Materials and Methods. *Left*, flow cytometry images; *middle*, percentage of neutrophils in $CD45^+$ granulocytes; *right*, number of neutrophils in 10^4 $CD45^+$ granulocytes. *Lower panel*: immunofluorescent staining of neutrophils. *Left*, FITC-labeled Ly6G and DAPI staining images, scale bar: 20 μm; *right*, Ly6G positive cell number per mm^2. **(B).** Mast cells. *Left*, toluidine blue and eosin staining images, scale bar: 100 μm; white arrow: mast cells. *Right,* mast cell number per section. **(C).** Expression levels of mast cell protease 1 and 2 in colonic epithelial crypts (cECs) and isolated LPLs. Data shown are quantitative RT-PCR results. WT, wild-type; KO, *AKR1B8 –/–*. Data denote mean ± SEM of four mice per group. $^*P < 0.05$; $^{**}P < 0.01$; $^{***}P < 0.001$, independent samples t-test.

We further examined the expression of immunoregulatory cytokines in cECs and data showed that immunoregulatory IL18 and CCL20 were downregulated while IL1β and CCL18 were upregulated in cECs of *AKR1B8 –/–* mice (**Figure 6B**).

We then explored the signaling transduction that results in deficiency and abnormal expression of cytokines in cECs. AKR1B10 (AKR1B8 in mice) promotes long chain fatty acid and membrane lipid synthesis and activates PIP_2 lipid messenger system (Ma et al., 2008; Huang et al., 2018). PIP_2 mediates PI3K/AKT and PKC/ERK signaling transduction (Luo et al., 2003). We thus evaluated AKT and ERK activity in cECs. Data showed that p-AKT (T308 & S473) and p-ERK decreased in *AKR1B8 –/–* cECs (**Figure 6C**); ERK downstream effectors p-RSK90 and p-MSK1 also decreased (**Figure 6C**).

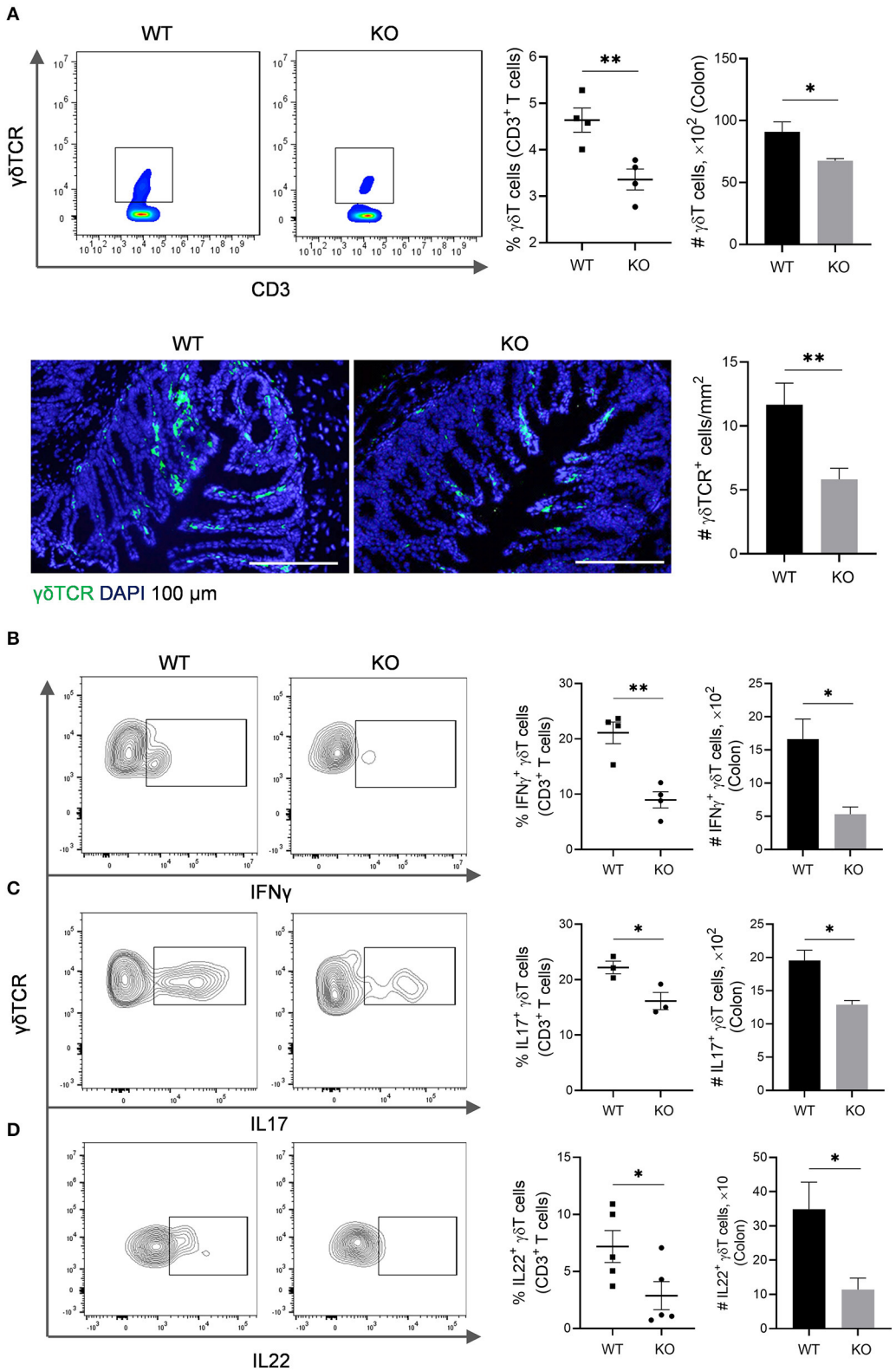

FIGURE 3 | γδT cells in the colon of *AKR1B8 –/–* mice. **(A)** γδT cell number. *Upper panel*: Flow cytometry. Lamina propria leukocytes (LPLs) were isolated from colons and subjected to flow cytometry analysis as described in Materials and Methods. *Left*, flow cytometry images; *middle,* percentage of γδT cells in $CD3^+$ T cells; *right*, number of γδT cells in 10^4 $CD3^+$ T cells. *Lower panel*: Immunofluorescent staining of γδT cells. *Left*, FITC-labeled γδTCR and DAPI staining images, scale

(Continued)

FIGURE 3 | bar: 20 μm; *right*, γδTCR positive cell number per mm^2. **(B–D)** IFNγ, IL17, and IL22-producing γδT cells. LPLs were isolated from colon and stimulated with PMA and ionomycin in presence of protein transport inhibitor for 5 h, followed by staining for CD3, γδTCR, and then IFN-γ, IL17, or IL22. *Left*, flow cytometry images; *middle,* percentage of IFNγ, IL17, and IL22-producing γδT cells in total γδT cells*; right*, number of IFNγ, IL17, and IL22-producing γδT in 10^4 γδT cells. WT, wild-type; KO, *AKR1B8 –/–*. Data indicate mean ± of SEM of four mice per group. $^*P < 0.05$; $^{**}P < 0.01$.

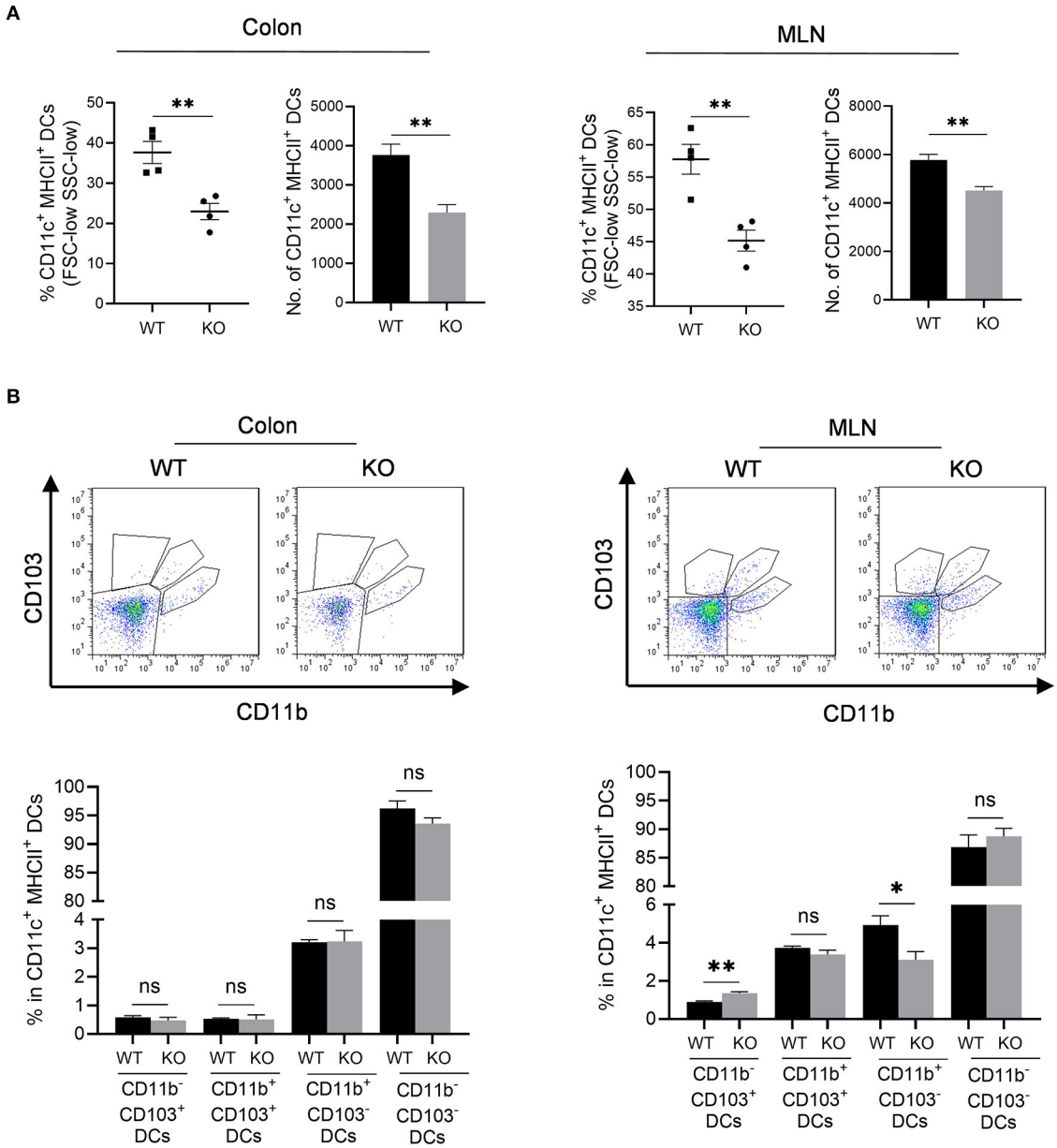

FIGURE 4 | Antigen presentation cells in colon and MLN of *AKR1B8 –/–* mice. Lamina propria leukocytes (LPLs) and mesenteric lymph node (MLN) cells were isolated and analyzed by flow cytometry as described in Materials and Methods. **(A)** $MHCII^+$ dendritic cells in colonic lamina propria and MLN. *Left*, percentage of $CD11c^+$ $MHCII^+$ DCs in FSC-low SSC-low mononuclear cells; *right,* number of $CD11c^+$ $MHCII^+$ DCs in 10^4 FSC-low SSC-low mononuclear cells. **(B)** DC subtypes in colon and MLN. *Upper*, flow cytometry images; *lower*, percentage of $CD103^+$ DC subsets in $CD11c^+$ $MHCII^+$ DCs. WT, wild-type; KO, *AKR1B8 –/–*. Data indicate mean ± SEM of four mice per group. $^*P < 0.05$; $^{**}P < 0.01$.

NF-κB is a master signaling cascade that regulates cytokine expression and immune response; IκB is a main negative regulator that holds NF-κB homo- or heterodimers in cytosol. AKT phosphorylates Thr23 of IKKα and activates IKKα, which in turn phosphorylates IκBα and triggers NF-κB nuclear translocation (Romashkova and Makarov, 1999). ERK

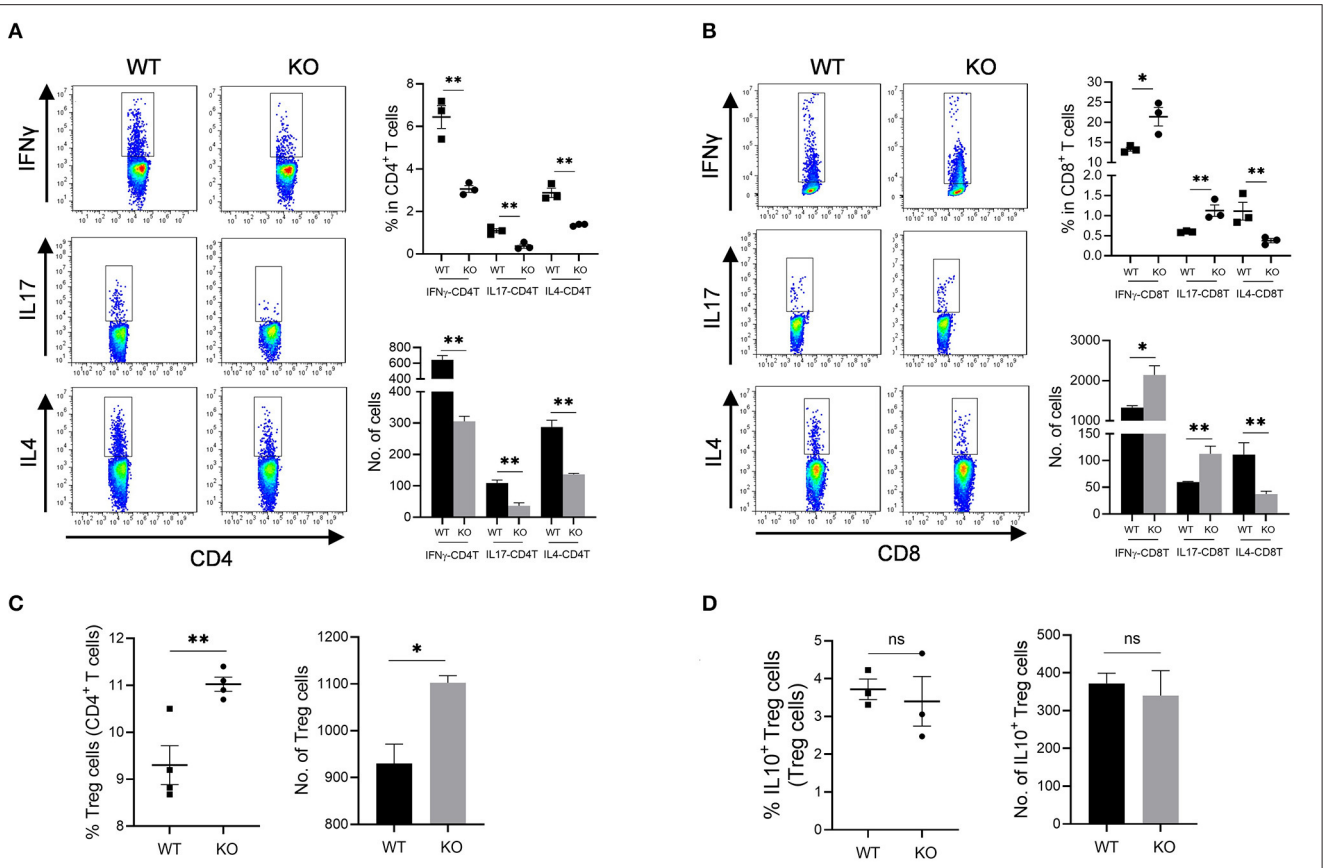

FIGURE 5 | Adaptive CD4T and CD8T cells in MLN of *AKR1b8 –/–* mice. Mesenteric lymph node (MLN) cells were isolated and analyzed by flow cytometry as described in Materials and Methods. **(A)** IFNγ, IL17, and IL4-producing CD4T helper cells. *Left panel*, flow cytometry images of IFNγ-CD4T (Th1), IL17-CD4T (Th17), and IL4-CD4T (Th2) cells; *right upper,* percentage of IFNγ, IL17, and IL4-CD4T in total CD4T cells, *right lower*, number of IFNγ, IL17, and IL4-CD4T cells in 10^4 CD4T cells. **(B).** IFNγ, IL17 and IL4-producing cytotoxic CD8T cells. *Left panel*, flow cytometry images of IFNγ-CD8T (Tc1), IL17-CD8T (Tc17), and IL4-CD8T (Tc2) cells; *right upper,* percentage of IFNγ, IL17 and IL4-CD8T in CD8T cells, *right lower*, number of IFNγ, IL17, and IL4-CD8T cells in 10^4 CD8T cells. **(C)** $CD4^+$ Treg cells. *Left,* percentage of $CD4^+$ Treg cells in CD4T cells; *right,* number of Treg cells in 10^4 CD4T cells. **(D)** IL10-producing Treg cells. *Left,* percentage of IL10-producing Treg cells in total Treg cells; *right,* number of IL10-producing Treg cells in 10^4 total Treg cells. WT, wild-type; KO, *AKR1B8 –/–*. Data represent mean ± SEM form four mice per group. $^*P < 0.05$; $^{**}P < 0.01$.

also activates NF-κB signaling through phosphorylation and activation of RSK90 and MSK1 that in turn phosphorylate p65/RelA at Ser536 (Wang et al., 2010). Our data showed that in cECs of *AKR1B8 –/–* mice, p-IKKα/β, p-IKBα and p-p65 (Ser536) all decreased (**Figure 6D**). Together our data suggest that AKR1B8 deficiency inhibits AKT and ERK signaling activity in cECs that in turn impedes the NF-κB signaling cascade, deregulating immunoregulatory cytokine expression and intestinal immunity.

DISCUSSION

Muc2 is produced by goblet cells and secreted to line on the epithelial layer of intestine, where it functions as a physical barrier to block luminal pathogen invasion. Decreased Muc2 production associates with UC in humans (Van der Sluis et al., 2006), and *Muc2 –/–* causes spontaneous colitis in mice (Van Klinken et al., 1999), suggesting its critical role in intestinal health. AKR1B8 deficiency disrupts self-renewal and injury repair of colon epithelial cells and thus the mice were susceptibility to DSS-induced colitis and associated carcinogenesis (Shen et al., 2015). This study investigated the function of AKR1B8 in intestinal epithelial barrier and immunity under naïve status. We found that Muc2 expression in goblet cells decreased and mucosal permeability increased; the intestinal immunity was re-shaped.

Innate immune cells respond as the first line and function for extracellular clearance of pathogens. Results showed that neutrophils and mast cells increased in the colon of *AKR1B8 –/–* mice. Mast cell proteases, mCPT1 and mCPT2, are predominant products expressed by mast cells and function for extracellular microbial or parasite clearance (Urb and Sheppard, 2012). The increased expression of mCPT1 and mCPT2 in crypts and LPL isolates of *AKR1B8 –/–* colon confirmed the mast cell infiltrations. Mast cell proteases induce tissue injury and

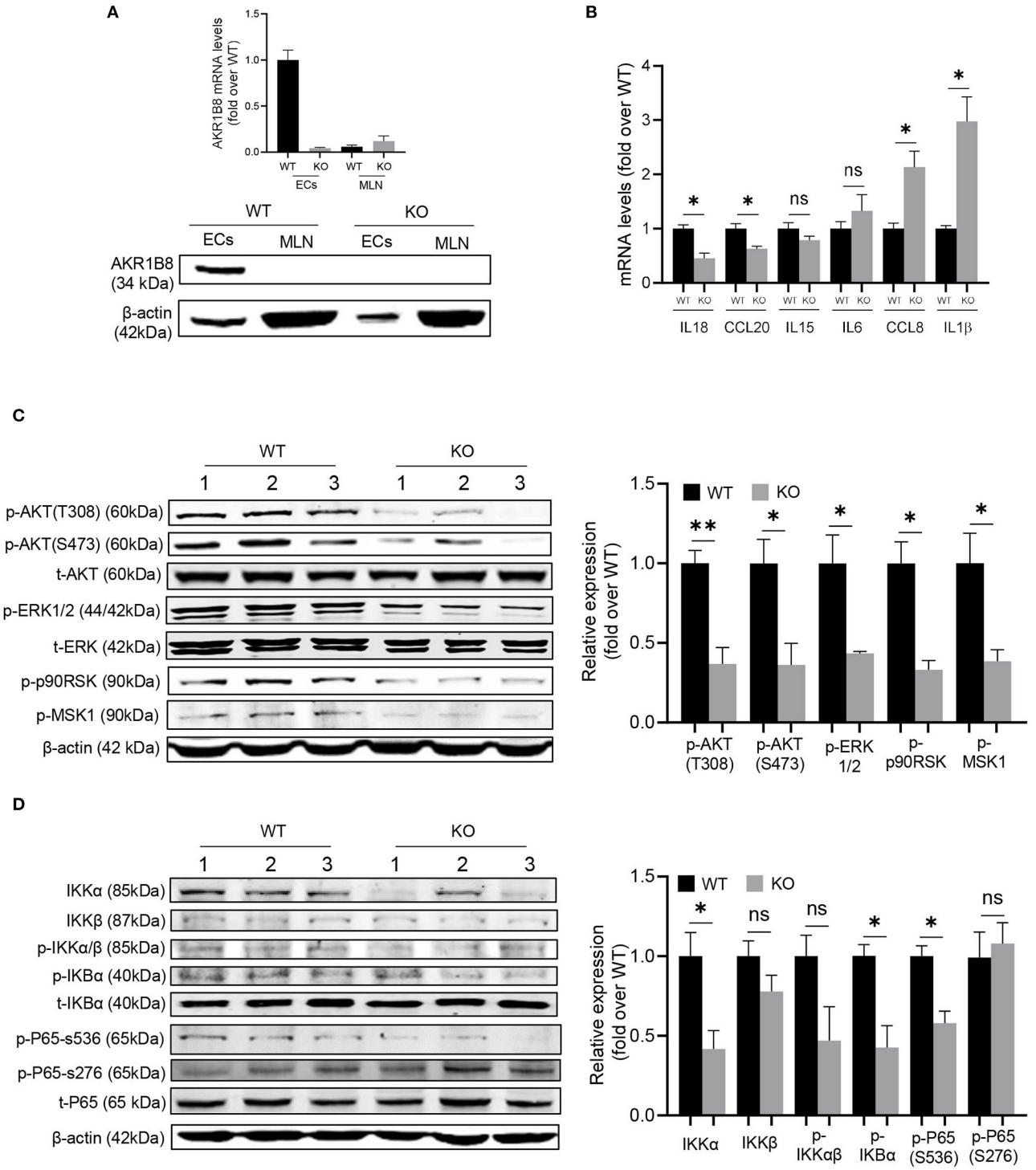

FIGURE 6 | Molecular mechanisms of intestinal immune defects in *AKR1B8 –/–* mice. **(A)** AKR1B8 expression in colonic epithelial cells (ECs) and immune cells from mesenteric lymph nodes (MLN). RNA and proteins were extracted for qRT-PCR (*upper panel*) and Western blot (*lower panel*) analyses as described in Materials and Methods. **(B)** Expression of IL18, CCL20, IL15, IL6, CCL8, and IL1β cytokines in ECs. Data indicate qRT-PCR results as described in Materials and Methods. **(C)** AKT and ERK signaling activity. The p-AKT (Ser473), p-AKT (Thr308), t-AKT, p-ERK (1/2), t-ERK, p-p90RSK and p-MSK1 proteins were analyzed by Western blot as described in Materials and Methods. β-actin was used as an internal control. *Left panel*, representative images; *right panel*, quantitative data of band intensity by Image J software. Data were normalized by respective total proteins. **(D)** NF-κB signal activity. IKKα, IKKβ, p-IKKα/β, p-IKBα, t-IKBα, p-P65 (S536), p-P65 (S276), and t-P65 protein levels were analyzed by Western blot. *Left panel*, representative images; *right panel*, quantitative data of band intensity by Image J software. Data of phosphorylated proteins were normalized by respective total proteins. Data of IKKα and IKKβ were normalized by β-actin. WT, wild-type; KO, *AKR1B8 –/–*. Data represent mean ± SEM of three to four mice per group. $^{*}P < 0.05$; $^{**}P < 0.01$.

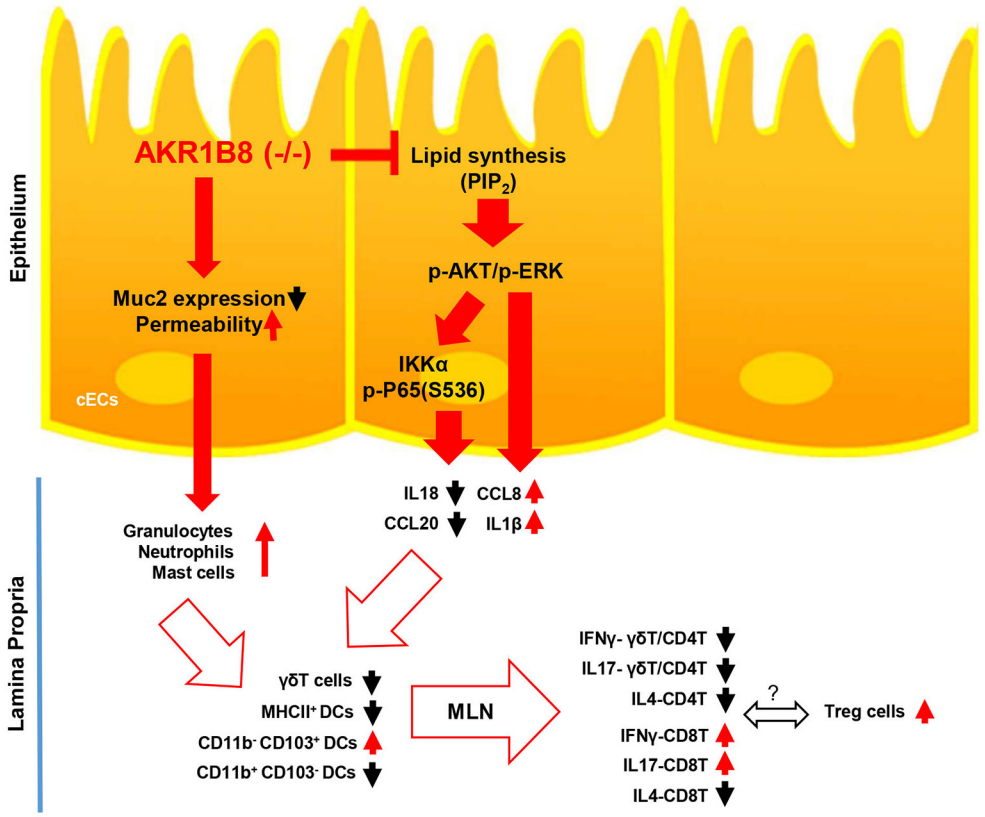

FIGURE 7 | Hypothetic model of AKR1B8 in regulation of intestinal immunity. AKR1B8 deficiency leads to decrease of Muc2 expression and increase of epithelial permeability, triggering inflammatory cell infiltration; AKR1B8 deficiency diminishes synthesis of long chain fatty acid/membrane lipids (e.g., PIP_2), which attenuates AKT and ERK signaling activity and in turn inhibits NF-κB signaling activity. Diminished AKT, ERK, and NF-κB signaling activity deregulates the expression of immunoregulatory cytokines, which together with infiltrated granulocytes impairs development and function of innate immune γδT cells and antigen presentation dendritic cells, eventually leading to defects of adaptive immune cells.

permeability, triggering inflammation (Urb and Sheppard, 2012), which supports the fact that *AKR1B8* –/– mice are susceptible to DSS-induced colitis and colitis associated carcinogenesis (Shen et al., 2015).

Neutrophils and mast cells suppress γδT and CD4T cell function (Kalyan et al., 2014; Sabbione et al., 2014). The γδT cells are critical immune mediators in intestine; mice that lack γδT cells are susceptible to DSS-induced colitis (Kober et al., 2014). Consistently, γδT cells were defective in number and function in the colon of *AKR1B8* –/– mice that are susceptible to DSS-induced colitis. Through a major histocompatibility complex class II (MHCII)-mediated mechanism, professional antigen presentation cells DCs uptake and present microbial antigens to naïve T lymphocytes, thus initiating adaptive immune response. MHCII deficiency inhibits antigen presentation and leads to immunodeficiency (Chen and Jensen, 2008). To our surprise, total $MHCII^+$ DCs decreased in the colon and MLN of *AKR1B8* –/– mice. Subtype analysis of $MHCII^+$ DCs revealed that $CD11b^-$ $CD103^+$ DCs increased, but $CD11b^+$ $CD103^-$ DCs decreased in MLN; the subtypes of $MHCII^+$ DCs were not altered notably in colon. This is understandable as $MHCII^+$ DCs are migratory to flare the adaptive immunity in MLN. Development and maturation of $MHCII^+$ DCs and subtypes are multifactorial, including antigen species and concentrations, uptake pathways and cytokine microenvironments (Randolph et al., 2008). Nevertheless, $CD11b^-$ $CD103^+$ DCs are involved in antigen cross-presentation and priming of CD8T cells (Ruane and Lavelle, 2011); $CD11b^-$ $CD103^+$ DCs are also a crucial mediator of Treg cells that works in immune tolerance (Coombes et al., 2007). In contrast, $CD11b^+$ $CD103^-$ DCs are involved in priming of Th1 and Th17 CD4T cells (Liang et al., 2016). Consistently, the IFNγ and IL17-producing CD8T and Treg cells increased, but Th1 and Th17 cells decreased in *AKR1B8* –/– mice. In summary, in the *AKR1B8* –/– colon, abnormal innate immune cell infiltration occurred, and γδT cells were dysfunctional and DC development was changed, eventually re-shaping the adaptive immunity.

CD8T cells are cytotoxic T cells (Tc) and function to defense against intracellular pathogens. The increased IFNγ (Tc1) and IL17 (Tc17)-producing CD8T cells may represent a compensatory mechanism to the decreased IFNγ (Th1) and IL17 (Th17)-producing CD4T for pathogen clearance. This makes the

colonic immunity at a new balance in *AKR1B8* deficiency, thus being free of spontaneous colitis. However, IL4-producing CD4T and CD8T cells both decreased, which may indicate vulnerability of *AKR1B8* –/– mice to external stimuli, such as DSS. This is consistent to literature reports that IL-4 knockout mice are susceptible to infection (Noben-Trauth et al., 1996). Treg cells are immune suppressors of effector T cells, i.e., Th1 and Th17 (Paust and Cantor, 2005). In the MLN and colon of *AKR1B8* –/– mice, Treg cells increased, but functional IL-10 producing Treg cells were not, which may represent a feedback to balance the Treg function in *AKR1B8* –/– mice.

AKR1B10 is an important regulator of fatty acid/lipid *de novo* synthesis, regulating the PIP_2 lipid second messenger. Mouse AKR1B8 is the ortholog of human AKR1B10 and mediates fatty acid and lipid synthesis (Joshi et al., 2010). PIP_2 is a central mediator of AKT and ERK signaling cascades that regulate IECs proliferation, adhesion and integrity (Zhao et al., 2018). NF-κB is a central signaling pathway that regulates cytokine expression. AKT and ERK are involved in the regulation of NF-κB signaling activity via controlling expression and phosphorylation of key effector molecules, such as IKKα and RelA/p65. The decreased p-AKT, p-ERK, p-IKKα/β, p-IKBα and p-p65 (Ser536) in cEC of *AKR1B8* –/– mice proved the concept that AKR1B8 mediates the PI3K/AKT and PKC/ERK signaling pathways and subsequently the NF-κB activity. AKT and ERK signaling also directly triggers IL-18 expression (Niyonsaba et al., 2005; Venkatesan et al., 2010). Therefore, inhibition of AKT and ERK signaling by AKR1B8 deficiency may induce intestinal immune defects directly or through a NF-κB mediated mechanism. In addition, both AKT (Lee et al., 2010) and ERK (Damiano et al., 2018) signaling regulate Muc2 expression, and accordingly Muc2 was downregulated in the goblet cells of *AKR1B8* –/– mice and barrier function of colonic epithelium was impaired, which in turn triggered innate immune cell infiltration. It is warranted to dissect in more detail the molecular regulation of cytokine expression and immune response in *AKR1B8* –/– mice.

In conclusion, this study demonstrated the essential role of AKR1B8 in control of intestinal epithelial function and immunity (**Figure 7**). AKR1B8 deficiency leads to barrier dysfunction and permeability, activating infiltration of granulocytes; AKR1B8 deficiency inhibits AKT and ERK activity and thus disrupts the expression of cytokines, leading to defects of intestinal innate and adaptive immunity. This work unraveled the key role of AKR1B8 in cECs function and intestinal immunity, providing new insights in the regulation of intestinal homeostasis and health.

DATA AVAILABILITY STATEMENT

The raw data supporting the conclusions of this article will be made available by the authors, without undue reservation.

ETHICS STATEMENT

The animal study was reviewed and approved by Southern Illinois University School of Medicine Laboratory Animal Care and Use Committee.

AUTHOR CONTRIBUTIONS

DC and XW designed the research. XW and YS performed animal experiments. XW, YC, and ML performed flow cytometry experiments and analysis. XW, RK, and YZ performed molecular biology experiments. DC and XW wrote the manuscript. D-FL and DC revised the manuscript. All authors contributed to the article and approved the submitted version.

SUPPLEMENTARY MATERIAL

The Supplementary Material for this article can be found online at: https://www.frontiersin.org/articles/10.3389/fcell.2021.632805/full#supplementary-material

REFERENCES

Birchenough, G., Johansson, M. E., Gustafsson, J., Bergström, J., and Hansson, G. (2015). New developments in goblet cell mucus secretion and function. *Mucosal Immunol.* 8, 712–719. doi: 10.1038/mi.2015.32

Bonneville, M., O'brien, R. L., and Born, W. K. (2010). [gamma][delta] T cell effector functions: a blend of innate programming and acquired plasticity. *Nat. Rev. Immunol.* 10:467. doi: 10.1038/nri2781

Cao, D., Fan, S. T., and Chung, S. S. (1998). Identification and characterization of a novel human aldose reductase-like gene. *J. Biol. Chem.* 273, 11429–11435. doi: 10.1074/jbc.273.19.11429

Chen, X., and Jensen, P. E. (2008). MHC class II antigen presentation and immunological abnormalities due to deficiency of MHC class II and its associated genes. *Exp. Mol. Pathol.* 85, 40–44. doi: 10.1016/j.yexmp.2008.03.011

Coombes, J. L., Siddiqui, K. R., Arancibia-Cárcamo, C. V., Hall, J., Sun, C.-M., Belkaid, Y., et al. (2007). A functionally specialized population of mucosal CD103+ DCs induces Foxp3+ regulatory T cells via a TGF-β-and retinoic acid–dependent mechanism. *J. Exp. Med.* 204, 1757–1764. doi: 10.1084/jem.20070590

Damiano, S., Sasso, A., De Felice, B., Di Gregorio, I., La Rosa, G., Lupoli, G. A., et al. (2018). Quercetin increases MUC*2* and MUC5AC gene expression and secretion in intestinal goblet cell-like LS174T via PLC/PKCα/ERK1-2 pathway. *Front. Physiol.* 9:357. doi: 10.3389/fphys.2018.00357

Guermonprez, P., Valladeau, J., Zitvogel, L., Théry, C., and Amigorena, S. (2002). Antigen presentation and T cell stimulation by dendritic cells. *Annu. Rev. Immunol.* 20, 621–667. doi: 10.1146/annurev.immunol.20.100301.064828

Hall, L. J., Murphy, C. T., Hurley, G., Quinlan, A., Shanahan, F., Nally, K., et al. (2013). Natural killer cells protect against mucosal and systemic infection with the enteric pathogen *Citrobacter rodentium*. *Infect. Immun.* 81, 460–469. doi: 10.1128/IAI.00953-12

Hanahan, D., and Weinberg, R. A. (2011). Hallmarks of cancer: the next generation. *Cell* 144, 646–674. doi: 10.1016/j.cell.2011.02.013

Harrington, L. E., Hatton, R. D., Mangan, P. R., Turner, H., Murphy, T. L., Murphy, K. M., et al. (2005). Interleukin 17–producing CD4+ effector T cells develop via a lineage distinct from the T helper type 1 and 2 lineages. *Nat. Immunol.* 6:1123. doi: 10.1038/ni1254

Huang, C., Cao, Z., Ma, J., Shen, Y., Bu, Y., Khoshaba, R., et al. (2018). AKR1B10 activates diacylglycerol (DAG) second messenger in breast cancer cells. *Mol. Carcinog.* 57, 1300–1310. doi: 10.1002/mc.22844

Joshi, A., Rajput, S., Wang, C., Ma, J., and Cao, D. (2010). Murine aldo-keto reductase family 1 subfamily B: identification of AKR1B8 as an ortholog of human AKR1B10. *Biol. Chem.* 391, 1371–1378. doi: 10.1515/bc.2010.144

Kalyan, S., Chandrasekaran, V., Quabius, E. S., Lindhorst, T. K., and Kabelitz, D. (2014). Neutrophil uptake of nitrogen-bisphosphonates leads to the suppression of human peripheral blood γδ T cells. *Cell. Mol. Life Sci.* 71, 2335–2346. doi: 10.1007/s00018-013-1495-x

Kober, O. I., Ahl, D., Pin, C., Holm, L., Carding, S. R., and Juge, N. (2014). γδ T-cell-deficient mice show alterations in mucin expression, glycosylation, and goblet cells but maintain an intact mucus layer. *Am. J. Physiol. Gastrointestinal Liver Physiol.* 306, G582–G593. doi: 10.1152/ajpgi.00218.2013

Lee, H. Y., Crawley, S., Hokari, R., Kwon, S., and Kim, Y. S. (2010). Bile acid regulates MUC2 transcription in colon cancer cells via positive EGFR/PKC/Ras/ERK/CREB, PI3K/Akt/IκB/NF-κB and p38/MSK1/CREB pathways and negative JNK/c-Jun/AP-1 pathway. *Int. J. Oncol.* 36, 941–953. doi: 10.3892/ijo_00000573

Liang, J., Huang, H. I., Benzatti, F. P., Karlsson, A. B., Zhang, J. J., Youssef, N., et al. (2016). Inflammatory Th1 and Th17 in the intestine are each driven by functionally specialized dendritic cells with distinct requirements for MyD88. *Cell Rep.* 17, 1330–1343. doi: 10.1016/j.celrep.2016.09.091

Luo, J., Manning, B. D., and Cantley, L. C. (2003). Targeting the PI3K-Akt pathway in human cancer. *Cancer Cell* 4, 257–262. doi: 10.1016/S1535-6108(03)00248-4

Ma, J., Yan, R., Zu, X., Cheng, J. M., Rao, K., Liao, D. F., et al. (2008). Aldo-keto reductase family 1 B10 affects fatty acid synthesis by regulating the stability of acetyl-CoA carboxylase-alpha in breast cancer cells. *J. Biol. Chem.* 283, 3418–3423. doi: 10.1074/jbc.M707650200

Maloy, K. J., and Powrie, F. (2011). Intestinal homeostasis and its breakdown in inflammatory bowel disease. *Nature* 474, 298. doi: 10.1038/nature10208

Ng, S. C., Shi, H. Y., Hamidi, N., Underwood, F. E., Tang, W., Benchimol, E. I., et al. (2017). Worldwide incidence and prevalence of inflammatory bowel disease in the 21st century: a systematic review of population-based studies. *Lancet* 390, 2769–2778. doi: 10.1016/S0140-6736(17)32448-0

Niyonsaba, F., Ushio, H., Nagaoka, I., Okumura, K., and Ogawa, H. (2005). The human β-defensins (-1,-2,-3,-4) and cathelicidin LL-37 induce IL-18 secretion through p38 and ERK MAPK activation in primary human keratinocytes. *J. Immunol.* 175, 1776–1784. doi: 10.4049/jimmunol.175.3.1776

Noben-Trauth, N., Kropf, P., and Müller, I. (1996). Susceptibility to *Leishmania* major infection in interleukin-4-deficient mice. *Science* 271, 987–990. doi: 10.1126/science.271.5251.987

Paust, S., and Cantor, H. (2005). Regulatory T cells and autoimmune disease. *Immunol. Rev.* 204, 195–207. doi: 10.1111/j.0105-2896.2005.00247.x

Peterson, L. W., and Artis, D. (2014). Intestinal epithelial cells: regulators of barrier function and immune homeostasis. *Nat. Rev. Immunol.* 14, 141–153. doi: 10.1038/nri3608

Randolph, G. J., Ochando, J., and Partida-Sánchez, S. (2008). Migration of dendritic cell subsets and their precursors. *Annu. Rev. Immunol.* 26, 293–316. doi: 10.1146/annurev.immunol.26.021607.090254

Romashkova, J. A., and Makarov, S. S. (1999). NF-κB is a target of AKT in anti-apoptotic PDGF signalling. *Nature* 401:86. doi: 10.1038/43474

Ruane, D. T., and Lavelle, E. C. (2011). The role of CD103+ dendritic cells in the intestinal mucosal immune system. *Front. Immunol.* 2:25. doi: 10.3389/fimmu.2011.00025

Sabbione, F., Gabelloni, M. L., Ernst, G., Gori, M. S., Salamone, G., Oleastro, M., et al. (2014). Neutrophils suppress γδ T-cell function. *Eur. J. Immunol.* 44, 819–830. doi: 10.1002/eji.201343664

Salim, S. Y., and Söderholm, J. D. (2011). Importance of disrupted intestinal barrier in inflammatory bowel diseases. *Inflamm. Bowel Dis.* 17, 362–381. doi: 10.1002/ibd.21403

Shen, Y., Ma, J., Yan, R., Ling, H., Li, X., Yang, W., et al. (2015). Impaired self-renewal and increased colitis and dysplastic lesions in colonic mucosa of AKR1B8-deficient mice. *Clin. Cancer Res.* 21, 1466–1476. doi: 10.1158/1078-0432.CCR-14-2072

Shen, Y., Zhong, L., Johnson, S., and Cao, D. (2011). Human aldo-keto reductases 1B1 and 1B10: a comparative study on their enzyme activity toward electrophilic carbonyl compounds. *Chem. Biol. Interact.* 191, 192–198. doi: 10.1016/j.cbi.2011.02.004

Siegel, R. L., Miller, K. D., and Jemal, A. (2017). Cancer statistics, 2017. *CA Cancer J. Clin.* 67, 7–30. doi: 10.3322/caac.21387

Tariq, K., and Ghias, K. (2016). Colorectal cancer carcinogenesis: a review of mechanisms. *Cancer Biol. Med.* 13:120. doi: 10.20892/j.issn.2095-3941.2015.0103

Taskoparan, B., Seza, E. G., Demirkol, S., Tuncer, S., Stefek, M., Gure, A. O., et al. (2017). Opposing roles of the aldo-keto reductases AKR1B1 and AKR1B10 in colorectal cancer. *Cell. Oncol.* 40, 563–578. doi: 10.1007/s13402-017-0351-7

Urb, M., and Sheppard, D. C. (2012). The role of mast cells in the defence against pathogens. *PLoS Pathog.* 8:e1002619. doi: 10.1371/journal.ppat.1002619

Van der Sluis, M., De Koning, B. A., De Bruijn, A. C., Velcich, A., Meijerink, J. P., Van Goudoever, J. B., et al. (2006). Muc2-deficient mice spontaneously develop colitis, indicating that MUC2 is critical for colonic protection. *Gastroenterology* 131, 117–129. doi: 10.1053/j.gastro.2006.04.020

Van Klinken, B. J., Van der Wal, J. G., Einerhand, A., Büller, H., and Dekker, J. (1999). Sulphation and secretion of the predominant secretory human colonic mucin MUC2 in ulcerative colitis. *Gut* 44, 387–393. doi: 10.1136/gut.44.3.387

Venkatesan, B., Valente, A. J., Prabhu, S. D., Shanmugam, P., Delafontaine, P., and Chandrasekar, B. (2010). EMMPRIN activates multiple transcription factors in cardiomyocytes, and induces interleukin-18 expression via Rac1-dependent PI3K/Akt/IKK/NF-κB andMKK7/JNK/AP-1 signaling. *J. Mol. Cell. Cardiol.* 49, 655–663. doi: 10.1016/j.yjmcc.2010.05.007

Wang, C., Yan, R., Luo, D., Watabe, K., Liao, D. F., and Cao, D. (2009). Aldo-keto reductase family 1 member B10 promotes cell survival by regulating lipid synthesis and eliminating carbonyls. *J. Biol. Chem.* 284, 26742–26748. doi: 10.1074/jbc.M109.022897

Wang, H., Moreau, F., Hirota, C. L., and MacNaughton, W. K. (2010). Proteinase-activated receptors induce interleukin-8 expression by intestinal epithelial cells through ERK/RSK90 activation and histone acetylation. *FASEB J.* 24, 1971–1980. doi: 10.1096/fj.09-137646

Wang, X., Darcy, J., Cai, C., Jin, J., Bartke, A., and Cao, D. (2018). Intestinal immunity in hypopituitary dwarf mice: effects of age. *Aging.* 10, 358–370. doi: 10.18632/aging.101393

Yan, R., Zu, X., Ma, J., Liu, Z., Adeyanju, M., and Cao, D. (2007). Aldo–keto reductase family 1 B10 gene silencing results in growth inhibition of colorectal cancer cells: implication for cancer intervention. *Int. J. Cancer* 121, 2301–2306. doi: 10.1002/ijc.22933

Zhao, S., Xia, J., Wu, X., Zhang, L., Wang, P., Wang, H., et al. (2018). Deficiency in class III PI3-kinase confers postnatal lethality with IBD-like features in zebrafish. *Nat. Commun.* 9:2639. doi: 10.1038/s41467-018-05105-8

Zhong, L., Liu, Z., Yan, R., Johnson, S., Zhao, Y., Fang, X., et al. (2009). Aldo-keto reductase family 1 B10 protein detoxifies dietary and lipid-derived alpha, beta-unsaturated carbonyls at physiological levels. *Biochem. Biophys. Res. Commun.* 387, 245–250. doi: 10.1016/j.bbrc.2009.06.123

Zu, X., Yan, R., Pan, J., Zhong, L., Cao, Y., Ma, J., et al. (2017). Aldo-keto reductase 1B10 protects human colon cells from DNA damage induced by electrophilic carbonyl compounds. *Mol. Carcinog.* 56, 118–129. doi: 10.1002/mc.22477

Conflict of Interest: The authors declare that the research was conducted in the absence of any commercial or financial relationships that could be construed as a potential conflict of interest.

frontiers in Cell and Developmental Biology

REVIEW
published: 01 April 2021
doi: 10.3389/fcell.2021.649045

Ferroptosis Is a Potential Novel Diagnostic and Therapeutic Target for Patients With Cardiomyopathy

*Zhenyu Zhai†, Pengtao Zou†, Fuxiang Liu, Zirong Xia and Juxiang Li**

Department of Cardiovascular Medicine, The Second Affiliated Hospital of Nanchang University, Nanchang, China

Cardiomyocyte death is a fundamental progress in cardiomyopathy. However, the mechanism of triggering the death of myocardial cells remains unclear. Ferroptosis, which is the nonapoptotic, iron-dependent, and peroxidation-driven programmed cell death pathway, that is abundant and readily accessible, was not discovered until recently with a pharmacological approach. New researches have demonstrated the close relationship between ferroptosis and the development of many cardiovascular diseases, and several ferroptosis inhibitors, iron chelators, and small antioxidant molecules can relieve myocardial injury by blocking the ferroptosis pathways. Notably, ferroptosis is gradually being considered as an important cell death mechanism in the animal models with multiple cardiomyopathies. In this review, we will discuss the mechanism of ferroptosis and the important role of ferroptosis in cardiomyopathy with a special emphasis on the value of ferroptosis as a potential novel diagnostic and therapeutic target for patients suffering from cardiomyopathy in the future.

Keywords: ferroptosis, regulated necrosis, cardiac damage, cardiomyopathy, heart failure

OPEN ACCESS

Edited by:
Brian C. Schaefer, Uniformed Services University of the Health Sciences, United States

Reviewed by:
Jason Karch, Baylor College of Medicine, United States
Takashi Matsui, University of Hawaii, United States
Dezhao Lu, Zhejiang Chinese Medical University, China

***Correspondence:**
Juxiang Li
ljx912@126.com; 892744649@qq.com

†These authors share first authorship

Specialty section:
This article was submitted to Cell Death and Survival, a section of the journal Frontiers in Cell and Developmental Biology

Received: *15 January 2021*
Accepted: *08 March 2021*
Published: *01 April 2021*

Citation:
Zhai Z, Zou P, Liu F, Xia Z and Li J (2021) Ferroptosis Is a Potential Novel Diagnostic and Therapeutic Target for Patients With Cardiomyopathy. Front. Cell Dev. Biol. 9:649045. doi: 10.3389/fcell.2021.649045

INTRODUCTION

The death of myocardial cells is a crucial aspect of cardiac pathophysiology. Damaged cardiomyocytes are eliminated through the activation of six major forms of regulated cell death including necroptosis, ferroptosis, pyroptosis, mitochondrial-mediated necrosis, apoptosis, and autophagic cell death under different conditions (Galluzzi et al., 2018). These regulated myocardial cell death mechanisms participate in the onset and progression of cardiovascular diseases. For example, the mechanism of cardiomyocyte apoptosis has been investigated to a great depth, has been linked to inflammation, infection, ischemia, and immunologically induced damnification in the heart and subsequently heart failure (Kerr et al., 1972; Kang and Izumo, 2003; Wencker et al., 2003; Abbate et al., 2006). Among different necrotic cell deaths, necroptosis contributes significantly to ischemic injuries of the heart, worsening heart function, as well as adverse cardiac remodeling reported by several studies (Luedde et al., 2014; Adameova et al., 2016, 2017; Zhu and Sun, 2018; Ghardashi Afousi et al., 2019). Compared with other forms of myocardial cell death mechanisms, autophagic cell death is not a process that customarily commands the destruction of the cell, it is believed to act as a protective mechanism that recycles the molecular components and unwanted or damaged cellular constituents, thereby maintaining cell vitality. Akazawa et al. (2004) reported that autophagic cell death played a certain part in the pathophysiology of heart failure in transgenic mice. Ferroptosis is another newly identified programmed cell death mechanism that is distinguished from necroptosis and apoptosis; it is iron-dependent and characterized by the toxic

lipid reactive oxygen species (ROS) accumulation (Lu et al., 2017), which were also associated with the pathogenesis of several diseases, such as tumors, stroke, ischemia-reperfusion injury, etc. (Guiney et al., 2017; Stockwell et al., 2017). Recently, several studies have demonstrated that ferroptosis played a crucial role in myocardial homeostasis and pathology (Akazawa, 2015; Conrad and Proneth, 2019; Chen et al., 2020; Li W. et al., 2020). However, the biological roles and regulation pathways of ferroptosis in cardiovascular diseases have not been entirely understood.

Ferroptosis is a nonapoptotic, abundant and accessible cellular iron-dependent, and peroxidation-driven programmed cell death pathway, was not discovered until recently with the aid of a pharmacological approach (Dixon et al., 2012). Surprisingly, the erastin and RSL3 induced mode of cell death which was revealed through high-throughput screening of small-molecule libraries, was deemed to be nonapoptotic – as cell death in those treated with erastin and RSL3 occurred without biochemical apoptotic hallmarks. The principle apoptotic machinery with regards to cells treated with erastin and RSL3 – caspases, Bcl-2-associated X protein (Bax) and Bcl-2 homo-logous antagonist/killer (Bak) – was suppressed in the meantime (Dolma et al., 2003; Yagoda et al., 2007; Yang and Stockwell, 2008; Wolpaw et al., 2011). Further studies identified that the requirement for cellular iron, disruption of the intracellular redox homeostasis controlled by glutathione (GSH), glutathione peroxidase 4 (GPX4), and lipid peroxidation were incorporated in this cell death process (Rui et al., 2020). Recent literature has established key enzymes and metabolites of the ferroptosis pathway and specified chemical modulators (Stockwell et al., 2017). The research about ferroptosis has attached much attention in the context of tumors, pathophysiologically degenerative conditions, and other areas (Guiney et al., 2017; Stockwell et al., 2017; Lin et al., 2020). However, ferroptosis is discovered in cardiac tissue more recently, and there are many studies reported concerning ferroptosis specifically in cardiovascular diseases by using several methods of inducing and inhibiting ferroptosis in cardiac tissue (Baba et al., 2018; Bai et al., 2018; Liu et al., 2018, 2020; Li W. et al., 2019, 2020; Li et al., 2021; Wu et al., 2021). This article will explain the mechanism of ferroptosis and summarized advances of ferroptosis in cardiomyopathy. We hope to deliver novel insights for the research of cardiomyopathy in the future.

THE MECHANISM OF FERROPTOSIS

The present definition of ferroptosis is a programmed cell death (PCD) that is reliant on a large number of cellular iron and lipid hydroperoxide, subsequently inducing copious lipid accumulation in cells, interfering with the homeostasis of redox reactions, and eventually promoting cell death (Xie et al., 2016; Dixon, 2017; Imai et al., 2017; Stockwell et al., 2017). This concept distinguishes from canonical signaling cascades for apoptosis or necroptosis, in which the main antioxidant system essentially comprises of various metabolic processes. The associated mechanism of ferroptosis is involved in amino acid metabolism, which was affected by GSH consumption and reduced activity and availability of glutathione peroxidases 4 (GPX4), iron metabolism, lipid peroxidation metabolism, etc. (**Figure 1**).

Glutathione Consumption

Xc-system, known as the glutamate-cystine reverse transport system, transports glutamate (Glu) into the extracellular space and, meanwhile, cystine is transported into the cell on an equal ratio. P53 can specifically inhibit Xc-system through down-regulating the expression of SLC7A11 (Kang et al., 2019). The study conducted by Jiang et al. (2015) demonstrated that the antioxidant capacity of human lung cancer H1299 cells remarkably decreased after activation of the P53 gene and cells were prone to ferroptosis (Han et al., 2020). Apart from P53, clinical drugs for cancer cells, including sulfasalazine and sorafenib, and erastin can also induce ferroptosis by inhibiting the activity of cystine/glutamate antiporter Xc-system (Dixon et al., 2012, 2014; Xie et al., 2016). After cystine is transported into the cell, it is converted to cysteine and readily used for GSH production with glutamate-cysteine ligase (GCLC) and glutathione synthetase (GSS) acting as catalysts (Griffith, 1999; Dickinson and Forman, 2002). GSH, as one of major intracellular antioxidant buffers, is widely distributed in tissues of higher organisms. The concentration of intracellular GSH decreases with aging due to variations of numerous factors, including changes in activity of GSH synthetic and metabolic enzymes as well as availability of precursor amino (Jones, 2006). Under normal conditions, intracellular free GSH exists almost exclusively in its reduced form. Reduced GSH is critical in sustaining redox balance under the action of GPX4 *in vivo* (Kalinina and Gavriliuk, 2020). GSH is able to protect important cellular components against damage induced by ROS including free radicals, peroxides, lipid peroxides, and heavy metals (Pompella et al., 2003; Pompella and Corti, 2015). Oxidized glutathione (GSSG) can be converted to free GSH from under the action of GSH reductase. In mammalian cells, the ratio of GSH/GSSG is conservatively estimated at approximately 10,000:1∼50,000:1 within the cytosol under physical condition (Morgan et al., 2013; Lv et al., 2019). The lower ratio of GSH/GSSG, decreasing to values of 10:1 and even 1:1, was observed stimulated by various oxidative stress models (Zitka et al., 2012). The ratio of GSH/GSSG is regarded as one of indicators of oxidative stress in the body (Owen and Butterfield, 2010; Zitka et al., 2012; Sentellas et al., 2014; Kalinina and Gavriliuk, 2020). The finding above was consistent with the results of study by Wu et al. (2018). They found that ferroptosis and mitochondrial dysfunction were induced after co-treatment with 100 μM t-BHP for 1 h in PC12 cells, which was a widely used oxidative stress stimulus, accompanied by GSH depletion, decrease of the ratio of GSH/GSSG, reduced Gpx4 expression, and increased lipid ROS (Wu et al., 2018). The results of study by Wu et al. (2018) indicated that the ratio of GSH/GSSG is tightly related to ferroptosis as well as GSH depletion. Importantly, Sun et al. (2018b) conducted the study to explore the association between GSH consumption and ferroptosis for the first time, and the results demonstrated that GSH deletion could trigger ferroptosis by generating lipid peroxidation build-up in retinal pigment epithelial (RPE) cells (Qiu et al., 2020). Therefore, it

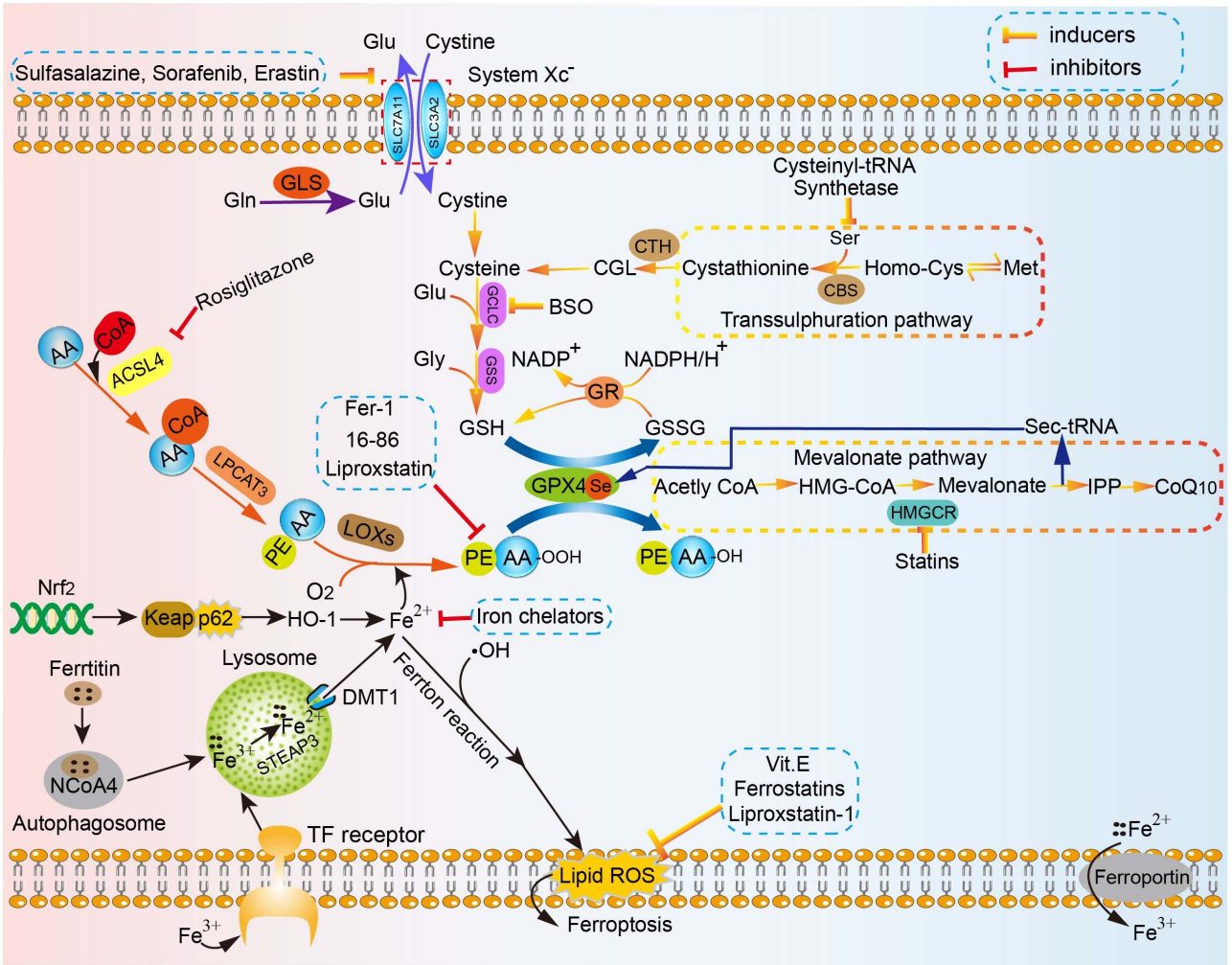

FIGURE 1 | The mechanism of ferroptosis in cell. Amino acid metabolism, which can be affected by GSH consumption and reduced activity and availability of GPX4, iron metabolism, lipid peroxidation metabolism, the high concentration of glutamic acid outside the cell, etc. are strongly implicated in the mechanism of ferroptosis. Homocysteine is converted to cystathionine under the catalysis of the cystathionine b-synthase (CBS), and in the final step, cystathionine is converted to cysteine under the action of the corresponding cystathionine g-lyase in the reverse *trans*-sulfurylation pathway, which can help maintain homeostasis of intracellular cysteine level and subsequently reduce the sensitivity to ferroptotic cell death. The sec-tRNA and CoQ10 produced in the mevalonate pathway can also affect ferroptosis. SLC7A11, the glutamate/cystine antiporter solute carrier family 7 member 11; SLC3A2, the glutamate/cystine antiporter solute carrier family 3 member 2; GSL, glutaminase; Glu, glutamate; Gln, glutamine; GCLC, glutamate-cysteine ligase; GSS, glutathione synthetase; Gly, glycine; GSH, glutathione; GPX4, glutathione peroxidases 4; GR, glutathione reductase; CBS, cystathionine b-synthase; CTH, ceramide trihexoside; Met, Methionine; ACSL4, acyl-CoA synthetase long-chain family member 4; LPCAT3, lysophosphatidylcholine acyltransferase 3; LOXs, lipoxygenases; DMT1, divalent metal transporter 1; ROS, reactive oxygen species; IPP, isopentenyl pyrophosphate; HMGCR, HMG-CoA reductase.

can be concluded that GSH consumption is regarded as an indispensable process leading up ferroptosis.

The upstream factors mediating deprivation of intracellular GSH can be summarized in three aspects: glutamine (Gln) decomposition, reduced concentration of cysteine and high concentration of extracellular glutamate. More than half of the free amino acids in the human body are in the form of glutamine in muscles and other tissues. Extracellular glutamine could be transformed to Glu, under the action of glutaminase 1 (GLS1) and glutaminase 2 (GLS2), which is then converted to a-ketoglutarate (a-KG) by using the deamination reaction. In a final step, a-KG is degraded by the mitochondrial tricarboxylic acid cycle (TCA). The research proposed by Gao M. et al. (2019) demonstrated that knockdown of GLS2 to inhibit glutamine decomposition pathway could suppress ferroptosis. Cells can maintain levels of intracellular cysteine by the glutamate–cystine reverse transport system as described earlier, which can offer the oxidized form of cellular cysteine–cystine, and the reverse *trans*-sulfurylation pathway, which can convert methionine to homocysteine, cystathionine, in turn, and eventually to cysteine (Hayano et al., 2016). Factors contributing to decreased availability of cysteine greatly promoted the occurrence of ferroptosis. The glutamate/cystine antiporter solute carrier family 7 member11 (SLC7A11), cationic amino acid transporter,

promotes the synthesis of GSH by mediating cystine uptake and Glu release, protects cells from oxidative stress, maintains cell redox balance, and prevents lipids peroxidation induced ferroptosis. The study by Jiang et al. (2015) indicated that p53 could limit the availability of cysteine via suppression of SLC7A11 expression, making cells prone to ferroptosis. Cysteinyl-tRNA synthetase encoded by the CARS gene is associated with protein translation of tRNAs by using cysteine. The conclusion has been proven by Hayano et al. (2016) that the knockout of *CARS* gene by three additional Ambion Silencer Select siRNA sequences could make the increase of intracellular free cysteine, preventing Erastin-induced ferroptosis. Homocysteine is converted to cystathionine under the catalysis of the cystathionine b-synthase (CBS), and in the final step, cystathionine is converted to cysteine under the action of the corresponding cystathionine g-lyase in the reverse *trans*-sulfurylation pathway. In a study to explore the influence of the reverse *trans*-sulfurylation pathway on the resistance of drugs, the researchers discovered that sensitivity of these resistant cells to ferroptosis might be restored through upregulating the pathway, whereas the pathway cannot prevent Ras-selective lethal small molecule 3 (RLS3), the GPX4 inhibitor, induced ferroptosis due to acting on the "upstream" of ferroptosis (Hayano et al., 2016). In addition, when the concentration of extracellular glutamate increases abnormally, the concentration gradient of glutamate inside and outside the cell changes, subsequently affecting the cellular exchange of Glu and cystine in a 1:1 manner, ultimately leading to lipid peroxidation accumulation, and consequently ferroptosis (Yang and Stockwell, 2016; Yang et al., 2016; Latunde-Dada, 2017). Studies have indicated that oxidation toxicity mediated by high extracellular glutamate could induce nerve cell injury manifesting as ferroptosis (Yang et al., 2014; Zheng et al., 2017), and the results of the research conducted by Liu further support the view above (Liu et al., 2017). In a nutshell, changes based on Gln decomposition, reduced availability of cysteine and high concentration of extracellular glutamate can silence the Xc- system, causing GSH- consumption induced ferroptosis.

Decreased Activity or Availability of GPX4

If GSH metabolism is the crux of the amino acid metabolism mechanism of ferroptosis, GPX4 is the channel that join all the modifications. GPX4, as a crucial antioxidant enzyme, is different from the other GPX family members in the fields of its monomeric structure, a less restricted dependence on GSH as reducing substrate, and the ability to reduce lipid-hydroperoxides inside biological membranes. Reduced GSH is converted to the oxidized form of glutathione (glutathione disulfide, GSSG), which is recycled by GSH reductase and $NADPH/H^+$, under the catalysis of GPX4 during the reduction of hydrogen peroxide, organic hydroperoxides, and lipid peroxides, protecting cells from oxidative stress. GPX4, the GSH-dependent antioxidant enzyme, can reduce lipid hydroperoxides (PUFAs-OOH) to the corresponding alcohol by using two units of GSH as a donor, inhibiting the oxidative stress induced ferroptosis (Lv et al., 2019). Inactivation of the system XC (−)/glutathione/glutathione peroxidase 4 (Gpx4) axis can bring about an accumulation of lipid peroxides, subsequently leading to ferroptotic cell death (Friedmann Angeli et al., 2014; Yang et al., 2014). The factors contributing to reduced activity or availability of GPX4 will increase oxidative stress and make cells prone to the occurrence of ferroptosis. At present, specific ferroptosis-inducing agents included Erastin, RSL3, and ferroptosis-inducing agents 56 (FIN56) (Yang and Stockwell, 2008; Shimada et al., 2016). In particular, RSL3 and FIN56 are usually used to trigger ferroptosis by limiting the activity or availability of GPX4. Yang et al. (2014) found that RSL3 through the mechanism silencing GPX4 could increase oxidative stress, resulting in ferroptosis. Moreover, the research led by Shimada et al. (2016) has demonstrated that FIN56 can reduce GPX4 abundance by consuming GPX4 protein. Moreover, the study conducted by Dabkowski et al. (2008) reported that, for the first time, mitochondria-specific transgenic overexpression of GPX4 could attenuate myocardial ischemia/reperfusion (I/R)-associated cardiac contractile dysfunction, which was relevant to enhanced mitochondrial electron transport chain (ETC) complex activities.

Recently, ferroptosis suppressor protein 1 (FSP1), which was previously known as apoptosis-inducing factor mitochondrial 2 (AIFM2), is regarded as another potent factor to protect cells against ferroptosis.

Bersuker et al. (2019) reported that myristoylation was capable of recruiting FSP1, which was identified through a synthetic lethal CRISPR–Cas9 screen, to the plasma membrane and reduced coenzyme Q10 (CoQ_{10}) as an oxidoreductase, subsequently keeping lipid peroxides from propagation within membranes in the absence of GPX4. The results of the study demonstrated that a novel ferroptosis suppression pathway tightly related to FSP1 acted in parallel to the canonical GSH-based GPX4 pathway. The findings by Bersuker et al. (2019) was consistent with, to some extent, the results of the study conducted by Doll et al. (2017, 2019). They also found that FSP1 was able to protect cells from ferroptosis induced by GPX4 depletion in a cDNA overexpression screen complementing for *GPX4* loss and CoQ_{10}, known as ubiquinone, could be regenerated under the catalysis of FSP1 using NAD(P)H. CoQ_{10} was capable of scavenging small-molecule lipophilic radical, such as ferrostatin-1 (Fer-1) and liproxstatin-1, leading to halting ferroptosis (Dixon et al., 2012; Bebber et al., 2020). The findings above indicated that pharmacological inhibition of FSP1 may be an effective therapeutic method to sensitize cancer cells to ferroptosis-inducing chemotherapeutic agents.

Lipid Peroxidation Metabolism

Recent evidence has demonstrated that lipid peroxidation metabolism is associated with the form of ferroptosis, which participates in the establishment of membranous micelles and pores (Borst et al., 2000; Yang et al., 2016; Doll et al., 2017; Agmon et al., 2018). At present, it is believed that the formation of lipid hydroperoxides is related to lipoxygenase (LOXs)-catalyzed autoxidation and enzymatic reactions rather than cyclooxygenases (COXs) (Yang et al., 2016). Currently, studies on lipid peroxidation metabolism related to ferroptosis mainly

focus on enzyme-catalyzed lipid peroxidation reactions. Under ferroptosis, the peroxidation of polyunsaturated fatty acids (PUFAs) seems to be mainly regulated by LOXs and GPX4 (Seiler et al., 2008; Yang et al., 2016). In particular, LOXs, which are iron-containing nonheme dioxygenases, directly catalyze lipid peroxidation by promoting the di-oxygenation of free and esterified PUFAs (Kuhn et al., 2015), whereas GPX4 indirectly inhibits lipid peroxidation (Seiler et al., 2008). Friedmann Angeli et al. (2014) found that multiple LOXs were associated with PUFA peroxidation and under GPX4 inactivity the accumulation of oxidized PUFAs could make cells to occur ferroptosis (Dixon et al., 2012). Additionally, ROS scavengers, such as liproxstatin-1 (Lip-1), ferrostatin-1 (Fer-1), as well as coenzyme Q10, vitamin E and their analogs can inhibit the lethal cascade related to ferroptosis (Yagoda et al., 2007; Friedmann Angeli et al., 2014; Matsushita et al., 2015; Kagan et al., 2017; Zilka et al., 2017). The metabolism of arachidonic and adrenic acids, which are groups of PUFAs, are associated with two important enzymes – acyl-CoA synthetase long-chain family member 4 (ACSL4) and lysophosphatidylcholine acyltransferase 3 (LPCAT3), both of which engage with the incorporation of long PUFAs into lipid membranes, and several studies have proven that inhibition of ACSL4 and 3 LPCAT3 by genetic and/or pharmacological can protect cells from ferroptosis in some settings (Dixon et al., 2015; Yuan et al., 2016b; Doll et al., 2017; Kagan et al., 2017). PUFAs can be converted to PUFA-CoA under the catalysis of acyl-CoA synthase. Arachidonic acid (AA) is usually preferentially thioesterified under the action of ACSL4, subsequently are involved in the formation of phospholipids, when oxidized, it forms phosphatidy-lethanolamine to make cells prone to ferroptosis in a final step (Golej et al., 2011). Doll et al. (2017) has highlighted that inactivating ACSL4 gene and pharmacologically inhibiting ACSL4 with distinct thiazolidinediones (TZDs), namely rosiglitazone (ROSI), pioglitazone (PIO) and troglitazone (TRO), can effectively obstruct ferroptosis as this hinders the assembly and movement of PUFAs-OOH, indicating that Acsl4 inhibition is a viable therapeutic method to prevent diseases related to ferroptosis.

Although enzyme-catalyzed lipid peroxidation reactions have become the focus of many researchers, it is also essential not to ignore the importance of non-enzymatic lipid peroxidation. The progression of oxygen-driven free radical chain reaction, namely non-enzymatic lipid peroxidation, includes three main processes in turn (Frank, 1950). Initiation refers to the generation of early lipid radical L·, since a hydrogen atom is pumped away from the lipid molecule LH under the premise of generating a large number of sufficiently reactive free radicals such as ·OH; During the next step propagation, L· undergoes a series of stages including hydrogen pumping, addition, fracture, etc. This process continuously repeats to produce a chain reaction. The oxidation process will not be stopped as long as the reaction remains dominant. The progress of termination occurs with a limited amount of antioxidants acting as free radical scavengers, and eventually, the reaction slows down and becomes terminated. Moreover, lipid molecules are constantly recruited to free radical reactions by PLOO· and PLO· produced through the spontaneous oxidation of lipid peroxidation (Davies and Guo, 2014). Fenton reaction discovered in 1984 by H. J. H. Fenton is currently believed to be the provider of free radicals for lipid peroxidation metabolism, so are the Fenton-like reaction (Lai and Piette, 1978).

Iron Metabolism

Iron is known as one of important trace elements for cell survival in the body, the majority of which is distributed in cells and stored in ferritin and incorporated into heme and iron-sulfur (Fe-S) cluster proteins (Wang and Pantopoulos, 2011). Iron is closely related to a variety of biological processes under physiological states, such as delivering oxygen to cells by binding to heme for cellular generation of ATP and that is energy metabolism, deoxyribonucleic acid (DNA) synthesis and repair, cellular respiration, and electron transfer, participation in redox reactions, and the generation (Fe-S) protein clusters which can regulate gene expression, as well as overall metabolism (Johnson et al., 2005; Pantopoulos et al., 2012; Hirst, 2013; Lawen and Lane, 2013; Abbaspour et al., 2014; Loreal et al., 2014; Sumneang et al., 2020). Similar to other cell types, the endogenous levels of iron concentration in cytosol, mitochondria, nuclei, or lysosomes within cardiomyocytes is approximately 6, 16, 7, and 16 μM, respectively, under normal conditions (Petrat et al., 2001; Rauen et al., 2007; Nakamura et al., 2019; Sumneang et al., 2020). There is only one pathway for iron export from cardiomyocytes and that is through Fpn1. Nevertheless, iron is able to enter cardiomyocytes through several ways, which makes cardiomyocytes particularly prone to iron overload under pathological conditions. A detailed discussion with regard to the mechanism of cellular iron regulation in the heart has been reviewed elsewhere (Abbaspour et al., 2014; Gao G. et al., 2019; Ghafourian et al., 2020; Ravingerova et al., 2020). Moreover, cellular excess iron makes cardiomyocytes vulnerable to ferroptosis through the production of ROS. There exists a close relationship between the ferroptosis and the homeostasis of iron metabolism in cells.

Gao et al. (2015) confirmed the significance of iron in the formation of ferroptosis through experimental methods and established that cells became more susceptible to ferroptosis after a rise in iron level within the redox-active labile iron pool (LIP) (Hou et al., 2016). The study by Dixon et al. (2012) indicated that reduce iron in LIP by several methods could suppress the formation of ferroptosis (Kwon et al., 2015). Notably, ferritinophagy is a critical mechanism to regulate the level of LIP. LIP is composed of ferrous iron in a soluble, chelatable state within the cytoplasm and is regulated by ferritin, the substrate of ferritinophagy, which is a highly conserved iron storage protein and is made up of two subunits including H-ferritin and L-ferritin (Cordani et al., 2019; Zhang et al., 2019). Ferritinophagy is a process that ferritin is sequestered into autophagosomes and delivered to lysosomes for degradation and is important for maintaining iron homeostasis in cells (Kidane et al., 2006; Asano et al., 2011; Mancias et al., 2014; Masaldan et al., 2018). Previous studies have reported that iron chelator, such as DFO and DpdtC, is capable of inducing ferritinophagy (Mancias et al., 2014; Huang et al., 2018). The study conducted by Gao et al. (2015)

demonstrated that ferritinophagy could trigger ferroptosis by promoting the accumulation of iron and ROS, which was consistent with the finding by Hou et al. (2016) and Tang et al. (2018). Controlling iron level in cells by interrupting ferritinophagy may be a new therapeutic target for inhibiting ferroptosis in the future (Sui et al., 2019; Li N. et al., 2020). However, the human body can sustain iron homeostasis in both the cell and the whole by several proteins and pathways, such as the iron-responsive element (IRE)-binding proteins, also known as IRE-BP, IRBP, IRP and IFR, which attach to IREs during the regulation of iron metabolism within human bodies (Gray and Hentze, 1994; Eisenstein, 2000). In addition, transferrin, which is an important carrier glycoprotein of serum iron that becomes endocytosed into cells through transferrin receptor (TFRC). Both transferrin and its receptor are perceived as important participants of regulating iron metabolism (Gao et al., 2015). Yang and Stockwell (2008) found that increasing unstable iron intake by upregulating TFRC could increase the sensitivity of cells toward ferroptosis. Iron is a central co-factor for several molecules and enzymes and is particularly involved with regulating mitochondrial function (Levi and Rovida, 2009; Stehling and Lill, 2013). In the context of cardiomyocyte, mitochondria is predominantly crucial for sustaining the normal functions of cardiomyocyte, hence further highlighting the indispensable role of iron during cardiac function, since mitochondria fuel the cardiac muscles to constantly contract (Barth et al., 1992). Disturbance of iron homeostasis including iron deficiency and accumulation of iron can impair the normal cardiac function and result in various cardiovascular diseases (von Haehling et al., 2015; de Montalembert et al., 2017; Fujikura et al., 2018; Lakhal-Littleton, 2019). Excess iron can be transported and accumulated into cardiac tissue and cardiomyocytes from iron-overload disorders or other cardiac pathologies (Oudit et al., 2003). Accordingly, excess iron will cause the overproduction of mitochondrial ROS. When the surplus of iron is also taken into the mitochondria, it consequently becomes a hotbed of ROS production from oxidation phosphorylation and H2O2 production (Oudit et al., 2003; Levi and Rovida, 2009; Bolduc et al., 2019; Fang et al., 2019; Gao M. et al., 2019). In addition, Fe^{3+} can be converted to Fe^{2+}, under the action of the metal reductase STEAP3, and then divalent metal transporter 1 (DMT1) releases Fe^{2+} in lysosome into cytoplasmic LIP through. These soluble, redox-active free iron in the LIP is considered as the catalyst that induces the elevated ROS production in ferroptosis, thereby causing cardiomyocytes more sensitive to oxidative stress in the presence of excess iron (Thomas et al., 2013; Melenovsky et al., 2017; Xu et al., 2019).

Other Pathways Related to Ferroptosis

Apart from GSH consumption, reduced activity and availability of GPX4, lipid peroxidation metabolism, iron metabolism, and other pathways are also correlated with the mechanism of ferroptosis; for instance, organelle-mediated pathways, Nrf2 pathway, TP53 pathway, etc. Importantly, Statin drugs is capable of making cells vulnerable to ferroptosis through inhibiting the rate-limiting enzyme of the mevalonate pathway, HMG CoA reductase, presumably by depleting CoQ10 and possibly by also inhibiting downstream tRNA isopentenylation via TRIT1, which is necessary for the biosynthesis of GPX4 (Fradejas et al., 2013; Shimada et al., 2016; Viswanathan et al., 2017). Moreover, several cell structures including mitochondria, endoplasmic reticulum (ER), lysosomes are involved in the formation of ferroptosis by mediating multiple pathways. The research led by Gao M. et al. (2019) have confirmed that mitochondria have a central role in ferroptosis, which can affect the pathway of glutamine decomposition and subsequently result in ferroptosis (Tadokoro et al., 2020). Yuan et al. (2016a) also discovered that inhibition of CDGSH iron sulfur domain 1 (CISD1), which is an iron sulfur protein that can suppress iron transportation during the aforementioned progression, could prevent lipid peroxidation and ferroptosis by suppressing mitochondrial iron uptake through RNAi technology or pioglitazone pharmacology. The evidence indicated that ER oxidative stress markers that activate cation transport regulator homolog 1 (CHAC1), transcription factor 4 (ATF4), and phosphorylation of eIF2a were all upregulated during ferroptosis (Dixon et al., 2014). However, the precise correlation between ER and ferroptosis still remains vague, and further research is needed to explore its function in ferroptosis. Recent researches suggest that lysosomes are also related to ferroptosis. Mancias et al. (2014) found that the cargo receptor NCOA4 transferring ferritin to lysosomes also participates in ferroptosis. In addition, the study by Hou et al. (2016) proposed that the knockout of autophagy-related genes Atg5 and Atg7 also limits Erastin-induced ferroptosis in cells, since ferroptosis is dependent on autophagy. Abdalkader et al. (2018) found multiple genes controlled by the transcription factor nuclear factor erythroid 2-related factor 2 (Nrf2) were involved in ferroptosis, such as GCLM, GSS, SLC7A11, MT1G, TFRC, and so on. The study conducted by Jennis et al. (2016) indicated that the up-regulated GLS2 targeting for TP53 (p53 genes) could result in p53-dependent ferroptosis.

THE ROLE OF FERROPTOSIS IN CARDIOMYOPATHY

Cardiomyopathy is closely related to the progress of heart failure, especially lethal heart failure, such as diabetic cardiomyopathy (DCM), doxorubicin (DOX)-induced cardiotoxicity, dilated cardiomyopathy, hypertrophic cardiomyopathy, and so on (Maron et al., 2018; Fang et al., 2019; Rosenbaum et al., 2020; Wei et al., 2020). Loss of terminally differentiated cardiomyocytes is identified as a principle risk factor in the onset of multiple cardiomyopathies. However, the mechanism of cardiomyocyte death has not been completely unveiled. Literature has indicated that the newly discovered iron-dependent ferroptosis is implicated in many cardiomyopathies including ischemia/reperfusion (I/R)- and DOX-induced cardiomyopathy (DIC), iron overload cardiomyopathy (IOC), DCM, septic cardiomyopathy, etc. The focus of this study will be on the role of ferroptosis in the pathophysiology

of the four kinds of cardiomyopathy above, and we hope to provide a fresh insight for the diagnosis and treatment of cardiomyopathy.

Ferroptosis and Doxorubicin-Induced Cardiomyopathy

There are two main classifications for DOX-induced myocardial injuries: contractile dysfunction and loss of myocyte. Though both are deemed crucial in the progression of DIC, loss of myocyte could be more important as it is an irreversible process and generates a poorer prognosis, even fatal decades after onset (Felker et al., 2000). However, the mechanisms that lead to cardiomyocyte death are not fully understood. Fang et al. (2019) proposed that ferroptosis, which is an iron-dependent, and peroxidation-driven programmed cell death form, was observed in the murine model of DIC, and suppression of ferroptosis by ferrostatin-1 (Fer-1) substantially alleviated DIC. The outcomes of the study also revealed hemeoxygenase-1 (Hmox1), which is widely acknowledged for its robust cardioprotection (Yet et al., 2001; Wang et al., 2010), was significantly stimulated in heart induced by DOX, and free iron released on heme degradation by Nrf2-mediated up- regulation of Hmox1 was necessary for inducing cardiac injury. Importantly, Fer-1 and iron chelation also alleviated both acute and chronic I/R induced heart failure in mice models. The results above were consistent with the finding by Liu et al. (2020) that Fer-1was capable of inhibiting ferroptosis, subsequently preventing cardiac injury, along with the ultrastructural changes of cardiomyocyte mitochondria. The study conducted by Liu et al. (2020) also showed ferroptosis was a crucial mechanism in DIC and highlighted the crucial role of Acyl-CoA thioesterase 1 (Acot1) during the process, which was related to its biochemical function by shaping the lipid composition, indicating that Acot1 bears the potential of becoming a therapeutic target in preventing DIC by inhibition of ferroptosis. The findings by Tadokoro et al. (2020) suggested that mitochondria-dependent ferroptosis played an important role for cardiomyopathy induced by DOX (DIC) in the mice model via downregulated glutathione peroxidase 4 (GPX4) and excessive lipid peroxidation caused by DOX through DOX-Fe^{2+} complex in mitochondria, which could be reversed by GPX4 overexpression or iron chelation targeting Fe^{2+} in mitochondria in cardiomyocytes. They also reported that Fer-1 and zVAD-FMK, which were concomitant inhibitors of ferroptosis and apoptosis, were capable of fully protecting cardiomyocytes against death induced by DOX (Tadokoro et al., 2020). These researches emphasize that targeting ferroptosis would be a reasonable protective approach for preventing DIC. Interestingly, although Fang et al. (2019) demonstrated that ferroptosis induced by iron overload is a major pathogenesis factor of the DIC, knocking out receptor interacting serine/threonine kinase 3 (Ripk3) could increase survival rates compared with Fer-1 treatment alone, which indicated that ferroptosis and necroptosis were simultaneously involved in tissue damage as researchers had reported before (Linkermann et al., 2014). The link between ferroptosis and necroptosis warrants further investigation in DIC.

Ferroptosis and Iron Overload Cardiomyopathy

At the cellular level, iron is involved in multiple biochemical reactions, which serves as crucial component of a variety of enzymes participating energy metabolism, cellular respiration, synthesis and repair of DNA (Lawen and Lane, 2013; Loreal et al., 2014). However, excessive iron accumulation, namely iron overload, in cells is an important implication of several diseases disrupting the homeostatic systemic iron regulatory mechanism, such as primary hemochromatosis and transfusion-dependent anemia (Gujja et al., 2010; Gao et al., 2014; Kontoghiorghe and Kontoghiorghes, 2016). Importantly, iron overload in cardiomyocyte can result in IOC, the major reason of fatality in patients suffering from hemochromatosis. IOC manifests as progressive electromechanical deterioration of the heart (Nakamura et al., 2019). It is well known that the lethal level of lipid peroxidation is the significant feature of ferroptosis, which can be influenced by several factors, such as ROS, lipoxygenases (LOX), cyclooxygenases (COX), and GPX4. Hence, excessive accumulation of ROS, enhanced activities of LOX and/or COX, and decreased activity or availability of GPX4 are capable of inducing irresistible lipid peroxidation, subsequently resulting in ferroptotic cell death (Friedmann Angeli et al., 2014; Yang et al., 2014; Galluzzi et al., 2018; Lei et al., 2019). In this regard, iron overload in cardiomyocyte is able to trigger ferroptosis through several means, including using the Fenton reaction to catalyze the reactions for ROS production, and serving as a co-factor for LOX, allowing this enzyme to oxidize PUFAs, indicating that ferroptosis may be tightly related to IOC (Friedmann Angeli et al., 2014; Yang et al., 2014; Baba et al., 2018; Galluzzi et al., 2018; Lei et al., 2019). However, the mechanism underling how iron overload leads to IOC has not been fully elucidated and more studies need to be conducted to investigate the role of ferroptosis in IOC in the future (Ravingerova et al., 2020; Sumneang et al., 2020). In addition, Baba et al. (2018) reported that erastin (8 μM), RSL3 (1 μg/ml), and isoprenaline (1 μM), which were specific ferroptosis-inducing compounds, could lead to ferroptosis by reducing GSH availability, suppressing GPX4 activity, and interfering with many of the molecules involved in regulating iron concentration and iron-mediated redox reactions, such as GPX4, NADPH oxidase 4 (Nox4), and ferritin heavy chain (Liu et al., 2018). Ferroptosis in cardiomyocyte can be inhibited by ferrostatin-1, increased mechanistic rapamycin signaling target (mTOR), overexpression of ectonucleotide pyrophosphatase/phosphodiesterase family member 2 (ENPP2), and administration of puerarin (Baba et al., 2018; Bai et al., 2018; Liu et al., 2018).

Ferroptosis and Diabetic Cardiomyopathy

Diabetic cardiomyopathy, which manifests as hypertrophy and fibrosis in the heart, can result in early ventricular diastolic dysfunction and late ventricular systolic dysfunction in a chronological order without changes in blood pressure and coronary disease in clinic (Bugger and Abel, 2014; Kurmus et al., 2018; Parim et al., 2019), which is perceived as one

of the most common complications of diabetes that is linked with increased risk of heart failure (Paolillo et al., 2019). DCM is a kind of multifactorial disorder, and the mechanism of DCM are involved in insulin resistance, hyperglycemia, oxidative stress, fatty acids, myocardial fibrosis, inflammatory response, mitochondrial dysfunction, hypertrophy, ER stress, etc. (Wang et al., 2014; Cao et al., 2015; Chen et al., 2018). Basically, the terminal pathway of cardiomyocytes during DCM is cell death. Many studies have found that myocardial cell death patterns in DCM include four types, such as apoptosis, autophagy, necrosis, and entosis (Martins et al., 2017; Tang et al., 2019). More recent researches have elucidated that ferroptosis, which is a recently discovered form of cell death first proposed by Dixon et al. (2012), is linked with the pathological progress of DCM. Oxidative stress, which can interfere the balance between antioxidant capacity and the production of ROS, has been widely accepted as a common mechanism of DCM (Khullar et al., 2010; Huynh et al., 2014). Considering that ROS formation promotes ferroptosis, it is very likely that ferroptosis is involved in DCM (Anandhan et al., 2020; Chen et al., 2020). Zang et al. (2020) showed that diabetes was capable of inducing autophagy deficiency with time, resulting in Nuclear factor-erythroid factor 2-related factor 2 (Nrf2)-mediated defense was turned off. Subsequently, Nrf2-operated pathological program was turned on, which made cells prone to ferroptosis, leading to worsening the progression of DCM (Zang et al., 2020). This indicated that more attention should be given with regard to ferroptosis mediated by the Nrf2 pathway. A growing number of evidence showed that Nrf2 and its target genes, which possessed the anti-oxidant, anti-inflammatory, anti-apoptotic, anti-ferroptotic, and anti-fibrotic functions, could protect β islet cells of the pancreas against the oxidative damage induced by high glucose in DCM. Studies demonstrated that many natural and synthetic activators of Nrf2 might have the promising therapeutic values on DCM in in animal models of DCM (Ge et al., 2019). Pharmacological inhibition of Nrf2-mediated pathway may be a therapeutic target for preventing DCM in the future. Bruni et al. (2018) reported that β islet cells of the pancreas in the body were vulnerable to ferroptosis induced by erastin or RSL3, and the damage to the human β islet cells could be reversed by Fer-1. However, they also found that the function of β islet cells, which were treated with erastin, RSL3, or both compounds, were not weakened before transplantation into an immunodeficient recipient mouse, indicating that the relation between ferroptosis and the dysfunction of β islet cells needs further investigation. Moreover, Li W. et al. (2020) indicated that ferroptosis was implicated in the ischemia/reperfusion injury of DCM through endoplasmic reticulum stress (ERS), which is a cellular response to ER dysfunction and can be induced by ROS, and suppression of ferroptosis could alleviate diabetes mellitus myocardial ischemia/reperfusion injury (DIR), which may provide a new therapeutic target for DCM.

Ferroptosis and Septic Cardiomyopathy

Septic cardiomyopathy is a kind of reversible complication in patients suffering from sepsis, and is also one of the major causes of high mortality of sepsis (Zechendorf et al., 2020). A prominent feature in the progress of septic cardiomyopathy is death of terminally differentiated myocardial cells. Previous studies demonstrated that lipopolysaccharide (LPS) or stimulator of interferon genes (STING) were closely implicated in sepsis-induced cardiac dysfunction by causing apoptosis, autophagy, pyroptosis, or cardiomyocytes necroptosis (Suzuki et al., 2003; Wang et al., 2015; Sun et al., 2018a; Li N. et al., 2019). Nevertheless, evidence shows that other kinds of cell death may be part of the pathogenesis of septic cardiomyopathy, because the suppression of autophagy, pyroptosis, or apoptosis alone is able to partially relieve the sepsis-induced cardiac injury (Suzuki et al., 2003; Sun et al., 2018a; Li W. et al., 2019). The higher expression level of cyclooxygenase-2 (COX-2), also known as prostaglandin endoperoxide synthase 2 (PTGS2) – a recognized marker of ferroptosis – was observed in the heart of murine model with sepsis (Shen et al., 2007; Frazier et al., 2012; Yang et al., 2014). In addition, mitochondria changes in myocardial cell damage induced by LPS were consistent with mitochondrial characteristics of ferroptosis in cardiomyocytes (Xie et al., 2016; Sun et al., 2018a). The findings above indicated that ferroptosis may be closely linked to the progression of septic cardiomyopathy induced by LPS. Importantly, the study conducted by Li W. et al. (2020), which aimed to investigate the role and underlying mechanism of ferroptosis on septic cardiac injury induced by LPS, demonstrated that LPS was able to promote the expression of nuclear receptor coactivator 4 (NCOA4) but decrease the level of ferritin, which was degraded in a ferritinophagy-dependent manner through the interaction between NCOA4 and ferritin, leading to a higher level of Fe^{2+} was released into cytoplasm. Subsequently, the expression of siderofexin (SFXN1) on mitochondrial membrane was activated by Cytoplasmic Fe^{2+}, which in turn transported cytoplasmic Fe^{2+} into mitochondria, resulting in the accumulation of mitochondrial ROS and making cardiomyocyte sensitive to ferroptosis. This indicated that ferroptosis mediated by ferritinophagy could confer damage upon cardiomyocyte for sepsis-induced cardiac injury. The results of the study were consistent with the discovery of previous research that mitochondrial iron reduction could avert cardiac ischemic damage through suppressing mitochondrial ROS production (Chang et al., 2016; Sumneang et al., 2020). Therefore, aiming ferroptosis in cardiomyocyte could be a novel clinical approach of treating cardiac injury induced by sepsis.

SUMMARY AND PROSPECT

This review has outlined our knowledge about the mechanism of ferroptosis, and described the role of ferroptosis in cardiomyopathy. An emphasis in the duality of ferroptosis, including amino acid metabolism and iron-overload counterparts, is evident throughout the manuscript, derived mostly from recent studied aiming to investigate the role and underlying principles of ferroptosis on cardiomyopathy.

However, apart from amino acid metabolism and iron metabolism, lipid peroxidation metabolism, the high concentration of glutamic acid outside the cell, organelle-mediated pathways, Nrf2 pathway, TP53 pathway, etc. are also

implicated in the mechanism of ferroptosis. Oxidative stress, which is the final downstream event of the pathway related to ferroptosis, could be induced either by way of a lack of enzymatic antioxidants, or loss of iron homeostasis, subsequently causing ferroptosis. Ferroptosis was also involved in pathological cell death of other diseases of cardiovascular system, for instance heart failure and myocardial infarction (Liu et al., 2018; Chen et al., 2019; Park et al., 2019; Yoshimura et al., 2020). However, there is no study conducted to explore the relationship between ferroptosis and the pathogenesis of arrhythmia, such as ventricular tachycardia, atrial fibrillation, and ventricular fibrillation. Interestingly, to identify atrial fibrillation (AF) - related mRNAs, we collected human right atrial appendage tissues from five patients suffering persistent AF (AF group) and five patients with normal sinus rhythm (NSR group) and characterized the global changes in mRNA expression with high-throughput sequencing technology. We found that SLC7A11 was significantly downregulated (the results of our study have not been published), which is a cystine/glutamate transporter gene, a key gene regulating "iron overload-mediated ferroptosis," and an important part of the amino acid reverse transport system (Fang et al., 2020). Additionally, further research is called for to clarify the mechanism of triggering of ferroptosis at the molecular level in various chronic and acute cardiovascular system disorders; and whether there exists any difference in the regulation of ferroptosis based on myocardial cell type, patient age, and other factors. To respond to the questions above, it is imperative to establish methods to identify the specific cells that undergo ferroptosis in the heart.

Considering that many studies have successfully observed ferroptosis in animal models of multiple cardiomyopathy and that inhibition of ferroptosis by several methods can relieve cardiomyocyte injury, the major problem is how to immediately apply these findings to the diagnosis and treatment of cardiomyopathy in clinic. Combining existing information of antioxidant function with the growing mechanistic knowledge of ferroptosis to design novel approaches that may help in the identification and advancement of materials that can result in more specific methods to block iron-dependent ROS accumulation *in vivo*. While there are many obstacles to overcome, researching in the area has the possibility to illuminate new insights into cardiomyopathy and generate more efficient treatment modalities.

AUTHOR CONTRIBUTIONS

ZZ drafted the manuscript. ZZ, JL, PZ, FL, and ZX revised the manuscript. All authors have read and approved the final version of manuscript.

FUNDING

This work was supported by grants from Jiangxi Graduate Innovation Fund (YC2019-B040 to ZZ) and Jiangxi Natural Jiangxi Provincial Health Committee (20195194 to ZX and JL).

REFERENCES

Abbaspour, N., Hurrell, R., and Kelishadi, R. (2014). Review on iron and its importance for human health. *J. Res. Med. Sci.* 19, 164–174.

Abbate, A., Bussani, R., Amin, M. S., Vetrovec, G. W., and Baldi, A. (2006). Acute myocardial infarction and heart failure: role of apoptosis. *Int. J. Biochem. Cell Biol.* 38, 1834–1840. doi: 10.1016/j.biocel.2006.04.010

Abdalkader, M., Lampinen, R., Kanninen, K. M., Malm, T. M., and Liddell, J. R. (2018). Targeting Nrf2 to suppress ferroptosis and mitochondrial dysfunction in neurodegeneration. *Front. Neurosci.* 12:466. doi: 10.3389/fnins.2018.00466

Adameova, A., Goncalvesova, E., Szobi, A., and Dhalla, N. S. (2016). Necroptotic cell death in failing heart: relevance and proposed mechanisms. *Heart Fail Rev.* 21, 213–221. doi: 10.1007/s10741-016-9537-8

Adameova, A., Hrdlicka, J., Szobi, A., Farkasova, V., Kopaskova, K., Murarikova, M., et al. (2017). Evidence of necroptosis in hearts subjected to various forms of ischemic insults. *Can. J. Physiol. Pharm.* 95, 1163–1169. doi: 10.1139/cjpp-2016-0609

Agmon, E., Solon, J., Bassereau, P., and Stockwell, B. R. (2018). Modeling the effects of lipid peroxidation during ferroptosis on membrane properties. *Sci. Rep.* 8:5155. doi: 10.1038/s41598-018-23408-0

Akazawa, H. (2015). Mechanisms of cardiovascular homeostasis and pathophysiology–from gene expression, signal transduction to cellular communication. *Circ. J.* 79, 2529–2536. doi: 10.1253/circj.CJ-15-0818

Akazawa, H., Komazaki, S., Shimomura, H., Terasaki, F., Zou, Y., Takano, H., et al. (2004). Diphtheria toxin-induced autophagic cardiomyocyte death plays a pathogenic role in mouse model of heart failure. *J. Biol. Chem.* 279, 41095–41103. doi: 10.1074/jbc.M313084200

Anandhan, A., Dodson, M., Schmidlin, C. J., Liu, P., and Zhang, D. D. (2020). Breakdown of an ironclad defense system: the critical role of NRF2 in mediating ferroptosis. *Cell Chem. Biol.* 27, 436–447. doi: 10.1016/j.chembiol.2020.03.011

Asano, T., Komatsu, M., Yamaguchi-Iwai, Y., Ishikawa, F., Mizushima, N., and Iwai, K. (2011). Distinct mechanisms of ferritin delivery to lysosomes in iron-depleted and iron-replete cells. *Mol. Cell Biol.* 31, 2040–2052. doi: 10.1128/MCB.01437-10

Baba, Y., Higa, J. K., Shimada, B. K., Horiuchi, K. M., Suhara, T., Kobayashi, M., et al. (2018). Protective effects of the mechanistic target of rapamycin against excess iron and ferroptosis in cardiomyocytes. *Am. J. Physiol. Heart Circ. Physiol.* 314, H659–H668. doi: 10.1152/ajpheart.00452.2017

Bai, Y. T., Chang, R., Wang, H., Xiao, F. J., Ge, R. L., and Wang, L. S. (2018). ENPP2 protects cardiomyocytes from erastin-induced ferroptosis. *Biochem. Biophys. Res. Commun.* 499, 44–51. doi: 10.1016/j.bbrc.2018.03.113

Barth, E., Stammler, G., Speiser, B., and Schaper, J. (1992). Ultrastructural quantitation of mitochondria and myofilaments in cardiac muscle from 10 different animal species including man. *J. Mol. Cell Cardiol.* 24, 669–681. doi: 10.1016/0022-2828(92)93381-s

Bebber, C. M., Muller, F., Prieto Clemente, L., Weber, J., and von Karstedt, S. (2020). Ferroptosis in cancer cell biology. *Cancers (Basel)* 12:164. doi: 10.3390/cancers12010164

Bersuker, K., Hendricks, J. M., Li, Z., Magtanong, L., Ford, B., Tang, P. H., et al. (2019). The CoQ oxidoreductase FSP1 acts parallel to GPX4 to inhibit ferroptosis. *Nature* 575, 688–692. doi: 10.1038/s41586-019-1705-2

Bolduc, J. A., Collins, J. A., and Loeser, R. F. (2019). Reactive oxygen species, aging and articular cartilage homeostasis. *Free Radic. Biol. Med.* 132, 73–82. doi: 10.1016/j.freeradbiomed.2018.08.038

Borst, J. W., Visser, N. V., Kouptsova, O., and Visser, A. J. W. G. (2000). Oxidation of unsaturated phospholipids in membrane bilayer mixtures is accompanied by membrane fluidity changes. *BBA Mol. Cell Biol. L.* 1487, 61–73. doi: 10.1016/S1388-1981(00)00084-6

Bruni, A., Pepper, A. R., Pawlick, R. L., Gala-Lopez, B., Gamble, A. F., Kin, T., et al. (2018). Ferroptosis-inducing agents compromise *in vitro* human islet viability and function. *Cell Death Dis.* 9:595. doi: 10.1038/s41419-018-0506-0

Bugger, H., and Abel, E. D. (2014). Molecular mechanisms of diabetic cardiomyopathy. *Diabetologia* 57, 660–671. doi: 10.1007/s00125-014-3171-6

Cao, H., Chen, T., and Shi, Y. (2015). Glycation of human serum albumin in diabetes: impacts on the structure and function. *Curr. Med. Chem.* 22, 4–13. doi: 10.2174/0929867321666140912155738

Chang, H. C., Wu, R., Shang, M., Sato, T., Chen, C., Shapiro, J. S., et al. (2016). Reduction in mitochondrial iron alleviates cardiac damage during injury. *EMBO Mol. Med.* 8, 247–267. doi: 10.15252/emmm.201505748

Chen, X., Xu, S., Zhao, C., and Liu, B. (2019). Role of TLR4/NADPH oxidase 4 pathway in promoting cell death through autophagy and ferroptosis during heart failure. *Biochem. Biophys. Res. Commun.* 516, 37–43. doi: 10.1016/j.bbrc.2019.06.015

Chen, X. F., Li, X. L., Yang, M., Song, Y., and Zhang, Y. (2018). Osteoprotective effects of salidroside in ovariectomized mice and diabetic mice. *Eur. J. Pharmacol.* 819, 281–288. doi: 10.1016/j.ejphar.2017.12.025

Chen, Y., Hua, Y., Li, X., Arslan, I. M., Zhang, W., and Meng, G. (2020). Distinct types of cell death and the implication in diabetic cardiomyopathy. *Front. Pharmacol.* 11:42. doi: 10.3389/fphar.2020.00042

Conrad, M., and Proneth, B. (2019). Broken hearts: iron overload, ferroptosis and cardiomyopathy. *Cell Res.* 29, 263–264. doi: 10.1038/s41422-019-0150-y

Cordani, M., Donadelli, M., Strippoli, R., Bazhin, A. V., and Sanchez-Alvarez, M. (2019). Interplay between ROS and autophagy in cancer and aging: from molecular mechanisms to novel therapeutic approaches. *Oxid. Med. Cell. Longev.* 2019:8794612. doi: 10.1155/2019/8794612

Dabkowski, E. R., Williamson, C. L., and Hollander, J. M. (2008). Mitochondria-specific transgenic overexpression of phospholipid hydroperoxide glutathione peroxidase (GPx4) attenuates ischemia/reperfusion-associated cardiac dysfunction. *Free Radic. Biol. Med.* 45, 855–865. doi: 10.1016/j.freeradbiomed.2008.06.021

Davies, S. S., and Guo, L. (2014). Lipid peroxidation generates biologically active phospholipids including oxidatively N-modified phospholipids. *Chem. Phys. Lipids* 181, 1–33. doi: 10.1016/j.chemphyslip.2014.03.002

de Montalembert, M., Ribeil, J. A., Brousse, V., Guerci-Bresler, A., Stamatoullas, A., Vannier, J. P., et al. (2017). Cardiac iron overload in chronically transfused patients with thalassemia, sickle cell anemia, or myelodysplastic syndrome. *PLoS One* 12:e0172147. doi: 10.1371/journal.pone.0172147

Dickinson, D. A., and Forman, H. J. (2002). Cellular glutathione and thiols metabolism. *Biochem. Pharmacol.* 64, 1019–1026. doi: 10.1016/s0006-2952(02)01172-3

Dixon, S. J. (2017). Ferroptosis: bug or feature? *Immunol. Rev.* 277, 150–157. doi: 10.1111/imr.12533

Dixon, S. J., Lemberg, K. M., Lamprecht, M. R., Skouta, R., Zaitsev, E. M., Gleason, C. E., et al. (2012). Ferroptosis: an iron-dependent form of nonapoptotic cell death. *Cell* 149, 1060–1072. doi: 10.1016/j.cell.2012.03.042

Dixon, S. J., Patel, D. N., Welsch, M., Skouta, R., Lee, E. D., Hayano, M., et al. (2014). Pharmacological inhibition of cystine-glutamate exchange induces endoplasmic reticulum stress and ferroptosis. *Elife* 3:e02523. doi: 10.7554/eLife.02523

Dixon, S. J., Winter, G. E., Musavi, L. S., Lee, E. D., Snijder, B., Rebsamen, M., et al. (2015). Human haploid cell genetics reveals roles for lipid metabolism genes in Nonapoptotic cell death. *ACS Chem. Biol.* 10, 1604–1609. doi: 10.1021/acschembio.5b00245

Doll, S., Freitas, F. P., Shah, R., Aldrovandi, M., da Silva, M. C., Ingold, I., et al. (2019). FSP1 is a glutathione-independent ferroptosis suppressor. *Nature* 575, 693–698. doi: 10.1038/s41586-019-1707-0

Doll, S., Proneth, B., Tyurina, Y. Y., Panzilius, E., Kobayashi, S., Ingold, I., et al. (2017). ACSL4 dictates ferroptosis sensitivity by shaping cellular lipid composition. *Nat. Chem. Biol.* 13, 91–98. doi: 10.1038/nchembio.2239

Dolma, S., Lessnick, S. L., Hahn, W. C., and Stockwell, B. R. (2003). Identification of genotype-selective antitumor agents using synthetic lethal chemical screening in engineered human tumor cells. *Cancer Cell* 3, 285–296. doi: 10.1016/S1535-6108(03)00050-3

Eisenstein, R. S. (2000). Iron regulatory proteins and the molecular control of mammalian iron metabolism. *Annu. Rev. Nutr.* 20, 627–662. doi: 10.1146/annurev.nutr.20.1.627

Fang, X., Cai, Z., Wang, H., Han, D., Cheng, Q., Zhang, P., et al. (2020). Loss of Cardiac Ferritin H facilitates cardiomyopathy via Slc7a11-mediated ferroptosis. *Circ. Res.* 127, 486–501. doi: 10.1161/CIRCRESAHA.120.316509

Fang, X., Wang, H., Han, D., Xie, E., Yang, X., Wei, J., et al. (2019). Ferroptosis as a target for protection against cardiomyopathy. *Proc. Natl. Acad. Sci. U.S.A.* 116, 2672–2680. doi: 10.1073/pnas.1821022116

Felker, G. M., Thompson, R. E., Hare, J. M., Hruban, R. H., Clemetson, D. E., Howard, D. L., et al. (2000). Underlying causes and long-term survival in patients with initially unexplained cardiomyopathy. *N. Engl. J. Med.* 342, 1077–1084. doi: 10.1056/NEJM200004133421502

Fradejas, N., Carlson, B. A., Rijntjes, E., Becker, N. P., Tobe, R., and Schweizer, U. (2013). Mammalian Trit1 is a tRNA([Ser]Sec)-isopentenyl transferase required for full selenoprotein expression. *Biochem. J.* 450, 427–432. doi: 10.1042/BJ20121713

Frank, C. E. (1950). Hydrocarbon autoxidation. *Chem. Rev.* 46, 155–169. doi: 10.1021/cr60143a003

Frazier, W. J., Xue, J., Luce, W. A., and Liu, Y. (2012). MAPK signaling drives inflammation in LPS-stimulated cardiomyocytes: the route of crosstalk to G-protein-coupled receptors. *PLoS One* 7:e50071. doi: 10.1371/journal.pone.0050071

Friedmann Angeli, J. P., Schneider, M., Proneth, B., Tyurina, Y. Y., Tyurin, V. A., Hammond, V. J., et al. (2014). Inactivation of the ferroptosis regulator Gpx4 triggers acute renal failure in mice. *Nat. Cell Biol.* 16, 1180–1191. doi: 10.1038/ncb3064

Fujikura, K., Golive, A. D., Ando, T., Corado, F. M., Shitole, S. G., Kizer, J. R., et al. (2018). Increased iron deposition is directly associated with myocardial dysfunction in patients with sickle cell disease. *JACC Cardiovasc. Imaging* 11, 279–280. doi: 10.1016/j.jcmg.2017.02.011

Galluzzi, L., Vitale, I., Aaronson, S. A., Abrams, J. M., Adam, D., Agostinis, P., et al. (2018). Molecular mechanisms of cell death: recommendations of the Nomenclature Committee on Cell Death 2018. *Cell Death Differ.* 25, 486–541. doi: 10.1038/s41418-017-0012-4

Gao, C., Li, L., Chen, B., Song, H., Cheng, J., Zhang, X., et al. (2014). Clinical outcomes of transfusion-associated iron overload in patients with refractory chronic anemia. *Patient Prefer. Adherence* 8, 513–517. doi: 10.2147/PPA.S56238

Gao, G., Li, J., Zhang, Y., and Chang, Y. Z. (2019). Cellular iron metabolism and regulation. *Adv. Exp. Med. Biol.* 1173, 21–32. doi: 10.1007/978-981-13-9589-5_2

Gao, M., Monian, P., Quadri, N., Ramasamy, R., and Jiang, X. (2015). Glutaminolysis and transferrin regulate ferroptosis. *Mol. Cell* 59, 298–308. doi: 10.1016/j.molcel.2015.06.011

Gao, M., Yi, J., Zhu, J., Minikes, A. M., Monian, P., Thompson, C. B., et al. (2019). Role of mitochondria in ferroptosis. *Mol. Cell* 73:e353. doi: 10.1016/j.molcel.2018.10.042

Ge, Z. D., Lian, Q., Mao, X., and Xia, Z. (2019). Current status and challenges of NRF2 as a potential therapeutic target for diabetic cardiomyopathy. *Int. Heart J.* 60, 512–520. doi: 10.1536/ihj.18-476

Ghafourian, K., Shapiro, J. S., Goodman, L., and Ardehali, H. (2020). Iron and heart failure: diagnosis, therapies, and future directions. *JACC Basic Transl. Sci.* 5, 300–313. doi: 10.1016/j.jacbts.2019.08.009

Ghardashi Afousi, A., Gaeini, A., Rakhshan, K., Naderi, N., Darbandi Azar, A., and Aboutaleb, N. (2019). Targeting necroptotic cell death pathway by high-intensity interval training (HIIT) decreases development of post-ischemic adverse remodelling after myocardial ischemia / reperfusion injury. *J. Cell Commun. Signal.* 13, 255–267. doi: 10.1007/s12079-018-0481-3

Golej, D. L., Askari, B., Kramer, F., Barnhart, S., Vivekanandan-Giri, A., Pennathur, S., et al. (2011). Long-chain acyl-CoA synthetase 4 modulates prostaglandin E(2) release from human arterial smooth muscle cells. *J. Lipid. Res.* 52, 782–793. doi: 10.1194/jlr.M013292

Gray, N. K., and Hentze, M. W. (1994). Iron regulatory protein prevents binding of the 43S translation pre-initiation complex to ferritin and eALAS mRNAs. *EMBO J.* 13, 3882–3891. doi: 10.1002/j.1460-2075.1994.tb06699.x

Griffith, O. W. (1999). Biologic and pharmacologic regulation of mammalian glutathione synthesis. *Free Radic. Biol. Med.* 27, 922–935. doi: 10.1016/s0891-5849(99)00176-8

Guiney, S. J., Adlard, P. A., Bush, A. I., Finkelstein, D. I., and Ayton, S. (2017). Ferroptosis and cell death mechanisms in Parkinson's disease. *Neurochem. Int.* 104, 34–48. doi: 10.1016/j.neuint.2017.01.004

Gujja, P., Rosing, D. R., Tripodi, D. J., and Shizukuda, Y. (2010). Iron overload cardiomyopathy: better understanding of an increasing disorder. *J. Am. Coll. Cardiol.* 56, 1001–1012. doi: 10.1016/j.jacc.2010.03.083

Han, C., Liu, Y., Dai, R., Ismail, N., Su, W., and Li, B. (2020). Ferroptosis and its potential role in human diseases. *Front. Pharmacol.* 11:239. doi: 10.3389/fphar.2020.00239

Hayano, M., Yang, W. S., Corn, C. K., Pagano, N. C., and Stockwell, B. R. (2016). Loss of cysteinyl-tRNA synthetase (CARS) induces the transsulfuration pathway and inhibits ferroptosis induced by cystine deprivation. *Cell Death Differ.* 23, 270–278. doi: 10.1038/cdd.2015.93

Hirst, J. (2013). Mitochondrial complex I. *Annu. Rev. Biochem.* 82, 551–575. doi: 10.1146/annurev-biochem-070511-103700

Hou, W., Xie, Y., Song, X., Sun, X., Lotze, M. T., Zeh, H. J. III, et al. (2016). Autophagy promotes ferroptosis by degradation of ferritin. *Autophagy* 12, 1425–1428. doi: 10.1080/15548627.2016.1187366

Huang, T., Sun, Y., Li, Y., Wang, T., Fu, Y., Li, C., et al. (2018). Growth inhibition of a novel iron chelator, DpdtC, against hepatoma carcinoma cell lines partly attributed to ferritinophagy-mediated lysosomal ROS generation. *Oxid. Med. Cell. Longev.* 2018:4928703. doi: 10.1155/2018/4928703

Huynh, K., Bernardo, B. C., McMullen, J. R., and Ritchie, R. H. (2014). Diabetic cardiomyopathy: mechanisms and new treatment strategies targeting antioxidant signaling pathways. *Pharmacol. Ther.* 142, 375–415. doi: 10.1016/j.pharmthera.2014.01.003

Imai, H., Matsuoka, M., Kumagai, T., Sakamoto, T., and Koumura, T. (2017). Lipid peroxidation-dependent cell death regulated by GPx4 and ferroptosis. *Curr. Top. Microbiol. Immunol.* 403, 143–170. doi: 10.1007/82_2016_508

Jennis, M., Kung, C. P., Basu, S., Budina-Kolomets, A., Leu, J. I., Khaku, S., et al. (2016). An African-specific polymorphism in the TP53 gene impairs 53 tumor suppressor function in a mouse model. *Genes Dev.* 30, 918–930. doi: 10.1101/gad.275891.115

Jiang, L., Kon, N., Li, T. Y., Wang, S. J., Su, T., Hibshoosh, H., et al. (2015). Ferroptosis as a 53-mediated activity during tumour suppression. *Nature* 520, 57–62. doi: 10.1038/nature14344

Johnson, D. C., Dean, D. R., Smith, A. D., and Johnson, M. K. (2005). Structure, function, and formation of biological iron-sulfur clusters. *Annu. Rev. Biochem.* 74, 247–281. doi: 10.1146/annurev.biochem.74.082803.133518

Jones, D. P. (2006). Extracellular redox state: refining the definition of oxidative stress in aging. *Rejuvenation. Res.* 9, 169–181. doi: 10.1089/rej.2006.9.169

Kagan, V. E., Mao, G., Qu, F., Angeli, J. P., Doll, S., Croix, C. S., et al. (2017). Oxidized arachidonic and adrenic PEs navigate cells to ferroptosis. *Nat. Chem. Biol.* 13, 81–90. doi: 10.1038/nchembio.2238

Kalinina, E. V., and Gavriliuk, L. A. (2020). Glutathione synthesis in cancer cells. *Biochemistry (Mosc)* 85, 895–907. doi: 10.1134/S0006297920080052

Kang, P. M., and Izumo, S. (2003). Apoptosis in heart: basic mechanisms and implications in cardiovascular diseases. *Trends Mol. Med.* 9, 177–182. doi: 10.1016/s1471-4914(03)00025-x

Kang, R., Kroemer, G., and Tang, D. (2019). The tumor suppressor protein 53 and the ferroptosis network. *Free Radic. Biol. Med.* 133, 162–168. doi: 10.1016/j.freeradbiomed.2018.05.074

Kerr, J. F., Wyllie, A. H., and Currie, A. R. (1972). Apoptosis: a basic biological phenomenon with wide-ranging implications in tissue kinetics. *Br. J. Cancer* 26, 239–257. doi: 10.1038/bjc.1972.33

Khullar, M., Al-Shudiefat, A. A., Ludke, A., Binepal, G., and Singal, P. K. (2010). Oxidative stress: a key contributor to diabetic cardiomyopathy. *Can. J. Physiol. Pharmacol.* 88, 233–240. doi: 10.1139/Y10-016

Kidane, T. Z., Sauble, E., and Linder, M. C. (2006). Release of iron from ferritin requires lysosomal activity. *Am. J. Physiol. Cell Physiol.* 291, C445–C455. doi: 10.1152/ajpcell.00505.2005

Kontoghiorghe, C. N., and Kontoghiorghes, G. J. (2016). Efficacy and safety of iron-chelation therapy with deferoxamine, deferiprone, and deferasirox for the treatment of iron-loaded patients with non-transfusion-dependent thalassemia syndromes. *Drug Des. Devel. Ther.* 10, 465–481. doi: 10.2147/DDDT.S79458

Kuhn, H., Banthiya, S., and van Leyen, K. (2015). Mammalian lipoxygenases and their biological relevance. *BBA Mol. Cell Biol. L.* 1851, 308–330. doi: 10.1016/j.bbalip.2014.10.002

Kurmus, O., Aslan, T., Ekici, B., Baglan Uzunget, S., Karaarslan, S., Tanindi, A., et al. (2018). Impact of admission blood glucose on coronary collateral flow in patients with ST-Elevation myocardial infarction. *Cardiol. Res. Pract.* 2018:4059542. doi: 10.1155/2018/4059542

Kwon, M. Y., Park, E., Lee, S. J., and Chung, S. W. (2015). Heme oxygenase-1 accelerates erastin-induced ferroptotic cell death. *Oncotarget* 6, 24393–24403. doi: 10.18632/oncotarget.5162

Lai, C. S., and Piette, L. H. (1978). Spin-trapping studies of hydroxyl radical production involved in lipid peroxidation. *Arch. Biochem. Biophys.* 190, 27–38. doi: 10.1016/0003-9861(78)90250-3

Lakhal-Littleton, S. (2019). Iron deficiency as a therapeutic target in cardiovascular disease. *Pharmaceuticals (Basel)* 12:125. doi: 10.3390/ph12030125

Latunde-Dada, G. O. (2017). Ferroptosis: role of lipid peroxidation, iron and ferritinophagy. *Biochim. Biophys. Acta Gen. Subj.* 1861, 1893–1900. doi: 10.1016/j.bbagen.2017.05.019

Lawen, A., and Lane, D. J. (2013). Mammalian iron homeostasis in health and disease: uptake, storage, transport, and molecular mechanisms of action. *Antioxid Redox Signal.* 18, 2473–2507. doi: 10.1089/ars.2011.4271

Lei, P., Bai, T., and Sun, Y. (2019). Mechanisms of ferroptosis and relations with regulated cell death: a review. *Front. Physiol.* 10:139. doi: 10.3389/fphys.2019.00139

Levi, S., and Rovida, E. (2009). The role of iron in mitochondrial function. *Biochim. Biophys. Acta* 1790, 629–636. doi: 10.1016/j.bbagen.2008.09.008

Li, N., Jiang, W., Wang, W., Xiong, R., Wu, X., and Geng, Q. (2021). Ferroptosis and its emerging roles in cardiovascular diseases. *Pharmacol. Res.* 166:105466. doi: 10.1016/j.phrs.2021.105466

Li, N., Wang, W., Zhou, H., Wu, Q., Duan, M., Liu, C., et al. (2020). Ferritinophagy-mediated ferroptosis is involved in sepsis-induced cardiac injury. *Free Radic. Biol. Med.* 160, 303–318. doi: 10.1016/j.freeradbiomed.2020.08.009

Li, N., Zhou, H., Wu, H., Wu, Q., Duan, M., Deng, W., et al. (2019). IRF3 contributes to lipopolysaccharide-induced cardiac dysfunction, inflammation, apoptosis and pyroptosis by activating NLRP3. *Redox Biol.* 24:101215. doi: 10.1016/j.redox.2019.101215

Li, W., Feng, G., Gauthier, J. M., Lokshina, I., Higashikubo, R., Evans, S., et al. (2019). Ferroptotic cell death and TLR4/Trif signaling initiate neutrophil recruitment after heart transplantation. *J. Clin. Invest.* 129, 2293–2304. doi: 10.1172/JCI126428

Li, W., Li, W., Leng, Y., Xiong, Y., and Xia, Z. (2020). Ferroptosis is involved in diabetes myocardial ischemia/reperfusion injury through endoplasmic reticulum stress. *DNA Cell Biol.* 39, 210–225. doi: 10.1089/dna.2019.5097

Lin, X., Ping, J., Wen, Y., and Wu, Y. (2020). The mechanism of ferroptosis and applications in tumor treatment. *Front. Pharmacol.* 11:1061. doi: 10.3389/fphar.2020.01061

Linkermann, A., Skouta, R., Himmerkus, N., Mulay, S. R., Dewitz, C., De Zen, F., et al. (2014). Synchronized renal tubular cell death involves ferroptosis. *Proc. Natl. Acad. Sci. U.S.A.* 111, 16836–16841. doi: 10.1073/pnas.1415518111

Liu, B., Zhao, C., Li, H., Chen, X., Ding, Y., and Xu, S. (2018). Puerarin protects against heart failure induced by pressure overload through mitigation of ferroptosis. *Biochem. Biophys. Res. Commun.* 497, 233–240. doi: 10.1016/j.bbrc.2018.02.061

Liu, Y., Zeng, L., Yang, Y., Chen, C., Wang, D., and Wang, H. (2020). Acyl-CoA thioesterase 1 prevents cardiomyocytes from Doxorubicin-induced ferroptosis via shaping the lipid composition. *Cell Death Dis.* 11:756. doi: 10.1038/s41419-020-02948-2

Liu, Y., Zhao, N., Li, C., Chang, Q., Liu, X., Liao, Y., et al. (2017). Longistyline C acts antidepressant in vivo and neuroprotection *in vitro* against glutamate-induced cytotoxicity by regulating NMDAR/NR2B-ERK pathway in C12 cells. *PLoS one* 12:e0183702. doi: 10.1371/journal.pone.0183702

Loreal, O., Cavey, T., Bardou-Jacquet, E., Guggenbuhl, P., Ropert, M., and Brissot, P. (2014). Iron, hepcidin, and the metal connection. *Front. Pharmacol.* 5:128. doi: 10.3389/fphar.2014.00128

Lu, B., Chen, X. B., Ying, M. D., He, Q. J., Cao, J., and Yang, B. (2017). The role of ferroptosis in cancer development and treatment response. *Front. Pharmacol.* 8:992. doi: 10.3389/fphar.2017.00992

Luedde, M., Lutz, M., Carter, N., Sosna, J., Jacoby, C., Vucur, M., et al. (2014). RIP3, a kinase promoting necroptotic cell death, mediates adverse remodelling after myocardial infarction. *Cardiovasc. Res.* 103, 206–216. doi: 10.1093/cvr/cvu146

Lv, H., Zhen, C., Liu, J., Yang, P., Hu, L., and Shang, P. (2019). Unraveling the potential role of glutathione in multiple forms of cell death in cancer therapy. *Oxid. Med. Cell. Longev.* 2019:3150145. doi: 10.1155/2019/3150145

Mancias, J. D., Wang, X., Gygi, S. P., Harper, J. W., and Kimmelman, A. C. (2014). Quantitative proteomics identifies NCOA4 as the cargo receptor mediating ferritinophagy. *Nature* 509, 105–109. doi: 10.1038/nature13148

Maron, B. J., Rowin, E. J., Udelson, J. E., and Maron, M. S. (2018). Clinical spectrum and management of heart failure in hypertrophic cardiomyopathy. *JACC Heart Fail* 6, 353–363. doi: 10.1016/j.jchf.2017.09.011

Martins, I., Raza, S. Q., Voisin, L., Dakhli, H., Law, F., De Jong, D., et al. (2017). Entosis: the emerging face of non-cell-autonomous type IV programmed death. *Biomed. J.* 40, 133–140. doi: 10.1016/j.bj.2017.05.001

Masaldan, S., Clatworthy, S. A. S., Gamell, C., Meggyesy, P. M., Rigopoulos, A. T., Haupt, S., et al. (2018). Iron accumulation in senescent cells is coupled with impaired ferritinophagy and inhibition of ferroptosis. *Redox Biol.* 14, 100–115. doi: 10.1016/j.redox.2017.08.015

Matsushita, M., Freigang, S., Schneider, C., Conrad, M., Bornkamm, G. W., and Kopf, M. (2015). T cell lipid peroxidation induces ferroptosis and prevents immunity to infection. *J. Exp. Med.* 212, 555–568. doi: 10.1084/jem.20140857

Melenovsky, V., Petrak, J., Mracek, T., Benes, J., Borlaug, B. A., Nuskova, H., et al. (2017). Myocardial iron content and mitochondrial function in human heart failure: a direct tissue analysis. *Eur. J. Heart Failure* 19, 522–530. doi: 10.1002/ejhf.640

Morgan, B., Ezerina, D., Amoako, T. N., Riemer, J., Seedorf, M., and Dick, T. P. (2013). Multiple glutathione disulfide removal pathways mediate cytosolic redox homeostasis. *Nat. Chem. Biol.* 9, 119–125. doi: 10.1038/nchembio.1142

Nakamura, T., Naguro, I., and Ichijo, H. (2019). Iron homeostasis and iron-regulated ROS in cell death, senescence and human diseases. *Biochim. Biophys. Acta Gen. Subj.* 1863, 1398–1409. doi: 10.1016/j.bbagen.2019.06.010

Oudit, G. Y., Sun, H., Trivieri, M. G., Koch, S. E., Dawood, F., Ackerley, C., et al. (2003). L-type Ca2+ channels provide a major pathway for iron entry into cardiomyocytes in iron-overload cardiomyopathy. *Nat. Med.* 9, 1187–1194. doi: 10.1038/nm920

Owen, J. B., and Butterfield, D. A. (2010). Measurement of oxidized/reduced glutathione ratio. *Methods Mol. Biol.* 648, 269–277. doi: 10.1007/978-1-60761-756-3_18

Pantopoulos, K., Porwal, S. K., Tartakoff, A., and Devireddy, L. (2012). Mechanisms of mammalian iron homeostasis. *Biochemistry* 51, 5705–5724. doi: 10.1021/bi300752r

Paolillo, S., Marsico, F., Prastaro, M., Renga, F., Esposito, L., De Martino, F., et al. (2019). Diabetic cardiomyopathy: definition, diagnosis, and therapeutic implications. *Heart Failure Clin.* 15, 341–347. doi: 10.1016/j.hfc.2019.02.003

Parim, B., Sathibabu Uddandrao, V. V., and Saravanan, G. (2019). Diabetic cardiomyopathy: molecular mechanisms, detrimental effects of conventional treatment, and beneficial effects of natural therapy. *Heart Fail Rev.* 24, 279–299. doi: 10.1007/s10741-018-9749-1

Park, T. J., Park, J. H., Lee, G. S., Lee, J. Y., Shin, J. H., Kim, M. W., et al. (2019). Quantitative proteomic analyses reveal that GPX4 downregulation during myocardial infarction contributes to ferroptosis in cardiomyocytes. *Cell Death Dis.* 10:835. doi: 10.1038/s41419-019-2061-8

Petrat, F., de Groot, H., and Rauen, U. (2001). Subcellular distribution of chelatable iron: a laser scanning microscopic study in isolated hepatocytes and liver endothelial cells. *Biochem. J.* 356, 61–69. doi: 10.1042/0264-6021:3560061

Pompella, A., and Corti, A. (2015). Editorial: the changing faces of glutathione, a cellular protagonist. *Front. Pharmacol.* 6:98. doi: 10.3389/fphar.2015.00098

Pompella, A., Visvikis, A., Paolicchi, A., De Tata, V., and Casini, A. F. (2003). The changing faces of glutathione, a cellular protagonist. *Biochem. Pharmacol.* 66, 1499–1503. doi: 10.1016/s0006-2952(03)00504-5

Qiu, Y., Cao, Y., Cao, W., Jia, Y., and Lu, N. (2020). The application of ferroptosis in diseases. *Pharmacol. Res.* 159:104919. doi: 10.1016/j.phrs.2020.104919

Rauen, U., Springer, A., Weisheit, D., Petrat, F., Korth, H. G., de Groot, H., et al. (2007). Assessment of chelatable mitochondrial iron by using mitochondrion-selective fluorescent iron indicators with different iron-binding affinities. *Chembiochem* 8, 341–352. doi: 10.1002/cbic.200600311

Ravingerova, T., Kindernay, L., Bartekova, M., Ferko, M., Adameova, A., Zohdi, V., et al. (2020). The molecular mechanisms of iron metabolism and its role in cardiac dysfunction and cardioprotection. *Int. J. Mol. Sci.* 21:7889. doi: 10.3390/ijms21217889

Rosenbaum, A. N., Agre, K. E., and Pereira, N. L. (2020). Genetics of dilated cardiomyopathy: practical implications for heart failure management. *Nat. Rev. Cardiol.* 17, 286–297. doi: 10.1038/s41569-019-0284-0

Rui, T., Li, Q., Song, S., Gao, Y., and Luo, C. (2020). Ferroptosis-relevant mechanisms and biomarkers for therapeutic interventions in traumatic brain injury. *Histol. Histopathol.* 35, 1105–1113. doi: 10.14670/HH-18-229

Seiler, A., Schneider, M., Forster, H., Roth, S., Wirth, E. K., Culmsee, C., et al. (2008). Glutathione peroxidase 4 senses and translates oxidative stress into 12/15-lipoxygenase dependent- and AIF-mediated cell death. *Cell Metab.* 8, 237–248. doi: 10.1016/j.cmet.2008.07.005

Sentellas, S., Morales-Ibanez, O., Zanuy, M., and Alberti, J. J. (2014). GSSG/GSH ratios in cryopreserved rat and human hepatocytes as a biomarker for drug induced oxidative stress. *Toxicol. In Vitro* 28, 1006–1015. doi: 10.1016/j.tiv.2014.04.017

Shen, E., Fan, J., Chen, R., Yee, S. P., and Peng, T. (2007). Phospholipase Cgamma1 signalling regulates lipopolysaccharide-induced cyclooxygenase-2 expression in cardiomyocytes. *J. Mol. Cell Cardiol.* 43, 308–318. doi: 10.1016/j.yjmcc.2007.06.007

Shimada, K., Skouta, R., Kaplan, A., Yang, W. S., Hayano, M., Dixon, S. J., et al. (2016). Global survey of cell death mechanisms reveals metabolic regulation of ferroptosis. *Nat. Chem. Biol.* 12, 497–503. doi: 10.1038/nchembio.2079

Stehling, O., and Lill, R. (2013). The role of mitochondria in cellular iron-sulfur protein biogenesis: mechanisms, connected processes, and diseases. *Cold Spring Harb. Perspect. Biol.* 5:a011312. doi: 10.1101/cshperspect.a011312

Stockwell, B. R., Friedmann Angeli, J. P., Bayir, H., Bush, A. I., Conrad, M., Dixon, S. J., et al. (2017). Ferroptosis: a regulated cell death nexus linking metabolism. *Redox Biology, and Disease. Cell* 171, 273–285. doi: 10.1016/j.cell.2017.09.021

Sui, S., Zhang, J., Xu, S., Wang, Q., Wang, P., and Pang, D. (2019). Ferritinophagy is required for the induction of ferroptosis by the bromodomain protein BRD4 inhibitor (+)-JQ1 in cancer cells. *Cell Death Dis.* 10:331. doi: 10.1038/s41419-019-1564-7

Sumneang, N., Siri-Angkul, N., Kumfu, S., Chattipakorn, S. C., and Chattipakorn, N. (2020). The effects of iron overload on mitochondrial function, mitochondrial dynamics, and ferroptosis in cardiomyocytes. *Arch. Biochem. Biophys.* 680:108241. doi: 10.1016/j.abb.2019.108241

Sun, Y., Yao, X., Zhang, Q. J., Zhu, M., Liu, Z. P., Ci, B., et al. (2018a). Beclin-1-dependent autophagy protects the heart during sepsis. *Circulation* 138, 2247–2262. doi: 10.1161/CIRCULATIONAHA.117.032821

Sun, Y., Zheng, Y., Wang, C., and Liu, Y. (2018b). Glutathione depletion induces ferroptosis, autophagy, and premature cell senescence in retinal pigment epithelial cells. *Cell Death Dis.* 9:753. doi: 10.1038/s41419-018-0794-4

Suzuki, J., Bayna, E., Dalle Molle, E., and Lew, W. Y. (2003). Nicotine inhibits cardiac apoptosis induced by lipopolysaccharide in rats. *J. Am. Coll. Cardiol.* 41, 482–488. doi: 10.1016/s0735-1097(02)02820-6

Tadokoro, T., Ikeda, M., Ide, T., Deguchi, H., Ikeda, S., Okabe, K., et al. (2020). Mitochondria-dependent ferroptosis plays a pivotal role in doxorubicin cardiotoxicity. *JCI Insight* 5:e132747. doi: 10.1172/jci.insight.132747

Tang, D., Kang, R., Berghe, T. V., Vandenabeele, P., and Kroemer, G. (2019). The molecular machinery of regulated cell death. *Cell Res.* 29, 347–364. doi: 10.1038/s41422-019-0164-5

Tang, M., Chen, Z., Wu, D., and Chen, L. (2018). Ferritinophagy/ferroptosis: iron-related newcomers in human diseases. *J. Cell Physiol.* 233, 9179–9190. doi: 10.1002/jcp.26954

Thomas, C., Mackey, M. M., Diaz, A. A., and Cox, D. P. (2013). Hydroxyl radical is produced via the Fenton reaction in submitochondrial particles under oxidative stress: implications for diseases associated with iron accumulation. *Redox Rep.* 14, 102–108. doi: 10.1179/135100009x392566

Viswanathan, V. S., Ryan, M. J., Dhruv, H. D., Gill, S., Eichhoff, O. M., Seashore-Ludlow, B., et al. (2017). Dependency of a therapy-resistant state of cancer cells on a lipid peroxidase pathway. *Nature* 547, 453–457. doi: 10.1038/nature23007

von Haehling, S., Jankowska, E. A., van Veldhuisen, D. J., Ponikowski, P., and Anker, S. D. (2015). Iron deficiency and cardiovascular disease. *Nat. Rev. Cardiol.* 12, 659–669. doi: 10.1038/nrcardio.2015.109

Wang, G., Hamid, T., Keith, R. J., Zhou, G., Partridge, C. R., Xiang, X., et al. (2010). Cardioprotective and antiapoptotic effects of heme oxygenase-1 in the failing heart. *Circulation* 121, 1912–1925. doi: 10.1161/CIRCULATIONAHA.109.905471

Wang, J., Liu, H., Li, N., Zhang, Q., and Zhang, H. (2014). The protective effect of fucoidan in rats with streptozotocin-induced diabetic nephropathy. *Mar. Drugs* 12, 3292–3306. doi: 10.3390/md12063292

Wang, J., and Pantopoulos, K. (2011). Regulation of cellular iron metabolism. *Biochem. J.* 434, 365–381. doi: 10.1042/BJ20101825

Wang, Y., Wang, Y., Yang, D., Yu, X., Li, H., Lv, X., et al. (2015). beta(1)-adrenoceptor stimulation promotes LPS-induced cardiomyocyte apoptosis through activating PKA and enhancing CaMKII and IkappaBalpha phosphorylation. *Crit. Care* 19:76. doi: 10.1186/s13054-015-0820-1

Wei, X. M., Yang, W. B., Su, X. X., Zhang, A. D., Jin, W., and Fang, Y. H. (2020). Plasma free fatty acid is associated with ischemic cardiomyopathy and cardiac dysfunction severity in systolic heart failure patients with diabetes. *Chin. Med. J. (Engl)* 134, 472–474. doi: 10.1097/CM9.0000000000001167

Wencker, D., Chandra, M., Nguyen, K., Miao, W., Garantziotis, S., Factor, S. M., et al. (2003). A mechanistic role for cardiac myocyte apoptosis in heart failure. *J. Clin. Invest.* 111, 1497–1504. doi: 10.1172/JCI17664

Wolpaw, A. J., Shimada, K., Skouta, R., Welsch, M. E., Akavia, U. D., Pe'er, D., et al. (2011). Modulatory profiling identifies mechanisms of small molecule-induced cell death. *Proc. Natl. Acad. Sci. U.S.A.* 108, E771–E780. doi: 10.1073/pnas.1106149108

Wu, C., Zhao, W., Yu, J., Li, S., Lin, L., and Chen, X. (2018). Induction of ferroptosis and mitochondrial dysfunction by oxidative stress in C12 cells. *Sci. Rep.* 8:574. doi: 10.1038/s41598-017-18935-1

Wu, X., Li, Y., Zhang, S., and Zhou, X. (2021). Ferroptosis as a novel therapeutic target for cardiovascular disease. *Theranostics* 11, 3052–3059. doi: 10.7150/thno.54113

Xie, Y., Hou, W., Song, X., Yu, Y., Huang, J., Sun, X., et al. (2016). Ferroptosis: process and function. *Cell Death Differ.* 23, 369–379. doi: 10.1038/cdd.2015.158

Xu, T., Ding, W., Ji, X., Ao, X., Liu, Y., Yu, W., et al. (2019). Molecular mechanisms of ferroptosis and its role in cancer therapy. *J. Cell. Mol. Med.* 23, 4900–4912. doi: 10.1111/jcmm.14511

Yagoda, N., von Rechenberg, M., Zaganjor, E., Bauer, A. J., Yang, W. S., Fridman, D. J., et al. (2007). RAS-RAF-MEK-dependent oxidative cell death involving voltage-dependent anion channels. *Nature* 447, 864–868. doi: 10.1038/nature05859

Yang, W. S., Kim, K. J., Gaschler, M. M., Patel, M., Shchepinov, M. S., and Stockwell, B. R. (2016). Peroxidation of polyunsaturated fatty acids by lipoxygenases drives ferroptosis. *Proc. Natl. Acad. Sci. U.S.A.* 113, E4966–E4975. doi: 10.1073/pnas.1603244113

Yang, W. S., SriRamaratnam, R., Welsch, M. E., Shimada, K., Skouta, R., Viswanathan, V. S., et al. (2014). Regulation of ferroptotic cancer cell death by GPX4. *Cell* 156, 317–331. doi: 10.1016/j.cell.2013.12.010

Yang, W. S., and Stockwell, B. R. (2008). Synthetic lethal screening identifies compounds activating iron-dependent, nonapoptotic cell death in oncogenic-RAS-harboring cancer cells. *Chem. Biol.* 15, 234–245. doi: 10.1016/j.chembiol.2008.02.010

Yang, W. S., and Stockwell, B. R. (2016). Ferroptosis: death by lipid peroxidation. *Trends Cell Biol.* 26, 165–176. doi: 10.1016/j.tcb.2015.10.014

Yet, S. F., Tian, R., Layne, M. D., Wang, Z. Y., Maemura, K., Solovyeva, M., et al. (2001). Cardiac-specific expression of heme oxygenase-1 protects against ischemia and reperfusion injury in transgenic mice. *Circ. Res.* 89, 168–173. doi: 10.1161/hh1401.093314

Yoshimura, C., Nagasaka, A., Kurose, H., and Nakaya, M. (2020). Efferocytosis during myocardial infarction. *J. Biochem.* 168, 1–6. doi: 10.1093/jb/mvaa051

Yuan, H., Li, X., Zhang, X., Kang, R., and Tang, D. (2016a). CISD1 inhibits ferroptosis by protection against mitochondrial lipid peroxidation. *Biochem. Biophys. Res. Commun.* 478, 838–844. doi: 10.1016/j.bbrc.2016.08.034

Yuan, H., Li, X. M., Zhang, X. Y., Kang, R., and Tang, D. L. (2016b). Identification of ACSL4 as a biomarker and contributor of ferroptosis. *Biochem. Biophys. Res. Commun.* 478, 1338–1343. doi: 10.1016/j.bbrc.2016.08.124

Zang, H., Wu, W., Qi, L., Tan, W., Nagarkatti, P., and Nagarkatti, M. (2020). Inhibition enables Nrf2 to exaggerate the progression of diabetic cardiomyopathy in mice. *Diabetes* 69, 2720–2734. doi: 10.2337/db19-1176

Zechendorf, E., O'Riordan, C. E., Stiehler, L., Wischmeyer, N., Chiazza, F., Collotta, D., et al. (2020). Ribonuclease 1 attenuates septic cardiomyopathy and cardiac apoptosis in a murine model of polymicrobial sepsis. *JCI Insight* 5:e131571. doi: 10.1172/jci.insight.131571

Zhang, H., Zhabyeyev, P., Wang, S., and Oudit, G. Y. (2019). Role of iron metabolism in heart failure: from iron deficiency to iron overload. *Biochim. Biophys. Acta Mol. Basis Dis.* 1865, 1925–1937. doi: 10.1016/j.bbadis.2018.08.030

Zheng, D. W., Lei, Q., Zhu, J. Y., Fan, J. X., Li, C. X., Li, C., et al. (2017). Switching apoptosis to ferroptosis: metal-organic network for high-efficiency anticancer therapy. *Nano Lett.* 17, 284–291. doi: 10.1021/acs.nanolett.6b04060

Zhu, H., and Sun, A. (2018). Programmed necrosis in heart disease: molecular mechanisms and clinical implications. *J. Mol. Cell Cardiol.* 116, 125–134. doi: 10.1016/j.yjmcc.2018.01.018

Zilka, O., Shah, R., Li, B., Friedmann Angeli, J. P., Griesser, M., Conrad, M., et al. (2017). On the mechanism of cytoprotection by ferrostatin-1 and liproxstatin-1 and the role of lipid peroxidation in ferroptotic cell death. *ACS Cent. Sci.* 3, 232–243. doi: 10.1021/acscentsci.7b00028

Zitka, O., Skalickova, S., Gumulec, J., Masarik, M., Adam, V., Hubalek, J., et al. (2012). Redox status expressed as GSH:GSSG ratio as a marker for oxidative stress in paediatric tumour patients. *Oncol. Lett.* 4, 1247–1253. doi: 10.3892/ol.2012.931

Conflict of Interest: The authors declare that the research was conducted in the absence of any commercial or financial relationships that could be construed as a potential conflict of interest.

frontiers in Cell and Developmental Biology

BRIEF RESEARCH REPORT
published: 31 May 2021
doi: 10.3389/fcell.2021.689951

Identification of the Bok Interactome Using Proximity Labeling

*Laura M. Szczesniak, Caden G. Bonzerato and Richard J. H. Wojcikiewicz**

Department of Pharmacology, SUNY Upstate Medical University, Syracuse, NY, United States

The function of the Bcl-2 family member Bok is currently enigmatic, with various disparate roles reported, including mediation of apoptosis, regulation of mitochondrial morphology, binding to inositol 1,4,5-trisphosphate receptors, and regulation of uridine metabolism. To better define the roles of Bok, we examined its interactome using TurboID-mediated proximity labeling in HeLa cells, in which Bok knock-out leads to mitochondrial fragmentation and Bok overexpression leads to apoptosis. Labeling with TurboID-Bok revealed that Bok was proximal to a wide array of proteins, particularly those involved in mitochondrial fission (e.g., Drp1), endoplasmic reticulum-plasma membrane junctions (e.g., Stim1), and surprisingly among the Bcl-2 family members, just Mcl-1. Comparison with TurboID-Mcl-1 and TurboID-Bak revealed that the three Bcl-2 family member interactomes were largely independent, but with some overlap that likely identifies key interactors. Interestingly, when overexpressed, Mcl-1 and Bok interact physically and functionally, in a manner that depends upon the transmembrane domain of Bok. Overall, this work shows that the Bok interactome is different from those of Mcl-1 and Bak, identifies novel proximities and potential interaction points for Bcl-2 family members, and suggests that Bok may regulate mitochondrial fission via Mcl-1 and Drp1.

Keywords: Bcl-2 related ovarian killer, B-cell lymphoma 2 (Bcl-2) family, proximity labeling, myeloid-cell leukemia 1, apoptosis

OPEN ACCESS

Edited by:
Jochen H. M. Prehn, Royal College of Surgeons in Ireland, Ireland

Reviewed by:
Thomas Kaufmann, University of Bern, Switzerland
Michelle Miller, Walter and Eliza Hall Institute of Medical Research, Australia

***Correspondence:**
Richard J. H. Wojcikiewicz
wojcikir@upstate.edu

Specialty section:
This article was submitted to Cell Death and Survival, a section of the journal Frontiers in Cell and Developmental Biology

Received: *01 April 2021*
Accepted: *06 May 2021*
Published: *31 May 2021*

Citation:
Szczesniak LM, Bonzerato CG and Wojcikiewicz RJH (2021) Identification of the Bok Interactome Using Proximity Labeling. Front. Cell Dev. Biol. 9:689951. doi: 10.3389/fcell.2021.689951

INTRODUCTION

The Bcl-2 family mediates the intrinsic apoptosis pathway through the coordinated actions of pro- and anti-apoptotic proteins (Kale et al., 2018). The pro-apoptotic proteins include Bax and Bak, which mediate the release of cytochrome c from mitochondria via mitochondrial outer membrane permeabilization (MOMP), an effect opposed by the anti-apoptotic proteins Bcl-2, Mcl-1, and Bcl-x_L. Pro-apoptotic sensitizer proteins, including Bad and Noxa, bind the anti-apoptotic proteins to prevent inhibition of apoptosis, while pro-apoptotic activator proteins, such as Bid and Bim, bind and activate Bax and Bak to facilitate MOMP. Many "non-apoptotic" roles for Bcl-2 family members have also been identified, including regulation of mitochondrial dynamics, Ca^{2+} homeostasis, and autophagy (Chong et al., 2020).

Bcl-2 related ovarian killer (Bok) was initially categorized as a pro-apoptotic Bcl-2 family member that can trigger MOMP (Hsu et al., 1997; Llambi et al., 2016), but many recent studies

Abbreviations: BioID/TurboID, proximity-dependent biotin identification; Bok, Bcl-2-related ovarian killer; cC3, cleaved caspase-3; ER, endoplasmic reticulum; IP, immunoprecipitation; IP_3R, inositol 1,4,5-trisphosphate receptor; KO, knock-out; MAM, mitochondrial-associated membrane; MEF, mouse embryonic fibroblast; MERC, mitochondria-ER contact site; MOMP, mitochondrial outer membrane permeabilization; MS, mass spectrometry; pDrp1, phosphorylated Drp1; PM, plasma membrane; SOCE, store-operated calcium entry; T-Bak, TurboID-Bak; T-Bok, TurboID-Bok; T-Mcl-1, TurboID-Mcl-1; TM, transmembrane.

have also identified non-apoptotic functions (Ke et al., 2012; D'Orsi et al., 2016; Naim and Kaufmann, 2020; Shalaby et al., 2020). For instance, Bok "knock-out" (KO) from mouse embryonic fibroblasts (MEFs) causes mitochondrial fragmentation, which can be rescued by re-introduction of Bok (Schulman et al., 2019). This phenotype is intriguing, given that Bok is predominantly endoplasmic reticulum (ER)-localized (Echeverry et al., 2013) and constitutively bound to inositol 1,4,5-trisphosphate receptors (IP_3Rs) (Schulman et al., 2013, 2016), which are tetrameric channels that release Ca^{2+} from ER stores. Bok has also been reported to protect IP_3Rs from proteolysis (Schulman et al., 2013), mediate ER stress-induced apoptosis (Carpio et al., 2015), and positively regulate uridine metabolism (Srivastava et al., 2019).

Proximity-dependent biotin identification (BioID) was developed after the discovery that a point mutation, R118G, in the *Escherichia coli* biotin ligase protein BirA created a promiscuous ligase that could biotinylate proteins within an approximately 20 nm radius *in situ,* after the addition of exogenous biotin (Roux et al., 2012). Since the inception of BioID, multiple iterative modifications have been made to the original biotin ligase, the most recent being TurboID, which contains 16 mutations, permitting efficient biotin labeling *in situ* in as little as 15 min (Branon et al., 2018).

Here we show using TurboID that the Bok interactome is wide-ranging, but importantly, contains numerous ER and mitochondrial proteins, including mediators of mitochondrial fission, proteins involved in ER-plasma membrane (PM) contact, and Mcl-1. Further, we show that Bok and Mcl-1 interact physically and functionally and that the interactomes for Bok, Bak, and Mcl-1 are distinct, but overlap somewhat. These results shed light on the cellular roles of Bok and other Bcl-2 family members.

MATERIALS AND METHODS

Materials

HeLa cells were maintained as described (Pearce et al., 2007). Antibodies raised in rabbits were: anti-Mcl-1 #D35A5 (for immunoblot), anti-Bcl-x_L #54H6, anti-Bax #2772, anti-Bcl-2 #50E3, anti-caspase-3 #9662, anti-pDrp1-616 #D9A1 and anti-pDrp1-637 #4867S (Cell Signaling Technology), anti-Bak #06-536 (Millipore), anti-IP_3R1, anti-IP_3R2 and anti-IP_3R3 (for immunoprecipitation; IP) (Wojcikiewicz, 1995), anti-erlin2 (Pearce et al., 2007), and anti-Bok (Ke et al., 2012). Mouse monoclonal antibodies were: anti-Flag epitope (M2, Sigma), anti-IP_3R3 #610313 (for immunoblot) and anti-Drp1 #611112 (BD Biosciences), anti-V5 epitope tag (GenScript), anti-Mcl-1 #RC13 (for IP) and anti-streptavidin #S10D4 (ThermoFisher), and anti-p97 (Research Diagnostics Inc.). Purified streptavidin was from BioLegend. PCR and Gibson reagents were from New England BioLabs. SDS-PAGE reagents were from Bio-Rad. Lipofectamine 2000 was from ThermoFisher. Cell culture dishes were from Corning. HRP-conjugated secondary antibodies and all other reagents not listed were from Sigma. Vectors encoding mouse and human Mcl-1 and Bok, and human Bak were kind gifts from Dr. T. Kaufmann (Echeverry et al., 2013). pCag-mouse Bok^{WT} (Schulman et al., 2016) and associated mutants used in **Figure 4** (Bok^{L34G} and $Bok^{\Delta TM}$, which lacks amino acids 188-213) were created by PCR using existing primers (Schulman et al., 2013). BioRender was used to generate **Figures 1A**, **2A**, **3B** and **Supplementary Figures 2, 3**.

Generation of Bok KO HeLa Cell Lines

The CRISPR-Cas9 system using the pCas-Guide-EF1a-GFP vector (#GE100018, OriGene) was used to generate Bok KO HeLa cells by targeting exon 2 (GTCTGTGGGCGAGCGGTCAA) or exon 4 (GCCCCGCGGCCACCGCATAC). Cells were transfected using Lipofectamine 2000, medium was changed after 24 h, and 48 h post-transfection, EGFP-expressing cells were selected by fluorescence-activated cell sorting and were seeded at one cell/well in a 96-well plate. Colonies were expanded and assessed for Bok immunoreactivity as described (Schulman et al., 2016). Multiple independent Bok KO cell lines for each exon target were used for all experiments.

Generation of TurboID Fusion Proteins and Proximity Labeling

cDNAs were subcloned from vectors containing mouse Bok^{WT}, mouse Bok^{L34G}, mouse Mcl-1^{WT}, and human Bak^{WT} (Echeverry et al., 2013; Schulman et al., 2016), and were ligated to the 3' end (C terminus) of V5-TurboID in place of the stop codon (Addgene #107169) (Branon et al., 2018) using Gibson assembly, creating TurboID-Bok^{WT}, TurboID-Bok^{L34G}, TurboID-Mcl-1, and TurboID-Bak, respectively; the authenticity of all constructs was confirmed by DNA sequencing (Genewiz).

Bok KO HeLa cells in 10 cm dishes were transfected (0.325–1.25 μg cDNA/22.5 μL Lipofectamine), and ∼16 h later, medium was changed, cells were incubated with 50 μM biotin for 2 h, washed thrice with ice-cold PBS, and harvested with ∼500 μL ice-cold lysis buffer for IP as described (Schulman et al., 2016) or for streptavidin pull-down. To purify biotinylated proteins, lysates were incubated with 300μg/mL streptavidin C1 magnetic beads (ThermoFisher) for ∼16 h at 4°C, and beads were washed stringently with buffers containing SDS and detergents as described (Firat-Karalar and Stearns, 2015). All samples were re-suspended in gel loading buffer, boiled for 5 min, and subjected to SDS-PAGE. For pilot experiments (**Figures 1B**, **3A**), lysates were transferred to nitrocellulose, and biotinylated species were detected by incubation with 100 ng/mL purified streptavidin (which binds to biotin with high affinity) for 1 h, anti-streptavidin for ∼16 h, and then developed similarly to other immunoblots. Once biotinylation was confirmed, purified biotinylated proteins were again subjected to SDS-PAGE until the dye front ran ∼2 cm, and lanes were excised for mass spectrometry (MS) analysis (described in **Supplementary Methods**).

Analysis of MS Results

The MS data for each TurboID fusion protein underwent two stages of refinement (depicted in **Supplementary Figure 3**). In the first stage, for each experiment (i) proteins were excluded from further analysis if the q value > 0.01, (ii) keratin proteins

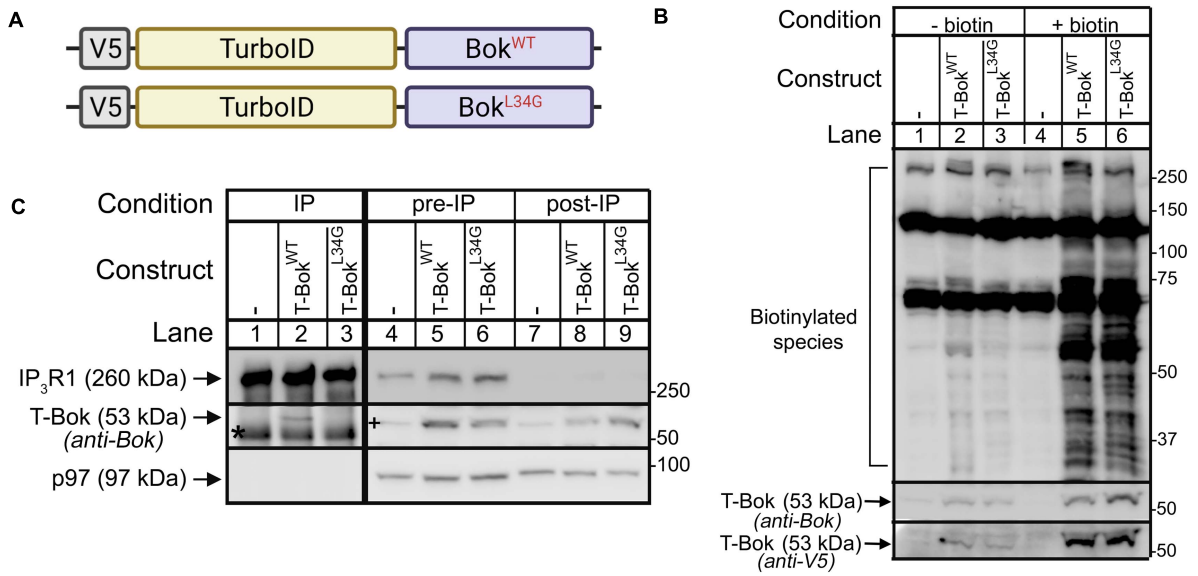

FIGURE 1 | TurboID-Bok construct characterization. **(A)** V5-TurboID-Bok fusion constructs, T-Bok^{WT} and T-Bok^{L34G}. **(B)** Immunoblot for biotin-labeled species (detected with streptavidin/anti-streptavidin) in lysates from Bok KO HeLa cells transfected as indicated to express T-Bok^{WT} or T-Bok^{L34G}, without or with 2 h media supplementation with 50 μM biotin. Immunoreactivity of T-Bok constructs was assessed with either anti-Bok or anti-V5 (middle and lowest panels, respectively). **(C)** Anti-IP$_3$R1/IP$_3$R3 IP (lanes 1–3) and lysates (either pre- or post-IP; lanes 4–9) from Bok KO HeLa cells transfected as indicated, probed in immunoblots for the proteins indicated; p97 serves as a loading control. Co-migrating IgG heavy chain seen in the Bok probe of IPs is indicated by the asterisk. A 53kDa background band seen in the Bok probe of Bok KO cell lysates (lane 4) is indicated by the plus sign. Because Bok^{L34G} is relatively unstable (Schulman et al., 2016), to obtain equal expression, the amount of cDNA transfected for T-Bok^{L34G} was double that for T-Bok^{WT}.

were excluded, and (iii) proteins were included only if they were unique or if abundance was 5× increased in TurboID samples versus control samples (abundance = peptide spectrum match number divided by the total number of amino acids in the parent protein). In the second stage, lists of included proteins from a number (n) of independent experiments were compared, and proteins were considered to be "strongly labeled" if they were present in multiple (e.g., at least 6/7) lists. For each TurboID construct, lists of proteins after the first stage of refinement, plus the strongly labeled proteins, are shown in **Supplementary Tables 1–4**. Protein localization is described in the **Supplementary Methods**.

Cell Lysis, IP and Immunoblotting

Lysates were prepared with ice-cold lysis buffer containing 1% Triton X-100, IPs were prepared with Protein A-Sepharose CL-4B beads (GE Healthcare), and lysates and washed IPs were subjected to SDS-PAGE and immunoblotting as described (Schulman et al., 2013, 2016).

RESULTS

Bok Deletion in HeLa Cells Causes Mitochondrial Fragmentation

We selected HeLa cells for TurboID as they are relatively easy to transfect and have been used previously in proximity labeling studies (Roux et al., 2012). To facilitate analysis of the Bok interactome, we deleted endogenous Bok by CRISPR-Cas9 targeting of Bok exons 2 and 4, with no off-target effects on expression of other Bcl-2 family members or IP$_3$Rs (**Supplementary Figure 1A**). Interestingly, imaging of these Bok KO cells indicated that Bok deletion causes mitochondrial fragmentation (**Supplementary Figure 1B**), with image quantification revealing significantly reduced mitochondrial particle length, area, and aspect ratio, while mitochondrial width was unchanged (**Supplementary Figures 1C–F**). Similar effects of Bok KO have been observed in MEFs (Schulman et al., 2019).

TurboID-Bok as a Method to Identify the Bok Interactome

We performed TurboID experiments using wild-type Bok (Bok^{WT}) and an L34G Bok mutant that cannot bind IP$_3$Rs (Bok^{L34G}) (Schulman et al., 2013) to determine if the proteins proximal to Bok are dependent on the interaction of Bok and IP$_3$Rs. Both Bok^{WT} and Bok^{L34G} were fused to V5-tagged TurboID, creating TurboID-Bok^{WT} and TurboID-Bok^{L34G} (T-Bok^{WT} and T-Bok^{L34G}, respectively, **Figure 1A**). TurboID was fused to the N- termini to minimize the possibility of mislocalization, since Bok is localized to the ER by its C-terminal transmembrane (TM) domain (Echeverry et al., 2013).

Expression of T-Bok^{WT} and T-Bok^{L34G} in Bok KO HeLa cells resulted in an exogenous biotin-dependent smear of biotinylated species (**Figure 1B**, lanes 5, 6). The two prominent bands at ∼130 and 70 kDa, seen in all lanes, were identified by MS analysis as the endogenously biotinylated proteins pyruvate carboxylase and

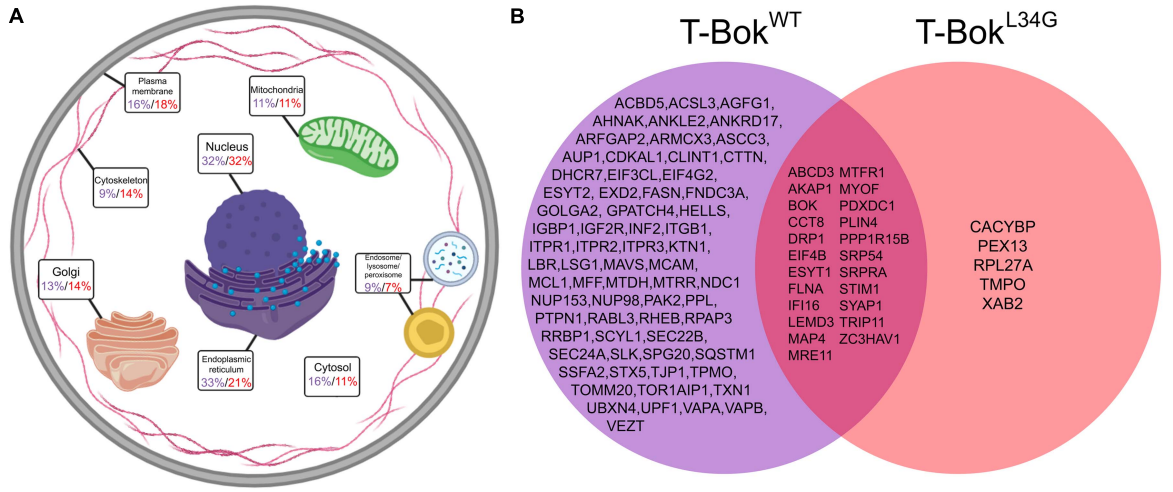

FIGURE 2 | TurboID-Bok^{WT} and TurboID-Bok^{L34G} interactomes. **(A)** Localization of proteins identified by T-Bok^{WT} (purple) and T-Bok^{L34G} (red). Percentage values are the percent of proteins assigned to the specified subcellular compartment; as proteins were assigned to 1–3 compartments, percentages add to >100%. For further information, see **Supplementary Tables 1, 2**. **(B)** Comparison of proteins identified by T-Bok^{WT} and T-Bok^{L34G}. The proteins shown were present in at least 6/7 and 4/5 independent experiments, respectively.

propionyl-CoA carboxylase (Tong, 2013), respectively. It is also noteworthy that the immunoreactivity of the T-Bok constructs increased after the addition of biotin (**Figure 1B**, lanes 2–3 versus 5–6), consistent with previous findings that TurboID constructs are stabilized by exogenous biotin (Branon et al., 2018).

To determine how well the T-Bok constructs interact with IP_3Rs, we examined their ability to co-IP with endogenous IP_3Rs (**Figure 1C**). This showed, as expected, that T-Bok^{WT}, but not T-Bok^{L34G}, binds IP_3Rs (lane 2 versus 3) (Schulman et al., 2013). Importantly, the difference between pre-IP versus post-IP lysates suggest that most of T-Bok^{WT} is associated with IP_3Rs (lane 5 versus 8).

From cells incubated with biotin as in **Figure 1B** (lanes 4–6), biotinylated proteins were purified using streptavidin-coated beads followed by SDS-PAGE, trypsin digestion, and MS analysis (**Supplementary Figure 2**). The initial list of proteins obtained for each T-Bok sample underwent two stages of data refinement to remove non-specifically interacting proteins (**Supplementary Figure 3**). The first stage excluded any proteins that were also found in control (non-transfected) samples analyzed on the same day, and the second stage included proteins present only in multiple independent experiments; for T-Bok^{WT} and T-Bok^{L34G}, only proteins present in at least 6/7 and 4/5 experiments, respectively, were included. These "strongly labeled" proteins were categorized for subcellular localization (**Supplementary Tables 1, 2** and **Figure 2A**) and were compared to determine similarities and differences (**Figure 2B**). Interestingly, fewer proteins were identified by T-Bok^{L34G} than T-Bok^{WT} (28 versus 90 proteins, respectively), Bok was present on both lists due to self-biotinylation, and only T-Bok^{WT} labeled IP_3Rs (Itpr1-3), indicating that the approach is valid.

T-Bok^{WT} was proximal to a broad array of proteins at different sites (**Figure 2A**), although ER and nuclear localizations were predominant (33 and 32% of labeled proteins, respectively). While the identification of ER proteins is to be expected due to Bok's constitutive ER localization with IP_3Rs (Echeverry et al., 2013; Schulman et al., 2016), the high number of nuclear proteins is surprising. However, proteins were assigned up to 3 locations, and many of the multi-located proteins included a nuclear assignment. Additionally, several of the nucleus-assigned proteins were nuclear membrane proteins, which is understandable given the contiguous nature of the ER and nuclear membrane (English and Voeltz, 2013). Also in the T-Bok^{WT} protein list were several PM (16%), cytosolic (16%), Golgi (13%), and mitochondrial proteins (11%).

More detailed consideration of proteins identified for T-Bok^{WT} (**Figure 2B**) revealed clusters of proteins known to regulate mitochondrial fission (Drp1, Mff, Inf2, Akap1, etc.) (Czachor et al., 2016; Kraus et al., 2021) and ER-PM contact sites (Itpr1-3, Stim1, Vapa, Vapb, etc.) (Murphy and Levine, 2016; Prole and Taylor, 2019). Drp1 is a GTPase well-known for being the main effector protein for mitochondrial fission (Kraus et al., 2021), Stim1 is an ER protein involved in store-operated Ca^{2+} entry (SOCE) and ER-PM junctions (Prole and Taylor, 2019), and Akap1 is a mitochondrial membrane scaffolding protein that regulates a variety of mitochondrial functions (Czachor et al., 2016). Notably, no Bcl-2 family members were labeled by T-Bok^{WT} aside from Mcl-1. Surprisingly, we did not detect uridine monophosphate synthetase, despite recent reports that Bok regulates uridine metabolism by enhancing its activity (Srivastava et al., 2019), or key proteins involved in mitochondrial fusion (e.g., Mfn1/2), despite evidence that Bok can regulate fusion rate (Schulman et al., 2019).

The result that T-Bok^{WT} strongly labeled three times as many proteins as T-Bok^{L34G} was initially perplexing. However, it is likely that T-Bok^{L34G} is rapidly turned over because it cannot interact with IP_3Rs (Schulman et al., 2016), and this may impair biotin ligase activity. Indeed, to achieve comparable expression

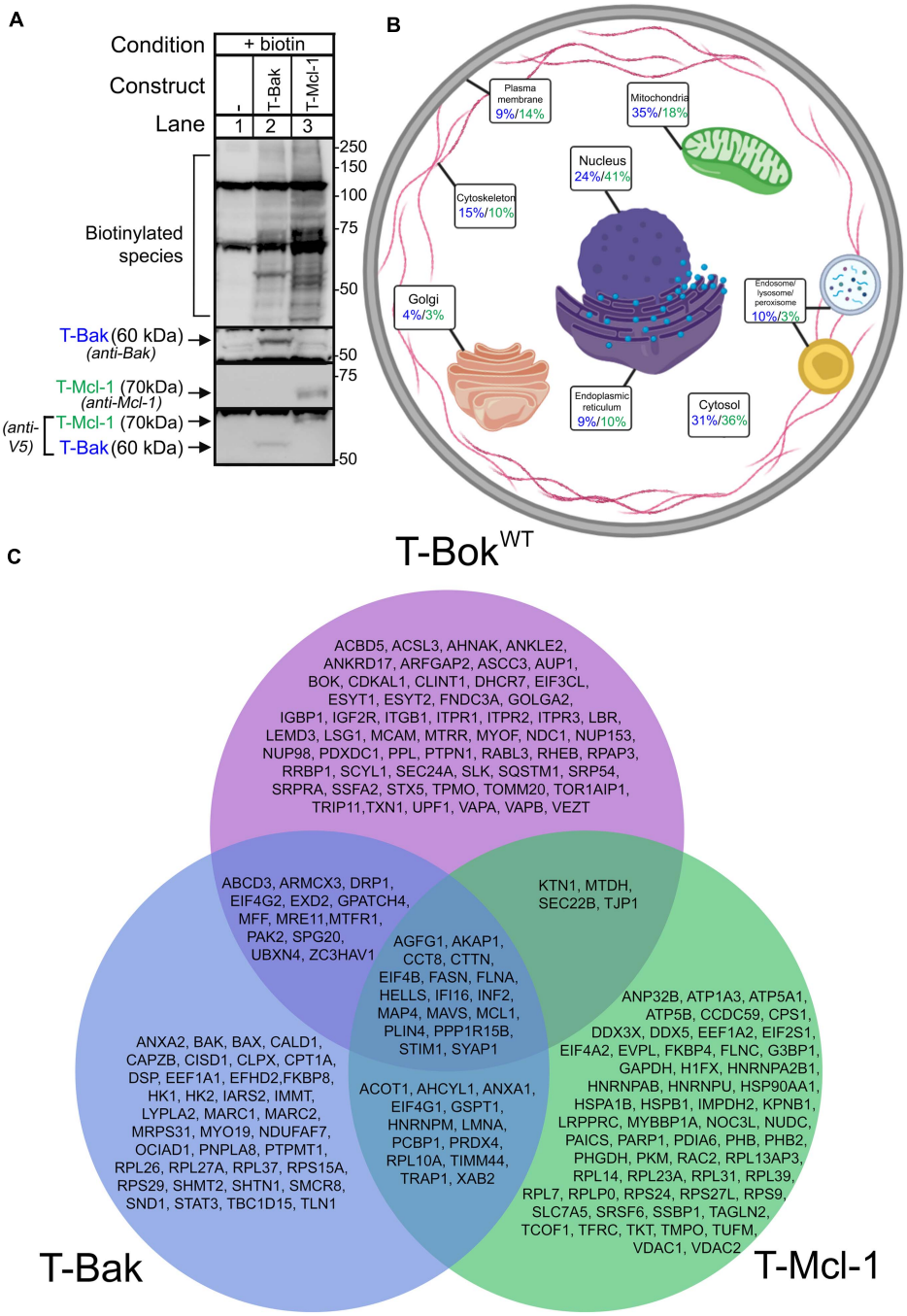

FIGURE 3 | TurboID-Bak and TurboID-Mcl-1 interactomes. **(A)** Immunoblot for biotin-labeled species (detected with streptavidin/anti-streptavidin) in lysates from Bok KO HeLa cells transfected as indicated to express T-Bak or T-Mcl-1, without or with 2 h media supplementation with 50 μM biotin. Immunoreactivity of TurboID constructs was assessed with either anti-Bak, anti-Mcl-1, or anti-V5 (2nd-4th panels, respectively). **(B)** Localization of proteins identified by T-Bak (blue) and T-Mcl-1 (green). Percentage values are the percent of proteins assigned to the specified subcellular compartment; as proteins were assigned to 1–3 compartments, percentages add to >100%. For further information, see **Supplementary Tables 3, 4**. **(C)** Comparison of proteins identified by T-Bok^{WT}, T-Bak, and T-Mcl-1. The proteins shown were present in at least 6/7, 2/3, and 2/3 independent experiments, respectively.

and biotinylation required using twice as much T-Bok^{L34G} cDNA than T-Bok^{WT} cDNA (**Figures 1B,C**). Nevertheless, the protein list for T-Bok^{L34G} overlapped significantly with that of T-Bok^{WT}, suggesting that the mutant protein still localizes to the ER despite not binding to IP$_3$Rs. A comparison of the two T-Bok constructs with a lower threshold for T-Bok^{L34G} (i.e., addition of proteins in 3/5 experiments, **Supplementary Figure 4**) identified more proteins that were also present in the T-Bok^{WT} list, including

more of the proteins involved in mitochondrial fission (Inf2 and Mff). Overall, the interactome of T-Bok^{L34G} has some similarities to that of T-Bok^{WT}, but also major differences. Some of these differences may result from localization of T-Bok^{WT} to IP_3Rs, but likely also reflect the marked differences in T-Bok^{WT} and T-Bok^{L34G} stability.

TurboID-Bak and TurboID-Mcl-1 Interactomes

To assess T-Bok^{WT} proximity labeling specificity and better understand other Bcl-2 family members, we generated TurboID constructs for Bak, which localizes predominantly to mitochondria, and Mcl-1, which also localizes to mitochondria, but is also found at the ER and in the cytosol (Kale et al., 2018). Both TurboID-Bak (T-Bak) and TurboID-Mcl-1 (T-Mcl-1) expressed and induced biotinylation similarly to T-Bok^{WT} (**Figure 3A**).

TurboID was performed in Bok KO HeLa cells to allow for direct comparison with T-Bok^{WT} results. The possible impact of the presence of endogenous Mcl-1 and Bak in these cells (**Supplementary Figure 1A**) on labeling was not examined in this study. Localization of strongly labeled proteins (**Figure 3B** and **Supplementary Tables 3, 4**) demonstrates that both T-Bak and T-Mcl-1 did not identify as many ER proteins as T-Bok^{WT} (9, 10, and 33%, respectively), as expected. In order of abundance, T-Bak identified mitochondrial (35%), cytosolic (31%), and nuclear proteins (24%), whereas T-Mcl-1 identified nuclear (41%), cytosolic (36%), and mitochondrial proteins (18%). Again, as expected, both T-Bak and T-Mcl-1 labeled more mitochondrial proteins than T-Bok^{WT}.

Comparison of the protein lists for the three Bcl-2 family proteins (**Figure 3C**) demonstrated that each interactome is quite distinct, although there was significant overlap. In particular, Inf2 and Mavs, which are involved in mitochondrial fission (Kraus et al., 2021) and fusion (Koshiba et al., 2011), respectively, were present in all lists, as were Akap1 and Stim1. Also, both T-Bok^{WT} and T-Bak labeled Mcl-1, which is consistent with studies indicating that Bok (Hsu et al., 1997) and Bak (Cuconati et al., 2003) can physically interact with Mcl-1.

The protein lists for T-Bak and T-Bok^{WT} showed some overlap, and notably, the mitochondrial fission proteins Mff and Mtfr1 were common to both. Many of the proteins unique to the T-Bak list were mitochondrial proteins, and not surprisingly, Bax was among them (Kale et al., 2018). T-Mcl-1 showed only minor overlap with T-Bok^{WT}, and uniquely labeled Vdac1/2, consistent with findings that Mcl-1 physically interacts with Vdac and can facilitate Vdac-dependent mitochondrial Ca^{2+} uptake (Huang et al., 2014). Overall, the discrete proximity labeling patterns for T-Bok^{WT}, T-Bak, and T-Mcl-1 validate the TurboID approach, and comparison of the three protein lists reflects the complexity of the Bcl-2 family network and identifies potential novel interactions.

Analysis of the Bok-Mcl-1 Interaction

Since T-Bok^{WT} labeled Mcl-1 but no other Bcl-2 family member (**Figure 2**), we wondered whether this signified mere proximity between Bok and Mcl-1, or whether they interact directly. Interestingly, when co-expressed, Bok^{WT} did co-IP with 1F-Mcl-1 (Mcl-1 with an N-terminal Flag tag), and 1F-Mcl-1 increased Bok immunoreactivity (**Figure 4A**, lane 4), suggesting that the interaction stabilizes Bok. This was still observed with Bok^{L34G} (lane 8), indicating that it was not mediated by the BH4 domain of Bok that is critical for the interaction with IP_3Rs (Schulman et al., 2013), but was markedly reduced for Bok$^{\Delta TM}$ (lane 6), indicating that Bok localization to membranes is important for the interaction, or that it is directly mediated by the Bok TM domain itself (Lucendo et al., 2020). Under the same conditions, endogenous Bok did not co-IP with endogenous Mcl-1 (**Supplementary Figure 5**), as noted in some other studies (Echeverry et al., 2013; Schulman et al., 2016), indicating that the Bok-Mcl-1 interaction is relatively weak and is only detectable upon protein overexpression. Nevertheless, the interaction between exogenous Bok^{WT} and 1F-Mcl-1 has functional significance, as Bok^{WT}-mediated increases in cleaved caspase-3 (cC3), were suppressed significantly by 1F-Mcl-1 (**Figure 4B**, lanes 3 versus 4). Interestingly, Bok$^{\Delta TM}$ increased cC3 levels similarly to Bok^{WT}, but the effect of Bok$^{\Delta TM}$ was not significantly suppressed by 1F-Mcl-1 (lanes 5 versus 6), consistent with their much weaker physical interaction (**Figure 4A**, lane 6). Further, Bok^{L34G} induced significantly more cC3 than Bok^{WT} (**Figure 4B**, lanes 3 versus 7), presumably because Bok^{L34G} is not sequestered by IP_3Rs, although Mcl-1 suppressed the response (lanes 7 versus 8). Overall, these data indicate that the proximity labeling approach can identify fleeting protein-protein interactions of functional significance that might not be detectable by conventional (e.g., co-IP) analysis of endogenous proteins, and that Mcl-1 likely mediates or modulates the effects of Bok. It should be noted that in these studies, we utilized mouse Bok and Mcl-1 expressed in human HeLa cells. However, mouse and human Bok and Mcl-1 amino acid sequences are 95% and 76% identical, respectively, and human Bok and Mcl-1 co-IP like their mouse counterparts when over-expressed in Bok KO HeLa cells (**Figure 4C**), indicating that the mouse and human proteins behave identically in the HeLa cell context.

Bok Deletion in HeLa Cells Does not Alter Drp1 Phosphorylation Status or Ca^{2+} Mobilization

Since Drp1 is a crucial mediator of mitochondrial fission (Kraus et al., 2021) and was strongly labeled by T-Bok^{WT} (**Figure 2**), we sought to determine if Bok regulates Drp1 activity, which can be measured through Drp1 phosphorylation (pDrp1). pDrp1^{S616} is associated with increased mitochondrial fission, whereas pDrp1^{S637} is associated with decreased mitochondrial fission (Kraus et al., 2021). Using validated antibodies, we examined pDrp1 levels among HeLa cell lines and found that pDrp1^{S616} and pDrp1^{S637} levels were not substantially changed by Bok deletion (**Supplementary Figure 6**). Likewise, given that several proteins related to intracellular Ca^{2+} signaling at the ER or at ER-PM contact sites were labeled by T-Bok^{WT}, we sought to determine whether Bok KO altered Ca^{2+} mobilization. However, WT and Bok KO HeLa cells responded essentially identically to trypsin

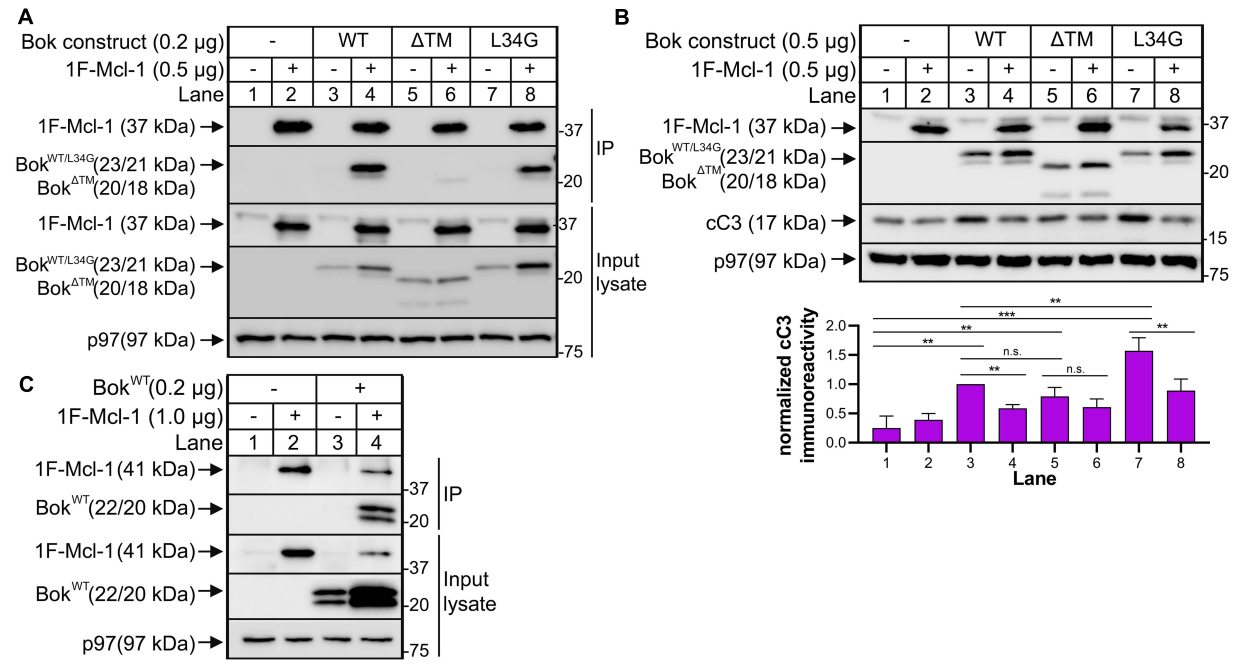

FIGURE 4 | Overexpressed Mcl-1 and Bok interact with consequences on apoptotic signaling. **(A)** Bok KO HeLa cells were transfected to express 1F-mouse Mcl-1 and mouse Bok^{WT} and mutants as indicated for ∼18 h, and cell lysates and anti-Flag IPs were probed as indicated; p97 serves as a loading control. **(B)** Cleaved caspase-3 (cC3) immunoreactivity, visualized as an ∼17kDa band, was measured and quantified in Bok KO HeLa cells expressing 1F-mouse Mcl-1 and mouse Bok^{WT} and mutants as indicated for ∼18 h; a representative immunoblot is shown together with quantification of cC3 immunoreactivity using Image Lab software (mean ± SEM, $n = 4$). An unpaired t-test with Welch's correction was used to determine significance; $p < 0.005$ is denoted by **, $p < 0.0005$ is denoted by ***, n.s. = not statistically significant. Data were graphed and analyzed using GraphPad Prism software. **(C)** Bok KO HeLa cells were transfected to express 1F-human Mcl-1 and human Bok^{WT} as indicated for ∼18 h, and cell lysates and anti-Flag IPs were probed as indicated; p97 serves as a loading control.

(**Supplementary Figure 7**), indicating that Bok KO does not affect Ca^{2+} signaling.

DISCUSSION

Proximity labeling was developed to identify the interactome for a given protein by labeling transient interactions and nearby proteins, providing an alternative to the traditional co-IP or co-purification approaches that reveal only the highest affinity protein-protein interactions (Roux et al., 2012). Here we show that TurboID can efficiently and specifically identify the interactomes for Bok, Mcl-1, and Bak. T-Bok-labeled proteins are predominantly found in the ER, consistent with Bok's reported subcellular localization. In contrast, T-Bak and T-Mcl-1 mostly labeled mitochondrial and nuclear proteins, respectively, consistent with Bak's known localization to the mitochondrial membrane, and a more mixed distribution for Mcl-1 (Kale et al., 2018).

While the proteins labeled by T-Bok^{WT} were predominantly ER-residents, protein groups in other locations were also identified, indicating a role for Bok at the interface of the ER and other organelles. As Bok deletion causes mitochondrial fragmentation, we particularly focused on mitochondrial proteins. Mitochondria-ER contacts (MERCs), sometimes referred to as mitochondrial-associated membranes (MAMs) when isolated in biophysical protocols, are transient microdomains where ER and mitochondria come within 10-80 nm of each other (Giacomello and Pellegrini, 2016). Several studies report that MERCs are essential for numerous signaling processes, including Ca^{2+} transfer, lipid trafficking/metabolism, and regulation of cell death or survival (Perrone et al., 2020), and interestingly, a recent study suggests that Bok is integral to the stability of MERCs/MAMs (Carpio et al., 2021). However, aside from IP_3Rs, T-Bok did not label any of the proteins reported to be important in the coupling of the ER to mitochondria at MERCs/MAMs, including Vdac1, Grp75, or Mfn2 (Perrone et al., 2020). Rather, T-Bok identified several proteins important for mitochondrial fission, including Drp1, Mff, Akap1, and Inf2 (Czachor et al., 2016; Kraus et al., 2021). This suggests that the role of Bok at the interface of ER and mitochondria is not to maintain MERC/MAM structure or function, but rather to regulate mitochondrial fission. This notion is consistent with findings that the ER is highly involved in mitochondrial fission (Perrone et al., 2020), and that ER projections can wrap around mitochondria to mediate the division process (Friedman et al., 2011).

Could an inhibitory effect of Bok on key fission mediators, such as Drp1, explain the mitochondrial fragmentation seen in Bok KO cells? This is a distinct possibility, since although we were unable to see an effect of Bok KO on Drp1 levels or phosphorylation (a measure of Drp1 activity), Drp1 function is

regulated by several post-translational modifications aside from phosphorylation (Chang and Blackstone, 2010), and other fission mediators (e.g., Inf2, Mff), could also be regulated by interfacing with Bok. Further, as indicated below, Mcl-1 could mediate effects of Bok on mitochondrial fission.

That the protein list for T-Bok^{L34G}, which does not bind IP_3Rs, was considerably shorter than that for T- Bok^{WT} and other TurboID-fusion proteins, is likely explained by the instability of T-Bok^{L34G} (Schulman et al., 2016); presumably, the rapid turnover of T- Bok^{L34G} impairs its ability to elicit significant biotinylation. Unfortunately, this unexpected finding made it impossible to accurately assess the effect of localization to IP_3Rs on the T-Bok^{WT} interactome. Nevertheless, it is interesting that almost all of the proteins strongly labeled by T-Bok^{L34G} were also labeled by T-Bok^{WT}, indicating that T-Bok^{L34G} is localized similarly to T-Bok^{WT}. This is consistent with the ability of Bok^{L34G} to restore normal mitochondrial morphology when introduced into Bok KO cells (Schulman et al., 2019).

The overlap in proteins labeled by T-Bok, T-Bak, and T-Mcl-1 is intriguing and may open new research avenues. For example, the scaffolding protein Akap1, which modulates numerous signaling pathways at the mitochondrial surface (Czachor et al., 2016), was labeled by T-Bok, T-Bak, and T-Mcl-1, suggesting that it may be a general mediator of Bcl-2 family-related processes at the mitochondrial membrane. Likewise, all 3 proteins labeled Stim1, an ER membrane protein involved in ER-PM coupling for SOCE (Prole and Taylor, 2019). To the best of our knowledge, interactions between Stim1 and Bok, Bak, or Mcl-1 have not been previously reported, and although we did not detect an effect of Bok KO on Ca^{2+} signals that include SOCE, Bcl-2 does regulate SOCE (Vanden Abeele et al., 2002; Chiu et al., 2018), suggesting that many Bcl-2 family members may regulate this pathway. Lastly, both T-Bok and T-Bak identified Mcl-1, and Mcl-1 was the only Bcl-2 family member identified by T-Bok. This is consistent with the widespread distribution of Mcl-1 (Kale et al., 2018) and indicates that analysis of the Bok-Mcl-1 interaction may be a fruitful approach to solving the puzzle of how Bok acts within the cell.

Indeed, we were able to show that Bok and Mcl-1 interact physically, albeit only when overexpressed, and that this binding has functional consequences, since Mcl-1 inhibited Bok-mediated apoptotic signaling. These finding are broadly consistent with those of others (Hsu et al., 1997; Stehle et al., 2018; Lucendo et al., 2020), but with some significant differences. In particular, our findings that Bok$^{\Delta TM}$ mediates apoptotic signaling similarly to Bok^{WT} contradict a recent study (Stehle et al., 2018) indicating that the TM domain of Bok is required for apoptosis, although this could be accounted for by the different experimental systems used. The Bok-Mcl-1 interaction also provides a potential mechanism for Bok to regulate mitochondrial morphology, since Mcl-1 regulates mitochondrial fission, at least in part, by acting through Drp1 (Moyzis et al., 2020). As we find that T-Bok^{WT} strongly labels both Mcl-1 and Drp1, it is possible that Bok inhibits mitochondrial fission rate by modulating the action of Mcl-1. Thus, upon Bok KO, fission rate would be accelerated, explaining the mitochondrial fragmentation observed in Bok KO MEFs (Schulman et al., 2019) and Hela cells (**Supplementary Figure 1**). Interestingly, in our previous studies on the mechanism of Bok KO-induced mitochondrial fragmentation we could not measure mitochondrial fission rate directly, but found that Bok KO inhibits fusion rate. Since T-Bok identified mitochondrial fission mediators but not fusion mediators, we speculate that the effect of Bok KO on fusion rate may be an adaptation to a direct effect of Bok KO on fission mediators and fission rate.

It is important to note that the proteins identified by TurboID constructs reveal proximity, but not necessarily functional interactions. As a "shotgun" approach to the study of possible protein-protein interactions, deriving meaning from proximity labeling still requires functional studies, such as those we performed with Bok and Mcl-1. In that particular case, we were able to demonstrate functional consequences from the Bok-Mcl-1 interaction, but it is also inevitable that some, perhaps most, identified proteins will not interact physically, and other methods (e.g., CRISPR-Cas9-mediated protein KO) will be required to establish significance of proximity. Overall, we hope that this study serves to drive further research into Bok and Bcl-2 family interactions, with outcomes that will lead to a better understanding of Bok and cell physiology.

Going forward, it will be particularly interesting to determine if stably expressed Bcl-2 family proteins biotinylate more specifically than the transient expression method used in the present study, how the interactomes might change when apoptosis is triggered, how endogenous Mcl-1 and Bak impact the labeling seen with T-Mcl-1 and T-Bak, and how certain proteins strongly labeled by T-Bok might help explain the various putative roles of Bok. In particular, the interaction with anti-apoptotic Mcl-1 and thus the Bcl-2 family network may explain how manipulating Bok levels can have various effects on apoptotic signaling (Naim and Kaufmann, 2020; Shalaby et al., 2020), the identification of Drp1 and other fission mediators may explain how Bok can influence mitochondrial morphology (Schulman et al., 2019), and the identification of ER-PM and ER-Golgi junctional proteins (e.g., Stim1, Vapa and Vapb) suggest new possible roles for Bok in inter-organelle contact sites.

DATA AVAILABILITY STATEMENT

The authors acknowledge that the data presented in this study must be deposited and made publicly available in an acceptable repository, prior to publication. Frontiers cannot accept a manuscript that does not adhere to our open data policies.

AUTHOR CONTRIBUTIONS

LS performed, guided, and analyzed all the experiments shown and was the primary author of the manuscript. CB designed and implemented screening of HeLa Bok KO cell lines and assisted with image acquisition for **Supplementary Figure 1B**. RW conceived and coordinated the study with substantial editorial input into the manuscript. All authors reviewed the results and approved the final version of the manuscript.

FUNDING

The research performed in this article was funded by National Institutes of Health Grants DK107944, GM121621, and GM134638.

ACKNOWLEDGMENTS

We thank Thomas Kaufmann, University of Bern, Switzerland, for providing anti-Bok and cDNAs, Ebbing de Jong for assistance with mass spectrometry analysis, Bruce Knutson for providing TurboID cDNA and helpful suggestions, Jacqualyn Schulman for assistance with gRNA vector design, and Katherine Keller and Pranav Suri for technical assistance and helpful suggestions.

SUPPLEMENTARY MATERIAL

The Supplementary Material for this article can be found online at: https://www.frontiersin.org/articles/10.3389/fcell.2021.689951/full#supplementary-material

REFERENCES

Branon, T. C., Bosch, J. A., Sanchez, A. D., Udeshi, N. D., Svinkina, T., Carr, S. A., et al. (2018). Efficient proximity labeling in living cells and organisms with TurboID. *Nat. Biotechnol.* 36, 880–887. doi: 10.1038/nbt.4201

Carpio, M. A., Means, R. E., Brill, A. L., Sainz, A., Ehrlich, B. E., and Katz, S. G. (2021). BOK controls apoptosis by Ca(2+) transfer through ER-mitochondrial contact sites. *Cell Rep.* 34:108827. doi: 10.1016/j.celrep.2021.108827

Carpio, M. A., Michaud, M., Zhou, W., Fisher, J. K., Walensky, L. D., and Katz, S. G. (2015). BCL-2 family member BOK promotes apoptosis in response to endoplasmic reticulum stress. *Proc. Natl. Acad. Sci. U. S. A.* 112, 7201–7206. doi: 10.1073/pnas.1421063112

Chang, C. R., and Blackstone, C. (2010). Dynamic regulation of mitochondrial fission through modification of the dynamin-related protein Drp1. *Ann. N. Y. Acad. Sci.* 1201, 34–39. doi: 10.1111/j.1749-6632.2010.05629.x

Chiu, W. T., Chang, H. A., Lin, Y. H., Lin, Y. S., Chang, H. T., Lin, H. H., et al. (2018). Bcl(-)2 regulates store-operated Ca(2+) entry to modulate ER stress-induced apoptosis. *Cell Death Discov.* 4:37.

Chong, S. J. F., Marchi, S., Petroni, G., Kroemer, G., Galluzzi, L., and Pervaiz, S. (2020). Noncanonical Cell Fate Regulation by Bcl-2 Proteins. *Trends Cell Biol.* 30, 537–555. doi: 10.1016/j.tcb.2020.03.004

Cuconati, A., Mukherjee, C., Perez, D., and White, E. (2003). DNA damage response and MCL-1 destruction initiate apoptosis in adenovirus-infected cells. *Genes Dev.* 17, 2922–2932. doi: 10.1101/gad.1156903

Czachor, A., Failla, A., Lockey, R., and Kolliputi, N. (2016). Pivotal role of AKAP121 in mitochondrial physiology. *Am. J. Physiol. Cell Physiol.* 310, C625–8.

D'Orsi, B., Engel, T., Pfeiffer, S., Nandi, S., Kaufmann, T., Henshall, D. C., et al. (2016). Bok Is Not Pro-Apoptotic But Suppresses Poly ADP-Ribose Polymerase-Dependent Cell Death Pathways and Protects against Excitotoxic and Seizure-Induced Neuronal Injury. *J. Neurosci.* 36, 4564–4578. doi: 10.1523/jneurosci.3780-15.2016

Echeverry, N., Bachmann, D., Ke, F., Strasser, A., Simon, H. U., and Kaufmann, T. (2013). Intracellular localization of the BCL-2 family member BOK and functional implications. *Cell Death Differ.* 20, 785–799. doi: 10.1038/cdd.2013.10

English, A. R., and Voeltz, G. K. (2013). Endoplasmic reticulum structure and interconnections with other organelles. *Cold Spring Harb. Perspect. Biol.* 5:a013227. doi: 10.1101/cshperspect.a013227

Firat-Karalar, E. N., and Stearns, T. (2015). Probing mammalian centrosome structure using BioID proximity-dependent biotinylation. *Methods Cell Biol.* 129, 153–170. doi: 10.1016/bs.mcb.2015.03.016

Friedman, J. R., Lackner, L. L., West, M., DiBenedetto, J. R., Nunnari, J., and Voeltz, G. K. (2011). ER tubules mark sites of mitochondrial division. *Science* 334, 358–362. doi: 10.1126/science.1207385

Giacomello, M., and Pellegrini, L. (2016). The coming of age of the mitochondria-ER contact: a matter of thickness. *Cell Death Differ.* 23, 1417–1427. doi: 10.1038/cdd.2016.52

Hsu, S. Y., Kaipia, A., McGee, E., Lomeli, M., and Hsueh, A. J. (1997). Bok is a pro-apoptotic Bcl-2 protein with restricted expression in reproductive tissues and heterodimerizes with selective anti-apoptotic Bcl-2 family members. *Proc. Natl. Acad. Sci. U. S. A.* 94, 12401–12406. doi: 10.1073/pnas.94.23.12401

Huang, H., Shah, K., Bradbury, N. A., Li, C., and White, C. (2014). Mcl-1 promotes lung cancer cell migration by directly interacting with VDAC to increase mitochondrial Ca2+ uptake and reactive oxygen species generation. *Cell Death Dis.* 5:e1482. doi: 10.1038/cddis.2014.419

Kale, J., Osterlund, E. J., and Andrews, D. W. (2018). BCL-2 family proteins: changing partners in the dance towards death. *Cell Death Differ.* 25, 65–80. doi: 10.1038/cdd.2017.186

Ke, F., Voss, A., Kerr, J. B., O'Reilly, L. A., Tai, L., Echeverry, N., et al. (2012). BCL-2 family member BOK is widely expressed but its loss has only minimal impact in mice. *Cell Death Differ.* 19, 915–925. doi: 10.1038/cdd.2011.210

Koshiba, T., Yasukawa, K., Yanagi, Y., and Kawabata, S. (2011). Mitochondrial membrane potential is required for MAVS-mediated antiviral signaling. *Sci. Signal.* 4:ra7. doi: 10.1126/scisignal.2001147

Kraus, F., Roy, K., Pucadyil, T. J., and Ryan, M. T. (2021). Function and regulation of the divisome for mitochondrial fission. *Nature* 590, 57–66. doi: 10.1038/s41586-021-03214-x

Llambi, F., Wang, Y. M., Victor, B., Yang, M., Schneider, D. M., Gingras, S., et al. (2016). BOK Is a Non-canonical BCL-2 Family Effector of Apoptosis Regulated by ER-Associated Degradation. *Cell* 165, 421–433. doi: 10.1016/j.cell.2016.02.026

Lucendo, E., Sancho, M., Lolicato, F., Javanainen, M., Kulig, W., Leiva, D., et al. (2020). Mcl-1 and Bok transmembrane domains: unexpected players in the modulation of apoptosis. *Proc. Natl. Acad. Sci. U. S. A.* 117, 27980–27988. doi: 10.1073/pnas.2008885117

Moyzis, A. G., Lally, N. S., Liang, W., Leon, L. J., Najor, R. H., Orogo, A. M., et al. (2020). Mcl-1-mediated mitochondrial fission protects against stress but impairs cardiac adaptation to exercise. *J. Mol. Cell Cardiol.* 146, 109–120. doi: 10.1016/j.yjmcc.2020.07.009

Murphy, S. E., and Levine, T. P. (2016). (VAP), a Versatile Access Point for the Endoplasmic Reticulum: review and analysis of FFAT-like motifs in the VAPome. *Biochim. Biophys. Acta* 1861, 952–961. doi: 10.1016/j.bbalip.2016.02.009

Naim, S., and Kaufmann, T. (2020). The Multifaceted Roles of the BCL-2 Family Member BOK. *Front. Cell Dev. Biol.* 8:574338. doi: 10.3389/fcell.2020.574338

Pearce, M. M., Wang, Y., Kelley, G. G., and Wojcikiewicz, R. J. (2007). SPFH2 mediates the endoplasmic reticulum-associated degradation of inositol 1,4,5-trisphosphate receptors and other substrates in mammalian cells. *J. Biol. Chem.* 282, 20104–20115. doi: 10.1074/jbc.m701862200

Perrone, M., Caroccia, N., Genovese, I., Missiroli, S., Modesti, L., Pedriali, G., et al. (2020). The role of mitochondria-associated membranes in cellular homeostasis and diseases. *Int. Rev. Cell Mol. Biol.* 350, 119–196. doi: 10.1016/bs.ircmb.2019.11.002

Prole, D. L., and Taylor, C. W. (2019). Structure and Function of IP3 Receptors. *Cold Spring Harb. Perspect. Biol.* 11:a035063. doi: 10.1101/cshperspect.a035063

Roux, K. J., Kim, D. I., Raida, M., and Burke, B. (2012). A promiscuous biotin ligase fusion protein identifies proximal and interacting proteins in mammalian cells. *J. Cell Biol.* 196, 801–810. doi: 10.1083/jcb.201112098

Schulman, J. J., Szczesniak, L. M., Bunker, E. N., Nelson, H. A., Roe, M. W., Wagner, L. E. II, et al. (2019). Bok regulates mitochondrial fusion and morphology. *Cell Death Differ.* 26, 2682–2694. doi: 10.1038/s41418-019-0327-4

Schulman, J. J., Wright, F. A., Han, X., Zluhan, E. J., Szczesniak, L. M., and Wojcikiewicz, R. J. (2016). The Stability and Expression Level of Bok Are

Governed by Binding to Inositol 1,4,5-Trisphosphate Receptors. *J. Biol. Chem.* 291, 11820–11828. doi: 10.1074/jbc.m115.711242

Schulman, J. J., Wright, F. A., Kaufmann, T., and Wojcikiewicz, R. J. (2013). The Bcl-2 protein family member Bok binds to the coupling domain of inositol 1,4,5-trisphosphate receptors and protects them from proteolytic cleavage. *J. Biol. Chem.* 288, 25340–25349. doi: 10.1074/jbc.m113.496570

Shalaby, R., Flores-Romero, H., and Garcia-Saez, A. J. (2020). The Mysteries around the BCL-2 Family Member BOK. *Biomolecules* 10:1638. doi: 10.3390/biom10121638

Srivastava, R., Cao, Z., Nedeva, C., Naim, S., Bachmann, D., Rabachini, T., et al. (2019). BCL-2 family protein BOK is a positive regulator of uridine metabolism in mammals. *Proc. Natl. Acad. Sci. U. S. A.* 116, 15469–15474. doi: 10.1073/pnas.1904523116

Stehle, D., Grimm, M., Einsele-Scholz, S., Ladwig, F., Johanning, J., Fischer, G., et al. (2018). Contribution of BH3-domain and Transmembrane-domain to the Activity and Interaction of the Pore-forming Bcl-2 Proteins Bok. Bak, and Bax. *Sci. Rep.* 8:12434.

Tong, L. (2013). Structure and function of biotin-dependent carboxylases. *Cell Mol. Life Sci.* 70, 863–891. doi: 10.1007/s00018-012-1096-0

Vanden Abeele, F., Skryma, R., Shuba, Y., Van Coppenolle, F., Slomianny, C., Roudbaraki, M., et al. (2002). Bcl-2-dependent modulation of Ca(2+) homeostasis and store-operated channels in prostate cancer cells. *Cancer Cell* 1, 169–179. doi: 10.1016/s1535-6108(02)00034-x

Wojcikiewicz, R. J. (1995). Type I, II, and III inositol 1,4,5-trisphosphate receptors are unequally susceptible to down-regulation and are expressed in markedly different proportions in different cell types. *J. Biol. Chem.* 270, 11678–11683. doi: 10.1074/jbc.270.19.11678

Conflict of Interest: The authors declare that the research was conducted in the absence of any commercial or financial relationships that could be construed as a potential conflict of interest.

frontiers in Cell and Developmental Biology

REVIEW
published: 24 June 2021
doi: 10.3389/fcell.2021.675617

Fatty Acids Metabolism: The Bridge Between Ferroptosis and Ionizing Radiation

Zhu-hui Yuan[1†], Tong Liu[2†], Hao Wang[1], Li-xiang Xue[2,3] and Jun-jie Wang[1*]*

[1] Department of Radiation Oncology, Peking University Third Hospital, Beijing, China, [2] Center of Basic Medical Research, Institute of Medical Innovation and Research, Peking University Third Hospital, Beijing, China, [3] Biobank, Peking University Third Hospital, Beijing, China

Exposure of tumor cells to ionizing radiation (IR) alters the microenvironment, particularly the fatty acid (FA) profile and activity. Moreover, abnormal FA metabolism, either catabolism or anabolism, is essential for synthesizing biological membranes and delivering molecular signals to induce ferroptotic cell death. The current review focuses on the bistable regulation characteristics of FA metabolism and explains how FA catabolism and anabolism pathway crosstalk harmonize different ionizing radiation-regulated ferroptosis responses, resulting in pivotal cell fate decisions. In summary, targeting key molecules involved in lipid metabolism and ferroptosis may amplify the tumor response to IR.

Keywords: fatty acid metabolism, ferroptosis, irradiation, cancer, cell death

OPEN ACCESS

Edited by:
Jiyan Zhang,
Independent Researcher,
Beijing,China

Reviewed by:
Hou Yuzhu,
University of Chicago, United States
Ella L. Kim,
Johannes Gutenberg University Mainz, Germany

****Correspondence:***
Li-xiang Xue
lixiangxue@hsc.pku.edu.cn
Jun-jie Wang
junjiewang@pku.edu.cn

[†] These authors have contributed equally to this work

Specialty section:
This article was submitted to Cell Death and Survival, a section of the journal Frontiers in Cell and Developmental Biology

Received: *03 March 2021*
Accepted: *04 June 2021*
Published: *24 June 2021*

Citation:
Yuan Z-h, Liu T, Wang H, Xue L-x and Wang J-j (2021) Fatty Acids Metabolism: The Bridge Between Ferroptosis and Ionizing Radiation. Front. Cell Dev. Biol. 9:675617. doi: 10.3389/fcell.2021.675617

INTRODUCTION

Aggressively proliferating cancer cells have an increased demand for energy and macromolecules. Thus, cancer cells prefer to expedite glycolysis utilization and glutamine consumption, as well as uptake or endogenous synthesis of lipids. Exogenous sources and endogenous lipids provide essential components to the tumor cell membrane and organelles. Fatty acids (FAs) are indispensable substrates for lipid biosynthesis and function execution, and the *de novo* synthesis of endogenous FAs is considered the major pathway for lipid recruitment by cancer cells (Menendez and Lupu, 2007). FAs are divided into saturated and unsaturated FAs according to the number of carbon-carbon bonds. Given that saturated membrane lipids are less sensitive to oxidative stress, high saturation levels of membrane phospholipids can protect cancer cells from damage induced by reactive oxygen species (ROS). Unsaturated FAs are able to subject tumor cells to oxidative stress and toxicity, and studies have recently found that metabolic stress can promote polyunsaturated FA (PUFA) binding membrane phospholipids (PLs) and make tumor cells more sensitive to ferroptosis.

Ferroptosis, a programmed cell death dependent on iron, is triggered by metabolic stress and interruption of homeostasis, especially the imbalance between the accumulation of lipid peroxide (LPO) and inactivity of antioxidant molecules, such as glutathione-dependent peroxidase (GPX4) and reduced glutathione (GSH) (Dixon et al., 2012; Yang and Stockwell, 2016). In addition, morphological, biochemical, and genetic changes in ferroptotic cells differ from those of other cells during programmed cell death. Ferroptosis cannot be induced by apoptosis inducers, even at high concentrations (Xie et al., 2016). Biochemically, the widely accepted views on the molecular

mechanism of ferroptosis can be separated into three classes: cytotoxicity of PL-PUFAs, redox-active iron, and loss of lipid peroxide repair. Among these cytotoxic molecules, ROS and divalent iron ions are essential in the regulation of ferroptosis. Moreover, lipid peroxidation is considered a pivotal trigger in the final step of ferroptosis. Recently, some studies have found that ferroptosis that occurs after ionizing radiation may be a novel target for decreasing radiation resistance and promoting clinical benefits.

Ionizing radiation induces cell death by transferring energy to the molecules of the absorbing matter. Water molecules are the most important matter in the human body, and radiation can interact with water molecules to induce lethal effects in cells by generating radicals, inducing oxidative stress, or directly ionizing deoxyribonucleic acid (DNA). With the exception of target DNA, recent studies have found that ionizing radiation can change the lipid profile in several cancers, including glioma, breast, colorectal, and skin cancer (Benais-Pont et al., 2006; Bougnoux et al., 2010; Antal et al., 2014; Narayanan et al., 2015; Shaikh et al., 2017), whereas the abnormal metabolism of lipids is the central trigger for ferroptosis. Thus, increasing attention has been focused on the crosstalk between radiation, lipid metabolism, and ferroptosis.

Several studies have shown that the interplay between FA metabolism and ferroptosis is linked to oncogenesis, tumor progression, metastasis, and radiotherapy resistance. Moreover, irradiation can regulate both ferroptosis and FA metabolism. At the same time, ferroptosis may render tumor cells more vulnerable to therapies that further stress their ability to regulate redox homeostasis, thereby generating opportunities for novel therapies. Targeting substrates of lipid metabolism and regulating ferroptosis in radiotherapy could decrease toxicity and increase clinical benefits. Therefore, we reviewed the interplay between FA metabolism, ionizing radiation, and ferroptosis. We focus our discussions on the biological mechanisms by which FA metabolism might be altered by radiation, as well as the contribution it makes to radiation-regulated ferroptosis and/or the possibility of radioresistance. We also suggest directions that could guide future clinical development and research of novel combination approaches, particularly combining ferroptosis agonists with radiotherapy, as well as lipid metabolism regulators, to improve the efficacy of cancer treatment and promote radiosensitivity.

FATTY ACID METABOLISM AND FERROPTOSIS

Metabolic reprogramming in uncontrolled-proliferation tumor cells requires lipids, proteins, and nucleotides to develop and maintain cellular structure and function, and the metabolism is significantly different from that in relative normal tissues. The considerable development of lipidomic technologies has broadened our understanding of the relevance of lipid metabolism to cancer biology.

Fatty acid metabolism has been implicated in a variety of oncogenic processes, including tumorigenesis, metastatic colonization, treatment resistance, and cell differentiation (Beloribi-Djefaflia et al., 2016). However, unlike normal cells, in which exogenous FAs play a dominant role, tumor cells have the capacity to synthesize FAs *de novo* (Ookhtens et al., 1984). The primary source of carbon for FA synthesis in cancer cells comes from glucose, which is broken down into acetyl-CoA and then citrate in the mitochondria. The *de novo* synthesis of FAs can be divided into saturated and unsaturated FAs. Unsaturated FAs bind membrane phospholipids and subject tumor cells to oxidative stress, while saturated FAs play a protective role in tumor cell biology. As most studies have revealed the relationship between unsaturated FAs and ferroptosis, the following reviews are concentrated on unsaturated FAs. Unsaturated FAs with carbon-carbon bonds can be divided into monounsaturated fatty acids (MUFAs, only one double bond) and polyunsaturated fatty acids (PUFAs, at least two double bonds).

In recent years, increasing attention has been focused on PUFA peroxides and ferroptosis. PUFAs bind to biological membrane phospholipids and tend to be oxidized to generate ferroptotic cell death under oxidative or energy stress. This form of cell death is known to be dependent on substrates that maintain redox homeostasis. Under oxidative or energetic stress, PUFA, particularly arachidonoyl (AA) and adrenic acid (AdA), is catalyzed by acyl-CoA synthetase long-chain family member 4 (ACSL4), lysophosphatidylcholine acyltransferase (LPCAT), and 15-lipoxygenase (15-LOX/ALOX15) to generate PUFA-containing phospholipids and induce ferroptosis to maintain redox homeostasis. Thus, the following section discusses the prominent effects of abnormal FA metabolism in triggering ferroptosis.

PUFA-PL Impinges on Tumor Cell's Susceptibility to Ferroptosis

With increasing levels of ROS, PUFA-PL is oxidized to generate PUFA-PL-OOH, which is the most important substrate for inducing ferroptosis. Among PUFA-PL, long-chain PUFAs, particularly AA or AdA, seem to be indispensable for navigating cells to ferroptosis. Indeed, genetic or pharmacological inhibition of acyl-CoA synthase 4 (ACSL4) to suppress AA or AdA esterification into PE has been shown to inhibit ferroptosis (Kagan et al., 2017). The ACSL4, LPCAT3, and ALOX family, which are involved in the synthesis of PUFA-PL-OOH, can also regulate cellular sensitivity to ferroptosis. Suppression of ferroptosis has also been observed by targeting or knockout of these enzymes (Doll et al., 2017). In breast cancer cell panels, which have diverse expression levels of ACSL4, the level of GPX4 is inversely proportional to that of ACSL4 and cell viability, and is correlated with the effect of ACSL4 in the esterification of AA and AdA into phosphatidylethanolamines (PE). Moreover, ACSL4 and ACSL3 can also catalyze AA; however, given the lower expression of free AA in the cytoplasm, other FAs can outcompete AA by combining with ACSL3. Thus, ACSL4 is a privileged enzyme that promotes ferroptosis (Doll et al., 2017). It should be noted that that regulation of ferroptosis by ACSL4 is necessary for glutathione peroxidase 4 (GPX4) inhibition, but is dispensable for the p53-mediated ferroptosis pathway, in which

ALOX12 is essential for tumor suppression. The p53-mediated pathway downregulates the transcriptional level of SLC7A11 and contributes to the activation of ALOX12 (Chu et al., 2019). Following the generation of AA-CoA by ACSL4, LPCAT3 esterifies these derivatives into phosphatidylethanolamines (AA-PE and AdA-PE, also known as PL-PUFAs) in the plasma or internal membrane. PL-PUFAs are then oxidized into PL-PUFA-OOH under the assistance of ALOX15, and ultimately trigger ferroptotic cell death. Therefore, PL-PUFA-OOH acts as the main executor, triggering ferroptosis. While PUFAs stimulate cells to undergo ferroptosis, MUFA has the opposite effect.

Monounsaturated fatty acids suppresses ROS accumulation at the plasma membrane and decreases the level of PUFA-PL, inhibiting ferroptosis in an ACSL3-dependent manner (Magtanong et al., 2019). Tumor cells have the capacity to use MUFA to facilitate metastasis, and previous studies have demonstrated that some tumor types prefer to initially metastasize through the lymphatic system before metastasizing systemically through the blood. Although the mechanism underlying the phenomenon remains unclear, the Ubellacker group revealed the possible role of oleic acid, a MUFA, which can incorporate into the cell membrane as a "suit of armor" and protect cancer cells in lymph from ferroptosis and facilitate distant metastasis (Ubellacker et al., 2020). In this study, tumor cells injected intranodally were more resistant to ferroptosis due to high level of oleic acid and GSH. Furthermore, some researchers found that stearyl CoA desaturase 1 (SCD1) converts saturated FAs into MUFAs and is highly expressed in several cancers (Wang et al., 2015; Igal, 2016). In line with this, inhibition of SCD1 increases cell sensitivity to ferroptosis, with decreasing levels of CoQ10 and MUFAs (Tesfay et al., 2019).

Polyunsaturated fatty acids can be obtained from acid hydrolases from lipophage (Singh and Cuervo, 2012) and function to regulate ferroptosis. Intracellular surplus FAs do not exist as free FAs because high concentrations of free FAs are cytotoxic; thus, after executing its biological function, surplus free FAs are stored in the form of a neutral biomolecule in lipid droplets (LD), which have been shown to be abundant in tumor cells (Unger, 2002; Martin and Parton, 2006; Thiele and Spandl, 2008; Qiu et al., 2015; Klemm and Ikonen, 2020). A phase II clinical trial evaluating bortezomib monotherapy for advanced renal cancer revealed partial responses in only 12% of patients with renal cell carcinoma (Kondagunta et al., 2004). HIF-2α/PLIN2/LD-dependent lipid storage and endoplasmic reticulum stress resistance is thought to contribute to this limited response rate. In addition, LD can combine with ras-related protein rab-7a (RAB7A) and be degraded by lipophagy. In a previous study on liver cancer where HepG2 cells were treated with RSL3, the level of LD increased initially, but later decreased, and LD degradation was found to be associated with increasing levels of lipid peroxidation (Bai et al., 2019). This result highlights the balance between lipid storage and degradation, which determines the cell response to ferroptosis stress. However, the role of lipophages remains controversial. Apart from its tumor suppressor role, lipophagy-dependent degradation of lipids may provide rapidly proliferating cancer cells with energy substrates and intermediates for the synthesis of biomolecules, which contribute to the survival of tumor cells (Gomez and de Molina, 2016).

Of note, the uptake of omega-3 and omega-6 PUFAs is essential for cell function, while their precursors (linoleic acid and α-linolenic acid, respectively) are solely exogenic and cannot be provided through the *de novo* pathway (Swinnen et al., 2003). Epidemiological studies recommend that a diet rich in omega-3 PUFA is beneficial for decreasing cancer incidence. Omega-3 PUFAs can inhibit tumor cell proliferation via different pathways, including cyclooxygenase-2 (COX-2), nuclear factor-kappa B (NF-κB), Akt, and PPAR signaling pathways (Dolcet et al., 2005; Schley et al., 2005; Wu and Kral, 2005; Bai et al., 2009). In contrast, high intake of omega-6 PUFAs shows inverse effects on tumorigenesis (Pozzi et al., 2010; Panigrahy et al., 2012). Interestingly, FA transformation between pro-tumorigenesis and anti-tumorigenesis FAs dramatically promotes tumor repression. Berquin et al. (2007) used the *fat*1 transgene, which encodes omega-3 desaturase, to successfully convert most omega-6 PUFAs into omega-3 PUFAs in PTEN-knockout mice. The results suggest that pharmacological or genetic means to convert PUFAs with diverse functions may have unexpected effects on the treatment response.

In summary, considering the role of FAs, including FFA and PUFA, in ferroptosis, targeting PUFA-PL may inhibit tumorigenesis and metastasis by triggering ferroptosis.

Disruption of Redox Homeostasis Is the Final Component in Ferroptosis Induction

Given the requirement of lipid homeostasis in normal cells, once the interruption of redox homeostasis occurs, reduced protein or molecules is initiated to scavenge excess lipid peroxidase. Glutathione (GSH) and coenzyme Q10 (CoQ10) are important antioxidants in cells.

Cysteine can act as both as a basic unit for protein translation and as an essential substrate of the antioxidative system. Two pathways have been shown to contribute to increased cysteine levels. One is the glutamate-cystine antiporter system Xc-, which can import extracellular cystine into cells and export intracellular glutamate at a 1:1 ratio, and the other is transsulfuration, which converts methionine into cysteine when extracellular sources of cysteine are limited (Zhu et al., 2019). Thus, imported cystine is reduced immediately, transformed into cysteine in cells, and used to synthesize reduced GSH under the catalysis of glutamate-cysteine ligase and glutathione synthetase. GPX4 then cleans LPO and maintains cellular redox homeostasis by using two GSH molecules as electron donors to reduce phospholipid hydroperoxides (PL-OOH) to the corresponding alcohols and leaving GSSG (oxidized GSH) as a byproduct (Yang et al., 2014). GSSG is reduced to GSH by glutathione reductase using NADPH. Thus, inhibition of the Xc- system, GSH, or GPX4 can induce intracellular accumulation of LPO and ultimately lead to cell ferroptosis.

The NAD(P)H-ferroptosis suppressor protein 1 (FSP1)-coenzyme Q10 (CoQ10, also named ubiquinone) pathway is an emerging pathway associated with ferroptosis suppression.

The suppression of ferroptosis by FSP1 is mediated by CoQ10. The reduced form of CoQ10 is ubiquinol, which promotes the generation of lipid peroxyl radicals and stimulates the accumulation of lipid peroxidation using NAD(P)H. Thus, FSP1 catalyzes ubiquinol into CoQ10 and decreases the level of lipid peroxidation. FSP1-mediated suppression of ferroptosis is an independent pathway parallel to the Xc/GSH/GPX4 axis.

In short, the loss of the scavenging system for eliminating lipid hydroperoxides from PUFA-PLs is one of the hallmarks of ferroptosis.

Peroxisomes Act as the Achilles' Heel of FA Metabolism During Ferroptosis

Peroxisomes perform many essential lipid metabolism functions, including the catabolic and anabolic processes of FAs. Peroxisomes play particularly important roles in FAO, ether-phospholipid biosynthesis, and ROS metabolism (**Figure 1**). Previous studies have shown that β-oxidation of FAs predominantly occurs in mitochondria;, although peroxisomes also participate in FA oxidation (Chen X. et al., 2020; Luppi et al., 2020). Although the integral compounds and full-scale function of peroxisomes remain unclear, it has been demonstrated that peroxin (PEX) families are essential components that maintain their structure and function, and peroxisome proliferator-activated receptors (PPARs), a set of three receptor subtypes (PPARα, γ, and δ) regulate a broad range of genes in many metabolically active tissues.

Peroxisomes are involved not only in catabolic processes but also in anabolic processes, such as ether phospholipids. Ether phospholipids account for 20% of phospholipids in humans, are characterized by an alkyl chain attached at the position of sn-1 (Lodhi and Semenkovich, 2014; Lodhi et al., 2015), and are the major type of ether phospholipids is plasmalogen. Given that the alkenyl-ether group of plasmalogen represents a major lipid-soluble antioxidant component, plasmalogen can scavenge ROS and mitigate cellular oxidative stress. A reduction of ether phospholipids has been observed to correlate with increasing colorectal cancer and lymph node metastasis because the high level of ROS consumes plasmalogen (Wang Y. et al., 2020). Ether was recently reported to bind phospholipids characterized by an alkyl chain attached at the sn-1 position (Lodhi and Semenkovich, 2014; Lodhi et al., 2015). Previous studies have focused on the effects of PUFA and MUFA oxidation on ferroptosis regulation; however, a recent study has found that ether phospholipids also participate in ferroptosis. Peroxisomes contribute to ferroptosis by synthesizing polyunsaturated ether phospholipids (PUFA-ePL). The downregulation of PUFA-ePL is associated with tumor cell resistance to ferroptosis peroxisomal biogenesis factor 3 (PEX3), peroxisomal biogenesis factor 10 (PEX10), peroxisomal biogenesis genes, and alkylglycerone phosphate synthase (AGPS), and fatty acyl-CoA reductase 1 (FAR1) encoding peroxisomal enzymes is considered to contribute to these effects. Alteration of PEX3, PEX10, AGPS, and FAR1 showed no connection with ACSL4 and LPCAT3 (Zou et al., 2020). In our previous work, PEX5 was found to be involved in radioresistance in hepatocellular carcinoma (HCC) (Wen et al., 2020). However, the functions of peroxisomes in regulating ferroptosis sensitivity are dispensable given that the alkenyl-ether group is not critical to ferroptosis sensitivity. PUFA-PL can complement the depletion of PUFA-ePL, and, more importantly, the ether lipid precursor 1-O-alkyl-glycerol-3-phosphate (AGP) is required for dispatch to the endoplasmic reticulum to synthesize plasmalogens (critical ethers for PUFA-ePL); however, it remains unknown how the ultimate step of PUFA-ePL synthesis is executed and regulated.

As mentioned above, PPARs play an indispensable role in peroxisome function. The expression of many genes involved in peroxisomal FA β-oxidation and proliferation is controlled by transcription factors of the PPAR family. Intriguingly, researchers have found that PPARα activity is regulated by MDM2/MDMX and drove the resistance of glioblastoma cells to ferroptosis. In addition, PPARα is associated with increased levels of saturated FAs and MUFAs (Strand et al., 2019), which may partially explain the reason for ferroptosis resistance. PPARγ also showed inhibitory effects on ferroptosis (Venkatesh et al., 2020). These findings are consistent with other publications that have shown that PPARγ can regulate SCD1 (Shi et al., 2013). SCD1 is a rate-limiting enzyme in MUFA biosynthesis; thus, PPARγ can facilitate MUFA synthesis and inhibit ferroptosis. Moreover, a recent study found inhibition of ferroptosis in tumor cells with high density due to up-regulation of E-cadherin and epithelial mesenchymal transition (EMT) (Wu et al., 2019). Pharmacological or genetic approaches to inhibit E-cadherin could rescue ferroptosis sensitivity. Interestingly, previous studies have suggested that PPARγ may increase EMT by upregulating E-cadherin (Yang et al., 2019; Kim et al., 2020). PPARδ is another isoform of PPARs, and evidence has shown that activation of PPARδ could increase ACSL3 mRNA and protein *in vitro* and *in vivo* (Cao et al., 2010). As mentioned above, ACSL3 is a negative enzyme for ferroptosis as it functions to synthesize MUFA. Moreover, in a hamster model fed with different fat diets, PPARδ was found to upregulate ACSL4 expression in liver tissue, one of the key enzymes for synthesizing PUFA-PL-OOH to trigger ferroptosis (Kan et al., 2015). These contradictory findings suggest that the response of cells to ferroptosis may be affected by different PPAR isoforms with different effects on the lipid profile. Thus, PPARs not only act as organelles to maintain redox homeostasis, but also function to regulate ferroptosis and lipid metabolism, which directly affect tumorigenesis, metastasis, and therapeutic response; thus, the specific effects under different conditions should be considered.

IONIZING RADIATION: A VERSATILE REGULATOR IN THE INITIATION OF FERROPTOSIS

Radiotherapy has attracted significant attention for the treatment of over 50% of all cancers, either alone or in combination with other anti-cancer therapies. Despite the expansive research on delivery techniques and dosing schedules, the outcome of radiotherapy for many cancers remains unsatisfactory, particularly with respect to radio-resistance, regardless of the original and/or acquired resistance. Thus, a deep understanding

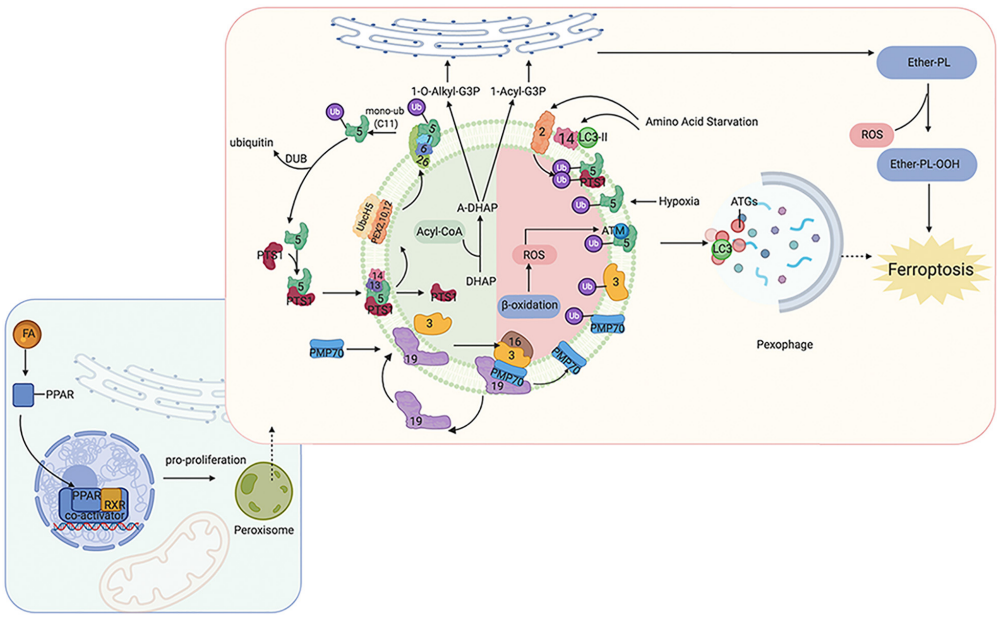

FIGURE 1 | Overview of molecular and proteins, which are involved in ferroptosis, localized at the peroxisome membrane in mammals. Ferroptosis can be regulated by peroxisome synthesized ether-linked phospholipid and PPARs. G3P would be imported into peroxisomal membrane, then dehydronated by G3PDH and introduce DHAP. Then, DHAP acyltransferase (DHAPAT) uses fatty acyl CoA to acylate dihydroxyacetone phosphate (A-DHAP). Besides, fatty acyl CoA can be reduced to fatty alcohol by a peroxisomal membrane-associated fatty acyl CoA reductase with NADPH. Subsequently, acyl-DHAP is converted to alkyl-DHAP by peroxisomal fatty alcohol. Acyl- or alkyl-DHAP reductase (ADHAP) can reduce acyl-DHAP and alkyl-DHAP to 1-acyl-G3P and 1-O-alkyl-G3P, respectively. 1-acyl-G3P and 1-O-alkyl-G3P are imported into ER, and converted to diacylphospholipid or ether-linked phospholipids (ether-PL). Ether-PL can be oxidized to ether-PL-OOH, which has been considered a trigger of ferroptosis. PPARs have three receptor sub-types (PPARα, γ, and δ). PPARα and γ could facilitate MUFA synthesis to suppress ferroptosis. Although PPARδ has been reported to up-regulate the expression of ACSL3 to promote the synthesis of MUFA, PPARδ could also up-regulate ACSL4 which is a promoter of ferroptosis. PPAR, peroxisome proliferator-activated receptors; G3P, glycerol 3-phosphate; G3PDH, glycerol 3-phosphate dehydrogenase; DHAP, dihydroxyacetone phosphate; DHAPAT, DHAP acyltransferase; A-DHAP, acyl-DHAP; ADHAPR, acyl-/alkyl-DHAP reductase; PL, phospholipid; MUFA, monounsaturated fatty acids; ACSL, acyl-CoA synthetase long-chain family member; GSR, glutathione-disulfide reductase.

of the interaction between radiation and aberrant tumoral biological context is urgently required. In recent years, FAO-generated ferroptosis has gained increasing attention, and the understanding of the correlation between IR and ferroptosis, as well as their crosstalk in the tumor microenvironment, is increasing. According to previous studies, IR can influence several processes of FA metabolism, including synthesis (Catalina-Rodriguez et al., 2012; Martius et al., 2014; Kan et al., 2015; Koritzinsky, 2015; Benedetti et al., 2017; Gonnissen et al., 2017; Tan et al., 2018; Chuang et al., 2019; Gottgens et al., 2019; Kaur et al., 2019; Chen J. et al., 2020), transport (Zammit et al., 1989; Martius et al., 2015), oxidation, and reduction (Meister and Anderson, 1983; Martius et al., 2015; Ma et al., 2018; Ye et al., 2020), and is involved in generating FA metabolites (Richards et al., 2009; Zhong and Yin, 2015; **Table 1**). In other words, by taking advantage of ionizing radiation affecting lipid peroxidation, RT can further sensitize tumor cells to ferroptosis, which could be considered as a new treatment strategy to achieve better outcomes (shown in **Figure 2**).

IR Induces Ferroptotic Cell Death by Promoting Lipid Peroxidation

In addition to DNA, membranes are also considered critical targets of ionizing radiation. Several studies have supported the idea that membrane damage induced by radiation is a critical event and an initial step in triggering cell death. The plasma membrane lipid bilayer is exposed to radiation and radiation-induced ROS, resulting in lipid peroxidation, including PUFA peroxidation (**Figure 2A**).

After radiation exposure, PUFAs can be converted to various lipid peroxide derivatives, including malondialdehyde (MDA) (Richards et al., 2009). Moreover, 4-hydroxy-2-non-enal (4HNE), produced by lipid peroxidation, reacts easily with amino or thiol groups, and modifies and cross-links proteins, including oxidoreductases, transferases, and kinases (Poli et al., 2008). High 4HNE levels can trigger an unfolded protein response (UPR) through pathways involving protein kinase R (PKR)-like endoplasmic reticulum kinase (PERK). This signaling cascade activates the transcription factor 6 (ATF6) and inositol requirement 1 (IRE1), accompanied by JNK and p38 signaling, suggesting that 4HNE acts as an upstream modulator of the radiation-induced ROS response and endoplasmic reticulum stress (Lin et al., 2014).

As discussed above, PUFA-PL-OOH plays an important role in triggering ferroptosis. ACSL4 catalyzes AA/AdA to generate acyl-CoA and is known to be required for ferroptosis induction by generating the lipid target pool for peroxidation (Doll et al., 2017; Friedmann Angeli et al., 2019). Evidence has shown that IR can

TABLE 1 | Proteins or enzymes influenced by ionizing radiation in fatty acids metabolism and ferroptosis.

	Proteins/enzymes	Expression/Level	Radio-resistance	Functions	References
FAs transport					
	FAT/CD36	↑	NA	Transport exogenous FAS across plasma membrane	Martius et al., 2014, 2015; Gonnissen et al., 2017
FAs biogenesis					
	CTP	↑	↑	Carries citrate from the mitochondria to the cytosol, associates with cancer aggressiveness	Catalina-Rodriguez et al., 2012
	ACLY	↑	↑	Key enzyme of *de novo* fatty acid synthesis, cleaves cytosolic citrate into acetyl-CoA and oxaloacetate.	Gottgens et al., 2019
	ACC	↑	↑	Converts acetyl-CoA into malonyl- CoA	Koritzinsky, 2015; Gonnissen et al., 2017
	FASN	↑	↑	Catalyzes the final step of FAs *de novo* synthesis	Chuang et al., 2019; Chen J. et al., 2020
	ACSL4	↑	↓	Catalyzes AA/AdA to generate acyl-CoA	Ye et al., 2020
Ether synthesis					
	PEX5	↑	↑	Receptor for PTS1, target of phosphorylation and ubiquitination,	Wang Y. et al., 2020
	PPARα/γ	↑	↑	Acts as lipid sensors to regulate peroxisomal fatty acid β-oxidation and proliferation	Benedetti et al., 2017; Kaur et al., 2019
	PPARδ	↓	NA	Acts as lipid sensors to regulate peroxisomal fatty acid β-oxidation and proliferation	Kan et al., 2015
Fatty acid oxidation					
	CTP1	↓	↑	The rate-limiting enzyme of FAO	Zammit et al., 1989; Tan et al., 2018
Redox					
	SLC7A11	↓	↓	Transport cystine into cytoplasm	Richards et al., 2009
	GPX4	↓	↓	Major antioxidant enzyme, reduces phospholipid hydroperoxides, inhibits lipid peroxidation	Ye et al., 2020
	GSH	↓	↓	The major cellular thiol participating in cellular redox reactions and thioether formation	Meister and Anderson, 1983; Ye et al., 2020
	GSSG	↓	↓		Meister and Anderson, 1983; Ye et al., 2020
Derivation					
	4-HNE	↑	NA	Unfold protein response (upr)	Poli et al., 2008; Zhong and Yin, 2015
	MDA	↑	NA	Modifies and cross-links proteins	Richards et al., 2009

FA, fatty acid; IR, ionizing radiation; CTP, mitochondrial citrate transporter protein; ACLY, ATP citrate lyase; ACC, Acetyl-CoA Carboxylase; FASN, fatty acid synthase; ACSL4, acyl-CoA synthetase long-chain family member 4; PEX, peroxisomal biogenesis factor; PPAR, peroxisome proliferator-activated receptors; FAT/CD36, fatty acid transposase; CTP1, carnitine palmitoyl transferase 1; GPX4, Phospholipid hydroperoxide glutathione peroxidase; GSH Glutathione; GSSG, glutathione disulfide; MDA, malondialdehyde; 4HNE, 4-Hydroxy-2-non-enal.

upregulate the level of ACSL4, and, in ACSL4-knockout cells, IR failed to induce ferroptosis with a decrease in lipid peroxidation. In turn, ACSL4-regulated ferroptosis can sensitize tumors to radiation. However, the mechanism by which IR regulates ACSL4 expression remains unknown. A previous study found that BMP4 could increase the level of ACLS4 and decrease the expression of p53 in epidermal growth factor receptor (EGFR)-mutant non-small cell lung cancer *in vivo* and *in vitro*(Bach et al., 2018).

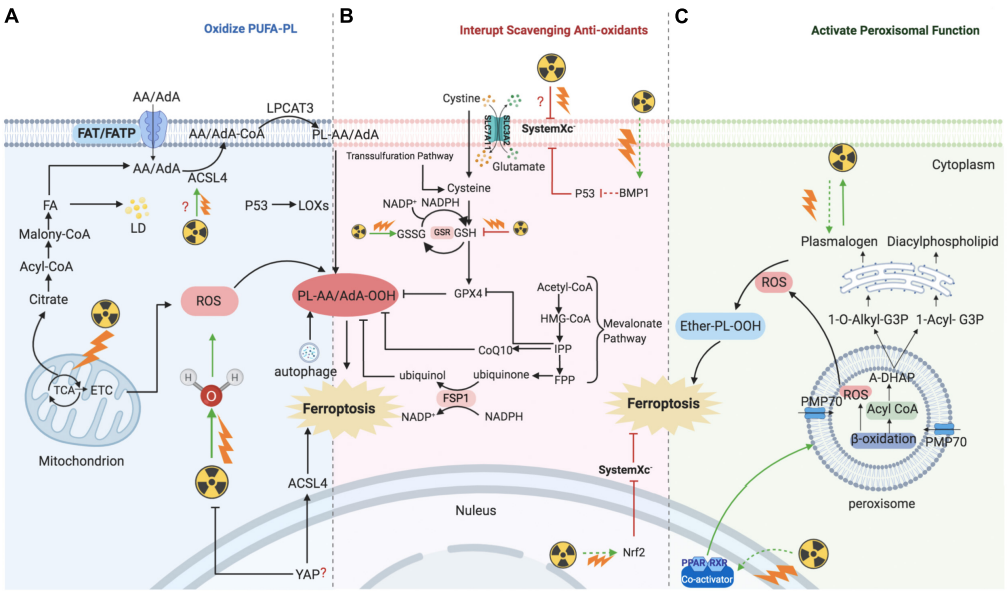

FIGURE 2 | Mechanism of ionizing radiation – regulated ferroptosis. IR introducing excessive lipid peroxidation and decreasing antioxidants levels are key mechanism for regulating ferroptosis. **(A)** IR induces ferroptosis by introducing excessive lipid peroxidases. IR could up-regulate the level of ACSL4, and then ACSL4 catalyzes AA/AdA to generate Acyl-CoA. After AA generating AA-CoA by ACSL4, LPCAT3 esterifies these derivatives into AA-PL or AdA-PL in plasma membrane or internal membrane. Then, PL-AA/AdA is oxidized into PL-PUFA-OOH under the assistance of LOXs, and ultimately triggers ferroptotic cell death. In addition, IR could also provide amounts of ROS to directly oxidize PL-PUFA via ionizing water molecular or mitochondria. **(B)** IR induces ferroptosis by interrupting redox homeostasis. IR suppresses the expression of SLC7A11 and inhibits the import of extracellular cystine into cell to synthesis GSH, whereas the level of GSSG is increased. **(C)** IR induces ferroptosis by activating functions of peroxisome. IR stimulates PPARs which promote the proliferation and fatty acid β-oxidation of peroxisome. Then, peroxisome would synthesize A-DHAP which is transported to endoplasmic reticulum to synthesize plasmalogen. Plasmalogen binds PL, and under the stress of ROS, ether-PL is oxidized to ether-PL-OOH. Once the redox homeostasis is broke, ether-PL-OOH would become an inducer of ferroptotic cell death. IR, ionizing radiation; ACSL, acyl-CoA synthetase long-chain family member; AA, arachidonoyl; AdA, adrenic acid; LPCAT3, lyso-phosphatidylcholine acyltransferase; PL, phospholipid; PUFA, polyunsaturated fatty acids; LOX, lipoxygenase; ROS, reactive oxygen species; GSH, glutathione; GSSG, oxidized GSH; GPX4, glutathione-dependent peroxidase; PPAR, peroxisome proliferator-activated receptors; A-DHAP, acyl-dihydroxyacetone phosphate; FAT; FATP; FA, fatty acid; TCA, tricarboxylic acid cycle; ETC, electron transport chain; LD, lipid droplet; IPP; FPP; CoQ10, ubiquinone; FSP1, NAD(P)H-ferroptosis suppressor protein 1; PMP, peroxisomal membrane proteins.

Moreover, IR can stimulate adipogenesis in the bone marrow by increasing the secretion of BMP4 (Bajaj et al., 2016). Notably, BMP4 may have diverse effects depending on the tumor type. For instance, BMP4 has been observed to be correlated with tumorigenesis and resistance to anti-cancer treatment by affecting FA metabolism in lung cancer (Bach et al., 2018). However, high levels of BMP4 have also been shown to be associated with promising survival rates in patients with glioma, as BMP4 promotes glioma cancer stem-like cell differentiation, and in turn, increases the tumor response to radiotherapy and chemotherapy (Xi et al., 2017).

Recently, *in vivo* and *in vitro* studies have provided mechanistic insights into the observation that cancer cells cultured at high density are resistant to ferroptosis due to the Merlin-Hippo signaling axis, which suppresses the proto-oncogenic transcriptional co-activator YAP to upregulate ACSL4 and the transferrin receptor (Wu et al., 2019; Yang and Chi, 2020). Nonetheless, if ferroptosis is consistently associated with radiosensitivity, YAP may have a positive effect on tumor cell response to IR. Indeed, several studies have demonstrated that YAP is frequently activated during the growth and progression of many solid tumors and may also confer resistance to radiotherapy. For example, YAP overexpression promotes medulloblastoma tumorigenesis, as well as the survival of cerebellar granule neuron precursor cells upon irradiation (Fernandez et al., 2012). Furthermore, YAP knockdown in urothelial carcinoma cells has been shown to increase the DNA damage response induced by γ-irradiation (Ciamporcero et al., 2016). Various biochemical and immunological methods have revealed that IR increases the expression of glucose-regulated protein 78kDa (GRP78) on the surface of cancer cells. GPR78 acts upstream of YAP/TAZ signaling and promotes migration and radiation-resistance in pancreatic ductal adenocarcinoma cells (Gopal et al., 2019). GRP78 is a member of the heat shock protein 70 (HSP70) family and acts as a centrally located sensor of stress, which responds and adapts to alterations in the tumor microenvironment. Thus, we hypothesize that ferroptosis increases the tumor response to radiation and may independently of the YAP signaling axis. Further work is needed to clarify how YAP and its upstream and downstream regulators confer resistance to radiotherapy.

In addition to regulating ACSL4 expression, it is clear that IR can directly target the tumor cell membrane PUFA-PL by generating an abundance of ROS. As discussed above, the

formation of lipid peroxide by PUFA-PL-OOH plays a significant role in triggering ferroptosis, and the contribution of PUFA-PL to ferroptosis depends on oxidation by ROS. The biological effects of IR are executed by the radiolysis of water and the generation of ROS ($^{\cdot}OH$, $H^{\cdot}$, $O_2^{\cdot -}$, H_2, H_2O_2). Among these free radicals, $^{\cdot}OH$ radicals are recognized as the major ROS in the ferroptosis process because of their high activity and sufficient energy. $O_2^{\cdot -}$ influences lipid peroxidation mainly through the Fenton reaction as opposed to directly abstracting hydrogen from pure PUFA due to the relatively low activity of $O_2^{\cdot -}$ compared to $^{\cdot}OH$ radicals.

Ferroptosis requires ROS, and the most significant source of ROS is the tricarboxylic acid cycle (TCA cycle) and the electron transport chain (ETC). It is clear that mitochondria are one of the most important targets of radiotherapy through the generation of mitochondrial ROS (mROS). In cancer cells, mROS amplify the tumorigenic phenotype and accelerate the accumulation of additional mutations that lead to metastatic behavior. Moreover, lipid ROS initially colocalizes with mitochondria, suggesting that mROS is the major source of ROS during ferroptosis (Gao et al., 2019). Of note, suggestive evidence of the involvement of mitochondria in ferroptosis highlights that mitochondria are not only mandatory for initiating ferroptosis by providing ROS, but also cause morphological and functional damage to themselves (Xie et al., 2016; Yu et al., 2017; Gao et al., 2019; Wang H. et al., 2020). IR-mediated mROS is reportedly involved in the immune response, gene expression, nuclear DNA damage, genomic instability, activity of metabolic and antioxidant enzymes, and radiosensitivity (Kim et al., 2006, 2017; Saenko et al., 2013; Xu et al., 2018). Moreover, a previous study demonstrated that targeting mitochondrial antioxidants, including manganese superoxide dismutase (MnSOD), glutathione peroxidase 2 (Gpx2), and thioredoxin reductase 2 (TrxR2) by microRNA-17-3p remarkably sensitized prostate cancer cells to IR. In addition, the use of nanosensitizers targeting mitochondria to increase mROS accumulation can promote IR-induced cell death (Chen Y. et al., 2019). Taken together, these results suggest that IR targeting of mitochondria and promotion of mROS accumulation oxidizes PUFA-PL and makes tumor cells more vulnerable to ferroptosis. However, the role of mitochondria in regulating ferroptosis remains unclear. IR can damage mitochondrial DNA (mtDNA), whereas loss of mtDNA or removal of mitochondria does not affect ferroptosis (Dixon et al., 2012; Gaschler et al., 2018).

IR Induces Ferroptosis by Interrupting the Scavenging Capacity of PUFA-PL-OOH

Under normal conditions, dysfunction of PUFA-PL-OOH scavenging capacity is another important means to regulate ferroptosis (**Figure 2B**). SLC7A11, GPX4, and GSH are essential substrates for the scavenging of peroxides. SLC7A11 expression is related to tumor invasion and metastasis via affecting the redox status or exporting glutamate in the tumor microenvironment. A previous study in prostate cancer showed that SLC7A11 expression is increased in the metastatic stromal area and is related to a low survival rate (Zhong et al., 2018). Moreover, SLC7A11 is essential for eliciting tumor formation and maintaining tumorigenicity by relieving oxidative stress in some oncogenic KRAS-mutant cancers, such as pancreatic ductal adenocarcinoma, colorectal adenocarcinoma, and lung adenocarcinoma (Lim et al., 2019). Moreover, recent studies have shown that KEAP1-NRF2 mutant lung cancer cells have high expression of SLC7A11 and are prone to resist radiation. Using ferroptosis inducers or agonists targeting SLC7A11 has the potential to sensitize radioresistant tumor cells. Moreover, abnormal expression of SLC7A11, regulated by IR, has been reported recently; high expression was found to correspond to poor survival in patients diagnosed with glioma, whereas SLC7A11 methylation indicated increased overall survival and disease-free survival. Interestingly, these associations only exist in patients who received radiotherapy and not those who did not (Ye et al., 2020). Moreover, a combination of IR and immune checkpoint inhibitors showed synergistic effects on SLC7A11 expression, and interferon-γ derived from immunotherapy-activated CD8 + T cells and IR-activated ATM both act as core regulators (Lang et al., 2019).

Recent studies revealed that p53 serves as an agonist of ferroptosis by repressing SLC7A11 and activating ALOX12 (Jiang et al., 2015; Chu et al., 2019). The diverse response of tissue to IR could contribute to the tissue specificity of p53 gene expression. A decline in radiosensitivity was accompanied by a reduction in p53 expression (Rogel et al., 1985; Komarova et al., 1997). Moreover, similar to the tumor suppression function of p53, BRCA1-associated protein 1 (BAP1) also acts as a tumor suppressor by targeting SLC7A11. Cancer genomic analysis revealed that SLC7A11 is a key target gene of BAP1 (Li C. et al., 2019). BAP1 decreases histone 2A ubiquitination occupancy on the SLC7A11 promoter and represses SLC7A11 expression in a deubiquitinating-dependent manner, leading to elevated lipid peroxidation and ferroptosis (Zhang et al., 2018). In patients with head and neck squamous cell cancer, overexpression of BAP1 was associated with higher failure rates after radiotherapy, possibly via deubiquitylation of H2Aub and modulation of homologous recombination, and was associated with poor outcomes (Liu et al., 2018). Although p53 and BAP1 have been suggested to be correlated with IR-induced SLC7A11 repression, IR-regulated ferroptosis did not affect the DNA damage response because both pharmacological (ferrostatin-1 treatment) and genetic (SLC7A11 or GPX4 overexpression) approaches did not affect phosphorylated H2AX foci formation and release of DNA damage response signals (Chk2 and p53 phosphorylation) (Lei et al., 2020).

Conversely, to gain resistance to ferroptosis, cancer cells show a tendency to upregulate SLC7A11 expression following IR treatment (Lei et al., 2020). Although we considered the increase in SLC7A11 as an adaptive response, IR-activated molecular factors should be taken into account. Nuclear factor E2-related factor 2 (NRF2) is considered an upstream signaling molecule that inhibits ferroptosis by regulating SLC7A11 under conditions of stress. NRF2 is also activated by radiation, which operates as an antioxidant adaptive response system, while activating transcription factor 4 (ATF4) is another SLC7A11-related transcription factors (McDonald et al., 2010; Chen et al.,

2017). Similarly, IR has been shown to increase ATF4 in certain cancer cells (Kim et al., 2014). However, contrary to the pro-tumorigenic role of ferroptosis, the IR-regulated AFT4 increase is associated with radiotherapy sensitivity. Thus, whether IR-mediated ferroptosis depends on the repression of SLC7A11, and how IR regulates the level of SLC7A11 remains to be clarified.

The anti-oxidation molecules GSH and GSH/GSSG are also significantly decreased after radiation treatment (Ye et al., 2020), suggesting that high levels of GSH consumes ROS generated by radiation and greatly reduces the efficacy of IR. Indeed, numerous studies have revealed that depletion or inhibition of GSH can increase the tumor response to radiation (Dethmers and Meister, 1981; Bump et al., 1982; Estrela et al., 1995).

Based on these findings, IR is implicated in ferroptosis not only by forming PUFA-PL-OOH but also by inhibiting the production of reduced molecules. Conversely, the radiosensitivity of tumor cells is enhanced after treatment with ferroptosis inducers. Other anticancer treatments such as immunotherapy, show synergistic effects with IR on ferroptosis. Together, ferroptosis may provide an emergent research direction for promoting the clinical benefits of radiotherapy.

IR Induces Ferroptosis via Activating Peroxisome

Despite the abovementioned functions of peroxisomes in FA metabolism and ferroptosis, several studies have shown the interplay between peroxisomes and ionizing irradiation and indicated a novel mechanism of IR-regulated ferroptosis (**Figure 2C**).

Peroxisome proliferator-activated receptors α has been shown to enhance the radiosensitivity of pancreatic cancer cells via the Wnt/β-catenin pathway, and the Wnt/β-catenin has been shown to increase intracellular bivalent iron and result in ferroptosis following asbestos exposure (Xue et al., 2018; Ito et al., 2020). Furthermore, knockout of PPARα could lead to the inhibition of radiation-induced apoptosis. The specific mechanism involved in PPARα-regulated radiosensitivity may be associated with time-dependent increases in NF-κB DNA-binding activity (Zhao et al., 2007). In human endothelial cells exposed to individual dietary FAs, linoleic acid stimulates NF-κB transcriptional activation (Toborek et al., 2002), and previous studies have found that NF-κB is abrogated by overexpression of GPX4 (Li L. et al., 2019; Brigelius-Flohe and Flohe, 2020). Similarly, in addition to PPARα, PPARγ agonists can also inhibit tumor growth by enhancing radiosensitivity (Kim et al., 2020). Moreover, activation of peroxisome function by IR may partially explain the increased expression of ACSL4 following radiation exposure. In line with this, a selective increase in ACSL4 was observed in the testes and livers of high-fat diet animals through the activation of PPARδ (Kan et al., 2015). Consistent with these findings, RT increases PPAR δ in normal tissue and decreases it in tumor tissue (Linard et al., 2008; Yang et al., 2011; Gao et al., 2012; Mangoni et al., 2017; Kaur et al., 2019). These findings imply that peroxisomes act as a dominant linker between FA metabolism and IR to generate ferroptosis.

As we have demonstrated, PEX genes are essential for peroxisomal structure and function. In mammalian cells, at least 12 PEX genes have been found to be involved in the assembly of the peroxisomal membrane, interacting with peroxisomal targeting sequences (PTSs), allowing proteins to be shuttled to peroxisomes, and acting as docking receptors for peroxisomal proteins. PEX 3 is critical for the assembly of the peroxisomal membrane and import of peroxisomal membrane proteins (PMPs). Moreover, based on Zou's research, PEX3 contributes to ether-promoting ferroptosis, and plasmalogen, synthesized by peroxisomes, has been shown to promote ferroptosis by binding membrane phospholipids (Zou et al., 2020). Some researchers have explored the interaction, especially the synergistic effects, between IR and ether lipids, and found that ether lipids showed supra-additive cytotoxic effects with ionizing radiation and the could be considered a sensitizer to IR in radio-resistant tumor cells (Berkovic et al., 1997). Recently, CLR127, a clinical-grade antitumor alkyl phospholipid ether analog, was shown to increase the tumor response to IR *in vivo* and *in vitro* (Elsaid et al., 2018). However, the functions of other PEX genes in ferroptosis have not yet been revealed. For instance, our previous study revealed that PEX5, the cargo receptor of peroxisomes, functions to transport cargo to docking sites at the peroxisomal membrane and is highly expressed in HepG2 cells (Wen et al., 2020). Moreover, the upregulation of PEX5 in liver cancer cells was also found to be associated with radioresistance; however, whether PEX5 is a regulator of peroxisomal ferroptosis remains unclear.

Although direct evidence supporting IR-regulated ferroptosis by altering peroxisomes is scarce, considering the crosstalk between peroxisome-regulated FA metabolism, IR, and ferroptosis, it is conceivable that IR could also induce ferroptosis with the alteration of peroxisomes. However, the novel mechanism underlying the synergistic effect of IR and peroxisome requires further exploration. Taken together, research on peroxisome functions in regulating FA metabolism, ferroptosis, and radiobiology is increasingly, and the findings not only expand our knowledge on the mechanistic underpinnings of tumorigenesis and metastasis, but also highlight the need for therapeutic strategies using targeted agonists or inhibitors to be more context-dependent and personalized.

FUTURE PERSPECTIVES

As the interplay between lipid metabolism and ferroptosis is linked to the tumor biological context and efficiency of anticancer treatments, our knowledge of the molecular mechanism and regulation of the ionizing effect has greatly advanced in recent years. However, several key questions remain to be answered.

Applying a Systematic and Precise Approach to Dissect the Effect of IR-Regulated Ferroptosis

Selecting a compatible dose and dose rate are important factors in radiation treatment of tumor cells. Varying the dose rate is known to alter the levels of lipid peroxidation in that lipid peroxidation shows an "inverse dose rate effect," namely increasing lipid

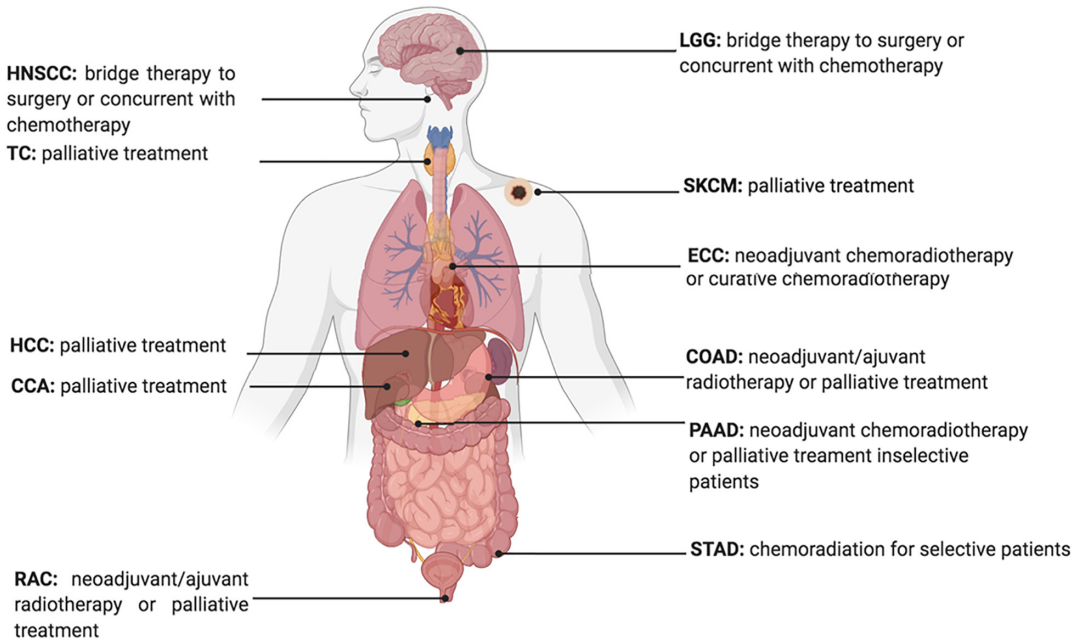

FIGURE 3 | Current Status of Radiotherapy for treatment of high ACSL4 expression tumors. HNSCC, Head and Neck squamous cell carcinoma; TC, Thyroid carcinoma; HCC, hepatocellular carcinoma; CCA, cholangiocarcinoma; RAC, Rectum adenocarcinoma; ECC, Esophageal carcinoma; LGG, Brain Lower Grade Glioma; STAD, Stomach adenocarcinoma; PAAD, Pancreatic adenocarcinoma; COAD, Colon adenocarcinoma; SKCM, Skin Cutaneous Melanoma.

peroxidation at a constant absorbed dose rate, with decreasing radiation dose rate (Stark, 1991; Kumar et al., 2003; Klepko et al., 2014; Mao et al., 2016). Decreased lipid peroxidation at high dose rates is probably due to greater recombination effects when the number of positive and negative ion pairs is assembled. Thus, irradiation-related biological damage occurs rapidly without the combination of free radicals and PUFAs.

The "oxygen effect" is another explanation for the inverse dose-rate effect. The oxygen effect is widely accepted as a key element of radiosensitivity, and it is a well-established fact that IR damages significantly more tumor cells in normoxic compared to hypoxic conditions. This is partly due to molecular oxygen reacting with the induced DNA radicals to produce chemically irreparable peroxyl radicals. In addition, some studies further explored the effect of different dose rates on the oxygen effect and revealed that the oxygen effect was decreased at a lower dose rate (0.3). According to these findings, ROS generated by higher dose rate IR tends to bind DNA, while ROS introduced by lower dose rate IR is prone to peroxidize FAs. While further studies are required to validate these results, the characteristics of FA metabolism are now a reasonable option to select candidates who are unable or unsuitable for low-dose IR.

Although the "inverse dose rate effect" seems to suggest a low dose rate in order to obtain more obvious response LPO, low doses of low LET radiation (^{137}Cs γ rays) delivered at a low dose-rate upregulates antioxidant defense (e.g., an increase in the level of glutathione together with upregulation of γ-glutamylcysteine synthetase expression) (Bravard et al., 1999; Kojima et al., 2002; de Toledo et al., 2006). In contrast, high LET radiation propagates oxidative stress in irradiated cells and their neighboring bystanders (Narayanan et al., 1997, 1999; Azzam et al., 2002).

In addition to the effects of dose and dose rate, other unanswered questions involve the extent to which variation in the level of expression and activity of DNA repair enzymes (DNA double-strand break repair, a predominant phenomenon of radiobiology) and proteins involved in downstream signaling after IR plus enzymes and proteins involved in ferroptosis, influence the outcome of RT. Given the highly ordered nature of the protein, a few structural changes introduced by single amino acid changes in individual proteins may significantly alter the activity of the complex. Indeed, there is increasing evidence that crosstalk among glucose, FA, and amino acid metabolism (Li and Zhang, 2016) affects cancer predisposition, and, by inference, may also modulate the response to radiation treatment.

Heterogeneity Is Considered to Have a Significant Impact on the Outcome of IR-Regulated Ferroptosis

Cancer heterogeneity (intertumoral and intratumoral) remains a key hurdle in cancer medicine. Thus, we propose that tumoral heterogeneity, including special and temporal heterogeneity, affects the tumor response to IR-regulated ferroptosis. Different organs show different capacities and activities of FA metabolism, which may lead to diverse responses to IR-regulated ferroptosis. In addition, a single tumor over different timepoints may also present different responses. For example, hypoxia can trigger genetic mechanisms that may confer additional survival

advantages to tumor cells. Hypoxia induces the expression of several genes, particularly genetic programs that are under the control of hypoxia inducible factor 1 (HIF-1). Importantly, HIF-1 can inhibit ferroptosis via a mechanism dependent on the GSH/GPX4 axis, and this process can provide selective pressure for the emergence of ferroptosis-resistant subclones. Similarly, hypoxia may select for cells with p53 mutations (since cells expressing wild-type p53 tend to undergo ferroptosis more readily), generating tumors with an anti- ferroptosis, highly malignant phenotype. Moreover, cells that are initially hypoxic may become more oxygenated during a fractionated course of RT. Following a fraction of RT, most radiosensitive aerobic cells in a tumor will be killed and the surviving fraction will be predominantly hypoxic. If sufficient time is allowed before the next fraction of radiation, some of the tumor cells will oxygenate through the process of reoxygenation, and, if this is efficient, the presence of hypoxic cells will not significantly affect the tumor response. However, the speed of reoxygenation varies widely, from a few hours in some tumors to several days in others. As a result, the treatment window of a combination of radiotherapy and ferroptosis inducer/inhibitor holds great promise for ensuring treatment efficiency.

Targeting PUFA-PL May Lead to a New Epoch Against Malignant Disease

Developing therapeutic strategies to target lipid metabolism and ferroptosis in cancers may be of great interest for anticancer treatment. For example, erastin, a widely used ferroptosis inducer that influences the ferroptotic process by inhibiting the Xc^- Xc-system directly and decreasing the intake of cystine, is reported to decrease the radio-resistance of non-small cell lung cancer (Pan et al., 2019). Furthermore, given the increased expression of ACSL4 in tumor cells treated with IR, ACSL4 could be used as an effective biomarker to show tumor response to IR (**Figure 3**; Lei et al., 2020).

The contribution of ferroptosis inducers or inhibitors has been reported to alter the clinical efficacy of radiotherapy. Indeed, the erastin-promoting effects of radiosensitivity indicate that combining radiotherapy and ferroptosis inducers might increase tumor response (Pan et al., 2019; Shibata et al., 2019). Moreover, it has been reported that ferroptosis is associated with radiotherapy complications. The GPX4 level was decreased in radiated lungs, and liproxstatin-1 could protect lung tissue from radiation-induced lung fibrosis by activating the Nrf2 pathway and increasing GPX4 (Li X. et al., 2019). Thus, selecting candidates that are prone to radiation damage induced by ferroptosis, and combining ferroptosis inhibitors and radiotherapy to avoid injury would introduce a new therapeutic approach to enhance treatment efficacy.

Ferroptosis is also associated with several immunological processes, and immunotherapy combined with IR appears to synergistically suppress SLC7A11 and promote tumor cell ferroptosis (Lang et al., 2019). Thus, this may offer new options for further understanding and resolving issues in immunotherapy and radiotherapy.

Outstanding Issues for Future Research

Despite the rapid growth of research on ferroptosis-based cancer therapy, some challenges remain to be overcome. First, direct evidence supporting the effects of MUFA on tumor cell proliferation is insufficient, and some evidence has shown that converting pro-tumorigenesis FAs (e.g., omega-6 PUFA) into anti-tumorigenic FAs (e.g., omega-3 PUFA) inhibits tumor growth. Second, evidence has shown that the most specific signals of ferroptosis in humans remain sparse. Numerous experiments have measured 4-HNE and MDA, two final degradation products of LPO, to determine the level of ferroptosis in human tissue. In addition, Li W. et al. (2019) found that the recruitment of neutrophils to coronary vascular endothelial cells is initiated through ferroptosis in heart transplantation. However, neutrophils are not unique markers for predicting the cellular response to ferroptosis. Abnormal recruitment of neutrophils can also be induced by inflammation, cancer, treatment approaches, or certain physical conditions. Therefore, considering future clinical applications, more accurate, specific, convenient, and economic signals are required. Third, some classic pathways, such as Wnt, P53, NF-κB, mTOR, MAPK, and BMP, all of which are involved in tumor growth, have been reported to be involved in ferroptosis. However, how these signaling pathways regulate IR-regulated ferroptosis, and how FA metabolism changes following their activation, are questions for further work, the answers to which are necessary to resolve the relationship between radiation and ferroptosis. Finally, given that mitochondria are targets of radiation, whether mitochondrial functions are complemented by peroxisomes, another organelle involved in FA metabolism following IR, needs to be explored.

CONCLUSION

Emerging research has progressively increased the understanding of ferroptosis mechanisms, interpreted ionizing radiation effects on ferroptosis, and revealed the interplay among irradiation, ferroptosis, and lipid metabolism. In the future, more efforts should be focused on the crosstalk between ferroptosis and radiotherapy in terms of different metabolic states, not only from the lipid metabolic profile, but from a broader view to integrate the entire metabolic environment at a given dose and given cancer type by a series of comprehensive studies. The interactome strategy, including the novel techniques and probes in the field of chemoproteomics, will deepen our understanding of this subject.

AUTHOR CONTRIBUTIONS

Z-hY and TL wrote the original draft of the manuscript. Z-hY, TL, L-xX, and J-jW wrote, reviewed, and edited the manuscript. All authors have read and agreed to the published version of the manuscript.

FUNDING

This study was supported by the National Natural Science Foundation of China (Grant Number 82073335), National Natural Science Foundation of China (Grant Number 81972966), Beijing Natural Science Foundation (Grant Number 7202228), National Natural Science Foundation of China (Grant Number 82073057), and Clinical Medicine plus X Project of Peking University (Grant Number PKU2020LCXQ024).

ACKNOWLEDGMENTS

We thank all authors of the review for thoughtful comments and discussions.

REFERENCES

Antal, O., Hackler, L. Jr., Shen, J., Man, I., Hideghety, K., Kitajka, K., et al. (2014). Combination of unsaturated fatty acids and ionizing radiation on human glioma cells: cellular, biochemical and gene expression analysis. *Lipids Health Dis.* 13:142.

Azzam, E. I., De Toledo, S. M., Spitz, D. R., and Little, J. B. (2002). Oxidative metabolism modulates signal transduction and micronucleus formation in bystander cells from alpha-particle-irradiated normal human fibroblast cultures. *Cancer Res.* 62, 5436–5442.

Bach, D. H., Luu, T. T., Kim, D., An, Y. J., Park, S., Park, H. J., et al. (2018). BMP4 Upregulation Is Associated with Acquired Drug Resistance and Fatty Acid Metabolism in EGFR-Mutant Non-Small-Cell Lung Cancer Cells. *Mol. Ther. Nucleic Acids* 12, 817–828. doi: 10.1016/j.omtn.2018.07.016

Bai, D., Ueno, L., and Vogt, P. K. (2009). Akt-mediated regulation of NFkappaB and the essentialness of NFkappaB for the oncogenicity of PI3K and Akt. *Int. J. Cancer* 125, 2863–2870. doi: 10.1002/ijc.24748

Bai, Y., Meng, L., Han, L., Jia, Y., Zhao, Y., Gao, H., et al. (2019). Lipid storage and lipophagy regulates ferroptosis. *Biochem. Biophys. Res. Commun.* 508, 997–1003. doi: 10.1016/j.bbrc.2018.12.039

Bajaj, M. S., Kulkarni, R. S., Ghode, S. S., Limaye, L. S., and Kale, V. P. (2016). Irradiation-induced secretion of BMP4 by marrow cells causes marrow adipogenesis post-myelosuppression. *Stem Cell Res.* 17, 646–653. doi: 10.1016/j.scr.2016.11.015

Beloribi-Djefaflia, S., Vasseur, S., and Guillaumond, F. (2016). Lipid metabolic reprogramming in cancer cells. *Oncogenesis* 5:e189. doi: 10.1038/oncsis.2015.49

Benais-Pont, G., Dupertuis, Y. M., Kossovsky, M. P., Nouet, P., Allal, A. S., Buchegger, F., et al. (2006). Omega-3 polyunsaturated fatty acids and ionizing radiation: combined cytotoxicity on human colorectal adenocarcinoma cells. *Nutrition* 22, 931–939. doi: 10.1016/j.nut.2006.05.012

Benedetti, E., d'Angelo, M., Ammazzalorso, A., Gravina, G. L., Laezza, C., Antonosante, A., et al. (2017). PPARalpha Antagonist AA452 Triggers Metabolic Reprogramming and Increases Sensitivity to Radiation Therapy in Human Glioblastoma Primary Cells. *J. Cell Physiol.* 232, 1458–1466. doi: 10.1002/jcp.25648

Berkovic, D., Grundel, O., Berkovic, K., Wildfang, I., Hess, C. F., and Schmoll, H. J. (1997). Synergistic cytotoxic effects of ether phospholipid analogues and ionizing radiation in human carcinoma cells. *Radiother. Oncol.* 43, 293–301. doi: 10.1016/s0167-8140(97)01909-9

Berquin, I. M., Min, Y., Wu, R., Wu, J., Perry, D., Cline, J. M., et al. (2007). Modulation of prostate cancer genetic risk by omega-3 and omega-6 fatty acids. *J. Clin. Invest* 117, 1866–1875.

Bougnoux, P., Hajjaji, N., Maheo, K., Couet, C., and Chevalier, S. (2010). Fatty acids and breast cancer: sensitization to treatments and prevention of metastatic re-growth. *Prog. Lipid Res.* 49, 76–86. doi: 10.1016/j.plipres.2009.08.003

Bravard, A., Luccioni, C., Moustacchi, E., and Rigaud, O. (1999). Contribution of antioxidant enzymes to the adaptive response to ionizing radiation of human lymphoblasts. *Int. J. Radiat. Biol.* 75, 639–645. doi: 10.1080/095530099140285

Brigelius-Flohe, R., and Flohe, L. (2020). Regulatory Phenomena in the Glutathione Peroxidase Superfamily. *Antioxid Redox Signal* 33, 498–516. doi: 10.1089/ars.2019.7905

Bump, E. A., Yu, N. Y., and Brown, J. M. (1982). Radiosensitization of hypoxic tumor cells by depletion of intracellular glutathione. *Science* 217, 544–545. doi: 10.1126/science.7089580

Cao, A., Li, H., Zhou, Y., Wu, M., and Liu, J. (2010). Long chain acyl-CoA synthetase-3 is a molecular target for peroxisome proliferator-activated receptor delta in HepG2 hepatoma cells. *J. Biol. Chem.* 285, 16664–16674. doi: 10.1074/jbc.m110.112805

Catalina-Rodriguez, O., Kolukula, V. K., Tomita, Y., Preet, A., Palmieri, F., Wellstein, A., et al. (2012). The mitochondrial citrate transporter, CIC, is essential for mitochondrial homeostasis. *Oncotarget* 3, 1220–1235. doi: 10.18632/oncotarget.714

Chen, D., Fan, Z., Rauh, M., Buchfelder, M., Eyupoglu, I. Y., and Savaskan, N. (2017). ATF4 promotes angiogenesis and neuronal cell death and confers ferroptosis in a xCT-dependent manner. *Oncogene* 36, 5593–5608. doi: 10.1038/onc.2017.146

Chen, J., Zhang, F., Ren, X., Wang, Y., Huang, W., Zhang, J., et al. (2020). Targeting fatty acid synthase sensitizes human nasopharyngeal carcinoma cells to radiation via downregulating frizzled class receptor 10. *Cancer Biol. Med.* 17, 740–752. doi: 10.20892/j.issn.2095-3941.2020.0219

Chen, X., Shang, L., Deng, S., Li, P., Chen, K., Gao, T., et al. (2020). Peroxisomal oxidation of erucic acid suppresses mitochondrial fatty acid oxidation by stimulating malonyl-CoA formation in the rat liver. *J. Biol. Chem.* 295, 10168–10179. doi: 10.1074/jbc.ra120.013583

Chen, Y., Li, N., Wang, J., Zhang, X., Pan, W., Yu, L., et al. (2019). Enhancement of mitochondrial ROS accumulation and radiotherapeutic efficacy using a Gd-doped titania nanosensitizer. *Theranostics* 9, 167–178. doi: 10.7150/thno.28033

Chu, B., Kon, N., Chen, D., Li, T., Liu, T., Jiang, L., et al. (2019). ALOX12 is required for p53-mediated tumour suppression through a distinct ferroptosis pathway. *Nat. Cell Biol.* 21, 579–591. doi: 10.1038/s41556-019-0305-6

Chuang, H. Y., Lee, Y. P., Lin, W. C., Lin, Y. H., and Hwang, J. J. (2019). Fatty Acid Inhibition Sensitizes Androgen-Dependent and -Independent Prostate Cancer to Radiotherapy via FASN/NF-kappaB Pathway. *Sci. Rep.* 9:13284.

Ciamporcero, E., Shen, H., Ramakrishnan, S., Ku, S., Chintala, S., Shen, L., et al. (2016). YAP activation protects urothelial cell carcinoma from treatment-induced DNA damage. *Oncogene* 35, 1541–1553. doi: 10.1038/onc.2015.219

de Toledo, S. M., Asaad, N., Venkatachalam, P., Li, L., Howell, R. W., Spitz, D. R., et al. (2006). Adaptive responses to low-dose/low-dose-rate gamma rays in normal human fibroblasts: the role of growth architecture and oxidative metabolism. *Radiat Res.* 166, 849–857. doi: 10.1667/rr0640.1

Dethmers, J. K., and Meister, A. (1981). Glutathione export by human lymphoid cells: depletion of glutathione by inhibition of its synthesis decreases export and increases sensitivity to irradiation. *Proc. Natl. Acad. Sci. U S A* 78, 7492–7496. doi: 10.1073/pnas.78.12.7492

Dixon, S. J., Lemberg, K. M., Lamprecht, M. R., Skouta, R., Zaitsev, E. M., Gleason, C. E., et al. (2012). Ferroptosis: an iron-dependent form of nonapoptotic cell death. *Cell* 149, 1060–1072. doi: 10.1016/j.cell.2012.03.042

Dolcet, X., Llobet, D., Pallares, J., and Matias-Guiu, X. (2005). NF-kB in development and progression of human cancer. *Virchows Arch.* 446, 475–482. doi: 10.1007/s00428-005-1264-9

Doll, S., Proneth, B., Tyurina, Y. Y., Panzilius, E., Kobayashi, S., Ingold, I., et al. (2017). ACSL4 dictates ferroptosis sensitivity by shaping cellular lipid composition. *Nat. Chem. Biol.* 13, 91–98. doi: 10.1038/nchembio.2239

Elsaid, M. Y., Shahi, A., Wang, A. R., Baiu, D. C., Li, C., Werner, L. R., et al. (2018). Enhanced Radiosensitivity in Solid Tumors using a Tumor-selective Alkyl Phospholipid Ether Analog. *Mol. Cancer Ther.* 17, 2320–2328. doi: 10.1158/1535-7163.mct-17-0897

Estrela, J. M., Obrador, E., Navarro, J., Lasso De la Vega, M. C., and Pellicer, J. A. (1995). Elimination of Ehrlich tumours by ATP-induced growth inhibition, glutathione depletion and X-rays. *Nat. Med.* 1, 84–88. doi: 10.1038/nm0195-84

Fernandez, L. A., Squatrito, M., Northcott, P., Awan, A., Holland, E. C., Taylor, M. D., et al. (2012). Oncogenic YAP promotes radioresistance and

genomic instability in medulloblastoma through IGF2-mediated Akt activation. *Oncogene* 31, 1923–1937. doi: 10.1038/onc.2011.379

Friedmann Angeli, J. P., Krysko, D. V., and Conrad, M. (2019). Ferroptosis at the crossroads of cancer-acquired drug resistance and immune evasion. *Nat. Rev. Cancer* 19, 405–414. doi: 10.1038/s41568-019-0149-1

Gao, M., Yi, J., Zhu, J., Minikes, A. M., Monian, P., Thompson, C. B., et al. (2019). Role of Mitochondria in Ferroptosis. *Mol. Cell* 73:e353.

Gao, S., Wu, R., and Zeng, Y. (2012). Up-regulation of peroxisome proliferator-activated receptor gamma in radiation-induced heart injury in rats. *Radiat. Environ. Biophys.* 51, 53–59. doi: 10.1007/s00411-011-0390-9

Gaschler, M. M., Hu, F., Feng, H., Linkermann, A., Min, W., and Stockwell, B. R. (2018). Determination of the Subcellular Localization and Mechanism of Action of Ferrostatins in Suppressing Ferroptosis. *ACS Chem. Biol.* 13, 1013–1020. doi: 10.1021/acschembio.8b00199

Gomez, C. M., and de Molina, A. R. (2016). Microtargeting cancer metabolism: opening new therapeutic windows based on lipid metabolism. *J. Lipid Res.* 57, 193–206. doi: 10.1194/jlr.r061812

Gonnissen, A., Isebaert, S., McKee, C. M., Muschel, R. J., and Haustermans, K. (2017). The Effect of Metformin and GANT61 Combinations on the Radiosensitivity of Prostate Cancer Cells. *Int. J. Mol. Sci.* 2017:18.

Gopal, U., Mowery, Y., Young, K., and Pizzo, S. V. (2019). Targeting cell surface GRP78 enhances pancreatic cancer radiosensitivity through YAP/TAZ protein signaling. *J. Biol. Chem.* 294, 13939–13952. doi: 10.1074/jbc.ra119.009091

Gottgens, E. L., van den Heuvel, C. N., de Jong, M. C., Kaanders, J. H., Leenders, W. P., Ansems, M., et al. (2019). ACLY (ATP Citrate Lyase) Mediates Radioresistance in Head and Neck Squamous Cell Carcinomas and is a Novel Predictive Radiotherapy Biomarker. *Cancers* 11:1971. doi: 10.3390/cancers11121971

Igal, R. A. (2016). Stearoyl CoA desaturase-1: New insights into a central regulator of cancer metabolism. *Biochim. Biophys. Acta* 1861, 1865–1880. doi: 10.1016/j.bbalip.2016.09.009

Ito, F., Yanatori, I., Maeda, Y., Nimura, K., Ito, S., Hirayama, T., et al. (2020). Asbestos conceives Fe(II)-dependent mutagenic stromal milieu through ceaseless macrophage ferroptosis and beta-catenin induction in mesothelium. *Redox Biol.* 36:101616. doi: 10.1016/j.redox.2020.101616

Jiang, L., Kon, N., Li, T., Wang, S. J., Su, T., Hibshoosh, H., et al. (2015). Ferroptosis as a p53-mediated activity during tumour suppression. *Nature* 520, 57–62. doi: 10.1038/nature14344

Kagan, V. E., Mao, G., Qu, F., Angeli, J. P., Doll, S., Croix, C. S., et al. (2017). Oxidized arachidonic and adrenic PEs navigate cells to ferroptosis. *Nat. Chem. Biol.* 13, 81–90. doi: 10.1038/nchembio.2238

Kan, C. F., Singh, A. B., Dong, B., Shende, V. R., and Liu, J. (2015). PPARdelta activation induces hepatic long-chain acyl-CoA synthetase 4 expression in vivo and in vitro. *Biochim. Biophys. Acta* 1851, 577–587. doi: 10.1016/j.bbalip.2015.01.008

Kaur, S., Nag, A., Gangenahalli, G., and Sharma, K. (2019). Peroxisome Proliferator Activated Receptor Gamma Sensitizes Non-small Cell Lung Carcinoma to Gamma Irradiation Induced Apoptosis. *Front. Genet.* 10:554.

Kim, E. J., Lee, Y. J., Kang, S., and Lim, Y. B. (2014). Ionizing radiation activates PERK/eIF2alpha/ATF4 signaling via ER stress-independent pathway in human vascular endothelial cells. *Int. J. Radiat. Biol.* 90, 306–312. doi: 10.3109/09553002.2014.886793

Kim, G. J., Chandrasekaran, K., and Morgan, W. F. (2006). Mitochondrial dysfunction, persistently elevated levels of reactive oxygen species and radiation-induced genomic instability: a review. *Mutagenesis* 21, 361–367. doi: 10.1093/mutage/gel048

Kim, S., Choe, J. H., Lee, G. J., Kim, Y. S., Kim, S. Y., Lee, H. M., et al. (2017). Ionizing Radiation Induces Innate Immune Responses in Macrophages by Generation of Mitochondrial Reactive Oxygen Species. *Radiat. Res.* 187, 32–41. doi: 10.1667/rr14346.1

Kim, T. W., Hong, D. W., Park, J. W., and Hong, S. H. (2020). CB11, a novel purine-based PPAR ligand, overcomes radio-resistance by regulating ATM signalling and EMT in human non-small-cell lung cancer cells. *Br. J. Cancer* 123, 1737–1748. doi: 10.1038/s41416-020-01088-w

Klemm, R. W., and Ikonen, E. (2020). The cell biology of lipid droplets: More than just a phase. *Semin. Cell Dev. Biol.* 108, 1–3. doi: 10.1016/j.semcdb.2020.06.016

Klepko, A. V., Motrina, O. A., Bulavytska, V. M., Kondratova, Y. A., Vatlitsova, O. S., Chernyshov, A. V., et al. (2014). Analysis of the antioxidantive qualities of sperm after total body X-irradiation of animals. *Probl. Radiac. Med. Radiobiol.* 19, 407–418.

Kojima, S., Ishida, H., Takahashi, M., and Yamaoka, K. (2002). Elevation of glutathione induced by low-dose gamma rays and its involvement in increased natural killer activity. *Radiat. Res.* 157, 275–280. doi: 10.1667/0033-7587(2002)157[0275:eogibl]2.0.co;2

Komarova, E. A., Chernov, M. V., Franks, R., Wang, K., Armin, G., Zelnick, C. R., et al. (1997). Transgenic mice with p53-responsive lacZ: p53 activity varies dramatically during normal development and determines radiation and drug sensitivity in vivo. *EMBO J.* 16, 1391–1400. doi: 10.1093/emboj/16.6.1391

Kondagunta, G. V., Drucker, B., Schwartz, L., Bacik, J., Marion, S., Russo, P., et al. (2004). Phase II trial of bortezomib for patients with advanced renal cell carcinoma. *J. Clin. Oncol.* 22, 3720–3725. doi: 10.1200/jco.2004.10.155

Koritzinsky, M. (2015). Metformin: A Novel Biological Modifier of Tumor Response to Radiation Therapy. *Int. J. Radiat. Oncol. Biol. Phys.* 93, 454–464. doi: 10.1016/j.ijrobp.2015.06.003

Kumar, M., Sharma, M. K., Saxena, P. S., and Kumar, A. (2003). Radioprotective effect of Panax ginseng on the phosphatases and lipid peroxidation level in testes of Swiss albino mice. *Biol. Pharm. Bull.* 26, 308–312. doi: 10.1248/bpb.26.308

Lang, X., Green, M. D., Wang, W., Yu, J., Choi, J. E., Jiang, L., et al. (2019). Radiotherapy and Immunotherapy Promote Tumoral Lipid Oxidation and Ferroptosis via Synergistic Repression of SLC7A11. *Cancer Discov.* 9, 1673–1685. doi: 10.1158/2159-8290.cd-19-0338

Lei, G., Zhang, Y., Koppula, P., Liu, X., Zhang, J., Lin, S. H., et al. (2020). The role of ferroptosis in ionizing radiation-induced cell death and tumor suppression. *Cell Res.* 30, 146–162. doi: 10.1038/s41422-019-0263-3

Li, C., Deng, X., Zhang, W., Xie, X., Conrad, M., Liu, Y., et al. (2019). Novel Allosteric Activators for Ferroptosis Regulator Glutathione Peroxidase 4. *J. Med. Chem.* 62, 266–275. doi: 10.1021/acs.jmedchem.8b00315

Li, L., Sun, S., Tan, L., Wang, Y., Wang, L., Zhang, Z., et al. (2019). Polystyrene Nanoparticles Reduced ROS and Inhibited Ferroptosis by Triggering Lysosome Stress and TFEB Nucleus Translocation in a Size-Dependent Manner. *Nano Lett.* 19, 7781–7792. doi: 10.1021/acs.nanolett.9b02795

Li, W., Feng, G., Gauthier, J. M., Lokshina, I., Higashikubo, R., Evans, S., et al. (2019). Ferroptotic cell death and TLR4/Trif signaling initiate neutrophil recruitment after heart transplantation. *J. Clin. Invest.* 129, 2293–2304. doi: 10.1172/jci126428

Li, X., Duan, L., Yuan, S., Zhuang, X., Qiao, T., and He, J. (2019). Ferroptosis inhibitor alleviates Radiation-induced lung fibrosis (RILF) via down-regulation of TGF-beta1. *J. Inflamm.* 16:11.

Li, Z., and Zhang, H. (2016). Reprogramming of glucose, fatty acid and amino acid metabolism for cancer progression. *Cell Mol. Life Sci.* 73, 377–392. doi: 10.1007/s00018-015-2070-4

Lim, J. K. M., Delaidelli, A., Minaker, S. W., Zhang, H. F., Colovic, M., Yang, H., et al. (2019). Cystine/glutamate antiporter xCT (SLC7A11) facilitates oncogenic RAS transformation by preserving intracellular redox balance. *Proc. Natl. Acad. Sci. U S A* 116, 9433–9442. doi: 10.1073/pnas.1821323116

Lin, M. H., Yen, J. H., Weng, C. Y., Wang, L., Ha, C. L., and Wu, M. J. (2014). Lipid peroxidation end product 4-hydroxy-trans-2-nonenal triggers unfolded protein response and heme oxygenase-1 expression in PC12 cells: Roles of ROS and MAPK pathways. *Toxicology* 315, 24–37. doi: 10.1016/j.tox.2013.11.007

Linard, C., Gremy, O., and Benderitter, M. (2008). Reduction of peroxisome proliferation-activated receptor gamma expression by gamma-irradiation as a mechanism contributing to inflammatory response in rat colon: modulation by the 5-aminosalicylic acid agonist. *J. Pharmacol. Exp. Ther.* 324, 911–920. doi: 10.1124/jpet.107.129122

Liu, X., Kumar, M., Yang, L., Molkentine, D. P., Valdecanas, D., Yu, S., et al. (2018). BAP1 Is a Novel Target in HPV-Negative Head and Neck Cancer. *Clin. Cancer Res.* 24, 600–607. doi: 10.1158/1078-0432.ccr-17-1573

Lodhi, I. J., and Semenkovich, C. F. (2014). Peroxisomes: a nexus for lipid metabolism and cellular signaling. *Cell Metab.* 19, 380–392. doi: 10.1016/j.cmet.2014.01.002

Lodhi, I. J., Wei, X., Yin, L., Feng, C., Adak, S., Abou-Ezzi, G., et al. (2015). Peroxisomal lipid synthesis regulates inflammation by sustaining neutrophil membrane phospholipid composition and viability. *Cell Metab.* 21, 51–64. doi: 10.1016/j.cmet.2014.12.002

Luppi, P., Drain, N., To, R., Stolz, D., Wallace, C., Watkins, S., et al. (2020). Autocrine C-peptide protects INS1 beta cells against palmitic acid-induced

oxidative stress in peroxisomes by inducing catalase. *Endocrinol. Diabetes Metab.* 3:e00147.

Ma, Y., Temkin, S. M., Hawkridge, A. M., Guo, C., Wang, W., Wang, X. Y., et al. (2018). Fatty acid oxidation: An emerging facet of metabolic transformation in cancer. *Cancer Lett.* 435, 92–100. doi: 10.1016/j.canlet.2018.08.006

Magtanong, L., Ko, P. J., To, M., Cao, J. Y., Forcina, G. C., Tarangelo, A., et al. (2019). Exogenous Monounsaturated Fatty Acids Promote a Ferroptosis-Resistant Cell State. *Cell Chem. Biol.* 26, 420–432e429.

Mangoni, M., Sottili, M., Gerini, C., Desideri, I., Bastida, C., Pallotta, S., et al. (2017). gamma agonist protects from radiation-induced intestinal toxicity. *U Eur. Gastroenterol. J.* 5, 218–226. doi: 10.1177/2050640616640443

Mao, X. W., Nishiyama, N. C., Pecaut, M. J., Campbell-Beachler, M., Gifford, P., Haynes, K. E., et al. (2016). Simulated Microgravity and Low-Dose/Low-Dose-Rate Radiation Induces Oxidative Damage in the Mouse Brain. *Radiat. Res.* 185, 647–657. doi: 10.1667/rr14267.1

Martin, S., and Parton, R. G. (2006). Lipid droplets: a unified view of a dynamic organelle. *Nat. Rev. Mol. Cell Biol.* 7, 373–378. doi: 10.1038/nrm1912

Martius, G., Alwahsh, S. M., Rave-Frank, M., Hess, C. F., Christiansen, H., Ramadori, G., et al. (2014). Hepatic fat accumulation and regulation of FAT/CD36: an effect of hepatic irradiation. *Int. J. Clin. Exp. Pathol.* 7, 5379–5392.

Martius, G., Cameron, S., Rave-Frank, M., Hess, C. F., Wolff, H. A., and Malik, I. A. (2015). The anti-TNF-alpha antibody infliximab inhibits the expression of fat-transporter-protein FAT/CD36 in a selective hepatic-radiation mouse model. *Int. J. Mol. Sci.* 16, 4682–4697. doi: 10.3390/ijms16034682

McDonald, J. T., Kim, K., Norris, A. J., Vlashi, E., Phillips, T. M., Lagadec, C., et al. (2010). Ionizing radiation activates the Nrf2 antioxidant response. *Cancer Res.* 70, 8886–8895. doi: 10.1158/0008-5472.can-10-0171

Meister, A., and Anderson, M. E. (1983). Glutathione. *Annu Rev. Biochem.* 52, 711–760.

Menendez, J. A., and Lupu, R. (2007). Fatty acid synthase and the lipogenic phenotype in cancer pathogenesis. *Nat. Rev. Cancer* 7, 763–777. doi: 10.1038/nrc2222

Narayanan, A., Baskaran, S. A., Amalaradjou, M. A., and Venkitanarayanan, K. (2015). Anticarcinogenic properties of medium chain fatty acids on human colorectal, skin and breast cancer cells in vitro. *Int. J. Mol. Sci.* 16, 5014–5027. doi: 10.3390/ijms16035014

Narayanan, P. K., Goodwin, E. H., and Lehnert, B. E. (1997). Alpha particles initiate biological production of superoxide anions and hydrogen peroxide in human cells. *Cancer Res.* 57, 3963–3971.

Narayanan, P. K., LaRue, K. E., Goodwin, E. H., and Lehnert, B. E. (1999). Alpha particles induce the production of interleukin-8 by human cells. *Radiat Res.* 152, 57–63. doi: 10.2307/3580049

Ookhtens, M., Kannan, R., Lyon, I., and Baker, N. (1984). Liver and adipose tissue contributions to newly formed fatty acids in an ascites tumor. *Am. J. Physiol.* 247, R146–R153.

Pan, X., Lin, Z., Jiang, D., Yu, Y., Yang, D., Zhou, H., et al. (2019). Erastin decreases radioresistance of NSCLC cells partially by inducing GPX4-mediated ferroptosis. *Oncol. Lett.* 17, 3001–3008.

Panigrahy, D., Edin, M. L., Lee, C. R., Huang, S., Bielenberg, D. R., Butterfield, C. E., et al. (2012). Epoxyeicosanoids stimulate multiorgan metastasis and tumor dormancy escape in mice. *J. Clin. Invest.* 122, 178–191. doi: 10.1172/jci58128

Poli, G., Schaur, R. J., Siems, W. G., and Leonarduzzi, G. (2008). 4-hydroxynonenal: a membrane lipid oxidation product of medicinal interest. *Med. Res. Rev.* 28, 569–631. doi: 10.1002/med.20117

Pozzi, A., Popescu, V., Yang, S., Mei, S., Shi, M., Puolitaival, S. M., et al. (2010). The anti-tumorigenic properties of peroxisomal proliferator-activated receptor alpha are arachidonic acid epoxygenase-mediated. *J. Biol. Chem.* 285, 12840–12850. doi: 10.1074/jbc.m109.081554

Qiu, B., Ackerman, D., Sanchez, D. J., Li, B., Ochocki, J. D., Grazioli, A., et al. (2015). HIF2alpha-Dependent Lipid Storage Promotes Endoplasmic Reticulum Homeostasis in Clear-Cell Renal Cell Carcinoma. *Cancer Discov.* 5, 652–667. doi: 10.1158/2159-8290.cd-14-1507

Richards, G. A., White, H., Grimmer, H., Ramoroka, C., Channa, K., Hopley, M., et al. (2009). Increased oxidants and reduced antioxidants in irradiated parenteral nutrition solutions may contribute to the inflammatory response. *J. Intensive Care Med.* 24, 252–260. doi: 10.1177/0885066609332744

Rogel, A., Popliker, M., Webb, C. G., and Oren, M. (1985). p53 cellular tumor antigen: analysis of mRNA levels in normal adult tissues, embryos, and tumors. *Mol. Cell Biol.* 5, 2851–2855. doi: 10.1128/mcb.5.10.2851-2855.1985

Saenko, Y., Cieslar-Pobuda, A., Skonieczna, M., and Rzeszowska-Wolny, J. (2013). Changes of reactive oxygen and nitrogen species and mitochondrial functioning in human K562 and HL60 cells exposed to ionizing radiation. *Radiat. Res.* 180, 360–366. doi: 10.1667/rr3247.1

Schley, P. D., Jijon, H. B., Robinson, L. E., and Field, C. J. (2005). Mechanisms of omega-3 fatty acid-induced growth inhibition in MDA-MB-231 human breast cancer cells. *Breast Cancer Res. Treat* 92, 187–195. doi: 10.1007/s10549-005-2415-z

Shaikh, S., Channa, N. A., Talpur, F. N., Younis, M., and Tabassum, N. (2017). Radiotherapy improves serum fatty acids and lipid profile in breast cancer. *Lipids Health Dis.* 16:92.

Shi, H. B., Luo, J., Yao, D. W., Zhu, J. J., Xu, H. F., Shi, H. P., et al. (2013). Peroxisome proliferator-activated receptor-gamma stimulates the synthesis of monounsaturated fatty acids in dairy goat mammary epithelial cells via the control of stearoyl-coenzyme A desaturase. *J. Dairy Sci.* 96, 7844–7853. doi: 10.3168/jds.2013-7105

Shibata, Y., Yasui, H., Higashikawa, K., Miyamoto, N., and Kuge, Y. (2019). Erastin, a ferroptosis-inducing agent, sensitized cancer cells to X-ray irradiation via glutathione starvation in vitro and in vivo. *PLoS One* 14:e0225931. doi: 10.1371/journal.pone.0225931

Singh, R., and Cuervo, A. M. (2012). Lipophagy: connecting autophagy and lipid metabolism. *Int. J. Cell Biol.* 2012:282041.

Stark, G. (1991). The effect of ionizing radiation on lipid membranes. *Biochim. Biophys. Acta* 1071, 103–122. doi: 10.1016/0304-4157(91)90020-w

Strand, E., Lysne, V., Grinna, M. L., Bohov, P., Svardal, A., Nygard, O., et al. (2019). Short-Term Activation of Peroxisome Proliferator-Activated Receptors alpha and gamma Induces Tissue-Specific Effects on Lipid Metabolism and Fatty Acid Composition in Male Wistar Rats. *PPAR Res.* 2019:8047627.

Swinnen, J. V., Van Veldhoven, P. P., Timmermans, L., De Schrijver, E., Brusselmans, K., Vanderhoydonc, F., et al. (2003). Fatty acid synthase drives the synthesis of phospholipids partitioning into detergent-resistant membrane microdomains. *Biochem. Biophys. Res. Commun.* 302, 898–903. doi: 10.1016/s0006-291x(03)00265-1

Tan, Z., Xiao, L., Tang, M., Bai, F., Li, J., Li, L., et al. (2018). Targeting CPT1A-mediated fatty acid oxidation sensitizes nasopharyngeal carcinoma to radiation therapy. *Theranostics* 8, 2329–2347. doi: 10.7150/thno.21451

Tesfay, L., Paul, B. T., Konstorum, A., Deng, Z., Cox, A. O., Lee, J., et al. (2019). Stearoyl-CoA Desaturase 1 Protects Ovarian Cancer Cells from Ferroptotic Cell Death. *Cancer Res.* 79, 5355–5366. doi: 10.1158/0008-5472.can-19-0369

Thiele, C., and Spandl, J. (2008). Cell biology of lipid droplets. *Curr. Opin. Cell Biol.* 20, 378–385.

Toborek, M., Lee, Y. W., Garrido, R., Kaiser, S., and Hennig, B. (2002). Unsaturated fatty acids selectively induce an inflammatory environment in human endothelial cells. *Am. J. Clin. Nutr.* 75, 119–125. doi: 10.1093/ajcn/75.1.119

Ubellacker, J. M., Tasdogan, A., Ramesh, V., Shen, B., Mitchell, E. C., Martin-Sandoval, M. S., et al. (2020). Lymph protects metastasizing melanoma cells from ferroptosis. *Nature* 585, 113–118. doi: 10.1038/s41586-020-2623-z

Unger, R. H. (2002). Lipotoxic diseases. *Annu. Rev. Med.* 53, 319–336. doi: 10.1146/annurev.med.53.082901.104057

Venkatesh, D., O'Brien, N. A., Zandkarimi, F., Tong, D. R., Stokes, M. E., Dunn, D. E., et al. (2020). MDM2 and MDMX promote ferroptosis by PPARalpha-mediated lipid remodeling. *Genes Dev.* 34, 526–543. doi: 10.1101/gad.334219.119

Wang, H., Klein, M. G., Zou, H., Lane, W., Snell, G., Levin, I., et al. (2015). Crystal structure of human stearoyl-coenzyme A desaturase in complex with substrate. *Nat. Struct. Mol. Biol.* 22, 581–585. doi: 10.1038/nsmb.3049

Wang, H., Liu, C., Zhao, Y., and Gao, G. (2020). Mitochondria regulation in ferroptosis. *Eur. J. Cell Biol.* 99:151058. doi: 10.1016/j.ejcb.2019.151058

Wang, Y., Hinz, S., Uckermann, O., Honscheid, P., von Schonfels, W., Burmeister, G., et al. (2020). Shotgun lipidomics-based characterization of the landscape of lipid metabolism in colorectal cancer. *Biochim. Biophys. Acta Mol. Cell Biol. Lipids* 1865:158579. doi: 10.1016/j.bbalip.2019.158579

Wen, J., Xiong, K., Aili, A., Wang, H., Zhu, Y., Yu, Z., et al. (2020). PEX5, a novel target of microRNA-31-5p, increases radioresistance in

hepatocellular carcinoma by activating Wnt/beta-catenin signaling and homologous recombination. *Theranostics* 10, 5322–5340. doi: 10.7150/thno.42371

Wu, J. T., and Kral, J. G. (2005). The NF-kappaB/IkappaB signaling system: a molecular target in breast cancer therapy. *J. Surg. Res.* 123, 158–169. doi: 10.1016/j.jss.2004.06.006

Wu, J., Minikes, A. M., Gao, M., Bian, H., Li, Y., Stockwell, B. R., et al. (2019). Intercellular interaction dictates cancer cell ferroptosis via NF2-YAP signalling. *Nature* 572, 402–406. doi: 10.1038/s41586-019-1426-6

Xi, G., Best, B., Mania-Farnell, B., James, C. D., and Tomita, T. (2017). Therapeutic Potential for Bone Morphogenetic Protein 4 in Human Malignant Glioma. *Neoplasia* 19, 261–270. doi: 10.1016/j.neo.2017.01.006

Xie, Y., Hou, W., Song, X., Yu, Y., Huang, J., Sun, X., et al. (2016). Ferroptosis: process and function. *Cell Death Differ* 23, 369–379. doi: 10.1038/cdd.2015.158

Xu, Z., Zhang, Y., Ding, J., Hu, W., Tan, C., Wang, M., et al. (2018). miR-17-3p Downregulates Mitochondrial Antioxidant Enzymes and Enhances the Radiosensitivity of Prostate Cancer Cells. *Mol. Ther Nucleic Acids* 13, 64–77. doi: 10.1016/j.omtn.2018.08.009

Xue, J., Zhu, W., Song, J., Jiao, Y., Luo, J., Yu, C., et al. (2018). Activation of PPARalpha by clofibrate sensitizes pancreatic cancer cells to radiation through the Wnt/beta-catenin pathway. *Oncogene* 37, 953–962. doi: 10.1038/onc.2017.401

Yang, L., Zhang, H., Zhou, Z. G., Yan, H., Adell, G., and Sun, X. F. (2011). Biological function and prognostic significance of peroxisome proliferator-activated receptor delta in rectal cancer. *Clin. Cancer Res.* 17, 3760–3770. doi: 10.1158/1078-0432.ccr-10-2779

Yang, P., Chen, S., Zhong, G., Kong, W., and Wang, Y. (2019). Agonist of PPAR-gamma Reduced Epithelial-Mesenchymal Transition in Eosinophilic Chronic Rhinosinusitis with Nasal Polyps via Inhibition of High Mobility Group Box1. *Int. J. Med. Sci.* 16, 1631–1641. doi: 10.7150/ijms.35936

Yang, W. H., and Chi, J. T. (2020). Hippo pathway effectors YAP/TAZ as novel determinants of ferroptosis. *Mol. Cell Oncol.* 7:1699375. doi: 10.1080/23723556.2019.1699375

Yang, W. S., and Stockwell, B. R. (2016). Ferroptosis: Death by Lipid Peroxidation. *Trends Cell Biol.* 26, 165–176. doi: 10.1016/j.tcb.2015.10.014

Yang, W. S., SriRamaratnam, R., Welsch, M. E., Shimada, K., Skouta, R., Viswanathan, V. S., et al. (2014). Regulation of ferroptotic cancer cell death by GPX4. *Cell* 156, 317–331. doi: 10.1016/j.cell.2013.12.010

Ye, L. F., Chaudhary, K. R., Zandkarimi, F., Harken, A. D., Kinslow, C. J., Upadhyayula, P. S., et al. (2020). Radiation-Induced Lipid Peroxidation Triggers Ferroptosis and Synergizes with Ferroptosis Inducers. *ACS Chem. Biol.* 15, 469–484. doi: 10.1021/acschembio.9b00939

Yu, H., Guo, P., Xie, X., Wang, Y., and Chen, G. (2017). Ferroptosis, a new form of cell death, and its relationships with tumourous diseases. *J. Cell Mol. Med.* 21, 648–657. doi: 10.1111/jcmm.13008

Zammit, V. A., Corstorphine, C. G., and Kolodziej, M. P. (1989). Target size analysis by radiation inactivation of carnitine palmitoyltransferase activity and malonyl-CoA binding in outer membranes from rat liver mitochondria. *Biochem. J.* 263, 89–95. doi: 10.1042/bj2630089

Zhang, Y., Shi, J., Liu, X., Feng, L., Gong, Z., Koppula, P., et al. (2018). BAP1 links metabolic regulation of ferroptosis to tumour suppression. *Nat. Cell Biol.* 20, 1181–1192. doi: 10.1038/s41556-018-0178-0

Zhao, W., Iskandar, S., Kooshki, M., Sharpe, J. G., Payne, V., and Robbins, M. E. (2007). Knocking out peroxisome proliferator-activated receptor (PPAR) alpha inhibits radiation-induced apoptosis in the mouse kidney through activation of NF-kappaB and increased expression of IAPs. *Radiat. Res.* 167, 581–591. doi: 10.1667/rr0814.1

Zhong, H., and Yin, H. (2015). Role of lipid peroxidation derived 4-hydroxynonenal (4-HNE) in cancer: focusing on mitochondria. *Redox Biol.* 4, 193–199. doi: 10.1016/j.redox.2014.12.011

Zhong, W., Weiss, H. L., Jayswal, R. D., Hensley, P. J., Downes, L. M., St Clair, D. K., et al. (2018). Extracellular redox state shift: A novel approach to target prostate cancer invasion. *Free Radic Biol. Med.* 117, 99–109. doi: 10.1016/j.freeradbiomed.2018.01.023

Zhu, J., Berisa, M., Schworer, S., Qin, W., Cross, J. R., and Thompson, C. B. (2019). Transsulfuration Activity Can Support Cell Growth upon Extracellular Cysteine Limitation. *Cell Metab.* 30:e865.

Zou, Y., Henry, W. S., Ricq, E. L., Graham, E. T., Phadnis, V. V., Maretich, P., et al. (2020). Plasticity of ether lipids promotes ferroptosis susceptibility and evasion. *Nature* 585, 603–608. doi: 10.1038/s41586-020-2732-8

Conflict of Interest: The authors declare that the research was conducted in the absence of any commercial or financial relationships that could be construed as a potential conflict of interest.

frontiers in Cell and Developmental Biology

ORIGINAL RESEARCH
published: 09 November 2020
doi: 10.3389/fcell.2020.529544

Vi4-miR-185-5p-Igfbp3 Network Protects the Brain From Neonatal Hypoxic Ischemic Injury via Promoting Neuron Survival and Suppressing the Cell Apoptosis

Liu-Lin Xiong[1,2,3†], Lu-Lu Xue[1,4†], Ruo-Lan Du[1], Hao-Li Zhou[1], Ya-Xin Tan[4,5], Zheng Ma[4], Yuan Jin[4], Zi-Bin Zhang[1], Yang Xu[1], Qiao Hu[1], Larisa Bobrovskaya[3], Xin-Fu Zhou[3], Jia Liu[4*] and Ting-Hua Wang[1,4*]*

[1] Institute of Neurological Disease, Translational Neuroscience Center, West China Hospital, Sichuan University, Chengdu, China, [2] Department of Anesthesiology, The Affiliated Hospital of Zunyi Medical University, Zunyi, China, [3] School of Pharmacy and Medical Sciences, Division of Health Sciences, University of South Australia, Adelaide, South Australia, [4] Animal Zoology Department, Institute of Neuroscience, Kunming Medical University, Kunming, China, [5] Shijiazhuang Maternity and Child Healthcare Hospital, Shijiazhuang, China

Neonatal hypoxic ischemic encephalopathy (HIE) due to birth asphyxia is common and causes severe neurological deficits, without any effective therapies currently available. Neuronal death is an important driving factors of neurological disorders after HIE, but the regulatory mechanisms are still uncertain. Long non-coding RNA (lncRNA) or ceRNA network act as a significant regulator in neuroregeneration and neuronal apoptosis, thus owning a great potential as therapeutic targets in HIE. Here, we found a new lncRNA, is the most functional in targeting the Igfbp3 gene in HIE, which enriched in the cell growth and cell apoptosis processes. In addition, luciferase reporter assay showed competitive regulatory binding sites to the target gene Igfbp3 between TCONS00044054 (Vi4) and miR-185-5p. The change in blood miR-185-5p and Igfbp3 expression is further confirmed in patients with brain ischemia. Moreover, Vi4 overexpression and miR-185-5p knock-out promote the neuron survival and neurite growth, and suppress the cell apoptosis, then further improve the motor and cognitive deficits in rats with HIE, while Igfbp3 interfering got the opposite results. Together, Vi4-miR-185-5p-Igfbp3 regulatory network plays an important role in neuron survival and cell apoptosis and further promote the neuro-functional recovery from HIE, therefore is a likely a drug target for HIE therapy.

Keywords: IGFBP3, Vi4, cell apoptosis, hypoxic ischemic encephalopathy, miRNA-185-5p, neuron survival

OPEN ACCESS

Edited by:
Nu Zhang,
The University of Texas Health Science Center at San Antonio, United States

Reviewed by:
Zhiping Wang,
Zhejiang University, China
Yansheng Feng,
The University of Texas Health Science Center at San Antonio, United States

***Correspondence:**
Ting-Hua Wang
Wangth_email@163.com
Jia Liu
liujiaaixuexi@126.com
Liu-Lin Xiong
499465010@qq.com

† These authors have contributed equally to this work

Specialty section:
This article was submitted to Cell Death and Survival, a section of the journal Frontiers in Cell and Developmental Biology

Received: *25 January 2020*
Accepted: *14 September 2020*
Published: *09 November 2020*

Citation:
Xiong L-L, Xue L-L, Du R-L, Zhou H-L, Tan Y-X, Ma Z, Jin Y, Zhang Z-B, Xu Y, Hu Q, Bobrovskaya L, Zhou X-F, Liu J and Wang T-H (2020) Vi4-miR-185-5p-Igfbp3 Network Protects the Brain From Neonatal Hypoxic Ischemic Injury via Promoting Neuron Survival and Suppressing the Cell Apoptosis. Front. Cell Dev. Biol. 8:529544. doi: 10.3389/fcell.2020.529544

INTRODUCTION

Hypoxic ischemic encephalopathy (HIE) is an important cause of death and disability in neonates and typically results in serious long-term sequelae including behavioral and cognitive dysfunction, learning difficulties, cerebral palsy and epilepsy (Busl and Greer, 2010; Shankaran et al., 2012; Yang and Kuan, 2015). For the pathological changes, cerebral hypoxia-ischemia (HI) causes the continued injury cascade including cytotoxicity, oxidative stress and mitochondrial disorders, which subsequently lead to neuronal injury and obvious cell death (Brekke et al., 2017). Although the survival rate of HIE has increased as treatments have improved, there is a high risk of permanent neurological deficits in the survivors (Dailey et al., 2013). As a result, HIE affects considerably the health and quality of life of patients and impose significant social and economic burdens. Thus, the key to avoid the HIE-induced long term neurological deficits is to present the neuronal death and enhance synaptic plasticity in the acute time. Hence, this is an unmet medical problem which requires investigation to elucidate mechanisms and to find effective neurotherapeutic targets for HIE. Long non-coding RNAs (lncRNA) are currently thought to be crucial regulators of genomic imprinting, chromatin remodeling, transcription, and cell cycles, and their expression is spatially and temporally restricted to cell types and stages of development (Clark and Blackshaw, 2014). Although their function and mechanism of action are not fully clear, perturbations in lncRNA expression have been implicated in many diseases, including Alzheimer's disease, heart pathology, and multiple forms of cancer (Clark and Blackshaw, 2014). In the central nervous system (CNS), lncRNAs are particularly abundant and their expression is spatially restricted and temporally regulated (Aprea et al., 2013), playing an important role in brain development. Growing evidence has also demonstrated the functional significance of lncRNAs in neuronal differentiation, maintenance and plasticity (Clark and Blackshaw, 2014). Thus, analysis of lncRNAs may broaden our understanding of the molecular mechanisms of HIE, and provide targets for new therapeutics. It has been documented that there is a crosstalk between lncRNAs and miRNAs (microRNAs), lncRNAs contain miRNA-binding sites, and can function as competing endogenous RNAs (ceRNAs) for miRNAs and protein coding mRNAs, then participate in disease development, such as cardiac hypertrophy and prostate cancer (Chiyomaru et al., 2013; Tay et al., 2014; Wang et al., 2014, 2016). However, the role of this crosstalk in the neurological deficits induced by HIE requires further exploration. Advances in molecular biology technology have led to a more in-depth understanding of HIE pathogenesis.

Therefore, in this study, using gene sequencing and a high throughput functional screening, we have shown that TCONS00044054 (Vi4) plays a crucial role in the neuron survival and cell apoptosis after HIE. Via microRNA sequencing, target scan and RNA22 prediction and quantitative Polymerase Chain Reaction (qPCR) verification, miR-185-5p stands out a site-regulated relationship with Insulin-like growth factor-binding protein 3 (Igfbp3) and Vi4. Moreover, to better understand the potential roles of Vi4, miR-185-5p, and Igfbp-3 crosstalk implicated in the neuron survival, cell apoptosis and further long-term neurological impairments caused by HIE, we further demonstrated their functions via lentivirus-mediated or CRISPER/Cas9 technologies. Taken together, our findings reveal a new pluripotent regulatory circuit that functions via a miRNA competitive mechanism mediated by Vi4.

MATERIALS AND METHODS

Animal Care

The animal protocol of this study has been approved by the Animal Care & Welfare committee of Kunming Medical University. Timed pregnant female Sprague-Dawley rats were purchased from Animal Centre of Kunming Medical University and housed in individual cages. After birth, pups were housed with their dam under a 12 h light/dark cycle, with food and water available *ad libitum* throughout the study. Then 7-days-old SD rat pups (weighing 12–15 g) were used in the later study. MiR-185-5p knock-out (KO) rats were constructed in Cyagen Biosciences (Cyagen, Guangzhou, China). All experiments were performed in consistence with the Guide for the Care and Use of Laboratory Animal published by the United States National Institutes Health.

Neonatal HI Insult

A modified hypoxic-ischemic model of HIE was generated as previously described (Ferrari et al., 2010). Briefly, 7-days-old (P7) postnatal pups were anesthetized with 3% isoflurane. Following 0.5 cm skin incision in the midline of the neck, the right common carotid artery of each pup was identified, exposed and permanently ligated with an electrocoagulator (Spring Medical Beauty Equipment Co., Ltd., Wuhan, China). After recovering in their dams for 1 h, the pups were then placed in an airtight chamber maintaining hypoxia [8% O_2, 92% N_2 at 4 L/min (min)] inside the chamber at a constant 37°C for 2 h. A constant temperature of 37°C was maintained throughout all the procedures. After hypoxia, the animals returned to their dams and the ambient temperature was maintained throughout the entire experimental period. Sham animals underwent anesthesia and the common carotid artery was exposed without ligation and hypoxia.

Behavioral Studies

Sensorimotor, cognitive, learning, and memory functions were assessed by behavioral tests-NSS test (Shohami et al., 1995), Morris Water maze test (Yang et al., 2017), rotarod (Hamm et al., 1994), Y-maze (Hu et al., 2017), and Open field tests.

Neurological Severity Score (NSS Score)

Severity of neurological deficit was assessed by use of NSS system (Shohami et al., 1995). The evaluations included the sensory (visual, tactile, proprioceptive), motor (muscle status, abnormal movement), balance tests, and reflex were recorded on a scale of 0–18 (0, normal score; 18, maximal deficit score).

Morris Water Maze Test

Morris Water maze test was employed to investigate the spatial learning and memory deficits 1 month after HIE as previously described (Yang et al., 2017). In brief, the test was conducted including acquisition phase and probe trial. Initial training was conducted for the first 5 days; during the training period, the rats were guided to locate a hidden and 1 cm submerged platform using peripheral visual information, the water temperature was maintained at 22–24°C. The rats were introduced into the pool for five consecutive days, and four times a day, and 15 to 20 min between training sessions. The rats were given 90 s to locate the platform and were allowed to remain on the platform for 10 s before being removed, while rats that were unable to locate the platform within 90 s were placed on the platform for 10 s before being removed. And the escape latency was recorded. On the 6th day, a probe trial was conducted, in which the platform was removed and the number of crossings over the previous platform location was recorded over one 90 s trial. Tracking System SMART 3.0 (Panlab, Spain) was used to record all the trials and track the movements of the animals automatically.

Rotarod

Rotarod test was used to assess the animals' ability to balance, motor coordination and physical condition (Hamm et al., 1994). Each group of rats was subjected to adaptive training for 3 days before the experiment. That means rats were placed on a rotating stick to accommodate the movement on the stick and trained once a day, each time 30–35 revolutions per minute (RPM), training for 5–10 min. After training, rats were placed on a rotating rod suspended 35–40 cm above the table surface, and the speed was 0–40 rpm with the increment of 2 rpm per every 10 s for 3 min. Thereafter, the time of duration (seconds) on the rod was recorded at a constant speed of 40 rpm, the longest time among the three consecutive tests were the final results.

Y-Maze

In the present study, Y-maze test was performed to detect the distinctiveness, working memory and reference memory of rats. The Y-maze device, provided by Shanghai Xinsoft (Shanghai, China), consisted of three arms including initial, wrong, and food arms. To inspire the animal's desire to ingest food, all animals should be fasted 1 day in advance. In the adaptation period, the animals were placed in the Y maze, each time for 10 min, adapted to 2–3 times a day, a total of 1 day, and there is no need to put food (this adaption can be synchronized with the fasting period). During 1-day training period, the training frequencies were kept the same for all rats, and the food (chocolate or bait) was placed in one arm of Y maze. Then the door of the other arm was closed, and the rats were placed in the initial arm to find the food. This training lasted for 5–10 min each time. Afterward, the animals could attend the formal test, in this period, the doors of the three arms were opened, the fasted rats were then put into the initial arm, the entry number and duration in each arm within 5 min were recorded with a video camera for each rat, and estimated by SuperMaze V2.0. Under the same moving time on the Y-maze, higher values of the two parameters in the food arm reflected higher spatial memory ability (Hu et al., 2017).

Open Field Tests

The open field test was selected to further assess locomotion (motor function), autonomous behavior, inquiry behavior and the tension of experimental animals in new environments. The experiment was conducted in a free exploration open-field apparatus, which was 100 cm × 100 cm × 40 cm (length × width × height) and divided into twenty-five 4 × 4 squares. Each rat was carried into the open field and allowed to adapt to the apparatus (10 min daily; three consecutive days) before testing. On the 4th day, rats were re-exposed to the open field for 5 min tests. These rats in stressful situations may lead to a rearrangement of hairs, feathers, and other appendages and sensory stimulation of the skin. In most cases these immediate effects, such as grooming, undoubtedly represent stressful behaviors. Contrarily, rearing (standing upright on the hind legs) is used to indicate a rats' behavior in a relaxed state. During testing, the time spent grooming and rearing of each rat was recorded by a video camera, and estimated by SuperMaze V2.0.

Positron Emission Tomography-Computed Tomography (PET-CT)

Positron Emission Tomography-Computed Tomography was carried out to observe the glucose uptake in brains, presented by SUV max. In detail, rats were fasted for 8 h and deprived of water for 4 h before examination. Then rats were anesthetized using Sumianxin II for induction (0.1 mg/kg), and fixed in the supine position in PET/CT scanning table (Discovery 690/Elite, GE, United States). The whole-body CT and PET data were obtained with a standard protocol using AW VolumeShare 5 software for 20 min. The scanning parameters were as follows: voltage for 120 kV, electricity for 260 μA, screw pitch for 0.561, rotational speed for 0.5 s/cycle, thickness and interval for 3.75 mm, 512 × 512 for CT matrix and fov = 50 cm × 50 cm. Thereafter, the PET scan of the same region followed at 2.5 min per bed table position was performed. Attenuation correction and iterative reconstruction of PET images was performed using the CT data and 47 frames of PET cross-sectional images were obtained. Moreover, the CT and PET images were transferred to AW VolumeShare 5 workstation, respectively, and the coronal, sagittal, cross-sectional, and three-dimensional images as well as the fusion images of CT and PET images were obtained. Finally, the PET/CT images were read by two PET/CT reporters via double blind method, and the average value of WB-SUVmax was determined by drawing the ROI of cerebral hemorrhage.

Tissue Harvest

According to diverse experiments, the preparation of samples was different. After behavioral studies, animals performed for gene analysis were anesthetized, then, their brains were removed, cortex including peri-infarct tissue (approximately 3 mm around the infarcted area of the ipsilateral hemisphere) and hippocampus were separated carefully. The tissues can be stored at −80°C for further use. For morphological detection, the samples were obtained after intracardiac perfusion with 0.9% physiological saline followed by 4% paraformaldehyde (at 4°C, pH 7.4), the

brain samples were post-fixed for 5 h at 4°C. The tissue was kept in 30% sucrose in 0.1 Mol (M) phosphate buffer, pH 7.4, for 72 h at 4°C. Then, the brains were embedded in the paraffin. The paraffin-embedded sections were cut into serial horizontal sections (5 μm thickness) and processed simultaneously. For immunocytochemical analysis of neurons, cells were cultured on glass coverslips in 6-well plates. Following washes in PBS, the cells were rinsed and fixed with 4% paraformaldehyde at room temperature for 30 min.

Triphenyl Tetrazolium Chloride (TTC) Staining and Evaluation of Infarction Volume

The rats were anesthetized with isoflurane and decapitated at 24 h post HI. The brains were rapidly removed and sliced into 2-mm-thick coronal sections in a rat brain matrix (Seino Co., Ltd., Beijing, China). The sections were immediately immersed in 2% 2,3,5-triphenyltetrazolium chlorides (Sigma Co., St. Louis, MO, United States) at 37°C for 30 min in the dark, washed in PBS and then fixed by 4% formaldehyde in phosphate buffered solution. The infarction area of each section was traced and measured using Image J Software (Version 1.43 u; National Institutes of Health, Bethesda, MD, United States). To abolish the error caused by brain edema, we corrected the infarct volume by standard methods as described in the previous report (contralateral hemisphere volume – volume of non-ischemic ipsilateral hemisphere), with infracted volume expressed as a percentage of the contralateral hemisphere. In addition, the brain swelling was determined by subtracting the total volume of the non-ischemic hemisphere from that of the ischemic hemisphere (Hu et al., 2009).

Hematoxylin and Eosin Staining (HE Staining)

Pathological changes in the brains of rats were observed by HE staining. In brief, the prepared brain sections were exposed to HE staining, and morphology changes in the brain tissues were observed using a light microscope (CX40, Shunyu, Ningbo, China) to detect morphologic changes. Moreover, the average cell size in cortex and hippocampus from five fields of each section (three sections/each animal and five animals/group) was quantitatively analyzed using Image-Pro Plus 6.0 software (Media Cybernetics, Silver Spring, MD, United States). Each section was evaluated by three investigators blinded to the experimental information.

Nissl Staining

The neuronal cells of the cortex and hippocampus section were visualized by a Nissl staining assay. Briefly, brain slides (5 μm) were stained with 0.1% cresyl violet stain for 1 h at 60°C. The sections were then placed in 0.1% Nissl differentiation, and then they were subsequently washed with distilled water, dehydrated by gradient concentrations of ethanol (70, 80, 90, and 100%), cleared in xylene, and finally coverslipped with neutral balsam. The dark neurons and surviving neurons were observed using a light microscope (magnification, × 200, × 400, Shunyu, Ningbo, China). Five random fields were chosen by a blinded observer and used to quantify positive cell numbers. Cell counts from the left and right hippocampus and cortex on each of the six sections were averaged to provide a single value for each animal.

Bioinformatics Analysis

The differentially expressed lncRNAs, mRNAs and miRNAs in brain after HI were screened using gene sequencing. Furthermore, in order to predict the relationship among lncRNA, miRNA, and mRNA, ceRNA analysis was performed by Biomarker Technologies in Beijing. In addition, RNA22[1] was used to predict the binding site between lncRNA and miRNA, the website is. TargetScan[2] was used to predict miRNAs that target Igfbp3. Venny 2.1[3] was applied to perform the intersection analysis.

Luciferase Reporter Assays

Igfbp3 3′UTR luciferase plasmids as well as the corresponding Mut plasmids were generated by RiboBio (Guangzhou, China). The Vi4-ORF-mut was constructed by GeneCopoeia Company (Guangzhou, China). The pmiR-RB-REPORT™ Dual luciferase-expressing vector contained hRlucc DNA encoding *Renilla* luciferase as a reporter and hLucc DNA encoding firefly luciferase as an internal control. Constructs of WT luciferase plasmid contained the full-length 3′-UTR of Igfbp3 mRNA, and the mutant plasmids contained a 3′UTR mutation (mutated from "TCTCTCC" to "AGAGAGG") could effectively abrogate the binding of Igfbp3 to miR-185-5p. The constructs were confirmed by *Xho*I and *Not*I restriction enzyme digestion and sequencing. Then, 293Tα cells (4×10^3 cells per well) were seeded into triplicate wells of 96-well plates 1 day before transfection. Afterward, the mixture of 3′UTR luciferase plasmids of Igfbp3 or control or port or plasmid (100 ng/ml, Guangzhou RiboBio, China) and miR-185 -5p mimic/mimic-nc (final concentration 80 nM) were transfected into 293Tα cells using SuperFectinTM II *in vitro* DNA Transfection Reagent (Pufei Biotech, China). For the detection between Vi4-ORF-mut and miR-185-5p, Vi4-ORF-mut was transfected into cells 1 day before mimic transfection. 48 h after transfection, luciferase activity was measured with a Dual-Luciferase Reporter Assay Kit (Promega, E1910). The fluorescence value of Renilla fluorescence/firefly is the final relative luciferase activity.

LncRNA-ORF-Vector Generation

ORF-vector was verified by Enzyme Digest and Electrophoresis and recombinant lentivirus production. Briefly, sequences of lncRNAs were acquired from gene sequencing was sent to GeneChem Company (Shanghai, China) to construct recombinant overexpressed vector (ORF-vector) and then verified by Enzyme Digest and Electrophoresis and sequencing. After that, the lentiviral particles were generated following a standardized protocol using highly purified plasmids and EndoFectin-Lenti™ and TiterBoost™ reagents. Then, the titer

[1]https://cm.jefferson.edu/rna22/Interactive/

[2]http://www.targetscan.org/vert_72/

[3]http://bioinfogp.cnb.csic.es/tools/venny/

of each lentivirus was quantified and lentiviral stocks were stored at −80°C to keep the activity.

Construction of Igfbp3-sh/Vi4-sh Vectors

Three potential shRNA sequences targeting the Igfbp3 and Vi4 mRNA were designed by GeneChem Company (Shanghai, China), according to the sequence detected in gene sequencing. At the same time, a nonsense shRNA was also designed and synthesized for NC. Then three Igfbp3-sh and Vi4-sh vectors were also provided by GeneChem Company (Shanghai, China). After successful construction, PC12 cells were prepared to single out the most effective shRNA sequence. In brief, when the PC12 cells were 30% confluence, fresh medium containing shRNA lentivirus and 4 μg/ml polybrene, was added to cells. After 3-days transfection, the effects of shRNA were detected by qRT-PCR. Subsequently, the most efficient shRNA-lentivirus-vector was used for the later experiment. In this study, for Igfbp3-shRNA, target sequence (TGACTGATTCCAAGTTCCA) is the most efficient one, for the Vi4-shRNA, target sequence (CGCCAGGTCATCAAGA AGCAA) is the most efficient one, which were used in the later experiment.

Construction of miR-185 Mimic/Inhibitor

miR-185 mimic/inhibitor [provided by RiboBio (Guangzhou, China)]. The inhibitor, a chemically modified RNA single-strand, is the complementary strand of the miR-185-5p sequence. The sequence of Hsa-miR-185-5p/rno-miR-185-5p is 5′UGGAGAGAAAGGCAGUUCCUGA 3′; the binding sequence of miR-185-5p is 5′TCTCTC3′; miR-185-5p predicts the target sequence to be 5′AGAGA 3′.

Lentivirus Injection in the Neonatal Rats

To detect the role of Vi4 in the rats with HIE, 3-days old postnatal pups were anesthetized with 3% isoflurane and 5 μl (2×10^8/ml) Vi4-ORF was injected into rats at the right lateral ventricle via microscopic device, and physiological saline was a negative-control (HI-NC). Injection coordinates were 4 mm depth at the following coordinate: 1.5 mm perpendicular to the front cymbal, and further 1.0 mm apart. Infusion was performed at a rate of 100 nl/min. After injection, the glass pipette was left in place for an additional 2 min before being slowly retracted.

Genotype Identification of miR-185-5p KO Rats

For the rats at 7–10 days after birth, the toes and tail tips were collected and numbered. Then, rats' genomic DNA was extracted using Transgen's genomic DNA extraction kit (ee101-12), and PCR detection was performed with the amplification primer: Rat Mir185-F: 5′-CTGATGTGCTCAGGGTGTTGACC-3′; Rat Mir185-R: 5′-GC TGCTGATGTTAGGGAGGAGGC-3′.

Primary Cortical and Hippocampal Neuron Cultures

The 1-day SD rats were anesthetized and the cortexes/hippocampus were harvested, minced, and isolated by 0.25% trypsin for 10 min at 37°C, then eluted with 10% fetal bovine serum (FBS). Afterward, the tissue suspension was centrifuged at 1000 rpm for 10 min, and complete culture medium (Hyclone) composed of DMEM/HIGH GLUCOSE, 10% fetal calf serum and 1% penicillin-streptomycin solution as used to resuspended the pellets in the bottom. Neurons were then plated in 6-well plates (Corning, United States) coated with poly-d-lysine and laminin (Sigma-Aldrich, St. Louis, MO, United States) at a density of 5×10^5 cells/ml, and incubated at 37°C, 5% CO_2. In addition, for immunofluorescence staining, we put three cover slips in the 6-well plates before coating. Four hours later, the complete culture medium was replaced with neurobasal medium with the addition of 2% B27 (Invitrogen, Carlsbad, CA, United States). The culture medium was changed the next day, then one-half change was doing every 3 days. The neurons were identified by Tuj1 staining to confirm the purity.

Transfection of Vi4-ORF or miR-185 Mimic/Inhibitor or Igfbp3-shRNA Into Cortical Neurons

To detect the role of Vi4, miR-185-5p and Igfbp3 on the cell growth or viability, Vi4-ORF-vector, miR-185 mimic/inhibitor [provided by RiboBio (Guangzhou, China)], or Igfbp3-shRNA were transfected into cortical neurons after culturing for 3 days. The transfection system of miR-185-5p was the mixture of 1x riboFECTTMCPBuffber, 100 ng/μlriboFECTTMCP Regent and miR-185-5p mimic (80 nM) or miR-185-5p inhibitor (100 nM), the mixture was added drop-wise to the appropriate wells, respectively. Then, the medium with miRNA transfection was changed immediately before OGD. The transfection system of Vi4-ORF and Igfbp3-sh lentivirus included corresponding lentivirus with no polybrene. Briefly, the lentiviral infection was performed in the titer of two multiplicity of infection (MOI) in primary neurons. After incubation at 37°C for 8 h, the original medium was replaced with fresh medium. eGFP was set as the NC group, and was observed under the Inversed Fluorescent Microscope (Leica, Wetzlar, Germany) to evaluate the transfection efficiency. Moreover, for the rescue experiment between miR-185-5p and Igfbp3, as well as Vi4 and miR-185-5p, we added miR-185-5p mimic into the cells with Vi4-ORF lentivirus or Igfbp3-sh/Vi4-sh into miR-185-5p KO cells. OGD was performed 3 days after transfection. Then the cell growth and viability and cell apoptosis were detected at 24 h post OGD.

OGD

Neurons were prepared to mimic for HI *in vitro* conditions, according to OGD protocol. Briefly, the cells were washed with 0.01 mM PBS for one time before the medium was changed to glucose-free medium. Then cells were transferred into a hypoxia chamber (Thermo Fisher Scientific, Waltham, United States) with a gas mixture composed of 5% CO_2 and 95% N_2 for 2 h. The control cells were incubated normally, and without exposing to OGD.

Immunofluorescence Staining

Immunocytochemical analysis of Tuj1 was performed to detect the neuron growth. Briefly, for neuronal immunocytochemistry,

slices were directly permeated in PBS containing 3% goat serum for 30 min at 37°C. Then, the slices were incubated with primary antibody of Tuj1 (1:200, Rabbit, ABclonal) or Tuj1 (1:200, mouse, ABclonal) and species-specific secondary antibodies of 488 (1:100, goat anti-rabbit, Abbkine) and 594 (1:100, goat anti-mouse, Abbkine). The average length of neuron axon was calculated using Image-Pro Plus 6.0 software (Media Cybernetics, Silver Spring, MD, United States).

TUNEL Assay

Apoptotic cells were tested by TUNEL assay, the brain tissues and cells were prepared as previously described. In brief, the TUNEL reaction mixture of enzyme solution and labeling solution was added at a ratio of 1:9 (v/v), and the slices of cells were stored at 4°C overnight in the dark. After three washes with PBS, the slices were stained with DAPI for 5 min at room temperature, and images were observed via high-content imaging system (Evons, Thermo, United States). Sixteen fields were randomly selected from each section, and apoptosis was quantified by determining the percentage of TUNEL/DAPI using high-content quantitative system.

Counting Kit-8 Assays (CCK8)

Neuron viability was assayed by CCK-8 (Dojindo Laboratories, Kumamoto, Japan), according to the manufacturer's instructions. In brief, neurons were plated at a density of 1×10^5 cells per well in 96-well plates. At the end time, 10 μl CCK-8 solution containing a highly water-soluble tetrazolium salt WST-8 [2-(2-methoxy-4-nitrophenyl)-3-(4-nitrophenyl)-5-(2,4-disulfophenyl)-2H-tetrazolium, monosodium salt] was added into each well, followed by incubation for 3 h at 37°C. Cell proliferation/viability was determined by measuring the OD at 450 nm. Percentage over control was calculated as a measure of cell viability.

Flow Cytometry

Cell apoptosis was also observed by flow cytometry using a cell apoptosis analysis kit (APC Annexin V Apoptosis Detection Kit with PI). Briefly, at 24 h post OGD, the cells were digested by 0.25% trypsin (EDTA free), followed by centrifuging for 5 min at 1000 rpm. Then, the collected cells were rinsed by 1 × PBS (4°C) for two times, and the cell number was quantified at 1×10^6/sample. Afterward, cells were resuspended by 500 μl 1 × binding buffer, then 5 μl Annexin V-APC and 5 μl PI were mixed with 100 μl cell suspension, followed by incubating for 15 min at room temperature without light. Ultimately, the cells were analyzed by a flow cytometer (Becton Dickinson United States) after being added another 400 μl 1 × Binding Buffer. Apoptosis rate was decided by the sum of the first, second and fourth quadrants.

Collection of Human Samples

For the serum samples, the patient's whole blood was gathered through a coagulant tube. After gathering the blood, gently reverse the coagulated tube to mix the blood, then stand them upright at room temperature until the blood was completely coagulated. All serum samples were retrieved and transferred to the laboratory of the Institute of Neuroscience, Kunming Medical University within 2 h after blood collection. After the filtration treatment according to the standard, the serum of 23 people in the BI-3rd group of coagulant tubes was centrifuged for 1000 × 10 min to isolate the serum. Then the collected serum was transferred to 1.5 ml microtubules. All samples were immediately frozen in liquid nitrogen and stored at 80°C. Furthermore, same procedures were performed for the serum obtained from a control group. This experiment was approved by the ethic committee of 2014-2, and all the patients and controls got the informed consent before blood sample collection.

In addition, we also collected a 29-day-old human fetus to culture the primary cortical neurons, this was approved in September 30, 2015 by the Ethics Committee of Kunming Medical University, China (approval No. 2015-9). Informed consent was obtained from the mother. An abort d 29-day-old fetus was collected from the first affiliated hospital of Kunming Medical University and immediately stored on ice. The brain was dissected and placed in 75% alcohol for 2 min. The cortical neurons were then isolated and cultured as described above for the rat neuron culture.

Quantitative Real-Time Polymerase Chain Reaction (qRT-PCR)

Total RNA was isolated with TRIzol reagent (Takara Bio Inc., Otsu, Japan) and was reverse transcribed to cDNA with the Revert Aid^{TM} First Strand cDNA Synthesis kit (Thermo, United States) and All-in-One miRNA First Strand cDNA Synthesis Kit (GeneCopoeia). The qRT-PCR was then performed to detect the relative expression of mRNA, miR-185-5p and LncRNATCONS00044054 were detected in 24 h after HI and Igfbp3 was detected in 6 h, 24 h and 1 week after HI. The primer sequences were shown as in **Table 1**. Next, reaction was performed in a DNA thermal cycler (ABI 7300) according to the following standard protocol: one cycle of 95°C for 5 min; 40 cycles of 95°C for 10 s; annealing of 58°C (miR-185-5p) for 20 s, 53°C (Igfbp3) for 10 s, 55°C (lncRNATCONS00044054) for 10 s; and extension of 72°C for 20 s. Relative expressions were calculated with normalization to GAPDH values by using the $2^{-\Delta\Delta Ct}$ method.

TABLE 1 | The primer information.

	Forward	Reverse
TCONS00044054 (rat)	5′TGTTCAATT GTCGGTCTTGGTG 3′	5′GAGTTCTGCT GGCTAGTGCTG 3′
Igfbp3 (rat)	5′GGCTCCTT GGGTCGCTTCGT 3′	5′CCCGCCTGAG TTGGACTTCAC 3′
Igfbp3 (human)	5′AGGAAGG AGGAATGGCTTGC 3′	5′CCTCAGTC ATGGCCACAGTT 3′
MiR-185-5p (rat)	HmiRQP0247(GeneCopoeia)	
MiR-185-5p (human)	HmiRQP0247 GAGAGAAAGGCAGTTCCTGAAA	
MiR-380-5p (rat)	HmiRQP0478(GeneCopoeia)	

Western Blot

Both cortical and hippocampal brain tissues were frozen immediately and stored at 80°C until assessment. To testify the protein expression of Igfbp3 in 6 h after HI, protein was extracted from each group using RIPA lysis buffer (Beyotime, Jiangsu, China) containing 2% of cocktail pill (Roche). Then, the protein concentration was detected by BCA protein assay kit (Beyotime Institute). Afterward, protein (60 μg) was separated by sodium dodecyl sulfate-polyacrylamide gel electrophoresis at 60 V for 30 min and then at 120 V for 1.2 h, and followed by transferring to polyvinylidene fluoride membranes (Millipore, Billerica, MA, United States) over 4 h at 350 mA. After being blocked by 5% non-fat milk for 1 h, the membranes were then incubated with Igfbp3 primary antibody (1:500; Ab6672, rabbit) overnight at 4°C. β-actin (1:2000, A01010, mouse) was set as an internal control. Thereafter, the membranes were rinsed in TBST and incubated with secondary antibody (goat anti-rabbit IgG and goat anti-mouse IgG; ZSGB-BIO, Beijing, China, 1:5000) for 1 h. Finally, after being rinsed in TBST, the membrane was detected using Alpha Innotech (Bio-Rad Laboratories, Berkeley, CA, United States) with ECL.

Statistical Analysis

All data in the experiment are presented as mean ± SD. Comparisons among groups were analyzed using one-way or two-way repeated-measures ANOVA analysis with the SPSS version 19.0 (IBM Corporation, New York, NY, United States). For multiple group comparison, ANOVA with Tukey's *post hoc* multiple comparisons were applied. And Student's *t*-test was used to analyze the data between two groups. $P < 0.05$ was considered statistically significant.

RESULTS

The Expression of Vi4 (TCONS00044054) Increased After HIE

The result of qRT-PCR showed that Vi4 was upregulated by HIE (**Figure 1A**, $P < 0.05$). It is worth noting that Vi4 expression have the same trend as the microarray (**Figure 1B**). Moreover, it was further found that the expression of Vi4 in OGD was higher than that of normal cortical neurons (**Figure 1C**, $P < 0.05$). The name of vector was GV367 with *Age*I/*Nhe*I enzymes digestion, showing the plasmid molecular weight of the digested products (**Figure 1D**). The results of positive clonal sequencing, indicating the plasmid clone is ok (**Figures 1E,F**). Then, the transfection of Vi4 over-expressed vector (Vi4-ORF) into the PC12 cell line, the green color emerged by GFP represents the successful transfection (**Figure 1G**).

Vi4 Overexpression (Vi4-ORF) Protected neurons and Improved the Long-Term Neurological Deficits in Rats With HIE

Postnatal day 3 rats were injected with 5 μl (2×10^8/ml) Vi4-ORF or Vi4-negative control (Vi4-NC) into the right lateral ventricle via microscopic device, Vi4-NC was used as a control (HI-NC) (**Figure 2A**). HIE model was then established 4 days (d) after virus injection. The TTC staining in the HI-NC group showed a clear cerebral infarction on the right side of the brain, and Vi4-ORF significantly decreased the infarction area (**Figures 2B,C**, $P < 0.05$). In addition, Nissl-staining was used to detect the neuron survival, as a result, Nissl-stained neurons including the normal and dark ones were detected in the both cortex and hippocampus (**Figure 2D**). Quantitative analysis showed that the number of total neurons was markedly deceased after HI, and the dark neurons was increased as compared with the sham group, while the number of dark neurons in the Vi4-ORF group significantly decreased in comparison to the NC group in those areas (**Figure 2E**, $P < 0.05$). In addition, Vi4-ORF group showed the more total neurons than NC group both in cortex and hippocampus (**Figure 2F**, $P < 0.05$). Additionally, spatial learning was evaluated for consecutive 5 days and a probe trial for spatial memory was conducted on the 6th day at two time points of 1-month post HIE. As expected, at both times points the rats injected with Vi4-ORF performed better in learning and memory than that of rats in NC groups (**Figures 2G,I**, $P < 0.05$). Compared with animals in the HI-NC group, Vi4-ORF-treated rats had significantly more crossings over the previous platform location (**Figure 2H**, $P < 0.05$). Y-maze was performed to measure the spatial memory of rats 1 month after HIE. As shown in **Figure 2J**, the time spent in food arm in the Vi4-ORF group was longer than that in the NC group ($P < 0.05$), while time in the initial arm and wrong arm was shorter ($P < 0.05$), indicating that the ventricle injection of Vi4-ORF ameliorated the spatial memory of rats with HIE (**Figure 2J**, $P < 0.05$). Besides, open field test indicated that Vi4-ORF rats showed less grooming time and significant increase rearing time with respect to the NC group (**Figures 2K,L**, $P < 0.05$). Similarly, Vi4-ORF-treated rats exhibited increased time on the rotor bar compared to the NC littermates (**Figure 2M**, $P < 0.05$). However, the treatment with Vi4-ORF of HIE rats had no significant effect on the number of arm entries compared with NC animals. NSS in HI-NC group was obviously increased compared with the sham and Vi4-ORF group at 1 month after HIE, (**Figure 2N**, $P < 0.05$).

Vi4 Reduced the OGD-Caused Inhibition of Neuron Growth and Cell Apoptosis

Furthermore, PET-CT was carried out to measure the glucose uptake in the brain, quantified by Standardized Uptake Value (SUV) max. As a result, Vi4-ORF injection induced a better glucose uptake in the brain, demonstrated by higher SUV max than that in the NC group (**Figures 3A,B**, $P < 0.05$). To further explore the effect of Vi4 on the growth of cortical and hippocampal neurons, Vi4-ORF and Vi4-negative control (NC) vectors were transfected into the primary cortical neurons (**Figure 3C**). The CCK8 results showed that Vi4 increased the cortical and hippocampal neurons viability under OGD in primary neurons compared with NC group (**Figure 3D**, $P < 0.05$). In addition, through Tuj1 and TUNEL staining, we found that Vi4 reduced apoptotic cells and reserved the length of

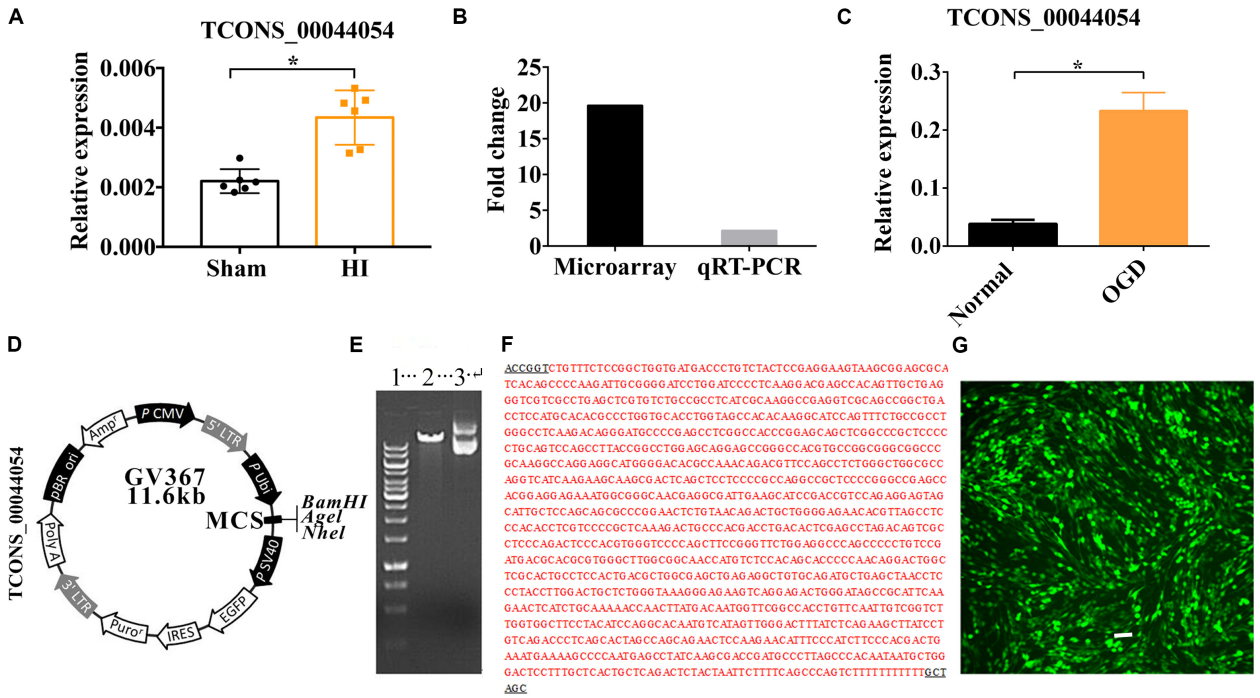

FIGURE 1 | The relative expression of TCONS00044054 (Vi4) in HIE. **(A)** Quantitative histogram for Vi4 expression in sham and HI groups, n = 6/group **(B)** The fold change of Vi4 in the microarray and qRT-PCR analysis. **(C)** Quantitative histogram for Vi4 expression in sham and HI groups. **(D,E)** The name of vector was GV367 with *AgeI*/*NheI* enzymes digestion, showing the plasmid molecular weight of the digested products. 1 was for marker (from up to down: 10 kb, 8 kb, 6 kb, 5 kb, 4 kb, 3.5 kb, 3 kb, 2.5 kb, 2 kb, 1.5 kb, 1 kb, 750 bp, 500 bp, and 250 bp), 2 was for digested vector (11.6 kb), and 3 was for non-digested vector. **(F)** The results of positive clonal sequencing, indicating the clone is ok. **(G)** The transfection of Vi4-ORF into the PC12 cell line, the green color emerged by GFP represents the successful transfection. Scale bar = 100 μm. The relative expression was relative to that of the sham or normal group HI group: hypoxic ischemic group. All data are presented as mean ± SD, $^*P < 0.05$.

neuronal axons after OGD in cortical and hippocampal neurons (**Figures 3E–H**, $P < 0.05$).

The Upregulation of Igfbp3 by Vi4 in HI Is Competitively Silenced by Negative Regulation of miR-185-5p

The analysis of ceRNA was used to explore the relationship among lncRNA, miRNA, and mRNA, to predict the target candidate of Vi4. As predicted by bioinformatics analysis on Vi4 and conjoint analysis of gene sequencing, Igfbp3 was finally determined as the target of Vi4 (**Figures 4A,B**). This target was further validated by q-PCR verification in OGD cortical neurons after Vi4-ORF transfection, which showed 300-fold upregulation of Igfbp3. In addition, the expression of Igfbp3 was detected in brain of HIE rats at 6 h, 24 h and 1 week after HI (**Supplementary Figure 1**), and elevated at 24 h after HI. The relative protein expression of Igfbp3 in 6 h after HI group was down-regulation than that of the sham group (**Figure 4C**, $P < 0.05$). In addition, we asked a question whether Vi4 shares regulatory miRNAs with Igfbp3. Therefore, we applied cross matching of RNA22, TargetScan and miRNA sequencing using rat cortex with HIE to determine common matching miRNAs. As a result, miR-185-5p and miR-380-5p were found most likely miRNAs silencing both Vi4 and Igfbp3 (**Figures 4D,E**). To confirm the expression of miR-185-5p and miR-380-5p and Igfbp3 after HIE, q-PCR was employed to quantify their levels in the cortex and hippocampus. The results showed that HIE induced significantly increase in the expression of Igfbp3 at 24 h, but decrease in miR-185-5p and miR-380-5p (**Figures 4F,G**, $P < 0.05$). Then the regulatory relationships among Vi4, miR-185-5p and miR-380-5p and Igfbp3 were also investigated in the primary cortical neurons after OGD. We found that miR-185-5p was markedly down regulated after OGD, and Vi4-ORF treatment can further enhance this effect. However, there was no significant difference in the expression of miR-380-5p, thus miR-185-5p was the focus for the further study (**Figure 4H**, $P < 0.05$). The relative expression of Igfbp3 in OGD group was up-regulation than that of the normal group (**Figure 4I**, $P < 0.05$). Moreover, we constructed miR-185-5p mimic and inhibitor to transfect the neurons. We found that miR-185-5p mimic could cause down-regulation of Igfbp3, whereas the miR-185-5p inhibitor or Vi4-ORF could counteract OGD-induced decrease of Igfbp3, indicating both miR-185-5p and Vi4-ORF exhibit competitive regulation of Igfbp3 expression after ODG (**Figure 4I**, $P < 0.05$). Moreover, the expression of Igfbp3 protein in these groups showed the same trend as qRT-PCR (**Figures 4J,K**, $P < 0.05$).

Afterward, RNA22 and TargetScan were used to predict the binding sites between Vi4 and miR-185-5p, miR-185-5p and

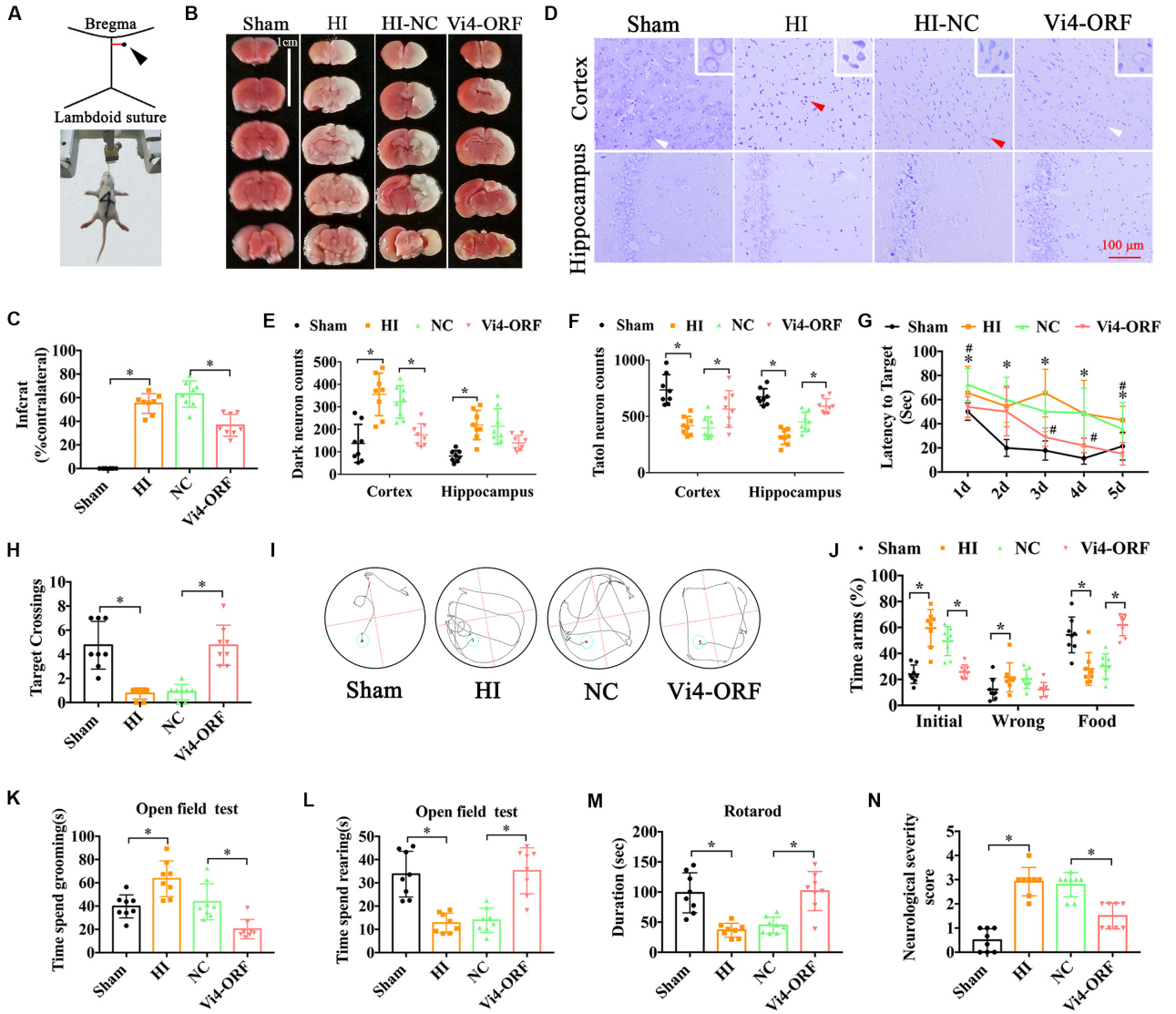

FIGURE 2 | The neurobehavioral tests of rats after intraventricular injection of Vi4-ORF *in vivo*. **(A)** Coordinates of the right ventricle for the Vi4-ORF injection in the P3 rats. **(B)** TTC staining among the sham, HI-NC and Vi4-ORF groups at 24 h after HI. Scale bar = 1 cm. Pale white represents the infarct area, red shows the normal staining. **(C)** Quantitative histogram for the infarct ratio (% contralateral) between NC and Vi4-ORF groups, *n* = 8/group. **(D)** Nissl staining in the groups of sham, HI-NC and Vi4-ORF. The white arrow represents surviving neurons. The red arrow represents dark neurons. Scale bar = 100 μm. **(E,F)** The number of dark neuron and total neuron in cortex and hippocampus among sham, HI, NC and Vi4-ORF groups, *n* = 8/group. **(G)** The latency to target during 5 days training among the sham, HI, NC, and Vi4-ORF groups at 1 month after HI in MWM test. $^{*}P < 0.05$ vs. Sham. $^{\#}P < 0.05$ vs. NC, *n* = 8/group. **(H)** Target crossings in MWM test at 1 month after HI, respectively. **(I)** The walking path of the platform in probe trial of Morris Water Maze test at day 5 of 1 month after HI. **(J)** The time arms (%) of initial, wrong and food arms in the sham, HI, NC and Vi4-ORF groups at 1 month after HI in the Y-maze test, *n* = 8/group. **(K,L)** The time spent grooming and rearing in the open field experiment 1 month after HI, *n* = 8/group. **(M)** The duration of rats on rotary bar in the rotarod test 1 month after HI, *n* = 8/group. **(N)** NSS score among the sham, HI, NC and Vi4-ORF groups 1 month post HI, *n* = 8/group. The N number is the number of biological repeats. HI, hypoxia-ischemia; NC, negative control; H, hours; D, days; MWM, Morris water maze; Vi4-ORF, Vi4 overexpression. All data were presented as mean ± SD, $^{*}P < 0.05$.

Igfbp3 (**Figure 4L**). To ascertain whether this observed effect depends on their regulation of the Igfbp3 3′UTR, we constructed luciferase reporters containing Igfbp3 3′UTR [Igfbp3-Wild Type (WT), Igfbp3-Mutant (Mut)]. Luciferase plasmid (Igfbp3-WT, Igfbp3-Mut) and miR-185-5p mimic/miR-185-5p mimic-nc were transfect d into the 293T cell clones. Vi4-ORF-WT/Mut was also constructed. The sequence bound by miR-185-5p is TCTCTC. As a result, in cells transfected with plasmids containing the Igfbp3 3′-UTRs (**Figures 4La,b**), the relative luciferase activity was significantly decreased after treatment with miR-185-5p, whereas the inhibitory effect of miR-185-5p was abolished in the plasmid containing the mutant 3′-UTRs of Igfbp3 (**Figure 4M**, $P < 0.05$). For the rescue experiment, Vi4-ORF or Vi4-ORF-Mut was also transfected into the cells with Igfbp3-WT plus miR-185-5p mimic/miR-185-5p-mimic-nc. Vi4 didn't directly combine with Igfbp3. Vi4 could regulate Igfbp3 by competitively

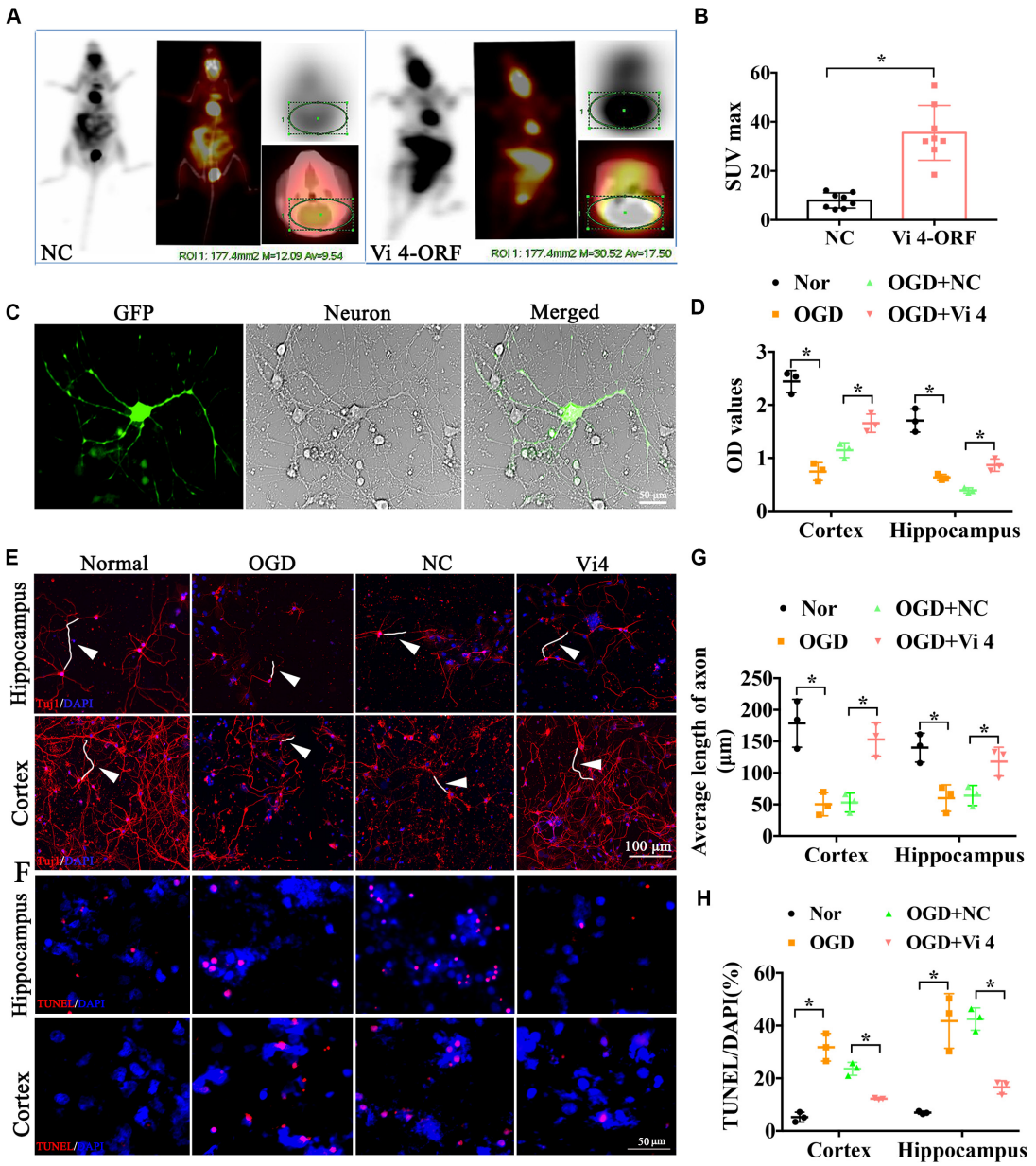

FIGURE 3 | The functional examination on the hippocampal and cortical neurons after the transfection of the Vi4-ORF. **(A)** Images of glucose uptake in the brain by PET-CT in NC and Vi4-ORF groups 2-month after HI. **(B)** The quantified bar chart of SUV max, $n = 8$/group. **(C)** The successful transfection of Vi4-ORF vectors in the cortical neurons, demonstrated by green fluorescence in the cells. Scale bar = 50 μm. **(D)** Cell viability showed by relative CCK8 values in both normal and OGD cells with lentivirus transfection 24 h after OGD in hippocampal and cortical neurons. **(E)** Immunofluorescent staining of Tuj1 to observe the cell state after the ORF-Vi4 vector transfection in the hippocampal and cortical neurons 24 h after OGD. Red fluorescence represents the positive Tuj1 cells, and the blue is the nuclear staining. White arrow represents axon. Scale bar = 100 μm. **(F)** Cell apoptosis detected by TUNEL staining in the cortical neurons 24 h after OGD. Scale bar = 100 μm. Red fluorescence represents TUNEL positive cells, and the blue is the nuclear staining. **(G)** Bar chart for average axon length of cortical and hippocampal neurons at 24 h post OGD. **(H)** Cell apoptosis presented by TUNEL/DAPI (%) in both normal and OGD cells with lentivirus transfection 24 h after OGD. PET-CT, Positron Emission Tomography-Computed Tomography; SUV, Standardized Uptake Value; OGD, oxygen glucose deprivation; Tuj1, neuronal class III β-Tubulin; CCK8, cell counting kit-8; TUNEL, Terminal deoxynucleotidyl Transferase Mediated Nick End Labeling. All data are presented as mean ± SD, $^*P < 0.05$, $n = 3$/group.

binding miR-185-5p and weaken the combination of Igfbp3 and miR-185-5p. Therefore, overexpression of Vi4 but not the mutant Vi4-ORF-Mut, overcame the decreased luciferase activity of Igfbp3 (**Figure 4N**, $P < 0.05$). Furthermore, we verified the expressional changes of Igfbp3 and miR-185-5p in the serum of normal and patients with brain ischemia (BI). We found that the expression level of Igfbp3 in BI patients was much higher than that in normal ones, while the expression level of miR-185-5p in BI patients was lower than that of normal subjects (**Figure 4O**, $P < 0.05$). Additionally, the aborted fetal neurons

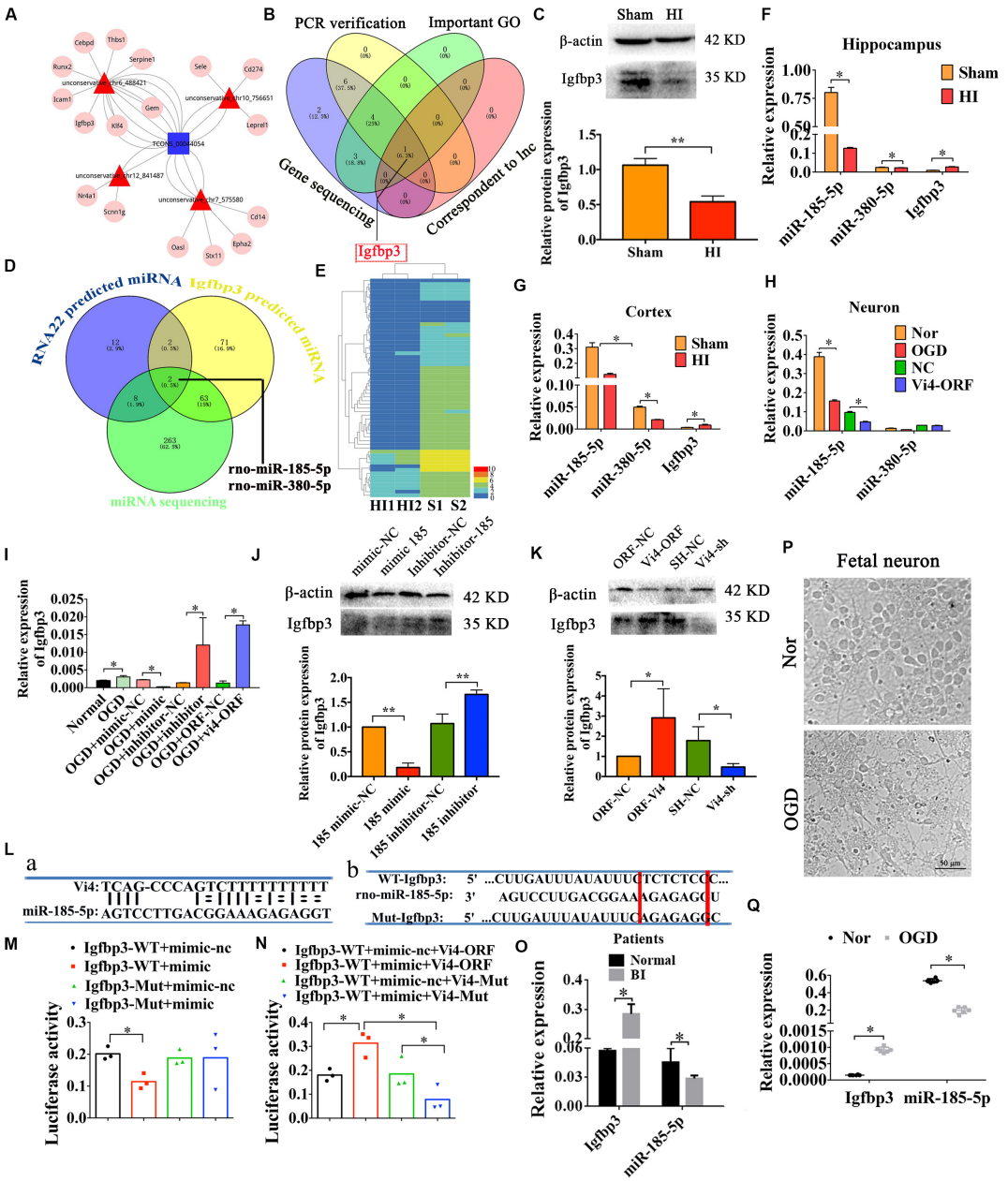

FIGURE 4 | Regulatory relationships among Vi4, miR-185-5p and Igfbp3 in sites and expression. **(A)** ceRNA analysis of Vi4 among diverse miRNAs and mRNAs. The blue square represents Vi4, the red triangles represent miRNAs, and the pink circles represent related genes. **(B)** Intersection of PCR verification, important GO analysis, gene sequencing and correspondent to lnc via bioinformatics analysis for selecting the target gene to Vi4 in the venny 2.1 software. **(C)** Western blot detection of the cortical brain tissues in the sham and HI rats, *n* = 6/group. **(D)** Intersection of RNA22 prediction, TargetScan for Igfbp3-predicted miRNAs and miRNA sequencing to further find the miRNAs that is the most relevant to Igfbp3 and Vi4. **(E)** The heat map of miRNA sequencing between Sham (S1, S2) and HI (H1, H2) groups at 24 h after HI, *n* = 2 in each group. miR-185-5p and miR-380-5p were finally obtained. Red indicates high expression, and blue low expression. **(F)** Relative expression of miR-380-5p, miR-185-5p and Igfbp3 in the sham and HI groups in hippocampus 24 h post HI, *n* = 8/group. **(G)** Relative expression miR-380-5p, miR-185-5p and Igfbp3 in cortex 24 h after HI, *n* = 8/group. **(H)** Relative expression of miR-380-5p and miR-185-5p in neurons 24 h after OGD, *n* = 6/group. **(I)** Relative expression of Igfbp3 in neurons 24 h after OGD, *n* = 6/group. **(J,K)** Western blot detection of the expression of Igfbp3 protein in the cortical neurons in 24 h after OGD, *n* = 6/group. **(L,a)** The binding sites between Vi4 and miR-185-5p predicated by RNA22 software. **(L,b)** The binding sites between miR-185-5p and Igfbp3 3′UTR predicted by TargetScan. The Mut sequences designed for Igfbp3 3′UTR in luciferase reporter assay. **(M,N)** Relative luciferase activities in each group at 48 h after transfection, *n* = 6/group. **(O)** Relative expression of Igfbp3, and miR-185-5p in the serum of BI patients and normal controls. *n* = 23/group. **(P)** The primary cortical neurons from the aborted fetus in the normal and OGD condition. Scale bar = 50 μm. **(Q)** Quantitative detection of the expressional level of miR-185-5p and Igfbp3 in the human neurons after OGD insults, *n* = 6/group. For **(C,F–I,O,Q)**, the relative expression was relative to that of the sham or normal group. For **(J)**, the relative expression was relative to that of the 185-mimic-nc group. For **(K)**, the relative expression was relative to that of the ORF-NC group. WT, wild type; BI, brain ischemia; Mut, mutant. Data are shown as mean ± SD, $^*P < 0.05$.

were further applied to investigate effect of Igfbp3 and miR-185-5p following OGD condition (**Figure 4P**) and found that the expression of Igfbp3 was obviously elevated in OGD compared with normal neurons (**Figure 4Q**, $P < 0.05$). Whereas, miR-185-5p had the lowest expression level in OGD (**Figure 4Q**, $P < 0.05$). These results imply an important role of Vi4 in modulating Igfbp3 by competitively binding miR-185-5p in HI. Therefore, Vi4 is likely to function as a ceRNA for miR-185-5p.

Neurological Deficits Induced by Neonatal HI Were Improved After miR-185-5p Knockout (KO)

To investigate the function of miR-185-5p in rats with HIE, we established the miR-185-5p KO rats through CRISPR/CAS9 technology. Briefly, two single gRNA (sgRNA) action targets for miR-185 gene were designed. Oligonucleotide chains were synthesized according to the sticky end formed by sgRNA vector through *Bsa*I, then the chains were connected to pRP [CRISPR]-hCas9-U6 carrier after annealing. Construction of sgRNA vector was completed and was confirmed by sequencing (**Figure 5A**). After microinjection for F0, we began to reproduce to acquire Fragment 1 (F1), and verified the genetic modification of miR-185-5p caused by CRISPR/CAS9 via PCR gel electrophoresis to determine WT, homozygote (KO), and heterozygote (HET) off springs. WT and KO were used for the later experiment (**Figure 5B**). The result of qRT-PCR showed that there was lower expression of miR185-5p in the cortex and hippocampus of the miR-185-5p-KO rats than that of WT rats (**Figure 5C**, $P < 0.05$). Intracerebral glucose intake was observed by PET-CT, and quantified by the SUV-max. The glucose intake was increased in miR-185-5p-KO, compared to that of WT rats (**Figure 5D**, $P < 0.05$). As shown in **Figure 5E**, the TTC staining in the miR185-5p-WT group showed a clear cerebral infarction on right side of the brain, and the cerebral infarction as significantly reduced in the miR-185-5p-KO group, as demonstrated by the reduced infarct ratio (% contralateral) (**Figure 5H**, $P < 0.05$). Because of the swelling of cells after HIE injury and the cell layer of the hippocampus was thickened. However, the swelling of cells was attenuated in miR-185-5p-KO group. HE staining of the hippocampus showed that the cell layer size of the miR-185-5p-KO group was significantly thinner than that of the miR185-5p-WT group (**Figures 5F,I**, $P < 0.05$). Besides, Nissl-stained neurons were observed in cortex and hippocampus from miR185-5p-WT and miR185-5p-KO rats (**Figure 5G**). The miR185-5p-KO group showed the more total neurons and the lower dark neurons in both cortex and hippocampus than that of miR185-5p-WT group (**Figures 5J,K**, $P < 0.05$).

In order to observe the exploratory behavior, general activity and anxiety of experimental animals in new environments, the open field experiment was performed. Compared with WT rats, the rearing time spent by KO rats was clearly increased (**Figure 5L**, $P < 0.05$), but the grooming time spent by KO rats was largely decreased (**Figure 5M**, $P < 0.05$). In addition, compared with animals in the WT group, miR-185-5p KO rats had a reduced NSS score at both 1 month after HIE (**Figure 5N**, $P < 0.05$). Additionally, the running time on the rotarod by miR-185-5p KO rats was longer than that by WT rats (**Figure 5O**, $P < 0.05$) in the rotarod test, indicating these KO rats possessed better motor function and coordination ability 1 month after HIE. Similarly, spatial learning and memory were evaluated via Morris water maze at 1-month post HI induction. As a result, the KO rats performed better than the WT rats in finding the platform with a better learning performance through 5 days of training (**Figure 5P**, $P < 0.05$). On the 6th day, these KO rats also exhibited more crossings to the previous platform, indicating a better spatial memory (**Figure 5Q**, $P < 0.05$). In the test of Y-maze, KO animals spent shorter time in the wrong arm and longer time in the food arm than the WT animals. However, there was no significant difference in each arm entries (**Figure 5R**, $P > 0.05$). All these findings above suggest that knockout of miR-185-5p could ameliorate the motor, learning and memory dysfunctions induced by HIE.

miR-185-5p KO Decreased Cell Apoptosis and Enhanced Cell Viability in Primary Cortical Neurons and Hippocampal Neurons After OGD Associated With Vi4 and Igfbp3 Regulation

As shown in **Figure 6A**, after knocking out miR-185-5p in the rats, the protein level of Igfbp3 was significantly upregulated when compared to the WT rats, as indicated by western blot detection in both cortex and hippocampus (**Figure 6A**, $P < 0.05$). The expression of Igfbp3 mRNA in hippocampus of miR-185-5p-KO rats was obviously increased compared to WT rats (**Figure 6B**, $P < 0.05$). Similarly, the mRNA level of Vi4 was significantly upregulated in cortex of miR-185-5p-KO rats when compared to the WT rats (**Figure 6C**, $P < 0.05$). Consequently, Igfbp3 siRNA was constructed to silence the expression of Igfbp3. The result of WB showed the expression of Igfbp3 protein was remarkably reduced after interfering Igfbp3 (**Figure 6D**, $P < 0.05$). After OGD, the cortical and hippocampal neurons were damaged significantly compared with the normal neurons, especially the neurites, as indicated by Tuj1 staining. Igfbp3 knockdown aggravated the neuron injury, as demonstrated by shorter neurites and lower cell viability detected by CCK8 assay as compared with the NC group (**Figures 6E–G**, $P < 0.05$). These demonstrated that Igfbp3 played an important role in neuroprotection after OGD. Furthermore, to investigate whether miR-185-5p regulates cell growth through modulating Igfbp3 or functioning together with Vi4, we performed immunofluorescent staining of Tuj1 and TUNEL as well as CCK8 in WT and KO neurons from both cortex and hippocampus with OGD. For the rescue experiment, interference of Vi4 by shRNA (Vi4-shRNA) or Igfbp3-shRNA was added to KO cells. As a result, OGD induced serious neuron damage, such as cell apoptosis and axonal injury, while miR-185-5p KO reduced cell apoptosis and showed better axon growth. This protective role was abolished by the inhibition of Vi4 or Igfbp3 (**Figures 6H,I**), as demonstrated by lower CCK8 values and shorter neurites as well as more cell apoptosis in both cortical and hippocampal neurons (**Figures 6J–L**, $P < 0.05$). These findings further ascertain that miR-185-5p KO could protect neurons from OGD via modulating Igfbp3 and Vi4.

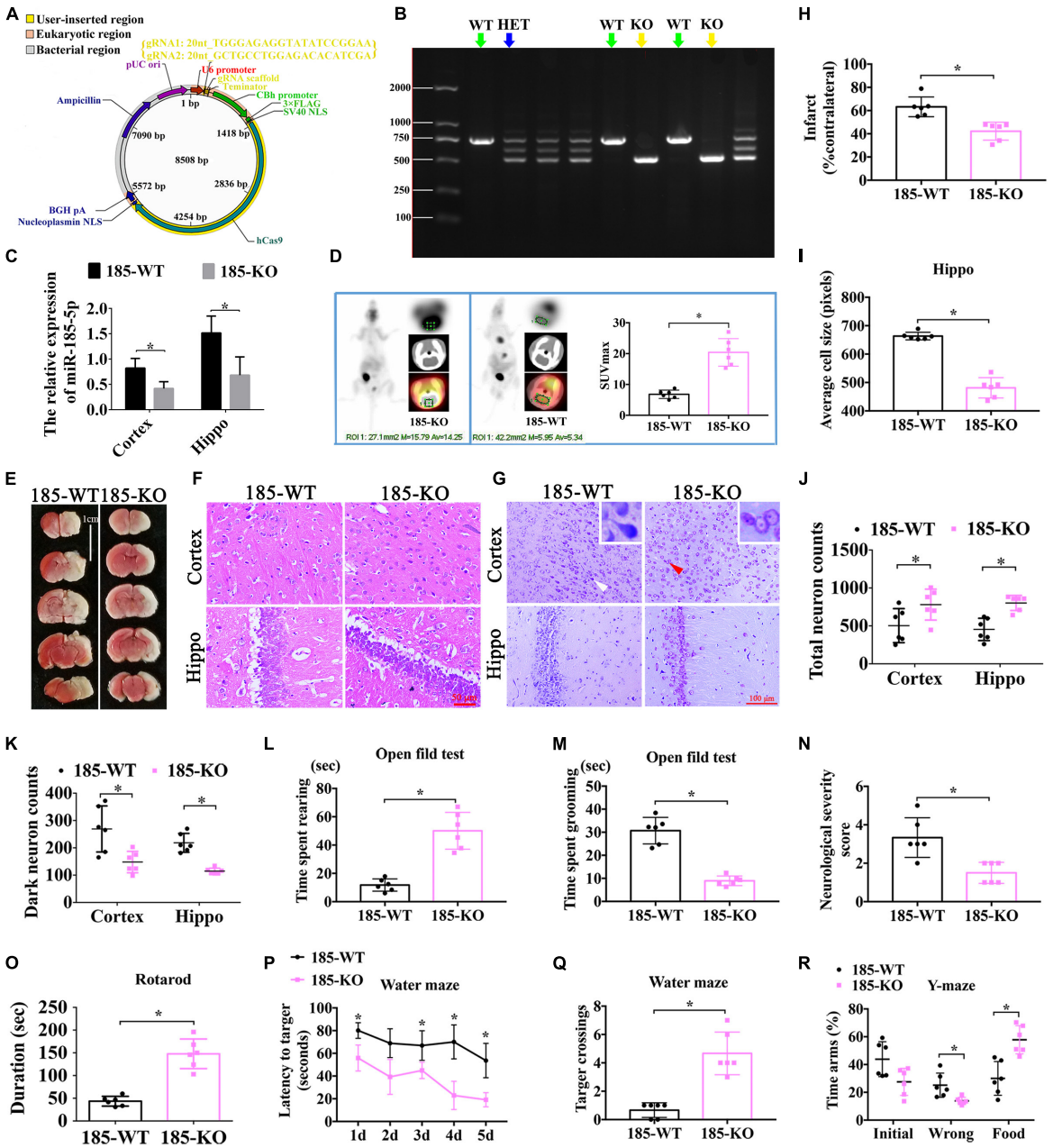

FIGURE 5 | The role of miR-185-5p KO in the improvement of neurological function after HIE. **(A)** The vector map for miR-185-5p vector builder. U6 promoter: Human U6 promoter. {gRNA1: 20nt_TGGGAGAGGTATATCCGGAA; gRNA2: 20nt_GCTGCCTGGAGACACATCGA}: the component entered by user. gRNA scaffold, Chimeric gRNA scaffold; Terminator, U6 terminator; CBh promoter, Chicken beta Act n hybrid promoter; 3xFLAG, 3 tandem flag epitopes; SV40 NLS, SV40 nuclear localization signal; hCas9, Human codon-optimized Cas9; Nucleoplasmin NLS, Nucleoplasmin nuclear localization signal; BGH pA, Bovine growth hormone polyadenylation; Ampicillin, Ampicillin resistance gene; pUCori, pUC origin of replication. **(B)** Electrophoretic band chart for genotype detection. Green arrows represent WT rats, yellow represent KO, and blue arrow represents HET. The markers exhibit 100 bp, 250 bp, 500 bp, 750 bp, 1000 bp, and 2000 bp, respectively. **(C)** The relative expression of Igfbp3 in the rats of 185-WT and 185-KO. The relative expression was relative to that of the 185-WT in cortex group. **(D)** The glucose-uptake images in the brain and SUV max detected by PET-CT 2-month post HIE. **(E,H)** TTC staining and quantitative analysis of infarct ratio, respectively, in the rats of 185-WT and 185-KO. Scale bar = 1 cm. Pale color represents infarct area, *n* = 6/group. **(F,I)** HE staining and the cell size analysis of cortex and hippocampus, respectively, in the rats of 185-WT and 185-KO. Scale bar = 50 μm, *n* = 6/group. **(G)** Nissl staining in cortex and hippocampus between 185-WT and 185-KO groups. The white arrow represents surviving neurons. The red arrow represents dark neurons. Scale bar = 100 μm. **(J,K)** Quantitative histogram for total neuron and dark neuron in cortex and hippo in these groups, *n* = 6/group. **(L,M)** The time spent rearing and grooming in the open field test 1 month after HIE, respectively, *n* = 6/group. **(N)** NSS score at 1 month after HIE. **(O)** The duration of on the rotarod bar 1 month after HIE, *n* = 6/group. **(P)** The latency to target for the first 5 days training in the MWM test, *n* = 6/group. **(Q)** Target crossings in MWM test in the 6th day of testing. **(R)** The time spent in the initial, wrong and food arms of Y-maze at 1-month post HIE, *n* = 6/group. HET: heterozygote. 185-WT: miR-185-5p wild type. 185-KO: miR-185-5p knockout. PET-CT, Positron Emission Tomography-Computed Tomography; SUV, standardized uptake value; HE, hematoxylin-eosin; Hippo, hippocampus. All data are presented as mean ± SD, $^*P < 0.05$.

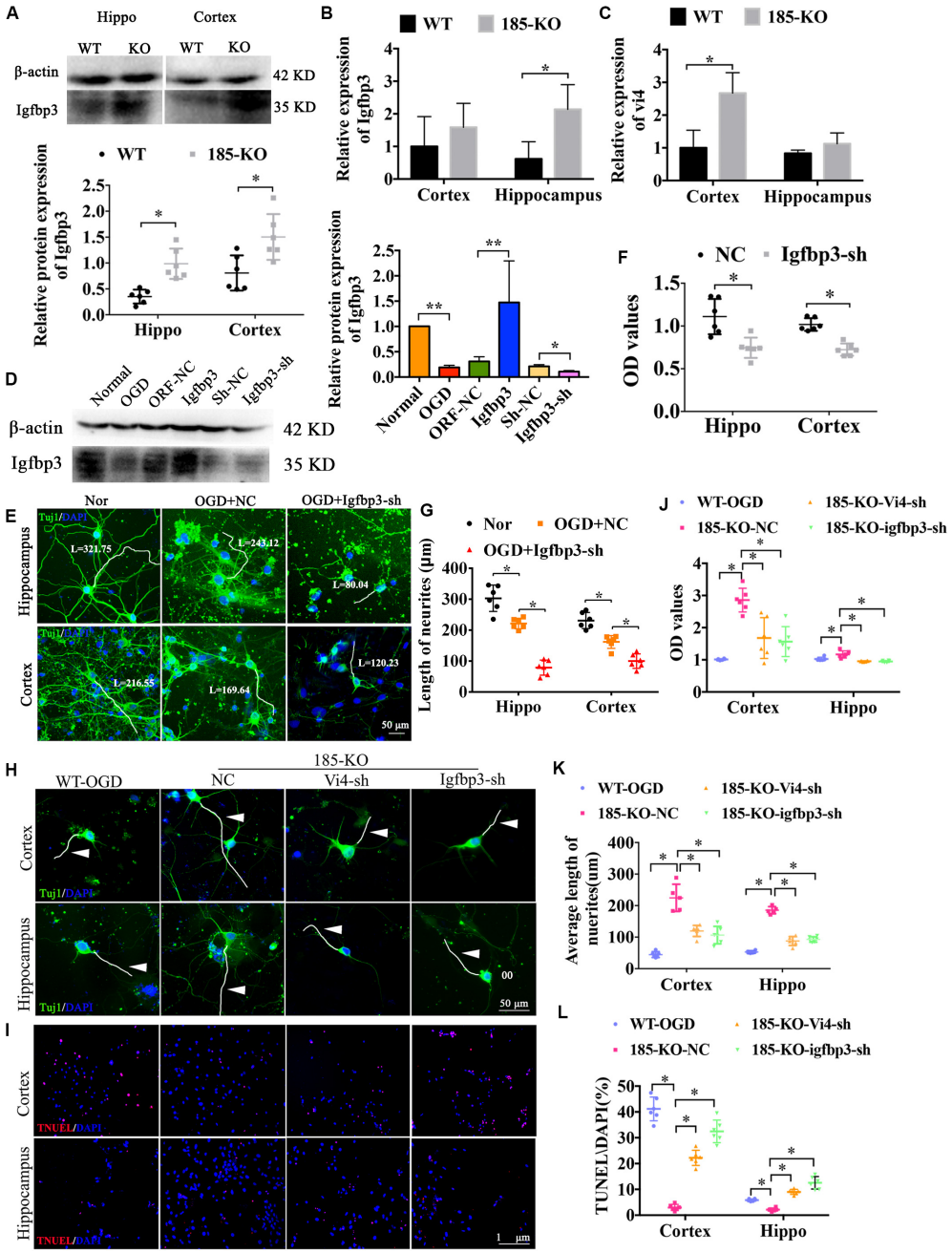

FIGURE 6 | The role of miRNA-185-5p KO in the growth of neurons and cell apoptosis as well as the regulatory relationship with Vi4 and Igfbp3 in function. **(A)** Western blot detection of the expression of Igfbp3 protein in the cortical and hippocampal brain tissues of the WT and 185-KO rats, *n* = 6/group. The relative expression was relative to that of the 185-WT in hippocampus group. **(B,C)** The expression of Igfbp3 and Vi4 in cortex and hippocampus from WT and 185-KO rats. The relative expression was relative to that of the 185-WT in cortex group. **(D)** Western blot detection of the expression of Igfbp3 protein in the cortical neurons in the groups of normal, OGD, NC, Igfbp3 and Igfbp3-sh. The relative expression was relative to that of the sham or normal group. **(E,G)** Immunofluorescent staining of Tuj1 in Nor, OGD + NC, and OGD + Igfbp3-sh groups to detect the cell phenotype and axon growth. The neurons are stained by green colors, which are Tuj1 positive. Blue represents the nucleus. Scale bar = 50 μm. **(F)** Relative CCK8 values in the cortical and hippocampal neurons between NC and Igfbp3-si groups, *n* = 6/group. **(H)** Immunofluorescent staining of Tuj1 in the cortical and hippocampal neurons, respectively, in the groups of WT, miR-185-5p-KO + NC (185-KO-NC), miR-185-5p-KO + Vi4-sh (185-KO-Vi4-sh) and miRNA-185-5p-KO + Igfbp3-sh (185-KO-Igfbp3-sh) 24 h after OGD. Scale bar = 50 μm, green staining represents the Tuj1 positive cells, and the nucleus s stain d by blue. White arrow represents axon. **(I)** TUNEL staining in the WT, miR-185-5p-KO + NC (185-KO-NC), miR -185-5p-KO + Vi4-sh (185-KO-Vi4-sh) and miRNA-185-5p-KO + Igfbp3-sh (185-KO-Igfbp3-sh) groups 24 h after OGD in both cortical and hippocampal neurons. Scale bar = 100 μm. Apoptotic cells are stained by red color, and the nucleus is stained by blue. **(J–L)** Quantitative histograms of relative CCK8 values, the average length of axon and cell apoptosis presented by TUNEL/DAPI (%). Nor, normal; Vi4-sh, Vi4-shRNA, interference of Vi4 by shRNA; Igfbp3-sh, interference of Igfbp3 by shRNA. All data are shown as mean ± SD, $^{*}P < 0.05$, $^{**}P < 0.01$, *n* = 6/group.

Inhibition of Vi4 and Igfbp3 Aggravated the Neuron Damage and Neurological Deficits in Rats With HIE

Postnatal day 3 rats were injected with 5 μl (2×10^8/ml) Igfbp3-sh or Vi4-sh or sh-NC into the right lateral ventricle via microscopic device. The results of HE staining showed that the cell layer size of the Igfbp3-sh group was significantly thicker than that of the NC group in the cortex and hippocampus (**Figures 7A,B**, $P < 0.05$). Moreover, Nissl-staining revealed (**Figure 7C**) that the number of total neurons was obviously reduced in HI group, and the dark neurons was increased in comparison to sham group. Whereas, the number of total neurons was remarkably decreased in the Igfpb3-sh group as compared with NC group (**Figure 7D**, $P < 0.05$). Furthermore, Igfpb3-sh group showed more dark neurons in both cortex and hippocampus than that of NC group (**Figure 7E**, $P < 0.05$). In addition, spatial learning was evaluated for consecutive 5 days and a probe trial for spatial memory was conducted on the 6th day at post HIE. As expected, at both times points the rats injected with Igfbp3-sh performed worse in learning and memory than rats in the sham or NC groups (**Figures 7F,H**, $P < 0.05$) Compared with the NC group, the rats of Igfbp3-sh group had significantly less crossings over the previous platform location (**Figure 7G**, $P < 0.05$). Additionally, NSS in Igfbp3-sh group was obviously increased compared with the NC group after HIE (**Figure 7I**, $P < 0.05$). Similarly, Igfbp3-sh rats exhibited decreased time on the rotor bar compared to the NC littermates (**Figure 7J**, $P < 0.05$). Furthermore, the Y-maze was performed to measure the spatial memory of rats 1 month after HIE. The time spent in food arm in the Igfbp3-sh group was shorter than that in the NC group ($P < 0.05$), while time in the error arm was longer ($P < 0.05$), indicating that the ventricle injection of Igfbp3-sh damaged the spatial memory of rats with HIE (**Figures 7K,L**, $P < 0.05$). Open field test indicated that Igfbp3-sh rats showed more grooming time and less rearing time compared to the NC group (**Figures 7M,N**, $P < 0.05$). Moreover, knocking down Vi4 showed the same trend as Igfbp3-sh, which increased neuronal apoptosis and worsen the motor and cognitive deficits in rats with HIE (**Figure 7**, $P < 0.5$).

DISCUSSION

Accumulating evidence showed that lncRNAs and miRNAs played important roles in physiological and pathological conditions. As a result, new drugs were under development to target miRNAs and lncRNAs for the treatment of cancers and other diseases. In this study, we reported that a novel lncRNA (Vi4) as upregulated in the brain of HIE rats and in cortical neurons under OGD conditions, promoted neurite growth and reduces cell apoptosis of cortical and hippocampal neurons after HI. We have elucidated a functional mechanism of Vi4 which upregulated the Igfbp3 gene via competitively binding miR-185-5p in HI. *In vivo* studies showed that, overexpression of Vi4 or silencing (or KO) of miR-185-5p improved long-term motor functions and reduced the deficiencies in learning and memory of HIE rats.

In the present study, we have successfully established a HIE model in neonatal rats and found Vi4 has a function of promoting the cell growth and neuroprotection in rats with HIE. Accumulating evidence has indicated that the brain was the organ with the most abundant and varied lncRNAs which also existed in the other parts of mammalian body except reproductive cells (Goff et al., 2015). Many lncRNAs were specifically expressed in nerve cells with different levels of expression in different brain regions (Aprea et al., 2013; Luo et al., 2013). For example, a high level of expression of lncRNA HOTAIR facilitated the onset of ischemic infarct induced by hypoxia (Yang and Lu, 2016). MALAT 1 protects brain microvasculature and parenchyma after brain ischemic injury by suppressing endothelial cell death and inflammation (Zhang et al., 2017). The present study has for the first time identified the novel function of Vi4 involved in neuroprotection in the rat model of HIE. It is highly expressed in the brain of HI and in neurons with OGD. Lentivirus-mediated overexpression of Vi4 promoted growth of neurites, increased viability and reduced apoptosis of primary neurons of cortex and hippocampus after OGD *in vitro*. Consistently, neonatal HIE rats with Vi4-ORF treatment showed a reduced infarction size and better performance in motor behavior and cognitive functions after acute and long-term HI. PET-CT showed these rats treated with Vi4-ORF also exhibited more glucose-uptake in the brain. Thus, our results indicated that a higher level of Vi4 was associated with the recovery of neurological deficits induced by neonatal HIE. Through conjoint analysis of bioinformatics prediction and PCR verification, we found that Igfbp3 was closely correlated with Vi4 in both regulatory sites and function. We observed that the overexpression of Vi4 was enough to increase the mRNA level of Igfbp3 and promote neurological recovery. It is known that Igfbp3 on the surface of vascular endothelial cells may help attracting IGF-I, which stimulates angiogenesis (Danis and Bingaman, 1997), and the level of Igfbp3 mRNA in cerebral vascular endothelial cells is increased at 1 h after HI, and reaches its highest level at 24 h after recovery (Lee et al., 1999). In contrast, after HI (1, 5, 24, and 72 h), neuronal Igfbp3 mRNA expression levels in the area of normal middle cerebral artery supply decreased significantly within 24 h (Lee et al., 1999), which was consistent with our findings of down-regulation of Igfbp3 protein expression at 6 h after HI. These results suggested that Igfbp3 downregulation was detrimental to neurological function after HIE injury. Accumulating evidence showed that Igfbp3 could promote axonal growth, cellular proliferation and differentiation (Devesa et al., 2014 and Kartal et al., 2016). In this sense, the lack or deficiency of hormones may lead to acute and subacute consequences, such as hypoglycemia, growth retardation, mental-motor deficiency, disturbances in cognitive functions and cardiovascular system (Volpe, 2001), indicating an important role of Igfbp3 in HIE. Our data in the present study showed that Vi4 was an upstreaming positive regulator of the Igfbp3 gene in HIE was consistent with these published results, indicating the Vi4-Igfbp3 signal was a critical neuroprotective factor in HI injury. Furthermore, to answer a question of how Vi4 functions with Igfbp3, and if some other

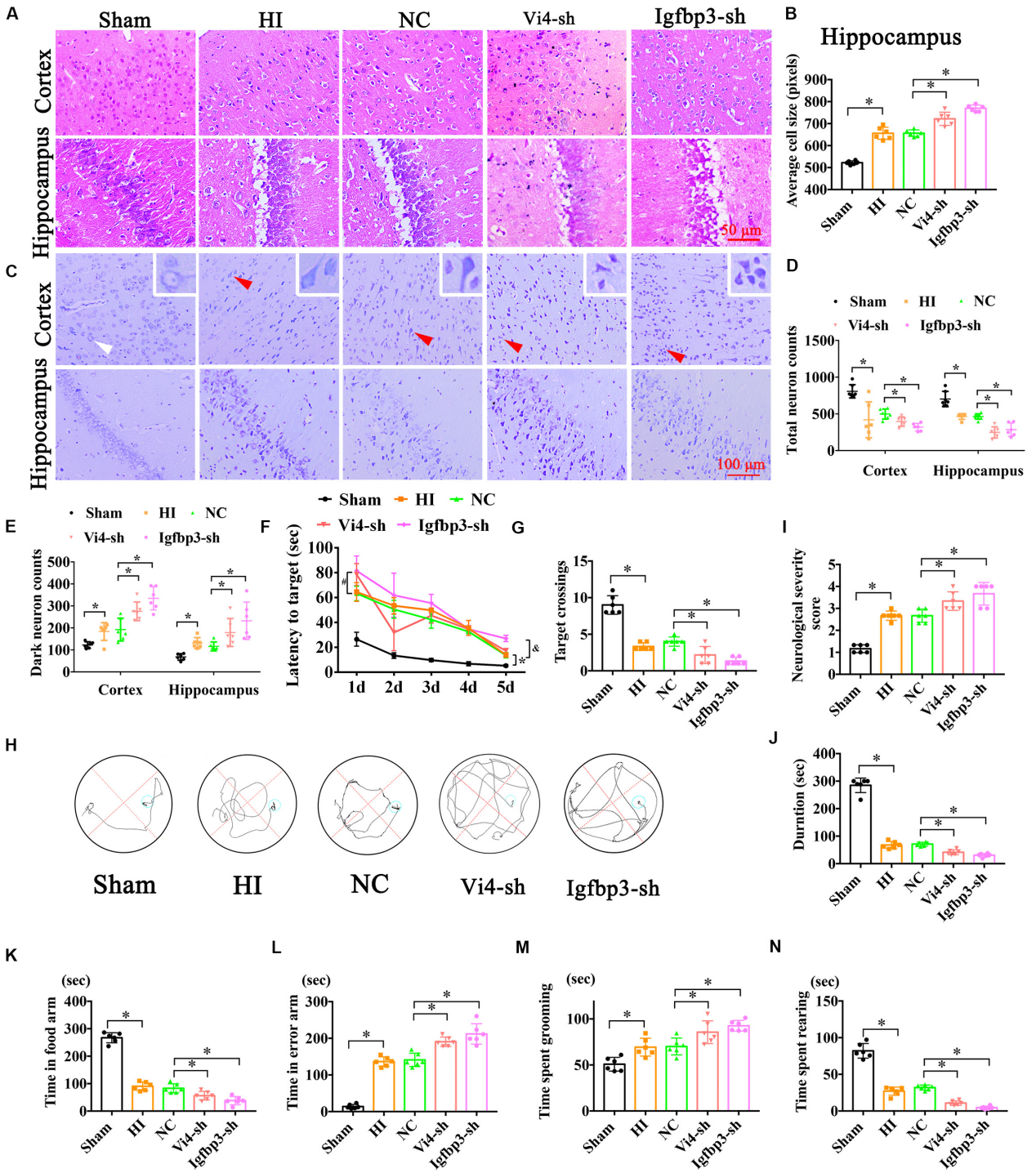

FIGURE 7 | The neurobehavioral tests of rats after intraventricular injection of Vi4-sh and Igfbp3-sh *in vivo*. **(A,B)** HE staining and the cell size analysis of cortex and hippocampus, respectively, in the rats of Sham, HI, NC, Vi4-sh and Igfbp3-sh. Scale bar = 50 μm, n = 6/group. **(C)** Nissl staining in cortex and hippocampus among sham, HI, NC, Vi4-sh and Igfbp3-sh groups. The white arrow represents surviving neurons. The red arrow represents dark neurons. Scale bar = 100 μm. **(D,E)** Quantitative histogram for total neuron and dark neuron in these groups, n = 6/group. **(F)** The latency to target during 5 days training among the sham, HI, NC, Vi4-sh and Igfbp3-sh groups after HI in MWM test. $^{*}P < 0.05$: HI vs. Sham.$^{\#}P < 0.05$: Vi4-sh vs. NC. $^{\&}P < 0.05$: Igfbp3-sh vs. NC, n = 6/group. **(G)** Target crossings in MWM test after HI, respectively, n = 6/group. **(H)** The walking path of the platform in probe trial of Morris Water Maze test at day 5 after HI. **(I)** NSS score among the sham, HI, NC, Vi4-sh and Igfbp3-sh groups post HI, n = 6/group. **(J)** The duration of rats on rotary bar in the rotarod test after HI, n = 6/group. **(K,L)** The time arms of food and error arms in the sham, HI, NC, Vi4-sh and Igfbp3-sh groups after HI in the Y-maze test, n = 6/group. **(M,N)** The time spent grooming and rearing in the open field experiment after HI, n = 6/group. All data were presented as mean ± SD, $^{*}P < 0.05$.

pathways exist in the regulation between Vi4 and Igfbp3, we performed double prediction via RNA22 and TargetScan, then combined with luciferase reporter assay and functional detection. Our results indicated that Vi4 shared the response element of Igfbp3 with miR-185-5p. To confirm our prediction, we constructed miR-185-5p KO rats, and examined their regulatory relationship *in vivo* in the model of HIE and *in vitro* neurons under OGD. We have found that rats with miR-185-5p KO perform better in the long-term spatial learning and memory and motor tests. In addition, after miR-185-5p knockout, the cortical and hippocampal neurons grew better than WT neurons, and cell apoptosis was also decreased after OGD. Furthermore, these positive effects were partially reversed by interfering with Vi4 or Igfbp3. Evidence in the past few years has shown that miR-185 was a novel tumor suppressor and was one of the most well-defined miRNAs in cancer biology. It was associated with cell proliferation and apoptosis and plays a major role in tumorigenesis and tumor progression (Dong-Xu et al., 2015; Sun et al., 2017). However, there is no study to show it is associated with HIE. Our result in present study indicated that miR-185-5p could be a therapeutic target in HIE, and Vi4 may function as a ceRNA by competitively binding miR-185-5p, and modulate Igfbp3 in the process of HI-induced neuronal injury. In order to further validate this finding, we also verified their expressional levels in patients with brain ischemia, and indeed showed that the level of Igfbp3 was increased and miR-185-5p decreased after brain ischemia in the blood of patients. The changes of Igfbp3 and miR-185-5p after brain ischemia may represent early compensatory mechanisms for self-protection in the body (Purushothuman and Stone, 2015).

Taken together, our research has demonstrated that Vi4 and miR-185-5p act as key regulators of the Igfbp3 gene, whereby Vi4 positively promotes its gene expression but miR-185-5p negatively counteracts Vi4. Our study has also elucidated important roles of Vi4-miR-185-5P-Igfbp3 signaling network in regulating neuron survival and cell apoptosis after HIE, showing Vi4-Igfbp3 signal promotes functional recovery whereas miR185-5p aggravates the brain damage after HIE. Vi4-miR185-5p-Igfbp3 could be potential therapeutically targets for HIE treatment.

DATA AVAILABILITY STATEMENT

The datasets generated for this study can be found in the Vi4-miR-185-5p-lgfbp3 network protects the brain from neonatal hypoxic ischemic injury via promoting neuron survival and suppressing the cell apoptosis.

ETHICS STATEMENT

The studies involving human participants were reviewed and approved by the Ethics Committee of Kunming Medical University, China (Approval No. 2015-9) in September 30, 2015. The patients/participants provided their written informed consent to participate in this study. The animal study was reviewed and approved by the Animal Care and Welfare Committee of Kunming Medical University. Written informed consent was obtained from the owners for the participation of their animals in this study and individual(s) for the publication of any potentially identifiable images or data included in this article.

AUTHOR CONTRIBUTIONS

L-LXi, L-LXu, R-LD, H-LZ, Y-XT, ZM, YJ, Z-BZ, YX, QH, LB, X-FZ, JL, and T-HW performed the material preparation and data collection and analysis. L-LXi, L-LXu, H-LZ, QH, and T-HW wrote and revised the first draft of the manuscript. All authors contributed to the study conception and design, commented on previous versions of the manuscript, and read and approved the final manuscript.

FUNDING

This study was supported by grant from the National Natural Science Foundation of China (Grant Nos. 82001604 and 82060243) and Joint Fund of Zunyi Science and Technology Bureau-Affiliated Hospital of Zunyi Medical University No. HZ2020250. This work was also supported by Program of Science and Technology, Department of Sichuan Province (2020YFS0043) and Doctoral Start-up Fund of Affiliated Hospital of Zunyi Medical University No. 201903.

ACKNOWLEDGMENTS

We would like to thank Prof. Zhao-Qiong Zhu from Department of Anesthesiology, the Affiliated Hospital of Zunyi Medical University and Prof. Fei Liu from Department of Anesthesiology, West China Hospital, Sichuan University for their technical support.

SUPPLEMENTARY MATERIAL

The Supplementary Material for this article can be found online at: https://www.frontiersin.org/articles/10.3389/fcell.2020.529544/full#supplementary-material

REFERENCES

Aprea, J., Prenninger, S., Dori, M., Ghosh, T., Monasor, L. S., Wessendorf, E., et al. (2013). Transcriptome sequencing during mouse brain development identifies long non-coding RNAs functionally involved in neurogenic commitment. *EMBO J.* 32, 3145–3160. doi: 10.1038/emboj.2013.245

Brekke, E., Berger, H. R., Wideroe, M., Sonnewald, U., and Morken, T. S. (2017). Glucose and intermediary metabolism and astrocyte-neuron interactions following neonatal hypoxia-ischemia in

rat. *Neurochem. Res.* 42, 115–132. doi: 10.1007/s11064-016-2149-9

Busl, K. M., and Greer, D. M. (2010). Hypoxic-ischemic brain injury: pathophysiology, neuropathology and mechanisms. *NeuroRehabilitation* 26, 5–13. doi: 10.3233/nre-2010-0531

Chiyomaru, T., Yamamura, S., Fukuhara, S., Yosh, H., Kinoshita, T., Majid, S., et al. (2013). Genistein inhibits p ostate cancer cell growth by targeting miR-34a and oncogenic HOTAIR. *PLoS One* 8:e70372. doi: 10.1371/journal.pone.0070372

Clark, B. S., and Blackshaw, S. (2014). Long non-coding RNA-dependent transcriptional regulation in neuronal development and disease. *Front. Genet.* 5:164. doi: 10.3389/fgene.2014.00164

Dailey, T., Mosley, Y., Pabon, M., Acosta, S., Tajiri, N., van Loveren, H., et al. (2013). Advancing critical care medicine with stem cell therapy and hypothermia for cerebral palsy. *Neuroreport* 24, 1067–1071. doi: 10.1097/wnr.0000000000000062

Danis, R. P., and Bingaman, D. P. (1997). Insulin-like growth factor-1 retinal microangiopathy in the pig eye. *Ophthalmology* 104, 1661–1669. doi: 10.1016/s0161-6420(97)30081-5

Devesa, P., Agasse, F., Xapelli, S., Almengló, C., Devesa, J., Malva, J. O., et al. (2014). Growth hormone pathways signaling for cell prolifera-tion and survival in hippocampal neural precursors from postnatalmice. *BMC Neurosci.* 15:100. doi: 10.1186/1471-2202-15-100

Dong-Xu, W., Jia, L., and Su-Juan, Z. (2015). MicroRNA-185 is a novel tumor suppressor by negatively modulating the Wnt/beta-catenin pathway in human colorectal cancer. *Indian J. Cancer* 52(Suppl. 3), E182–E185. doi: 10.4103/0019-509x.186576

Ferrari, D. C., Nesic, O. B., and Perez-Polo, J. R. (2010). Oxygen resuscitation does not ameliorate neonatal hypoxia/ischemia-induced cerebral edema. *J. Neurosci. Res.* 88, 2056–2065. doi: 10.1002/jnr.22358

Goff, L. A., Groff, A. F., Sauvageau, M., Trayes-Gibson, Z., Sanchez-Gomez, D. B., Morse, M., et al. (2015). Spatiotemporal expression and transcriptional perturbations by long noncoding RNAs in the mouse brain. *Proc. Natl. Acad. Sci. U.S.A.* 112, 6855–6862. doi: 10.1073/pnas.1411263112

Hamm, R. J., Pike, B. R., O'Dell, D. M., Lyeth, B. G., and Jenkins, L. W. (1994). The rotarod test: an evaluation of its effectiveness in assessing motor deficits following traumatic brain injury. *J. Neurotrauma* 11, 187–196. doi: 10.1089/neu.1994.11.187

Hu, F., Li, T., Gong, H., Chen, Z., Jin, Y., Xu, G., et al. (2017). Bisphenol A impairs synaptic plasticity by both pre- and postsynaptic mechanisms. *Adv. Sci. (Weinh)* 4:1600493. doi: 10.1002/advs.201600493

Hu, Q., Chen, C., Yan, J., Yang, X., Shi, X., Zhao, J., et al. (2009). Therapeutic application of gene silencing MMP-9 in a middle cerebral artery occlusion-induced focal ischemia rat model. *Exp. Neurol.* 216, 35–46. doi: 10.1016/j.expneurol.2008.11.007

Kartal, Ö, Aydınöz, S., Kartal, A. T., Kelestemur, T., Caglayan, A. B., Beker, M. C., et al. (2016). Time dependent impact of perinatal hypoxia on growth hormone, insulin-like growth factor 1 and insulin-like growth factor binding protein-3. *Metab. Brain Dis.* 4, 827–835. doi: 10.1007/s11011-016-9816-z

Lee, W. H., Wang, G. M., Yang, X. L., Seaman, L. B., and Vannucci, S. I. (1999). Perinatal hypoxia-ischemia decreased neuronal but increased cerebral vascular endothelial IGFBP3 expression. *Endocrine* 11, 181–188. doi: 10.1385/endo:11:2:181

Luo, H., Sun, S., Li, P., Bu, D., Cao, H., and Zhao, Y. (2013). Comprehensive characterization of 10,571 mouse large intergenic noncoding RNAs from whole transcriptome sequencing. *PLoS One* 8:e70835. doi: 10.1371/journal.pone.0070835

Purushothuman, S., and Stone, J. (2015). The reaction of cerebral cortex to a nearby lesion: damage, survival, self-protection. *Brain Res.* 1601, 52–63. doi: 10.1016/j.brainres.2015.01.003

Shankaran, S., Pappas, A., McDonald, S. A., Vohr, B. R., Hintz, S. R., and Yolton, K. (2012). Childhood outcomes after hypothermia for neonatal encephalopathy. *N. Engl. J. Med.* 366, 2085–2092. doi: 10.1056/NEJMoa1112066

Shohami, E., Novikov, M., and Bass, R. (1995). Long-term effect of HU-211, a novel non-competitive NMDA antagonist, on motor and memory functions after closed head injury in the rat. *Brain Res.* 674, 55–62. doi: 10.1016/0006-8993(94)01433-i

Sun, C. C., Zhang, L., Li, G., Li, S. J., Chen, Z. L., Fu, Y. F., et al. (2017). The lncRNA PDIA3P interacts with miR-185-5p to modulate oral squamous cell carcinoma progression by targeting cyclin D2. *Mol. Ther. Nucleic Acids* 9, 100–110. doi: 10.1016/j.omtn.2017.08.015

Tay, Y., Rinn, J., and Pandolfi, P. P. (2014). The multilayered complexity of ceRNA crosstalk and competition. *Nature* 505, 344–352. doi: 10.1038/nature12986

Volpe, J. J. (2001). Perinatal brain injury from pathogenesis to neuroprotec-tion. *Ment. Retard. Dev. Disabil. Res. Rev.* 7, 56–64. doi: 10.1002/1098-2779(200102)7:1<56::AID-MRDD1008<3.0.CO;2-A

Wang, K., Liu, F., Zhou, L. Y., Long, B., Yuan, S. M., and Wang, Y. (2014). The long noncoding RNA CHRF egulat s cardiac hypertrophy by targeting miR-489. *Circ. Res.* 114, 1377–1388. doi: 10.1161/circresaha.114.302476

Wang, W. T., Sun, Y. M., Huang, W., He, B., Zhao, Y. N., and Chen, Y. Q. (2016). Genome-wide long non-coding RNA analysis identified circulating LncRNAs as novel non-invasive diagnostic biomarkers for gynecological disease. *Sci. Rep.* 6:23343. doi: 10.1038/srep23343

Yang, B., Xia, Z. A., Zhong, B., Xiong, X., Sheng, C., and Wang, Y. (2017). Distinct hippocampal expression profiles of long non-coding RNAs in an Alzheimer's disease model. *Mol. Neurobiol.* 54, 4833–4846. doi: 10.1007/s12035-016-0038-5

Yang, D., and Kuan, C. Y. (2015). Anti-tissue plasminogen activator (tPA) as an effective therapy of neonatal hypoxia-ischemia with and without inflammation. *CNS Neurosci. Ther.* 21, 367–373. doi: 10.1111/cns.12365

Yang, L., and Lu, Z. N. (2016). Long non-coding RNA HOTAIR promotes ischemic infarct induced by hypoxia through up-regulating the expression of NOX2. *Biochem. Biophys. Res. Commun.* 479, 186–191. doi: 10.1016/j.bbrc.2016.09.023

Zhang, X., Tang, X., Liu, K., Hamblin, M. H., and Yin, K. J. (2017). Long noncoding RNA Malat1 regulates cerebrovascular pathologies in ischemic stroke. *J. Neurosci.* 37, 1797–1806. doi: 10.1523/jneurosci.3389-16.2017

Conflict of Interest: The authors declare that the research was conducted in the absence of any commercial or financial relationships that could be construed as a potential conflict of interest.

Advantages of publishing in Frontiers

OPEN ACCESS
Articles are free to read for greatest visibility and readership

FAST PUBLICATION
Around 90 days from submission to decision

HIGH QUALITY PEER-REVIEW
Rigorous, collaborative, and constructive peer-review

TRANSPARENT PEER-REVIEW
Editors and reviewers acknowledged by name on published articles

Frontiers
Avenue du Tribunal-Fédéral 34
1005 Lausanne | Switzerland

Visit us: www.frontiersin.org
Contact us: frontiersin.org/about/contact

REPRODUCIBILITY OF RESEARCH
Support open data and methods to enhance research reproducibility

DIGITAL PUBLISHING
Articles designed for optimal readership across devices

FOLLOW US
@frontiersin

IMPACT METRICS
Advanced article metrics track visibility across digital media

EXTENSIVE PROMOTION
Marketing and promotion of impactful research

LOOP RESEARCH NETWORK
Our network increases your article's readership